THESIS, SUBMITTED FOR THE DEGREE OF DOCTOR OF PHILOSOPHY IN THE UNIVERSITY OF OXFORD

METAMORPHIC EVOLUTION OF THE CRUST OF SOUTH-WESTERN NORWAY: AN EXAMPLE FROM SOGNEFJORD



by

DAVID ELLIOTT BAILEY

of UNIVERSITY COLLEGE

and the DEPARTMENT OF EARTH SCIENCES,

UNIVERSITY OF OXFORD

SHORT ABSTRACT

Metamorphic evolution of the crust of south-western Norway: An example from Sognefjord, D.Phil thesis by D. E. Bailey of University College (Trinity Term, 1989)

Part of the Western Gneiss Region (WGR) of Norway has been mapped in western Sognefjord. Five major tectonostratigraphic units underlying low-grade Devonian metasediments have been recognized: the Basement Gneisses (BG), Lower, Middle, and Upper Mafic Units (LMU, MMU, UMU), and Hyllestad Schists (HS). All the units have been affected by polyphase deformation. Five different styles of deformation have been recognized across the field area, representing up to five discrete tectonic episodes.

Eclogite facies mineral assemblages have been found in the BG, either forming mafic pods or as relicts in garnet amphibolites. Temperature and pressure conditions of metamorphism in all units have been estimated using various calibrated reactions. Temperatures range from about 400 °C to 700 °C and pressures from about 4 kbar in post-D_2 assemblages to 15 kbar in eclogites. Estimated conditions of eclogite formation are consistent with regional studies.

High-pressure (eclogitic) conditions have also been inferred from mineral textures in the highest unit (Hyllestad Schists). Mineral assemblages in parts of this unit may represent pressures as high as 14 kbar at temperatures of 600 °C.

It is suggested that the Mafic Units and HS are allochthonous and were emplaced onto the WGR during an early stage of the Caledonian Orogeny. All units, including the Basement Gneisses, have suffered retrogression during a late extensional phase which continued into at least the Middle Devonian.

LONG ABSTRACT

An area in Sognefjord has been mapped on the western margin of the Western Gneiss Region (WGR). Petrographic studies have also been carried out on basement rocks sampled between Lavik and Vangsnes from both the north and south shores of Sognefjord. In the main field area of study, between Hyllestad and Lavik, five major tectonostratigraphic units have been recognized. Each unit is separated from the others by tectonic contacts in which blastomylonitic fabrics are developed. The basal unit, the Basement Gneisses (BG), is characterized by migmatites and gneisses of acidic to intermediate compositions, and supracrustal origins. It is overlain by three units comprising mainly mafic to intermediate plutonic rocks overprinted by amphibolite and lower grades of metamorphism during the Caledonian orogeny. These units have been named the Lower, Middle, and Upper Mafic Units (LMU, MMU, UMU). The highest unit, the Hyllestad Schists (HS), chiefly comprises quartzose and pelitic metasediments, with metavolcanites, minor intrusives, and two large bodies of deformed granite. The grade of these rocks varies from Lower Greenschist in the west to amphibolite, and possibly even eclogite, facies in the east. They are, in turn, overlain by Devonian conglomerates along a low-angle contact, which also shows a tectonic fabric.

All units show polyphase deformation, but different episodes of the tectonic history are better developed in some units than others. Five deformation "events" have been recognized in the BG and characteristic structural elements have been correlated with structures of similar style, and with similar relations to metamorphic events, in the other

units. All units are believed to have shared broadly the same tectonic history since D_3 and all show evidence of a pre-D_3 event in which a strong foliation was developed (D_2). F_3 folds in the west of the field area are recumbent and have a consistent northwesterly vergence. D_4 structures are confined to open warps of the foliation seen only in the BG. However, a low-angle extensional shear banding is developed during D_5, also with a "top-to-northwest" vergence. The intensity of Caledonian deformation decreases eastwards. In the Hyllestad-Lavik region very little of the pre-Caledonian fabric is preserved but, between Höyanger and Balestrand, Precambrian textures in basement migmatites can be seen and Caledonian deformation is mainly confined to discrete shear zones.

Metamorphism in the BG is generally of amphibolite grade, and shows ample evidence of retrogression to epidote amphibolite and upper greenschist facies. However, relict eclogites can still be recognized by symplectitic replacement of clinopyroxene by hornblende and albite, and of phengite by biotite and albite. At some localities, relict omphacite can still be seen, and numerous mafic pods containing almost unaltered eclogite minerals forms a large body at Helleböstölane. Conditions of eclogite formation are estimated to be 600 °C at 15 kbar, which are consistent with regional studies on country-rock eclogites by Griffin et al (1985). Field relations suggest that eclogite metamorphism occurred <u>in situ</u> with respect to the adjacent basement rocks, and depression of supracrustal material to depths of about 50km followed by uplift to near-surface conditions during the Caledonian orogeny is inferred.

Staurolite-bearing schists from the BG may have formed at temperatures as high as 700 °C. Other rock-types in the BG give temperatures of about 450 to 500 °C.

Assemblages characteristic of high-pressure metamorphism have not been found in the Mafic Units. Barometric calculations give pressures from 5 to 10 kbar, the best constrained estimates being obtained from rocks showing the inversion of kyanite to sillimanite at temperatures of 500 to 525 °C.

Mineral assemblages in the HS suggest a range of P-T conditions. To the west of Kolgrovheia, the grade of metamorphism is generally low, falling in the greenschist facies. In the eastern (and structurally lower) part of the unit, much higher pressures and temperatures are recorded. A variety of geothermometers applied to a range of rock-types yield temperatures of about 600 to 650 °C. Geobarometers suggest that equilibration pressures in some rocks were in excess of 7 kbar, or even 9 to 10 kbar. However, the presence in a few outcrops of rocks containing the assemblage garnet + kyanite + staurolite + chloritoid in the matrix, and as inclusions in garnet imply "eclogitic" pressures, possibly greater than 14 kbar.

There is a general up-section decrease in temperature and pressure of metamorphism, with garnet amphibolites overprinting eclogites in the BG, amphibolites and epidote-amphibolites in the Mafic Units and HS, and greenschist facies metamorphism in the upper parts of the HS. The range of Caledonian P-T conditions represents a greater tectono-stratigraphic thickness than is now present.

The Mafic Units and HS are considered to be allochthonous and to have been emplaced onto the WGR during the Caledonian Orogeny, probably contemporaneously with the emplacement of the major Caledonian nappes to the east of the Jostedal culmination. The high-pressure rocks of the HS are believed to have formed at very similar temperatures and pressures to the eclogites of the Basement Gneisses. This may be explained by a relatively simple tectonic model, in which the Mafic Units and Hyllestad Schists were emplaced onto the Basement Gneisses during, or prior to, high-pressure metamorphism in which case the whole area suffered deep burial and the Mafic Units must be assumed to have had any evidence of eclogite facies metamorphism thoroughly overprinted during the subsequent history.

Alternatively, if the lack of high-pressure mineral assemblages in the Mafic Units is taken to indicate that they have never suffered deep burial, high-pressure metamorphism in the HS may have occurred in a different setting to eclogite metamorphism in the BG and a more complex tectonic model is required to explain the observed tectonic succession.

The Mafic Units and HS may represent the "trailing-edge" of the major Caledonian nappes.

Brittle extensional deformation in the upper parts of the section probably continued into the Devonian during deposition of the Solund conglomerates.

CONTENTS

CHAPTER 1: INTRODUCTION TO THE SCANDINAVIAN CALEDONIDES AND THE AREA 1

1.1 Aims and scope of project 1

1.2 Location and Geological Setting 2

1.2.1 Location 2

1.2.2 Geological setting 4

1.3 Structural setting 9

1.3.1 Regional geophysical characteristics 9

1.3.2 Regional structure 10

1.3.3 Formation and deformation of Devonian sediments 13

1.3.4 Structure in the field area 15

1.4 Geochronology of the WGR and surrounding areas 17

1.5 Metamorphism in the WGR 21

1.6 Plate reconstructions of the Scandinavian Caledonides 27

CHAPTER 2: THE TECTONOSTRATIGRAPHY AND STRUCTURE OF THE AREA 35

2.1 Structural setting of the field area 35

2.2 Basement Gneisses 37

2.3 Amphibolites and Gabbros 42

2.3.1 The Lower Mafic Unit (Lavik Amphibolites) 43

2.3.2 The Middle Mafic Unit (Gråfjell Gneisses) 47

2.3.3 The Upper Mafic Units (Mölmesdal Gabbro) 50

2.4 The Hyllestad Schists 52

2.5 Synopsis 57

2.6 Summarized structural and metamorphic chronology with criteria for correlating deformation phases across different units 62

CHAPTER 3: METAMORPHISM OF THE BASEMENT GNEISSES 68

3.1 Metamorphic history of the Basement Gneisses between Lavik and Balestrand 68

3.2 Metamorphic history of the Basement Gneisses between Lavik and Soetevik 70

3.2.1 Mineral assemblages in amphibole-bearing gneisses 71

3.2.2 Mineral chemistry in amphibole-bearing gneisses 72

3.2.3 Mineral assemblages in pelitic and semi-pelitic gneisses 74

3.2.4 Mineral chemistry in pelitic and semi-pelitic gneisses 76

3.3 Geothermobarometry of the Basement Gneisses 79

3.3.1 Amphibole-bearing gneisses 79

3.3.2 Pelitic and semi-pelitic gneisses 82

3.3.3 Thermobarometric results 84

CHAPTER 4: ECLOGITE FACIES METAMORPHISM IN THE BASEMENT GNEISSES 87

4.1 Location of eclogites 87

4.2 Field relations of eclogite bodies 88

4.3 Petrography and mineral chemistry of the eclogites 89

4.3.1 Least retrogressed eclogites (containing clinopyroxene) 89

4.3.2 Amphibolitized eclogites with no relict clinopyroxene 94

4.3.3 Orthopyroxene-plagioclase gneisses at Ytre Hellebö 97

4.4 Thermobarometry of the eclogites and related rock-types 100

4.4.1 Discussion of results 105

CHAPTER 5: METAMORPHISM IN THE MAFIC UNITS 110
5.1 Introduction 110
5.2 Petrography and mineral chemistry of the Lower and Middle Mafic Units 112
5.2.1 Petrography and mineral chemistry of garnet amphibolites in the LMU and MMU 114
5.2.2 Petrography of pelites in the LMU and MMU 116
5.3 Petrography and mineral chemistry of the UMU 117
5.3.1 Distribution of rock-types in the UMU 118
5.3.2 Mineral chemistry of gabbros and related rocks in the UMU 120
5.3.3 Formation of coronas in gabbros of the UMU 121
5.3.4 Mineral chemistry of garnet amphibolites in the UMU 125
5.3.5 Mineral chemistry of pelites at Löland 126
5.4. Thermobarometry of the Lower Mafic Unit 129
5.4.1 Thermobarometry of garnet amphibolites 129
5.4.2 Thermobarometry of pelites and granitic gneisses 130
5.5 Thermobarometry of the Middle Mafic Unit 131
5.6 Thermobarometry of the Upper Mafic Unit 132
5.6.1 Thermobarometry of the Upper Mafic Unit at Löland 132
5.6.2 Thermobarometry of other parts of the UMU 133
5.7 Conclusions 134

CHAPTER 6: METAMORPHISM OF THE HYLLESTAD SCHISTS 137
6.1 Location and geological setting of the Hyllestad Schists 137
6.2 Petrology of the Hyllestad Schists 138
6.2.1 Petrography and mineral chemistry of biotite-chlorite schists 138

6.2.2 Petrography and mineral chemistry of almandine-kyanite schists 140
6.2.3 Petrography and mineral chemistry of calc-silicate schists 146
6.2.4 Petrography and mineral chemistry of carbonate rocks 147
6.2.5 Petrography and mineral chemistry of garnet amphibolites 148
6.2.6 Petrography and mineral chemistry of schists between Råsvikheia and Espelandsvatnet 148
6.3 Thermobarometry of the Hyllestad Schists 149
6.3.1 Thermobarometry of schists containing kyanite-almandine and compatible assemblages east of Kleivevatnet 149
6.3.2 P-T grids, the compatability of different assemblages in the Hyllestad Schists, and implications for P-T conditions 156
CHAPTER 7: CONCLUSIONS 165
REFERENCES 161
TABLES
FIGURES
APPENDICES
Appendix 1: Equal area stereonet plots of structural data
Appendix 2: Analytical techniques
A2.1: Mineral analyses
A2.2: Rock analyses
Appendix 3: Representative mineral analyses
(i) Garnet
(ii) Amphibole
(iii) Biotite

(iv) Chlorite

(v) Epidote

(vi) Feldspar

(vii) Ilmenite

(viii) Muscovite

(ix) Staurolite

(x) Chloritoid

(xi) Pyroxene

Appendix 4: Abbreviations of mineral names used in the text and figures

ACKNOWLEDGMENTS

My grateful thanks go to my supervisor, Dr S. L. Harley, for introducing me to Norway, for his steadfast support, and for his strenuous attempts to improve the manuscript, including innumerable constructive comments.

I am also indebted to Professors A. G. Milnes and A. G. Koestler, and Dr Thomas Dietler for instructive discussions, encouragement and hospitality during the course of the fieldwork. For cheerful help in the field, under the most trying of conditions, many thanks to Katherine Harwood, Sian May, Jonathon Henton, and Dan Bishop. Special thanks should also go to Mr and Mrs Oskar Ringereide, of Mosemyra Camping for their hospitality during my visits to Norway.

N. Charnley, K. Parish, S. Wyatt, C. Fagg, S. Baker, P. Jackson, J. Hyde, J. Wells, and R. McAvoy gave invaluable technical assistance in Oxford. Joan Morall in the Department library must also be thanked for her patient help over the years. Claire and Jude Carlton, Julia York, and Caroline Beckley provided excellent draughting assistance for which, again, many thanks. I am especially grateful to Sally Thompson and Sriyanee De Silva for their invaluable support and assistance during the final frantic days and hours. Thanks also to Nina Phipps, Prof. E. A. Vincent, and the Department of Earth Sciences, Oxford for generous financial assistance during the early stages of the research.

It goes without saying that the past few years would not have been the same without the support, encouragement, and companionship of the post-graduate community of the Department of Earth Sciences at Oxford University. Martin Whitehouse, Steve Wade, Peter Cunningham, Charles Harper, Steve Knott, Jon Woodhead, and Rhoda Tait are just those unlucky enough to have shared an office with me. Special thanks to Clive Mitchell, Sriyanee De Silva, Dave Prescott, Peter Weston, Colin Devey, Nigel Platt, Joe Cartwright, Mike Widdowson, and Chris Elders, even though they didn't share an office with me, and to Stuart Taylor, even though he isn't a geologist. Space is too limited to name all the rest - you know who you are: ta.

Many thanks to my parents, for their forebearance during the last quarter century, or so.

The project was funded partly by NERC, and partly by Vicky, to whom I cannot express enough gratitude for all the time, effort, and love she has lavished on me, especially towards the end.

Chapter 1: Introduction to the Scandinavian Caledonides and the Study Area

1.1 Aims and scope of project

This study is concerned with metamorphic rocks from the Western Gneiss Region (WGR) and overlying units of southwestern Norway. In particular, it concentrates on some relatively high grade rocks in the Sogn og Fjordane region. One of the initial aims of the project was to determine whether the "country rock" eclogites in western Norway have been metamorphosed *in situ*, or whether they are of exotic origin, principally through a study of metamorphism in the "basement" rocks, rather than a detailed study of the eclogites themselves.

An area of the WGR between Lavik and Hyllestad was chosen for detailed study. This area contains examples of rocks with relicts of high-pressure metamorphism and a variety of "basement" rock-types, mostly of amphibolite grade. The detailed field studies were supported by reconnaissance studies of the structural and metamorphic history of basement rocks along an east-west section across the WGR in Sognefjord. In the absence of published geological maps of the area showing appropriate detail, extensive field mapping was carried out to determine the structural relations between eclogite-bearing basement rocks and other parts of the area. A sequential deformation history has been constructed from field evidence to provide a framework for studies on the thermal evolution of the area.

In addition to the field studies outlined above, the metamorphic P-T conditions and their evolution in different

areas have been elucidated through mineral texture relations in thin-section, and delineation of mineral chemistry and zoning relations based on electron microprobe analysis. These techniques have been used to compare P-T conditions in different rocks units, and to address the question of whether amphibolite facies assemblages now seen in basement rocks have overprinted an earlier history of high-pressure metamorphism.

Since Norwegian eclogites are now widely believed to be of Caledonian age, the field and structural relations, and the mineral chemistry of the Cambro-Silurian schists of the Hyllestad arc have been examined, to determine whether they have shared the history of high-pressure metamorphism apparently suffered by the basement. Analysis of structural controls on deposition in the Solund basin is beyond the scope of the project, but the thermal and tectonic evolution of basement rocks in the field area has implications for models of Devonian deposition in a tectonic setting.

1.2 Location and Geological Setting

1.2.1 Location

Sognefjord is Norway's longest and deepest fjord. It runs approximately east-west at a latitude of 61 °N and the main study area is situated between Lavik and Hyllestad towards the western end (figure 1.1). From the precipitous cliffs of Solund on the west coast to the foot of the Jotunheim mountains, 150 km inland, the fjord provides spectacular scenery and almost unbroken exposure across the southern part of the Western Gneiss Region (WGR) (figures 1.2, 1.3). Access to some parts of the peneplain, now at an average elevation of about 1000 m above sea level, is gained only with difficulty,

particularly on the southern shore of Sognefjord.

The area between Hyllestad and Lavik, has a less elevated topography than the internal parts of Sognefjord, although the landscape is nevertheless rugged. The highest part of the area is the eastern edge of the Solund massif which rises over 750 m above ordnance datum, with cliffs falling almost unbroken to the sea (figure 1.4). The hills formed by rocks of the basement gneisses, amphibolites, and gabbros reach about 600 m, while the granitic rocks of the Hyllestad Arc protrude from the low ground occupied by the surrounding schists (figure 1.5).

Hillsides not covered with coarse scree deposits are generally thickly wooded between sea level and about 400-500m, hence outcrop is confined mainly to the fjord and road sections, and to bare hill-tops. Fjord exposure is excellent and nearly continuous between Leirvik and Lavik, and large-scale structures are well-exposed in the cliffs.

Map references quoted on the 1:20,000 and 1:5,000 sheets published by the Fylkeskartkontoret i Sogn og Fjordane, which have been used as base maps for this study, are based on a meridian to the east of the field area with grid numbers increasing from south to north and from east to west. An ad hoc system with grid numbers increasing from west to east (mimicking the British Ordnance Survey system) was found to be more convenient in the field; these grid numbers, as well as adjusted south-north grid numbers also appear on figures in the text, and are listed with their equivalent Norwegian grid references in table 1.1.

1.2.2 Geological Setting

The Norwegian Caledonides form an elongate north-south belt, with an average width of 200 km, and extend 1800 km for almost the entire length of the country. The crystalline basement of the Baltic Shield crops out to the south and east of the Caledonian front. In addition, a number of tectonically bounded inliers of a similar crystalline nature occur in the central and southwestern parts of the orogen. The largest of these extends from Namsos to Bergen (figure 1.2) and has been variously referred to as the Western (or Basal) Gneiss Region (WGR), the Namsos-Bergen Coastal Gneiss area, and the Basement Gneiss Complex etc (e.g. Bryhni and Sturt, 1985, Oftedahl, 1980, Cuthbert et al, 1983).

Sognefjord crosses the entire width of the southern part of the WGR, from the Valdres thrust sheet in the east, to the Cambro-Silurian schists of the Hyllestad Arc and Solund conglomerates in the west. The field area of the present study includes the western margin of the WGR and extends into its overlying units.

The WGR is overlain in the south by the thrust sheets of the Bergen Arcs (Middle and Upper Allochthons) and, in the southeast, by a thin sequence of autochthonous-parautochthonous sediments, overlain in turn by "sparagmite" and the Precambrian crystalline Jotun thrust sheets (Middle Allochthon) (figure 1.2). To the northeast and around Trondheim it is overlain by the lateral equivalents of the Valdres sheets and by the largely ophiolitic rocks of the Trondheim supergroup (Upper Allochthon), (Cuthbert et al, 1983, Oftedahl, 1980, Bryhni and Sturt, 1985, Hossack and Cooper, 1986, Gee et al, 1985). In the west, the boundary of

the WGR is less well defined. Caledonian nappes have been identified, e.g. the Precambrian Dalsfjord and Cambro-Silurian Stavfjord nappes of the Melvær and Askvoll area (Skjerlie, 1984), and have been interpreted as corresponding to parts of the Lower, Middle, and Upper Allochthons (Gee et al, 1985). Other metasupracrustals on the west coast (notably those of the "Fjordane complex") which are usually regarded as part of the Western Gneiss Complex, may be the more intensely deformed equivalents of rocks to the east of the Jostedal culmination such as the Jotun and Seve thrust units (Bryhni, 1966, Bryhni and Sturt, 1985).

A wide variety of rocks occur within the WGR, but the predominant types are granitoid migmatites, gneisses, and augen gneisses with, locally, granites, pegmatites, gabbroic rocks, and banded amphibolites. Lenticular inclusions of eclogites, granulites, ultramafites, and anorthosites showing retrogressive textures also occur within the gneisses. The supracrustal rocks mentioned above comprise quartzites, meta-arkoses, garnetiferous schists and gneisses (occasionally with kyanite or sillimanite), banded amphibolites, marbles, and calc-silicates. The southeastern basement rocks of the pre-Caledonian foreland include Proterozoic granites, migmatites, and heterogeneous and banded gneisses. The gneisses have been strongly interfolded with metamorphic supracrustals, and all these rock-types have suffered deformation and metamorphism during the Sveconorwegian (Grenvillian) orogeny. In addition, there are augen gneisses with Grenvillian intrusion ages and post-kinematic granites, gabbros, anorthosites, and charnockites.

It is not clear whether rocks of truly "basement"

character (that is, autochthonous crystalline gneisses of equivalent status to the foreland gneisses of southern Norway) are exposed in the present study area. The reconnaissance study of Bryhni (1966) assigns all the rocks which have been grouped together as "Basement Gneisses" in this study (see chapters 2 and 3) to the Fjordane Complex as, with minor exceptions, does Kildal (1970). Bryhni and Sturt (1985) state that these rocks, along with the overlying amphibolite units and rocks of the Hyllestad Arc, are of "uncertain position" and suggest that they may be allochthonous. In the eastern part of the field area the basement gneisses comprise homogeneous pink or grey augen gneisses and granitoid migmatites which are interbanded with biotite-gneisses and quartzites containing pink muscovite. In the central and western parts of the area, banded amphibole-biotite gneisses and migmatites together with quartzites, schists, and amphibolites are found. Porphyritic feldspar, possibly of metasomatic origin, is common in most horizons. Some of the thick augen gneisses and granitic migmatites recognized, particularly those in the central and possibly in the eastern parts of the area, may correspond to the Jostedal Complex of Bryhni (1966), as partially indicated by Kildal (1970), while the lithological associations of the remainder correspond closely to the Fjordane Complex. The Jostedal and Fjordane Complexes cannot always be readily distinguished; migmatization, metamorphism, and deformation shared by both groups blurs distinctions in the best exposed areas (Carswell, 1973) and, in the present study area, Caledonian deformation is particularly intense (Dietler et al, 1985).

Overlying the Basement Gneisses, several thick units of

amphibolitic gneisses and schists have been distinguished comprising predominantly doleritic or gabbroic compositions, and occupying the central and eastern parts of the area. The geometry of these units and the nature of their contacts with each other and with the Basement Gneisses indicate a tectonic, rather than igneous, emplacement into their present position. At these contacts, conformity between the foliations has been imposed during deformation of presumably Caledonian age. These amphibolites and gabbros (with minor ultramafic pods) correspond to part of the units interpreted by Bryhni and Grimstad (1970) as metasupracrustals, possibly allochthonous, and distinct from the Basement Gneisses. If these rocks are truly allochthonous they may be correlatives of the Jotun thrust sheets, with their associations of syenites, anorthosite-gabbros, and gabbroic gneisses (indeed, Bryhni and Sturt, 1985, draw attention to similarities between the Jotun and Seve nappes and supracrustals of the westernmost parts of the Gneiss Complex). It should be mentioned, however, that similar rock-types occur elsewhere in Norway; for example, coronitic gabbros from the field area bear close comparison with rocks from Lofoten and Vesteralen (Griffin and Heier, 1973).

The eugeoclinal metasediments and metavolcanics of the Hyllestad Arc have long been regarded as Lower Palaeozoic in age (Kolderup, N-H., 1928, Kolderup, N-H., 1952, Kildal, 1970, Sigmond et al, 1984). Recent tectonic interpretations suggest they may represent the trailing edge of the Upper Allochthon (figure 1.2) (Gee et al, 1985). As with the case of the amphibolites discussed above, the status of these rocks is unlikely to be unequivocally resolved on the basis of field

comparisons or radiometric age determinations alone, owing to the intense Caledonian reworking of rocks both above and below the contact. Macro- and microstructural observations (this study) suggest that the Hyllestad Schists were also subjected to a late-stage reworking by extensional shearing. This is probably related to extensional deformation noted in the overlying Devonian and, although probably late Caledonian in age, may be as late as Permian or Mesozoic in age (Torsvik et al, 1989).

The youngest rocks in the field area are the Devonian conglomerates of the Solund archipelago, described in detail by C.F. Kolderup (1926) and Nilsen (1968), which, along with the Håsteinen, Kvamshesten, and Hornelen Devonian, have attracted a great deal of interest in recent years (Hossack, 1984, Torsvik et al, 1986, 1987, 1988, Norton, 1986, 1987, Seranne and Seguret, 1985). Sedimentation was clearly related to tectonic activity during the Devonian, but the style and timing of tectonism with respect to deposition is still a matter of controversy (see below), not least because the major depocentres, although sharing many characteristics, nevertheless show differences in sediment type, degree of metamorphism, and fault geometry (Steel et al, 1985). Whether the various Devonian basins were linked to form one large sheet prior to erosion (e.g. Hossack, 1984), or whether deposition occurred at discrete centres (Steel et al, 1985), remains in doubt.

The similarity in rock-types, tectonostratigraphic position, and Proterozoic history (Kullerud et al, 1986, Corfu, 1980) have led many authors to assume contiguity at depth between the WGR and other basement "windows" in the main

Caledonian belt and the foreland gneisses of southernmost Norway (e.g. Cuthbert et al, 1983, Bryhni and Sturt, 1985, Hossack and Cooper, 1986). In other models the WGR has been interpreted as an allochthonous unit overlying low-grade metasediments (Mykkeltveit et al, 1980). However, as pointed out by Cuthbert et al (1983), such a model would seem to preclude the development of high-pressure assemblages in the WGR. Their cartoon (figure 1.6) indicates underthrusting of the WGR by the foreland and cover, with the Laurentia-Baltica suture located off the present Norwegian coast.

Caledonian deformation of the Proterozoic gneiss of southern Norway increases in intensity towards the northwest and the main Caledonian thrust belt. Inverted basement-cover relations are known in the western area, but large-scale undulations, late faulting and local shearing are more generally seen. The southeastern areas of the WGR also show mild Caledonian effects, but there is a similar, if more marked, northwestward intensification in the overprinting of the gneisses culminating in the complex and obscure relations between crystalline basement and metasupracrustals (Bryhni and Sturt, 1985, Dietler et al, 1985).

1.3 Structural setting

1.3.1 Regional Geophysical Characteristics

The broad-scale crustal structure of the Scandinavian peninsula has been investigated by means of a regional gravity survey (Wolff, 1985). The 250 km low-pass map reveals a line of negative Bouguer anomalies, corresponding closely to the Caledonian mountain chain, and a roughly parallel gravity high running along the coast (figure 1.7). The former feature

reflects the thickening of light crustal rocks in the Caledonian thrust sheets, while the offshore positive anomaly may be due to crustal thinning during the opening of the Atlantic. A geophysical survey by Talwani and Eldholm (1972) disclosed a narrow high-gradient positive anomaly trending parallel to the coast from Lofoten and across the Norwegian Sea towards northeast Scotland. The anomaly on Lofoten can be attributed to the presence of mafic granulites and Talwani and Eldholm explain the linear extension as an intrabasement density contrast in Precambrian rocks. Cuthbert et al (1983) interpret the anomaly as an ophiolite-lined geosuture between the Baltic shield and the leading edge of an over-riding Greenland plate.

The residual gravity map (Wolff, 1983) is characterized by the presence of negative gravity anomalies, which correspond to the granitoid Precambrian basement rocks (including the WGR), and by positive gravity anomalies associated with the Caledonian thrust sheets as a result of their high average densities. Positive anomalies are particularly marked in the case of the crystalline Jotun sheets and the nappes of the Trondheim region.

1.3.2 Regional Structure

The allochthonous elements of the Norwegian Caledonides have been grouped into two major units by Hossack and Cooper (1986): the External Thrust Sheets, and the Internal or "Exotic" Nappe Complex. The External Thrust Sheets comprise three major units (figure 1.8):

i) the Baltic Cover Thrust Sheets, in which there is limited basement involvement. This unit corresponds roughly to

the Lower Allochthon, but includes the Autochthon and Middle Allochthons (figure 1.2), of Gee et al (1985)

ii) the Crystalline Thrust Sheets in which a high proportion of basement is involved. These are mainly Precambrian metamorphic rocks and include the Jotun thrust sheet. The unit corresponds to parts of the Lower and Upper Allochthons, and most of the Middle Allochthon

iii) the Oceanic Thrust Sheets, comprising Lower Palaeozoic sediments and volcanics with ophiolitic fragments, and corresponding to parts of the Upper Allochthon.

The Baltic Cover Thrust Sheets and Crystalline Thrust Sheets are inferred to be derived from the Baltic Craton. The Oceanic Thrust Sheets include faunas of Baltic and of North America affinities and are interpreted by Hossack and Cooper as obducted slices of oceanic crust.

The Internal (or "Exotic) Nappe Complex corresponds roughly to the Uppermost Allochthon, is characterized by folded isoclinal folds separated by slide zones, and possesses fold nappe geometry. Rb/Sr whole-rock isochrons suggest that the rocks are Precambrian in age and pre-Caledonian deformation histories have been distinguished for some elements. The structure and history of the complex have been reviewed by Hossack and Cooper (1986) and Oftedahl (1980) and, since they are only indirectly relevant to the tectonic evolution of the study area, will not be considered further here.

The External Thrust Sheets are distinct from the Internal Nappe Complex in possessing typical wedge-shaped thrust sheet geometries thinning down-dip to trailing branch-lines, as described from the Appalachians and the Canadian Rockies

(Dahlstrom, 1970, Boyer and Elliott, 1982).

Deformation in the Upper and Uppermost Nappes of Gee et al (1985) is broadly Upper Ordovician in age, while in the Autochthon and the Lower and Middle Allochthons, it occurred during the Silurian (Gee and Roberts, 1983) (figure 1.9). The rocks of the External Thrust Sheets are considered by many authors to have originated far to the west of their present positions, and the dominant transport direction in southern Norway appears to have been towards the southeast (Strand, 1961, Oftedal, 1980). However, structures interpreted as lateral ramps suggest that easterly and southeasterly thrusting also occurred (figure 1.10). If a piggy-back thrusting model is assumed for the region, the variation in apparent transport directions may be due to clockwise rotation of thrust slip vectors with time, from easterly as thrusting started, through southeasterly during the major phase of thrusting, and finally southerly. Balanced sections in which a constant southeasterly slip direction is assumed, imply a minimum of 400 km shortening, with an original section length of 900 km (Hossack and Cooper, 1986).

In central Southern Norway, the Caledonian nappe units occupy a synclinal depression referred to by Goldschmidt (1912) as the "Faltungsgraben". At the eastern end of Sognefjord, the Jotun thrust sheets are believed to have a wedge-shaped geometry and a thickness, based on gravity surveys, of 10-15 km (Smithson et al, 1974). However aeromagnetic surveying suggests this figure should be no more than 5 km (Aalstad et al, 1977).

Reusch (1908) and Goldschmidt (1916) postulated that the Jotun Nappe was locally derived by upward movement of a large

mass of deeply rooted material followed by lateral spreading. Later authors have pointed out that there is evidence for northwesterly movement of the Jotun thrust sheets along the southeast margin of the WGR and have suggested that emplacement was as an "Ivrea-type" flake (Banham et al, 1979, Battey and McRitchie, 1973). A deep root of this sort would explain the large gravity anomaly observed. Banham et al (1979) have suggested that the northern margin of the Jotun nappes represents a Caledonian suture zone. In such a model, the Jotun-like rocks to the west of the Jostedal culmination could not represent the "trailing-edge" of a large far-travelled nappe, as suggested elsewhere (e.g. Hossack, 1984, Gee et al, 1985). It is possible that the northwesterly directed slip vectors described from parts of the Jotun nappe may be due to a later, reversed, phase of thrusting or backthrusting.

The complete encirclement of the outcrop of the nappe complex by a basal mylonite zone supports a distant source; and the recognition, in the coastal area of the WGR, of the Stavfjord nappe comprising rocks of Cambro-Silurian age, emplaced onto the WGR during the late Silurian (Skjerlie, 1984), demonstrates that eastward thrusting was active during the Caledonian orogeny across the entire width of the WGR.

1.3.3 Formation and deformation of Devonian sediments

The final phase of the Caledonian orogeny in Norway is recorded by the deformation of late Silurian to Middle Devonian sediments in the Nordfjord-Sognefjord region (figure 1.2). Generally speaking, these sediments occur in basins bounded to the east, north, and south by faults, and to the

west by unconformable contacts (Steel et al, 1985). In older studies low-angle basal contacts have been interpreted as thrust planes (C.F. Kolderup, 1923, Nilsen, 1968, Kildal, 1970, Höisæter, 1971, Skjerlie, 1971, Bryhni, 1978), and the asymmetric distribution of sediment type within the basins has been related to syn-sedimentary vertical or strike-slip movement on steeply-dipping east-west marginal faults (Bryhni, 1964, Nilsen, 1968, Bryhni and Skjerlie, 1975, Steel et al, 1977, Steel and Gloppen, 1980). In these interpretations, open folding along east-west to northeast-southwest axes with later high and low-angle faulting, pebble-stretching lineations, locally penetrative cleavage, and low-grade metamorphism (anchizone to lower greenschist) are attributed to a post-depositional "Svalbardian" or "Solundian" event.

More recent studies have led to interpretations of the basal contacts of the Hornelen, Kvamshesten, and Solund basins as sections of a single, partially eroded, low-angle extensional detachment with a displacement of up to 40 km or more: the Målöy Fault (Hossack, 1984) or Nordfjord-Sogn Detachment, (Norton, 1986, 1987). The approximately east-west trending high-angle faults are re-interpreted as syndepositional extensional "lateral ramps" (Hossack, 1984), or as late to post-Devonian faults post-dating both the low-angle faults and sedimentation, but broadly following the original faulted margins of the basin (Norton et al, 1989). In such models most, or all, of the deformation and metamorphism of the Devonian sediment is considered to be <u>contemporaneous</u> with sedimentation and extensional collapse of the Baltic margin during isostatic rebound of underthrusted continental crust. Extensional fabrics in the rocks forming the basement

to the Devonian are reported in this study and by Norton et al (1989).

Palaeomagnetic data (Torsvik et al, 1986, 1987, 1988) suggests that most of the deformation observed in the coastal Devonian basins is post-depositional and related to north-south compression, in contradiction to the sedimentary-structural studies noted above. Extensional criteria could be of Permian or younger age, as palaeomagnetic results support the hypothesis that reactivation of Caledonian structures during the Upper Palaeozoic or Mesozoic has occurred (Torsvik et al, 1989, Torsvik pers. comm.). Calculated palaeomagnetic pole positions for the Kvamshesten and Håsteinen basins closely correspond to Upper Devonian to Lower Carboniferous poles for the British Isles and Spitsbergen (Torsvik et al, 1989, Watts, 1985). Resetting of palaeomagnetic fabrics requires higher temperatures, and consequently deeper burial than would be expected in models of synsedimentary deformation, and the late ages obtained for such fabrics by comparison of poles with well-constrained apparent polar wander paths, would seem to support a post-sedimentary tectonic phase (the "Solundian Orogeny"). The apparent contradictions of the various lines of evidence may yet be resolved by consideration of the uplift history and tectonic evolution of the pre-Devonian basement.

1.3.4 Structure of the field area

The regional orientation of the compositional foliation of the WGR is observed in the Sognefjord profile to vary from moderate easterly dips, in the east, to moderate southerly or westerly dips, in the west, across a culmination near Lavik.

There are indications of at least two Caledonian shearing events, the intensity of the later and more pervasive increases towards the west (Dietler et al, 1985). The present study area is located mainly in regime three of Dietler et al (1985), where the Caledonian mylonitic or blastomylonitic foliation becomes the dominant fabric (figure 1.11). By contrast, in the internal parts of Sognefjord deformation is confined to discrete, narrow zones cutting essentially "un-Caledonized" Precambrian gneisses and migmatites. The most ductile deformation in the field area generally occurs around Lavik and in the amphibolite units; in contrast to the regional trend, to the west of Lavik strain becomes more brittle in type in a westerly direction, and during later events.

In the coastal area of Sognefjord, the pre- and early Caledonian foliations dip between north and northwest or south and southeast, and are deformed around easterly or westerly plunging Caledonian fold hinges (chapter 2). Five styles of deformation are recognized in the area between Avenfjord and Hyllestad, possibly representing up to five "phases" of deformation. An early, possibly pre-Caledonian foliation ("S_1") is developed in basement gneisses and. where preserved, is generally deformed into tight or isoclinal "F_2" folds. The "S_1" foliation is formed by the rotation and drawing out of migmatitic differentiates and pre-existing foliations into a well-defined compositional banding. F_2 isoclines with their associated axial planar cleavage ("S_2") may form as a consequence of the same episode of deformation. Isoclines are refolded in the hinges of later recumbent folds with a relatively open profile ("F_3"). Crenulation of the mica S_2

foliation, is common but a well-developed "S_3" axial planar foliation is not seen. "F_4" folds are characterized by upright open warping of earlier foliations and are not easily distinguished except in coastal exposures.

The "D_5" event is characterized by a pervasively developed extensional crenulation cleavage ("S_5") in the schists of the Hyllestad Arc, and by widely spaced anastomosing fractures in the schists and gneisses around Böfjorden. D_5 is almost certainly related to extensional structures observed in the Solund conglomerate and is therefore presumably of late Caledonian (Devonian or later) age.

The strong north-south pattern of drainage is the result of jointing which also controls the orientation of minor fjords in the Solund peninsula and may be the result of Tertiary extension (Nilsen, 1973).

1.4 Geochronology of the WGR and surrounding areas

The age of the rocks forming the WGR and the timing of metamorphic events have been matters of controversy and the objects of apparently conflicting studies. The region has a complex and extended history during which rocks of many disparate types have been brought together. In contrast to other parts of the Norwegian Caledonides (such as the nappes of the central Scandinavian Caledonides (Stephens and Gee, 1985), biostratigraphic control on tectonic evolution is lacking within the WGR. A limited biostratigraphic constraint on the age of rocks in the WGR and a minimum age for the Caledonian metamorphism is provided by evidence from the overlying units. Deposition at Trondheimsfjord had started by

the Lower Downtonian (and possibly uppermost Silurian). Abundant fossils of the plants Psilophyton sp. and, less commonly Aphyllopteris, thought to be early Middle Devonian in age, occur on Lamholmen, near the margins of the Solund basin (Kolderup, 1916). Nilsen (1968) suggests an approximately Middle Devonian age for the rocks of the Solund district from comparison with other Devonian rocks of the Sognefjord-Nordfjord region.

The lower age limit of Caledonian deformation in the WGR is constrained by the age of the youngest rocks known to have been deposited before the development of the allochthon, i.e. the Llandoverian of the Köli Supergroup (Gee, 1978, Cuthbert et al, 1983). It has been suggested that collision of Baltica and Laurentia began in the late Llandovery, resulting in the appearance of coarse sediment in south Norway and Sweden derived from the west (Bassett, 1985). More recently McKerrow et al (1989) have presented a palaeogeographic reconstruction in which sediment supplied to the Southern Uplands was derived from the Mongolian Arc. This model does not allow for continental collision between Baltica and Laurentia until the late Wenlock/Ludlow (see below).

A considerable number of radiometric age determinations have been carried out on rocks from the WGR and surrounding areas, but the results should be considered in terms of the local field relations and metamorphic history, as not all the components of the WGR can be assumed to have suffered congruent histories. Compilations of radiometric ages (Neumann, 1960, Broch, 1964, Bryhni, 1973, Kullerud et al, 1986, Mearns, 1986) have allowed a general chronological framework for the timing of metamorphic events in the WGR to

emerge.

Kullerud et al (1986) recognise three main age ranges based mostly on Rb/Sr WR and mineral-pair isochrons: broadly Caledonian, 350-450 Ma; late Proterozoic, 900-1250 Ma; and middle Proterozoic, 1450-1750 Ma (cf Corfu, 1980). The oldest reliable ages come from Rb-Sr WR determinations on gneisses (K-Ar dating of eclogites also yields high ages but this is probably due to a large component of excess Ar, particularly in pyroxenes - McDougall and Green, 1964). Low initial $^{87}Sr/^{86}Sr$ ratios (mostly about 0.705) in the gneisses suggest that the period 1450-1750 Ma represents the main episode of crust formation. Large 2 sigma errors and MSWD values are attributed to the disturbance of isotopic equilibrium during later metamorphic events.

Late Proterozoic (900-1250 Ma) ages are mainly recorded by Rb-Sr WR analyses (e.g. Priem et al 1973), but also some mineral data from Rb-Sr, K-Ar, and Ar-Ar methods. Initial $^{87}Sr/^{86}Sr$ values greater than 0.71 imply that this event involved crustal reworking.

Both the Jostedal and Fjordane complexes of the southern part of the WGR (Bryhni, 1966, Kildal, 1970) have yielded Rb/Sr ages of about 1700 Ma (Brueckner, 1979) while a late intrusive phase is represented by the Hestbrepiggan granite (about 1000 Ma) and Geiranger Granodiorite (960 Ma) (Oftedahl, 1980).

Caledonian (350-450 Ma) isochrons based on isotopic analyses of mineral separates are given by a wide range of decay systems. Garnet-WR-clinopyroxene Sm-Nd isochrons from eclogites suggest that closure of the system in the WGR occurred between about 400-420 Ma (e.g. Mearns, 1986, Griffin

and Brueckner, 1985). Oftedahl (1980) reports eclogites with a Rb/Sr "formation" age of 1800 Ma and with a weak metamorphic event at 1100 Ma and stronger one at 400 Ma. Eclogites of Caledonian age have been shown to be derived from gabbros intruded at nearly 1200 Ma BP (Mörk and Mearns, 1986). These conclusions are supported by U-Pb zircon ages of 400 Ma in eclogites (Gebauer et al, 1985). The main phase of the Caledonian orogeny in the central part of the Caledonides was over by the beginning of the Devonian (Strand, 1961, McKerrow et al, 1989). Lower Devonian mica ages (e.g. Priem et al, 1973, Skjerlie and Pringle, 1978) are probably a reflection of slow post-orogenic cooling rate. Kullerud et al (op cit) calculate a minimum cooling rate of 7 °C/Ma. Post-Caledonian ages are found only in syenite dykes in Sunnfjord (261 Ma) and Tustna (291 Ma) (Furnes, 1982, Råheim, 1974).

Eclogites from the Seve Nappes have older ages (about 500 Ma compared to approximately 400 Ma) than those from the WGR (Mörk et al, 1988), suggesting that a separate high-pressure event took place in some of the allochthonous units before they were emplaced over the WGR.

The schists and gneisses of the Hyllestad Arc are generally considered to be of Lower Palaeozoic age (N-H. Kolderup, 1952, Nilsen, 1968, Kildal, 1970, Oftedahl, 1980). Schists and amphibolites of a similar type, crop out in Nordfjord and Sunnfjord. At the latter locality, nappes of Cambro-Silurian schist contain Precambrian mangerites and related rocks. Rugose corals of Lower Ordovician to Lower Silurian, and crinoids of Upper Ordovician to Lower Silurian age, are reported from limestone on West Atlöy (Skjerlie, 1969). However, the exact age of the Hyllestad schists has

still to be established. Attempts to date the large bodies of granite which intrude into the schists (A.G. Koestler, pers comm, Bailey unpublished results) have been unsuccessful because of homogeneity in Rb/Sr ratios.

Only a few radiometric age determinations have been carried out in the vicinity of the present study area. Two are reported by Kullerud et al (1986): one from Ortnevik on the southern shore of Sognefjord, the other from northwest of Hyllestad. The first has been obtained by the K-Ar method on muscovite from a pegmatite (Broch, 1964). The age, as recalculated by Kullerud et al (1986) following Dalrymple (1979), is 574.5 Ma (the uncertainty is not given). The second age determination, a Rb-Sr, clinopyroxene-WR analysis (Griffin and Brueckner, 1985) on a large body of kyanite eclogite is given as 267 ± 42 Ma and is not considered meaningful. In addition to these a "Caledonian" intrusion age for granitic bodies in Sognefjord is reported by Dietler et al, 1985.

1.5 Metamorphism in the WGR

A wide range of metamorphic conditions are seen in the WGR from the Caledonian greenschist overprinting of Precambrian amphibolites to high P-T granulite and eclogite facies rocks, themselves showing evidence of retrogression through amphibolite and lower grades of metamorphism. The wide variety of mineral assemblages observed thus represents not only various levels of exhumation at different locations, but a complex polyphase tectonic and metamorphic evolution.

Much of the WGR shows evidence of metamorphism at amphibolite grade or lower. In the coastal areas amphibolite facies metamorphism overprints high pressure assemblages

believed to be of Caledonian age, whereas in other areas amphibolite facies metamorphism pre-dates Caledonian structures and appears to belong to a Precambrian tectonothermal event. Since Eskola's classic paper "On the eclogites of Norway" (1921), much attention has focussed on eclogites and the frequently associated garnet peridotites, whilst other aspects of metamorphism in the WGR have been relatively poorly studied.

Recent work on the occurrence of high pressure metamorphism in the Scandinavian Caledonides has been reviewed by Griffin et al (1985) and Griffin (1987). It has been suggested that the eclogites are in general the products of "in situ" alteration of low pressure supracrustal rocks (e.g. Cuthbert et al, 1983, Griffin and Carswell, 1985, Jamtveit, 1987). The very high pressures and temperatures of formation estimated for such rocks has led others to challenge this hypothesis. Furthermore the host rocks appear to be of lower metamorphic grade, and have, in some cases, yielded different radiometric ages to the eclogites and their associated rock-types. Contacts between eclogitic and country rocks are usually sheared and opponents of in situ metamorphism have proposed that pods and lenses containing high-pressure assemblages have been tectonically emplaced into their current positions from deeper levels. In the latter case an origin in the upper mantle, or in subducted (or deeply obducted) oceanic crust has been postulated (O'Hara and Mercy, 1963, Lappin, 1966, Carswell, 1966, O'Hara et al, 1971, O'Hara, 1976, Lappin and Smith, 1981, Gebauer et al, 1982, Mearns and Lappin, 1982, Smith, 1981).

Norwegian eclogite occurrences belong to the Group B of

Coleman et al (1965) and are traditionally divided into "internal", and "external" (or "country-rock") types. The former are enclosed by bodies of garnet peridotite, the latter by other rock types, particularly paragneisses or augen gneisses. Within the field area of the present study, the eclogites are all of "external" type. It now appears that the two types may be of different age and distinct origin and that it is not appropriate to relate both types to a single tectonothermal event.

Two types of garnet peridotite have been distinguished in the WGR (Carswell et al, 1983). "Fe-Ti" peridotites form small isolated pods, or layers in garnet websterite-eclogite lenses. The more widespread "Mg-Cr" type form large masses up to several kilometres in diameter. Peridotite bodies typically have retrograde margins. "Internal" eclogites occur with dyke-like geometries, as layers of garnet-clinopyroxenite and garnet-websterite grading into garnet peridotite (Carswell, 1981), or as boudinaged dykes of superferrian basalt composition (Griffin and Qvale, 1985).

Sm-Nd dating of rocks from Almklovdalen suggest old ages for internal eclogites. A garnet-clinopyroxene-whole rock age of about 1700 Ma has been determined for a garnet peridotite (Mearns, 1986). Jacobsen and Wasserburg (1980) obtain an age for a garnet pyroxenite of about 1475 Ma. Mearns (1986) has suggested that the latter date, and an age of 1050 Ma also obtained from a similar garnet pyroxenite may represent disturbance of the isotopic system during Sveconorwegian and Caledonian thermal events.

"External" eclogites occur as lenticular pods from tens of centimetres to hundreds of metres long. They also typically

show retrogression of the margins, where garnet amphibolite overprints garnet-omphacite assemblages. Symplectitic replacement of high pressure minerals is common and foliations developed within pods may be continuous with Caledonian fabrics in the country-rock, or may be deflected into parallelism with the margins of the pods. Contacts between the eclogite pods and country-rock are usually highly modified by boudinage or folding, but igneous relations including back-veining of eclogite by anatectic melts are reported (Griffin and Carswell, 1985, Krogh, 1980) and the dyke-like form of some retrogressed eclogites (for example, this study) also suggests an original igneous relation between gneiss and eclogite. External eclogite protolith intrusion ages have been dated to about 1550 Ma, 1250 Ma (Mörk and Mearns, 1986), and about 550 Ma (Griffin and Brueckner, 1985). The age of the external eclogite mineral parageneses has been established as Caledonian by Sm-Nd mineral pair isochrons, and U-Pb dating of zircons ([Griffin and Brueckner, 1980, Mearns, 1986, Mörk and Mearns, 1986, Gebauer et al, 1985, Krogh et al, 1974).

Recent studies of the external eclogites have increasingly indicated that such rocks had low pressure protoliths, and hence have been metamorphosed <u>in situ</u>. Griffin (1987) summarizes the three main lines of evidence as follows:

1. Lithological associations and geochemistry. A few eclogites have igneous relations with respect to supracrustal associations which demonstrates a shallow, or at least crustal, origin for the protolith. This is supported by geochemical evidence (e.g. positive Eu anomalies, Gebauer et al, 1985) that many eclogite bodies had cumulate protoliths formed through plagioclase fractionation. Eclogites occurring

as layers in anorthosites have gradational contacts and geochemical affinities with the anorthosite (Brastad, 1985). The protolith, which appears to have been olivine + pyroxene + plagioclase bearing, is constrained to have formed at less than 8 kbar.

2. Arrested reactions. Partial conversion to eclogitic assemblages is observed in coronitic gabbros throughout the WGR (Gjelsvik, 1952, Griffin and Råheim, 1973, Griffin and Heier, 1973, Mörk, 1985a,b, 1986) and is apparently due to prograde reaction as metamorphism occurred long after gabbro intrusion (Mörk and Mearns, 1986).

3. Inclusion suites and mineral zoning. Garnets in external eclogites have been shown to preserve, as inclusions, amphibolite facies or glaucophane-schist mineral assemblages (Krogh, 1982, Krogh, 1980). Zoning in garnets towards higher values of Mg/Fe at the rim than the core suggest growth during prograde metamorphism (Krogh, 1980, 1982, this study); a subsequent retrograde reversal of the trend is sometimes noted. Strong zoning in Ca, from high core to low rim values observed in some eclogites has been related to early growth in the presence of plagioclase (Jamtveit, 1987a, Mörk, 1985b). Essentially unzoned garnets from high temperature eclogites can be explained as having suffered homogenization after or during prograde growth.

Fe/Mg distribution between garnet and clinopyroxene has been measured for a large number of eclogite bodies in the WGR. The results show a regional variation (Krogh, 1977a, b) probably representing a generalized westward (coastal) increase in equilibration temperature (Griffin et al, 1985) (figure 1.12). Calculated temperatures presented by Griffin et

al (1985) range from between 500 and 600 °C (in Sunnfjord) to 800 °C in the northern parts of the WGR. Pressures of eclogite formation estimated by Griffin et al (1985) show a corresponding increase towards the coast with a range of about 11 - 20 kbar, however, the methods used mostly only indicate minimum rather than absolute pressure values. A P-T-t path reaching a maximum pressure of 25 kbar has been calculated for the Eiksunddal body by Jamtveit (1987a). Such a high P_{max} approaches the quartz-coesite phase boundary of Bohlen and Boettcher (1982) and is therefore consistent with reported occurrences of coesite preserved as inclusions in eclogitic pyroxenes (Smith, 1984). Even higher pressures, up to 40 kbar, have been suggested for external garnet websterites but such estimates are probably spurious (Griffin, 1987).

High pressure rocks in the Norwegian coastal area are generally enclosed in gneisses at amphibolite grade and this has been regarded as strong evidence against in situ eclogite metamorphism. Eskola (1921) regarded the garnet amphibolites as retrogressed eclogites which had suffered retrogression in an event of regional significance. Evidence of previous high pressure metamorphism in the gneisses includes the former presence of omphacite, now represented by symplectites of clinopyroxene or amphibole with plagioclase, and intergrowths of plagioclase + quartz + pyroxene ± amphibole (Mysen and Heier, 1972). Pseudomorphs of biotite + K-feldspar + kyanite, after phengite, are reported to be widespread in the gneisses (Griffin, 1987). Hydration of pyroxenes in the gneisses and in the rims of eclogite pods can be attributed to release of water by phengite breakdown during decompression, without requiring an external source for fluid. Mafic eclogites can be

expected to retain high pressure assemblages more readily than non-mafic rocks (Koons and Thompson, 1985).

In the present study area there is little evidence for high-pressure metamorphism in the gneisses. Symplectitic intergrowths of biotite and feldspar are observed but kyanite and clinopyroxene are absent from assemblages in felsic gneisses. However, the eclogites themselves have suffered strong retrogression at amphibolite and epidote-amphibolite grades with, in many cases, complete hydration of pyroxenes, so retrograde overprinting can be inferred to have been particularly pervasive in this part of the WGR.

Basic dykes within the Basement Gneisses of the WGR show evidence of at least two phases of metamorphism, each with a thermal gradient increasing towards the west (figure 1.13). Most of the fjord section is characterized by epidote-amphibolite overprints on garnet amphibolite assemblages. To the west of Avenfjord (figure 2.2), amphibolite and epidote-amphibolite facies assemblages overprint eclogites, whereas in the Leikanger area, dykes of epidote-amphibolite grade show retrogression to upper greenschist facies. Epidote-amphibolite and greenschist facies metamorphism are found in Basement Gneisses and overlying rocks to the south and west of Hyllestad, with a similar up-section decrease in thermal conditions.

1.6 Plate reconstructions of the Scandinavian Caledonides

Following early attempts (e.g. Dewey, 1969) several models have been presented to explain deformation and metamorphic events related to the Caledonian orogeny in terms of plate tectonic processes. A successful model should explain

the regional structure of the Scandinavian Caledonides, including the emplacement of thrust sheets (some of which contain rocks of ophiolitic affinity), the timing of deformation events within the autochthonous and allochthonous units, and the widespread and deep-seated metamorphism in the WGR with its apparent increase in pressure and temperature towards the west. It should also take into account the distribution of sediment types and faunal associations found within the various allochthonous units and the unconformable deposition of coarse, clastic sequences of Devonian age on rocks showing Caledonian deformation (e.g. Kvamshesten basal conglomerate overlying syenite mangerites emplaced as part of the Dalsfjord nappe during the Ordovician, Bryhni and Skjerlie, 1975, Skjerlie, 1984). Other constraints on tectonic models are imposed by the disposition of other continental masses during the time interval of interest. These have been deduced from palaeomagnetism, climatically related lithofacies, and faunal provenance studies.

Dewey (1969) presented a relatively simple model for the Scandinavian Caledonides in which Greenland, as part of a North American plate, over-rides a westerly subducted slab of the Iapetus Ocean. Closure of the ocean is indicated to have occurred by the Devonian, with eastward thrusting of allochthonous units over the Baltic Shield and back-thrusting of basement and cover rocks towards the west in the over-riding Laurentian margin. Continental subduction of coastal Norway is not indicated.

More recently, Stephens and Gee (1985) have presented a detailed account, based on studies in central Norway and Sweden, where the superior biostratigraphic data constrain

palaeogeographic reconstructions more closely than in other part of the Scandinavian Caledonides. They base their model largely on faunal provinciality and the recognition of late Precambrian and Lower Palaeozoic platform, miogeoclinal, and eugeoclinal successions within different parts of the allochthon. Thin Vendian to Lower Cambrian quartzites overlain by black, uraniferous, mid to upper Cambrian shales passively underlie the sole thrust of the lower allochthon along the thrust front, and are also known from borehole data 30 km west of the front. Similar successions in basement windows imply that the Baltoscandinavian platform extended westwards at least as far as the present Norwegian coastline during the Vendian and Cambrian. Miogeoclinal successions in the Lower and Middle Allochthons have also been correlated with Vendian to Cambrian sequences in the parautochthon and are believed to have been deposited offshore of the present coastline.

The highest unit of the Middle Allochthon - the Särv nappe - contains a swarm of dolerite dykes of approximately MORB tholeiite, but partly alkaline, composition. These may represent incipient opening of the Iapetus in the Vendian. Restoration of the Lower and Middle Allochthon suggests the Baltoscandinavian miogeocline extended up to 300 km offshore of the present coast of central Norway. The lowest part of the Upper Allochthon, the Seve nappe, shows some similarity to the Särv nappe and is interpreted by Stephens and Gee (op. cit.) as the outer part of the Baltoscandinavian miogeocline.

The Seve nappe is succeeded by the Köli nappes, which make up the remainder of the Upper Allochthon, and comprise mainly greenschist facies volcanics and sediments of Ordovician (or possibly Cambrian) to Silurian age,

representing island arc, back-arc, fore-arc, and oceanic environments. Obduction of ophiolites in the highest Köli unit occurred to a location with North American faunal associations only, and is therefore interpreted as occurring on the Laurentian margin. The development of a volcanic arc is believed to have occurred with an oceanic segment separating Laurentia from the Baltoscandinavian margin. Three "suspect" terranes of eugeoclinal characteristics are recognized by Stephens and Gee (1985) in the Köli nappes of the central Scandes: the Virisen, Gjersvik, and Hölonda terranes (see figures 1.14, 1.15).

Miogeoclinal sequences in the Uppermost Allochthon are believed to be related to a western (Laurentian) margin due to dissimilarities in sediment type, intrusive rock-types and timing of metamorphism in this unit compared to those in underlying tectonic units.

The tectonic model of Stephens and Gee (op. cit.) is shown in figure 1.15. Imbrication of basement rocks on the Baltoscandinavian margin is assumed to have begun in the early Ordovician. Closure of the Iapetus Ocean is thought to have started in the Tremadoc and culminated in A-subduction involving underthrusting of Laurentia by Baltica.

Andresen and Færseth (1982) have considered the evolution of the southern Scandinavian Caledonides in a similar setting of ocean closure (figure 1.16). They describe an autochthonous basement comprising a heterogeneous gneiss complex, Proterozoic volcanics and sedimentary supracrustals, and post-orogenic Sveconorwegian intrusive bodies. This is overlain by a parautochthonous or autochthonous metasedimentary platform sequence, the Vidda Group, which changes westward to a deeper

water miogeocline. In the east, the succession is dominated by euxinic black shales of Lower Cambrian to mid Ordovician (or younger) age. In turn, the parautochthonous cover is succeeded by the Holmasjö Formation, showing three major episodes of thrusting with associated folding. The basal thrust cuts down to the southwest into the basement. The Holmasjö Nappe is capped by the Nupsfonn Nappe comprising crystalline thrust sheets. The latter unit shows Precambrian migmatization and amphibolite facies metamorphism overprinted by a Caledonian penetrative cataclastic fabric, and by lower greenschist facies assemblages. Overlying the Nupsfonn Nappe are three "exotic" Precambrian nappes probably assembled in the Precambrian, and collectively referred to as the Dyrskard-Kvitenut-Revsegg Allochthon.

The highest part of the nappe pile is occupied by the Sunnhordland Nappe Complex, which represents a thick Lower Palaeozoic eugeoclinal development and is composed of three major units:

1. The Hardangerfjord Group
2. The Sunnhordland Igneous Complex
3. The Dyvikågen Group

Andresen and Færseth correlate the Sunnhordland Nappe Complex with the Trondheim Nappes (Upper Allochthon) of the central Scandes. The Kvitenut and Nupsfonn nappes are considered to be lateral equivalents of the Jotun and Valdres Nappes, respectively. The rocks of the Dyvikågen Group, or possibly the Hardangerfjord group, are correlated with the Lower Palaeozoic schists of the Hyllestad Arc. Such correlations are broadly in agreement with the map of Gee et al (1985).

Evidence from Karmöy Island suggests the occurrence of a pre-Arenig episode of deformation and ophiolite obduction, possibly related to the "Finnmarkian" orogeny of northern Scandinavia, occurred prior to the emplacement of the allochthonous units over the Baltoscandinavian and Lower Palaeozoic platform during the mid to late Silurian. An alternative interpretation is that obduction of the ophiolite onto an island arc development near the Laurentian margin occurred at about 450 Ma BP, and was followed by emplacement of the whole complex onto the Baltoscandinavian margin in the Scandian orogeny. McKerrow et al (1989) suggest that the Finnmarkian Orogeny may be related to closure of a "Neo-Iapetus" Ocean which formed by rifting of the Laurentian margin prior to Tremadoc times.

One possibility is that the island arc "terrane" represented by the Sunnhordland Nappe Complex may be the equivalent of the Gjersvik and Hölonda terranes of the central Scandes which were deformed during displacement towards the Laurentian margin in the early Ordovician. Successions in these terranes are not directly comparable with those in the Sunnhordland Nappe Complex, but do contain mid-Ordovician clastic sequences. More evidence regarding the faunal provinciality of sediments in the Sunnhordland Nappe Complex is required before it can be related to deformation on either margin.

Cuthbert et al (1983) and Jamtveit (1987a) also favour a model involving westward underthrusting of the Laurentian continent by the Baltic Shield, with the suture zone lying to the west of an internally imbricated WGR. The deep burial of the present Norwegian coastal area resulted from overthrusting

of Baltica by Laurentia. During the development of the nappe pile, rapid compression of basement rocks would have occurred, followed by thermal relaxation due to conduction of heat from the mantle and radiogenic decay. Widespread evidence of disequilibrium amongst the high pressure assemblages, including low temperature eclogites suggests the heating event during decompression was of limited duration; a figure of 33 Ma is suggested by Cuthbert et al from isostatic modelling. Krogh (1982) calculated a P-T-t path for Norwegian eclogites with almost adiabatic decompression during uplift (see also Krogh 1977a, Griffin et al, 1985, Jamtveit, 1987a). Exhumation of high-pressure rocks in the basement is also widely considered to have been the result of the eastward translation of the nappe pile under conditions of gravitational instability (Cuthbert et al, 1983), and may also have been caused by the extensional "collapse" of the western part of the orogen during the Devonian (Seguret et al, 1989, Chauvet et al, 1989).

The model of McKerrow et al (1989) draws together faunal, sedimentological, radiometric, and palaeomagnetic lines of evidence from several continental masses and "suspect terranes". The relations between Laurentia and Baltica are broadly similar to those suggested by Stephens and Gee (1985). However, they present new biostratigraphic data suggesting the derivation of sediment deposited to the south of Laurentia and Baltica, and now forming the Southern Uplands, from a volcanic arc fringing the Siberian-Mongolian continent. Westerly subduction of the Iapetus Ocean beneath Laurentia provided a trench which directed sediment derived from the arc towards the south, where it was incorporated into the Southern Uplands

accretionary wedge (figure 1.17). The model is supported by the recent discovery of a coral of the genus Ceriaster, previously known only from Afghanistan and China, in Llandovery turbidites of the Southern Uplands. Sedimentation continued in the Southern Uplands until the late Wenlock implying that final closure of the Iapetus occurred no earlier than 420 Ma (McKerrow pers. comm.). This is a little later than some estimates for the timing of high pressure metamorphism (e.g. Griffin and Brueckner, 1980, upper estimate of Griffin and Brueckner, 1985), especially since elimination of the ocean basin should be an early consequence of continental underthrusting. The closure date suggested by McKerrow et al favours metamorphic ages of 390 to 400 Ma (e.g. Krogh et al, 1974, Gebauer et al, 1985, Mearns, 1986).

A Lower Palaeozoic scenario involving A-type subduction of the Baltic Shield beneath a North American continental mass during the late Silurian has become widely accepted during recent years as a model for the Scandinavian Caledonides. The consequences of such a collision have been the emplacement of a thick nappe pile, containing elements derived from both the Baltic and Laurentian continents, onto the Baltic Shield; high pressure metamorphism in the Norwegian coastal region; and imbrication of the WGR. Subsequent isostatic uplift led to tectonic stripping of the nappe pile and extensional collapse during the closing stages of the orogeny.

CHAPTER 2: TECTONOSTRATIGRAPHY AND STRUCTURE

The study area is situated on the western margin of the Western Gneiss Region (WGR), which exposes a large area of basement gneiss. The structure of these gneisses and their relation to the overlying Lower Palaeozoic schists is examined in this chapter.

2.1 Structural setting of the Field Area

An area of approximately 200km^2 between Råsholm and Lifjorden has been mapped (figure 2.1) during the present study. This area is situated on the western margin of the WGR in which the parautochthonous basement gneisses are exposed (figure 1.1) (Cuthbert et al, 1983, Gee et al, 1985). The central and eastern parts of the area fall within this basement window.

The reconnaissance mapping of Bryhni (1966) places the "Basement Gneisses" and "Mafic Units" of this study in the Fjordane complex of metasupracrustal gneisses and schists, which overlies the more easterly, and largely migmatitic, Jostedal complex. Later workers (e.g. Kildal, 1970, Bryhni and Sturt, 1985) make similar distinctions between metasupracrustal and migmatitic complexes. Such subdivisions are of limited use in this study since both "Fjordane" and "Jostedal" complexes are typified by the presence of granitic and augen gneisses and migmatites. Skjerlie (1984) recognizes two divisions of the basement rocks in the Melvær and Askvoll area (figure 1.1): the lowermost Jostedal Complex, corresponding to the definition of Bryhni (1966), and the Vevring Complex, consisting of dioritic and quartz-dioritic

gneisses overlain by eclogite-amphibolites and amphibolites. These "complexes" may be equivalent to the Basement Gneisses and Mafic Units, respectively, of the present study (table 2.1).

The WGR has been overprinted by Caledonian deformation which progressively increases in intensity to the west (Strand, 1960, Dietler et al, 1985). Within the study area the WGR has been thoroughly reworked and the correlation of lithologies is considerably hampered by the development of blastomylonitic textures and the destruction of original fabrics. Together with marked differentiation of micaceous and quartzo-feldspathic components in strongly mylonitised granitic or tonalitic gneisses, this overprint can render even broad distinctions (e.g. between orthogneisses and paragneisses) difficult to make with certainty.

To the west of Lavik the general strike of lithologies is east-west with moderate to steep dips, mainly towards the north. Between Lavik and Råsholm major folds are developed. Strong mineral elongation lineations are present across the whole area and have a gentle or moderate plunge to the east or west outwards from the central part of the area.

In the western part of the study area the WGR is overlain along a discordant tectonic contact by the "Hyllestad Schists", a sequence mainly comprising pelitic, semi-pelitic, and psammitic schists which exhibit chlorite to kyanite grade mineral assemblages. Their composition suggests a eugeosynclinal sequence with volcaniclastic influence. They have been tectonostratigraphically correlated with the Caledonian Upper Allochthon and are assumed to be of Lower Palaeozoic age (Gee et al, 1985; Kildal, 1970; Nilsen, 1968).

Associated with these schists are coarse garnet-amphibolites, discontinuous calc-silicate bands, banded gneisses and granodioritic bodies. Minor folds and shear bands are ubiquitous. The compositional layering in this area dips moderately towards directions between north and west. In the extreme west of the study area, at Gygrekjeften (025126), the "Cambro-Silurian" schists are overlain by the Devonian Solund Conglomerates (Nilsen, 1968), which rest upon a planar tectonic contact shallowly-dipping to the west (figure 1.4) and described variously as a thrust (C.F. Kolderup, 1926; Nilsen, 1968) or low-angle extensional fault (Hossack, 1984, Norton, 1986, 1987).

2.2 The Basement Gneisses

The structurally lowermost horizons in the study area comprise a thick unit of intensely deformed gneisses, migmatites and metabasites. These are almost continuously exposed along the shore of Sognefjord between Nesje (023055) and Avenfjord (235100). The term "Basal Gneiss Complex" has been used to describe the parautochthonous rocks of the WGR; here the term "Basement Gneisses" is used more specifically for a particular unit of the WGR exposed in the field area. The structurally lowest part of the Basement Gneisses consists of at least 600m (maximum thickness exposed) of coarse-grained augen gneiss with abundant porphyroblasts of pink or white alkali feldspar up to 3cm in length. A steep foliation is folded around mesoscopic, northward-vergent hinges, which are cut by small southward-vergent shear zones. In places coarse-grained bands with migmatitic texture are developed. Mafic horizons, 1 to 2m thick, possibly corresponding to deformed

doleritic dykes occur in this unit.

Above the augen gneisses is a sequence of banded gneisses with occasional thin (2-3m) horizons of staurolite schists and acidic orthogneisses (table 2.2). This sequence probably represents a psammitic and semi-pelitic supracrustal sequence.

A deformation of supposed Caledonian age (Dietler et al, 1985) is ubiquitous (figure 2.2), but where it is only weakly developed on a mesoscopic scale, diffuse stromatic leucosomes may be recognized. A few outcrops of virtually unaffected migmatite in which this foliation is poorly developed may be found between Brensdal and Stavsneset (113023, 090047, figure 2.2) in which at least 2 generations of melt may be distinguished in granitic and monzonitic migmatites (figure 2.7). In these areas of lower Caledonian strain the main compositional foliation is cross-cut by pegmatite veins and mafic dykes (figure 2.5). Phenocrysts and ophitic texture may frequently be recognized in the latter, which are generally doleritic in chemistry, if rather rich in potassium. The mineralogy of the mafic dykes is characteristic of the amphibolite facies (table 2.2) and there is no evidence that higher metamorphic grades have been attained. Despite a lack of radiometric data concerning the age of these dykes, they are considered to be pre-Caledonian, possibly Precambrian: they frequently show foliations parallel with external foliations and they are occasionally folded around open hinges. In areas of higher strain, boudinaged or lensoid mafic bodies with biotite-rich selvedges occur and, if originally present, cross-cutting intrusive relations are destroyed. The margins are parallel to locally anastomosing late shear bands and may be folded around isoclinal hinges.

Mafic pods and sheets showing evidence of eclogite facies metamorphism occur at several horizons. The geographically most extensive, representing the largest volume of material, is between 250-500m thick and crops out at Brensdal, Helleböstölane and Ytre Hellebö (110032, 130025, 140020). Eclogitic assemblages are occasionally preserved (table 2.2), but are more commonly partially replaced by amphibolite-facies assemblages. Mafic pods showing no relict clinopyroxene, but with similar field associations are exposed at Indredalen, Alværen and also near Takle (on the southern shore of Sognefjord). These occurrences are characterised by the podiform nature of the mafic bodies (from a few centimetres to 2m in length) and their association with tightly folded white-weathering quartzitic gneisses, which enclose the pods.

Horizons rich in coarse K-feldspar porphyroblasts are common throughout the "basement" complex, increasing in thickness and abundance towards the upper parts of the sequence studied. On the western shore of Avenfjord (figure 2.2), the augen gneisses have the appearance of a granite orthogneiss. However, between Alværnipa and Råsholm (205070, 285085) gneisses containing coarse feldspar porphyroblasts are interbanded with schists of an apparently metasedimentary nature. In many parts of the study area the growth of feldspar porphyroblasts preceded the latest episode of shearing deformation and may be related to earlier migmatisation of country rock gneisses. Stromatic migmatites and ophthalmites (McLellan, 1983) are recognized at some horizons.

The maximum structural thickness of the "basement" gneisses and migmatites in the study area, measured

perpendicular to the main compositional banding, is at least 7000m. The original "stratigraphic" thickness has been considerably modified with repetition by minor folds and shear zones, and attenuation or boudinage of fold limbs. The pervasiveness of overprinting blastomylonitic textures increases, in general, towards the north and with proximity to the overlying units. At the contact with the overlying units (see below), blastomylonitic textures are ubiquitous, feldspar porphyroblasts become elongated and develop diffuse margins, and a platy fabric is commonly found. Such platy zones have a width of several tens or even hundreds of metres. However, the overlying units are typically amphibolitic schists with a lower competency and it is these which appear to have accommodated much of the strain.

The earliest minor structures which can be recognized are tight to isoclinal hinges folding a compositional banding. The origin of the folded banding, however, is not immediately obvious; it typically consists of layers of a few centimetres thickness which are parallel or subparallel to major variations in composition. It is not equally well-developed everywhere and where less intense is apparently produced by the "smearing-out" of compositional inhomogeneities such as leucosomes in granitic migmatites, basic pods (dykes and sills?) etc. The development of this early foliation ("S_1") is in general less intense east of the field area, becoming mainly confined to discrete shear zones between Höyanger and Balestrand (Dietler et al, 1985, Bailey and Harley, unpubl. results). In these areas S_1 foliations post-date the intrusion of dykes and pegmatite veins and several migmatization events (figures 2.6, 2.7). Minor structures

associated with S_1 have not been recognized in the field area. The isoclines mentioned above (F_2) have an axial planar fabric, S_2, defined by the preferred orientation of micas, and sometimes amphiboles (figure 2.8, appendix 1). F_2 folds are quite common in the basement gneisses but their axes are difficult to measure, as the gneisses do not generally part easily along the S_1 foliation. A mineral elongation lineation parallel to F_2 axes is sometimes seen, defined mainly by quartz rodding, but also preferred orientations of biotite and amphibole grains. F_2 folds may be quite large with amplitudes of 10m or so, but commonly have amplitudes of a metre or less (figures 2.9, 2.10).

F_2 folds are most easily recognized when refolded by folds of F_3 type (figures 2.11, 2.12). In the basement gneisses these frequently have rounded open hinges. F_3 hinges are ubiquitous in the field area and generally have axes gently plunging, very approximately, east-west with axial planes dipping gently or moderately to the east (figures 2.8, 2.13, and appendix 1). To the east of Lavik, F_3 folds have very variable geometry: axes are oriented more or less east-west but poles to axial planes scatter widely on the stereonet. At Beksneset (112013) a large (10m) rounded pair of F_3 folds in banded gneisses, verge northwest (figure 2.14). Incompetent bands form complex accommodation structures in the hinge regions. To the north of this locality meso- to macro-scale F_3 folds are common, with almost exclusively northwesterly or northerly vergence, sharp to rounded hinges and flat-lying or gently northward-dipping axial planes. Similar structures may be seen at Nesholmsundet (038051) (figure 2.15) where folds of 0.5m wavelength are parasitic on

northerly vergent folds an order of magnitude larger. Crenulation of S_2 is developed in F_3 hinges in schistose horizons, but forms a poor parting. F_3 folding is responsible for the pi-girdle of poles to compositional foliations (figure 2.8).

At one or two localities a broad warping of the compositional foliation which also deforms F_3 axes may be seen (eg at Ytre Hellebö and northeast of Alværen (208064). These "F_4" warps have axes oriented roughly north-south, subhorizontal axial planes, and may be related to a broad updoming of the area between Brensdal and Hellebö.

In the western part of the area, notably between Nesholmsundet and Spisskammersvika (038051, 041057), an extensional crenulation cleavage (Platt and Vissers, 1980) is developed in garnet-biotite schists (figure 2.16). The parting is too weak to obtain good orientation data in the field but thin-section studies suggest that the shear bands have a consistent northwesterly dip and shear sense is "top-to-northwest". Minor conjugate shear bands of opposite shear sense are sometimes seen. Vertical shear zones near Leirvik and very small, brittle faults also belong to a phase of late extension, and may be related to the extensional crenulation cleavage mentioned above (figure 2.17). The shear zones trend north-south and contain quartz-filled tension gashes showing sinistral shear sense. The faults, up to 30cm in length, trend north-south, and have an offset of a few centimetres.

2.3 Amphibolites and Gabbros

The rocks immediately overlying the gneisses have been subdivided for the purpose of mapping into three major units,

referred to as the Lower, Middle, and Upper Mafic Units, on the basis of their composition and fabric. Together they share some similarities with the Vevrings complex of Skjerlie (1984) in the Melvær and Askvoll district. They mainly comprise mafic or intermediate schists and gneisses of predominantly igneous origin. Relict ophitic, cumulate and xenolithic textures are widespread though, more commonly, a strong linear or platy fabric overprints or obliterates igneous features. Where a schistosity is well-developed, open to tight minor folds, chevron-folds, and crenulations are often observed. Interference structures representing the overprinting of early folds by subsequent fold episodes are rare (figure 2.18).

2.3.1 The Lower Mafic Unit (Lavik Amphibolites)

This unit rests directly on the basement gneisses (figure 2.19), with an apparently concordant contact, and extends from east of Tjönnebakkane (195075) to the west of Bö Kapell (080078). The contact is well-exposed at Hanen (086068), and between Laviksåta and Sausnuken (140060, 105065), but elsewhere is generally obscured. The thickness is about 1000m. Near Lavik (175050) the apparent thickness is 1300m but some of the increased thickness is probably due to tectonic repetition of the strata (figure 2.19).

The commonest rock-type is a dark-green, medium-grained mafic amphibolite, frequently banded with white oligoclase-rich layers less than a millimetre to tens of centimetres in thickness. Lineated fabrics commonly occur with elongate dark and light patches up to 10 centimetres in length by 2cm. The dark areas are composed of aggregates of actinolite with

chlorite and biotite while pale areas are mainly oligoclase with accessory quartz. These are thought to represent coarse or pegmatoid gabbroic precursors. In the central and eastern portions of the unit several discontinuous bands, 2-20m thick, of markedly different composition occur, including granitic gneisses, and ultramafic and pelitic schists (table 2.2).

The major element chemistry of the mafic amphibolites is essentially that of a tholeiitic dolerite (Cox et al, 1979). Original igneous textures are preserved at several localities, most notably near Djupevik, Vasslitjörna, and Sausnuken (094076, 178064, 105065), where ophitic and intergranular textures, randomly oriented feldspar phenocrysts and idiomorphic pyroxene grain shapes may be discerned although the constituent grains have been partially replaced by assemblages of amphibolite or lower grade. A small dyke-like body intruding the amphibolites has been recognized at Djupevik. The massive, rounded outcrops comprising such material are dissected by near vertical joints and low-angle, anastomosing shear zones filled with platy actinolite + biotite + chlorite schist or with chloritic gouge. Peak conditions of metamorphism are represented by hornblende-garnet bearing assemblages. There is no field or petrographic evidence that conditions of eclogite metamorphism have ever been attained. Chlorite, magnetite, and frequently, biotite and actinolite are late, retrogressive phases. Retrogressive replacement of garnet-amphibole assemblages by biotite + epidote or biotite + chlorite is widespread but is associated, in particular, with the basal contact, e.g. at Kjörnes (078071). Schistose fabrics are invariably developed in the Lower Mafic Unit at this contact although massive amphibolites

with igneous textures may be found within a few metres of it. At Tjönnebakkane (195065) a "train" of massive amphibolites and gabbros occurs within 10m of, and parallel to, the contact; each occurrence has a podiform shape and is enclosed by actinolite-biotite schists.

Although the igneous nature of most of the rocks in this unit is clear, any originally igneous contacts have been tectonically modified and structural elements are nowhere observed to be cross-cut by igneous contacts. The widespread, if infrequent, preservation of early igneous features is due to the heterogeneity of fabric development during later deformation events. The development of penetrative fabrics may be controlled, in part, by original textures and composition.

The earliest evidence of deformation is the presence of differentiated, banded amphibolites consisting of 2-5mm layers of plagioclase interbanded with hornblende, such as those seen at Lavikstölane (155062). These rocks are rather rich in Al and Na compared with "average" basalt compositions (Cox et al, 1979) although otherwise closely similar in major chemistry, presumably due to higher normative plagioclase. The banding may be an original igneous feature, such as cumulate layering, modified by differentiation and is denoted as S_1; its identification depends on the recognition of early folds by which it is deformed.

Isoclinal folds of F_2 type are rarely seen and may be almost identical to later folds. It is possible to positively identify them only when their axial planes are deformed by open to tight folds of F_3 type, (figure 2.18) and where the rock-type has a compositional foliation (usually S_1). A

strong axial planar fabric ("S_2") is always present in these mafic schists. F_2 folds are rarely encountered, even where the rock-type is suitable for their preservation, so the geometry of very few examples could be determined. A quartz-rodding and mineral elongation lineation is parallel with F_2 axes. However, the axial planar fabric, S_2, appears to correspond to the "regional" foliation in this unit and except in the hinges of F_2 folds, is virtually indistinguishable from S_1; hence its variation throughout the unit may be inferred (figures 2.8, 2.13). Large-scale structures associated with D_2 have not been recognized in this unit, but the conformity of an S_2 schistosity at the basal contact suggests that it may be tectonic and of D_2 age. The peak metamorphic conditions of garnet-amphibolite experienced by the LMU are probably syn-D_2 in age. Hornblende aligned in S_2 wraps around garnet porphyroblasts whereas plagioclase and quartz moats resulting from the breakdown of garnet appear unaffected by the presence of an S_2 foliation.

Folds of F_3 type are almost ubiquitous in the LMU, being absent, or undetectable, only in parts lacking both S_1 and S_2 foliations. They take the form of open to tight folds or chevrons, usually with an amplitude of a few tens of centimetres but occasionally up to a metre or two. Axes have a shallow to moderate plunge mainly between northeast and southeast, clustering around 40° towards 080°. Axial planar orientations also have a wide scatter, but tend to have a shallow to moderate dip towards the east. The vergence of minor, or mesoscale, F_3 folds varies within the unit but appears to define a number of larger folds with hinges persistent for only several hundred metres or so. A mineral

elongation lineation parallel to F_3 axes is well-developed but may be confused with L_2 lineations. It is best seen in coarse-grained rock-types where earlier platy fabrics are not developed. The L_3 lineation is defined by quartz rodding, elongate biotite and actinolite grains and, very occasionally, by "tails" on porphyroblastic feldspars. Crenulation of S_2 schistosity is frequently observed in F_3 hinges, but only a weak axial planar fabric results with little or no differentiation. Metamorphism associated with D_3 is retrograde with respect to earlier episodes, involving the replacement of hornblende amphibole with more actinolitic compositions and the growth of new biotite. Zoning in plagioclase to more sodic compositions is most probably related to a general tendency towards low amphibolite/upper greenschist facies conditions during D_3.

The open warps which gently fold D_3 structures in the basement gneisses have not been observed in the amphibole schists of the Lower Mafic Unit, except at Djupevik (094076), where the main S_2 schistosity is very undulose; axial planes of F_3-type folds are apparently also disturbed by these very broad flexures which may be due to D_4. F_4 folding around approximately north-north-west trending axes may be responsible for the scatter in lineations and F_3 fold axis measurements.

2.3.2 The Middle Mafic Unit (Gråfjell Gneisses)

The Middle Mafic Unit forms a wide band of outcrops which extend from the western coast to the area at Nesje through Leirvik and Stöldal, to Vetlenipa (025067, 090087, 180075). It has a maximum thickness of approximately 2000m, though the

effect of tectonic thickening is difficult to assess with the absence of reliable stratigraphic marker horizons.

At Fjellheim (127077) the basal parts of the unit are not in contact with the LMU but rest on quartzo-feldspathic gneisses, commonly with large feldspar porphyroblasts, quartzites and garnet-mica schists. Petrographically, these are indistinguishable from the "basement gneisses" and appear to represent a basement window. Contacts are not exposed in this densely-wooded area. In the cliffs between Hanen and Leirvik (089083) a sharp, planar contact may be seen at the base of the unit, but here the basement window is not seen.

The dominant rock-types are medium to coarse-grained tonalitic gneisses, showing a blastomylonitic texture with a strong lineation and weakly developed foliation. Other rock types include massive orange-grey gneisses of syenogranitic to granodioritic composition (Cox et al, 1979); ultramafic tremolitic schist forming large ovoid pods (100-200m diameter); and actinolitic schists, 5-50m thick and continuous over several kilometres along strike (representative assemblages are shown in table 2.2). To the north of Indrefjord (060090) the unit passes into actinolitic schists and more acidic gneisses banded on the scale of 20-60m and totalling approximately 800m in thickness. On the whole igneous textures are poorly preserved, but at Leirvik (088085) faint, shadowy xenoliths of darker material may be discerned in grey-green medium- to coarse-grained tonalites. In addition trondhjemitic veins (figure 2.20) show strong lineations and folding and have been cut by thin (1-3cm) mylonitic shear zones. Fairly massive, coarse-grained textures are seen in amphibolites to the north of Leirvik at

Stigestrondevatnet (094094).

Strongly lineated rocks with weak or spaced planar fabrics are most common in this unit. Infrequent actinolitic and tremolite-rich assemblages develop strong schistosities.

A differentiated S_1 schistosity is absent from some rocks and in others, if present, is overprinted by later foliations. A penetrative S_2 foliation occurs in actinolitic and tremolitic rocks but is weakly developed in the tonalitic gneisses. A major fold is seen between Leirvik and Indrefjord, apparently predating F_3 minor folds which show constant northerly vergence across the structure. The compositional banding is folded around axes roughly parallel to subhorizontal westerly plunging mineral elongation lineations. The vergence of the major structure is opposed to the prevailing northerly vergence of F_3 structures in this part of the area. Mapping of bands of actinolitic schists reveal tight, mesoscopic folds of similar vergence and style in the central part of the area. Minor refolded folds, possibly of F_2 type are found to the east of Kleivevatnet (figure 2.21).

Northwestward-vergent F_3 folds with axes approximately parallel to a mineral elongation lineation are seen at Leirvik and at Arefjellet (135077). Stretching lineations plunge gently away from a "culmination" near Fjellheim (128076) to approximately 5° north of west, and between due east and 30° south of east (figures 2.8 and 2.13). There is a tendency for mineral elongation lineations to have more consistent orientations to the west. Minor fold axis orientations are much more scattered, with most plunging gently or moderately to the east. The axes of F_3 folds are often closely

coincident with those of F_2 structures and L_2 and L_3 mineral elongation lineations are sometimes indistinguishable. D_2 structures may have been rotated during D_3 into the stretching direction.

Undulose and anastomosing shear-zones of low-grade deform trondhjemitic veins at Leirvik; they are not seen to be deformed by any later events (figures 2.8, 2.20). The shear sense of the rotated veins is "top-to-north". Such shear zones appear to be confined to the area around, and to the west of, Leirvik. Extensional crenulation cleavage dipping shallowly towards the northwest is developed in some rock-types in the west of the area (e.g. north of Rysjedalsvåg). Boudinaged pods of saussuritized feldspar, showing extensional cracks infilled with albite, occur in isolation within amphibolites (figure 2.22).

2.3.3 The Upper Mafic Unit (Mölmesdal Gabbro)

The Upper Mafic Unit extends across the northern part of the area between Espelandsvatnet (108108) and Råsberg (225090). It attains 1600m in thickness, although some of this may be due to tectonic thickening. The base of the unit is exposed between Stöldal and Kjönas, where the contact is sharp and a highly schistose fabric is developed in the Upper Mafic Unit.

The main rock-types are coarse gabbros and banded hornblende or actinolite schists. There are also less mafic, coarse-grained, intrusive rocks, particularly at Löland (130110) where granitic and monzonitic rocks crop out. The unit is also distinguished from the Lower and Middle Mafic Unit by the common occurrence of basic dykes. At Kjönas

(155085), pegmatoid gabbros (grain-size about 2-3cm but up to 20cm) are cut by doleritic dykes with relicts of chilled margins, subophitic texture and discontinuous comb layering. The gabbros themselves are rather variable in composition. At Kjönas they have coarse labradorite laths with intergranular clinopyroxene and orthopyroxene. At Mölmesdal plagioclase laths form up to 70-80% of some rock-types which show cumulate layering with intergranular clinopyroxene. At Råsberg and Kjönas, coronas are developed on olivine and orthopyroxene (table 2.2). Ilmenite is almost ubiquitous, frequently present in sufficient quantity to make compass readings inaccurate, especially at Råsberg, Mölmesdal and Löland (220087, 183080, 156084).

Deformation is extremely heterogeneous: in some places intricate igneous or metamorphic textures are preserved with very little overprint. In the quarry at Kjönas, the only deformation is an elongation of coronas and a few low- to moderately-angled easterly-dipping shear zones whereas in the road-cutting nearby massive pegmatoid gabbros pass into sheared gabbros, gabbroic amphibolitic gneisses, and banded amphibolites with F_3-type minor folds and chevrons, or strongly lineated biotite-actinolite schists. Trondhjemite veins in less-deformed parts preserve sheared margins with northerly vergence (figures 2.23, 2.24). The categorization of folds, shear zones, and other structural elements into a classification based on a number of discrete deformation episodes is frequently impossible because of the heterogeneity of deformation. The coarse-grained rocks, on the whole, seem to have been most robust in resisting deformation. At Råsberg the Upper Mafic Unit rests on basement, the ilmenite mine road

passing through the contact several times. The margins of the unit consist of fine-grained amphibolites in which a fine banding defined by the segregation of amphibole and plagioclase is folded about tight to isoclinal hinges with an axial planar foliation developed. The banding, fold hinges and axial planar schistosity are probably related to S_1, F_2 and S_2 as seen in the Lower Mafic Unit, and are similarly refolded around F_3-type hinges. This is the only locality known at which interference of two phases of folding is clearly seen in the Upper Mafic Unit.

The Upper Mafic Unit is structurally overlain by the Hyllestad Schists (see below) to the west, and by a sequence of folded granitic augen gneisses and metasediments, resembling those of parts of the Basement Gneisses, to the north. The contact with the latter is not well-exposed but can be seen to the west of Bogsvatnet, where the base of the uppermost unit is an augen gneiss crowded with coarse K-feldspar porphyroblasts and locally exhibiting a strong mylonitic fabric (figure 2.27). These rocks may be lateral equivalents of the Basement Gneisses tectonically emplaced over the Mafic Units.

2.4 The Hyllestad Schists

A sequence of mica schists, banded and massive gneisses, amphibolites and granitic rocks crops out over a large area to the west of Aksevatnet, Kleivevatnet and Kolgrov (090120, 070115, 057098) and Båtevika (046078). It is bounded to the west by the basal contact of the Devonian Solund massif (figures 1.4, 2.1). The present preserved total thickness of the schists is 2000m or so, but as there is evidence of

considerable tectonic modification, the original "stratigraphic" thickness can only be guessed. The age of the sequence is taken to be Cambro-Silurian (Kolderup, 1952).

The base of the sequence is only well-exposed north of Soetevik, where the compositional foliation is concordant with underlying quartzo-feldspathic schists. Both rock-types exhibit highly mylonitized fabrics at this locality. Elsewhere the contact is obscured by farmland, but mapping of the underlying gneisses reveals an oblique discordancy. The contact is gently to moderately northwestward-dipping and is tectonic in nature. Recent models for the formation of the Devonian conglomerate (Hossack, 1984, Norton, 1987) imply that this contact is probably a thrust reactivated as a low-angle fault during the Lower or Middle Devonian. This is an attractive concept as it will accommodate many of the field observations, but cannot be, however, unequivocally confirmed or refuted from the study. Extensional minor and micro-structures, including boudinage, minor faults, and extensional crenulation cleavage (figures 2.26, 2.27), are seen throughout the unit and particularly near Soetevik.

The schists consist mainly of chlorite + Mn-garnet assemblages interbanded with quartzite and graphitic horizons. To the north of Nedre Lireidtjörna (040120) actinolite bearing horizons occur. Along the north shore of Sörefjorden and to the north of Kleivevatnet kyanite-schists occur, associated with "garbenschiefer" assemblages at the latter locality. Garnet-amphibolites and siliceous carbonates are present at a few horizons while epidote-amphibolites are fairly common (table 2.2). The sequence as a whole may represent a pile of eugeosynclinal sediments with some

volcaniclastic input and, possibly, submarine lavas.

The most elevated topography is formed by rocks of granitic to granodioritic composition. Around Kolgrovheia (053107) these form several thin northwesterly dipping sheets or slabs with a spaced planar mylonitic fabric. At Sogneskollen (030085) a more homogeneous mass is seen,cut by discrete shear zones and with a few minor intrusives preserved, some protruding from the main body (figure 2.28). At the western end of the contact with the surrounding schists (010085) an intrusive, cross-cutting contact is observed between the compositional banding in the schists and apophyses of the granite. Such apophyses are boudinaged and detached from the main body of the intrusion at Sognnes.

Deformation within the banded gneisses has a markedly contrasting style to that within the schists and granite. The gneisses show a regular banding on a 5-20cm scale defined by pale layers of quartzo-feldspathic material and dark grey layers of quartz, feldspar, biotite, amphiboles, and chlorite. The feldspars usually show partial saussuritization. The banding may be due to metamorphic differentiation (D_1?) modified by later shearing (D_2?). A schistosity defined by micas and amphiboles is developed parallel to the compositional banding of the rock and axial planar to the few isoclinal hinges (F_2?) which are still preserved. These early folds are tightly refolded by north or northwest-vergent folds (F_3?) with a wavelength of 30cm to a metre (figure 2.29). The later folds have a very "fluid", ductile profile with overturned or recumbent curved axial "planes" and curvilinear axes. A crenulated fabric is sometimes found in hinge regions. Boudinage of feldspathic horizons is common.

In the schists of highest grade (kyanite + staurolite + garnet and garnet + biotite assemblages etc.), which in general crop out to the east and southeast of Hyllestad, some differentiation into coarse- grained white mica- and quartz-rich foliae is developed. This is not always very marked and is generally poorly developed or absent in rocks of lower grade. Garnets, especially large euhedral porphyroblasts, occasionally include curved trails of dark minerals (ilmenite or rutile) and quartz indicating the formation of an early foliation which has been completely overprinted in the matrix. A variety of brittle crenulation is developed but little or no recrystallization is associated with it. Single mica flakes and elongate quartz grains are bent around tight hinges the former being fractured or kinked along the axial planes whilst the latter shows continuous undulose extinction from one limb to the next. In quartz grains recrystallization is confined mainly to serrated edges without the development of subgrains. Kyanite grains are also commonly fractured, often being crushed between two garnet "anvils" (figure 2.30, 2.31). This jostling of mineral elements affects all minerals in the rock with the exception of late chlorite and magnetite which fill fractures in garnet and kyanite grains and dislocation planes cutting the schistosity at a low angle. Recrystallization of quartz with much reduced grain-sizes, occurs along these mylonitic zones. Garnets generally cause the deflection of such shear zones, but are sometimes fractured. In chloritic schists from south of Kleivevatnet (069112) an extensional crenulation cleavage is developed with shear bands dipping gently westward or northwestward (figure 2.32). Similar fabrics are seen elsewhere in the unit although the number and

density of shear bands is usually less intense. To the west of Hyllestad the schists are of generally low grade (biotite or chlorite zone but with occasional garnet-amphibole "garbenschiefers") frequently preserving granular sedimentary textures. Calcite fibres infill fractures in actinolite grains extended along their length, but extensional crenulation cleavage is not always developed. Graphitic schists are cut by brittle shear planes and show asymmetric crenulations. The intensity of mylonitization increases again towards the contact with the Devonian conglomerate at Gygrekjeften (024128).

Deformation in the granitic rocks takes the form of a mylonitic foliation defined by shear bands in which the grain-size of quartz is greatly reduced. Feldspar grains are relatively strong and resist degradation. They are sometimes fractured or have spalled margins. Where they occur within shear zones the foliation is deflected, usually symmetrically. Samples collected from the Sogneskollen body are generally coarse-grained with much less evidence of mylonitization. Coarse quartz grains may show shadowy extinction without developing subgrains. These samples also have greater sericitization of feldspar and small radiating clusters of chlorite replacing biotite (the latter mineral being absent from mylonitised rocks near Kolgrovheia (053107)). Sericite-filled joints roughly parallel to and also perpendicular to the deformation foliation are common.

Rocks with a complicated metamorphic and tectonic history, such as the garnet-kyanite schists are juxtaposed out of sequence with rocks of much lower grade and relatively simple history. The contacts are mainly concordant with the

compositional layering (e.g. Sörefjord, Kleivevatnet, (070137,070115)). Minor "ramps" which truncate quartzose horizons occur (e.g. at Hyllestad, figure 2.33) and at Furnesvika (052123) shear zones truncating late tight folds bound a duplex-like structure in which large folds in chlorite schists are themselves truncated by a sheet of granitic material (figure 2.34). These are probably extensional shear zones related to the extensional crenulation cleavage seen elsewhere. Mineral elongation lineations on the contacts plunge gently or moderately to the west (figures 2.8, 2.13).

Stratigraphic marker horizons are not easily defined in the schists but the apparent repetition of granite "sheets" and of similar schistose lithologies, and the inversion of metamorphic gradients, suggest that the initial emplacement of these schists, amphibolites, and granite onto the underlying basement gneisses and amphibolite units was by thrusting. Subsequent deformations mainly show vergence to the northwest or north and have largely overprinted or reactivated earlier structures. Such structures would be consistent with certain models which suggest an extensional regime, for the formation of the Solund conglomeratic basin.

2.5 Synopsis (see also section 2.6 and table 2.3).

The wide variety of rock-types across the area may be considered to be partly responsible for (and partly the result of) the heterogeneity of the early Caledonian deformation. The development of anisotropic fabrics is extremely penetrative in parts of some units and yet may be almost absent in adjacent rocks and inevitably has a role in controlling the distribution and style of later structures.

The different units distinguished for mapping show some structural features in common:

[1] Open to tight folds of similar style which fold a pre-existing schistosity occur in the basement gneisses and the mafic units, and have been designated as F_3. It is proposed that the structural history of the basement gneisses from D_3 on has been shared with the Lower, Middle, and Upper Mafic Units and the augen gneisses of Bogsvatnet to Tonningsvatnet (154097, 116135).

[2] In addition it is noted that F_3 folds refold earlier isoclines (F_2) in the basement gneisses and the Lower and Upper Mafic Units. The main schistosity is parallel to the axial planes of these isoclines wherever they are found; and they fold an even earlier, differentiated foliation (S_1). The Middle Mafic Unit is affected by major pre-F_3 folds. It is thus deduced that the basement gneisses and mafic units probably share structural history from at least D_2 and possibly D_1 onwards and the constituent units were assembled syn-D_1 or -D_2. Prior to the development of this S_1 foliation very little can be deduced concerning the history of the Lower and Middle Mafic Units. The formation of coronas on mafic minerals from certain gabbroic rocks of the Upper Mafic Unit may be pre-D_1 or pre-D_2, while the basement gneisses show relicts of an early complex migmatization history, better preserved east of the field area especially around Vangsnes and Balestrand, and not recorded in units above the basement gneiss.

[3] The Hyllestad schists are more difficult to place and correlate in this structural sequence. Banded gneisses to the east of Hyllestad and around Kleivevatnet show F_3-type hinges

folding isoclines with axial planar schistosity while the garnet-bearing schists retain evidence of an early schistosity (S_2?) in curved garnet inclusion trails. Late, "brittle" crenulations and shear planes modify a pre-existing schistosity (again, S_2?) defined by mica orientations and quartz segregations. It is probable that these schists have also shared the post D_2 and, possibly D_1, history of the basement gneisses.

[4] A spaced extensional crenulation cleavage with top-to-west shear sense, which dips gently to the west or northwest, is present in the Hyllestad schists and is also seen in rocks of the Middle Mafic Unit and basement gneisses at Rysjedalsvåg (049074) and as far south as Nesje (030052). This is a late ("D_5") event cutting across earlier foliations and is confined to the west part of the area, encountered mainly west of Leirvik and increasing in intensity towards the west and northwest. Quartz-filled tension gashes forming north-south trending vertical shear zones (figure 2.17) and minor faults with offsets of a few centimetres and similar orientations (figures 2.22, 2.27) may also be of "D_5" age.

The overall structure of the area is shown in 17 north-south cross-sections in figure 2.19. These are drawn roughly perpendicular to the trend of D_3 mesoscale structures. In general, the units have a northerly dip but are overturned in the northeast of the area. The interpretation is based largely on the outcrop pattern, aerial photography, and interpolation of structures between well-constrained sections. Pre-D_3 minor structures are too infrequent to allow analysis of large-scale structures and are reoriented by later structures. Analysis of D_3 structures reveals the presence of

large mesoscale fold axes which fold contacts between the units. Between Fjellheim and Gråfjell the flat-lying basal contact of the Middle Mafic Unit branches from the basal contact of the Lower Mafic Unit, and the MMU is seen to rest directly on basement gneiss (figure 2.1). In the extreme east of the area the Upper Mafic Unit is also known to rest directly on Basement Gneisses and this contact is assumed to extend beneath the central part of the area, with the UMU/MMU and MMU/LMU contacts branching from it,and forming a "sole" structure. The tectonic nature of these contacts has been discussed in earlier sections. The direction and amount of movement along them is poorly constrained. The depth and dip-angle of the inferred "sole" contact is not known and is represented schematically in figure 2.19. The contacts branching from the "sole" contact may meet in a "roofing" structure (by analogy with thrust duplex structures) but this is not observed.

In this interpretation the "sole" contact is assumed to link the basal contact of the LMU with that of the UMU to the east of Bosdal (figures 2.1, 2.19). Exposure is lacking and the postulated contact cannot be observed in the field.

As mentioned above open to tight F_3 folds can be seen to deform the contact between the units, especially between the Basement Gneisses and Lower Mafic Unit between Hanen and Lavik. They also fold the mylonitic schistosity which is concordant to the contact. D_2 structures have not been observed deforming the contact, which may be because F_2 folds are usually isoclinal with limbs parallel to the S_1 foliation. The large fold pair between Leirvik and Lifjord believed to be of F_2 age (see above) does not appear to affect the

orientation of the contacts with units above or below (although exposure in this area is limited) and the structure is confined to the Middle Mafic Unit (figure 2.13). Deformation between D_1 and D_2 was probably progressive and continuous, and related to the initial emplacement of units into the present tectono-stratigraphic succession.

Where it was possible to identify and determine the vergence of F_2 folds, they are mainly consistent with a sense of asymmetry towards the south or east. Asymmetric delta-type tails on rotated feldspar porphyroclasts (Passchier & Simpson, 1986) give a sense of shear towards 310° but rotation of such porphyroclasts and development of tails with delta-type geometry probably occurred during D_3 and an exhaustive study was not within the scope of this project. Determination of C-axis orientations of quartz grains was carried out for some mylonitized rocks, but this type of analysis is hampered by unacceptably high concentrations of mica in most rock-types. More detailed analysis of rotated porphyroclasts and C-axis fabrics may reveal further information on the sense of emplacement of these rocks.

The emplacement of the Hyllestad schists onto the basement gneisses and amphibolites may have occurred during syn-D_2 thrusting. A subsequent phase of extensional tectonics in the Devonian (Hossack, 1984, Norton, 1986, 1987) during which the schists acted as an extremely incompetent zone may have been responsible for modifying the tectonostratigraphic succession of various horizons by reactivating early thrusts and resulting in a contraction of metamorphic zones. Many of the structures identified as of D_3 type, or later, have the correct vergence to support such a model.

2.6 Summarized structural and metamorphic chronology with criteria for correlating deformation phases across different units

In attempting to constrain the structural and metamorphic history of an area which has suffered polyphase deformation, it is necessary to construct a deformation chronology. In the present case, where individual units may not have shared the same deformation history, it is particularly important to correlate deformation episodes between different units. Deformation in the study area is heterogeneous and this results in rather crude comparisons being made between some units, particularly in respect of the earliest tectonic episodes.

The earliest phases of deformation are the least easy to correlate, having been overprinted and modified by subsequent "episodes", and the deformation chronology will be discussed taking the later episodes first (see also table 2.3).

D_5 deformation and metamorphism

The latest phase of deformation recognized, D_5, is most strongly expressed in the west of the field area, between Leirvik and Hyllestad. Structures of this age are rarely seen east of Leirvik, but are developed in all major units to the west of Leirvik. The typical structures associated with this event is an extensional crenulation cleavage, best seen in schistose horizons and therefore most widely developed in the Hyllestad Schists. This extensional crenulation cleavage has a consistent top-to-northwest vergence and a moderate to gentle westerly or northwesterly dip. Deformation took place under low-grade conditions (i.e. greenschist facies, or

lower). Chlorite and magnetite are developed along S_5 shear bands and, in schists of appropriate composition, replace staurolite, garnet, and chloritoid along cracks. Chlorite in such rocks is frequently decussate with respect to the D_5 extensional crenulation cleavage and is presumably post-kinematic.

D_4 deformation

D_5 structures have not been observed to overprint "D_4" structures. In this case the suggested order of deformation events is entirely arbitrary. "F_4" folds are only observed in parts of the Basement Gneisses to the east of Leirvik, and so cannot be correlated with deformation events in other units. They have upright axial planar with subhorizontal north-south axes. They deform the axes of folds recognized as of "D_3" age at Ytre Hellebö. Their regional significance beyond the field area cannot be assessed.

D_3 deformation and metamorphism

Structures assigned to the D_3 "event" are observed in all major units. In general, F_3 folds are open to tight, with moderately to gently plunging axes. In the east of the area, in the Basement Gneisses and Mafic Units, these mostly plunge to the east. In the west, in all major units (but particularly in the Hyllestad Schists), a westerly or northwesterly plunge is increasingly encountered (Appendix 1). The orientation of the compositional banding in all units appears to be controlled largely by F_3 folding. Plotted orientations of the compositional banding fall on the pi-girdle to F_3 fold axes. Crenluations are sometimes developed in F_3 hinges,

especially in schistose mafic or pelitic horizons, but a well-defined axial planar schistosity is not seen. Pre-existing garnet porphyroblasts in the Mafic Units and Basement Gneisses are sometimes broken down in F_3 crenulation hinges, with the formation of biotite, chlorite, magnetite, epidote, and plagioclase. Amphiboles often show zoning to more actinolitic compositions and this appears to be particularly developed in F_3 fold hinges, although it cannot be directly related to the D_3 event. Compositional markers are rotated by F_3 fold hinges, as are pre-F_3 schistosities defined by the orientation of biotite and hornblende in the Mafic Units and biotite, hornblende or white mica in the Basement Gneisses. Such schistosities must be, at latest, early D_3 in age, but in some cases can be shown to be parallel to the folded axial planes of F_2 isoclines in the Basement Gneisses and Mafic Units, and are therefore considered to be of D_2 age.

In the Hyllestad Schists, the axes of "F_3" folds have rather scattered orientations, the hinges of some folds also show slight curvature. They are correlated with F_3 folds in underlying units because they share the same broad geometrical features (axes plunging between W-E and NW-SE and axial planes which are subhorizontal or gently dipping into the NW or SE quadrants) as F_3 folds in the western parts of the Basement Gneisses and Mafic Units. In some horizons they can also be seen to fold an earlier biotite or amphibole foliation and, very rarely, to deform early isoclines.

F_3 folds can also be correlated between the Basement Gneisses and Mafic Units between Leirvik and Hanen where both units, and the contact between them, can be seen to be folded by F_3 hinges in the cliff section.

D_2 deformation and metamorphism

In both the Basement Gneisses and Mafic Units, F_3 folds are occasionally seen to deform earlier folds which are usually tight or isoclinal in profile (e.g. fig. 2.11, 2.18). These folds, designated as F_2, have a strong axial planar fabric - the "S_2" foliation defined by the orientation of rutile, biotite, white mica, and amphibole in the Mafic Units and Basement Gneisses. The S_2 schistosity is almost ubiquitous across the area. An absolute correlation between "D_2" structures in different units cannot readily be made, but all major units show isoclinal to very tight folds with an axial planar cleavage which are deformed by later "F_3" folds (although this situation is very rarely observed in the Hyllestad Schists).

In the Basement Gneisses and Mafic Units, garnet porphyroblasts sometimes show curved trails of inclusions, especially quartz, apatite, ilmenite, and rutile which appear to be continuous with the S_2 foliation and these garnets are interpreted as having grown syn-kinematically with D_2. In both the Basement Gneisses and Mafic Units such garnets form part of a garnet-amphibolite grade assemblage. In the Hyllestad Schists it is more difficult to relate the high-pressure garnet-kyanite-staurolite-chloritoid bearing assemblage to a particular deformation event. In rocks with the high-pressure assemblage, the pre-F_3 schistosity is strongly affected by the D_5 extensional crenulation cleavage. Garnet porphyroblasts have rutile and quartz defining curved or spiralled inclusion trails which may correspond to S_2 schistosities overgrown by synkinematic garnets in the other units, or may possibly be even earlier. In this case, the

correlation of the pre-"F_3" foliation in the Hyllestad Schists, designated as "S_2", with pre-F_3 foliations ("S_2") in the Basement Gneisses and Mafic Units is highly speculative.

In the Basement Gneisses, eclogite pods and the internal banding of eclogite assemblage minerals are deformed by isoclinal hinges and the high-pressure eclogite assemblage is interpreted as of early D_2 age at the latest, and possibly earlier.

D_1 deformation

The "D_1 event" can only be poorly characterized and it may really represent deformation related to the early stages of D_2 rather than a separate episode. F_1 folds have not been observed in any units and the only structural feature assigned to D_1 is the formation of an S_1 foliation which is deformed by F_2 isoclines. In the Basement Gneisses this "S_1" fabric is defined by the attentuation and flattening of compositional markers such as migmatitic leucosomes, pegmatite and aplite veins, and mafic dykes. The "S_1 foliation" is more properly a compositional banding which is best seen in granitic migmatites (e.g. fig. 2.6). Except in the hinges of F_2 isoclines this banding is parallel or subparallel to the S_2 schistosity.

In the Mafic Units compositional banding which outlines F_2 isoclines may be of "D_1" age, but no direct comparison with "S_1" in the Basement Gneisses can be made. No planar fabric analogous to S_1 has been observed in the Hyllestad Schists.

On structural criteria alone, all units appear to have suffered similar deformation during D_3 and D_5, although structures associated with the latter "event" are most

commonly seen in the west of the area. All units also appear to have suffered a pre-D_3 deformation ("D_2") with a well-developed schistosity, axial planar to isoclinal folds. Direct correlation, showing that this event occurred simultaneously in different units is not possible. However, it is noted that garnet amphibolite facies mineral assemblages believed to be of D_2 age occur in all units and that S_2 is parallel to the contacts between the major units, which suggests that they may have been emplaced together during a D_2 event which occurred under garnet-amphibolite conditions; or that they were emplaced together prior to D_2 and the contacts were reactivated during D_2.

In general, the earliest deformation "events" are more ductile in nature than the later ones. Since the later episodes are most intensely developed in the most of the area, this produces an apparent increase in the importance of brittle deformation in the west. The "episodic" scheme developed above, where separate "events" are discriminated by their structural geometry and overprinting relationships, tends to imply that deformation itself occurred in a series of temporally unconnected episodes. This of course may not have been the case. For instance, in the west of the area, the consistent top-to-west or top-to-northwest vergence of F_3 folds and of the D_5 extensional crenulation cleavage may both be related to a protracted episode of extension which also may have included the deposition of Devonian conglomerates in the Solund basin. However, no evidence has been found to show that D_3 folding was contemporaneous with D_5 at any one locality.

CHAPTER 3: METAMORPHISM OF THE BASEMENT GNEISSES

The metamorphic grade of the basement rocks along Sognefjord shows an overall increase from east to west: from upper greenschist facies overprinting epidote amphibolites near Leikanger, through epidote-amphibolites overprinting amphibolites between Balestrand and Lavik, to amphibolite facies overprinting eclogites between Lavik and Brensdal (figures 1.1, 1.13, 2.2). West of Leirvik the grade declines to upper greenschist or albite-epidote amphibolite overprinting amphibolite.

3.1 Metamorphic History of Basement Gneisses between Lavik and Balestrand

Between Balestrand and Avenfjord the metamorphic grade is mainly epidote-amphibolite facies, commonly showing evidence of earlier amphibolite facies metamorphism. The main rock-type is a grey migmatitic gneiss intruded by pegmatites, granitic rocks and basic to acidic dykes. There are at least two generations of basic dyke intrusion and several more of acidic dykes (figure 3.1). The basic dykes have been used to elucidate the metamorphic history and their mineral assemblages are shown in table 3.1. Hornblende-oligoclase assemblages typically show ilmenite rimmed by sphene, fine-grained amphibole surrounding larger amphibole and biotite grains, and optical zoning in epidote, plagioclase, and amphibole. These features suggest a reaction such as:

actinolite + Al-epidote + ilmenite + quartz

= hornblende + anorthite + sphene + H_2O (R3.1)

(Rambaldi, 1973). However, in many rocks there is "bleaching"

of amphiboles on rims and along cleavages to actinolite, and diffuse zoning of plagioclase to albite at grain edges, implying subsequent retrograde progress of the reaction. Sphene rimming ilmenite may also be produced by the reaction:

Al-amphibole + ilmenite + H_2O

= chlorite + sphene + quartz (R3.2)

which marks the boundary between the amphibolite and greenschist facies as defined by Liou et al, 1974. Chlorite replaces biotite, and feldspar shows saussuritisation or sericitisation. Garnets are occasionally present but, in general, there is no evidence of metamorphic grades higher than amphibolite having been attained. However, at Lia, to the west of Vadheim, an outcrop of garnet-amphibolite showing epidote-amphibolite overprint occurs which also shares many petrographic features with retrogressed eclogites seen within the study area (for example at Brensdal) and suggests that an early eclogite facies metamorphic event affected a wider area than previously recognised.

The age of the metamorphic events recorded in these dykes is uncertain. Intrusion of the dykes predates the formation of Caledonian shear zones and is assumed to be Precambrian but post-dates gneissification and subsequent migmatization of the Basement Gneisses. However, granitic bodies near Höyanger apparently associated with migmatization have been dated as Caledonian (Dietler et al, 1985). If the earlier, amphibolite grade, event is equivalent to that responsible for the formation of eclogite around Lavik, then both the early assemblages and the overprinting, assemblage are presumably Caledonian since eclogite facies metamorphism in the Western Gneiss Region is considered to be Caledonian, (Griffin et al,

1985). This interpretation is supported by the presence of garnet amphibolites showing indications of both an eclogite grade precursor and a retrograde history. However, migmatization of the Basement Gneisses also took place under amphibolite facies conditions. Milnes and Koestler (1985) report two phases of amphibolite facies metamorphism from basement windows in the Jotunheim - an early upper-amphibolite phase associated with widespread migmatization, and a later lower-amphibolite phase associated with post-orogenic shear zones.

3.2 Metamorphic History of the Basement Gneisses between Lavik and Soetevik

Within the main area of study the overprinting of early (Precambrian?) structures by Caledonian deformation obscures the early metamorphic history of the rocks. In some outcrops, pre-Caledonian migmatite textures are preserved with stromatic or cross-cutting leucosomes subparallel or oblique to the gneissose foliation (figure 3.2). Textural evidence for the former presence of melt, such as idiomorphic zoning of plagioclase or "primary replacement" textures (Ashworth and McLellan, 1985) are lacking. Myrmekite (sensu stricto) is frequently found, but probably represents subsolidus exsolution rather than eutectic crystallization, and although confined to migmatitic rocks from the Basement Gneisses, does not appear to be confined to leucosomes. Kyanite and sillimanite are not developed in muscovite + quartz-bearing horizons, hence conditions of migmatization are limited to the low temperature side of the reaction:

$$\text{muscovite} + \text{quartz} = \text{K-feldspar} + Al_2SiO_5 + H_2O \quad \text{(R3.3)}$$

but cannot be constrained further by melting reactions. Where undeformed mafic dykes are preserved cross-cutting the migmatitic foliation, the assemblages in these dykes are very similar to those observed in dykes between Höyanger and Balestrand (section 3.1 and table 3.1), indicating an earlier amphibolite or garnet-amphibolite grade event with retrograde zoning in amphiboles caused by overprinting at epidote-amphibolite grade. Some mafic bodies with dyke form show evidence of metamorphism under eclogite-facies conditions, these will be considered more fully in chapter 4.

3.2.1 Mineral assemblages in amphibole-bearing gneisses

Typical assemblages in amphibole-bearing migmatites are listed in table 3.2. Where garnet is developed it commonly forms coronas on amphibole and biotite grains (figure 3.3). Coronas on amphibole grains are apparently deformed in F_2 hinges (figure 3.4). However, the coronas are probably post-S_2, and merely follow the outline of previously deformed grains, since biotite grains aligned in the S_2 foliation also have coronas of garnet. In some cases garnet, amphibole, and biotite are intimately associated but coronas are not developed. Garnets are anhedral or skeletal forms with many quartz inclusions, or consist of small, partially-coalesced, euhedral grains. Untwinned albite forms a moat between garnet and surrounding grains, particularly amphibole or quartz, but not biotite. Retrogressive chlorite, which is deep green in thin-section, replaces biotite and amphibole along cleavage planes or forms more extensive patches. Metamict allanite, a common accessory is overgrown by zoned epidote (figure 3.5). The latter is a late decussate phase overgrowing the folded S_2

foliation in random orientations and replacing plagioclase. Sphene is the most common Ti-bearing accessory, whereas rutile is generally absent. Haematite and magnetite occur in the matrix of these rocks, the former sometimes overgrowing the rims of the latter. Magnetite is also found as inclusions throughout garnet porphyroblasts.

3.2.2 Mineral chemistry in amphibole-bearing gneisses

Garnets from coronas (see above) are CaFe-rich with significant amounts of Mn. Chemical profiles across individual crystals show a small gradual decrease in concentrations of Fe^{2+} from core to rims (figure 3.6) while Ca contents increase at first then decrease sharply at the rims where increases in Mn and Mg are observed.

In some rocks zoning profiles of garnets have irregular variations in chemistry, while retaining similar mean compositions to more smoothly zoned examples. Irregular profiles are found in garnets which appear to be formed by the coalescence of several smaller garnets nucleating in close proximity. In such cases, temperatures must have been low enough, or garnet growth fast enough (compared with diffusion rates), to inhibit complete homogenisation of growth zoning already present in individual grains. The ratio of Fe^{3+}/Fe^{2+} as calculated from charge balance criteria is not constant, varying from 0.05 to .22, but does not vary systematically with total iron content.

Skeletal garnets containing large quartz inclusions from a migmatized metasediment (sample 55G, figure 3.7) do not exhibit regular zoning profiles, but also show a tendency towards higher Mg at the rims.

Amphiboles from the Basement Gneisses are deep green in colour and those from orthogneisses are very similar in composition to those from sample 55G. The former may be classified as (potassian) magnesian hastingsitic hornblendes while the latter are ferro-tschermakitic hornblendes (Leake, 1978, and figure 3.8). Fe^{3+} has been calculated by the method of Laird and Albee (1981). Zoning profiles of amphiboles from orthogneisses show a decrease in Na, K, and Mg from core to rim (figure 3.6). In 55G amphiboles have much smaller grain-size and there is no significant difference in rim and core chemistry (table 3.3).

Biotite analyses are deficient in Al compared with the annite-phlogopite join (figure 3.9) possibly due to (Fe^{3+},Ti) = Al^{VI} substitution. Biotite grains have deep green to almost black absorption in thin-section. Manipulation of electron microprobe data by "MINFILE" (Afifi and Essene, 1988) suggests that $Fe_2O_3/(Fe_2O_3+FeO)$ is approximately 20-30 per cent in orthogneisses which is consistent with reported values for biotites coexisting with haematite (Guidotti, 1984), but may be as low as 2-5 per cent in sample 55G. However, the program does not give unique solutions to charge-balance calculations in micas owing to the possibility of cation deficiencies. Additional errors are introduced by the absence of H_2O from probe analyses and the possible loss of K and Na as volatiles in the electron beam. Ca and Na are present in minor amounts.

The plagioclase in this group of gneisses is albite-oligoclase (An_7-An_{11}) with zoning to higher values of An at the rims. Orthoclase is also present and is zoned to higher K at the rims.

3.2.3 Mineral assemblages in pelitic and semi-pelitic gneisses

Garnet-biotite pelitic and semi-pelitic gneisses occur throughout the area. They are generally amphibole-absent with less plagioclase and more biotite than the orthogneisses mentioned above. The most quartzose contain abundant coarse-grained white mica and, occasionally, staurolite.

In schists from the east and central parts of the area, biotite is usually oriented in an S_2 foliation. Garnets are inferred to have grown during the development of this fabric based on the observation of "syn-kinematic" inclusion trails (Spry, 1969) of opaque phases, sphene and quartz. The cores of such garnets are frequently S-shaped and poor in inclusions, whereas the rims are skeletal with abundant coarse quartz inclusions. F_3 crenulations of the mica foliations can be clearly seen to post-date garnet growth. Decussate chlorite, postdating D_3, fringes garnet and is intergrown with biotite along cleavage planes. At Kjörnes, in a schist from just below the contact with the overlying Lower Mafic Unit, garnets elongated parallel to the L_2 lineation lie within a well-defined S_2 mica foliation. In biotite-rich portions, garnets have retrogressive reaction coronas containing biotite, muscovite, albite, quartz, and magnetite, possibly due to a reaction such as:

almandine + K-feldspar + H_2O

= muscovite + biotite + quartz (R3.4)

At Rysjedalsvika biotite flakes lie in an S_2 foliation folded around mesoscopic F_3 hinges. In thin-section this S_2 foliation is seen to be overgrown obliquely by biotite lying in an overprinting extensional crenulation cleavage (see chapter 2). Chlorite replacing biotite is randomly oriented

and post-dates deformation. However, at Fort Nesje, 2km to the southwest, deformed chlorites lie within an extremely strong blastomylonitic foliation and show strained extinction. Here the chlorite is thought to have grown during shearing as extinction would be uniform if chlorite were mimetically replacing biotite.

Garnet-staurolite schists have been found at only two localities in the Basement Gneisses: to the northeast of Lavik and at Magnetjörndalen, to the north of Helleböstölane (L52A and 149B, respectively, figure 3.7). At both places, the staurolite-bearing rocks are confined to a thin unit of 2-3m thickness, comprising a coarse-grained quartz-muscovite schist, and may belong to a single continuous horizon. Garnets are up to 2mm across, elongate, rounded or embayed, and enwrapped by the muscovite foliation. Staurolites are found in small clusters, sometimes completely enclosed within large, decussate white micas. Some staurolite grains have euhedral outlines and overgrow the white mica foliation, others are cracked and have strained extinction. Both garnet and staurolite appear to have grown after formation of the S_2 foliation and prior to its crenulation during D_3. Muscovite has recrystallized in the hinges of F_3 crenulations and appears to replace biotite. The almost invariable association of staurolite and muscovite, the embayment of garnet (especially where in contact with mica), the lack of staurolite inclusions in garnet, and the replacement of biotite by muscovite suggest the retrograde reaction:

$$\text{garnet} + \text{biotite} + Al_2SiO_5 + H_2O = \text{staurolite} + \text{muscovite} + \text{quartz} \quad \text{(R3.5)}$$

However, no relict kyanite or sillimanite has been found.

Chlorite occurs as radiating rosettes overgrowing mica near to, and along cracks in, garnet and staurolite grains, and replacing mica along cleavage planes.

3.2.4 Mineral chemistry in pelitic and semi-pelitic gneiss

Garnets from pelitic and semi-pelitic schists generally have higher almandine, and lower grossular, spessartine and andradite components than those from amphibole-bearing gneisses (section 3.2.2 and figure 3.10). An exception is sample R1 from Rysjedalsvåg (figure 3.7) garnets from this sample resemble those from 55G in chemistry and in their skeletal form. In general, zoning profiles show core-to-rim increases in Mg and Fe with decreasing Ca and Mn (figure 3.6).

Exceptions to the typical zoning patterns are seen in sample FN1 from Nesje in which chemical profiles of three types may be recognised:

(i) "prograde" type

(ii) almost homogeneous (flat)

(iii) homogeneous core with a high-Mg, low-Ca plateau and flat, low-Mg, high-Ca rim compositions.

The patterns are interpreted as follows: (i) represents the prograde history of the rock.

(ii) represents a homogenization of (i) rather than later growth, as profiles are not absolutely flat and core compositions tend towards those in (i). There is a small retrograde rise in Mn at the rims which have a cloudier appearance than cores, suggesting that diffusion has occurred (Yardley, 1977).

(iii) core compositions are similar to rims of type (i) profiles and may represent nucleation of new garnets (this

type is found in much smaller garnets than the other two), later affected by retrogressive volume diffusion at the edges. However, there is a sharp break in the profile whereas a much smoother zoning curve would be expected if the zoning were produced by volume diffusion. The type (iii) profile may indicate rather that the chemical variation was produced during grain growth, possibly due to a sudden change in the availability of elements to the reaction site (by overgrowth of mica grain or a change in the mineral assemblage) or a rapid change in one or more of the intensive conditions.

Chemical zoning profiles across garnets from SF165, a schist collected from just beneath the contact with the Upper Mafic Unit at Råsholm, show twin peaks in Mn, corresponding to troughs in Ca, Mg and Fe^{2+}. Such a pattern is probably the result of growth at preferred sites during rotation of the grain. The distribution of cations suggests that the garnet was S-shaped during growth, with margins subparallel to S-shaped inclusion trails. This interpretation is supported by the outline of the contact between the inclusion-poor core and skeletal rims. The chemical zoning records a prograde history with no significant retrograde enrichment in Mn near rims (Yardley, 1977).

Elongate garnet grains in sample 446A have been mentioned above (section 3.2.3). Probe analyses were made along traverses parallel and perpendicular to the longest dimension of individual grains but the chemical profiles obtained were somewhat irregular. There is a slight increase in Fe and Mg and a decrease in Ca from "core" to "rim", however, these trends are sharply reversed in the vicinity of cracks in the grain. The variation in composition is not large and is

considered to be due to retrograde re-equilibration of garnet rims and matrix minerals, possibly imposed on an originally zoned garnet.

Biotites in pelitic and semi-pelitic rocks differ from those in amphibole-bearing gneisses in having excess Al compared with the phlogopite-annite join (figure 3.9) and are brown in thin-section with only a faint greenish tinge, suggesting a much lower Fe^{3+} content. Calculations using "MINFILE" (Afifi and Essene, 1988) suggest that Fe2O3/(Fe2O3+FeO) is generally about 10 to 20 per cent, but is as high as 50 per cent in staurolite-schists. Mg/(Mg+Fe) is approximately 42 to 46 per cent in most samples but is as low as 33 per cent in sample R1.

Muscovite has a small to moderate celadonite content and about 2 to 9 per cent paragonite, rising to 20 per cent in staurolite-schists. The deficiency of alkali cations in metamorphic micas has been related to grade recently by Wang and Banno (1987). This relation is not observed in the basement gneisses although Na in muscovite does appear to increase with grade (figure 3.11). Bright red micas occur in quartzitic schists between Alværen and Råsholm. They have been described in detail by Askvik (1972) who identified them as "manganiferous ferrian 2M muscovites" the red colour probably being due to Fe^{3+} together with Mn^{3+} and Ti^{3+}.

Plagioclase contents of these rocks are not large and grains are small or develop patchy subgrains. Compositions are mainly albite to oligoclase but anorthite contents are occasionally as high as An_{35}. Where grains are coarse enough for zoning to be detected, it is towards more calcic compositions on the rim. K-feldspar is also present and

frequently intergrown with biotite.

Large allanite grains are rimmed by epidote which shows marked zoning in all elements particularly Ca (increasing from core to rim) and Fe (decreasing, see figure 3.6), indicating retrogressive adjustment (Miyashiro and Seki, 1958)

Staurolite, if present, has ZnO up to 3 weight per cent. CoO and NiO combined are less than 0.1 weight per cent. Some zoning of Mg occurs with concentrations higher in the core of grains than at the rims.

3.3 Geothermobarometry of the Basement Gneisses

3.3.1 Amphibole-bearing gneisses

Three samples of garnet-amphibole gneiss from the Basement Gneisses were analysed by electron microprobe. Mineral assemblages suggest amphibolite facies overprinted by epidote-amphibolite to upper greenschist facies metamorphism.

Appropriate thermobarometric techniques are limited by the absence of such phases as muscovite and Al_2SiO_5 polymorphs and are restricted to Fe-Mg exchange thermometry between such phases as garnet, amphibole, and biotite. The application of such thermometers is prone to inaccuracy owing to the relatively large proportion of ferric over ferrous iron in most mafic phases. Charge balance considerations may be used to estimate the amount of ferric iron from electron microprobe analyses of garnet and, with less certainty, amphibole. According to Percival, 1983, the assumption that all Fe in biotite is divalent is likely to have only a small effect on garnet-biotite thermometry providing the same assumption is made for garnet. Estimates of Fe^{3+} in garnet and biotite for these rocks would lead to a negligible difference in

calculated temperature, amounting to only a few degrees.

The partitioning of iron and magnesium between biotite and garnet has been calibrated experimentally by Ferry and Spear (1978), and by comparing compositions of phases in natural rock specimens with independently determined temperature estimates by Thompson (1975) and Goldman and Albee (1977). Such calibrations assume ideal mixing of Fe and Mg in biotite and garnet solid solutions. The importance of nonideality in garnet solid solutions has been discussed by Ganguly and Kennedy (1974) and subsequent authors. Calibrations of the thermometer by Pigage and Greenwood (1982) and Perchuk (1985) make corrections for garnet components other than Fe and Mg, while Ganguly and Saxena (1984) and Hodges and Spear (1982) have presented solution models for garnet solid solutions which may be applied to the calibration of Ferry and Spear (op. cit.).

The accuracy of the thermometer may further be affected by nonideality in phlogopite-annite solutions or by substitutions such as $(Mg,Fe^{2+})Si = Al^{VI}Al^{IV}$ (tschermaks), $TiAl_2 = Si_2(Fe^{2+},Mg)$ (Ti-tschermaks, Dymek, 1983), $(Fe^{3+},Ti) = Al$, or $Mn = (Fe^{2+},Mg)$ in natural biotites.

In the garnet-amphibole gneisses of the Basement Gneisses the considerations outlined above have important consequences in the estimation of conditions of metamorphism. Garnets have "prograde" chemical profiles with little evidence of retrogressive Fe-Mg exchange at the rims, but have large spessartine and grossular components. Biotites have low concentrations of Ti and Al^{VI}, but are rather rich in Mn and ferric iron. Temperature estimates have been calculated using analyses from the "most prograde" compositions of garnet at

rims, or average compositions from flat profiles, and averaged biotite analyses, avoiding grains in contact with garnet where retrogressive Fe-Mg exchange would be greatest. In the amphibole-bearing gneisses there is little difference between the garnet-biotite temperatures determined from garnets with prograde profiles and those determined from garnets with flat profiles. In the semi-pelitic and pelitic schists (section 3.2.4), however, garnets with flat profiles sometimes show retrograde marginal zoning (figure 3.6, samples L52 and FN1). Such samples tend to give higher garnet-biotite temperatures than samples with only prograde-zoned garnets. This is consistent with the interpretation that they have suffered homogenization at high temperatures.

Graham and Powell (1984) have calibrated an Fe-Mg exchange thermometer for garnet and amphibole by empirical methods. Amphibole is assumed to contain only divalent iron, an assumption which is unlikely to be justified; recalculation by the method of Laird and Albee (1981) suggests that there is a significant ferric component in amphiboles from the Basement Gneisses. The spessartine content of garnet is high compared with compositions used in the calibration and may render the thermometer inaccurate when applied to these rocks. The results are higher than those obtained from garnet-biotite thermometry even if Fe^{3+} is estimated for amphiboles and deducted from the total iron when calculating the distribution coefficient. Results closer to garnet-biotite temperatures are obtained by the use of the calibration of Perchuk (1985); this is probably fortuitous as it does not take account of Ca or Mn components in garnet and the compositions of both phases differ widely from those used in the calibration.

The two feldspar thermometer of Powell and Powell (1977) has been criticised by Brown and Parsons (1981) but has been applied to some samples. Textural evidence suggests exsolution of feldspar has occurred during cooling and temperatures recorded may be expected to be post-peak.

3.3.2 Pelitic and semi-pelitic schists

The amphibole-absent schists analysed are more pelitic than the amphibole-bearing gneisses and compositions of garnet and biotite are closer to those recommended in most calibrations, with lower Fe^{3+} in garnets and biotite. The presence of white mica allows the application of garnet-muscovite Fe-Mg thermometers (e.g. Green and Hellman, 1982, Hynes and Forest, 1988) and barometers based on the reaction:

pyrope + grossular + muscovite

= 3anorthite + phlogopite (R3.6)

(Ghent and Stout, 1981, Hodges and Crowley, 1985).

In addition, the garnet-ilmenite Fe-Mn exchange thermometer of Pownceby et al, 1987 has been applied to appropriate assemblages where textural relations suggest equilibrium was achieved, but the calibration is extremely sensitive to small changes in the Mn content of ilmenite and matrix ilmenite analysed in this study were found to over-sequester Mn giving absurd results. Ilmenite inclusions in garnet are common but are frequently too small to analyse by electron microprobe.

The garnet-staurolite Fe-Mg exchange thermometer formulated by Perchuk (1977) may be applied to a limited number of samples. Temperatures obtained are lower than those given by garnet-biotite by about 150 °C. Garnet-biotite

temperatures are themselves high, falling outside the range of stability of Fe-staurolite (Richardson, 1968) and it is probable that garnet and biotite are not in equilibrium. Temperatures obtained by garnet-staurolite thermometry are also suspect as staurolite contains up to 3 wt% Zn (with minor Co and Ni) substituting for Fe. Baker (1985) has determined $K_{Fe/Mg}$ for coexisting staurolite and biotite from the Dalradian and his results are compared with average values for samples from the Basement Gneisses (figure 3.12). The main problem in applying geothermometers to the staurolite schists is that garnets show evidence of disequilibrium with a "retrograde" variation in chemistry at their rims, imposed on an overall prograde profile. The reaction responsible for staurolite formation in these schists is not known with certainty. The main features of the rock may be modelled by the petrogenetic grid of Harte (1975). Textural evidence (section 3.2.3) suggests the retrograde reaction:

garnet + biotite + Al_2SiO_5 + H_2O

=> staurolite + muscovite + quartz (R3.5)

The staurolite formed would be in equilibrium with high-Mg garnet compositions. However, analysed staurolite compositions fall outside the garnet-Al_2SiO_5 tie-line and may have been modified by the divariant reaction:

muscovite + H_2O + garnet

<= staurolite + biotite + quartz (R3.7)

Zoning to higher Fe/Mg ratios at the rims of staurolite and garnet (where it is superimposed on prograde zoning) could correspond to such a reaction. As noted above, the coexistence of garnet and staurolite probably represents a relict assemblage. The fall in X_{Mg} from cores to rims of

staurolite might correspond to a similar decline in X_{Mg} at the rims of garnets, but grains of staurolite are small, zoning is slight, and core compositions may not be those which co-existed with the highest Mg composition of garnet. Tie-lines between coexisting compositions of garnet and staurolite can not be drawn for these rocks.

The initial staurolite-out reaction noted above (3.5) is nearly isothermal in Harte's grid at approximately 650 °C, a temperature more consistent with those calculated for other assemblages in the Basement Gneisses than have been obtained by exchange thermometry with these schists. However, relict Al_2SiO_5 polymorphs are not observed and, if originally present, would require temperatures higher than 650 °C during the prograde history of the rock.

3.3.3 Thermobarometric results

Results obtained from the application of thermobarometric techniques outlined above are shown in figure 3.13 and table 3.4.

The limited amount of geobarometric evidence suggests that the Basement Gneisses as a whole have been subjected to pressures between about 6.7 and 10.8kbar (a higher value of 13.6kbar is obtained from sample L52A in which there is evidence of disequilibrium between garnet and mica). These are likely to be maximum pressures, since the determined anorthite content of plagioclase may be lower than that corresponding to peak metamorphic conditions due to retrograde re-equilibration and exsolution of feldspars. The highest pressure values are confined to the area west of Rysjedalsvika but the number of samples suitable for analysis was

unfortunately limited making general conclusions regarding variations in pressure across the area of limited worth. Barometers such as "STAGS","GULPS","GAILS", and "GRASP" (Essene and Bohlen, 1985) may be applicable to some of the Basement Gneisses but samples with appropriate assemblages have not yet been found.

Temperatures obtained from application of the garnet-biotite Fe-Mg exchange formulation of Ferry and Spear (1978) using the garnet solution model of Ganguly and Saxena (1984) range from about 438 to 647 °C (excluding results from staurolite schists, as discussed above) with limited evidence of an increase from east to west across the area. The garnet-muscovite thermometer of Hynes and Forest (1988) gives lower temperatures, by about 100 to 200 °C, than those given by garnet-biotite thermometers.

P-T paths for some rocks have been estimated from zoned garnets by the method of Spear and Selverstone (1983). These suggest that garnet growth occurred during a prograde, decompression path; but the absolute difference in core and rim compositions is slight and P and T calculated are small: about 1.5kbar and 20 °C, which is within the errors for estimated peak conditions.

Garnet-amphibole thermometry gives higher temperatures than those obtained by the garnet-biotite formulation of Ganguly and Saxena (op. cit.), although textural evidence suggests that equilibrium between garnet, amphibole and biotite has been attained, at least locally, and it is probable that the difference between the calculated values for the two thermometers (and between values calculated for garnet-biotite thermometers in amphibole-bearing and

amphibole-free rocks) is due to errors in the original formulations and, more significantly, to the application of the thermometers to phases with compositions differing widely from those used in the original calibration.

In conclusion, most rocks indicate temperatures of between about 425 and 525 °C, over a rather wide pressure range of about 4 to 9 kbar. These may represent a real metamorphic "event" corresponding roughly to D_2, with different rocks recording "closure" of exchange reactions at different stages of the cooling history. The much higher temperatures calculated for staurolite-bearing assemblages are almost certainly spurious, and have much larger errors, due to disequilibrium between peak assemblage phases. Temperatures calculated for sample FN1, from Nesje, are also high. In this rock, chlorite and biotite are intergrown, the development of the former phase being pre- or syn-D_5. Homogenization of zoning profiles of garnets suggest that high temperatures have been attained at some stage of the rock's history, but this is unlikely to be associated with the late growth of chlorite and biotite. The recent petrogenetic grid of Spear and Cheney implies a small temperature range, close to 550 °C for the equilibrium coexistence of chlorite with garnet containing such low spessartine components as those measured for FN1.

CHAPTER 4: ECLOGITE FACIES METAMORPHISM IN THE BASEMENT GNEISSES

Within the study area, rocks bearing mineral assemblages characteristic of the eclogite facies are restricted to the Basement Gneisses. They form lensoid or sheet-like mafic bodies which are usually enclosed by white-weathering quartzose schists (figures 4.1, 4.2). Isoclinal hinges with an axial planar foliation (probably S_2) are very rare but may be observed folding a weak compositional banding. The eclogites are thoroughly overprinted by amphibolite and epidote-amphibolite facies assemblages and the primary eclogitic mineralogy is only rarely preserved. Rocks closely associated with eclogites in the field include orthopyroxene-bearing gneisses and tremolitic schists.

4.1 Location of eclogites

Bodies of mafic rock identified as eclogites or having mineral assemblages and textures suggesting an eclogite precursor have been found at Helleböstölane, Brensdal, Ytre Hellebö, Alværen, and near Brekke (figure 1.1).

Rocks with similar field relations were found at Indredalen, but are too thoroughly amphibolitized to be certain that an eclogite assemblage precursor has been replaced. A garnet-amphibolite from Lia, to the west of Vadheim shares many textural and mineralogical similarities with retrogressed eclogites from the study area. In addition, a "lump of eclogite" is reported by Strand (1960, after "Reusch and others") probably from a locality in the area between Nesje and Rysjedalsvåg. No eclogites were found here,

but part of the area is occupied by a military installation to which access was not granted.

4.2 Field relations of eclogite bodies

Field relations between eclogite bodies and the surrounding Basement Gneisses are best exposed on the shore at Ytre Hellebö, where rocks of eclogitic character crop out over a 600m section. The eclogites form dark green to grey elongate or lensoid masses from approximately 0.5 to 10m across and 5 to 20m in length. They exhibit a variably-developed S_2 schistosity, best seen in the most amphibolitized examples, which is continuous with the biotite S_2 foliation in the Basement Gneisses and subparallel or oblique to the contact. Pegmatitic veins and stringers containing pale-blue rutilated quartz are developed at the contacts and may either extend from the basement migmatites into the mafic bodies, or enclose small pods of mafic material giving the margin a blebby appearance (figure 4.2). The migmatitic foliation in the gneisses is bent into parallelism with the contact, and there are southwesterly vergent folds at the sheared margin.

The sheet-like appearance of some of the eclogitic bodies (figures 4.3 and 4.4) suggests that they were originally intruded as doleritic dykes and subsequently metamorphosed at eclogite facies conditions. The quartz-albite pegmatites which fringe and intrude the mafic bodies may result from partial melting of the country rock at the time of intrusion, and back-veining of such melts into the doleritic magma. Griffin and Carswell (1985) describe such relations in eclogites from Midöy where the contact is well-preserved. Alternatively, since jadeite and other high-pressure minerals

are not preserved in these pegmatites, they may result from quartz-producing reactions in the mafic pods during retrogression.

4.3 Petrography and mineral chemistry of the eclogites

4.3.1 Least retrogressed eclogites (containing clinopyroxene)

The largest occurrence of eclogitic rocks is at Helleböstölane, where pod-shaped bodies up to 5 to 10m in length of variably amphibolitized eclogites and tremolitic schists occupy a lensoid area of approximately 300 by 600m. The pods are enclosed by a white-weathering gneiss comprising coarse-grained quartz with greenish biotite, tschermakitic amphiboles, epidote and white mica. This gneiss also contains small enclaves, up to 5cm in length of mafic material, mainly biotite, amphibole, albite, and epidote with ilmenite and sphene. They are similar in appearance to the larger pods of eclogite (although garnet has usually been completely replaced) and appear to have been separated from them by invading quartz veins and stringers. There are frequently selvages of coarsely crystalline quartz on the margins of the pods and forming veins which cut across them.

Eclogites found at Helleböstölane have, in general, suffered the least amphibolitization and, locally, primary eclogite assemblages are preserved with very little evidence of alteration, particularly where the S_2 cleavage is poorly developed and spaced at intervals of 5 to 10cm. Symplectites of pyroxene + albite and amphibole + albite after omphacite, and of biotite + albite, possibly after phengite, are best developed in the vicinity of cleavage planes (figure 4.5). Conversely, a few millimetres from such fractures, contacts

between garnet and pyroxene are sharp, with little sign of reaction. The least altered assemblage is omphacite + garnet + rutile + amphibole + apatite + quartz (+ white mica?) (table 4.1).

The compositions of garnets all fall within the field defined by Coleman et al (1965) for garnets of "type C" eclogites, that is eclogites associated with glaucophane schists in high-pressure, low-temperature terrains (figure 4.6). In contrast, the field relations and mineral assemblages (kyanite and glaucophane are absent) are typical of type B, in which eclogites showing retrograde metamorphism occur as bands or lenses within amphibolite grade migmatitic gneisses.

Chemical profiles across garnets do not show pronounced zoning but have slightly enhanced Mg contents at the rims (figure 4.7), mainly compensated by lower Ca. Fe^{2+} and Mn profiles are scattered with a tendency to higher Mn at rims for some profiles. A decrease in Ti concentrations from core to rim is also detected.

Clinopyroxenes from Helleböstölane are omphacites and also have compositions typical of type C eclogites (figure 4.8). The Fe-Mg distribution coefficient for cation exchange between omphacites and garnets is shown in figures 4.9. Recasting of probe results indicates that Fe^{3+} is a significant component comprising more than half the total iron. Chemical profiles do not show pronounced zoning but a minor decrease in Mg from core to rim (with increasing Fe^{TOT} and Ca) is present in some traverses (figure 4.7). Large grains of clinopyroxene often include smaller grains of the garnet, and vice versa. Small amphibole inclusions have also

been observed in garnet. Where the inclusion is entirely enclosed by the host (at least, no communication between inclusion and matrix can be seen within the plane of the thin-section) no reaction is observed at the contact. The compositions of garnet, clinopyroxene, and amphibole believed to be of primary origin are shown in figure 4.10. The plot also shows compositions of the same three phases in rocks from Ytre Hellebö which have suffered secondary alteration, and which are discussed in more detail below.

Amphiboles are barroisitic but, as recalculated (by Laird and Albee, 1981) fall on the boundary between calcic and sodic-calcic amphiboles. Recalculated analyses (figure 4.12) scatter across the compositional fields of barroisite, ferroan pargasite, magnesian hastingsite, and magnesio-kataphorite and taramite (Leake, 1978). Amphiboles included in garnets fall within the latter group and do not appear to differ significantly in composition from matrix amphiboles.

Muscovite with a high paragonite content is present, but is confined to shear zones where alteration is greatest. It is sometimes associated with symplectite of biotite and albite which may represent the products of phengite breakdown.

Zoisite, although common in amphibolitized eclogites in the area is not found in the least altered samples, and is presumably related to amphibolitization and subsequent retrogression.

As mentioned above, quartz and quartzo-feldspathic veins associated with eclogite pods may result from anatectic country rock melts. The examples studied have all been thoroughly amphibolitized and do not show the kyanite + clinopyroxene assemblages discussed in Griffin and Carswell

(1985). The strong planar fabric observed is S_2 in age and passes across margins of eclogite pods. Eclogite facies metamorphism may be assumed to pre-date D_2 deformation.

The first sign of amphibolitization seen is the formation of symplectitic rims on pyroxene grains. These are too fine for the composition of the constituent phases accurately to be measured, but analyses of the symplectite under a rastering beam are similar to omphacite analyses suggesting local breakdown of omphacite to albite and diopside (as noted by Hezner, 1903, Eskola, 1921, Wikström, 1970) either by oxidation:

ferrous omphacite + O_2 = ferric augite + plagioclase

or by diffusion of quartz into the reaction site from the matrix:

$$NaAlSi_2O_6 + SiO_2 = NaAlSi_3O_8$$

(Mysen and Griffin, 1973). The latter mechanism is probably involved in, if not entirely responsible for, jadeite breakdown since averaged symplectite analyses have rather high SiO_2 contents when recast as pyroxenes. However, although symplectites are frequently developed at quartz-omphacite grain contacts, this is not invariably the case. Chemical profiles across pyroxene grains do not show a significant decrease in Na as the symplectitic rim is approached, so the breakdown may occur virtually in situ. Other early signs of amphibolitization include the replacement of rutile by ilmenite, and graphic symplectites of biotite and albite.

At Ytre Hellebö, more complete amphibolitization is seen. At one roadside outcrop relict clinopyroxene is found. The compositions of such clinopyroxenes are more scattered than in less altered eclogites from Helleböstölane, are less sodic,

and plot near the limits of the omphacite field (fig 4.8a). This is probably due to the increased breakdown of the jadeite component to albite as there is a correspondingly greater modal volume of plagioclase in the rock. The trend away from jadeite is seen in figure 4.8b, with two distinct groups of pyroxene compositions belonging to the Helleböstölane and Ytre Hellebö occurrences.

In these more altered eclogites amphibole usually forms a dark green reaction rim where clinopyroxenes are in contact with garnets (figure 4.11, 4.13). The compositions of such amphiboles overlap those in less altered eclogites, but have a wider compositional range and show greater solid solution towards tremolite and away from tschermakite (figure 4.12). Although amphiboles are apparently the products of <u>in situ</u> hydration of pyroxenes, they are also seen to replace symplectitic pyroxene that has already "exsolved" albite. Amphiboles in the more retrogressed eclogites are lower in Na, in both the M4 and A sites, than those in rocks from Helleböstölane. There is also a tendency towards higher Si values, resulting in lower calculated Al^{IV} and higher Al^{VI}. The relative deficiency in Na and Fe^{3+} is balanced by increases in divalent cations, particularly Ca and Mg.

Garnets preserve marked "prograde" zoning in Mg (figure 4.7), although cracked and slightly resorbed at the margins. Core values of Fe/Mg are similar to garnet cores from "fresh" eclogites, but rim values are somewhat lower (figures 4.7, 4.10). The close association of garnet and omphacitic clinopyroxene, separated by reaction coronas of amphibole, implies that they are true relicts of an eclogite facies metamorphic event. The difference in garnet composition at

garnet edges may be due to different bulk rock Fe/Mg ratios. The "true" garnet and clinopyroxene rim compositions representing equilibrium under eclogite facies conditions are not preserved due to the formation of amphibole coronas. It is therefore difficult to be certain of the peak Fe/Mg garnet-clinopyroxene K_D but data presented in figure 4.9 suggests that (in SF68, at least) values may have been similar to those in samples 166A1 and 166A2. Prograde zoning of garnets cannot be used to constrain the early P-T evolution of the eclogites (cf Sunnmöre eclogites, Krogh, 1982) accurately because of the scarcity of suitable inclusions. Alternatively, the difference may be due to volume diffusion of Fe and Mg between garnet and clinopyroxene at grain boundaries during the formation of the hornblende coronas (figure 4.13). Volume diffusion in garnets is unlikely to have been an important process at the temperatures calculated for equilibration of eclogites. Zoning profiles in eclogite garnets, even where they have been partially resorbed during amphibolitization, may well represent the prograde evolution of the rocks prior to the peak of metamorphism under eclogite facies conditions.

As with less altered eclogites, all garnet compositions fall within group C of Coleman et al (1965), but there is a stronger trend towards group B in rim analyses (fig 4.6)

4.3.2 Amphibolitized eclogites with no relict clinopyroxene

Eclogites in a more advanced state of amphibolitization (eg sample SF20) are characterized by large, cracked, and partly resorbed garnets in a matrix consisting of a fine symplectite of hornblende and albite (figure 4.14). Despite evidence of resorption in some garnets, they nonetheless

retain prograde profiles (figure 4.7). Large amphibole grains, often rimmed by albite and with "bleached" centres, occur in the matrix and form rims on garnets. Tiny grains of magnetite form a collar at about 0.1mm distance from garnet margins. Rutile is abundant as inclusions in garnet or in the matrix and coarse apatite is present up to several modal per cent (table 4.1).

With progressive amphibolitization, garnets become more resorbed, there is a coarsening of the amphibole-albite symplectite, and plagioclase in such symplectites is slightly more calcic. Rutile becomes less abundant and Ti is probably taken up by the biotite which results from the breakdown of amphibole and garnet. In general garnets show a shift towards lower pyrope contents, compared to garnets in the well-preserved eclogites. This is true both for core and rim compositions (figure 4.6). Together with the difference in the direction of chemical trends on the grossular-almandine-pyrope plot between garnets in fresh and amphibolitized eclogites, this suggests that garnet zoning profiles may have been partially modified by volume diffusion during the later event, or that nucleation of new garnet with complete breakdown of the old accompanied amphibolitization, or that the bulk rock chemistry of these eclogites differs from that of sample 166A.

At Brensdal no relict clinopyroxenes were found in amphibolitized eclogites (table 4.1) and the lowest grade of retrogressive overprint is developed. This locality is at approximately the same structural level as Helleböstölane, if the effects of F_3 folding are taken into account. Garnets are rimmed, or completely replaced, by a radiating mass of epidote

and biotite (figure 4.15). An atoll of magnetite grains close to the outer margin of the reaction area marks the original extent of the garnet grain. Beyond the magnetite atoll a foliation defined by elongate biotite and amphibole grains wraps around the reaction corona. The biotite and amphibole occur as symplectitic intergrowths with sodic plagioclase. Relict rutile is present but in diminished amounts compared with fresh eclogites, and is overgrown by sphene. It is therefore deduced that garnet breakdown ensued after alteration of sodic pyroxene to amphibole-plagioclase symplectites.

Compositional trends are not well-defined in amphiboles from this group of rocks. In general, where there is a tendency for the scattered compositional data to define a weak trend, it seems to be related to the strength of the overprinting epidote-amphibolitization, although this factor is not easy to quantify. Thus, rocks such as SF24 and SF20 (in which amphibole-albite symplectites show extensive alteration, with the development of ilmenite), have lower Ca/Na^{M4} ratios than rocks such as SF138, in which amphibole does not show retrograde zoning and coarse symplectite textures are preserved with little sign of alteration. Other trends possibly associated with low-amphibolite grade overprint are a decline in total Si and in calculated Fe^{3+}/Fe^{2+}. Such trends are opposed to the changes in amphibole chemistry noted in the formation of secondary amphibole coronas, which is attributed to the crossing of compositional isopleths with positive dP/dT during decompression. Thus the (admittedly weak) reverse trends observed in more thoroughly amphibolitized rocks may represent the recrossing of the same

isopleths, at lower pressures, during cooling.

In addition to the occurrences at Helleböstölane, Ytre Hellebö, and Brensdal, where amphibolites of "eclogitic" type are associated with rocks containing relict omphacite, rocks lacking clinopyroxene have been identified as overprinted eclogites from field relations and petrographic features. These rocks, which contain up to 50% modal garnet and abundant rutile, crop out at Indredalen, Alværen, Brekke, and Lia, near Vadheim. They share many features shown by other amphibolitized eclogites in the field area, including the presence of coarse symplectites of amphibole and albite (after omphacite?), symplectites of biotite and albite (after phengite?), rutile with ilmenite developed on the rims, and atolls of iron ore on resorbed garnet.

The rocks from Lia differ from other examples in having large, twinned feldspar grains and small, recrystallized garnets. The locality falls at the eastern limit of recorded eclogite occurrences in the Sunnfjord area (Sigmond et al, 1984) and the amphibolitization features may be the result of decompression within the garnet-amphibolite facies, without necessarily indicating prior eclogite facies conditions.

4.3.3 Orthopyroxene-plagioclase gneisses at Ytre Hellebö

At Ytre Hellebö, eclogitic rocks are associated with hypersthene-plagioclase gneisses on the fjord shore section. Both rock-types occur as pods or lenses up to 10m across, with sheared margins, and with selvages of pale blue, rutilated quartz. The primary assemblage consists of hypersthene, up to 1cm or more across, and coarse-grained oligoclase with ilmenite, salitic clinopyroxene, and minor apatite (table

4.1).

Analysed plagioclase compositions average $An_{22} \pm An_{11}$, but original compositions in equilibrium with orthopyroxene may have been more calcic. Clinopyroxene is usually completely rimmed by orthopyroxene and is only present in minor amounts except where orthopyroxene is locally absent. In these parts of the rock clinopyroxene is the major mafic mineral and is much coarser grained. Biotite occurs both as coarse grains lying in an early foliation and as fine grains, randomly oriented in reaction coronas. The early gabbro assemblage may result from the assimilation of Al-rich crustal rocks by a basic magma (similar in composition to the eclogite precursor), and the textural relations between clinopyroxene and orthopyroxene may reflect an orthopyroxene-producing reaction such as:

$$Ca(Mg,Fe)Si_2O_6 + Al_2SiO_5 = (Mg,Fe)SiO_3 + CaAl_2Si_2O_8$$

salite — hypersthene — anorthite

However, no relict kyanite is preserved. Alternatively the texture might represent the reaction of diopside with garnet and quartz to form hypersthene and anorthite, under conditions of falling pressure.

The anorthite content of plagioclase as analysed is rather low but feldspar has clearly been involved in reactions with biotite and pyroxene, and is partially saussuritised. Garnet growth occurs at the expense of biotite, ilmenite, orthopyroxene, and clinopyroxene where they are in contact with plagioclase. The following (unbalanced) reactions appear to be recorded:

(1) plagioclase + orthopyroxene + H_2O = garnet + amphibole

(2) ilmenite + plagioclase + $biotite_1$ (+ quartz + O_2)
= garnet + $biotite_2$ (+ K-feldspar + H_2O)

(3) ilmenite + plagioclase + quartz + H_2O
= rutile + garnet + amphibole

(4) biotite + plagioclase (+ilmenite)
= garnet + amphibole + H_2O (+ K-feldspar)

(5) clinopyroxene + plagioclase + H_2O
= garnet + biotite (+ quartz)

(6) orthopyroxene + H_2O + quartz = cummingtonite

(7) clinopyroxene + ilmenite + plagioclase = garnet + quartz

(8) orthopyroxene + plagioclase = garnet + quartz

(9) biotite + ilmenite + plagioclase (+ quartz + O_2?)
= garnet (+ K-feldspar + H_2O)

Phases in parentheses are not observed but are likely to participate in reactions. Potassium feldspar is not observed in the rock, but if produced by reactions may be taken up in plagioclase, analyses of which have K-feldspar contents up to 10%, and is possibly present as cryptoperthite. In addition, pyroxenes have exsolved a large quantity of magnetite.

The rock shows no sign of eclogite facies metamorphism, the reactions above are more characteristic of the transition from the granulite to amphibolite facies and appear to be related to near-isobaric cooling, subsequent to some decompression, and are similar to those seen in granulites from Lofoten-Vesteraalen (Griffin and Heier, 1969). The hypersthene-plagioclase assemblage pre-dates the S_2 foliation, but the age of decompression and cooling "events" and their relation to the P-T path experienced by the eclogites are otherwise difficult to constrain from petrographic evidence.

Other rocks in the area pass from eclogite to amphibolite facies assemblages without recording any evidence of an excursion through the granulite field. However, the orthopyroxene gneisses and amphibolitized eclogites are closely associated in a small area of outcrop with no evidence of major tectonic breaks between bodies of each rock-type. Coarse plagioclase textures in the former rock-type suggest an igneous or prolonged high-grade metamorphic origin, whereas symplectitic plagioclase in the latter type are inferred to represent incomplete textural equilibration due to relatively rapid uplift following eclogite metamorphism. It is therefore suggested that the orthopyroxene gneisses are relicts of a pre-Caledonian decompression event. The corona textures are interpreted as a post-eclogite feature representing a segment of the cooling path.

4.4 Thermobarometry of the eclogites and related rock-types

Peak metamorphic temperatures for eclogite formation may be estimated by use of the garnet-clinopyroxene Fe-Mg exchange thermometer applied to the best-preserved eclogite samples. The calibration of Ellis and Green (1979) has been used, following the procedure of Griffin et al, 1985, in order that the results for the Helleböstölane locality may be compared directly with their results for the rest of the Western Gneiss Region. The assumptions made by Griffin et al (op. cit.) are as follows:

(i) that the eclogite facies metamorphism took place at 15 kbar

(ii) Fe^{+3} in clinopyroxenes may be calculated by the method of Neumann, 1976

(iii) all iron in garnet is assumed to be divalent, even

where the stoichiometry implies otherwise

(iv) the garnet composition with the lowest Fe:Mg ratio is taken to be in equilibrium with clinopyroxene.

(v) compositions used in thermometric calculations were measured at the rims of grains in contact and where no reaction textures (e.g. symplectitization) could be observed.

As in Griffin et al (op. cit.) the errors introduced by these assumptions lead to a bias towards lower temperatures due to overestimation of Fe^{+3} in clinopyroxene. If Fe^{+3} is calculated for garnet analyses, temperatures are only increased by about 5 °C.

The temperatures obtained from these calculations are consistent with the 600 °C isotherm determined by Griffin et al, 1985, for the Sunnfjord area (figure 1.12). Temperatures derived by applying the garnet-clinopyroxene thermometer to clinopyroxene inclusion and adjacent garnet compositions range from 520 to 590 °C. The lack of any textures indicating reaction between host and inclusion (see above, section 4.3) suggests that inclusions were effectively isolated from retrogressive re-equilibration with the matrix. Very few inclusions were available so it was not possible clearly to demonstrate increasing temperature by this method for any single garnet, but it seems reasonable to assume that eclogites formed on a prograde temperature path.

The assumption that pressure equalled 15 kbar during eclogite formation may be evaluated by use of the Diopside-Jadeite solid solution barometer of Gasparik and Lindsley, 1980, and Holland, 1980 (figure 4.19). Assuming the coexistence of albite, minimum pressure estimates may be made (albite is present in most eclogites from Helleböstölane, but

only in symplectites formed during decompression). The results are in good agreement with the assumed pressure and the pressures obtained by Griffin et al (1985) for the eclogite-bearing rocks of both the Sunnfjord area and the region as a whole (figure 4.19 and table 4.2). Kyanite is not observed in eclogites from Sognefjord. The stability of paragonite + $jadeite_{40}diopside_{60}$ + kyanite + H_2O is shown in figure 4.19. This reaction has been used in some studies to constrain the upper, or lower, limit of eclogite formation. (Holland, 1979). However, although the former presence of a paragonite component in white mica may be inferred from the occurrence of symplectites of biotite and albite, its activity cannot be calculated and may have been much less than unity. With no good estimate for this unknown, pressures are constrained only to less than about 30 kbar.

The estimated conditions fall at the lower end of the range for B-type eclogites (figure 4.9), which may account for the apparent anomaly between the field occurrence and the C-type compositions of garnets and pyroxenes (see section 4.3).

The stable assemblage in the least altered eclogites is unsuitable for other thermometers. Although amphibole is in textural equilibrium with garnet and omphacite, Graham and Powell (1984) specifically exclude eclogitic amphiboles from their calibration of the garnet-amphibole thermometer and the formulation of Perchuk (1985) is strictly for much less sodic amphibole compositions; both yield high temperatures by comparison with the garnet-clinopyroxene thermometer in this case. Perchuk (1968, 1969) has presented thermometers for the glaucophane schist and eclogite facies based on Fe-Mg and Ca-Na distribution between clinopyroxene and amphibole which,

despite uncertainty over Fe^{+3} in both phases, yield consistent temperatures, though rather low compared with garnet-clinopyroxene thermometry (table 4.2).

Some samples (SF68 and SF70) show disequilibrium between clinopyroxene and garnet, with the development of amphibole coronas at grain contacts (figure 4.13). Temperatures obtained by applying the clinopyroxene-garnet thermometer are anomalously high (table 4.2) and minimum pressures, as expected are somewhat lower than for the least altered eclogites. Ca contents in garnet and clinopyroxene are higher than in eclogites showing little amphibolitization, and Mg garnet rims also have higher Mg values than garnets from Helleböstölane. Mineral textures suggest that the grains analysed were formerly in equilibrium with omphacite. This suggests that bulk rock Fe/Mg ratios were different in each case or that during amphibolitization, preferential diffusion of Fe into hornblende coronas has affected garnet zoning profiles. Higher temperatures than those estimated for eclogite formation in the field area are probably necessary for the latter process to have more than a limited effect, but strong evidence for such elevated temperatures post-eclogite formation has not been found. It seems unlikely that equilibrium has been attained between garnet and amphibole except, perhaps, on an extremely localized scale, since hornblende compositions vary across the width of the corona.

Garnets from eclogites which show more complete amphibolitization also have generally "prograde" profiles. Hornblende appears to have reached textural equilibrium with garnets in some of these more completely altered rocks, and application of garnet-amphibole thermometers (Graham and

Powell, 1984, Perchuk, 1985) give temperatures between 700 and 780 °C (table 4.2). These thermometers are in better agreement than when applied to the Basement Gneisses (chapter 3). While this may be fortuitous, the compositions of the phases involved, in particular the concentrations of Mg and Mn, are closer to those used in the original calibrations and the calculated temperatures are probably correspondingly more accurate. Some amphiboles have $Na^{M4} > 0.4$ (figure 4.16), which is rather high compared with hornblendes accepted for use in the Graham and Powell formulation but, contrary to their suggestion, samples with the lowest Na^{M4} give the highest temperatures and high Na^{M4} seems to be related to higher values of Al^{VI} rather than of Fe^{3+}. Biotite is present in some rocks, possibly as a breakdown product of phengitic mica or, in rocks which have suffered post-amphibolitization retrogression, of amphibole and garnet. Garnet-biotite thermometry is not justified on grounds of textural disequilibrium, and calculated temperatures are anomalously high.

Reaction textures are seen in samples SF133 and Hö1 which resemble textures attributed by Griffin and Heier (1969) to the transition from granulite to the amphibolite facies. A number of potential thermobarometers may be applied, but the results must be viewed with circumspection as the analysed compositions of some phases (in particular pyroxenes and plagioclase, which have suffered low-grade decomposition) probably do not represent equilibrium. During corona development, equilibrium is likely to have been achieved only locally.

Using only secondary ("amphibolite") phases from coronas,

temperatures of about 610-650 °C are obtained. Pyroxene thermobarometry yields a wide range of temperatures and pressures with large errors, which cluster around 750-850 °C and (at these temperatures) 8-12 kbar (table 4.2).

4.4.1 Discussion of results

Results from thermobarometric calculations suggest that eclogite facies metamorphism occurred at around 15 kbar or more under prograde conditions, with eclogitic assemblages crystallizing initially at temperatures as low as 520 °C and subsequently reaching nearly 600 °C. Conditions such as these are in agreement with those suggested by Griffin et al, 1985, and Krogh, 1982, for eclogite formation in the Sunnfjord area of Norway. The subsequent P-T path would appear to represent decompression under increasing temperature, which in turn would imply that eclogite facies metamorphism represents peak pressures but, in contrast to the model of Griffin et al, not peak temperatures (figure 4.19). Unfortunately, the postulated prograde path from eclogite to amphibolite facies depends on the use of a different thermometer in each rock type. It would be more desirable, when comparing relative equilibration temperatures in a group of rocks, to use a single calibration, such as the garnet-clinopyroxene thermometer of Ellis and Green (op. cit.). However, Graham and Powell's original calibration for garnet-amphibole Fe-Mg exchange was made against the Ellis and Green formulation for garnet and clinopyroxene and should provide the most favourable alternative in clinopyroxene-free amphibolites. If the calibrations of the two thermometers are assumed to be directly comparable there is a clear difference between the

consistent results around 600 °C obtained for the rims of eclogite phases and the wider range of temperatures (630 to 770 °C) obtained from amphibolitized eclogites. In the latter case the lower values are obtained from rocks in which amphibolite facies assemblages are partially replaced by greenschist facies assemblages and in which garnets show a decrease in Mg and increase in Mn at the rims, attributed to retrograde re-equilibration (e.g. sample SF24, figure 4.7). In such rocks the temperature is calculated using the most "prograde" garnet composition and must therefore be regarded with caution as garnet and amphibole compositions probably do not represent equilibrium, and can be assumed only to approximate those of peak metamorphic conditions.

In one such sample (SF24), amphibole inclusions are commonly found in large garnet grains. Assuming that Fe-Mg exchange has not occurred between the amphibole and the matrix, or the adjacent garnet, since the amphibole was originally enclosed, temperatures at various stages of garnet growth may be estimated. Included amphiboles have higher Fe/Mg ratios than matrix examples and generally yield higher temperatures. The highest values come from inclusions near, but not at, the rim. Too few inclusions could be analysed to produce an isotherm map of a garnet but, as might be expected from the zoning profiles of garnets (figure 4.7), temperatures obtained fit a model of initially increasing temperatures, from about 600 to 700 °C. Low temperatures are found at the rims or near cracks, where garnet profiles are modified by retrogressive re-equilibration. Peak temperatures estimated by this method would therefore appear to be at least 700 °C, possibly higher. Sample SF20 gives a similar pattern of

results although inclusion temperatures range from about 770 to 800 °C. However, the assumption that equilibrium has been attained between garnet and amphibole in these rocks, which show so much evidence of disequilibrium between other phases, is probably not justified and therefore garnet-hornblende themometry is unreliable. As seen in samples SF68 and SF70, where secondary amphibole occurs at grain contacts between primary garnet and omphacitic clinopyroxene, zoning in garnet may be a relict of the prograde P-T evolution of the rock leading up to peak eclogite conditions. If the prograde zoning in the more thoroughly amphibolitized eclogites is also a relict of early eclogite formation, then the apparent increase in the garnet-amphibole "inclusion" temperatures may be completely spurious: the results obtained would merely reflect an increasing X_{Mg} gradient towards garnet rims which has been preserved from an earlier stage of the history, and amphibole inclusions may in fact have been in chemical communication with the matrix via cracks in the garnet which are not seen in the plane of the thin-section. Reliable constraints on the decompression P-T trajectory cannot be obtained by geothermobarometric analysis of this group of rocks alone.

The age of the corona development in sample SF133 relative to eclogite and amphibolite facies metamorphism is not known. The textures are consistent with (virtually) isobaric cooling (Griffin and Heier, 1969), and the temperatures given by thermometry of corona phases support this. Thermometry of primary phases is unreliable as there are obvious signs of disequilibrium (see above). However, since corona phases form a relatively small volume of the rock

it is reasonable to suggest that the growth of secondary minerals has not had a large effect on the average compositions of pyroxenes. If it is also assumed that retrograde Fe-Mg exchange between pyroxenes has been incomplete, then the high temperatures obtained from two-pyroxene thermometry (e.g. Wood and Banno, 1973, Lindsley, 1983), although probably not representing peak temperatures also indicate that coronas are retrograde.

In summary, the P-T path of eclogitic rocks from Sognefjord appears to have involved an initial prograde metamorphism from at least 520 to 600 °C followed by decompression and amphibolitization. The temperatures of eclogite metamorphism are estimated to have been about 600 °C at 15 kbar. Garnet-hornblende thermometry appears to indicate a post-eclogite prograde decompression path. However, the calculated temperatures for each part of the metamorphic history depend on the use of different thermometers and are not directly comparable, so such a prograde decompression history cannot be verified. It should be noted that, although the Graham and Powell thermometer is strictly not applicable to eclogite amphiboles, if it is used on eclogites where the primary assemblage clinopyroxene-amphibole-garnet <u>does</u> occur then it also yields temperatures which are higher than the garnet-clinopyroxene thermometer and which are similar to the, probably spurious, temperatures calculated for the peak of amphibolitization.

The time elapsed between eclogite and amphibolite facies metamorphism is not known but both events are believed to be of Caledonian age and therefore likely to belong to the same general cycle of burial and erosion. Textural evidence

suggests that the hypersthene-plagioclase-diopside assemblage observed in some gneisses is a pre-eclogite relict rather than post-eclogite granulite metamorphism, while corona phases may represent cooling on a low dP/dT path segment. The temperatures derived from the thermometry of corona phases from such gneisses are in reasonable agreement with a slight elevation in temperatures during decompression and amphibolitization of the eclogites.

CHAPTER 5: METAMORPHISM IN THE MAFIC UNITS

5.1 Introduction

The eclogite-bearing Basement Gneisses are immediately overlain by a thick succession of schists and gneisses, cropping out in a broad band across the central part of the area, which are mainly derived from igneous precursors of basic or intermediate composition. The contact between these rocks and the Basement Gneisses is tectonic in origin, as described in chapter 2. This sequence of amphibole schists, tonalitic gneisses and gabbroic coronites has been subdivided into three units separated by tectonic contacts: the Lower, Middle and Upper Mafic Units (LMU, MMU, and UMU, respectively). Each of these units has suffered several phases of deformation and metamorphism. A peak garnet-amphibolite metamorphic event which affects all the units is considered to have coincided with, or slightly post-dated the emplacement of the units in their present tectonostratigraphic position (i.e. it is of "D_2" age).

Doleritic dykes with intrusive contacts cut both the Mafic Units and Basement Gneisses. Those in the Basement Gneisses have rather higher K and Rb contents than examples in the Mafic Units but are otherwise similar in trace element chemistry (figure 5.1).

The age of the rocks comprising the Mafic Units is not known. As a group, they show some similarities to the "Vevring Complex" of the Melvær and Askvoll area (Skjerlie, 1984). This is a suite of intermediate and basic gneisses which develop amphibolite grade assemblages and blastomylonitic textures near their basal contacts with a

complex of anatectic and migmatized rocks (the "Jostedal Complex"). The Vevring Complex itself is thought by Skjerlie (1984) to be of Precambrian age, and is interpreted to be a thrust sheet emplaced during the Sveconorwegian (Grenvillian) orogeny (Skjerlie and Pringle, 1978), at least in the Gaular-Förde area.

Some of the coronite gabbros of the UMU show a close similarity to rocks from the Lofoten Islands of north Central Norway, as described by Griffin and Heier (1969) and ascribed by Gee et al (1985) to the parautochthon/lower allochthon. Broadly similar rocks are also seen in the Upper Jotun nappes (Emmett, pers. comm., 1986) in the eastern Jotunheim and assigned to the Middle Allochthon by Gee et al (op cit). Correlation of the Mafic Units with these nappes is beyond the scope of this thesis, but the occurrences elsewhere of similar rock-types at tectonostratigraphic levels higher than the WGR suggests that these Mafic Units may be more closely related to the allochthonous units than to the parautochthon. This possibility was suggested by Bryhni and Sturt (1985), who pointed out that similarities exist between the Caledonian nappes to the east of the Jostedal culmination and "supracrustal" rocks of the coastal area of the WGR.

The Mafic Units are overlain on the west and northwest of the area by the pelitic schists of the Hyllestad arc (Chapter 6), along another tectonic boundary. This chapter describes the petrography, metamorphic history, and thermobarometry of the Mafic Units.

5.2 Petrography and mineral chemistry of the Lower and Middle Mafic Units

The bulk of the LMU comprises mafic amphibolites, often with garnet. The bulk chemistry of some of these rocks has been determined for major and trace elements by X-ray fluorescence analysis (table 5.4). The major element chemistry of banded amphibolites is variable, but broadly that of tholeiitic to subalkaline basalts (Cox et al, 1979, Le Bas et al, 1986). In such rocks, a well-developed S_2 foliation is defined by the orientation of hornblende and biotite crystals, and is parallel (or occasionally sub-parallel) to the "S_1" compositional banding. CaFe-rich garnet ($Alm_{65}Grs_{25}Pyr_5Sps_5$) is common and rutile, biotite, and chlorite may also be present (table 5.1).

Ultramafic schists occur in both the LMU and MMU. They are best developed in the latter, where they form pods and lenses up to about 100m across. The S_2 schistosity is only poorly developed and the fabric usually comprises randomly oriented, or weakly aligned tremolite and chlorite, with relict olivine. Replacement textures involving epidote, talc, and cummingtonite in some samples suggest the former presence of plagioclase and orthopyroxene.

The Lower Mafic Unit (LMU, or Lavik Amphibolites) rests directly on the Basement Gneisses (figure 2.1). Coarse gabbroic textures and relict phases (e.g. clinopyroxene, figure 5.2) are sometimes preserved in samples from massively-textured pods or lenses up to tens of metres in size, where the S_2 cleavage is poorly developed. The S_2 foliation is deflected around these pods. A weak grain elongation sub-parallel to the S_2 foliation is sometimes present in schistose

material enclosing the pods, and actinolitic amphibole and biotite occur within discrete, anastomosing shear bands which cut the pods. The field association thus strongly suggests the derivation of the well-foliated amphibolites from gabbroic precursors. Variations in the thickness of compositional banding in enclosing amphibolites may at least partly reflect variations in original grain size, which range from 2mm to 10mm in the poorly foliated gabbro.

The Middle Mafic Unit crops out in a wide band between Vetlenipa and Soetevik. In the central part of the area the rock type is mainly tonalitic gneiss comprising plagioclase, biotite, and quartz, with allanite grains rimmed by thin overgrowths of epidote. In these rocks the S_2 foliation is only poorly developed, but a strong L_2 lineation is defined by coarse elongated biotite and plagioclase grains and ribbons of quartz, all showing post-tectonic recrystallization. Original igneous features are not common, but shadowy xenoliths are sometimes seen (e.g. at Leirvik). More mafic (i.e. approximately doleritic) gneisses are commonly found in the MMU, either as bands tens of metres thick striking parallel to the major contacts, or as more massive gneisses with randomly oriented relict plagioclase phenocrysts. In the former, a strong S_2 foliation defined by the orientation of elongate hornblende (or, more rarely, actinolite) prisms and biotite flakes is often developed parallel to the mafic horizon margins. The S_2 schistosity is subparallel to a compositional layering of hornblende + biotite and plagioclase + quartz, possibly the relict of an earlier differentiated schistosity (S_1 ?). Amphibole and biotite grains are folded by F_3 crenulations without recrystallization into an axial planar

orientation.

At a few localities, such as Tjönnebakkane, Fjellheim, and Böfjorden, garnet-mica schists are infolded with amphibolites of the LMU and MMU. These typically comprise garnet, biotite, plagioclase, quartz, and white mica; tourmaline and zircon are also usually present. Al_2SiO_5 polymorphs, staurolite, and chloritoid have not been found (cf the Hyllestad Schists and UMU).

5.2.1 Petrography and mineral chemistry of garnet amphibolites in the LMU and MMU

Garnets in amphibolites are almandine-rich with subordinate grossular and minor spessartine and pyrope components ($Alm_{65}Grs_{25}Pyr_5Sps_5$) (table 5.3), but almost invariably show slight compositional zoning (figure 5.3). Mg and Fe^{+2} profiles are saucer-shaped and are mirrored by variations in Ca and Mn. Small reversals in zoning trends seen at the extreme rims of some garnets are attributed to the retrograde re-equilibration of garnet margins with matrix phases; signs of resorption are frequently seen at grain boundaries. A thin and incomplete moat of plagioclase and quartz is commonly present separating garnet from amphibole grains forming the foliation. Large garnets contain curved, occasionally spiralled, trails of elongate quartz, ilmenite, rutile, sphene, or apatite inclusions. In some examples the trails are approximately continuous with the external S_2 foliation at the margins of the garnet, and garnet growth is inferred to be syn-kinematic with S_2 formation and rotation or crenulation. In others the internal and external foliations are discontinuous, suggesting that garnet growth stopped

before the cessation of D_2 deformation, or that the S_2 foliation has been reactivated subsequent to garnet growth (Bell, 1986).

In the west of the area, the relations between inclusion trails in garnets and external foliations in the matrix of the rock are obscured by overprinting of the S_2 foliation. These late (D_5), overprinting structures truncate garnet margins and inclusion foliae at a high angle. In some cases, the garnet has acted as a rigid porphyroclast and the sense of the late shearing is indicated by asymmetric "tails" formed by the external foliation. The internal foliations (S_2?) defined by inclusion trails seem to bear no structural relation to the shear sense indicated by asymmetric D_5 microstructures.

In the MMU garnets are not uncommon in doleritic schists and gneisses, but as in the LMU, garnet-absent assemblages are more usual. Where present, garnets are often embayed or cracked and may be surrounded by moats of plagioclase and quartz.

Most of the amphibole in rocks from the LMU crystallized during D_2 (see above). Amphibole analyses, as recalculated for ferric iron by the method of Laird and Albee (1981), fall in the compositional fields of hornblende, tschermakitic hornblendes and pargasite. More actinolitic compositions are sometimes found, usually in rocks showing well-developed D_3 structures such as F_3 chevrons, while tremolite occurs with chlorite in ultramafic schists. In thin-section, chemical zoning (figure 5.3) is often revealed by faint variations in absorption and birefringence. Zoning is strongest in Na, Al, and Ca with less pronounced variation in Mg and Fe (profiles of total iron, or total Na, are usually smoother than those of

Fe^{+2}, Fe^{3+} or Na_{M4}, suggesting imperfections in the recalculation scheme). Zoning in amphiboles trends from tschermakitic hornblende compositions at the core towards more actinolitic rim compositions (figure 5.3, 5.4). This trend opposes the gently prograde zoning observed in garnet and, although well-developed, is probably related to the small retrograde reversals in zoning seen in some garnet profiles The large body of literature on chemical zoning in garnets suggests that diffusion of cations may be slow at temperatures less than about 650 °C (Yardley, 1977, Freer, 1981, Elphick and Ganguly, 1985). Amphiboles, on the other hand, while widely reported to show zoning (e.g Holland and Richardson, 1979) seem to be less robust with respect to volume diffusion and retrogressive re-equilibration in these rocks. This is probably due in part to their significantly finer grain-size (compared to garnet) and possibly also to their well-developed cleavage. The widespread retrograde alteration of amphibole is probably responsible for the spread in calculated temperatures obtained from Fe-Mg thermometers.

Anorthite contents of plagioclase are highest at grain cores, where maximum values of about An_{46} are preserved. Rim values are as low as $An_{1.5}$ in some retrogressed samples. This zoning like that in amphiboles (see above) is probably related to a late (greenschist facies) retrogressive event.

5.2.2 Petrography of pelites in the LMU and MMU

As noted above, thin bands of pelitic schist are infolded with mafic amphibolites at a few localities in the LMU and MMU, frequently (but not invariably) occuring close to major tectonic contacts. The most common assemblage is garnet +

biotite + muscovite + quartz + albite + ilmenite ± graphite ± rutile ± tourmaline ± epidote. The history of garnet growth is similar to that in adjacent mafic schists and it is inferred that peak metamorphism was contemporaneous with D_2. Garnets (1-2cm diameter) include trails of elongate quartz, ilmenite, and graphite. These trails are curved or spiralled (i.e. the "axial surfaces" of microfolds defined by inclusion trails are curved), suggesting synkinematic (D_2) garnet growth and, possibly, rotation during growth (Schoneveld, 1977, Bell et al, 1986). However, included foliae are rarely continuous with the external schistosity and inconsistencies in the inferred rotation directions are frequently found for different garnets in a single sample. This may be due to reorientation of garnets during D_3 together with further rotation of garnets and reactivation of the external foliation during post-D_3 shearing (D_5). However, Bell (1986) has suggested that garnets with curved inclusion trails may not have rotated. In this model apparent rotational ambiguity may arise when the thin-section is cut in certain orientations with respect to internal foliation geometries. In the MMU, garnet inclusion trails are frequently truncated by a strong blastomylonitic foliation.

5.3 Petrography and mineral chemistry of the Upper Mafic Unit

The Upper Mafic Unit differs from the LMU and MMU mainly in the relative rarity of banded amphibolites and biotite-plagioclase gneisses and in the abundance of coarse-grained orthopyroxene- and olivine-bearing coronitic gabbros. Well-foliated mafic amphibolites are restricted in distribution mainly to the southern (lower margin), where they are

interpreted as mylonitized equivalents of coarse-grained gabbros.

The intensity of tectonic overprint is extremely variable. Between Kjönas and Råsholm outcrops of undeformed gabbros are cut by discrete shear zones. More commonly a weak L-S fabric is developed in which the original coarse-grained texture is still visible, although largely replaced by an amphibolite-grade mineralogy. Complete destruction of the original textures is relatively rare and relicts of the original assemblages are frequently preserved. Thick shear zones are developed near the margins of the unit in which the relation between amphibolitization and shearing can be seen. Deformation of large clinopyroxene crystals is accompanied by replacement by hornblende and quartz intergrowths. With further deformation, biotite becomes increasingly common and partially replaces hornblende.

5.3.1 Distribution of rock-types in the Upper Mafic Unit

The bulk of the unit between Kjönas and Råsholm consists of coarse-grained gabbro, usually containing small modal quantites of orthopyroxene or olivine and about 50 to 80% plagioclase. Orthocumulate textures are occasionally preserved, with idiomorphic laths of plagioclase (up to 5cm long), enclosed by poikilitic pyroxene (up to 2-3cm in size) and minor olivine. Olivine crystals up to 1cm in length have been observed. Coarse primary ilmenite and biotite are sometimes present, the latter usually showing evidence of oxidation. Ilmenite is sufficiently abundant to cause anomalous compass readings in the area of gabbro outcrops. Abandoned underground workings for ilmenite in the gabbro can

be seen at Råsholm and Löland.

Doleritic minor intrusions, in the form of thin dykes, (0.5 to 2m thick) are widespread within the gabbro body (figure 5.5). Intrusion into the gabbro pre-dated tectonic episodes and the dykes share all the metamorphic and deformational events recorded in the host rocks, including the development of minerals seen in corona assemblages. The major element chemistries of gabbro and dykes are similar. Trace element concentrations are rather variable, particularly in the gabbros and in elements expected to be mobile during metamorphism, such as K and Rb. The variation in trace element concentrations is probably due, at least in part, to the influx of fluid during corona formation. The trace elements expected to be the least affected during metamorphism (Zr, Ti, and Y) also show a large scatter, particularly in gabbroic samples (figure 5.6).

The greatest range of chemical compositions is seen in the northwest part of the unit near Löland. Coarse and medium-grained igneous rocks with granitic and monzonitic, as well as minor bodies with doleritic, compositions occur. Rocks of intermediate and acidic composition have a poorly developed S_2 foliation and garnet and amphibole have not been found. In contrast, rocks of doleritic composition (e.g. K3) are mostly completely altered to garnet amphibolite mineral assemblages (garnet + amphibole + ilmenite + plagioclase + quartz) and have a strongly developed foliation, suggesting that they may have behaved in the least competent fashion.

5.3.2 Mineral chemistry of gabbros and related rocks in the Upper Mafic Unit

Gabbros from the UMU consist mainly of labradorite and augite with ilmenite, forsterite, and enstatite. Olivines and othopyroxenes have similar X_{Mg} values (about 0.7 to 0.75) Plagioclase laths sometimes show zoning to lower anorthite contents (about An_{40}) at their margins.

Clinopyroxenes form coronas on some orthopyroxene grains. Analyses of this clinopyroxene are poor (appendix 3,xi), tending to be rather rich in Al and poor in Si. This may be due to very fine intergrowths of spinel, as noted by Griffin and Heier (1969) in rocks from the Lofoten-Vesteralen area. Spinel in these intergrowths are too fine to be distinguished optically but larger hercynite grains are seen in gabbros at Råsholm.

Amphiboles in late coronas (see below) vary from edenite and edenitic hornblende to pargasitic hornblende. Cummingtonite has been found in coronas on orthopyroxene at Kjönas. Garnets are not common, and are usually less than 0.1mm across, but where coarser garnets have been found, they have the composition $Alm_{60}Grs_{30}Pyr_{10}$. Very little compositional variation is seen, except for a minor decrease in Fe and increase in Ca at the margin of the grain.

In thoroughly amphibolitized rocks from the UMU, garnet compositions are similar to those noted above. Slight compositional zoning from core to rim occurs and is characterized by increasing XMg and decreasing spessartine contents. Amphiboles, as in the LMU and MMU, show the reverse trend in zoning, with Mg higher and Fe lower, at the core than at the rim (figure 5.3). This pattern is attributed to volume

diffusion during cooling, while that in garnets is believed to represent growth zoning during an earlier, prograde, episode which has been refractory to resetting by volume diffusion during cooling. Plagioclase shows a general decline in anorthite content, from about An_{35} in the centres of grains, to about An_{25} at the rims, also attributed to retrograde resetting. In sample K3, however, a slight increase in Ca is found at the rims of plagioclase and zoning in amphibole is less pronounced. Textural evidence suggests that the peak metamorphic assemblage is better preserved in this sample, and its mineral chemistry may therefore give the best indication of peak metamorphic conditions.

5.3.3 Formation of coronas in gabbros of the Upper Mafic Unit

Coronas in gabbros of the Upper Mafic Unit are of two general types. The first have been observed at Råsholm in undeformed gabbros. In this type, mafic phases (principally olivine and ilmenite) are rimmed by several distinct zones comprised of orthopyroxene, clinopyroxene, spinel, and garnet.

The second type is distributed over a wider area and range of rock-types. Amphibole, biotite, and chlorite (and in some cases dolomite, talc, garnet, and epidote) form a diffuse corona around any iron-bearing phase in the rock. This type of corona overprints the pyroxene-bearing type mentioned above and forms as a result of amphibolitization of the gabbro and post-tectonic retrogression under greenschist facies conditions. Orthopyroxene and olivine are usually more intensely affected than clinopyroxene (figure 5.7b)

Each type of corona is considered in more detail below.

(i) Early (pre-D_2) coronas

When fully developed (usually on olivine, where in contact with plagioclase) these consist of an inner ring of radiating orthopyroxene, succeeded by a layer of vermicular clinopyroxene intergrown with spinel, and usually surrounded by a further band of clinopyroxene, or sometimes pargasite, (figure 5.7a). At the outer margin of the orthopyroxene corona, a diffuse layer of dusty inclusions is sometimes seen extending into the clinopyroxene. This may be finely divided garnet, a mineral seen in many coronas, either as tiny isolated crystals, or as discontinuous bands within the clinopyroxene. These bands often show well-developed faces towards the clinopyroxene zone (i.e the exterior of the corona) but are skeletal towards the orthopyroxene zone. In most cases the pyroxenes form fine-grained, radiating needles, or columnar crystals. In others crystallization of orthopyroxene has been more complete and optically continuous grains, or "tabular" crystals (Ashworth, 1986), sometimes with irregular subgrain boundaries enclose several olivine grains with resorbed margins. Orthopyroxene, especially where it is in contact with ilmenite, is sometimes replaced by randomly oriented biotite.

Clinopyroxene grains in continuity with plagioclase do not exhibit well-developed coronas (although a very thin fringe of biotite and amphibole is usually present).

Coronas of this type have a striking similarity to those studied by Griffin and Heier (1969) from the Flakstadöy anorthosites of the Lofoten Islands, Norway, and by Joesten (1986) from Risör, Norway. Griffin and Heier interpret such features as having formed at about 9 kbar and 850 °C under

conditions of falling temperature. Joesten (1986) on the other hand, ascribes such textures to reaction between cumulus olivine and intercumulus melt, a controversial interpretation strongly disputed by Ashworth (1986) who points out that coronas only form at contacts between olivine and plagioclase and relates all the features of the multi-layered coronas to sub-solidus metamorphism. In either case, the presence of olivine and plagioclase as cumulus phases (as inferred here from igneous textures, implies a crystallization pressure of less than about 5 kbar. However, the coronas probably indicate burial of the cumulate, with or without a melt fraction, to about 7 to 9 kbar (Joesten, 1986, Griffin and Heierm 1969). The coronas are not thought to represent pressures as high as 12 to 15 kbar (eclogite facies). Although garnet occurs as a corona phase, it is not abundant and is usually found within coronas, rather than replacing plagioclase. Plagioclase breakdown and garnet development is not as advanced as in gabbro-eclogite coronites described by Mörk (1986) and corona clinopyroxene is not omphacitic (appendix 3xi, samples SF173 and SF179). The coronas described here are interpreted to have formed prior to D_2 during the cooling of the gabbro at a maximum of about 9 kbar.

(ii) Late (post-D_2) coronas

Coronas of edenitic amphibole and chlorite associated with minor dolomite with talc on orthopyroxene and olivine are commonly seen in gabbroic rocks between Mölmedal and Kjönas. Corona phases generally have radiating or randomly orientated textures even when coronas and their "host" phases have elongated outlines, although fabrics subparallel to the

mylonitic foliation, possibly mimetically developed on host mineral orientations are sometimes seen. This suggests they formed after the D_2 deformation event. Their relation to D_3 is less clear, since they are mainly confined to coarse-grained gabbros and anorthosites, or to dykes enclosed within such rocks which do not exhibit recognizable D_3 structures or microstructures.

Coronas of this type are multi-layered and occur where orthopyroxene or olivine are in contact with plagioclase. The "host" orthopyroxene may be a single large grain or, rarely, may itself be mantling relict serpentinized olivine grains (as in type (i) coronas). Orthopyroxene is completely replaced in most samples by pseudomorphs of talc, dolomite, and magnetite, with magnetite most abundant towards the margin of the former orthopyroxene crystal. This is usually surrounded by:

(1) a thin layer of talc with ferroan dolomite, succeeded in turn by

(2) magnesian chlorite with ferroan dolomite.

The sheet silicate phases are usually very fine-grained and show a weak preferred orientation subparallel to the long axis of the 'host' grain and its mantling coronas. At the junction between layers (1) and (2) fine-grained actinolitic amphibole occurs, which is idioblastic towards the chlorite. Throughout the chlorite-rich layer (2), but concentrated on its outer margin, is a thin layer of darker green (hornblendic) amphibole with a radiating habit. Small idioblasts of garnet are sparsely intergrown with amphibole at the extreme margin of the corona, but are more commonly found replacing plagioclase a millimetre or two beyond the edge of the corona.

Textures suggest that amphibole + chlorite + talc

crystallized simultaneously - amphiboles intergrown with chlorite are usually well-formed and fine-grained. Large corroded grains are not seen, nor are chlorite-absent coronas containing radiating amphibole crystals. Garnet is infrequently encountered and may represent relicts of an earlier granulite or garnet-amphibolite metamorphic event. The nature of relations between amphibole-chlorite coronas and the orthopyroxene-clinopyroxene coronas mentioned in the previous section clearly demonstrates that the latter formed first. The formation of the later coronas requires the influx of H_2O, under epidote-amphibolite to upper-greenschist facies conditions.

5.3.4 Mineral chemistry of garnet amphibolites in the Upper Mafic Unit

Fine-grained mafic bodies, in which equilibrium amphibolite facies assemblages rather than coronitic textures are developed, are commonly found in the Upper Mafic Unit. Occasionally, for instance in a road-cutting at Kjönas, a complete gradation of rock-types from gabbro to banded amphibolite is observed, where the transition is accompanied by increasing strain. A strong blastomylonitic schistosity in amphibolite grade assemblages is deformed by F_3 chevrons and is considered to be of D_2 age (see Chapter 2).

The common assemblage in these amphibolites is hornblende + biotite + plagioclase + quartz + ilmenite + apatite ± garnet ± rutile ± sphene ± epidote ± allanite. Similar assemblages are seen in the LMU and parts of the MMU. Epidote and sphene lie in the S_2 foliation but are most abundant in rocks strongly affected by F_3 folding. Large

grains of ilmenite and rutile (and occasionally apatite) are broken up to form discontinuous S_2-parallel stretching lineations.

The early stages of amphibolitization were of high grade with the development of garnet and rutile. In most amphibolites of the UMU, however, garnets have suffered limited reaction during the cooling history of the rock and they are surrounded by moats of plagioclase, quartz, biotite, and epidote. Elsewhere, garnet is absent and epidote is much more abundant, occurring as fine needles replacing plagioclase and lying within the S_2 foliation.

Garnet compositions are about $Alm_{65}Pyr_{10}Grs_{23}Sps_2$ and do not, on the whole, show strong zoning. Amphiboles by contrast often show marked zoning to lower Mg compositions at the rim, accompanied by rising Ca and Fe (figure 5.3). Such effects are attributed to post-D_2 retrograde re-equilibration and introduce errors into garnet-hornblende thermometry.

5.3.5 Mineral chemistry of pelites at Löland

Pelitic schists are infolded with gabbros and monzonites in a small outcrop near Löland. Two main rock-types occur: a mica schist and an amphibole-bearing garnet-mica schist. The first has the assemblage sillimanite + garnet + biotite + quartz + oligoclase + muscovite + rutile + ilmenite + tourmaline with relict kyanite. Sillimanite is extremely fine-grained and fibrous, and intimately intergrown with oligoclase. Kyanite exists as small prismatic crystals with embayed edges. Large garnets have curved inclusion trails of opaques with large irregular patches of quartz, possibly included quartz pressure shadows. Such xenoblastic garnet

cores are commonly rimmed by idioblastic garnet. Within these idioblastic rims opaque inclusions form tightly curved trails, interpreted here as crenulations formed within the matrix which were subsequently engulfed by late post-kinematic garnet, rather than as indicators of syn-kinematic garnet growth and rotation. The axial planes of these crenulations are sometimes continuous with those in the matrix. In addition, smaller idioblastic garnets in the matrix often show a highly regular concentric, hexagonal distribution of inclusions, inferred to represent garnet growth without rotation.

All analysed garnets from the sillimanite schist show zoning in Ca, Mn, Fe and Mg. Zoning in Mn and Fe is most marked, but is only poorly developed in late garnets containing concentric inclusion patterns. X_{Mg} values of about 0.10 are found throughout most garnets with a small, but sharp, rise of about 0.05 at the margins (figure 5.3). Rim compositions are $Alm_{66}Pyr_{11}Grs_{20}Sps_{3}$, with core compositions of $Alm_{54}Pyr_{7}Grs_{25}Sps_{14}$. As observed elsewhere (Carmichael, 1969, Foster, 1982), sillimanite pseudomorphs of kyanite are not seen. Nevertheless the textures of kyanite grains suggest that the overall sillimanite-producing reaction is due to the breakdown of kyanite, however complex the actual reaction path. Muscovite and quartz appear to coexist in equilibrium.

Mineral textures suggest an early metamorphic event in the amphibolite facies during which kyanite and zoned garnet were formed. The presence of curved inclusion trails probably related to the S_2 schistosity in garnet cores suggests early garnet growth occurred during D_2 in common with similar textures in the LMU and MMU. Post-kinematic growth of garnet,

as small idioblastic grains and rims on pre-existing porphyroblasts, was probably contemporaneous with the breakdown of kyanite to sillimanite (garnet zoning profiles suggest that later garnet growth occurred under prograde conditions). Although garnet growth is described here in terms of two discrete "episodes", it is not intended to imply that two discrete metamorphic events necessarily occurred. However, textures noted in some garnet grains are suggestive of resorption prior to the growth of idioblastic rims, and the nature of inclusion patterns implies variations in strain during rim and core growth. Idioblastic garnet growth and kyanite-sillimanite breakdown pre-date crenulations thought to be of D_3 age.

Aluminosilicates are not common in the area: sillimanite has not been found anywhere else, and kyanite is known only from schists of the Hyllestad arc. The small difference in chemistry between cores and rims of garnets and the presence of abundant kyanite relicts imply that the kyanite-sillimanite phase boundary was not overstepped by a large amount, or that garnet growth ceased soon after kyanite became metastable.

Sillimanite schists are interbanded with schists containing the assemblage garnet + amphibole + biotite + quartz + apatite + rutile + ilmenite. Both amphiboles and garnets are coarse-grained and show a slight increase in Mg at the rims. Garnet compositions are otherwise remarkably uniform ($Alm_{60}Pyr_9Grs_{30}Sps_1$), but amphiboles have irregular chemical profiles and are partially replaced by biotite and chlorite.

5.4 Thermobarometry of the Lower Mafic Unit

5.4.1 Thermobarometry of garnet amphibolites

Temperatures have been estimated using, where appropriate, the garnet-hornblende (Graham and Powell, 1984) and garnet-biotite (Ganguly and Saxena, 1984) Fe-Mg exchange thermometers, as discussed earlier. Each yields a broad range of temperatures, the former between 541 and 681 °C, the latter between about 520-640 °C (table 5.2). Temperatures have also been calculated for garnet-hornblende pairs where hornblende is included in garnet (dashed lines on figure 5.8b). These give lower values than matrix bornblende and garnet rim compositions, as expected from garnet zoning patterns (e.g. sample L150). Agreement between different thermometric calibrations, even when applied to the same sample, is generally poor. Most samples show some evidence of retrograde overprinting, including zoning in amphiboles and plagioclase, and the variations in calculated temperatures are probably mainly due to Fe-Mg re-equilibration during uplift. The data do not support or refute a regular geographic distribution of temperatures across the area.

The garnet-ilmenite thermometer (Pownceby et al, 1987) yields unreasonably high temperatures, apparently due to excess fractionation of Mn into ilmenite. However, the resolution of the thermometer is poor for garnet and ilmenite with such low Mn contents as those measured in these rocks.

Pressures have been estimated using the garnet-rutile-ilmenite-plagioclase-quartz barometer (GRIPS) of Bohlen and Liotta (1986). Since rutile is only present in very small modal volumes it is doubtful whether the titanium oxides co-existed in equilibrium (Bohlen and Liotta, op cit). In the

least altered samples plagioclase is zoned, with higher anorthite contents at the rim (a trend sometimes overprinted by a retrograde decrease). The most Ca-rich compositions were used in GRIPS barometry. The barometer yields pressures of about 8 to 9 kbar, although these results should be treated with caution given the likelihood of disequilibrium between Ti-bearing phases and the zoning of phases, such as feldspar and garnet, due to both prograde and retrograde metamorphism.

5.4.2 Geothermobarometry of pelites and granitic gneisses

Garnet-mica schists (T1, 449XZ) and a granitic gneiss (SF110) interbanded with garnet amphibolites in the LMU yield temperatures and pressures scattered over the same broad range as those obtained from the rest of the unit. Garnet-biotite temperatures range between 520 and 610 °C, two garnet-muscovite estimates are 497 and 509 °C, and a garnet-amphibole temperature of 524 °C was obtained from the granitic gneiss. The peak metamorphic assemblages in these rocks, as in the garnet-amphibolites, pre-date F_3 folding and crenulation and later shear bands. Phases such as micas, susceptible to low temperature re-equilibration, have probably been affected by disequilibrium Fe-Mg exchange during cooling which has produced a range of spurious temperatures. Application of the GRIPS barometer to the pelitic schists yields pressures similar to those obtained from garnet-amphibolites (8.2 and 8.5 kbar, at 500 °C). These may be compared with garnet-plagioclase-mica (MGMICA) pressures for the same samples - about 7.0 to 8.5 kbar - obtained using the most calcic plagioclase compositions.

Barometers appear to be more robust than exchange

thermometers for this suite of samples (figure 5.8). This may be a consequence of parallelism between cooling paths and the loci of barometer equilibrium constants in P-T space.

5.5 Thermobarometry of the Middle Mafic Unit

Garnet-bearing rocks are uncommon in the MMU. Only a few samples were collected which contained assemblages suitable for thermobarometric analysis. Most of these were found to the west of Leirvik in rocks cut by low-grade shear zones, or showing weakly developed extensional crenulation cleavage, related to the late D_5 event.

The results show a very broad overall scatter (figure 5.9). It is doubtful whether rutile is in equilibrium in peak metamorphic assemblages in any of these rocks and it is absent from most, so GRIPS barometry is not strictly appropriate and results should be regarded as maximum pressures.

Mafic samples containing hornblende (378, 498, 68, and SF119) yield garnet-amphibole temperatures from 496 - 582 °C. Garnet-biotite temperatures show an even wider spread, possibly because biotite is less refractory than amphibole to low-grade re-equilibration, and even breakdown to chlorite and magnetite, during late deformation and extensional crenulation cleavage development. However, three garnet-muscovite temperatures (485 - 515 °C) are close to garnet-muscovite results for the LMU (497 - 514 °C) and occur at the lower end of temperatures calculated by other methods.

Any systematic variation in peak metamorphic conditions from east to west across the unit is obscured by the poor data set.

5.6 Thermobarometry of the Upper Mafic Unit

5.6.1 Thermobarometry of the Upper Mafic Unit at Löland

Rocks of the UMU rarely show the peak metamorphic equilibrium assemblages comtemporaneous with, or post-dating, D_2 which are seen in other units. Where the development of a well-defined foliation is confined to discrete zones in largely undeformed gabbros, corona textures are post-D_3 and due to low-grade hydration. Amphibolite assemblages are confined mainly to the sheared boundaries of the unit where the S_2 schistosity is well-developed and, even there, garnet-bearing assemblages are not common. At Löland, the coincidence of a kyanite-sillimanite-garnet schist (K2a) with an amphibole-bearing mica schist (K2b), and a doleritic body containing a garnet-amphibole assemblage (K3) allows a number of thermobarometric equilibria to be considered including the kyanite-sillimanite transition. Calculated temperatures and pressures are shown in figure 5.10a and, compared to the rest of the Mafic Units, are well-constrained. The stippled area represents the range of pressures and temperatures calculated, rather than the limits of statistical errors. There is good agreement between the garnet-biotite and garnet-hornblende thermometers (using the calibrations of Ganguly and Saxena, 1984, and of Graham and Powell, 1984, respectively) for all relevant assemblages (table 5.2). The total range is about 490 to 530 °C at 5 kbar. Fairly close results are also obtained by use of the GRAIL, MGMICA and FEMICA barometers (Bohlen et al, 1983, Ghent and Stout, 1981, Hodges and Crowley, 1985), which suggest pressures of 4.3 to 5.3 kbar. The GRIPS barometer (Bohlen and Liotta, 1986) yields pressures of 6.7 to 9.5 kbar, which are inconsistent with experimental

determinations of the kyanite-sillimanite transition at these temperatures.

The garnet-biotite calibration of Hodges and Spear (1982) has been included on figure 5.10a as it gives temperatures more consistent with the kyanite-sillimanite transition than that of Ganguly and Saxena (1984). The Al_2SiO_5 triple points of Holdaway (1971) and of Richardson et al (1969) are also indicated, the latter being clearly inconsistent with P-T estimates for these rocks.

5.6.2 Thermobarometry of other parts of the Upper Mafic Unit

Conditions of peak metamorphism calculated for rocks from Löland may not apply to the whole of the UMU. Temperature estimates from garnet amphibolites cover a broad range roughly centred on estimates for rocks from Löland (figure 5.10b). Most garnet-amphibole temperatures (Graham and Powell, 1984) agree reasonably well with those in figure 5.10a and fall in a range of about 525-555 °C. The maximum temperature estimates of 659 °C is calculated using garnets and amphiboles from a coronitic gabbro (SF179), in which analyses of both phases are rather variable and possibly represent extremely localized areas of equilibrium within the thin-section. In addition, the average composition of amphibole does not correspond to hornblende and is not strictly suitable for the application of this thermometer.

The calibration of Hodges and Spear (1982) for the garnet-biotite geothermometer is indicated on figure 5.10b for comparison with that of Ganguly and Saxena (1984).

GRIPS barometry yields much higher pressure, for all rocks, than those estimated by other means for schists at

Löland (figure 5.10c), but are similar to GRIPS pressures calculated for those rocks. However, as in the LMU and MMU, rutile may not be an equilibrium phase in these rocks. Where present, it occurs only in small amounts, and textures suggest it is probably not in equilibrium with ilmenite and therefore calculated pressures represent maximum estimates.

5.7 Conclusions

The LMU, MMU, and UMU have all experienced an episode of metamorphism during D_2. This event occurred at conditions of about 550 °C in all units, with a general consistency between P-T estimates for pelites and mafics (figure 5.11). In the UMU, orthopyroxene-clinopyroxene-spinel coronas are developed at contacts between olivine and plagioclase. They are pre-D_2 in age and record a cooling event at between 7-9 kbar, which was probably unrelated to the Caledonian deformation and metamorphism recorded in this and other units, and not directly related to eclogite facies metamorphism in the Basement Gneisses. Pressure estimates have a broad range, but the UMU gives lower pressures than the LMU. The pressure interval may be from zero to 2 or 3 kbar, based on a variety of geothermobarometers. The results are probably not inconsistent with the total structural thickness, implying a negligible change in thickness of the three units since metamorphism took place. The Mafic Units all define P-T conditions significantly less than those of the eclogites in the Basement Gneisses, and preserve only a lower P history. This is also in contrast to the overlying Hyllestad Schists, which record evidence of P-T conditions as high as eclogite facies. Greenschist facies overprinting of the LMU, MMU, and

UMU is probably related mainly to D_5, although some retrogression may have occurred during D_3. The final crystallization/cooling pressure inferred for the undeformed gabbro in the UMU may be as high as about 9 kbar, yet the general deformation P-T conditions in the unit are at less than 9 kbar (5-6 kbar), even though the D_2 event involves strong folding. This sequence could suggest that either: (i) decompression occurred between cooling and emplacement to the present position (possibly as a consequence of previous erosion), or (ii) the emplacement itself involved decompressional unroofing (i.e. was extensional in nature).

It is significant that D_2 cannot be shown to have involved any obvious thickening here, as the pressure conditions during D_2 are not greater than conditions of early gabbro corona formation. It is conceivable that the Mafic Units may have suffered deep burial with the Basement Gneisses and eclogites without the development of eclogite facies assemblages, or with such assemblages having a very limited extent; perhaps confined to shear zones. Gabbroic rocks in which eclogite facies assemblages are only locally developed during deep burial have been reported from the Bergen Arcs and from Flemsöy (Mörk, 1986). No eclogite, or other uniquely high-pressure mineral assemblages have yet been identified from the Mafic Units. In view of the similarity of the bulk rock chemistry of many horizons in the Mafic Units to that of mafic rocks in the basement which do show eclogite mineralogy, this is surprising if these rocks have indeed suffered high-pressure conditions, especially when the large volume of rock exposed in the Mafic Units is considered. However, if eclogite assemblages were developed, but were confined to

shear zones or other areas in which strain was concentrated, and that these same highly strained zones were reactivated during D_2 when they were thoroughly overprinted in the garnet amphibolite facies.

Kyanite in a pelitic schist (sample K2a) from Löland could possibly be a relict of a high-pressure event, although it should be noted that kyanite is also stable at only moderate pressures at temperatures of 500-600 °C. Moderate pressures (about 4 - 5.5 kbar) are recorded by GRAIL and garnet-mica-plagioclase-quartz barometers (Bohlen et al, 1983, Ghent and Stout, 1981, Hodges and Crowley, 1985) in these schists (fig. 5.10a). Higher pressures, but still below eclogite facies conditions (about 7-10 kbar, fig. 5.10c) are recorded by GRIPS barometry (Bohlen and Liotta, 1986) in other parts of the UMU. These probably represent resetting of equilibria during D_2 and are similar to pressures recorded by the same barometers in the Hyllestad Schists, even where high-pressure conditions are inferred from petrographic considerations.

CHAPTER 6: METAMORPHISM OF THE HYLLESTAD SCHISTS

This chapter addresses the petrology and metamorphic history of the schists, mainly pelites, which structurally overlie the Mafic Units and are overlain, in turn, by the Devonian conglomerates of the Solund massif.

6.1 Location and geological setting of the Hyllestad Schists

The Hyllestad Schists occupy a broadly arcuate area centred on the town of Hyllestad and mainly comprise chlorite-muscovite-garnet and kyanite-staurolite-garnet schists, with calc-silicate schists and gneisses, meta-carbonates and quartzites. These schists are intercalated with garnetiferous mafic amphibolites and epidote-amphibolite gneisses, the latter possibly representing meta-spilites. The protoliths of the unit were probably aluminous greywackes, probably representing a "eugeoclinal" sequence. Thinly interbanded calc-silicate horizons containing abundant amphibole and, less commonly, garnet and chloritoid may represent occasional influxes of volcaniclastic sediment. Garnet-amphibole schists sometimes exhibit "garbenschiefer" textures.

The granitic bodies associated with the schists are considered as part of this unit. The sheet-like geometry and planar contacts are considered to be due mainly to local tectonic reworking. Intrusive contacts are locally preserved, showing that the granites may be regarded as part of the same tectonic unit as the mica-schists (see chapter2).

The upper contact of the unit is sharply defined by the base of the Devonian conglomerate, to the west of Hyllestad (figure 2.3) and overlies a zone of mylonitized rocks hundreds

of metres thick. The contact with the underlying mafic units is not exposed in the study area (see chapter2).

6.2 Petrology of the Hyllestad Schists

Micaceous schists of one sort or another form the bulk of the Hyllestad group. They have a wide range of chemical and mineralogical compositions, and mainly consist of muscovite-rich, biotite-poor schists, intercalated with garnet-amphibole and calc-silicate schists. Most of the "Barrovian" zonal index minerals seen in the Scottish Dalradian (Harte, 1975) are represented, but the sequence is not complete.

6.2.1 Petrography and mineral chemistry of biotite-chlorite schists

These schists comprise assemblages corresponding to the lower zones of the Barrovian sequence. They consist mainly of quartz, white mica, and albite or oligoclase feldspar. Chlorite is often the dominant mafic phase and, together with white mica and minor amounts of biotite defines the S_2 foliation. Assemblages are compatible with the biotite zone of the Dalradian. Sheet silicate minerals are deformed in late shear bands related to the extensional crenulation cleavage (see chapter 2). This is in contrast to the garnet-kyanite schists described below, where chlorite occurs only as a post-crenulation cleavage retrogressive phase and is decussate on the shearing foliation.

Biotite is much less abundant than chlorite and is sometimes only present in trace amounts. The scarcity of biotite is due to the rather aluminous bulk chemistry of the rock (figure 6.1).

White mica constitutes 50% or more of the modal volume of these schists and has a paragonite component of around 12 to 16%. Paragonite has not been found as a separate mineral phase, although it should be noted that electron microprobe analyses of sheet-silicates were mainly obtained with a rastering beam, and the apparently high Na content of these micas may result from the integration of analyses of finely interlayered paragonite and muscovite. However, results from several rock samples consistently yield paragonite components of less than 22% and no analyses show paragonite as the dominant component, thus the micas are inferred to be Na-K solid solutions.

Ilmenite is the predominant Ti-bearing phase, often being more abundant than biotite, and it forms flakes lying in the mica foliation. Rutile and sphene are absent. Other common accessories are tourmaline and apatite, and secondary pyrite.

Garnet is commonly present in schists with the chlorite-biotite assemblage. It has significant spessartine and grossular components, and shows pronounced chemical zoning (about $Alm_{55}Pyr_{11}Grs_{15}Sps_{19}$ in the core to $Alm_{61}Pyr_{23}Grs_{10}Sps_{6}$ in the rim). Garnets with such high Ca and Mn contents are not typical of the almandine zone and may occur with chlorite over a wide range of temperatures and pressures (Spear and Cheney, 1989). Mn typically displays bell-shaped profiles (figure 6.2) usually inferred to represent growth under prograde conditions. Zoning in Ca also declines from core to rim, but Fe, Mg, and XMg increase towards grain edges. Garnet grains occasionally attain a diameter of about a centimetre, but grain-sizes of less than 2mm are more frequent. In contrast to the kyanite-garnet schists (in which garnets are generally

large, skeletal, and full of inclusions), in the chlorite-biotite schists they are typically tiny and well-formed with few inclusions, but are nevertheless abundant.

6.2.2 Petrography and mineral chemistry of almandine-kyanite schists

These rocks contain zonal indices associated with higher grades of metamorphism than the Barrovian biotite zone. Chloritoid, almandine, staurolite, and kyanite all occur, often in a single hand-specimen. Garnet is always present in kyanite-bearing rocks, but staurolite and chloritoid are not abundant. No intervening "zones" containing staurolite-chloritoid-chlorite/garnet, garnet-staurolite-chlorite, or staurolite-garnet-biotite are seen, as would be expected in a sequence following the Barrovian piezothermal array (see table 6.1 assemblages and figure 6.3).

Original grain-boundary relations are affected by a late, low-grade shearing event (D_5) producing an extensional crenulation cleavage (see chapter 2). The result of this late deformation on the microstructure is to crush grains together, fracturing and fragmenting the most brittle minerals (figures 2.34, 2.35). Retrograde replacement of garnet and chloritoid by chlorite + magnetite is most complete in such grains. On a larger scale, any original metamorphic zonation of different assemblages may have been tectonically modified by the same deformation event, and also by folding during earlier events. In general, the higher-grade schists (i.e. kyanite-garnet and "garbenschiefer" assemblages) are found to the north of Katlenova and east of Hyllestad, towards the base of the unit. Higher in the sequence, south of Katlenova and to the west of

Hyllestad, lower grade schists are seen, biotite-chlorite assemblages are more abundant and garnet is frequently absent.

Kyanite is always abundant when present and always occurs with almandine garnet. Staurolite and chloritoid are usually also present. Quartz, white mica, rutile, apatite, and tourmaline are ubiquitous. Accessories include monazite, zircon, pyrite, and ilmenite.

Chlorite and biotite are only present in quantities up to a few modal per cent, but impart a greenish tinge to hand-specimens. They only occur in shear bands, or as decussate products of the breakdown of garnet, chloritoid, and staurolite and are usually intergrown with magnetite. Hence chlorite and biotite do not form part of the highest grade assemblage.

Staurolites have a deep golden colour in thin-section. Grains are small (less than 1mm) compared with garnet and kyanite, and are frequently xenoblastic. Those occurring in the matrix of the rock are often enclosed by large grains of sodic muscovite (X_{par} about 0.25) and, where included in garnet porphyroblasts are associated with paragonite (figure 6.4). Chloritoid and staurolite both occur in the matrix and within large garnet inclusion sites, but they have not been observed in contact in either case. Where staurolite is relatively abundant in the rock, chloritoid is often absent or present only in trace amounts. Rarely, a patchy replacement of staurolite by kyanite is seen (figure 6.5).

XMg in staurolite ranges from 0.15 to 0.25. The lower values are from grains included by garnet and are always observed to be lower than the values from adjacent garnet, which range from about 0.18 to 0.32 (figures 6.1, 6.2, table

6.2). This partitioning relation is the reverse of that observed for garnet-staurolite pairs from the Dalradian (Baker, 1985, Harte, 1975, Harte and Hudson, 1979), the Eastern Alps (Droop, 1981), or Southern Vermont, USA (Karabinos, 1985) but has been reported in high-pressure assemblages from the USSR (Udovkina et al, 1980). Vuichard and Ballèvre (1988) suggest that reversals in Fe-Mg partitioning between garnet and staurolite may occur at P-T conditions around 14 kbar and approximately 600 °C. These pressures are extremely high compared with those calculated using some barometers in this study (see section 6.3), but still could be significant. The ZnO content of staurolites from Hyllestad is about 2 to 3 per cent; lower than in other reported zincian staurolites from high-pressure assemblages (e.g. Deer et al, 1982, Spear and Franz, 1986).

Chloritoid occurs as a matrix phase and, rarely, as inclusions in garnet; XMg is about 0.30. It is sometimes replaced along cracks by late (post-D_5) chlorite, but matrix chloritoid is not observed in contact with staurolite, garnet, or kyanite; closely associated grains are separated by late shear bands. Original textural relations are partly obscured by the rotation and crushing of grains during late shearing.

White mica from the matrix of the schists has a significant paragonite component, with Na occupying up to 25 per cent of the A site. However, white mica associated with staurolite and kyanite inclusions in garnet (figure 6.4) contains about 75 mole per cent paragonite.

The main Ti phase in these schists is rutile. Ilmenite is present, usually intergrown with rutile, and is probably a retrogressive phase. Sphene is absent. Chlorite and biotite,

although both clearly retrograde phases, are similar in composition to those phases in chlorite and biotite schists where they occur in the primary assemblages.

Garnets are usually idioblastic and may form porphyroblasts up to 2-3cm across. Decussate chlorite is sometimes developed at the rims and along cracks; replacement may be well-advanced. Two distinct concentric zones are usually seen:

(i) A skeletal inner zone, or core, containing abundant inclusions of quartz. These are separated by thin strings of garnet to form a spongy or lacey texture. Core compositions have lower pyrope contents than garnet rims ($Alm_{72}Pyr_{13}Grs_{10}Sps_5$ compared with $Alm_{67}Pyr_{31}Grs_2Sps_0$). Quartz inclusions consist of single grains, and often have a shape fabric defining straight, curved, or spiralled trails, which are truncated by the "outer" zone of idioblastic garnet. Inclusions of rutile, apatite, white mica, and tourmaline also occur in this inner zone and are oriented parallel to the quartz inclusion foliations, if present. Trails of these minerals continue into the "outer" zone of the garnet and are truncated at the edge of the grain, but do not show a consistent orientation with respect to the external foliation in the matrix. Chloritoid and, less commonly, staurolite inclusions have been observed in contact with low-Mg garnet cores.

(ii) An outer zone, or rim, of garnet which contains - fewer quartz inclusions than the core and so is easily distinguished from it optically. It is also much richer in the pyrope end-member (see above). Such rims frequently contain inclusions of staurolite, chloritoid, and kyanite, as

well as rutile, tourmaline etc. "Collars" of garnet free of quartz inclusions also occur within the inner zone, where they enclose surrounding inclusions of staurolite and kyanite. These garnet areas have a high Mg content (about 25 mole per cent pyrope), close to, but slighty below, values in rim analyses. Although the staurolite and chloritoid inclusions are now apparently enclosed by garnet, they may have been in chemical communication with the matrix via cracks which resealed during subsequent stages of garnet growth.

Chemical zoning profiles across garnet grains (avoiding staurolite and kyanite inclusions and their associated high-Mg garnet collars) show a sharp increase in Mg from core to rim. The increase in pyrope content is most pronounced at grain edges; X_{Mg} rises from 13% in the core to 32% at the rims. The increase in pyrope content is balanced mainly by decreases in grossular and spessartine components (figure 6.2).

Grossular and spessartine contents are low, and are lower than those of garnets from chlorite-biotite schists (figures 6.1, 6.2, 6.6) (this is consistent with the interpretation of Spear and Cheney, 1989). In many traverses, core and rim have slightly flattened profiles connected by a steep chemical gradient. In one sample (from Ronset), in which staurolite and chloritoid are absent, chemical profiles are flat and intermediate in composition between cores and rims of more strongly zoned garnets. They may represent garnets which were originally zoned but which have been subsequently homogenized by intracrystalline diffusion. Such a process would probably require temperatures of 600 to 650 °C (Yardley, 1977).

The absence of kyanite as inclusions in garnet cores ("inner zones") and its abundance in garnet rims ("outer"

zones) suggests it was not present in early assemblages. From study of the distribution of inclusions in garnet grains, a staurolite-chloritoid-almandine assemblage is inferred to have given way to one containing kyanite in equilibrium with a more magnesian garnet. As noted above, staurolite in these rocks is less magnesian than co-existing garnet. This would permit the reaction:

staurolite + chloritoid = garnet + kyanite (Bi,Cd,Tc,Chl)

to take place. Petrographic evidence for this reaction includes:

(i) staurolite and chloritoid are relatively scarce in the matrix, compared with the abundance of kyanite and garnet

(ii) the relative abundances of matrix staurolite and chloritoid show an inverse relation, possibly representing domains in which garnet-staurolite-kyanite or garnet-chloritoid-kyanite assemblages develop, depending on the local Fe/Mg ratio.

(iii) staurolite is patchily replaced by kyanite both in the matrix and within garnet porphyroblasts (figure 6.5)

(iv) chloritoid, staurolite, and kyanite inclusions within garnet are enclosed by garnet "collars" which possess rim-like compositions, and which appear to have replaced spongy, low-Mg garnet (i.e. all four phases have occurred together in the past, and when this happens the relative X_{Mg} is staurolite < garnet < chloritoid).

Only one inclusion site has been found in which all three of the phases chloritoid, staurolite, and kyanite occur together. In this instance staurolite is partially replaced by kyanite and chloritoid is represented by a single tiny

grain. In most cases chloritoid is absent from multi-phase inclusion sites.

Paragonite is usually associated with staurolite and kyanite inclusions, where it is seen to replace the former and to form many small inclusions in the latter. The mode of occurrence of paragonite inclusions suggests that it is related to the breakdown of staurolite and chloritoid and the growth of garnet and kyanite. This is supported by the observation that "matrix" staurolite grains are, in fact, almost always included by coarse grains of post-S_2 muscovite with a high sodium content. No albite inclusions have been found in many probed garnet cores, so the source of the Na is somewhat enigmatic. A possible source is infiltrating fluid, which could introduce ionic sodium, as well as removing zinc released during the breakdown of staurolite (cf Mohr et al 1986). The significance of the AFM topology and its consequences for the petrogenetic grid are discussed later (section 6.3.2).

6.2.3 Petrography and mineral chemistry of calc-silicate schists

Hornblende-bearing schists are interbanded with garnet-muscovite pelites at Kleivevatnet and Soetevik. Amphibole crystals are up to 10cm in length and lie within the mica schistosity, either singly or in small, radiating or intersecting groups. They occur with quartz, fine-grained epidote, rutile and coarse garnets. The last of these contains inclusions of tourmaline, quartz, ilmenite, and rutile; inclusions of amphibole are not observed (although inclusions of garnet in hornblende are seen at Soetevik).

Calcite is present in small amounts and chlorite and magnetite are developed as secondary phases along cracks in hornblende and garnet. Garnets are almandine-rich, but have a higher grossular component than co-facial kyanite schists ($Alm_{60}Pyr_{15}Grs_{15}Sps_{10}$ at the core to $Alm_{64}Pyr_{22}Grs_{12}Sps_{2}$).

6.2.4 Petrography and chemistry of carbonate rocks

Small outcrops of calcite-rich schists occur near Soetevik and Kleivevatnet. They form thin, boudinaged layers up to 0.5m thick, interbanded with quartzose layers of similar thickness. Assemblages which have been observed include calcite + plagioclase + zoisite + tremolite + quartz ± chlorite; calcite + chlorite + quartz + zoisite + plagioclase; and calcite + tremolite + plagioclase + phlogopite + quartz. Quartz-rich interbanded horizons have the assemblage calcite + quartz + zoisite + amphibole. The occurrence of zoisite implies that any fluid present had a high XH_2O

At Soetevik, tremolite (strictly highly magnesian actinolite, Leake, 1978) grains have pinched ends and are replaced along cracks by calcite and chlorite. The latter phase also lies along shear bands associated with boudin necks. The assemblage tremolite + zoisite + quartz is replaced in boudin necks by chlorite + calcite + quartz (figure 6.7). This reaction is discontinuous in the end-member system $CaO-MgO-SiO_2-Al_2O_3-CO_2-H_2O$, but becomes continuous with the addition of the $FeMg_{-1}$ exchange vector. It represents retrogression under greenschist facies conditions, and its association with boudin necks suggest that this event probably corresponds to the formation of the D_5 extensional crenulation cleavage, observed nearby.

The phlogopite + tremolite + calcite bearing assemblages seen at Kleivevatnet have a high variance and reaction textures are not observed. The absence of diopside and microcline suggest that temperatures may not have exceeded about 600 °C (figure 6.9).

6.2.5 Petrography and mineral chemistry of garnet amphibolites

Garnet amphibolites forming small sheet-like doleritic bodies occur at Hyllestad, along the road to Dale. A well-developed S_2 amphibole foliation wraps around garnet grains. Garnets show a slight chemical zonation with Mg increasing from core to rim. Amphiboles, which are pargasitic hornblendes (figure 6.8), show a slight retrograde zoning. Oligoclase feldspar is zoned to albite at the rims. Rutile and ilmenite occur as accessories both as inclusions in garnets and in the matrix. Secondary calcite is also present in cracks and joints.

6.2.6 Mineral chemistry of schists between Råsvikheia and Espelandsvatnet

Garnet-mica schists of similar appearance to those of the Hyllestad arc (section 6.2.1) crop out on the west shore of Espelandsvatnet. They commonly contain large garnet porphyroblasts, sometimes up to 2 cm in diameter, which have curved, or spiral-shaped, inclusion trails of ilmenite, tourmaline, and quartz. The rocks differ from most of the Hyllestad schists mainly in containing abundant biotite. Kyanite, staurolite and chloritoid are all absent, but albite and, in the more calcic bulk compositions, hornblende porphyroblasts are usually present. The tectono-stratigraphic

relation of these schists to the rest of the Hyllestad group is ambiguous; they do not form part of the main arc and are structurally interleaved between rocks showing petrographic affinity with the mafic units. Kildal (1970) includes at least some of them with the Hyllestad schists and they are considered as a subdivision of that group here.

6.3 Thermobarometry of the Hyllestad Schists

The petrogenesis of schists and gneisses in the Hyllestad area suggests a range of peak P and T conditions have obtained across the area. The lowest temperatures and pressures occurred in rocks now to the west of Hyllestad which occupy the highest structural position. In some of these rocks original sedimentary grain shapes are preserved and mineral species such as chlorite, biotite, and epidote are developed.

6.3.1 Kyanite-almandine and compatible assemblages east of Kleivevatnet

A number of thermobarometers have been applied to a range of rock-types collected from near Kleivevatnet (figure 2.2). Temperatures are calculated to have been about 600 to 640 °C at pressures of around 8 kbar during the peak of metamorphism (table 6.3).

Metamorphic temperatures have been calculated using Fe-Mg exchange equilibria between garnet and biotite (Ganguly & Saxena, 1984), garnet and amphibole (Graham and Powell, 1985), garnet and staurolite (Perchuk, 1977), and garnet and muscovite (Hynes and Forest, 1988) in appropriate assemblages. Minimum pressure estimates have been obtained from the GRAIL barometer (Bohlen et al, 1983) in kyanite-bearing assemblages,

and from the garnet-plagioclase-mica (Ghent and Stout, 1981, Hodges and Crowley, 1985) equilibrium in kyanite-absent schists.

Although, garnet rim compositions are practically two component almandine-pyrope binaries, the absence of biotite from many equilibrium assemblages in these schists unfortunately restricts the use of the well-documented garnet-biotite thermometer. When present in kyanite-bearing schists, biotite usually only occurs in trace amounts. It forms reaction fringes on garnet, or is intergrown with late chlorite, apparently as a late disequilibrium phase.

a) Kyanite schists

White mica in kyanite-bearing schists generally has a significant celadonite component and the partitioning of Fe and Mg between garnet and white mica may be used to estimate temperatures (Krogh and Råheim, 1978, Green and Hellman, 1982, Hynes and Forest, 1988). The calibration of Hynes and Forest is preferred here as it is has been determined empirically from natural assemblages using the garnet-biotite thermometer of Ferry and Spear (1978) with the garnet mixing model of Ganguly and Saxena (1984) and results may thus be compared with temperatures obtained for garnet-biotite bearing rocks. Errors may be introduced into this calibration by differential partitioning of ferric and ferrous iron between garnet and muscovite, and by pressure dependence of Fe-Mg partitioning. The extent of the first effect is unknown, but it is probably not unreasonably great in these schists where magnetite and hæmatite are not primary phases (Hynes & Forest, 1988). Errors introduced by the pressure dependence of the equilibrium are

also likely to be small, particularly as the temperature range of interest is similar to that used in the calibration.

Staurolite co-exists with garnet in most kyanite-bearing schists from Hyllestad, both in the matrix and as inclusions in garnet. The garnet-staurolite Fe-Mg exchange thermometer of Perchuk (1977) has been applied to such schists. Temperatures obtained using analyses of staurolite inclusions and adjacent garnet, are in reasonable agreement with results from other exchange thermometers. Matrix staurolites and garnet rim analyses give rather high temperatures, mainly due to higher Fe/Mg ratios in the staurolite. Staurolite grains in the matrix are almost invariably enclosed by white mica or, less frequently, show alteration to kyanite. It is possible that matrix staurolites have been prevented from full equilibration with garnet rim compositions due to overgrowth by white mica. Inclusions have slightly lowered Zn contents compared to matrix staurolite.

Metamorphic pressures for garnet rims in equilibrium with kyanite can be estimated using the GRAIL barometer of Bohlen et al (1983). Pressures obtained (5.5 - 6.7 kbar) are very low compared with the garnet-plagioclase-mica-quartz barometer (7.4 to 8.5 kbar) (table 6.3, figure 6.10). GRAIL pressures should be regarded as <u>minimum</u> estimates for these rocks since ilmenite generally forms at the expense of rutile and may not have been present under peak conditions. Pressures have been calculated using the most pyrope-rich garnet rim compositions, which further minimises the calculated pressures. If core garnet compositions are used, higher pressures (up to about 6.5 kbar) are yielded by the calibration, but mineral textures suggest kyanite did not coexist with garnet cores.

Kyanite occasionally occurs partially included by garnet rims. In such situations adjacent garnet compositions are slightly richer in the almandine component and give higher "minimum" pressures (rutile and quartz inclusions are present throughout garnet grains). Kyanite-almandine schists from Ronset, north of Hyllestad, yield similar temperatures and pressures using the garnet-muscovite and GRAIL equilibria (table 6.3, figure 6.10). Qualitative P-T trajectories have been calculated for kyanite-almandine schists by applying the method of Spear and Selverstone (1983) to chemically zoned garnet porphyroblasts. P-T conditions during the growth of the low-Mg garnet cores cannot be constrained (e.g. by thermobarometry of inclusions with adjacent garnet). The trajectory has to be back-calculated from P-T estimates obtained from the compositions of garnet rims and matrix phase. Calculated P-T paths show almost adiabatic decompression during garnet growth. However, the method strictly should not be applied to these rocks since a kyanite is inferred to have appeared in the assemblage only during late garnet growth. For most of the history of the rocks represented by the garnet zoning profile, too few compositional variables can be determined to constrain the P-T trajectory of the rock.

b) Kyanite-absent schists

In kyanite-absent schists biotite, chlorite, and muscovite (in ascending order of abundance) all appear to be in equilibrium. They lie in a well-defined foliation, which has itself been cut by a later extensional crenulation cleavage. Garnet-biotite temperatures obtained from such rocks are in

good agreement with garnet-muscovite temperatures of about 630 °C (table 6.3), despite higher grossular and spessartine components in co-existing garnets. They also compare well with garnet-muscovite temperatures from nearby kyanite schists (see below).

The calibrations formulated by Ghent and Stout (1981) for the two end-member equilibria:

pyrope + grossular + muscovite = 3 anorthite + phlogopite

almandine + grossular + muscovite = 3 anorthite + annite

converge in the region of temperature estimates. Furthermore, the calibration of the Fe end-member reaction by Hodges and Crowley (1985) yields pressures which differ by less than 1 kbar. However, it should be noted that feldspars are sometimes partially saussuritized and a reduction in Ca-content would tend to elevate calculated pressures. A pressure of 8.9 kbar has been obtained by the application of the GRIPS barometer (Bohlen and Liotta, 1986) to a garnet-biotite-chlorite schist near Kleivevatnet (figure 6.10).

Garnet-biotite thermometry gives less consistent temperatures than garnet-muscovite thermometry. Assuming garnet to be relatively refractory to Fe-Mg re-equilibration during cooling, this may be due to retrograde equilibration between micas. The small modal volume of biotite would make this phase particularly susceptible to an alteration of its Fe/Mg ratio, compared with muscovite, and would result in larger discrepancies in garnet-biotite temperatures than in garnet-muscovite temperatures. A P-T path has been calculated for a sample from these schists using the method of Spear and Selverstone (1983) and chemical variations in garnet composition. The results are shown on figure 6.10.

plagioclase grains have suffered patchy alteration during late low-grade events and zoning profiles tend to be irregular. Variation in plagioclase composition during garnet growth was estimated from maximum and minimum anorthite contents from zoning profiles and from compositions of plagioclase inclusions in garnet, but values chosen had only a small effect on the slope of the P-T trajectory. In contrast to curves obtained from kyanite-bearing schists, the chlorite-biotite-garnet schist yielded a prograde P-T path with a small rise in pressure (about 0.4 kbar) near the core, flattening off at the rim, and with a total temperature range of about 50 °C. Core temperatures could not be verified (due to lack of suitable inclusions), and pressure estimates of the matrix assemblage are based mainly on barometers which may yield minimum, rather than absolute, values.

c) Calc-silicate schists and garnet amphibolites

Kyanite-almandine and chlorite-biotite schists are inter-banded with hornblende pelites and calc-silicates at Kleivevatnet and northwest of Hyllestad. The compositions of co-existing garnet and amphibole are suitable for the application of the garnet-hornblende thermometer of Graham and Powell (1984). Two samples from Kleivevatnet give temperatures of 628 and 657 °C, which are in reasonable agreement with those obtained by other methods. A third sample gives rather low temperatures (509 °C for the garnet-hornblende thermometer and 436 °C for the garnet-biotite thermometer). However, this sample shows evidence of extensive retrogression: garnet and amphibole grains are partially replaced by chlorite, and feldspar grains are saussuritized.

The low temperatures may be a consequence of re-equilibration of Fe and Mg at lower grades, possibly during the extensional phase of tectonics. A mafic garnet-amphibolite sample from Hyllestad gives a garnet- hornblende temperature of 646 °C.

Two samples of garnet-hornblende schist collected from the road-section to the northwest of Hyllestad yield GRIPS pressures (Bohlen and Liotta, 1986) of 13.4 and 14.7 kbar (the latter is a maximum estimate as ilmenite was assumed to be pure in this sample). These values are high compared with other estimates, but are close to pressures implied for Hyllestad assemblages by the petrogenetic grid of Vuichard and Ballèvre, 1988 (see below).

Samples collected from Sognnes and Soetevik are variably retrogressed and thermobarometers described above yield a range of temperatures and pressures, varying from nearly 600 to 466 °C at about 6.5 kbar. Temperatures decline with increased petrographic evidence of retrogression. In this area the schists have been intensely deformed by a mylonitic foliation and by a later extensional crenulation cleavage. Chlorite commonly replaces mafic phases. The least affected sample (R8) is a pelitic amphibolite with spongy hornblende porphyroblasts overgrowing garnet and intergrown with biotite. Garnet-biotite and garnet-amphibole thermometry yield similar results (592 and 591 °C, respectively). There is little evidence of reaction at grain contacts and the similarity to results from Kleivevatnet suggest that they are close to peak metamorphic conditions.

d) Schists at Råsvikheia-Espelandsvatnet

A sequence of garnet-biotite and garnet-actinolite

pelites crops out between Espelandsvatnet and Aksevatnet. Calculated temperatures are less consistent than for schists elsewhere but mainly cluster between 450 - 500 °C at pressures of around 6 to 8 kbar. The samples were collected from several units, with southerly-dipping tectonic boundaries and may represent rocks of different grades stacked together out of sequence. It is likely that Fe-Mg partitioning between various phases has been reset during tectonic reworking, and this would account for the poor precision of thermobarometric calculations. Some results suggest that peak temperatures may have been as high as 600 °C, consistent with peak temperatures from other parts of the Hyllestad schists.

Pressures have been estimated using the GRIPS barometer (Bohlen and Liotta, 1983). One value of 7.1 kbar was obtained, with four others falling between 8.7 and 9.0 kbar.

6.3.2 P-T grids, the compatibility of different assemblages in the Hyllestad Schists, and implications for P-T conditions

Muscovite-rich schists from Kleivevatnet contain many of the zonal index mineral species of a Barrovian-type sequence of regional metamorphism, covering the chlorite to the kyanite zone. However, calculated peak metamorphic temperatures for a variety of rock-types have a small range (about 630 ± 30 °C). Projections of peak assemblages in chlorite-biotite schists are compatible with those in kyanite-bearing schists since, in the latter, biotite is a late, retrogressive phase (figure 6.1). The sequence of mineral assemblages inferred from the distribution of inclusions in garnet grains and matrix phases would only be compatible with the Barrovian sequence for aluminous rocks very close to the A-F join in the Thompson

projection (figure 6.3), where the bulk composition does not "see" biotite-forming reactions. These rocks are also anomalous in that:

(i) staurolite is less magnesian than co-existing garnet

(ii) garnet and kyanite do not coexist until the lower kyanite zone in the Dalradian yet chloritoid, which deomposes terminally in the upper garnet zone, is still present as large, well-preserved grains in the matrix of many samples.

An alternative sequence of mineral assemblages for the Hyllestad Schists is illustrated in figure 6.11. The assemblage biotite-chlorite-garnet is compatible with these assemblages in less aluminous bulk compositions.

Vuichard and Ballèvre (1988) present a petrogenetic grid for high-pressure (eclogitic) metapelites. Staurolite is assumed always to be more magnesian than co-existing garnet, but the possibility of reversed partitioning is considered, in which case the staurolite-out reaction:

staurolite = garnet + kyanite + chloritoid (Bi,Cd,Tc,Chl)

would be replaced by:

staurolite + chloritoid = garnet + kyanite (Bi,Cd,Tc,Chl)

as predicted for the Hyllestad schists from petrographic and chemical considerations. Metapelites containing the assemblage garnet + kyanite, with inclusions of staurolite and chloritoid in garnet, have been reported from the Champtoceaux nappe, Brittany by Ballèvre et al (1987), and are interpreted to represent a metamorphic peak at 20 kbar and 700 °C.

The petrogenetic grid presented by Vuichard and Ballèvre (1988) for the system KFMASH assumes that there is no Fe/Mg partitioning reversal between staurolite and garnet. They

note, however, that such a reversal has been reported in high-pressure schists and suggest that it probably occurs at around 14 kbar at 600 °C. These are approximately the P-T conditions of the stable [Bi,Tc] invariant point, which also corresponds to the minimum P for the (Bi,Tc,Chl) reaction in their grid. The reversal of Fe/Mg partitioning discussed above may be represented on a Schreinemakers net by the occurrence of a singularity in one of the relevant univariant equilibria. Two arrangements are possible in the present case: the singularity can either occur at a pressure below the [Bi,Tc] invariant point on the chloritoid-absent reaction (figure 6.12b), or it can occur above the invariant point on the chlorite-absent reaction (figure 6.12c). In both instances the reaction:

chloritoid + staurolite = kyanite + garnet

is constrained to occur at pressures in excess of 14 kbar, however, the minimum pressure is lower in the former case than the latter.

Such pressures are very high compared with most estimates for the Hyllestad Schists based on available barometers, and are incompatible with amphibolite facies assemblages observed in interbanded, and presumably cofacial, mafic rocks. Glaucophane or barroisitic amphiboles and jadeitic pyroxene have not been observed. The assemblage chlorite-biotite-garnet seen in other schists has a broad stability range and does not constrain equilibrium conditions further, given that garnet is stabilized by non-system components, such as Mn and Ca (Spear and Cheney, 1989). Rocks with this assemblage commonly contain albite (not seen in the kyanite-schists where micas have a high paragonite component). The experimental work of Ganguly (1972) places the invariant point [Bi,Cd,Chl]

in the system KFASH at 18 kbar, 580 °C. This point terminates the (Bi,Tc,Cd,Chl) reaction at the low temperature, high pressure end. The suggested position in the P-T plane is in accord with geothermometric results in the present case, but gives no additional information on probable pressures of formation. Minimum pressure estimates may be provided by the solid solubility of phengite in mica (Massone and Schreyer, 1987). Like those obtained from GRAIL barometry these are much lower (about 6 kbar, with one or two analyses as high as 8-10 kbar) than those permitted by the nets of Vuichard and Ballèvre (op. cit.) and Spear and Cheney (1989) and provide little constraint. Furthermore, pressures of 6-8 kbar obtained using equilibria based on the assemblage garnet-plagioclase-biotite-muscovite-quartz (Ghent and Stout, 1981, Hodges and Crowley, 1985) in chlorite-biotite-garnet schists might be considered to be maximum estimates, since plagioclase tends to re-equilibrate to more sodic compositions during cooling.

Attempts to modify the topology of the relevant portion of the KFMASH reaction grid to allow the prograde (Bi,Tc,Cd,Chl) reaction to take place at pressures significantly less than 14 kbar have largely been unsuccessful.

A large shift in the position of the invariant point [Tc,Bi] has profound effects on invariant and univariant equilibria whose positions are reliably established; and if invariant points shown as metastable are assumed to be stable, large portions of the grid are effectively inverted. The problem may be partially overcome if components other than H_2O were present in the fluid phase. The effect of such a component on

the system would be to collapse the grid towards the origin. However, a large effect of this kind would also tend to lower the stability fields of metapelite assemblages observed in the Hyllestad Schists below the calculated temperature of approximately 630 °C. This is a serious consideration, since the grid of Vuichard and Ballèvre (1988) is based largely on that of Harte and Hudson (1979), which itself takes the Al_2SiO_5 triple point from Richardson et al (1969). Their determination of the triple point temperature (622 °C) is probably too high with respect to natural assemblages, with the consequence that temperature estimates for the Hyllestad Schists are probably already near the upper limits for some assemblages (e.g. chlorite-garnet-biotite).

Prior to the publication of the recent paper by Spear and Cheney (1989), and without knowledge of it, I considered the possibility that the invariant point [Bi,Tc] is metastable and that the assemblage garnet-kyanite-staurolite-chloritoid might occur at pressures less than 14 kbar if the (Bi,Chl,Tc,Cd) reaction emanates from [Tc,Chl] (figure 6.13). This renders an inversion in other parts of the grid. The stable portion of the (St,Ky,Tc) reaction, for example, although possessing a positive dP/dT slope, has the products and reactants reversed, so that biotite + chloritoid is stable at lower temperatures with respect to garnet + chlorite, a situation at odds with the KFMASH grid of Harte (1975) and of Harte and Hudson (1979). The assemblage garnet-biotite-chlorite, stable over a wide range of temperatures and pressures in the Vuichard and Ballèvre grid, is restricted in this case to relatively low pressure conditions and is not stable in the P-T region of the (Bi,Tc,Cd,Chl) reaction. However, the stability range would

be increased if MnO and CaO are added to the system.

Spear and Cheney (1989) present an alternative reaction grid to those of Vuichard and Ballèvre (1988) and Harte and Hudson (1979), which shares many of the features of figure 6.13. Their grid is calculated in end member systems using the Berman et al (1985) data set supplemented by newer data, and in the KFMASH system using $FeMg_{-1}$ partitioning data and the Gibbs method. Like other published examples this grid also indicates a high pressure stability field for the garnet-kyanite-chloritoid assemblage at greater than 15-16 kbar (figure 6.14) and implies garnet compositions more Fe-rich than $Mg_{0.35}$ at temperatures less than or equal to 600 °C (figure 6.15). These authors also assume that staurolites have higher X_{Mg} than garnet, in contrast to the relationship found in the assemblages here. Furthermore, the [Bi,Tc] invariant point of Vuichard and Ballèvre (1988) is metastable in the analysis of Spear and Cheney (1989), in favour of the point [Chl,Tc]. Another important and unusual aspect of the grid of Spear and Cheney is that the reaction:

chloritoid + biotite + quartz + H_2O

= garnet + muscovite + chlorite

proceeds to the right with increasing temperature, thus limiting garnet + chlorite assemblages to a narrow temperature stability field (520 - 570 °C) at pressures less than 9 kbar. In KFMASH therefore there is no overlap between the kyanite-pelite assemblages and the garnet-chlorite assemblages observed in the Hyllestad schists; however, in MnKFMASH garnet + chlorite stability is greatly enhanced and will overlap garnet + kyanite + chloritoid stability if garnet $X_{Mn+Ca} > 0.3$, a condition generally fulfilled for the garnet-chlorite

assemblages here (table 6.2, group B) if garnet cores are used.

Consideration of both this grid and that of Vuichard and Ballèvre (1988) - based on different assumptions and data-bases, indicate that pressure conditions in the pelites were in the range 14-16 kbar: much higher than most geobarometry suggests and not consistent with the assemblages developed in mafics.

Possible solutions to the conflicting lines of evidence are:

(i) kyanite and garnet-chlorite-biotite schists have indeed formed at very high pressures. GRAIL, plagioclase-mica- garnet-quartz, and phengite barometers yield minimum pressures, much lower than T_{max} values. These schists have been tectonically intercalated with lower pressure mafic and metasedimentary rocks of similar thermal grade.

(ii) The interpretation of mineral textures to represent the reaction staurolite + chloritoid = kyanite + garnet is misplaced. A possible alternative is that chloritoid has already disappeared from the "effective" mineral assemblage (being preserved only in garnets as inclusions or otherwise prevented from chemical interaction with other phases) by the continuous reaction:

chloritoid = garnet + staurolite

This alternative would still require Fe/Mg partitioning between garnet and staurolite to be reversed at pressures less than 14 kbar.

(iii) The position of the [Bi,Tc] invariant point on the grid of Vuichard and Ballèvre is at inappropriately high pressure, and the partitioning reversal may also take place at

a lower pressure than they suggest.

(iv) The Hyllestad Schists were metamorphosed under conditions of low water activity, such that the (Bi,Tc,Cd,Chl) reaction was stabilized at lower pressures than 14 kbar. However, the effect of diluting the water content of the fluid phase is not known and seems unlikely to reduce pressure to 8 kbar or so.

(v) staurolite is stabilized by ZnO and its relation to AFM phases is not rigorously depicted by the Thompson projection, or Schreinemakers grid. However, ZnO contents are not large compared with other reported staurolite analyses (e.g. in Deer et al, 1982) and are small compared with zincian staurolite from the Eastern Alps (e.g. Spear and Franz, 1986). Furthermore, the addition of extra-system components, such as Zn or Co, would tend to enlarge the stability field of, in this case, staurolite towards higher rather than lower pressures: a result which would only increase the problem.

Alternative (i) is preferred in this study. The low pressures recorded by the garnet-biotite-muscovite-plagioclase and GRIPS barometers are not easily reconciled with the constraints of the P-T reaction grid. It is suggested that these equilibria have been disturbed at low pressures, and that feldspar and ilmenite in particular may have suffered from low-grade overprinting during late shearing.

Summary

The absence of mineral assemblages typical of high-pressure facies in intercalated units, particularly the lack of jadeitic pyroxene, and the presence of garnet amphibolites and hornblende-bearing calc-silicate schists more typical of

medium-pressure amphibolite facies, strongly suggests that the [Bi,Tc] invariant point may be more appropriately placed at pressures below 14 kbar. However, modifications to the grid which would reduce minimum pressures for the (Bi,Tc,Cd,Chl) reaction to the region of 8-10 kbar (the upper range implied by exchange barometry) cannot be made without serously affecting other parts of the grid. In the light of field evidence for intense post-peak metamorphism reworking of rocks in the Hyllestad area, it seems likely that the kyanite-garnet schists, and possibly the garnet-chlorite-biotite schists, have been tectonically intercalated with garnet amphibolites etc. during the later stages of the Caledonian Orogeny (option (i) above).

If this is the case, then the occurrence of "eclogitic" assemblages within demonstrably supracrustal rocks, widely believed to be of Lower Palaeozoic age casts favourable light on models which assume low-pressure protoliths for Norwegian eclogites. However, since the Hyllestad Schists are thought to represent part of an allochthonous unit, and the age of metamorphism is not known, it cannot be determined precisely whether metamorphism in the schists is contemporaneous with eclogite facies metamorphism of basic rocks in the Basement Gneisses, or whether it pre-dates emplacement of the schists over the Basement Gneisses (in which case it may represent a subduction event on the Laurentian margin of the Iapetus Ocean).

CHAPTER 7: CONCLUSIONS

Some of the observations and apparent contradictions concerning the metamorphic histories, as deduced for different units in the field area, are reviewed and two possible tectonic models are discussed.

All the tectonostratigraphic units studied in the field area, the Basement Gneisses, Mafic Units, and Hyllestad Schists, have been subjected to polyphase deformation inferred, from regional considerations, to be mainly, or wholly, of "Caledonian" age. Five deformation "events" have been distinguished, based on the relations of minor structural elements to each other and to growth of metamorphic minerals. Different rock-types are characteristic of different units, and at least one of the deformation events (D_5) appears to vary in intensity across the area; this has resulted in stronger overprinting of early events by later ones in some units than in others. For instance, the development of D_5 is particularly notable in the Hyllestad Schists, whereas F_2 folds are rarely preserved outside of the Basement Gneisses. Parts of the Upper Mafic Unit (UMU), especially near Mölmesdal, appear to be virtually undeformed, although usually exhibiting evidence of metamorphic events seen elsewhere in the study area. Correlation of tectonometamorphic episodes between units can be made with reasonable confidence from D_3 onwards; F_3 folds are numerous within most units and fold contacts between the Basement Gneisses, Mafic Units, and Hyllestad Schists (figure 2.21). All units also show evidence of a pre-D_3 event characterized by foliation development and syn- kinematic garnet growth. Mylonitic fabrics associated with contacts between, and within, major units may also have

formed during an equivalent pre-D_3 event involving emplacement of the Mafic Units and Hyllestad Schists onto the Western Gneiss Region (WGR).

Eclogite metamorphism in the Basement Gneisses is believed to be of Caledonian, and probably of Scandian (approximately 400Ma), age in common with recent Sm-Nd and U-Pb isotopic age determinations on country-rock eclogite masses in the coastal region of the WGR (e.g. Gebauer et al, 1985, Griffin and Brueckner, 1985). Examination of eclogites found in the study area shows that they have suffered deformation during D_2. An S_2 foliation is seen in the best-preserved eclogite assemblages, at Helleböstölane, and shadowy isoclinal fold outlines, presumed to be of F_2 type and deforming banding of the eclogitic mineralogy has also been found. A minimum pressure of about 15 kbar has been estimated for these rocks, at a temperature of 600 °C. Such conditions are consistent with regional isotherms calculated for the WGR (Griffin et al, 1985). Evidence of extreme pressures, such as relict coesite, which have been claimed for some eclogites from the Norwegian Caledonides, has not been found. Nevertheless, the estimated pressure of eclogite formation are well in excess of reasonable estimates for metamorphic conditions in the surrounding Basement Gneisses, or the overlying Mafic Units (fig. 7.1). Although eclogite occurrences in the study area are mainly towards the base of the exposed section, the thickness of the overlying gneisses is insufficient to account for the lack of high-pressure assemblages in the mafic units. The chemistry of the bulk of the rocks in the Mafic Units is very similar to that of the eclogites themselves and should be equally suited to the formation and preservation of eclogitic

assemblages. Evidence for high pressure conditions prior to D_2 exists in the breakdown of olivine + plagioclase to form orthopyroxene and spinel-bearing coronas. Such coronas probably formed at temperatures of about 850 °C, much higher than the eclogite metamorphism in the basement, and at pressures of about 7-9 kbar. Pressure estimates are lower by 6 kbar or so than for the eclogites and the present structural thickness of, at most, 3-4km which separates the occurrences does not account for such a large pressure interval.

If the Mafic Units were buried with the Basement Gneisses, to almost equal depths, then it must be assumed that they did not develop an eclogite mineralogy, or that all traces of such an event have been erased by subsequent amphibolite facies metamorphism. In view of the large volume of mafic rocks in the Mafic Units it would seem unlikely that all traces of high-pressure metamorphism can have been effaced, since even thoroughly amphibolitized eclogites in the Basement Gneisses can be recognized as such, due to the presence of amphibole-albite symplectites etc. Completely effective overprinting of eclogite assemblages could conceivably occur if they were only developed within shear zones, or as corona phases in gabbroic rocks - sites where subsequent amphibolitization has been particularly intense.

An alternative tectonic model is that the Mafic Units were emplaced, either individually or <u>en masse</u>, onto Basement Gneisses already containing high-pressure assemblages, and that the extensive development of amphibolite facies metamorphism in the eclogites, Basement Gneisses, and Mafic Units was related to such an event. This D_2 amphibolite facies event occurred under conditions of about 550 °C. P-T

estimates for the Basement Gneisses and Mafic Units based on thermobarometric calculations vary over a broad range, but it may be inferred that the Basement Gneisses and Mafic Units suffered similar grades of metamorphism during this and later events, and thus have shared a similar uplift path. Rocks providing well-constrained P-T data occur near the top of the UMU and limit pressures to about 5-6 kbar. In this model it is implied that high-pressure assemblages also existed within the Basement Gneisses, at least immediately adjacent to sites of eclogite metamorphism. Such assemblages have not been found, but Koons and Thompson (1985) have shown that eclogitic assemblages in non-mafic rock-types are less easily preserved than in mafic rocks. In addition, the presence of blastomylonitic shear zones within the Basement Gneisses suggests that eclogite-bearing gneisses may have been tectonically juxtaposed against other "basement" gneisses which have never been subjected to pressures greater than 8-10 kbar.

The presence of kyanite relicts in metasedimentary rocks infolded with dolerites and monzonites of the UMU at Löland are not necessarily an indication of particularly high-pressures of metamorphism, and may represent conditions of no more than about 6 kbar. Sillimanite occurs in the post-D_2 assemblage implying that pressures fell to less than about 5 kbar between D_2 and D_3, rather low compared with estimates based on barometry elsewhere in the Mafic Units.

In simplified terms, there is a general decrease in pressure (by about 6 to 9 kbar) and grade of metamorphism towards the west from Brensdal to the Hyllestad Arc in which peak metamorphic assemblages range from eclogite facies,

through amphibolite, to lower greenschist, over a structural thickness of only 10km or so. The lower grades of metamorphism generally represent later overprinting events. The lower parts of the Hyllestad Schists present an anomaly in this pattern. Although the western (and structurally higher) portion of this unit is of lower grade than the underlying Mafic Units, schists to the east and north of Hyllestad include assemblages which represent substantially higher pressures than assemblages in underlying rocks. The assemblage garnet-kyanite-staurolite-chloritoid occurs in schists from at least two locations. It is not clear from petrographic studies that these phases are in equilibrium in the matrix (owing mainly to disruption of mineral grains during "D_5" deformation), but evidence from garnet inclusions demonstrates the former co-existence of all four species. Studies by Vuichard and Ballèvre (1988) and Spear and Cheney (1989) in the KFMASH system both suggest that this assemblage is only stable at pressures in excess of 14 kbar, despite significant differences in their petrogenetic grids. Pressures of this order are also implied in the grid of Harte and Hudson (1979). Such high pressures are not ruled out by barometric calculations, which tend only to give minimum estimates, but the particular rock-types in question are closely associated with amphibolites and schists characteristic of only moderate pressures of metamorphism. However, there is plentiful field evidence for tectonic "shuffling" of individual rock units along extensional shear zones during D_5, and possibly during earlier episodes.

Although "eclogitic" metamorphism in pelites of the Hyllestad Schists is contemporaneous with, or earlier than,

formation of an S_2-type foliation, it cannot be stated confidently that this was the same "D_2" event recorded by, and post-dating the formation of, mafic eclogites in the Basement Gneisses. A possible alternative is that the eugeoclinal sediments of the Hyllestad Schists are "exotic" in origin and that high-grade metamorphism occurred in a different setting to eclogite metamorphism in the Basement Gneisses (as defined in this study) and, possibly, to the WGR.

The presence of mineral assemblages representing high-pressures of metamorphism (in excess of 14 kbar) early in the history of the Hyllestad Schists, which overlie the Mafic Units, would seem to suggest that the whole area has suffered burial to lower crustal levels, with widespread development of eclogite facies assemblages in supracrustal rocks. This is clearly inconsistent with the lack of evidence, discussed above, that the Mafic Units have suffered deep burial at any stage of their metamorphic history. Two models are discussed below in which an attempt is made to resolve apparent paradox of the absence of high-pressure assemblages in the Mafic Units together with the presence of eclogitic metapelites in the Hyllestad Schists.

The simplest model, in terms of the tectonic evolution, is that all the major units were emplaced together at an early stage of the Caledonian orogeny and have shared essentially the same burial and uplift path. Such a model has many attractive features. All the Caledonian deformation events seen in any one unit can be assumed to correlate directly with those of the other units. The eclogite facies mineral assemblages seen in the Basement Gneisses can be assumed to be coeval with eclogitic metapelites in the Hyllestad Schists.

The estimated P-T conditions for each are extremely similar (fig. 7.1) and both occurrences could be the result of A-type subduction of the WGR (Cuthbert et al, 1983). Syn- to post-D_2 garnet amphibolite grade metamorphism observed in all major units occurred as the result of a pervasive overprint during uplift and decompression. It has been suggested (Cuthbert et al, 1983) that the major Caledonian nappes, including the Jotun nappes, became detached from their root zones and were translated eastwards by gravity spreading, resulting in exhumation of imbricated basement rocks forming the WGR. Such a mechanism may account for part of the early uplift history of basement rocks. However, extensional tectonism appears to have been more important, at least during the later history of the field area, with extension directed towards the west or northwest along low-angle contacts (Norton, 1986, 1987, Chauvet et al, 1989). Extensional collapse of the orogen could also be responsible for the down-faulting of low-grade metapelites in the western part of the Hyllestad Schists onto high-pressure metapelites. It is possible that extensional tectonics (combined with rapid erosion, at least during the Devonian) were responsible for most of the uplift experienced by these high-pressure rocks, and that such extenson may have started prior to D_3. Norton (1986, 1987) has suggested that Devonian extension occurred along pre-existing contacts from an earlier compressional phase of tectonics. Earlier phases of extension may also have occurred along pre-existing blastomylonitic shear zones within the Basement Gneisses, with preferential uplift of the parts which have suffered deepest burial. This could partly explain why eclogitic assemblages are restricted in distribution even within the Basement

Gneisses. For instance, mafic dykes in parts of the unit close to eclogite occurrences do not show any signs of high-pressure metamorphism. Selverstone and Spear (1985) report a similar juxtaposition of rocks metamorphosed at different depths by thinning of the intervening section and differential uplift in the Tauern Window of the Eastern Alps. Extensional tectonism may have continued through D_3, accounting for the preponderance of northwestward vergence in F_3 folds to the west of Brensdal. The extensional shear zones assigned to D_5 which are seen mainly to the west of Leirvik, and are best developed in the Hyllestad Schists, would represent the latest phase of extension, at the highest crustal levels. This phase may be as young as Middle Devonian in age according to models for the formation of Solund, Håsteinen, Kvamshesten, and Hornelen basins (Hossack, 1984, Norton, 1986, 1987).

The main problem with the above model is the absence of evidence for high-pressure metamorphism in the Mafic Units. As discussed above and in chapter 5, the early coronas seen in the UMU are not eclogitic in composition (cf coronas described in Mörk, 1986), but rather an early feature formed either during, or shortly following, the final stages of crystallization of the gabbro (Joesten, 1986, Ashworth, 1986). The pressures of formation of these coronas, although in excess of 5 kbar, are unlikely to have been higher than about 9 kbar and certainly less than 15 kbar (as estimated for the eclogites in the Basement Gneisses). If this model is accepted, it must be assumed that the Mafic Units, although buried to lower crustal levels, did not develop eclogite facies assemblages or that where such assemblages were developed they were thoroughly overprinted by garnet amphibolite assemblages during uplift.

This theory cannot be ruled out since occurrences are known from the Norwegian Caledonides (e.g. Mörk, 1986) where gabbros are only partially transformed to eclogite assemblages and, in the Bergen Arcs, eclogitization of gabbros and anorthosites is developed only in shear zones. Such shear zones might also be expected to suffer reactivation during later deformation, and to act as pathways for fluids and, as such, show the most complete overprinting of eclogite facies assemblages (if developed) during the uplift history of the area. Nevertheless it is surprising that, in such a large volume of rock, mostly of similar bulk chemistry to mafic material within the Basement Gneisses, that omphacitic clinopyroxene has not been found (even as inclusions in garnet porphyroblasts). Kyanite seen in schists infolded with the UMU at Löland could be a relict of a high-pressure metamorphism in the Mafic Units, but equally may only represent pressures in excess of about 5-6 kbar. In addition the P-T estimates based on geothermo-barometric calculations suggest that peak temperatures experienced by different rock units during D_2 were generally similar to or less than temperatures of high-pressure metamorphism. Garnet zoning profiles for rocks from the Mafic Units do not show a large chemical variation but do suggest that D_2 garnet amphibolite metamorphism was a prograde event (if only over a few tens of degrees). Possible explanations are that the zoning is a relict of the pre-burial prograde path, or that the area suffered a thermal perturbation during uplift

If, on the other hand, the Mafic Units are interpreted as never having suffered burial to pressures greater than 9 kbar, an alternative model is required, involving a more complex

history to allow the superposition of high-pressure Hyllestad Schists over the Mafic Units. An alternative model is presented below.

(1) High-pressure assemblages were developed in eugeoclinal pelites, in an active subduction setting, possibly located on the Laurentian margin of the Iapetus Ocean, or an island arc offshore of the Baltic margin, during the Caledonian orogeny. If this is the case, the similarity in P-T conditions experienced by parts of the Hyllestad Schists and eclogites in the Basement Gneisses must be regarded as coincidental.

(2) The high-pressure and greenschist facies pelites and granites (the "Hyllestad Schists") were thrust onto the WGR, during easterly-directed A-subduction of the Baltic margin, at a high structural level.

(3) The underthrusting of the WGR beneath the Greenland plate was responsible for the development of eclogite facies assemblages in deeply buried mafic rocks in the Basement Gneisses, at pressures of about 15 kbar. The timing of this event with respect to high-pressure metamorphism in the Hyllestad Schists is not known. Continent-continent collision also resulted in the stacking of high-pressure Hyllestad Schists at some structural position above the Mafic Units which were in turn superimposed over the Basement Gneisses. Prograde zoning of garnets in the Mafic Units may represent a metamorphic event related to this emplacement and of early D_2 age.

(4) Exhumation of the Basement Gneisses was caused by extension towards the west. In the field area, differential uplift of parts of the Basement Gneisses and the Mafic Units brought these two units into (broadly) their current

structural relationship and was accompanied by amphibolite facies metamorphism at about 550 °C, and between about 5-9 kbar. This event corresponds to D_2. Schists in the UMU show evidence of limited decompression (kyanite-sillimanite transition). For the eclogites, P-T estimates suggest decompression in the pressure interval 15-8 kbar occurred at temperatures of at least 600 °C, and was either nearly adiabatic or involved a relatively small initial temperature increase of about 30-50 °C.

(5) Continued extension into the Devonian resulted in rapid deposition in actively extending basins, with mylonitic fabrics developed in low competence units beneath the basal contact.

Further evidence is needed to constrain the relationship of the early compressional event responsible for emplacement of the Caledonian nappes to the deformation in the Mafic Units and Hyllestad Schists. The provenance of the Mafic Units and Hyllestad Schists has yet to be determined. The problem might be partly resolved by isotopic dating of tectonic and metamorphic episodes. Attempts to constrain the age of the Hyllestad Schists by Rb/Sr dating of the granitic intrusions were unsuccessful. Plutonic rock-types from the UMU have a wide range of compositions, from granites to gabbros, and it may be possible to determine the age of intrusion and subsequent metamorphic episodes. Detailed studies of the geochemistry of the Mafic Units, particularly little altered parts of the UMU, would allow comparisons with geochemical studies of the Jotun Nappe Complex and other units (e.g. Emmett, 1985).

A detailed study of kinematic indicators in the coastal

regions of Sognefjord would help to determine the extent and timing of extensional tectonism with respect to metamorphic events and the development of Devonian depocentres, and may allow them to be distinguished from early compressional episodes. Quartzose rocks suitable for analysis of quartz crystallographic c-axis orientations are probably fairly common in the Basement Gneisses, and possibly also the Hyllestad Schists (although most rock-types sampled in this study tended to be too micaceous). Feldspar porphyroclasts are also fairly common in parts of the Basement Gneisses and Middle Mafic Unit, and frequently show asymmetric features which could be used to determine shear sense. The limited analysis of these which was within the scope of this project yielded rather inconsistent results, but a detailed study relating porphyroblast growth and rotation to tectonic and metamorphic events should provide much useful information. These data could provide tests for the tectonic models suggested to account for the timing of the assembly of major structural units in the Lavik-Hyllestad area.

According to Kildal (1970), rock-types related to the Hyllestad Schists extend northwards and westwards beyond the boundaries of the present study area. More extensive sampling may reveal other assemblages which could be used to constrain petrogenetic grids for high-pressure pelites, such as those recently proposed by Vuichard and Ballèvre (1988), and Spear and Cheney (1989). A more extensive study could also yield further information on the reversal of partitioning of Fe and Mg between staurolite and garnet (from [garnet X_{Mg}] < [staurolite X_{Mg}] to [staurolite X_{Mg}] < [garnet X_{Mg}]) and on the role of Zn in staurolite from high-pressure assemblages.

REFERENCES

AALSTAD, I., ÅHM, K., HÅBREKKE, H., & KIHLE, O., 1977, Aeromagnetic investigations along the Norwegian geotraverse. In Heier, K.S. (ed) The Norwegian Geotraverse Project. 77-97

AFIFI, A.M. & ESSENE, E.J., 1988, MINFILE: A microcomputer program for storage and manipulation of chemical data on minerals. Am. Mineral. 73 446-448

ANDRESEN, A. & FÆRSETH, R., 1982, An evolutionary model for the southwest Norwegian Caledonides. Am. J. Sci. 282 756-782

ASHWORTH, J.R., 1986, The role of magmatic reaction, diffusion, and annealing in the evolution of coronitic microstructure in troctolitic gabbro from Risör, Norway: a discussion. Mineralog. Mag. London. 50 469-473

ASHWORTH, J.R. & MCLELLAN, E.R., 1985, Textures. In Ashworth, J.R. (ed) Migmatites. Blackie & Son Ltd., Glasgow. 180-203

ASKVIK, H., 1972, Red muscovite from a metasedimentary gneiss, Sogn, West Norway. Nor. geol. Unders. 273 7-12

AUSTRHEIM, H. & GRIFFIN, W.L., 1985, Shear deformation and eclogite formation within granulite-facies anorthosites of the Bergen Arcs, western Norway. Chem. Geol. 50 267-281

BAKER, A.J., 1985, Metamorphic studies in the Scottish Highlands. D.Phil. thesis, Oxford.

BALLEVRE, M., KIENAST, J.R., & PAQUETTE, J.L., 1987, Le métamorphism éclogitique dans la nappe hercynienne de Champtoceaux (Massif Armoricain). C.r. de l'Acad. des Sci. Paris. (II) 305 127-131

BANHAM, P.H., GIBBS, A.D., & HOPPER, F.W.M., 1979, Geological evidence in favour of a Jotunheimen Caledonian suture. Nature. London. 277, 289-291

BASSETT, M.G., 1985, Silurian stratigraphy and facies development in Scandinavia. In Gee & Sturt (eds) The Caledonide Orogen - Scandinavia and Related Areas, John Wiley & Sons Ltd. 283-292

BATTEY, M.H. & McRITCHIE, W.D., 1973, A geological traverse across the pyroxene-granulites of Jotunheimen in the Norwegian Caledonides. Nor. geol. Tiddskr. 53, 237-265

BELL, T.H., 1986, Foliation development and refraction in metamorphic rocks: reactivation of earlier foliations and decrenulation due to shifting patterns of deformation partitioning. J.metamorphic Geol. 4 421-444

BELL, T.H., RUBENACH, M.J., & FLEMING, P.D., 1986, Porphyroblast nucleation, growth and dissolution in regional metamorphic rocks as a function of deformation partitioning during foliation development. J.metamorphic Geol. 4 37-67

BERMAN, R.G., BROWN, T.H., & GREENWOOD, H.J., 1985, An internally consistent thermodynamic data base for minerals in the system Na_2O-K_2O-CaO-MgO-FeO-Fe_2O_3-Al_2O_3-SiO_2-TiO_2-H_2O-CO_2. At. Energy Can. Techn. Rep. 377 1-62

BISHOP, F.C., 1980, The distribution of Fe^{2+} and Mg betwen coexisting ilmenite and pyroxene with applications to geothermometry. Am. J. Sci. 280 46-77

BOHLEN, S.R. & BOETTCHER, A.L., 1982, The quartz-coesite transition: a precise determination and the effects of other components. J. geophys. Res. 87 749-756

BOHLEN, S.R. & LIOTTA, J.J., 1986, A barometer for garnet amphibolites and garnet granulites. J. Petrol. 27 1025-1034

BOHLEN, S.R., WALL, V.J., & BOETTCHER, A.L., 1983, Experimental investigation and geological application of equilibria in the system FeO-TiO_2-Al_2O_3-SiO_2-H_2O. Am. Mineral. 68 1049-1058

BOYER, S.E. & ELLIOTT, D., 1982, Thrust Systems. Bull. Am. Assoc. Petrol. Geol. 66 (9) 1196-1230

BRASTAD, K., 1985, Relationships between peridotites, anorthosites and eclogites in Björkedalen, western Norway. In Gee & Sturt (eds) The Caledonide Orogen - Scandinavia and Related Areas, John Wiley & Sons Ltd. 859-872

BROCH, O.A., 1964, Age determination of Norwegian minerals up to March 1964. Nor. geol. Unders. 228 84-114

BROWN, W.L. & PARSONS, I., 1981, Towards a more practical two-feldspar geothermometer. Contrib. Mineral. Petrol. 76 369-377

BRUECKNER, H.K., 1979, Precambrian ages from Geiranger-Tafjord-Grotli area of the Basal Gneiss Region, west Norway. Nor. geol. Tiddskr. 59, 141-153

BRYHNI, I., 1964, Relasjonen mellom senkaledonsk tectonikk of sedimentasjon ved Hornelens of Håsteinens devon. Nor. geol. Unders. 223, 10-25

BRYHNI, I., 1966, Reconnaissance studies of gneisses, ultrabasites, eclogites and anorthosites in outer Nordfjord, western Norway. Nor. geol. Unders. 241 1-68

BRYHNI, I., 1973, Radiometriske dateringer av bergater of mineraler i Gneis-regionen. Naturen 97, 223-230

BRYHNI, I., 1978, Flood deposits in the Hornelen basin, west Norway. Nor. geol. Tiddskr. 58, 273-300

BRYHNI, I. & GRIMSTAD, E., 1970, Supracrustal and infracrustal rocks in the gneiss region of the Caledonides west of Breimsvatn. Nor. geol. Unders. 266 105-140

BRYHNI, I. & SKJERLIE, F.J., 1975, Syndepositional tectonism in the Kvamshesten district (Old Red Sandstone), western Norway. Geol. Mag. 112 593-600

BRYHNI, I. & STURT, B.A., 1985, Caledonides of southwestern Norway. In Gee & Sturt (eds) The Caledonide Orogen - Scandinavia and Related Areas, John Wiley & Sons Ltd. 89-107

CARMICHAEL, D.M., 1969, On the mechanism of prograde metamorphic reactions in quartz-bearing pelitic rocks. Contrib. Mineral. Petrol. 20 244-267

CARSWELL, D.A., 1968, Picritic magma-residual dunite relationships in garnet peridotite at Kalskaret near Tafjord, south Norway. Contrib. Mineral. Petrol. 19 97-124

CARSWELL, D.A., 1973, The age and status of the basal gneiss complex of north-west southern Norway. Nor. geol. Tiddskr. 53 65-78

CARSWELL, D.A., 1981, Clarification of the petrology and occurrence of garnet lherzolites, garnet websterites and eclogite in the vicinity of Rödhaugen, Almklovdalen, West Norway. Nor. geol. Tiddskr. 61 249-260

CARSWELL, D.A. & CUTHBERT, S.J., 1986, Eclogite facies metamorphism in the lower continental crust. In Dawson, J.B., Carswell, D.A., Hall, J., & Wedepohl, K.H. (eds), The Nature of the lower continental crust. Geol. Soc. Spec. Publ. 24 193-209

CARSWELL, D.A., HARVEY, M.A., & AL-AMMAN, A., 1983, The petrogenesis of contrasting Fe-Ti and Mg-Cr garnet peridotite types in the high grade gneiss complex of Western Norway. Bull. Mineral. 106, 727-50

CHAUVET, A., et al, 1989, Terra Abstracts (in press).

CHAUVET, A. & SERANNE, M., 1988, Microtectonic evidence of Devonian extensional westward shearing in southwestern Norway. In Gayer, R. (ed) The Caledonide Geology of Scandinavia. Graham & Trotman, 245-254

COLEMAN, R.C., LEE, D.E., BEATTY, L.B., & BRANNOCK, W.W., 1965, Eclogites and eclogites: their difference and similarities. Bull. geol. Soc. Am. 76 483-508

CORFU, F., 1980, U-Pb and Rb-Sr systematics in a polyorogenic segment of the Precambrian shield, central southern Norway. Lithos 13 305-323

COX, K.G., BELL, J.D., & PANKHURST, R.J., 1979, The Interpretation of Igneous Rocks. Allen and Unwin, London.

CUTHBERT, S.J., HARVEY, M.A., & CARSWELL, D.A., 1983, A tectonic model for the metamorphic evolution of the basal gneiss complex, western South Norway. J. metamorphic Geol. 1 63-90

DAHLSTROM, C.D.A., 1970, Structural geology in the eastern margin of the Canadian Rocky Mountains. Bull. Can. Pet. Geol. 18, 332-406

DALRYMPLE, G.B., 1979, Critical tables for conversion of K-Ar ages from old to new constants. Geology. 7, 558-560

DEER, W.A., HOWIE, R.A., ZUSSMAN, J., 1978, Rock-forming minerals, Volume 2A: Single-chain silicates - 2nd edition. Halsted Press, John Wiley & Sons, New York.

DEER, W.A., HOWIE, R.A., ZUSSMAN, J., 1982, Rock-forming minerals, Volume1A: Orthosilicates - 2nd edition. Longman.

DEWEY, J.F., 1969, Evolution of the Appalachian/Caledonian Orogen. Nature. London. 222 124-129

DIETLER, T.N., KOESTLER, A.G., & MILNES, A.G., 1985, A preliminary structural profile through the Western Gneiss Complex, Sognefjord, southwestern Norway. Nor. geol. Tiddskr. 65 233-235

DROOP, G.T.R., 1981, Alpine metamorphism of pelitic schists in the South-East Tauern Window, Austria. Schweiz. mineral. petrogr. Mitt. 61 237-273

DYMEK, R.F., 1983, Titanium, aluminium and interlayer cation substitutions in biotite from high-grade gneisses, West Greenland. Am. Mineral. 68 880-889

ELLIS, D.J., & GREEN, D.H., 1979, An experimental study of the effect of Ca upon garnet-clinopyroxene Fe-Mg exchange equilibria. Contrib. Mineral. Petrol. 71 13-22

EMMETT, T.F., 1985, The trace element geochemistry of some high-grade Bergen-Jotun kindred gneisses from the Jotun Nappe around Gjendebu, central southern Norway. J.metamorphic Geol. 3 119-136

ESKOLA, P., 1921, On the eclogites of Norway. Vidensk.-Selsk. Skr. I. 8 1-118

ESSENE, E.J. & BOHLEN, S.R. 1985, New garnet barometers in the system CaO-FeO-Al_2O_3-SiO_2-TiO_2 (CFAST). (abs), Eos. 66 386

FERRY, J.M. & SPEAR, F.S., 1978, Experimental calibration of the partitioning of Fe and Mg between garnet and biotite. Contrib. Mineral. Petrol. 66 113-117

FOSTER, C.T., 1982, Textural variation of sillimanite segregations. Can. Mineral. 20 379-392

FURNES, H., MITCHELL, J.G., ROBINS, B., RYAN, P., & SKJERLIE, F.J., 1982, Petrography and geochemistry of peralkaline, ultrapotassic syenite dykes of Middle Permian age, Sunnmöre, W Norway. Nor. geol. Tiddskr. 62 147-159

GANGULY, J., 1972, Staurolite stability and related parageneses: theory, experiments, and applications. J. Petrol. 13 335-365

GANGULY, J. & KENNEDY, G.C., 1974, The energetics of natural garnet solid solutions. Contrib. Mineral. Petrol. 48 137-148

GANGULY, J. & SAXENA, S.K., 1984, Mixing properties of aluminosilicate garnets: constraints from natural and experimental data, and applications to geothermobarometry. Am. Mineral. 69 88-97

GASPARIK, T., & LINDSLEY, D.H., 1980, Phase equilibria at high pressure of pyroxenes containing monovalent and trivalent ions. In Prewitt, C. T. (ed) Reviews in Mineralogy. Volume 7. Pyroxenes 309-339. Mineral. Soc. Am.

GEBAUER, D., LAPPIN, M.A., GRÜNENFELDER, M., KOESTLER, A., & WYTTENBACH, A., 1982, Age and origin of some Norwegian eclogites: a U-Pb zircon and REE study. (abs) Terra Cognita 2 323

GEBAUER, D., LAPPIN, M.A., GRÜNENFELDER, M. & WYTTENBACH, A., 1985, The age and origin of some Norwegian eclogites: a U-Pb zircon and REE study. Chem. Geol. 52 227-247

GEE, D.G., 1978, Nappe displacement in the Scandinavian Caledonides. Tectonophysics. 47, 393-419

GEE, D.G., KUMPULAINEN, R., ROBERTS, D., STEPHENS, M.B., THON, A., & ZACHRISSON, E., 1985, Scandinavian Caledonides Tectonostratigraphic Map. Sver. geol. Unders. Ser. Ba NR 35. In Gee & Sturt (eds) The Caledonide Orogen - Scandinavia and Related Areas, John Wiley & Sons Ltd.

GEE, D.G. & ROBERTS, D., 1983, Timing of deformation in the Scandinavian Caledonides. In Schenk, P.E. (ed) Regional Trends in the Geology of the Appalachian-Caledonian-Hercynian-Mauritanide Orogen. D.Reidel Publ. Co., 279-292

GHENT, E.D. & STOUT, M.Z., 1981, Geobarometry and geothermometry of plagioclase-garnet-muscovite assemblages. Contrib. Mineral. Petrol. 76 92-97

GJELSVIK, T., 1952, Metamorphosed dolerites in the gneiss area of Sunnmöre on teh west coast of southern Norway. Nor. geol. Tiddskr. 30 33 -134

GOLDMAN, D. & ALBEE, A.L., 1977, Correlation of Mg/Fe partitioning between garnet and biotite with $^{18}O/^{16}O$ partitioning between quartz and magnetite. Am. J. Sci. 277 750-767

GOLDSCHMIDT, V.M., 1912, Die kaledonische Deformation der südnorwegischen Urbergstafel. Skr. Norske Vidensk. Selsk. Christiania Mat. nat. Kl 9 1-11

GOLDSCHMIDT, V.M., 1916, Übersicht der Eruptivgesteine im kaledonischen Gebierge zwischen Stavanger und Trondhjem. Skr. Norske Vidensk. Selsk. Christiania Mat. nat. Kl 2 1-140

GRAHAM, C.M. & POWELL, R., 1984, A garnet-hornblende geothermometer: calibration, testing, and application to the Pelona Schist, Southern California. J. metamorphic Geol. 2 13-31

GREEN, T.H., & HELLMAN, P.L., 1982, Fe-Mg partitioning between coexisting garnet and phengite at high pressure, and comments on a garnet-phengite geothermometer. Lithos 15 253-266

GRIFFIN, W.L., 1987, 'On the eclogites of Norway' - 65 years later. Mineralog. Mag. London. 51 333-343

GRIFFIN, W.L., AUSTRHEIM, H., BRASTAD, K., BRYHNI, I., KRILL, A.G., KROGH, E.J., MÖRK, M.B.E., QVALE, H., TÖRUDBAKKEN, B., 1985, High-pressure metamorphism in the Scandinavian Caledonides. In Gee & Sturt (eds) The Caledonide Orogen - Scandinavia and Related Areas, John Wiley & Sons Ltd. 783-802

GRIFFIN, W.L. & BRUECKNER, H.K., 1980, Caledonian Sm-Nd ages and a crustal origin for Norwegian eclogites. Nature. London. 285 319-321

GRIFFIN, W.L. & BRUECKNER, H.K., 1985, REE, Rb-Sr and Sm-Nd studies of Norwegian eclogites. Chem Geol 52 249-271

GRIFFIN, W.L. & CARSWELL, D.A., 1985, In situ metamorphism of Norwegian eclogites: an example. In Gee & Sturt (eds) The Caledonide Orogen - Scandinavia and Related Areas, John Wiley & Sons Ltd. 813-822

GRIFFIN, W.L. & HEIER, K.S., 1969, Parageneses of garnet, Lofoten-Vesteraalen, Norway. Contrib. Mineral. Petrol. 23 89-116

GRIFFIN, W.L. & HEIER, K.S., 1973, Petrological implications of some corona structures. Lithos. 6 315-335

GRIFFIN, W.L. & QVALE, H., 1985, Superferric eclogites and the crustal origin of garnet peridotites. In Gee & Sturt (eds) The Caledonide Orogen - Scandinavia and Related Areas, John Wiley & Sons Ltd. 803-812

GRIFFIN, W.L. & RÅHEIM, A., 1973, Convergent metamorphism of eclogites and dolerites, Kristiansund area, Norway. Lithos. 6 21-40

GUIDOTTI, C.V., 1984, Micas in metamorphic rocks. In Bailey, S.W. (ed) Reviews in Mineralogy, Volume 13: Micas, 357-467 Mineral. Soc. Am.

HARLEY, S.L. & GREEN, D.H., 1982, Garnet-orthopyroxene barometry for granulites and peridotites. Nature. London 300 697-701

HARTE, B., 1975, Determination of a pelite petrogenetic grid for the Eastern Scottish Dalradian. Carnegie Institute of Washington Year Book, 1974-75. 438-446

HARTE, B. & HUDSON, N.F.C., 1979, Pelite facies series and the temperatures and pressures of Dalradian metamorphism in east Scotland. In Harris, A.L., Holland, C.H., & Leake, B.E. (eds), The Caledonides of the British Isles - Reviewed. Spec. Publ. Geol. Soc. London 8 324-332

HEIM, M., SCHARER, U., & MILNES, A.G., 1977, The nappe complex in the Tyin-Bygdin-Vang region, central southern Norway. Nor. geol. Tiddskr. 57 171-178

HEZNER, L., 1903, Ein Beitrag zur Kenntnis der Eklogite und Amphibolite, mit besonderer Berücksichtigung der Vorkommnisse des mittleren Ötztales. Min. Petr. Mitt. 22 437-471 & 505-580

HODGES, K.V. & CROWLEY, P.D., 1985, Error estimation and empirical geothermobarometry for pelitic systems. Am. Mineral. 70 702-709

HODGES, K.V. & ROYDEN, L., 1984, Geologic thermombarometry of retrograded metamorphic rocks: an indication of the uplift trajectory of a portion of the Northern Scandinavian Caledonides. J. geophys. Res. 89 7077-7090

HODGES, K.V. & SPEAR, F.S., 1982, Geothermometry, geobarometry and the Al_2SiO_5 triple point at Mt. Moosilauke, New Hampshire. Am. Mineral. 67 1118-1134

HOLDAWAY, M.J., 1971, Stability of andalusite and the aluminium silicate phase diagram. Am. J. Sci. 271 97-131

HOLLAND, T.J.B., 1979, Experimental determination of the reaction paragonite=jadeite+kyanite+H_2O, and internally consistent thermodynamic data for part of the system Na_2O-Al_2O_3-SiO_2-H_2O, with applications to eclogites and blueschists. Contrib. Mineral. Petrol., 68, 293-301

HOLLAND, T.J.B., 1980, The reaction albite-jadeite+quartz determined experimentally in the range 600-1200 °C. Am. Mineral. 65 129-134

HOLLAND, T.J.B., & POWELL, R., "THERMO" pers. comm. July, 1988

HOLLAND, T.J.B., & POWELL, R., 1985, An internally consistent dataset with uncertainties and correlations: 2. Data and results. J. metamorphic Geol. 3 343-370

HOLLAND, T.J.B. & RICHARDSON, S.W., 1979, Amphibole zonation in metabasites as a guide to the evolution of metamorphic conditions. Contrib. Mineral. Petrol. 70 143-148

HOSSACK, J.R., 1984, The geometry of listric growth faults in the Devonian basins of Sunnfjord, W Norway. J. geol. Soc. London 141 629-638

HOSSACK, J.R. & COOPER, M.A., 1986, Collision tectonics in the Scandinavian Caledonides. In Coward, M.P., & Ries, A.C. (eds) Collision Tectonics. Geol. Soc. Spec. Publ. 19 287-304

HYNES, A. & FOREST, R.C., 1988, Empirical garnet-muscovite geothermometry in low-grade metapelites, Selwyn Range (Canadian Rockies). J. metamorphic Geol. 6 297-309

HÖISÆTER, T., 1971, Thrust Devonian sediments in the Kvamshesten area, Western Norway. Geol. Mag. 108 287-292

JACOBSEN, S.B. & WASSERBURG, G.J., 1980, Nd and Sr isotopes of the Norwegian garnet peridotites and eclogites. EOS 61, 389

JAMTVEIT, B., 1987a, Metamorphic evolution of the Eiksunddal eclogite complex, Western Norway, and some tectonic implications. Contrib. Mineral. Petrol. 95 82-99

JAMTVEIT, B., 1987b, Magmatic and metamorphic controls on chemical variations within the Eiksunddal eclogite complex, Sunnmöre, western Norway. Lithos, 20 369-389

JOESTEN, R., 1986, The role of magmatic reaction, diffusion, and annealing in the evolution of coronitic microstructure in troctolitic gabbro from Risör, Norway. Mineralog. Mag. London. 50 441-467

KARABINOS, P., 1985, Garnet and staurolite producing reactions in a chlorite-chloritoid schist. Contrib. Mineral. Petrol. 90 262-275

KILDAL, E.S. 1970, Geologisk kart over Norge, berggrunnskart. Målöy, 1:250 000, norsk utgave. Nor. geol. Unders.

KOLDERUP, C.F., 1916, Bulandets og Værlandets konglomerat og sandstensfelt. Bergens. Mus. Aarbog. 1915-1916. 3 1-6

KOLDERUP, C.F., 1923, Kvamshestens devonfelt. Bergens. Mus. Aarbog. 1920-21. 4 1-96

KOLDERUP, C.F., 1925, Haasteinens devonfelt. Bergens. Mus. Aarbog. 1923-24. 11 1-32

KOLDERUP, C.F., 1926, Solunds devonfelt. Bergens. Mus. Aarbog. 1924-1925. 8 1-73

KOLDERUP, N-H., 1928, Fjellbygningen i kystströket mellom Nordfjord of Sognefjord. Bergens. Mus. Aarbog. 1928. 1 1-222

KOLDERUP, N-H., 1952, The Age of Gneisses and Migmatites in the "North-West Block" of Southern Norway. Trans. geol. Soc. Edinburgh. 15 (Campbell Volume) 234-240

KOONS, P.O. & THOMPSON, A.B., 1985, Non-mafic rocks in the greenschist, blueschist and eclogite facies. Chem. Geol. 50 3-30

KROGH, E.J., 1977a, Evidence for a Precambrian continent-continent collision in western Norway. Nature. London. 267 17-19

KROGH, E.J., 1977b, Crustal and in situ origin of Norwegian eclogites. Reply. Nature. London. 269, 730

KROGH, E.J., 1980, Geochemistry and petrology of glaucophane-bearing eclogites and associated rocks from Sunnfjord, western Norway. Lithos 13, 355-380

KROGH, E.J., 1982, Metamorphic evolution of Norwegian country-rock eclogites as deduced from mineral inclusions and compositional zoning in garnets. Lithos 15 305-321

KROGH, E.J., MYSEN, B.O., & DAVIS, G.L., 1974, A Palaeozoic age for the primary minerals of a Norwegian eclogite. Carnegie Inst. Wash. Yearb., 73 575-576

KROGH, E.J. & RÅHEIM, 1978, Temperature and pressure dependence of Fe-Mg partitioning between garnet and phengite, with particular reference to eclogites. Contrib. Mineral. Petrol. 66 75-80

KULLERUD, L., TÖRUDBAKKEN, B.O., & ILEBEKK, S., 1986, A compilation of radiometric age determinations from the Western Gneiss Region, South Norway. Nor. geol. Unders. 406 17-42

LAIRD, J. & ALBEE, A.L., 1981, High-pressure metamorphism in mafic schist from Northern Vermont. Am. J. Sci. 281 97-126

LAPPIN, M.A., 1966, The field relationships of basic and ultrabasic masses in the basal gneiss complex of Stadlandet and Almklovdalen, Nordfjord, northwestern Norway. Nor. geol. Tiddskr. 46 439-495

LAPPIN, M.A. & SMITH, D.C., 1978, Mantle-equilibrated eclogite pods from the Basement Gneisses of the Selje district, Western Norway. J.Petrol. 19 530-584

LAPPIN, M.A. & SMITH, D.C., 1981, Carbonate, silicate and fluid relationships in eclogites, Selje district and environs, SW Norway. Trans. R. Soc. Edinburgh. 72 171-193

LEAKE, B.E., 1978, Nomenclature of amphiboles. Am. Mineral. 63 1023-1052

LE BAS, M.J., LE MAITRE, R.W., STRECKEISEN, A., & ZANETTON, B., 1986, A chemical classification of volcanic rocks based on the total alkali-silica diagram. J. Petrol. 27 745-750

LINDSLEY, D.H., 1983, Pyroxene thermometry. Am. Mineral. 68 477-493

LINDSLEY, D.H. & DIXON, S.A., 1976, Diopside-enstatite equilibria at 850-1400 °C, 5-35 kbar. Am. J. Sci. 276 1285-1301

LIOU, J.G., KUNIYOSHI, S., & ITO, K., 1974, Experimental studies of the phase relations between greenschist and amphibolite in a basaltic system. Am. Mineral. 274 613-632

MCDOUGALL, I. & GREEN, D.H., 1964, Excess radiogenic argon in pyroxenes and isotopic ages on minerals from Norwegian eclogites. Nor. geol. Tiddskr. 44 183-196

MCKERROW, W.S., DEWEY, J.F., & SCOTESE, C.R., 1989, The Ordovician and Silurian development of the Iapetus Ocean. Palaeontology. In press.

MCLELLAN, E.L., 1983, Contrasting textures in metamorphic and anatectic migmatites: an example from the Scottish Caledonides. J. metamorphic Geol. 1 241-262

MASSONE, H. & SCHREYER, W., 1987, Phengite geobarometry based on the limiting assemblage with K-feldspar, phlogopite, and quartz. Contrib. Mineral. Petrol. 96 212-224

MEARNS, E.W., 1986, Sm-Nd ages for Norwegian garnet peridotite. Lithos 19 269-278

MEARNS, E.W. & LAPPIN, M.A., 1982, A Sm-Nd isotopic study of 'internal' and 'external' eclogites, garnet lherzolites and grey gneiss from Almklovdalen, western Norway. (abs) Terra Cognita 2 324

MILNES, A.G. & KOESTLER, A.G., 1985, Geological structure of Jotunheimen, southern Norway (Sognefjell-Valdres cross-section). In Gee & Sturt (eds) The Caledonide Orogen - Scandinavia and Related Areas, John Wiley & Sons Ltd.

MITCHELL, C., 1988, Petrology and geochemistry of basaltic rocks of the Falkland Islands and Deccan Traps (India). Unpubl. D.Phil. Thesis. University of Oxford.

MIYASHIRO, A. & SEKI, Y., 1958, Enlargement of the composition field of epidote and piemontite with rising temperature. Am. J. Sci. 256 423-430

MOHR, D.W., BARNETT, R.L., & MICHIE, J., 1986, Chemical processes and migration of elements during retrogression of a staurolite-zone assemblage in western North Carolina. Contrib. Mineral. Petrol. 92 400-411

MYKKELTVEIT, S., HUSEBYE, E.S., & OFTEDAHL, C., 1980, Subduction of the Iapetus Ocean crust beneath the Möre Gneiss Region, southern Norway. Nature. London. 288 473-475

MYSEN, B. & GRIFFIN, W.L., 1973, Pyroxene stoichiometry and the breakdown of omphacite. Am. Mineral. 58 60-63

MYSEN, B.O. & HEIER, K.S., 1972, Petrogenesis of eclogites in high grade metamorphic gneisses, exemplified by the Hareidlandet eclogite, western Norway. Contrib. Mineral. Petrol. 36 73-94

MÖRK, M.B.E., 1985a, A gabbro to eclogite transition on Flemsöy, Sunnmöre, SW-Norway. Chem. Geol. 50 283-310

MÖRK, M.B.E., 1985b, Incomplete high P-T metamorphic transitions within the Kvamsöy pyroxenite complex, west Norway: a case study of disequilibrium. J. metamorphic Geol. 3 245-264

MÖRK, M.B.E., 1986, Coronite and eclogite formation in olivine gabbro (Western Norway): reaction paths and garnet zoning. Mineralog. Mag. London. 50 417-426

MÖRK, M.B.E., KULLERUD, K., & STABEL, A., 1988, Sm-Nd dating of Seve eclogites, Norrbotten, Sweden - Evidence for early Caledonian (505Ma) subduction. Contrib. Mineral. Petrol. 99 344-351

MÖRK, M.B.E. & MEARNS, E.W., 1986, Sm-Nd isotopic dating of minerals and whole-rocks from gabbros showing different degree of transition to eclogite. Lithos. 19 255-267

NEUMANN, E-R., 1976, Two refinements for the calculation of structural formulae for pyroxenes and amphiboles. Nor. geol. Tiddskr. 56 1-6

NEUMANN, H., 1960, Apparent ages of Norwegian minerals and rocks. Nor. geol. Tiddskr. 40, 173-191

NEWTON, R.C. & PERKINS, D., 1982, Thermodynamic calibration of geobarometers based on the assemblages garnet-plagioclase-orthopyroxene (clinopyroxene)-quartz. Am. Mineral. 67 203-222

NILSEN, T.H., 1968, The Relationship of Sedimentation to Tectonics in the Solund Devonian District of southwestern Norway. Nor. geol. Unders. 259 106pp.

NILSEN, T.H., 1973, The relation of joint patterns to the formation of fjords in western Norway. Nor. geol. Tiddskr. 53 183-194

NORTON, M.G., 1986, Late Caledonide Extension in Western Norway: A response to extreme crustal thickening. Tectonics 5 195-204

NORTON, M.G., 1987, The Nordfjord-Sogn Detachment, W. Norway. Nor. geol. Tiddskr. 67 93-106

NORTON, M.G., WILKS, W.J., & CUTHBERT, S.J., 1989, Palaeomagnetism, magnetic fabric and the structural style of the Hornelen Old Red Sandstone, western Norway. Discussion. J. geol. Soc. London (in press)

O'HARA, M.J., 1976, Origin of the Norwegian Eclogites. Progr. Expt. Petrol. NERC 3 252

O'HARA, M.J. & MERCY, E.L.P., 1963, Petrology and petrogenesis of some garnetiferous peridotites. Trans. R. Soc. Edinburgh.65 251-314

O'HARA, M.J. RICHARDSON, S.W., & WILSON, G., 1971, Garnet-peridotite stability and occurrence in crust and mantle. Contrib. Mineral. Petrol. 32 48-68

OFTEDAHL, C., 1980, Geology of Norway. Nor. geol. Unders. 356 3-114

PASSCHIER, C.W. & SIMPSON, C., 1986, Porphyroclast systems as kinematic indicators, J. struct. Geol. Oxford 8 831-843

PERCHUK, L.L., 1968, Pyroxene-garnet equilibrium and the depth facies of eclogites. Int. geol. Rev. 10 280-318

PERCHUK, L.L., 1969, The effect of temperature and pressure on the equilibrium of natural iron-magnesium minerals. Int. geol. Rev. 11 875-901

PERCHUK, L.L., 1977, Thermodynamic control of metamorphic processes. In Saxena, S.K. & Bhattacharji, S. (eds), Energetics of geological processes. Springer-Verlag, New York, 285-352

PERCHUK, L.L, 1985, Precambrian granulites of Siberia. J. metamorphic Geol. 3 265-310

PERCIVAL, J.A., 1983, High-grade metamorphism in the Chapleau-Foleyet area, Ontario. Am. Mineral. 68 667-686

PIGAGE, L.C. & GREENWOOD, H.J., 1982, Internally consistent estimates of pressure and temperature: the staurolite problem. Am. J. Sci. 282 943-969

PLATT, J.P. & VISSERS, R.L.M., 1980, Extensional structures in anisotropic rocks, J. struct. Geol. Oxford 2 397-410

POTTS, P.J., 1987, A handbook of silicate rock analysis. Blackie & Son Ltd, Glasgow & London. 622pp.

POWELL, M. & POWELL, R., 1977, Plagioclase-alkali feldspar geothermometry revisited. Mineralog. Mag. London. 41 253-256

POWELL, R. & HOLLAND, T.J.B., 1988, An internally consistent dataset with uncertainties and correlations: 3. Applications to geobarometry, worked examples and a computer program. J. metamorphic Geol. 6 173-204

POWNCEBY, M.I., WALL, V.J., & O'NEILL, H.St.C., 1987, Fe-Mn partitioning between garnet and ilmenite: experimental calibration and applications. Contrib. Mineral. Petrol. 97 116-126

PRIEM, H.N.A., BOELRIJK, N.A.I.M., HEBEDA, E.H., VERDURMEN, E.A.T., & VERSCHURE, R.H., 1973, A note on the geochronology of the Hestbrepiggan Granite in West Jotunheimen. Nor. geol. Unders. 289 31-35

RAMBALDI, E.R., 1973, Variation in composition of plagioclase and epidote in some metamorphic rocks near Bancroft, Ontario. Can. J. Earth Sci. 10 852-868

REUSCH, H., 1908, Tekst til Geologisk Kart over fjeldströkene mellem Jostedalsbræen og Ringerike. Nor. geol. Unders. 47 1-40

RICHARDSON, S.W., 1968, Staurolite stability in a part of the system Fe-Al-Si-O-H. J. Petrol. 9 467-488

RICHARDSON, S.W., GILBERT, M.C., & BELL, P.M., 1969, Experimental determination of kyanite-andalusite and andalusite-sillimanite equilibria; the aluminium silicate triple point. Am. J. Sci. 267 259-272

RÅHEIM, A., 1974, A post Caledonian syenite porphyry dyke in the western Gneiss Region Tustna, Central Norway. Nor. geol. Tiddskr. 54 139-147

SCONEVELD, C., 1977, A study of some typical inclusion patterns in strongly paracrystalline-rotated garnets. Tectonophysics 39 453-471

SEGURET, M., SERANNE, M., CHAUVET, A., & BRUNEL, M., 1989, Collapse basin: A new type of extensional sedimentary basin from the Devonian of Norway. Geology 17 127-130

SELVERSTONE, J. & SPEAR, F.S., 1985, Metamorphic P-T paths from pelitic schists and greenstones from the south-west Tauern Window, Eastern Alps. J.metamorphic Geol. 3 439-465

SERANNE, M., 1989, Palaeomagnetism, magnetic fabric and the structural style of the Hornelen Old Red Sandstone, western Norway. Discussion. J. geol. Soc. London (in press)

SERANNE, M. & SEGURET, M., 1985, Etirement ductile et cisaillement basal dans les bassins dévoniens de l'Ouest Norvège. C. r. Acad. Sc. Paris t. 300, Série II, no. 8

SIGMOND, E.M.O., GUSTAVSON, M., & ROBERTS, D.,1984, Berggrunnskart over Norge M 1:1 million. Nor. geol. Unders.

SKJERLIE, F.J., 1969, The pre-Devonian rocks in the Askvoll-Gaular area and adjacent districts, western Norway. Nor. geol. Unders. 258 325-

SKJERLIE, F.J., 1971, Sedimentasjon og tektonisk utvikling i Kvamshestens devonfelt, Vest-Norge. Nor. geol. Unders. 270 77-108

SKJERLIE, F.J., 1984, Melvær og Beskrivelse til de berggrunnsgeologiske kart 1017 1 og 1117 IV - M 1:50 000 (Med fargetrykte kart) Nor. geol. Unders. Skrifter 55, Universitetforlaget 1984, Trondheim

SKJERLIE, F.J. & PRINGLE, I.R., 1978, A Rb/Sr whole-rock isochron date from the loermost gneiss complex of the Gaular area, west Norway and its regional implications. Nor. geol. Tiddskr. 58 259-265

SMITH, D.C., 1981, A reappraisal of factual and mythical evidence concerning the metamorphic and tectonic evolution of eclogite-bearing terrain in the Caledonides. (abs) Terra Cognita 1 73

SMITH, D.C., 1984, Coesite in clinopyroxene in the Caledonides and its implications for geodynamics. Nature. London. 310 641-644

SMITHSON, S.B., RAMSBERG, I.B., & GRÖNLIE, G., 1974, Gravity interpretation of the Jotun Nappe of the Norwegian Caledonides. Tectonophysics 22 205-222

SPEAR. F.S., 1988, Metamorphic fractional crystallization and internal crystallization and internal metasomatism by diffusional homogenization of zoned garnets. Contrib. Mineral. Petrol. 99 507-517

SPEAR, F.S. & CHENEY, J.T., 1989, A petrogenetic grid for pelitic schists in the system SiO_2-Al_2O_3-FeO-MgO-K_2O-H_2O. Contrib. Mineral. Petrol.101 149-164

SPEAR, F.S. & FRANZ, G., 1986, P-T evolution of metasediments from the Eclogite Zone, south-central Tauern Window, Austria. Lithos 19 219-234

SPEAR, F.S., & SELVERSTONE, J., 1983, Quantitative P-T paths from zoned minerals: theory and tectonic applications. Contrib. Mineral. Petrol. 83 348-357

SPRY, A., 1969, Metamorphic Textures. Pergamon Press Ltd., Oxford.

STEEL, R.J. & GLOPPEN, T.G., 1980, Late Caledonian Devonian basin formation, western Norway: signs of strike-slip tectonics during infilling. Spec. Pub. Int. Ass. Sediment. 4, 79-103)

STEEL, R.J., MÆLE, S., NILSEN, H., RÖE, S.L., & SPINNAGER, Å., 1977, Coarsening-upward cycles in the alluvium of Hornelen Basin (Devonian) Norway: sedimentary response to tectonic events. Bull. geol. Soc. Am. 88 1124-1134

STEEL, R.J.. SIEDLECKA, A., & ROBERTS, D., 1985, The Old Red Sandstone basins of Norway and their deformation: a review. In Gee & Sturt (eds) The Caledonide Orogen - Scandinavia and Related Areas, John Wiley & Sons Ltd. 293-315

STEPHENS, M.B. & GEE, D.G., 1985, A tectonic model for the evolution of the eugeoclinal terranes in the central Scandinavian Caledonides. In Gee & Sturt (eds) The Caledonide Orogen - Scandinavia and Related Areas, John Wiley & Sons Ltd. 89-107

STRAND, T., 1960, The pre-Devonian rocks and structures in the region of Caledonian deformation. In Holtedahl, O. (ed) Geology of Norway. Nor. geol. Unders. 208 170-284

STRAND, T., 1961, The Scandinavian Caledonides: a review. Am. J. Sci. 259 161-172

SWEATMAN, T.R. & LONG, J.V.P., 1969, Quantitative electron-probe microanalysis of rock-forming minerals. J.Petrol. 10 332-379

TALWANI, M. & ELDHOLM, O., 1972, Continental margin off Norway: a geophysical study. Geol. Soc. Am. Bull. 83 3575-3606

THOMPSON, A.B., 1975, Mineral reactions in a calc-mica schist from Gassetts, Vermont, USA. Contrib. Mineral. Petrol. 53 105-127

TORSVIK, T.H., STURT, B.A., RAMSAY, D., & VETTI, V., 1987, The tecto-magnetic signature of the Old Red Sandstone and pre-Devonian strata in the Håsteinen area, western Norway, and implications for the later stages of the Caledonian Orogeny. Tectonics 3 305-322

TORSVIK, T.H., STURT, B.A., RAMSAY, D., BERING, D., & FLUGE, P.R., 1988, Palaeomagnetism, magnetic fabric and the structural style of the Hornelen Old Red Sandstone, western Norway. J. geol. Soc. London 145 413-430

TORSVIK, T.H., STURT, B.A., RAMSAY, D., BERING, D., & FLUGE, P.R., 1989, Palaeomagnetism, magnetic fabric and the structural style of the Hornelen Old Red Sandstone, western Norway. Reply. J. geol. Soc. London (in press)

TORSVIK, T.H., STURT, B.A., RAMSAY, D., KISCH, H.J., & BERING, D., 1986, The tectonic implications of Solundian (Upper Devonian) magnetization of the Devonian rocks of Kvamshesten, western Norway. Earth. Planet. Sci. Lett. 80 337-347

UDOVKINA, N.G., MURAVITSKAYA, G.N., & LAPUTINA, I.P., 1980, Talc-garnet-kyanite rocks of the Kokchetav Block, Northern Kazakhstan. Dokl. Akad. Nauk. SSSR. (English translation) 237 202-205

VUICHARD, J.P. & BALLEVRE, M., 1988, Garnet-chloritoid equilibria in eclogitic pelitic rocks from the Sesia zone (Western Alps): their bearing on phase relations in high pressure metapelites. J. metamorphic Geol. 6 135-157

WANG, G-F, & BANNO, S., 1987, Non-stoichiometry of interlayer cations in micas from low- to middle-grade metamorphic rocks in the Ryoke and the Sanbagawa belts, Japan. Contrib. Mineral. Petrol. 97 313-319

WATTS, A., 1985, Palaeomagnetism of the Lower Carboniferous Billefjorden Group, Spitsbergen. Geol. Mag. 122 383-388

WIKSTRÖM, A., 1970, Electron microprobe studies of the alteration of omphacite in eclogites from the Nordfjord area, Norway. Nor. geol. Tiddskr. 50 137-156

WOLFF, F.C., 1983, Crustal structure of the Scandinavian peninsula as deduced by wavelength filtering of gravity data. In Schenk, P.E. (ed) Regional Trends in the Geology of the Appalachian-Caledonian-Hercynian-Mauritanide Orogen. D.Reidel Publ. Co. 55-61

WOOD, B.J. & BANNO, S., 1973, Garnet-orthopyroxene and orthopyroxene-clinopyroxene relationships in simple and complex systems. Contrib. Mineral. Petrol. 42 529-534

YARDLEY, B.W.D., 1977, An empirical study of diffusion in garnet. Am. Mineral. 62 793-800

Table 1.1: Comparison of grid references used in this study with those used on published maps

	This study	Fylkeskart-contoret	M711 Series of US Army Map Service
Northings	00 000	341 000	$^{67}75170$
	05 000	346 000	$^{67}80170$
	10 000	352 000	$^{67}85170$
	15 000	356 000	$^{67}90170$
	20 000	361 000	$^{67}95170$
Eastings	00 000	47 000	$^{2}94\,650$
	05 000	42 000	$^{2}99\,650$
	10 000	37 000	$^{3}04\,650$
	15 000	32 000	$^{3}09\,650$
	20 000	27 000	$^{3}14\,650$

TABLE 2.1 SIMPLIFIED TECTONOSTRATIGRAPHY

This study	Bryhni, 1966	Kildal, 1970	Skjerlie, 1984 (Melvaer & Askvoll)
Devonian conglomerate	Devonian conglomerate	Devonian conglomerate	
		Greenschist	
Hyllestad Schists (Cambro-Silurian?)		Cambro-Silurian Schists	
UMU	Fjordane Complex	Metamorphic Supracrustals (Fjordane)	Vevring Complex
MMU			
LMU			
Basement Gneisses		including small inliers of "basal gneiss complex" at base (Jostedal)	Jostedal Complex

TABLE 2.2 REPRESENTATIVE MINERAL ASSEMBLAGES FROM SOGNEFJORD

Basement Gneisses	Ksp	qz	bi	mt	ilm	rut	sph	epi	white mica	chl	cpx	opx	oliv	sill	ky	st	ctd	gt	amph	plag	apat	calc	zirc
Augen gneiss	X	X	X		X															alb			
Banded migmatite	X	X	X															(X)	(X)	alb			
Quartzose schist		X	X		X				X	XR						X		X		olig			
Mafic dykes		X	X	X	(X)	(X)		X										(X)	hbl	X	(X)		
Orthogneiss			X	(X)			X	X										X	X	X	X		
Quartzite	X	X	(X)		X				rose mu											(alb)			
Eclogite					(X)	X			phen?		omph							X	bar		(X)		
Lower Mafic Unit (Lavik Amphibolites)																							
Amphibolite		X	(X)	X	(X)	(X)		(X)		(XR)	(X)							(X)	hbl	olig	(X)		
Granitic gneiss	X	X	X		X													(X)	(X)	olig			
Mica schists		X	X		X			(X?)	X									X		alb	X		
Middle Mafic Unit (Grafjell Gneisses)																							
Tonalitic gneiss	X	X	X	X?				X		XR								(X)	(X)	alb			
Tremolitic schist		(X)			X?					XR			X						tr			(X)	
Actinolitic schist		X			X?														act	alb	(X)		
Upper Mafic Unit (Molmesdal Gabbro)																							
Gabbro		(X)	X		X			(X)		(XR)	X	(X)	(X)					(X)	(XR)	lab	(X)		
Granite (K1A)	X	X	X	X																alb			(X)
Garbenschiefer		X	X				X		X	XR								X	X	alb			
Sillimanite schist		X	X			X			X	XR				X	XR			X		alb	X		
Amphibolite schist			X	X															X	X			
Hyllestad schists																							
Greenschist	X	X	(X)						phen(pa)	X								Mn-gt					
Gt-ky-st schist				(X)	X	X			phen(pa)	XR					X	X	(X)	Fe-gt					
Garbenschiefer		X	X			X		X	phen									X	X				
Gt amphibolite		X			X	X												X	X	X			
Siliceous dolomite		X					X	X		X									tr	X		X	
Granite	X	X	(X)	X						(XR)										alb	(X)		

XR=phase present as retrogressive phase;(X)=phase present in minor or trace amounts;mu=muscovite;pa=paragonite;phen=phengite;hbl=hornblende; tr=tremolite;bar=barroisite;act=actinolite
alb=albite;olig=oligoclase;lab=labradorite
Ksp=K-feldspar;qz=quartz;bi=biotite;mt=magnetite;ilm=ilmenite;rut=rutile; sph=sphene;epi=epidote;mica=white mica;chl=chlorite;cpx=clinopyroxene opx=orthopyroxene;ol=olivine;sill=sillimanite;ky=kyanite;st=staurolite ctd=chloritoid;gt=garnet;amph=amphibole;plag=plagioclase;apat=apatite calc=calcite;zirc=zircon

Table 2.3 Deformation and metamorphism in the field area

	Basement Gneisses	Eclogites (in Basement)	Lower & Middle Mafic Units	Upper Mafic Unit	Hyllestad Schists
D5	Extensional crenulation cleavage (e.c.c.) developed in schistose horizons in west of the area. Relation to D4 not established but post-dates F3 folding. Consistent vergence to W or NW. Some growth of biotite, shear bands often contain late chlorite.	Not observed in eclogites from Basement Gneisses.	E.c.c developed in west of area with top-to-NW vergence. Shear bands truncate inclusion trail foliation in garnets at high- angle. Low-grade anastomosing shear bands in Leirvik area are also assigned to D5. Chlorite, biotite, and actinolite are developed in shear bands.	Low-grade chlorite-filled anastomosing shear bands are seen in Loland area in massive meta-igneous rocks and may be of D5 age, but lack of well- foliated rocks in west of area means e.c.c. not well-developed.	E.c.c. widely developed throughout unit with top-to-NW vergence. Porphyroblasts of garnet, kyanite, chloritoid and staurolite are mechanically broken up by crushing in shear bands. Chlorite and magnetite are developed in shear zones and in cracks in porphyroblasts. Biotite forms fringes on garnet. White micas tightly crenulated and deformed in S5.
D4	Gentle upright warps which deform F3 hinges. Axial planes are approximately vertical, axes trend N-S. Age with respect to "D5" not known.	Effects of D4 not observed	Effects of D4 not observed	Effects of D4 not observed	Effects of D4 not observed
D3	Refolding of F2 isoclines and S2 foliation. S3 axial planar foliation absent or only weak crenulation fabric in F3 hinges. Garnet shows breakdown to biotite, chlorite, plagioclase, magnetite in F3 hinges. Zoning of hornblendes to actinolitic compositions at rims may be related to D3.	Horizons containing eclogite pods are folded by F3, but direct effects on eclogites are not observed. Garnet shows breakdown to radiating intergrowth of biotite, epidote, magnetite which are unaffected by D3 folding and decussate on D2 foliation.	Open to tight minor folds and chevrons deform F2 isoclines. In west of area folds mostly recumbent and asymmetric with vergence is consistently top-to-NW. Amphibole and biotite are folded without recrystallization into axial planar fabric. Breakdown of garnet to biotite, chlorite, magnetite occurs in F3 hinges.	F3 chevrons seen where foliation developed. At Loland crenulations post-date the breakdown of kyanite to sillimanite and the growth of idoblastic garnet.	Recumbent asymmetric F3 folds are commonly seen. Vergence consistently top-to-NW. In gneissose horizons biotite foliation is deformed around F3 hinges. In schistose horizons the D5 e.c.c. is usually the dominant fabric and F3 folds not often seen.

Table 2.3 Deformation and metamorphism in the field area

	Basement Gneisses	Eclogites (in Basement)	Lower & Middle Mafic Units	Upper Mafic Unit	Hyllestad Schists
D2	Isoclinal folding of "S1" is seen, sometimes isoclines are refolded in turn by F3 folds. A well-developed S2 foliation, axial planar to F2 is defined by the orientation of hornblende and biotite. isoclines. Garnets with S-shaped inclusion trails are interpreted to be syn-kinematic with D2. Contacts with other units are parallel to S2.	S2 foliation in amphibolitized eclogites is continuous with S2 foliation in surrounding gneisses. Banding of eclogite minerals rarely seen to be folded by F2 isoclines. Amphiboles and micas in hornblende-albite symplectite and biotite-albite symplectite after phengite is aligned in S2. Eclogite assemblages are considered to be early D2 at latest. Decompression and formation of symplectite textures is inferred to be of late D2 age.	S2 foliation defined by orientation of hornblende and biotite is well-developed and axial planar to rare isoclinal folds, which are themselves deformed by F3 folds. S2 foliation is particularly well-developed at contacts with major units. Garnet inclusions of rutile, ilmenite, quartz, sphene and apatite define a rotated foliation which is continuous with the external S2 foliation.	S2 is developed best at the margins of the unit. In much of the unit, massive textures are still preserved. At Loland amphiboles in a garbenschieter (K2b) is oriented in the S2 foliation. Sillimanite in smaple K2a is also aligned in the S2 foliation.	S2 defined by chlorite, biotite, and muscovite. High-pressure minerals (kyanite, staurolite, garnet) occur in schistose horizons where S2 foliation strongly overprinted by D5. Kyanite is usually sub-parallel to S2, where this can be determined. Kyanite and garnet contain inclusion trails of rutile and quartz which, in the case of garnet, are often curved or spiralled, but are discontinuous with the external foliation due to truncation by D5 micro-structures. These inclusion foliations may correspond to S2, or may be even earlier - direct correlation with other units cannot be made.
D1	Development of "S1" foliation is only structural feature observed. This fabric is formed by tectonic modification of pre-existing compositional markers (migmatite leucosomes, pegmatites, dykes etc), possibly with some further metamorphic differentiation. D1 may represent an early phase of D2 deformation.	D1 structures not observed in eclogite assemblages. Eclogite formation may be of D1 age, or early D2 at latest.	S1 not well-developed, and (assuming it is present) generally indistinguishable from S2. A compositional banding formed by the segregation of plagioclase and plagioclase-rich bands which is folded by F2 isoclines may be analogous to "S1" in Basement Gneisses.	D1 not observed in UMU Early coronas containing opx, cpx and spinel developed at plagioclase/olivine grain boundaries in gabbroic rocks are believed to have formed during the early cooling history of the rock, and pre-date Caledonian deformation.	D1 not observed in HS

TABLE 3.1 MINERAL ASSEMBLAGES IN DYKES FROM SOGNEFJORD

A) Dykes occurring between Lavik and Balestrand

	Amph	Biot	Plag	Qtz	Musc	Garn	Epid	Chl	Perth	K-fsp	Calc	Opaq	Rut	Apat
D10	H/A	X	lab		X							X		
SF2		X	X	X		X	X	X			X	il?		
SF3	H?	X	ab	X			X		X			il/sp		
SF4	H	X	X	X	(X)		(X)					il/sp		
SF5	H	X	X	X								il?		
SF1		X	ab	X		X	zo?				X	X		
D9A	A	X	ab?	X			al/ep				X	X		
D9B	H/A	X	X	X			X	(X)			(X)			X
D11	H/A	X	X	X	(X)						X	X		
D12	A?	X	ab	X			X					il/sp		
D13	(A)	X	X	X	(X)				X			il/sp		X
SF9	H/A	X	ab?	X			X					il/sp		
SF7		X		X	X	X?	X					X		
SF8		X		X	X		X			X		X		
D7	H/A	X	and	X		X		(X)				il/sp		X
D6	H/A	X	X	X			X					X		
SF6		X	X				X	(X)				il/sp		
D5	H/A	X	X	X				(X)				X		X
D4A		X	alb	X	(X)		al/ep		X	X		il/sp		X
D4B	H/A	X	alb	X	(X)		X	(X)				X		
D4C	H/A	X	X	X			(X)	(X)				mt?		
D3	H	X	X	X	(X)							il/sp		X
D14A		X	X	X	(X)		X					X		
D14C		X	X	X	X	X	al/ep	(X)	X	X		X		
D14D		X	X	X	X	X	X	X	X	X		X		
D14E		X	X	X	(X)	tr	al/ep	-	X	X		X		

TABLE 3.1 (con) MINERAL ASSEMBLAGES IN DYKES FROM SOGNEFJORD

A) Dykes occurring between Lavik and Balestrand (con)

	Amph	Biot	Plag	Qtz	Musc	Garn	Epid	Chl	Perth	K-fsp	Calc	Opaq	Rut	Apat
D2	H/A	X	X									il/sp		X
D8	A	X	X	X								X		X
D15	H	X	X	X		X	X		anti	(X)		X		X
D1	H	X	ab	X			X				X	X		X
D16	H/A	X	ab	X?		X	zo					il/sp	ru/il	
SF14		X	ab	X	(X)		X	X		X		mt?		
SF15		X	ab	X			al/ep	X	X	X				X
SF16		X	ab	X		X	al/ep			X				X
SF17	X	X	ab	X			al/ep	(X)		X				
327	H	X	ab	X			X	(X)				mt?		X
336	(H)/A	X	ab	X?			zo?	(X)				il/sp	ru/il	X

B) Dykes occurring between Lavik and Soetevik

	Amph	Biot	Plag	Qtz	Musc	Garn	Epid	Chl	Perth	K-fsp	Calc	Opaq	Apat
483A	H/(A)	X	ab-ol	X			al/ep	(X)				pyr?	X
483B	H	X	ab-ol	X			X					pyr?	X
92	H	X	alb	X		X	X					il/sp	X

Amph=amphibole, Biot=biotite, Plag=plagioclase, Qtz=quartz, Musc=muscovite, Garn=garnet, Epid=epidote, Chl=chlorite, Perth=perthite, K-fsp=K-feldspar, Calc=calcite, Opaq=opaque ore minerals, Rut=rutile, Apat=apatite

H=hornblende, A=actinolite, H/A=hornblende with actinolitic rims, alb=albite, olig=oligoclase, and=andesine, lab=labradorite, zois=zoisite, epi=epidote, all=allanite, all/epi=epidote rims on allanite, anti=antiperthite, il=ilmenite, sph=sphene, rut=rutile, mt=magnetite, pyr=pyrite, rut/il=ilmenite rims on rutile, il/sph=sphene rims on ilmenite, etc (X)=retrograde or vein phase

TABLE 3.2 MINERAL ASSEMBLAGES OF ROCKS FROM THE BASEMENT GNEISSES

	Garn	Amph	Staur	Biot	Musc	Qtz	Plag	K-fsp	Perth	Myrm	Epid	Chl	Calc	Opaq	Sph	Apat	
SF19	X	X		X		X	ab	X	X	X	al/ep	X		mt/hm	X	X	Orthogneiss
SF29		X		X		X	ab-ol	X	anti	X	X	(X)			X	X	Metasedimentary? migmatite
SF37				X		X	ol	X			X		X		X	X	Metasedimentary? migmatite
SF65		X		X	(X)	X	ab	X			X				X		Deformed dyke
SF125				X		X	X	X			al/ep	X			X	X	Metasedimentary? migmatite
SF126				X		X	X	X	anti	X	X	(X)		mt?	X	X	Metasedimentary? migmatite
SF143				X		X	ab	X	X		X	(X)		mt?	X	X	Augen gneiss
SF165	X			X	X	X	an	X						il	X		Pelitic schist
SF203	X	X		X		X	an	X			X	X		mt?			Orthogneiss
L52	X		X	X	X	X	ol					X		X			Quartz-staurolite schist
R1	X			X	X	X	ab	X		X	al/ep	X	X		X	X	Semi-pelite
55G	X	X		X		X	ol	X			al/ep			il?		X	Metasedimentary migmatite
149	X		X	X	X	X	ol					X		X			Quartz-staurolite schist
158				X		X	ab	X		X	al/ep	tr		X	X		Mylonitized gneiss
318				X		X	ab	X		X	X	(X)				X	Augen gneiss
330		X		X		X	ab	X	micro	X	X				X		Augen gneiss
446A	X			X	X	X	ol	X?			al/ep	X	X	X			Sheared gneiss
484		tr		X		X	ab	X	anti	X	al/ep	(X)		mt?	X	X	Metasedimentary migmatite
FN1	X			X	X	X	ol					X		X		X	Semi-pelitic schist

Amph=amphibole, Biot=biotite, Plag=plagioclase, Qtz=quartz, Musc=muscovite, Garn=garnet, Epid=epidote, Chl=chlorite, Perth=perthite, K-fsp=K-feldspar, Calc=calcite, Opaq=opaque ore minerals, Apat=apatite, Staur=staurolite, Myrm=myrmekite, Sph=sphene
ab=albite, ol=oligoclase, an=andesine, ep=epidote, al=allanite, il=ilmenite, mt=magnetite, hm=haematite (X)=retrograde or vein phase, tr=trace

Table 3.3 Mineral Chemistry of the Basement Gneisses (Structural formulae)

Garnets (12 Oxygens)

	149b	55G		SF19		SF203	R1		446A	FN1		SF165		L52A	
	rim	core	rim	core	rim	aver	core	rim	rim	core	rim	core	rim	core	rim
Mg	0.4675	0.0610	0.0804	0.0513	0.1684	0.0814	0.0516	0.0547	0.1146	0.1399	0.3718	0.0496	0.1132	0.2902	0.5696
Al	1.9823	1.8310	1.8401	1.7982	1.8270	1.8047	1.8958	1.8939	1.9674	1.9744	1.9665	1.9473	1.9752	1.9676	1.9762
Si	2.9917	2.9603	2.9943	3.0069	2.9757	2.8506	2.9672	2.9938	3.0064	2.9772	2.9994	2.9904	2.9904	3.0007	3.0018
Ca	0.1739	1.2053	1.2305	1.1483	1.0036	1.0665	1.2072	1.3066	0.9876	0.8236	0.5739	0.8736	0.8035	0.5563	0.2752
Ti	0.0010	0.0115	0.0043	nd	nd	0.0042	0.0129	0.0076	0.0053	0.0074	0.0052	0.0148	0.0063	0.0020	0.0051
Cr	nd	nd	nd	nd	nd	0.0008	nd	nd	nd	nd	nd	0.0000	0.0008	0.0000	0.0000
Mn	0.0295	0.5763	0.5650	0.2800	0.8659	0.4494	0.7556	0.5668	0.0142	0.1126	0.0452	0.2681	0.0170	0.0079	0.0348
Fe	2.3545	1.3546	1.2855	1.7154	1.1594	1.4254	1.1097	1.1768	1.9045	1.9650	2.0380	1.8563	2.0935	2.1754	2.1373
Fe3	0.0250	0.1972	0.1614	0.1950	0.1973	0.1396	0.1241	0.1048	0.0209	0.0411	0.0289	0.0476	0.0267	0.0297	0.0168
Fe2	2.3295	1.1574	1.1242	1.5204	0.9621	1.2858	0.9858	1.0720	1.8836	1.9239	2.0091	1.8087	2.0663	2.1456	2.1204
SUM	8.0004	8.0000	8.0001	8.0001	8.0000	7.6830	8.0000	8.0002	8.0000	8.0001	8.0000	8.0001	7.9999	8.0001	8.0000

Muscovite (22 Oxygens)

	149b	R1	446a	FN1	SF165	L52a
Na	0.3111	0.0498	0.0801	0.1753	0.0577	0.3673
Mg	0.2977	0.4714	0.3550	0.3621	0.3744	0.2113
Al	5.0289	4.3473	4.7570	4.9879	4.8276	5.2534
Si	6.3303	6.6606	6.4465	6.3481	6.5260	6.2281
K	1.5848	1.9499	1.9478	1.6962	1.7152	1.6055
Ca	0.0180	0.0035	0.0000	0.0000	0.0109	0.0011
Ti	0.0496	0.0578	0.0686	0.0660	0.0748	0.0534
Cr	nd	0.0006	0.0019	0.0023	0.0000	nd
Mn	0.0121	0.0058	0.0039	0.0020	0.0010	0.0008
Fe	0.4214	0.5641	0.4239	0.3867	0.2844	0.3583
SUM	14.0539	14.1108	14.0847	14.0266	13.8720	14.0792

Table 3.3 (con) Mineral Chemistry of the Basement Gneisses (Structural formulae)

Amphibole (23 Oxygens)

	55G	SF19 core	SF19 rim	SF203 aver
Na	0.4899	0.6221	0.3874	0.4177
Mg	1.2600	1.3189	1.2017	1.7578
Al	2.2497	2.1834	1.9923	2.0467
Si	6.1761	6.3173	6.7063	6.4226
K	0.3846	0.4221	0.2633	0.2349
Ca	1.8112	1.6709	1.6466	1.9046
Ti	0.0712	0.0811	0.0717	0.0639
Cr	nd	nd	nd	0.0020
Mn	0.2177	0.2013	0.1902	0.2161
Fe	3.4045	3.2149	3.0914	2.7490
SUM	16.0649	16.0320	15.5509	15.8153

Chlorite (14 Oxygens)

	149b	SF203	446a	FN1	L52a
Na	0.0219	0.0062	0.0077	0.0000	0.0010
Mg	2.2277	2.3874	0.4483	2.3425	2.3256
Al	2.8196	2.3842	2.4946	2.8111	2.8743
Si	2.5814	2.7650	2.7405	2.5785	2.5571
K	0.0976	0.0072	0.0103	0.0048	0.0099
Ca	0.0019	0.0306	0.0034	0.0032	0.0063
Ti	0.0103	0.0213	0.0014	0.0061	0.0087
Cr	0.0061	nd	0.0007	nd	0.0016
Mn	0.0147	0.1525	0.0493	0.0205	0.0107
Fe	2.3188	2.4237	4.2628	2.2417	2.2064
SUM	10.1000	10.1781	10.0190	10.0084	10.0016

Biotite (22 Oxygens)

	149b	55G	SF19	SF203	R1	446a	FN1	SF165	L52a
Na	0.0954	0.0280	nd	0.0214	0.0303	0.0308	0.0403	0.0175	0.0372
Mg	2.0007	1.9738	2.2746	2.5125	1.5620	2.2126	2.1747	1.9369	2.1837
Al	3.4596	2.6982	2.6837	2.7704	2.9811	2.9958	3.3004	3.1606	3.3653
Si	5.4652	5.5592	5.5853	5.5561	5.5202	5.5526	5.4311	5.4479	5.4133
K	1.7643	1.9879	1.9342	1.9135	1.9741	1.9392	1.8573	1.8534	1.8926
Ca	0.0019	0.0021	0.0000	0.0162	0.0013	0.0008	0.0086	0.0289	nd
Ti	0.1603	0.2854	0.2497	0.2298	0.3465	0.2990	0.2006	0.3655	0.1647
Cr	0.0097	nd	nd	nd	nd	0.0026	nd	0.0011	0.0028
Mn	0.0081	0.1352	0.0000	0.1359	0.0673	0.0442	0.0166	0.0127	0.0095
Fe	2.6046	3.1451	3.0632	2.6412	3.1631	2.5574	2.6374	2.7174	2.6340
SUM	15.5698	15.8149	15.7907	15.7970	15.6459	15.6350	15.6670	15.5419	15.7031

Epidote (25 Oxygens)

	SF203	R1 core	R1 rim	446a
Na	0.0156	0.0455	0.0000	0.000
Mg	0.0098	0.1649	0.0592	0.014
Al	4.5394	3.3359	4.6439	5.170
Si	6.0083	6.8274	6.3528	6.048
K	0.0098	0.0217	0.0137	0.010
Ca	3.9984	2.6780	3.5109	3.836
Ti	0.0186	0.3201	0.0105	0.028
Cr	0.0000	0.0000	0.0000	0.002
Mn	0.0244	0.0057	0.0631	0.006
Fe	1.3947	2.8199	1.6673	0.816
SUM	16.0190	16.2191	16.3214	15.930

Feldspars (8 Oxygens)

	SF19	SF203	R1	446a	FN1	SF165	L52a
Na	0.9021	0.0634	0.8586	0.691	0.612	0.6394	0.698
Mg	0.0039	0.0000	0.0026	0.001	0.003	0.0806	0.004
Al	0.9977	1.0223	1.1174	1.225	1.357	1.0656	1.269
Si	2.9805	2.9862	2.8879	2.774	2.657	2.8452	2.725
K	0.0144	0.9191	0.0090	0.064	0.006	0.0152	0.006
Ca	0.0694	0.0000	0.1098	0.232	0.336	0.1558	0.283
Ti	0.0000	nd	nd	0.001	0.000	0.0079	0.001
Mn	0.0028	nd	nd	0.000	0.000	0.0100	0.000
Fe	0.0080	0.0027	0.0016	0.002	0.002	0.1216	0.004
SUM	4.9788	4.9937	4.9869	4.990	4.973	4.9413	4.990

TABLE 3.4 THERMOBAROMETRY OF BASEMENT GNEISSES

		Garnet-Amphibole gneisses			Pelitic & semi-pelitic gneisses					
THERMOMETRY		SF19	SF203	55G	SF165	FN1	R1	446A	149B	L52
Garnet-amphibole	Per	474	428	509						
	G & P	630	561	618						
Garnet-biotite	G & Sa	522	421	505	441	638	536	428	695	769
	H & S	525	439	521	459	682	554	460	754	858
	P & G	730	585	692	499	743	751	507	787	923
	Thom	414	349	403	384	570	420	371	649	700
Garnet-muscovite	G & H				476	599	506	498	712	783
	H & F				388	549	355	426	606	678
Garnet-staurolite	Per								616	703
Two-feldspar	P & P	371		404	528					
Garnet-ilmenite	Fe-Mn Kd				-1.49				0.32	0.38
BAROMETRY										
Garnet-mica-feldspar	G & St (1)				3.9	8.2	8.2	6.7		9.1
	G & St (2)				4.8	8.4	9.5	7.5		8.9
	H & C				3.4	9.1	9.1	6.0		11.1
	H & P				5.6	10.0	16.6	6.9		10.9
CELAD	P & E					10.9				

All temperatures calculated at 8kbars, pressures calculated at Ganguly & Saxena garnet-biotite temperatures

Per=Perchuk, 1977; G & P=Graham & Powell, 1984; G & Sa=Ganguly & Saxena, 1984; H & S=Hodges & Spear, 1982; P & G= Pigage & Greenwood, 1982; Thom=Thompson, 1975; G & H=Green & Hellman, 1982; H & F=Hynes & Forest, 1988; P & P=Powell & Powell, 1977; G & St=Ghent & Stout (equilibria 1 & 2), 1981; H & C=Hodges & Crowley, 1985; H & P=Holland & Powell, 1985; P & E=Powell & Evans, 1983.

TABLE 4.1 MINERAL ASSEMBLAGES IN ECLOGITIC ROCKS

		LOCALITY	GARN	CPX	AMPH	OPX	PLAG	QTZ	RUT	OPAQ	EPID	BIOT	PHEN	CHL	APAT	SPH	CALC
(a)	166A	H	E	E	E		E	E	E	il		X	E		E		
(b)	SF68	Y	E	E	X		E		E	il	X				E		
	SF70	Y	E	E	X		E		E	il					E		
(c)	SF133	Y	X	X	X	X	X	X	X	il	X	X			X		
(d)	SF138	Y	E		X		E	E	E	il+pyr	X	X		(X)	E	X	X
	SF20	B	E		X		E	E	E	mt	X				E		
	SF21	B	E		X		E	E	E	mt+il	X	X	par	(X)	E	X	
	SF24	B	E		X		E	E	E	il	X				E		
	SF25	B	E		X		E	E	E		X	X	E		E		
	SF207	A	[E]		X		E	E	[E]	mt	X	X			E		
	SF227	I			X		E	E	[E]	mt+pyr		X			E		
	BK1C	BK	[E]		X		E	E	[E]	mt+il		X			E		
	D16	L	E		X		E	E	E	mt	X	X			E		

(a) eclogite showing little alteration (b) amphibolitized eclogite with relict clinopyroxene (c) noritic gneiss with coronas of garnet, amphibole, biotite etc. (d) amphibolitized eclogite lacking relict clinopyroxene. Square brackets indicate a relict phase present in trace amounts. Round brackets indicate a late, low-grade, retrogressive phase E=phases present in primary eclogite assemblage.
Localities: H=Hellebostolane, Y=Ytre Hellebo, B=Brensdal, A=Alvaeren, I=Indredalen, BK=Brekke, L=Lia

GARN=garnet, CPX=clinopyroxene, AMPH=amphibole, OPX=orthopyroxene, PLAG=plagioclase, QTZ=quartz, RUT=rutile, OPAQ=opaque ore mineral, EPID=epidote, BIOT=biotite, PHEN=phengite, CHL=chlorite, APAT=apatite, SPH=sphene, CALC=calcite, il=ilmenite, pyr=pyrite, mt=magnetite, par=paragonite

TABLE 4.2 GEOTHERMOBAROMETRY OF ECLOGITIC ROCKS

Thermometry		166A1	166A2	SF68	SF70	SF20	SF20#	SF24	SF24#	SF25	SF138	SF133
Garnet-Cpx	EG	593	597	(667)	(700)							(658)
Garnet-Amphibole	GP		*771	(813)	(826)	707	803	580	704	769	769	652
	P1		*812	(717)	(775)	700	746	545	650	728	779	540
Cpx-Amp Fe-Mg	P2	515	520	(880)	(700)							
Cpx-Amp Ca-Na	P3	500	500	(540)	(540)							
Garnet-Biotite	GS											645
Cpx-ilmenite	B											(773)
Opx-ilmenite	B											(800)
Two-pyroxene	LD											(759)
	WB											(805)
Barometry												
Di-Jd ss	GL	14.9	14.9									
Gt-Opx-Plag-Q	BWB											7.5
	PN											9.0
Garnet-Opx	HG											5.0

temperatures calculated using amphibole inclusion in garnet
* phase compositions differ widely from calibration
figures in parentheses: phases not in textural equilibrium
EG=Ellis & Green, 1979;GP=Graham & Powell, 1984;P1=Perchuk, 1985;
P2=Perchuk,1969;P3=Perchuk,1968,GS=Ganguly & Saxena,1984;B=Bishop,1980;
LD=Lindsley & Dixon,1976;WB=Wood & Banno,1973;GL=Gasparik & Lindsley,
1980;BWB=Bohlen et al,1983;PN=Perkins & Newton,****;HG=Harley & Green,
1982

Table 4.3 Mineral chemistry in eclogites and related rocks (structural formulae only)

Amphibole (23 Oxygens)

Sample	SF133	SF20 aver	SF24 rim	SF24 core	SF24 incl	SF25 aver	SF68 aver	SF70 nr gt	nr cpx
Na	0.4494	0.8152	0.9123	0.9140	1.1098	0.5739	0.9130	0.7156	0.7757
Mg	2.4798	2.2147	2.3960	2.6857	1.4509	2.0565	2.2250	1.9483	2.4522
Al	1.6501	2.3502	2.0123	1.5643	2.8489	1.9695	2.5764	2.7583	2.2799
Si	6.8076	6.4723	6.4532	6.9502	5.9472	6.6653	6.3972	6.2541	6.5152
K	0.1775	0.0490	0.0622	0.0501	0.0581	0.2659	0.0223	0.0177	0.0175
Ca	1.7316	1.3571	1.5409	1.1458	1.3946	1.7163	1.7445	1.7271	1.7390
Ti	0.0266	0.0508	0.0518	0.0192	0.0390	0.0346	0.0450	0.0203	0.0202
Cr	0.0019	0.0012	0.0000	0.0000	0.0019	0.0019	nd	nd	nd
Mn	0.0324	0.0151	0.0216	0.0128	0.0449	0.0169	0.0129	0.0255	0.0084
Fe	2.2959	2.4072	2.0650	1.7678	2.6672	2.4330	1.8016	2.2464	1.9137
SUM	15.6528	15.7328	15.5153	15.1099	15.5625	15.7337	15.7377	15.7133	15.7218

Sample	SF138 aver	SF138 (included by gt)		SF207 core	rim	166A1 aver	166A2 aver
Na	0.4562	0.4634	0.5005	0.4165	0.5006	1.3127	1.3946
Mg	1.8022	1.8350	1.8652	2.7562	2.2956	2.0755	1.9124
Al	2.4357	2.8390	2.8500	1.9952	2.3924	2.3752	2.6258
Si	6.3797	6.2174	6.1796	6.9463	6.5252	6.4646	6.3073
K	0.2272	0.1899	0.1971	0.0897	0.0882	0.0776	0.0692
Ca	1.7946	1.8106	1.8062	1.0563	1.7303	1.3169	1.3497
Ti	0.0357	0.0328	0.0411	0.0230	0.0343	0.0357	0.0549
Cr	0.0036	0.0019	0.0000	nd	nd	0.0000	0.0008
Mn	0.0581	0.0307	0.0222	0.0666	0.0357	0.0132	0.0178
Fe	2.5131	2.2348	2.2407	1.9358	1.9358	2.3639	2.3236
SUM	15.7060	15.6555	15.7026	15.2856	15.5381	16.0353	16.0560

Table 4.3 (con) Mineral chemistry in eclogites and related rocks (structural formulae only)

Biotite (22 Oxygens)

Sample	SF133	SF25	SF138	166A1
Na	0.0500	0.1200	0.0218	0.0873
Mg	2.4800	2.0568	2.1386	2.3830
Al	2.5460	3.2170	2.8516	3.3134
Si	5.4940	5.4732	5.5234	5.4003
K	1.8320	1.8623	1.8824	1.8591
Ca	0.0000	0.0909	0.0132	0.0000
Ti	0.4620	0.2739	0.2418	0.3963
Cr	nd	0.0015	0.0014	0.0000
Mn	0.0080	0.0141	0.0369	0.0089
Fe	2.6100	2.5257	3.0496	2.3902
SUM	15.4820	15.6354	15.7607	15.8385

Feldspars (8 Oxygens)

Sample	SF133	SF20	SF25	SF138
Na	0.6570	0.8760	0.7800	0.7870
Mg	0.0740	0.0010	0.0627	0.0012
Al	1.2300	1.0200	1.1694	1.1512
Si	2.5990	2.9730	2.7500	2.8463
K	0.0160	0.0040	0.0691	0.0108
Ca	0.4510	0.0600	0.1658	0.1664
Ti	0.0010	0.0010	0.0057	0.0009
Cr	nd	nd	nd	nd
Mn	0.0000	0.0000	nd	0.0003
Fe	0.0630	0.0140	0.0813	0.0114
SUM	5.0910	4.9490	5.0840	4.9755

Ilmenite (3 Oxygens)

Sample	SF133	SF25	SF138
Mg	0.0500	0.0362	0.0000
Al	0.0000	0.0000	0.0000
Si	0.0000	0.0000	nd
Ca	0.0000	0.0000	0.0000
Ti	0.9900	0.9859	0.9300
Cr	0.0000	0.0003	0.0000
Mn	0.0000	0.0075	0.0500
Fe3	0.0100	0.0000	0.1300
Fe2	0.9400	0.9877	0.8800
SUM	1.9900	2.0176	1.9900

Pyroxene (Fe3 calculated by method of Neumann, 1976)

Sample	SF133		SF68	SF70		166A1	166A2
	aver opx	aver cpx	cpx	cpx core	cpx rim	core	
Na	0.0144	0.1273	0.2966	0.3486	0.2723	0.4995	0.5101
Mg	0.8979	0.5900	0.5673	0.5304	0.5767	0.3910	0.3757
Al	0.0465	0.0685	0.2810	0.2927	0.3857	0.3670	0.3849
Si	1.9641	1.9416	1.9954	2.0028	1.8894	2.0029	1.9870
Ca	0.0524	0.8013	0.6802	0.6195	0.5188	0.4611	0.4541
Ti	0.0039	0.0040	0.0030	0.0015	0.0035	0.0032	0.0036
Cr	0.0003	0.0002	nd	nd	nd	nd	0.0000
Mn	0.0327	0.0104	0.0000	0.0000	0.0008	nd	0.0000
Fe	0.9878	0.4567	0.1765	0.2045	0.3506	0.2738	0.2847
Fe3	0.0411	0.1676	0.0190	0.0473	0.1051	0.1220	0.1442
Fe2	0.9467	0.2892	0.1575	0.1572	0.2455	0.1518	0.1405
SUM	4.0000	4.0000	4.0000	4.0000	3.9978	3.9985	4.0001

Table 4.3 (con) Mineral chemistry in eclogites and related rocks (structural formulae only)

Garnets (12 Oxygens)

Sample	SF133	SF20		SF24		SF25		SF68	
	corona	core	rim	core	rim	core	rim	core(AT)	rim(AY)
Mg	0.3122	0.2504	0.4753	0.2444	0.4944	0.2892	0.5646	0.3094	0.7813
Al	1.9500	1.9395	1.9915	1.9599	1.9691	1.9128	1.9682	1.9215	1.9555
Si	3.0668	2.9514	2.9326	2.9998	2.9843	2.9898	3.0009	3.0394	3.0432
Ca	0.8283	0.6655	0.5944	0.6827	0.6122	0.6513	0.6317	0.8410	0.7338
Ti	0.0029	0.0064	0.0031	0.0083	0.0031	0.0041	0.0031	nd	nd
Cr	nd	0.0000	0.0009	nd	nd	0.0009	0.0000	nd	nd
Mn	0.0733	0.3539	0.0142	0.2330	0.0125	0.0106	0.0272	0.0496	0.0179
Fe	1.7676	1.8330	1.9879	1.8720	1.9245	2.1413	1.8043	1.8391	1.4683
Fe3	0.0000	0.1028	0.0719	0.0320	0.0435	0.0924	0.0278	0.0391	0.3475
Fe2	1.7676	1.7302	1.9161	1.8399	1.8810	2.0489	1.7765	1.8000	0.2461
SUM	8.0011	8.0001	7.9999	8.0001	8.0001	8.0000	8.0000	8.0000	8.0000

Sample	SF70		SF138	166A1		166A2	
	core	rim		core	rim	core	rim
Mg	0.5223	0.6860	0.5691	0.4489	0.5362	0.3847	0.5445
Al	1.9410	1.9696	1.9192	1.9742	1.9585	1.9876	1.9626
Si	3.0449	3.0144	3.0382	2.9993	2.9770	3.0048	2.9812
Ca	0.6156	0.6245	0.4766	0.5230	0.4326	0.7269	0.4375
Ti	nd	nd	0.0040	0.0084	0.0027	0.0114	0.0062
Cr	nd	nd	0.0000	nd	nd	nd	nd
Mn	0.1105	0.0247	0.1682	0.0319	0.0428	0.0456	0.0462
Fe	1.7657	1.6809	1.8247	2.0144	2.0502	1.8388	2.0218
Fe3	0.0141	0.0161	0.0386	0.0181	0.0618	0.0000	0.0499
Fe2	1.7516	1.6648	1.7861	1.9963	1.9884	1.8388	1.9719
SUM	8.0000	8.0001	8.0000	8.0001	8.0000	7.9998	8.0000

Table 5.1: Mineral assemblages in rocks from Lower Mafic Unit

Sample	garn	biot	amph	cpx	plag	K-fsp	qtz	epid	chl	musc	calc	tour	apat	zirc	rut	sph	ilm	
Garnet amphibolites																		
SF32a		×	act		×				×									
SF35		×	×		×			×							×	×	×	*
SF36		×	×		×		×								×	×	×	*
SF104		×	×		×										×	×	×	*
SF105	×	×	×				×	×										
SF110	×	×	act		×	×							×		×			
L128	×	×	act		×				×					×	×	×	×	*
SF172	×	×	×		×				(×)		×		×		×		×	
SF194			×		×		×								×	×	×	*
SF196		×	×		×			(×)					×		×	×	×	*
L40	×	×	act		×		×							×			?	
L68	×	×	×	×	×												×	
L97	×	×	×		×						×							
L161	×		act	×	×				×								×	
L166		×	×		×			×	(×)	×			×					
176	×		×		×		×		×								×	
446b		×	×		×			×								×		
449	×	×	×		×						×				×	×	×	*
L168																		
SF112															×		×	
SF97	×		×												×		×	
Mica schists																		
L123		×			×		×		(×)	×			×	×				
381	×	×			×		×			×	×							
T1.1	×	×			×		×			×					×			
449XZ	×	×			×				(r)	×							×	
Ultramafic schist																		
L41a			tre						×									

garn=garnet, biot=biotite,
amph=amphibole,
cpx=clinopyroxene,
plag=plagioclase,
K-fsp=K-feldspar, qtz=quartz,
epid=epidote, chl=chlorite,
musc=muscovite, calc=calcite,
tour=tourmaline,
apat=apatite, zirc=zircon,
rut=rutile, sph=sphene,
ilm=ilmenite, pyr=pyrite,
mag=magnetite,
opx=orthopyroxene,
oliv=olivine,
sill=sillimanite, ky=kyanite,
spin=spinel

* These rocks show rutile being replaced by ilmenite, and ilmenite replaced by sphene.
Rounded brackets indicate late retrogressive phase.

Table 5.1 (con): Mineral assemblages in rocks from Middle Mafic Unit

Sample	garn	biot	amph	plag	epid	qtz	chl	musc	calc	pyr	mag	apat	ilm
68	×	×	hbl	×	×	?							×
498	×		×	×	zo	?							×
438	×	×		×			×	×					×
SF119	×	×	×	×			×		×	×			×
442	×	×		×		×	×	×					×
378	×	×	×	×	×	×				×			×
S7.1	×	×	×	×							×		
R3	×	×		×	×		×	×				×	×

Mineral assemblages in rocks from Upper Mafic Unit

Sample	garn	biot	amph	cpx	opx	oliv	plag	qtz	sill	ky	epid	chl	musc	talc	calc	tour	apat	rut	sph	ilm	pyr	mag	spin
SF58	×	×	×	×	×	×	×			×	×					×				×			×
SF156	×	×	×				×	×			×			×			?	×	×	×			
SF173	×	×	×	×	×	×	×				×									×			?
SF179	×	×	×	×	×	×	×				×									×			?
L25	×		×				×	×			×					×	×			×			
L27	×		×				×	×									×			×		×	
L41b	×		×				×	×								×				×		×	
L226		×		×	×		×	×														×	
L227			×	×			×														×	×	
B3	×	×	×				×	×						×		×	×			×	×		
B12	×	×	×				×				×	×	×				×			×			
K2a	×	×					×	×	×	×		×	×		×		×			×	×		
K2b	×	×	×				×	×				×				×	×			×	×		
K3	×	×	×				×	×						×			×			×			
KJ6	×	×	×	×			×					×			×					×			
KJ10b			×	×	×	×	×					×	×	×	dol		×						

Table 5.2 Thermobarometric results for Lower Mafic Unit

		Mica schists		Garnet amphibolites							
Sample		T1	449XZ	449	L128	L150	L168	SF97	SF110	SF112	SF172
Thermometers											
garnet-biotite											
	G & S	604	535	635	582		512		551	619	521
	H & S	663	564	711	664		531		600	659	544
garnet-muscovite											
	H & F	497	527								
	G & H	653	641								
	K & R	527	515								
garnet-hornblende											
	G & P			588	637	681	622	598	524	584	541
	Per			480	603	640	578	507	439	499	479
garnet-ilmenite											
	Fe-Mn Kd	0.22	0.42					4.48			1.77
Barometers											
GRIPS	B & L	8.2	8.5	8.1	7.0	7.8	8.1			7.8	8.9
garnet-mica-plag											
	G&St 1	8.5	7.1								
	G&St 2	7.7	7.0								
	H & C	7.0	6.3								

Pressures at 500 C, Temperatures at 8 kbar

G & S: Ganguly & Saxena, 1984; H & S: Hodges & Spear, 1982; G & H: Green & Hellman, 1982, (low-Mg pelite calibration); H & F: Hynes & Forest, 1988; Krogh & Raheim, 1978; G & P: Graham & Powell, 1984; Per: Perchuk, 1977; B & L: Bohlen & Liotta, 1986; G & St 2: Ghent & Stout, 1981 (calibrations 1 & 2); H & C: Hodges & Crowley, 1985.

Table 5.2 Thermobarometric results for Middle Mafic Unit

Sample		SF119	R3	57	68	378	438	442	498
Thermometers									
garnet-biotite									
	G & S	674	674	551	511	427	632	610	
	H & S	752	699	544	543	457	682	661	
garnet-muscovite									
	H & F		485				494	520	
	G & H		611				619	647	
	K & R		485				492	521	
garnet-hornblende									
	G & P	582		644	546	511			452
	Per	504		497	454	452			377
garnet-ilmenite									
	Fe-Mn Kd	3.558			1.095	2.959	1.348		0.825
Barometers									
GRIPS	B & L	8.4*			8.8*	8.2	7.8*	7.0*	
garnet-mica-plag									
	G&St 1		2.7				6.9	7.1	
	G&St 2		1.5				5.8	6.2	
	H & C		0.8				5.1	5.5	

Pressures at 500 C, Temperatures at 8 kbar

G & S: Ganguly & Saxena, 1984; H & S: Hodges & Spear, 1982; G & H: Green & Hellman, 1982, (low-Mg pelite calibration); H & F: Hynes & Forest, 1988; Krogh & Raheim, 1978; G & P: Graham & Powell, 1984; Per: Perchuk, 1977; B & L: Bohlen & Liotta, 1986; G & St 2: Ghent & Stout, 1981 (calibrations 1 & 2); H & C: Hodges & Crowley, 1985.

* rutile has not been observed in these assemblages, so GRIPS pressures should be regarded as maximum estimates

Table 5.2 Thermobarometric results for Upper Mafic Unit

Sample		SF156	SF179	L25	L27	L41b	B3	B12	K2a	K2b	K3	KJ6
Thermometers												
garnet-biotite												
	G & S	596	636				486	487	508	507	524	460
	H & S	648	685				542	544	567	564	558	518
garnet-hornblende												
	G & P	527	659	551	529	565	528	554		505	529	560
	Per	430	632	576	475	543	415	468		488	445	494
garnet-ilmenite												
	Fe-Mn Kd		1.473									
Barometers												
GRIPS	B & L			9.9	9.2		8.2		6.9	6.7	9.5	
GRAIL	BWB								4.3			
garnet-mica-plag												
	G&St 1								5.3			
	G&St 2								5.3			
	H & C								4.6			

Pressures at 500 C, Temperatures at 8 kbar

G & S: Ganguly & Saxena, 1984; H & S: Hodges & Spear, 1982; G & H: Green & Hellman, 1982, (low-Mg pelite calibration); H & F: Hynes & Forest, 1988; Krogh & Raheim, 1978; G & P: Graham & Powell, 1984; Per: Perchuk, 1977; B & L: Bohlen & Liotta, 1986; G & St 2: Ghent & Stout, 1981 (calibrations 1 & 2); H & C: Hodges & Crowley, 1985.

Table 5.3 Mineral chemistry of Mafic Units

Garnets structural formulae only

LMU

Garnet amphibolites

	176	449	L128		L150		L168	SF97		SF112		SF172		T1	
	rim		core	rim	core	rim	rim	core	rim	core	rim	core	rim	core	rim
Mg	0.4575	0.3798	0.1563	0.4847	0.1992	0.4555	0.1841	0.1439	0.2153	0.1283	0.2692	0.0848	0.1605	0.0930	0.3562
Al	1.9862	1.8910	2.0143	1.9587	1.9154	2.0085	1.8382	1.9730	1.9795	1.9607	1.9724	1.9607	1.9297	1.9591	1.9748
Si	3.0355	3.0454	2.9626	2.9618	3.0116	2.9171	3.0441	2.9744	2.9922	2.9302	2.9847	2.9962	3.0007	3.0383	2.9766
Ca	0.4384	0.9618	0.8498	0.6042	0.5829	0.6255	0.6988	0.8244	0.8406	0.8159	0.8201	0.6968	0.7285	0.6696	0.6484
Ti	0.0000	0.0042	0.0094	0.0021	0.0052	0.0042	0.0083	0.0084	0.0093	0.0114	0.0072	0.0093	0.0083	0.0072	0.0041
Cr	0.0000	0.0000	0.0009	0.0000	nd	nd	0.0000	nd	nd	nd	nd	0.0009	0.0000	0.0009	0.0000
Mn	0.0594	0.0276	0.2422	0.0383	0.1654	0.0151	0.1306	0.3494	0.0709	0.4937	0.1703	0.4456	0.1088	0.0482	0.0113
Fe	2.0231	1.6903	1.7645	1.9501	2.1109	1.9741	2.0960	1.7265	1.8923	1.6598	1.7761	1.8056	2.0636	2.1836	2.0286
Fe3	0.0000	0.0595	0.0128	0.0774	0.0678	0.0702	0.1094	0.0526	0.0284	0.0976	0.0358	0.0329	0.0613	0.0000	0.0045
Fe2	2.0231	1.6308	1.7517	1.8727	2.0431	1.9039	1.9866	1.6739	1.8640	1.5622	1.7404	1.7727	2.0022	2.1836	1.9842
SUM	8.0000	8.0001	8.0000	7.9999	7.9906	8.0000	8.0001	8.0000	8.0000	8.0000	8.0000	7.9999	8.0001	7.9999	8.0000

Orthogneiss

	449XZ		SF110	
	core	rim	core	rim
Mg	0.2777	0.1885	0.2094	0.3447
Al	1.9351	1.9783	1.9669	1.9909
Si	2.9900	2.9754	3.0194	2.9990
Ca	0.4885	0.6630	0.8896	0.5973
Ti	0.0031	0.0042	nd	nd
Cr	nd	nd	nd	nd
Mn	0.0185	0.0188	0.0561	0.1162
Fe	2.2871	2.1718	1.8587	1.9518
Fe3	0.0718	0.0421	0.0138	0.0101
Fe2	2.2153	2.1297	1.8449	1.9417
SUM	8.0000	8.0000	8.0000	7.9999

MMU

Garnet amphibolites

	68		378		498	
	core	rim	core	rim	core	rim
Mg	0.0952	0.1644	0.1736	0.2386	0.1110	0.1449
Al	1.9843	1.9896	1.9941	1.9423	1.9922	2.0005
Si	3.0044	3.0049	2.9677	2.9970	2.9956	2.9743
Ca	0.7982	0.8708	0.6179	0.7241	0.7765	0.7560
Ti	0.0114	0.0084	0.0064	0.0063	0.0073	0.0041
Cr	nd	nd	nd	nd	0.0000	0.0000
Mn	0.2775	0.0159	0.5069	0.1961	0.3656	0.1630
Fe	1.8290	1.9459	1.7334	1.8955	1.7519	1.9572
Fe3	0.0000	0.0000	0.0318	0.0543	0.0049	0.0211
Fe2	1.8290	1.9459	1.7016	1.8412	1.7470	1.9361
SUM	8.0000	7.9999	8.0000	7.9999	8.0001	8.0000

Mica schists

	SF119	438	
	rim	core	rim
Mg	0.2320	0.1950	0.3939
Al	1.9961	2.0004	1.9697
Si	2.9762	2.9704	2.9932
Ca	0.9423	0.2710	0.3351
Ti	0.0073	0.0053	0.0084
Cr	nd	nd	nd
Mn	0.0482	0.0918	0.0315
Fe	1.7979	2.4662	2.2682
Fe3	0.0204	0.0240	0.0287
Fe2	1.7775	2.4422	2.2395
SUM	8.0000	8.0001	8.0000

Table 5.3 (con) Mineral chemistry of Mafic Units

Garnets structural formulae only

	Orthogneiss					UMU Garnet amphibolites								
	442	R3		S7		B3		B12		L25		L27		L41b
	rim	core	rim	core	rim	core	rim	core	rim	core	rim	core	rim	rim
Mg	0.2332	0.3848	0.1969	0.0270	0.0268	0.2010	0.2321	0.1525	0.3045	0.2934	0.3590	0.1411	0.2396	0.2346
Al	1.9999	2.0155	1.9978	1.8960	1.8990	1.9743	1.9659	2.0447	1.9679	1.9670	1.9882	2.0062	1.9559	1.9804
Si	2.9723	2.9929	3.0152	2.9958	3.0002	2.9880	2.9998	3.0209	2.9892	2.9777	2.9938	3.0069	3.0064	2.9372
Ca	0.5579	0.0533	0.7951	1.0382	1.0649	0.9542	0.9709	0.9854	0.8359	0.6306	0.3990	0.9769	0.6712	0.5676
Ti	0.0052	0.0010	0.0103	0.0042	0.0031	0.0095	0.0074	0.0095	0.0063	0.0031	0.0020	0.0051	0.0031	0.0031
Cr	nd	nd	nd	0.0000	0.0000	nd	nd	nd	nd	nd	nd	0.0000	0.0000	0.0009
Mn	0.0580	0.1510	0.0218	0.6152	0.4689	0.1472	0.0446	0.0889	0.0416	0.0766	0.1224	0.1767	0.0609	0.1555
Fe	2.1737	2.4015	1.9627	1.4235	1.5371	1.7257	1.7793	1.6981	1.8546	2.0515	2.1356	1.6872	2.0628	2.1206
Fe3	0.0227	0.0000	0.0000	0.1040	0.0977	0.0282	0.0269	0.0000	0.0428	0.0522	0.0160	0.0000	0.0346	0.0783
Fe2	2.1510	2.4015	1.9627	1.3196	1.4394	1.6975	1.7524	1.6981	1.8117	1.9994	2.1196	1.6872	2.0283	2.0423
SUM	8.0000	8.0000	7.9998	7.9999	8.0000	7.9999	8.0000	8.0000	8.0000	7.9999	8.0000	8.0001	7.9999	7.9999

	Gabbro			UMU at Löland Mica schists				Gt-amph
	SF156		KJ6	K2A		K2B	K3	
	core	rim	rim	core	rim	rim	rim	
Mg	0.1536	0.2555	0.1873	0.1957	0.3181	0.2508	0.1942	
Al	1.9624	1.9991	1.9636	1.9731	1.9625	1.9722	1.9895	
Si	2.9947	3.0105	2.9912	2.9914	2.9929	2.9883	3.0425	
Ca	0.8076	0.8560	1.0339	0.6908	0.5995	0.8677	0.8319	
Ti	0.0104	0.0031	0.0084	0.0092	0.0052	0.0041	0.0072	
Cr	0.0009	0.0049	0.0000	nd	nd	nd	0.0000	
Mn	0.1971	0.0966	0.0158	0.4581	0.1061	0.0559	0.0440	
Fe	1.8733	1.7742	1.7998	1.6817	2.0157	1.8610	1.8907	
Fe3	0.0316	0.0000	0.0368	0.0263	0.0394	0.0354	0.0000	
Fe2	1.8416	1.7742	1.7630	1.6554	1.9763	1.8257	1.8907	
SUM	8.0000	7.9999	8.0000	8.0000	8.0000	8.0000	8.0000	

Table 5.3 (con)

Amphiboles (structural formulae calculated for 23 oxygens)

LMU (garnet amphibolites)

	SF172			L128	L150		449	MMU (garnet amphibolites) 68	378
	aver	core	rim	aver	aver	aver incl	aver	aver	
Na	0.6349	0.7453	0.5275	0.4786	0.4793	0.4515	0.4910	0.5096	0.4770
Mg	1.8878	1.8985	1.9268	2.0354	1.9268	1.6535	2.0907	1.7222	2.1927
Al	2.3886	2.5023	2.2543	2.9604	2.8810	2.6389	2.8034	2.6716	2.3236
Si	6.3822	6.3475	6.3881	6.2414	6.2290	6.3482	6.3296	6.3679	6.5895
K	0.1284	0.1385	0.1214	0.0816	0.0675	0.0505	0.0972	0.1372	0.0836
Ca	1.6367	1.5549	1.7692	1.7525	1.7117	1.4639	1.6666	1.7086	1.6253
Ti	0.0852	0.0737	0.0952	0.0527	0.0462	0.0422	0.0540	0.0635	0.0416
Cr	0.0034	0.0038	0.0058	0.0030	nd	nd	0.0029	0.0024	0.0039
Mn	0.0451	0.0291	0.0467	0.0136	0.0182	0.0103	0.0140	0.0138	0.0451
Fe	2.5256	2.4736	2.5756	1.8863	2.1976	2.8816	1.9576	2.4085	2.1028
SUM	15.7179	15.7672	15.7106	15.5045	15.5573	15.5407	15.5070	15.6053	15.4851

UMU (garnet amphibolites)

	B3		L25		L27		L41b	L227	SF156		UMU (Löland) K2b	K3	
	core	rim	core	rim	core	rim			core	rim		core	rim
Na	0.2970	0.4202	0.5454	0.6180	0.3817	0.5963	0.4129	0.6063	0.1536	0.1794	0.3559	0.3808	0.5321
Mg	2.6570	2.2533	2.2422	1.9289	2.5438	1.9789	1.8881	2.7909	4.1540	2.7352	2.1838	2.1155	1.9391
Al	2.1786	2.6487	2.2584	2.5452	1.6797	2.6881	2.1659	2.1972	1.0110	1.4041	2.6746	2.1535	2.3446
Si	6.6880	6.4308	6.5152	6.3128	6.9276	6.2076	6.5891	6.3208	7.0470	7.1686	6.5092	6.8578	6.5568
K	0.0601	0.1074	0.0585	0.0610	0.0955	0.0863	0.0838	0.1851	0.0346	0.0435	0.0745	0.1039	0.1087
Ca	1.6700	1.7205	1.5141	1.6708	1.5510	1.7865	1.5442	1.8182	1.7693	1.9048	1.5850	1.1243	1.6865
Ti	0.0370	0.0517	0.0598	0.0665	0.0304	0.0521	0.0562	0.2578	0.0321	0.0404	0.0479	0.0522	0.0490
Cr	0.0039	0.0039	0.0039	0.0019	0.0000	0.0000	0.0004	0.0017	0.0054	0.0038	nd	nd	nd
Mn	0.0171	0.0258	0.0224	0.0226	0.0220	0.0243	0.0385	0.0275	0.0281	0.0268	0.0165	0.0404	0.0443
Fe	1.7533	1.7922	2.3756	2.4588	2.2085	2.3170	2.7405	1.5126	1.2710	1.6914	1.8732	2.4268	2.2808
SUM	15.3620	15.4545	15.5955	15.6865	15.4402	15.7371	15.5195	15.7180	15.5061	15.1980	15.3206	15.2552	15.5419

Table 5.3 (con)

Biotite (Structural formulae based on 22 Oxygens)

	LMU					MMU				UMU	
	SF172	L128	T1	449	449XZ	68	378	438	442	B3	B12
Na	0.0215	0.0409	0.0455	0.0088	0.0204	0.0247	0.0294	0.0329	0.0343	0.0815	0.0357
Mg	2.3572	3.0448	1.4805	2.8257	2.2568	2.2300	3.2984	2.2370	2.3492	3.0066	3.0325
Al	2.9423	3.1353	3.3925	2.8977	3.2898	2.9470	2.8848	3.2420	3.3384	2.9637	3.0288
Si	5.4383	5.4517	5.4223	5.6027	5.4724	5.5226	5.5159	5.5406	5.4369	5.5680	5.5014
K	1.5305	1.8043	1.7912	1.8172	1.8659	1.8660	1.5913	1.6017	1.8702	1.6766	1.8257
Ca	0.0916	0.0083	0.0112	0.0074	nd	0.0029	0.0216	0.0052	0.0027	0.0297	0.0095
Ti	0.2768	0.1208	0.2447	0.2103	0.1982	0.2721	0.2192	0.1891	0.2006	0.2588	0.2374
Cr	0.0029	nd	0.0010	0.0034	0.0011	0.0029	nd	nd	nd	0.0035	nd
Mn	0.0197	0.0035	0.0179	0.0064	0.0051	0.0093	0.0113	0.0038	0.0230	0.0077	0.0023
Fe	2.9097	2.1728	3.1482	2.2702	2.5176	2.7995	2.0615	2.6144	2.3906	1.9730	2.0047
SUM	15.5894	15.7823	15.5550	15.6498	15.6273	15.6770	15.6334	15.4667	15.6459	15.5691	15.6780

	SF156	K2a	K2b	K3	KJ6	L226	SF173	SF179
Na	0.0108	0.0851	0.0466	0.2323	0.5801	nd	0.0625	0.1232
Mg	2.5467	2.9015	3.1798	2.3468	3.2150	3.5957	3.3049	3.0882
Al	3.1229	3.3249	3.1685	2.9417	3.4826	2.6069	2.8601	2.9855
Si	5.4178	5.5099	5.5230	5.5395	5.2439	5.5198	5.3837	5.3161
K	1.7035	1.6789	1.6179	1.6773	0.8919	1.7640	1.8297	1.5582
Ca	0.0254	0.0166	0.0044	0.0009	0.3959	nd	0.0074	0.0024
Ti	0.1951	0.1576	0.0787	0.2590	0.0143	0.4505	0.3107	0.2588
Cr	0.0146	nd	nd	nd	0.0099	nd	0.0039	0.0033
Mn	0.0199	0.0129	0.0142	0.0282	0.0227	0.0168	0.0103	0.0059
Fe	2.6190	1.8648	2.0131	2.6601	1.8746	1.6542	2.0470	2.4305
SUM	15.6757	15.5522	15.6462	15.6858	15.7309	15.6079	15.7577	15.6489

Table 5.3 (con)

Feldspars (Structural formulae based on 8 Oxygens)

	LMU				MMU			UMU								
	L128	L150	449XZ	68	378	438	442	B3 core	B3 rim	812	L25	L27	L41b	SF156 core	SF156 rim	K2a
Na	0.530	0.619	0.768	0.838	0.732	0.668	0.631	0.644	0.72	0.706	0.81	0.468	0.87	0.652	0.729	0.363
Mg	0.001	0.002	0.002	0.003	0.001	0.003	0.003	0.001	0.01	0.000	0.00	0.003	0.00	0.004	0.001	0.001
Al	1.439	1.373	1.231	1.151	1.252	1.273	1.329	1.329	1.26	1.272	1.15	1.488	1.12	1.322	1.277	1.595
Si	2.548	2.630	2.756	2.840	2.739	2.737	2.666	2.668	2.73	2.734	2.86	2.506	2.87	2.682	2.732	2.406
K	0.006	0.004	0.007	0.006	0.005	0.006	0.011	0.005	0.01	0.006	0.00	0.006	0.00	0.014	0.008	0.004
Ca	0.461	0.361	0.247	0.164	0.264	0.270	0.337	0.343	0.27	0.268	0.15	0.497	0.13	0.311	0.251	0.607
Ti	nd	0.000	0.000	0.001	nd	nd	nd	nd	nd	nd	nd	0.001	0.00	0.001	0.000	nd
Mn	nd	0.000	0.000	nd	nd	nd	nd	nd	nd	nd	nd	nd	nd	0.000	0.000	nd
Fe	0.010	0.005	0.003	0.004	0.011	0.006	0.010	0.001	0.01	0.002	0.01	0.018	0.01	0.005	0.001	0.004
SUM	4.995	4.994	5.015	5.005	5.004	4.963	4.987	4.991	4.999	4.986	4.976	4.986	5.006	4.989	4.998	4.980

	K2b	K3 core	K3 rim	KJ6	L226 core	L226 rim	L227	SF179
Na	0.576	0.790	0.740	0.351	0.485	0.549	0.348	0.495
Mg	0.004	0.000	0.000	0.001	0.023	0.001	0.003	0.001
Al	1.404	1.168	1.228	1.623	1.474	1.423	1.646	1.447
Si	2.588	2.835	2.773	2.379	2.498	2.572	2.353	2.568
K	0.006	0.006	0.009	0.002	0.023	0.007	0.003	0.003
Ca	0.418	0.173	0.231	0.626	0.486	0.430	0.639	0.438
Ti	nd	0.001	0.000	0.001	0.002	0.001	0.001	0.002
Mn	nd	0.005	0.003	0.000	nd	nd	nd	0.001
Fe	0.004	0.000	0.004	0.001	0.026	0.009	0.006	0.001
SUM	5.000	4.978	4.988	4.984	5.016	4.993	4.998	4.955

Table 5.3 (con)

Ilmenite (Structural formulae based on 3 Oxygens)

	LMU						MMU		UMU						
	SF172	L150	T1	449	449XZ	68	378	438	K2a	K3	L25	L27	L41b	KJ6	SF179
Si	0.000	0.000	0.001	0.000	0.000	0.000	0.000	0.00	0.000	0.001	0.000	0.00	0.000	0.006	0.000
Ti	0.961	0.933	1.021	1.004	1.002	0.982	0.995	1.01	0.991	0.969	0.965	0.89	0.932	0.963	0.956
Al	0.001	0.002	0.002	0.002	0.000	0.002	0.002	0.00	0.001	0.000	0.001	0.00	0.002	0.005	0.001
Cr	0.001	nd	nd	nd	0.000	nd	nd	nd	nd	nd	nd	nd	nd	0.011	0.000
Fe3	0.000	0.065	0.000	0.000	0.000	0.034	0.000	0.00	0.000	0.031	0.069	0.22	0.069	0.000	nd
Fe2	1.045	0.968	0.935	0.985	0.973	0.970	0.959	0.97	0.989	0.981	0.951	0.86	0.987	1.001	1.023
Mn	0.028	0.009	0.024	nd	0.022	0.008	0.034	0.01	0.030	0.019	0.010	0.01	nd	0.016	0.021
Mg	0.006	0.023	0.000	0.006	0.000	0.003	0.020	0.01	0.002	0.000	0.004	0.02	0.010	0.025	0.046
Ca	0.000	0.000	0.000	0.003	0.000	0.002	0.000	0.00	nd	0.000	0.000	0.00	0.000	0.000	0.000
SUM	2.042	2.000	1.982	1.999	1.996	2.000	2.008	1.997	2.012	2.000	2.000	2.000	2.000	2.026	2.047

Table 5.3 (con)

Muscovite (Structural formulae based on 22 Oxygens)

	LMU	MMU		UMU	
	T1	449XZ	438	442	K2a
Na	0.1067	0.2926	0.1971	0.1185	0.1755
Mg	0.2689	0.2424	0.1902	0.2966	0.4830
Al	5.1500	5.3481	5.4281	5.2801	4.8864
Si	6.3490	6.1669	6.2724	6.2406	6.5057
K	1.7141	1.6649	1.5834	1.7441	1.5295
Ca	0.0000	0.0021	0.0000	0.0005	0.0000
Ti	0.0756	0.0670	0.0496	0.0634	0.0461
Cr	0.0024	nd	nd	0.0011	nd
Mn	0.0036	0.0000	nd	0.0019	0.0011
Fe	0.2393	0.2872	0.1338	0.2400	0.2303
SUM	13.9096	14.0712	13.8546	13.9868	13.8576

Table 5.3 (con)

Pyroxene (Structural formulae based on 6 Oxygens)

	UMU					
	BO	EY	aver			
	L226	L227	KJ6	SF173	SF179	
				cpx	cpx	opx
Na	0.0483	0.0451	0.0614	0.0452	0.0356	0.0078
Mg	0.8064	0.7913	0.7490	0.7575	0.9049	1.2573
Al	0.1265	0.1263	0.2069	0.2111	0.1916	0.0782
Si	1.9334	1.9228	1.8916	1.8686	1.9203	2.0403
Ca	0.8186	0.8692	0.7561	0.7816	0.6060	0.0543
Ti	0.0099	0.0107	0.0255	0.0310	0.0330	0.0015
Cr	nd	0.0005	0.0016	0.0003	0.0005	0.0002
Mn	0.0146	0.0091	0.0047	0.0084	0.0057	0.0176
Fe	0.2424	0.2251	0.2997	0.2937	0.3024	0.5428
Fe3	0.0352	0.0515	0.2776	0.0398	0.0078	0.0000
Fe2	0.2072	0.1737	0.0221	0.2539	0.2946	0.5428
SUM	4.0001	4.0001	3.9965	3.9974	4.0000	4.0000

Table 5.3 (con)

Chlorite (Structural formulae based on 14 Oxygens)

	LMU		MMU		UMU					
	L128	L150	449XZ	438	442	B12	K2a	SF156	KJ6	KJ10b
Na	0.0107	0.0036	0.0000	0.0026	0.0197	0.0000	0.0080	0.0000	0.0542	0.0007
Mg	2.9616	2.9037	2.3807	2.2473	2.3939	2.7137	2.8504	1.6922	3.6077	3.8720
Al	2.5657	2.7260	2.7249	2.8331	2.7287	2.3419	2.6626	2.5319	2.0582	2.3218
Si	2.7212	2.6102	2.6529	2.5716	2.6129	2.4010	2.7217	2.8522	3.0547	2.8354
K	0.0458	0.0055	0.0236	0.0080	0.0112	0.0067	0.1462	0.1169	0.0074	0.0057
Ca	0.0039	0.0024	0.0189	0.0011	0.0056	0.0000	0.0040	0.0047	0.1785	0.0053
Ti	0.0110	0.0063	0.0083	0.0066	0.0064	0.0015	0.0250	0.0060	0.0107	0.0030
Cr	nd	nd	0.0000	nd	nd	nd	nd	0.0064	0.0006	nd
Mn	0.0047	0.0059	0.0113	0.0056	0.0298	0.0114	0.0119	0.0296	0.0056	0.0099
Fe	1.6884	1.7613	2.1677	2.3342	2.2234	2.9535	1.5689	2.6907	0.9581	0.9496
SUM	10.0130	10.0248	9.9881	10.0101	10.0314	10.4297	9.9987	9.9306	9.9357	10.0034

Table 5.4 Major and Trace Element analyses of rocks from Sognefjord

	GABBRO AND DYKES												AMPHIBOLITES				
	K1	K1B	K3	112C	112F	KJ1	KJ2	KJ3	KJ4	KJ5	KJ6	KJ7	SF40	SF41	SF32A	AV1	L68
SiO2	69.22	55.82	45.03	55.44	46.23	45.74	46.21	46.38	46.82	46.02	47.02	48.94	47.07	46.73	48.70	50.59	48.85
TiO2	0.27	0.62	3.31	0.66	2.31	2.64	2.24	2.08	2.18	2.59	0.67	0.65	1.95	2.03	0.17	0.75	0.88
Al2O3	15.62	19.10	13.32	19.46	15.84	15.15	15.58	16.03	15.18	15.05	19.06	17.01	19.01	16.29	23.53	16.61	16.50
Cr2O3	0.00	0.00	0.01	0.00	0.01	0.01	0.02	0.01	0.02	0.01	0.05	0.01	0.03	0.01	0.00	0.04	0.03
Fe2O3	2.82	7.11	19.62	7.14	16.10	17.02	15.91	14.87	14.62	16.29	11.80	10.20	13.45	14.87	7.07	10.67	12.17
MnO	0.04	0.15	0.19	0.14	0.22	0.21	0.20	0.19	0.20	0.21	0.15	0.16	0.14	0.18	0.08	0.17	0.18
MgO	0.42	2.87	6.39	2.62	6.15	5.77	6.50	6.43	6.58	6.03	9.37	9.60	5.58	6.52	6.65	6.95	8.52
CaO	1.34	6.01	8.26	5.87	9.22	7.93	8.38	8.57	9.23	8.41	8.46	9.85	8.08	8.22	9.89	8.75	10.29
Na2O	3.25	4.54	2.34	4.55	2.67	3.31	3.20	4.01	3.51	3.15	2.85	2.88	4.02	3.37	3.40	3.17	2.21
K2O	6.94	3.33	1.10	3.70	0.90	1.42	1.16	0.77	0.92	1.35	0.45	0.34	0.30	1.15	0.47	1.77	0.30
P2O5	0.08	0.45	0.44	0.42	0.33	0.80	0.61	0.66	0.72	0.88	0.12	0.36	0.36	0.62	0.03	0.53	0.06
Total	100.00	100.00	100.00	100.00	100.00	100.00	100.00	100.00	100.00	100.00	100.00	100.00	100.00	100.00	100.00	100.00	100.00
Rb	125.7	34.5	28.5	41.3	19.9	19.8	18.7	13.2	19.7	18.9	7.4	8.6	6.8	16.0	8.6	47.0	14.1
Sr	599.0	1266.9	191.4	1105.4	338.7	721.0	677.7	680.7	563.8	673.7	960.7	852.1	1283.8	715.2	556.8	1248.9	237.8
Y	15.5	16.6	47.4	16.5	34.9	29.7	27.7	29.1	33.8	32.0	4.0	17.1	10.7	25.8	2.4	16.5	18.0
Zr	207.9	17.9	247.2	18.1	181.6	80.5	75.7	73.5	96.5	75.2	22.4	43.4	32.6	66.2	13.1	62.8	58.3
Nb	12.7	2.1	10.8	2.7	12.5	8.1	8.4	7.2	11.5	6.7	2.8	4.4	2.8	6.3	2.0	4.6	4.0
Pb	31.6	15.4	9.1	17.0	7.0	10.6	6.2	8.4	10.2	8.8	4.3	4.1	9.2	5.3	17.1	8.7	6.0
Zn	33.3	83.4	204.9	84.8	131.0	151.7	111.5	124.9	122.7	144.5	84.0	75.1	96.7	126.8	54.0	84.9	77.8
Cu	76.5	45.3	47.5	69.1	73.9	72.9	91.0	82.5	78.8	66.0	28.9	34.4	98.7	82.8	2.4	60.3	87.1
Ni	1.3	8.8	44.8	8.5	76.4	81.1	109.2	111.4	85.6	75.3	195.2	161.8	107.9	108.2	181.1	82.3	156.3
Co	3.3	13.1	54.6	13.2	57.2	51.7	59.3	51.9	48.1	53.6	62.0	55.1	54.7	56.5	45.4	36.9	52.1
Cr	4.4	25.2	82.8	26.0	31.9	59.5	121.2	59.3	155.9	71.1	279.6	54.7	178.6	67.5	22.9	278.9	198.7
V	30.2	125.4	286.0	124.2	262.3	332.2	286.5	235.6	269.5	310.8	97.2	75.8	237.0	253.3	21.2	213.3	190.1
Ba	2750.1	2620.9	433.4	2379.9	428.5	1342.9	1055.2	910.0	1010.0	1276.2	451.7	519.3	447.8	1021.3	306.9	972.3	110.0

Table 5.4 (con) Major and Trace Element analyses of rocks from Sognefjord

	SOGNEFJORD DYKES																
	L161	V1	SF1	SF2	SF4	SF5	SF6	SF9	SF10	SF11	SF12	84D2	84D3	85D1	85D2	85D3	85D4A
SiO2	47.74	49.11	50.96	56.87	52.44	51.68	52.14	45.23	52.77	55.01	44.91	47.07	50.79	54.70	44.98	47.63	59.12
TiO2	0.55	0.70	3.13	1.82	1.62	1.57	1.86	2.19	2.51	2.47	3.39	1.31	3.15	1.91	3.33	2.10	0.87
Al203	19.91	16.93	15.17	15.21	15.65	15.38	18.18	16.00	15.43	14.98	15.26	15.49	15.00	14.96	15.39	15.52	17.07
Cr203	0.01	0.03	0.01	0.00	0.01	0.02	0.00	0.01	0.00	0.00	0.01	0.04	0.01	0.02	0.01	0.02	0.00
Fe203	9.09	10.64	12.04	8.98	11.10	12.44	8.92	15.34	11.14	10.87	16.34	13.19	12.07	8.44	16.13	14.45	8.70
MnO	0.13	0.16	0.15	0.17	0.22	0.19	0.12	0.21	0.13	0.18	0.23	0.20	0.15	0.11	0.22	0.36	0.21
MgO	9.49	8.55	3.98	3.42	4.93	5.39	2.67	6.54	3.52	3.34	5.50	7.75	3.98	5.10	5.65	5.68	0.87
CaO	10.93	11.30	6.50	4.40	6.36	7.12	6.62	8.40	6.61	5.22	7.38	11.08	6.62	4.82	7.57	6.96	2.80
Na20	1.95	2.26	2.92	4.28	4.70	4.03	5.06	2.79	3.45	3.35	3.41	2.69	2.99	2.71	3.56	4.06	4.41
K20	0.15	0.28	3.84	3.94	2.56	1.89	3.56	2.99	3.50	3.62	2.98	0.97	3.92	6.31	2.56	2.51	5.65
P205	0.04	0.04	1.29	0.91	0.41	0.29	0.85	0.30	0.93	0.95	0.61	0.21	1.33	0.93	0.60	0.70	0.32
Total	100.00	100.00	100.00	100.00	100.00	100.00	100.00	100.00	100.00	100.00	100.00	100.00	100.00	100.00	100.00	100.00	100.00
Rb	6.7	9.9	179.1	126.0	52.6	54.2	121.7	81.5	106.4	189.8	133.6	26.0	184.5	152.3	98.7	120.8	109.6
Sr	217.2	219.5	579.7	536.4	779.9	487.8	1630.8	340.9	1033.6	855.1	435.4	427.9	594.7	1166.1	520.4	381.9	336.8
Y	12.9	13.3	23.3	37.6	22.8	21.2	19.6	28.7	25.2	28.1	28.0	20.1	20.6	15.7	28.7	31.1	134.0
Zr	39.0	34.7	220.2	308.0	143.4	106.0	227.2	137.5	257.8	292.6	127.6	61.3	224.3	648.7	124.1	123.3	1476.9
Nb	2.8	3.1	12.0	14.5	9.9	9.1	11.5	11.1	14.0	14.3	8.5	4.9	11.1	16.9	8.5	7.8	66.6
Pb	5.8	3.7	19.7	54.8	17.5	13.5	20.9	21.7	18.8	19.8	12.4	7.6	19.5	26.4	13.0	12.8	32.7
Zn	58.2	71.3	148.3	131.6	118.8	117.0	74.5	116.8	133.0	187.4	164.6	95.0	150.7	122.9	149.1	173.6	211.4
Cu	60.0	67.1	38.8	18.7	28.9	30.6	34.8	19.1	25.5	23.3	77.8	128.8	32.7	0.0	48.9	24.2	12.5
Ni	222.4	164.4	38.2	21.5	44.6	88.7	20.6	87.9	26.7	22.7	47.2	61.7	34.6	131.1	53.5	78.6	3.9
Co	51.1	51.3	39.0	21.0	31.9	36.7	16.5	50.8	24.4	30.5	48.3	47.3	37.4	31.1	47.1	38.7	2.3
Cr	75.0	186.9	35.3	19.0	41.8	104.7	9.7	69.0	24.7	18.0	32.4	258.7	35.3	181.1	26.9	121.0	4.3
V	117.8	172.5	187.9	129.9	141.7	148.0	125.3	212.8	167.0	162.0	263.1	242.9	178.3	135.7	255.5	243.8	33.4
Ba	62.4	89.4	685.0	1251.1	1141.0	687.4	1312.3	424.7	1516.8	1258.7	865.6	182.3	686.5	2821.7	633.1	436.9	1929.3

Table 5.4 (con) Major and Trace Element analyses of rocks from Sognefjord

	85D4B	85D4C	85D5	85D6	85D7	85D8	85D9A	85D9B	85D10	85D11	85D12	85D13	85D14A	85D14B	85D14C	85D14D	85D14E
SiO2	50.60	47.66	44.62	44.78	41.55	55.68	52.55	53.20	47.59	52.83	53.40	54.47	52.59	49.96	66.31	75.88	65.17
TiO2	0.75	1.58	4.34	3.60	4.52	0.75	1.81	0.49	0.51	1.11	2.05	2.21	0.80	0.91	0.66	0.10	0.73
Al2O3	16.75	18.38	15.22	14.81	13.22	16.62	14.90	16.01	16.98	16.54	15.51	14.85	18.93	18.92	16.50	13.00	15.65
Cr2O3	0.02	0.00	0.00	0.01	0.02	0.01	0.01	0.02	0.01	0.01	0.00	0.00	0.00	0.00	0.00	0.00	0.00
Fe2O3	10.88	12.98	17.68	17.15	18.66	8.61	11.28	9.22	11.27	11.67	10.75	10.88	10.14	11.23	3.53	1.17	5.05
MnO	0.27	0.24	0.21	0.23	0.30	0.25	0.15	0.18	0.18	0.33	0.15	0.17	0.24	0.25	0.15	0.02	0.14
MgO	6.42	3.78	4.41	5.16	6.23	4.43	4.89	5.63	10.76	4.83	3.54	2.99	3.09	3.54	0.63	0.05	0.64
CaO	8.22	9.17	7.32	7.30	9.67	7.30	6.97	9.10	8.16	6.09	5.84	5.29	4.83	6.30	1.36	0.51	1.94
Na2O	3.05	3.95	4.32	3.35	1.91	4.74	3.07	4.72	2.44	4.14	4.14	4.14	4.76	4.57	4.75	4.18	4.24
K2O	2.87	1.23	1.25	2.95	2.19	1.33	3.74	1.26	1.96	2.33	3.43	3.64	4.16	3.79	5.95	5.08	6.30
P2O5	0.16	1.02	0.62	0.67	1.74	0.29	0.63	0.16	0.16	0.13	1.19	1.35	0.46	0.52	0.17	0.01	0.13
Total	100.00	100.00	100.00	100.00	100.00	100.00	100.00	100.00	100.00	100.00	100.00	100.00	100.00	100.00	100.00	100.00	100.00
Rb	91.0	29.8	33.7	171.0	79.2	70.7	131.3	34.1	54.4	137.6	75.3	93.9	132.7	125.0	107.0	102.9	132.1
Sr	795.6	909.5	655.9	441.1	250.7	406.6	573.7	396.2	691.2	332.1	1314.5	985.1	1076.2	1209.3	200.9	48.6	229.4
Y	43.4	34.8	31.1	33.9	81.1	67.0	21.3	31.1	16.8	47.7	37.2	42.2	16.0	18.5	45.2	2.5	91.1
Zr	79.2	32.9	124.0	142.6	455.4	50.4	163.6	31.5	84.3	65.8	434.4	442.7	86.9	82.0	367.0	42.6	993.6
Nb	8.1	3.7	8.3	8.8	20.9	16.7	9.2	7.7	5.0	17.0	18.7	19.8	5.4	5.2	19.8	4.7	50.4
Pb	19.7	29.2	4.4	10.9	8.1	15.7	17.2	14.0	10.3	12.0	31.3	32.7	28.8	23.9	23.5	20.5	44.2
Zn	148.3	192.1	122.5	133.6	167.6	101.0	131.4	80.6	89.5	205.7	155.5	171.2	168.0	135.3	95.1	17.5	168.1
Cu	43.7	30.5	37.9	111.0	38.0	17.1	30.0	5.4	44.7	4.4	22.1	23.4	0.3	15.7	16.7	3.1	5.4
Ni	80.8	19.1	30.9	44.2	67.5	31.8	62.0	34.3	146.6	51.7	24.9	8.5	2.9	2.8	0.8	0.1	2.2
Co	37.4	24.9	45.1	51.7	55.6	27.7	33.7	29.0	65.6	31.5	23.9	15.7	20.6	16.1	0.1	0.0	0.0
Cr	112.5	18.5	1.7	32.8	145.7	87.8	98.4	160.1	30.8	54.0	34.0	1.7	6.2	2.8	1.0	4.2	0.0
V	130.4	174.5	363.8	277.3	256.4	135.4	143.4	125.9	81.4	135.9	155.0	140.7	115.9	132.7	31.0	7.3	23.5
Ba	661.8	571.9	669.2	665.2	662.6	288.2	1245.1	240.2	591.0	314.8	2131.4	2239.9	1059.0	1557.1	1009.9	278.3	2006.7

Table 5.4 (con) Major and Trace Element analyses of rocks from Sognefjord

	ECLOGITES																
	85D15	92	327	336	483A	483B	SF27	166	BK1B	BK1C	BK1D	BK1E	BK1J	H01	H02	85D16A	85D16B
SiO2	53.50	46.75	47.27	47.11	46.60	45.03	45.04	45.02	45.54	46.49	45.70	54.52	45.13	46.06	46.03	47.59	46.69
TiO2	1.86	1.88	0.90	0.91	2.25	2.62	2.89	2.85	2.03	1.61	1.56	1.15	1.59	3.17	2.58	2.66	2.18
Al2O3	16.56	14.65	16.06	17.32	12.96	16.08	16.01	16.56	16.91	16.99	16.16	19.52	16.49	15.21	14.90	18.46	17.50
Cr2O3	0.01	0.01	0.02	0.01	0.00	0.01	0.01	0.01	0.01	0.01	0.01	0.00	0.01	0.01	0.02	0.00	0.00
Fe2O3	9.61	16.88	12.74	12.92	17.40	15.38	16.35	16.95	14.60	13.99	15.40	8.20	15.69	16.87	16.06	13.26	13.86
MnO	0.17	0.27	0.20	0.19	0.33	0.21	0.23	0.24	0.22	0.22	0.25	0.15	0.25	0.24	0.23	0.16	0.16
MgO	3.49	5.30	7.59	7.60	5.46	5.62	6.15	6.03	7.36	7.25	7.84	2.92	7.77	4.82	5.84	4.48	7.24
CaO	5.65	7.76	9.99	8.72	7.64	7.89	7.69	8.42	9.77	9.32	9.79	6.48	9.84	7.32	8.69	8.29	7.37
Na2O	4.93	3.56	3.50	2.90	3.28	3.65	3.28	2.74	2.72	2.99	2.90	5.35	2.80	3.33	2.81	3.64	3.57
K2O	3.14	2.26	1.44	2.11	2.70	2.74	1.72	0.68	0.77	0.97	0.28	1.24	0.33	2.29	2.45	0.95	0.96
P2O5	1.07	0.68	0.29	0.22	1.38	0.78	0.63	0.50	0.07	0.15	0.11	0.46	0.10	0.68	0.39	0.50	0.47
Total	100.00	100.00	100.00	100.00	100.00	100.00	100.00	100.00	100.00	100.00	100.00	100.00	100.00	100.00	100.00	100.00	100.00
Rb	72.0	50.9	22.7	83.5	68.2	65.5	62.8	21.6	32.7	39.5	12.2	34.7	13.4	121.1	142.4	17.7	16.9
Sr	1226.4	475.6	503.6	589.5	274.6	695.0	395.4	415.5	283.9	175.4	203.8	1368.1	232.8	268.0	163.1	1006.2	782.5
Y	34.1	41.6	24.1	21.1	36.0	27.3	36.6	37.8	32.9	27.6	34.4	22.7	32.7	79.7	49.3	23.7	20.7
Zr	378.6	101.4	48.3	42.2	84.9	119.8	211.4	172.8	89.0	80.9	79.2	255.8	86.9	228.1	183.4	106.9	100.8
Nb	19.3	4.9	3.6	3.1	5.0	4.8	10.2	10.0	6.6	5.1	7.0	7.2	6.6	16.3	8.1	6.7	5.5
Pb	26.9	12.4	17.9	9.6	12.6	10.0	14.0	12.1	19.6	9.3	8.2	14.0	9.5	25.6	14.2	6.6	5.5
Zn	159.3	139.0	95.8	95.1	160.2	105.2	141.6	139.3	111.9	109.1	128.5	70.1	130.4	235.1	162.0	94.6	98.6
Cu	9.8	105.1	30.5	76.4	21.2	30.0	40.4	28.0	3.5	15.3	8.8	11.0	4.2	56.3	108.7	28.2	23.8
Ni	36.4	53.2	87.0	113.9	23.0	48.8	88.2	70.7	110.6	104.8	121.2	18.4	125.7	44.3	71.2	40.8	107.5
Co	21.9	51.9	41.2	52.1	40.0	47.0	54.9	54.3	44.9	46.9	56.0	12.1	58.7	48.7	49.7	37.9	48.7
Cr	60.0	32.1	104.8	58.3	10.5	32.0	94.0	73.4	95.3	89.9	92.4	14.5	83.1	47.0	100.2	18.3	18.5
V	138.4	299.4	205.6	187.4	347.9	252.5	234.2	240.0	226.8	184.6	215.7	112.2	209.3	256.3	257.8	215.9	181.0
Ba	2283.3	1345.2	431.9	848.3	2510.8	1561.6	919.6	383.0	210.2	420.3	70.1	548.9	96.2	1068.8	464.8	737.2	645.6

Table 5.4 (con) Major and Trace Element analyses of rocks from Sognefjord

	GRANODIORITE			
	FF1A	FF1B	FF1C	FF1D
SiO2	70.24	70.59	70.51	71.16
TiO2	0.19	0.12	0.11	0.11
Al2O3	16.38	16.63	16.77	16.31
Cr2O3	0.00	0.00	0.00	0.00
Fe2O3	2.08	1.52	1.52	1.54
MnO	0.03	0.02	0.03	0.03
MgO	0.28	0.16	0.15	0.13
CaO	1.44	1.49	1.51	1.42
Na2O	5.67	5.98	5.92	5.73
K2O	3.61	3.46	3.44	3.54
P2O5	0.06	0.03	0.03	0.03
Total	100.00	100.00	100.00	100.00
Rb	52.6	41.8	41.8	56.9
Sr	1212.1	1488.5	1632.9	1156.2
Y	4.0	3.5	3.7	4.4
Zr	80.7	82.2	75.3	73.5
Nb	3.1	2.9	3.1	3.1
Pb	32.9	29.3	27.4	32.8
Zn	55.4	34.5	28.4	48.2
Cu	6.3	6.9	7.2	6.1
Ni	0.1	0.1	0.0	0.1
Co	3.1	0.0	0.0	0.2
Cr	3.0	6.1	5.9	5.9
V	13.8	9.4	8.6	9.4
Ba	1824.0	2017.5	2105.5	1692.7

Table 6.1 Mineral assemblages in Hyllestad Schists

	garn	ky	sta	musc	qtz	ctd	amph	biot	chl	epid	plag	K-fsp	calc	sph	rut	ilm	tour	mag	apat
Hyllestad area	Group A: kyanite-almandine schists																		
472	×	×	×	×	×	×			(×)	×					×	×	×	(×)	×
H12	×	×	×	×	×	×		(×)	(×)						×				
H16	×	×		×	×				(×)							×		(×)	
SF54	×	×	×	×	×	×		(×)	(×)						×	×	×	(×)	×
Hyllestad area	Group B: garnet-chlorite-biotite schists																		
421	×				×		×		×	×			×					×	
424	×			×	×			×	(×)							×	×	×	
427																			
543	×			×	×			×									×		×
550	×			×	×			×	×	×	×					×			
A3	×			×	×			×	(×)							×	×	×	
DAN13	×			×	×			×	×		alb						×	×	
DAN14					×			×		×	×			×					
H11				×	×			×	×	×	×		×			×	×		
SF52	×			×	×			×	×	×	alb		×			×	×		×
Hyllestad area	Group C: garnet-amphibole schists and mafic amphibolites (also carbonate rocks)																		
A2a				×		tre			×	×	×		×	×					
A4	×			×		×	(×)		(×)	×	×		×		×	×			×
H15	×		×	×		×	×		(×)	×					×		×		
H17	×		×	×		×	×		(×)	×	×		×	×		×			
H18	×			×		×			(×)	×	×		×			×		(×)	
SF46				×		×	×			×	×					×			×
SF47				×		×	×				×			×		×			×
SF84b			×	×		tre	phl			×	×		×	×					
Y29	×			×		×	×	×	×	×	×			×	×			×	×
Soetevik area	Group D																		
H10				×		×			×	×	×		×	×	×				
R6	×		×	×			×		×	×	×					×			
R8	×		×	×		×	×		××	×						×			
SF48	×		×	×	×	×	×	×	×							×		×	
Rasvikheia area	Group E																		
Y17.1	×		×	×			×		(×)							×	×		×
Y22	×		×	×		×	×		(×)	×	×					×			

Table 6.2 Mineral chemistry of assemblages in Hyllestad Schists (structural formulae given)

GARNET (O=12)

Group A

	SF54B		SF54C		472		H16	
	core	rim	core	rim	core	rim	core	rim
Mg	0.346	0.937	0.386	0.941	0.350	0.933	0.471	0.598
Al	1.967	1.983	1.971	1.966	2.015	2.015	1.963	1.971
Si	2.978	2.992	2.990	2.994	2.997	2.995	2.981	2.996
Ca	0.310	0.076	0.283	0.063	0.403	0.101	0.190	0.198
Ti	0.011	0.001	0.004	0.001	0.004	0.003	0.001	0.002
Mn	0.189	0.003	0.157	0.002	0.144	0.008	0.034	0.032
Fe	2.198	2.007	2.208	2.035	2.087	1.945	2.359	2.204
Fe3	0.044	0.024	0.035	0.039	0.000	0.000	0.055	0.032
Fe2	2.154	1.983	2.173	1.995	2.087	1.945	2.304	2.172
	8.000	8.000	8.000	8.000	8.000	8.000	8.000	8.000

Group B

	SF52		427		DAN13	
	core	rim	core	rim	core	rim
Mg	0.323	0.683	0.113	0.399	0.109	0.509
Al	1.967	1.981	2.003	2.024	1.978	2.029
Si	3.011	3.018	3.004	3.063	3.083	3.023
Ca	0.469	0.304	0.515	0.247	0.469	0.229
Ti	0.007	0.001	0.006	0.003	0.005	0.003
Mn	0.558	0.193	0.376	0.052	0.585	0.033
Fe	1.664	1.820	1.983	2.212	1.771	2.175
Fe3	0.015	0.000	0.000	0.000	0.000	0.000
Fe2	1.650	1.820	1.983	2.212	1.771	2.175
	8.000	8.000	8.000	8.000	8.000	8.000

Group C

	A3		A4*		H15		H17		H18		SF51*	
	core	rim	core	rim	core	rim	core	rim	core	rim	core	rim
Mg	0.111	0.566	0.362	0.450	0.444	0.674	0.319	0.422	0.188	0.272	0.109	0.147
Al	1.996	2.066	1.966	1.960	1.868	1.870	1.965	2.005	1.934	1.954	1.942	1.938
Si	2.987	3.053	2.974	2.984	3.078	3.033	3.048	3.023	3.037	3.033	2.990	2.987
Ca	0.629	0.260	0.436	0.643	0.463	0.353	0.763	0.848	0.603	0.758	0.888	0.888
Ti	0.008	0.001	0.006	0.002	0.006	0.001	0.012	0.003	-	-	0.012	0.012
Mn	0.390	0.027	0.177	0.039	0.299	0.043	0.190	0.033	0.413	0.036	0.344	0.096
Fe	1.878	2.026	2.074	1.922	1.842	2.026	1.703	1.666	1.827	1.947	1.791	1.932
Fe3	0.009	0.000	0.048	0.054	0.048	0.096	0.000	0.000	0.030	0.014	0.056	0.064
Fe2	1.870	2.026	2.025	1.868	1.794	1.931	1.703	1.666	1.797	1.934	1.735	1.868
	8.000	8.000	7.994	8.000	8.000	8.000	8.000	8.000	8.000	8.000	7.999	8.000

Group D

	R6		R8*	SF48
	core	rim		
Mg	0.141	0.324	0.434	0.119
Al	1.967	1.979	1.962	2.015
Si	3.005	3.003	2.981	2.994
Ca	0.484	0.367	0.425	0.442
Ti	0.004	0.004	0.002	0.005
Mn	0.681	0.104	0.088	0.092
Fe	1.718	2.219	2.107	2.334
Fe3	0.024	0.014	0.054	0.000
Fe2	1.694	2.206	2.053	2.334
	8.000	8.000	7.999	8.000

Group E

	Y4		Y11.2*		Y13a*	Y17.1*		Y22		368*	
	core	rim	core	rim		core	rim	core	rim	core	rim
Mg	0.088	0.257	0.094	0.426	0.242	0.151	0.383	0.059	0.133	0.113	0.317
Al	1.915	1.989	1.951	1.994	1.987	1.967	1.986	1.968	1.977	1.944	1.983
Si	3.010	3.001	3.027	3.009	3.005	2.994	3.012	2.990	2.983	2.994	3.000
Ca	0.448	0.308	0.478	0.357	0.630	0.718	0.507	0.947	0.943	0.538	0.304
Ti	0.007	0.003	0.005	0.004	0.004	0.013	0.006	0.004	0.004	0.007	0.002
Mn	0.831	0.007	0.850	0.089	0.100	0.401	0.111	0.772	0.095	0.602	0.079
Fe	1.701	2.435	1.593	2.119	2.031	1.756	1.990	1.260	1.865	1.802	2.315
Fe3	0.067	0.007	0.014	0.000	0.002	0.026	0.000	0.038	0.036	0.054	0.014
Fe2	1.633	2.428	1.579	2.119	2.029	1.730	1.990	1.222	1.829	1.748	2.301
	8.000	8.000	7.997	7.999	7.999	8.000	7.994	8.000	8.000	7.998	8.000

* analysis also contains small amounts of Cr

Group A: kyanite-almandine schists occurring at Kleivevatnet and Ronset (see fig 3.7)
Group B: chlorite-biotite-garnet schists from Kleivevatnet, Kolgrovheia, and Katlenova
Group C: garnet-amphibole schists and mafic amphibolites from Hyllestad and Kleivevatnet
Group D: schists from Soetevik
Group E: schists from Rasvikheia-Espelandet

Table 6.2 (con) Mineral chemistry of assemblages in Hyllestad Schists

MUSCOVITE (O=22)

	Group A						Group B				Group C	Group D
	SF54B		SF54C		472	H16	SF52	427	DAN13	A3	H17	R6
	inc	mat	inc	mat	mat							
Na	1.646	0.539	1.615	0.508	0.356	0.247	0.222	0.247	0.131	0.277	1.528	0.192
Mg	0.015	0.262	0.022	0.274	0.300	0.254	0.519	0.240	0.149	0.166	0.044	0.378
Al	5.919	5.303	5.951	5.199	5.086	5.014	5.095	4.931	5.226	5.136	6.073	4.934
Si	5.997	6.200	5.972	6.290	6.342	6.300	6.196	6.414	6.380	6.401	5.919	6.382
K	0.192	1.428	0.228	1.399	1.539	1.729	1.476	1.652	1.564	1.627	0.217	1.732
Ca	0.062	0.000	0.037	0.000	0.000	0.000	0.002	0.001	0.002	0.000	0.052	0.000
Ti	0.016	0.052	0.018	0.047	0.044	0.105	0.041	0.083	0.044	0.064	0.018	0.042
Cr	-	-	-	-	-	-	-	-	0.005	0.002	-	-
Mn	0.000	0.002	0.002	0.000	0.005	0.000	0.002	0.004	0.000	0.001	0.002	0.003
Fe	0.100	0.296	0.112	0.299	0.347	0.428	0.514	0.410	0.307	0.245	0.048	0.409
	13.946	14.081	13.956	14.017	14.019	14.076	14.065	13.983	13.808	13.918	13.900	14.072

BIOTITE (O=22)

	Group E					Group B					Group C		
	Y11.2	Y13a	Y17.1	Y22	368		SF52	427	DAN13	A3	H17	H18	SF51
Na	0.219	0.195	0.501	0.304	0.178	Na	0.024	0.024	0.049	0.035	0.067	0.043	0.019
Mg	0.309	0.383	0.265	0.245	0.443	Mg	3.147	2.056	2.953	1.838	3.597	2.641	2.652
Al	5.141	5.085	4.873	5.345	4.952	Al	3.172	3.113	3.124	3.283	2.986	2.818	3.027
Si	6.333	6.384	6.540	6.264	6.435	Si	5.507	5.855	5.734	5.663	5.501	5.638	5.481
K	1.757	1.715	1.419	1.672	1.678	K	1.621	1.765	1.733	1.872	1.625	1.705	1.641
Ca	0.000	0.005	0.150	0.001	0.000	Ti	0.145	0.162	0.177	0.210	0.015	0.106	0.197
Ti	0.051	0.048	0.041	0.038	0.051	Cr	-	-	0.003	0.005	0.153	0.201	0.002
Cr	0.003	0.003	0.007	0.002	0.004	Mn	0.024	0.019	0.023	0.022	0.002	0.015	0.012
Mn	0.002	0.001	0.003	0.002	0.001	Fe	1.947	2.320	1.620	2.507	1.753	2.459	2.598
Fe	0.217	0.161	0.142	0.140	0.222		15.586	15.314	15.416	15.433	15.699	15.626	15.630
	14.032	13.979	13.940	14.013	13.964								

	Group D		Group E					
	R6	R8	Y4	Y11.2	Y13a	Y17.1	Y22	368
Na	0.049	0.046	0.040	0.038	0.033	0.038	0.023	0.065
Mg	2.795	2.629	2.622	2.972	2.959	2.416	2.973	2.833
Al	3.096	2.970	3.142	3.199	3.139	3.304	3.035	3.342
Si	5.542	5.628	5.524	5.537	5.476	5.465	5.547	5.543
K	1.845	1.827	1.912	1.847	1.848	1.808	1.810	1.680
Ti	0.187	0.187	0.249	0.186	0.209	0.210	0.180	0.153
Cr	-	0.006	0.013	0.007	0.005	0.011	0.011	0.007
Mn	0.024	0.022	0.016	0.023	0.012	0.015	0.013	0.021
Fe	2.131	2.319	2.109	1.807	2.001	2.317	2.072	1.828
	15.669	15.634	15.626	15.616	15.681	15.584	15.665	15.471

Table 6.2 (con) Mineral chemistry of assemblages in Hyllestad Schists

CHLORITE (assuming O=20, OH=16)

	Group B				Group C			Group D	Group E			
	SF52	427	DAN13	A3	H15	H17	SF51	R6	Y11.2	Y13a	Y17.1	368
Na	0.008	0.008	0.007	0.012	0.000	0.000	0.000	0.007	0.021	0.018	0.014	0.000
Mg	5.888	4.116	5.466	3.870	5.626	5.099	5.095	2.812	6.214	5.904	5.441	5.895
Al	5.226	5.642	5.552	5.594	5.277	5.493	5.174	2.680	5.475	5.331	5.440	5.403
Si	5.439	5.362	5.352	5.454	5.460	5.217	5.404	2.668	5.234	5.356	5.257	5.314
K	0.181	0.102	0.050	0.044	0.016	0.016	0.017	0.038	0.016	0.064	0.012	0.065
Ti	0.027	0.026	0.014	0.016	0.012	0.011	0.012	0.010	0.012	0.018	0.011	0.016
Mn	0.074	0.056	0.075	0.056	0.052	0.007	0.030	0.032	0.046	0.029	0.041	0.047
Fe	3.174	4.516	3.345	4.700	3.459	4.191	4.253	1.754	3.008	3.269	3.732	3.250
	20.018	19.828	19.862	19.746	19.900	20.033	19.984	19.984	20.026	19.989	19.947	19.990

STAUROLITE (assuming O=22, OH=2)

	Group A					
	SF54B	SF54C	472 inc	472 mat	H12 inc	H12 mat
Mg	0.504	0.430	0.259	0.259	0.442	0.348
Al	8.708	8.688	9.185	8.833	8.571	8.711
Si	3.903	3.904	4.207	3.981	3.954	3.951
Ca	-	-	0.001	-	-	-
Ti	0.059	0.061	0.054	0.000	0.065	0.058
Mn	0.002	0.005	0.017	0.053	-	-
Fe	1.469	1.577	1.410	1.415	1.583	1.344
Zn	0.040	0.027	-	-	0.070	0.218
	14.684	14.692	15.133	14.542	14.685	14.630

CHLORITOID (assuming O=10, OH=4)

	Group A			Group D
	H12	SF54C	472	SF48
Na	-	0.007	-	-
Mg	0.606	1.125	1.212	0.394
Al	3.910	7.948	7.851	7.846
Si	2.032	4.010	4.018	4.071
K	-	0.010	0.006	-
Ca	-	0.060	0.001	0.000
Ti	0.001	0.004	0.001	0.002
Mn	0.004	0.009	0.023	0.026
Fe	1.455	2.848	2.946	3.666
	8.007	16.021	16.058	16.004

AMPHIBOLE (assuming O=22, OH=2)

	Group C					Group D		Group E	
	A4	H15	H17	H18	SF51	R8	SF48	Y13a	Y22
Na	0.745	0.631	0.606	0.669	0.398	0.752	0.429	0.393	0.403
Mg	2.156	2.199	1.905	1.593	2.007	1.931	1.146	1.939	2.158
Al	2.492	2.744	2.659	2.550	2.490	2.633	3.137	2.809	2.624
Si	6.482	6.409	6.416	6.489	6.485	6.460	6.178	6.352	6.502
K	0.138	0.086	0.086	0.147	0.098	0.089	0.079	0.091	0.089
Ca	1.537	1.458	1.682	1.490	1.751	1.464	1.759	1.661	1.655
Ti	0.090	0.053	0.038	0.079	0.044	0.048	0.039	0.040	0.042
Cr	0.002	-	-	-	0.003	0.003	-	0.009	0.005
Mn	0.006	0.013	0.015	0.029	0.035	0.011	0.021	0.019	0.020
Fe	1.974	1.932	2.155	2.519	2.161	2.205	2.681	1.832	1.889
	15.622	15.525	15.562	15.565	15.472	15.595	15.468	15.145	15.387

Group A: kyanite-almandine schists occurring at Kleivevatnet and Ronset (see fig 3.7)
Group B: chlorite-biotite-garnet schists from Kleivevatnet, Kolgrovheia, and Katlenova
Group C: garnet-amphibole schists and mafic amphibolites from Hyllestad and Kleivevatnet
Group D: schists from Soetevik
Group E: schists from Rasvikheia-Espelandet

Table 6.3 THERMOBAROMETRY OF HYLLESTAD SCHISTS

		Kyanite-almandine schists						Chl-bi-gt schists				Garnet-amphibole schists			
Thermometry/°C		H12	SF54	SF54B	SF54C	472	H16	SF52	427	DAN13	A3	A4	H15	H17	H18
Gt-hbl	G & P											646	628	697	669
	Per											601	657	597	593
Gt-bi	G & S							627	632	452	727			500	538
	H & S							734	682	520	788			581	584
Gt-mu	H & F	639	601	613	620	623	691	631	630	645	611			520	
	K & R	714	721	740	751	749	761	681	643	684	622			619	
	G & H	830	837	854	864	862	873	800	764	802	745			742	
Gt-st	Per (mat)	636	696	679	716	865									
	Per (inc)	617	699	711	640	597									
Gt-ilm	Fe-Mn Kd	0.60						10.64	0.44		0.25	2.53			0.44
BAROMETRY/kbar															
GRAIL	BWB	5.7	5.7	5.6	6.0	5.3	6.0								
Phengite (minimum)	M & S	6.5	7.0	5.5	6.0	6.0	6.0	6.0	7.5	8.0	8.5		7.5	4.5	
Gt-mica -fsp	G & St (1)							8.3	12.9	15.6	9.4			14.2	
	G & St (2)							7.7	12.6	16.7	8.0			15.5	
	H & C							8.5	13.3	17.4	9.8			16.7	
GRIPS	B & L										8.9			*14.7	13.4

Thermometry at 8 kbar, barometry at 630°C
* Pressure probably overestimated as ilmenite assumed to be pure

G & P: Graham & Powell, 1984; Per: Perchuk, 1977; G & S: Ganguly & Saxena, 1984; H & S: Hodges & Spear, 1982; H & F: Hynes & Forest, 1988; K & R: Krogh & Raheim, 1974; G & H: Green & Hellman, 1982 BWB: Bohlen et al, 1983; M & S: Massone & Schreyer, 1987; G & St: Ghent & Stout (equilibria 1 & 2), 1981; H & C: Hodges & Crowley, 1985; B & L: Bohlen & Liotta, 1986.

Table 6.3 (con) THERMOBAROMETRY OF HYLLESTAD SCHISTS

		Schists at Soetevik					Schists at Rasvikheia					
Thermometry/°C		SF51	SF55	R6	R8	SF48	Y4	Y11.2	Y13a	Y17.1	Y22	368
Gt-hbl	G & P	509			591	466			547		544	
	Per	416			608	474			515		511	
Gt-bi	G & S	436	657	469	592	494	415	469	459	614	499	413
	H & S	463	694	498	652	483	429	522	499	668	540	437
Gt-mu	H & F			542				508	387	439	444	441
	K & R			528				512	410	451	461	421
	G & H			654				638	536	577	587	547
Gt-st	Per (mat)											
	Per (inc)											
Gt-ilm	Fe-Mn Kd	1.64			1.11	2.99				4.33		
BAROMETRY/kbar												
GRAIL	BWB											
Phengite (minimum)	M & S			8.0	6.5	4.5		8.0	9.0	11.0	7.0	9.5
Gt-mica	G & St (1)			6.1				8.1	7.6	8.5	7.8	6.4
-fsp	G & St (2)			7.9				9.5	9.6	8.8	9.4	8.8
	H & C			8.7				10.2	10.3	9.5	10.0	9.5
GRIPS	B & L							7.1	8.9	9.0	8.7	7.3

Thermometry at 8 kbar, barometry at 630°C
* Pressure probably overestimated as ilmenite assumed to be pure

G & P: Graham & Powell, 1984; Per: Perchuk, 1977; G & S: Ganguly & Saxena, 1984; H & S: Hodges & Spear, 1982; H & F: Hynes & Forest, 1988; K & R: Krogh & Raheim, 1974; G & H: Green & Hellman, 1982 BWB: Bohlen et al, 1983; M & S: Massone & Schreyer, 1987; G & St: Ghent & Stout (equilibria 1 & 2), 1981; H & C: Hodges & Crowley, 1985; B & L: Bohlen & Liotta, 1986.

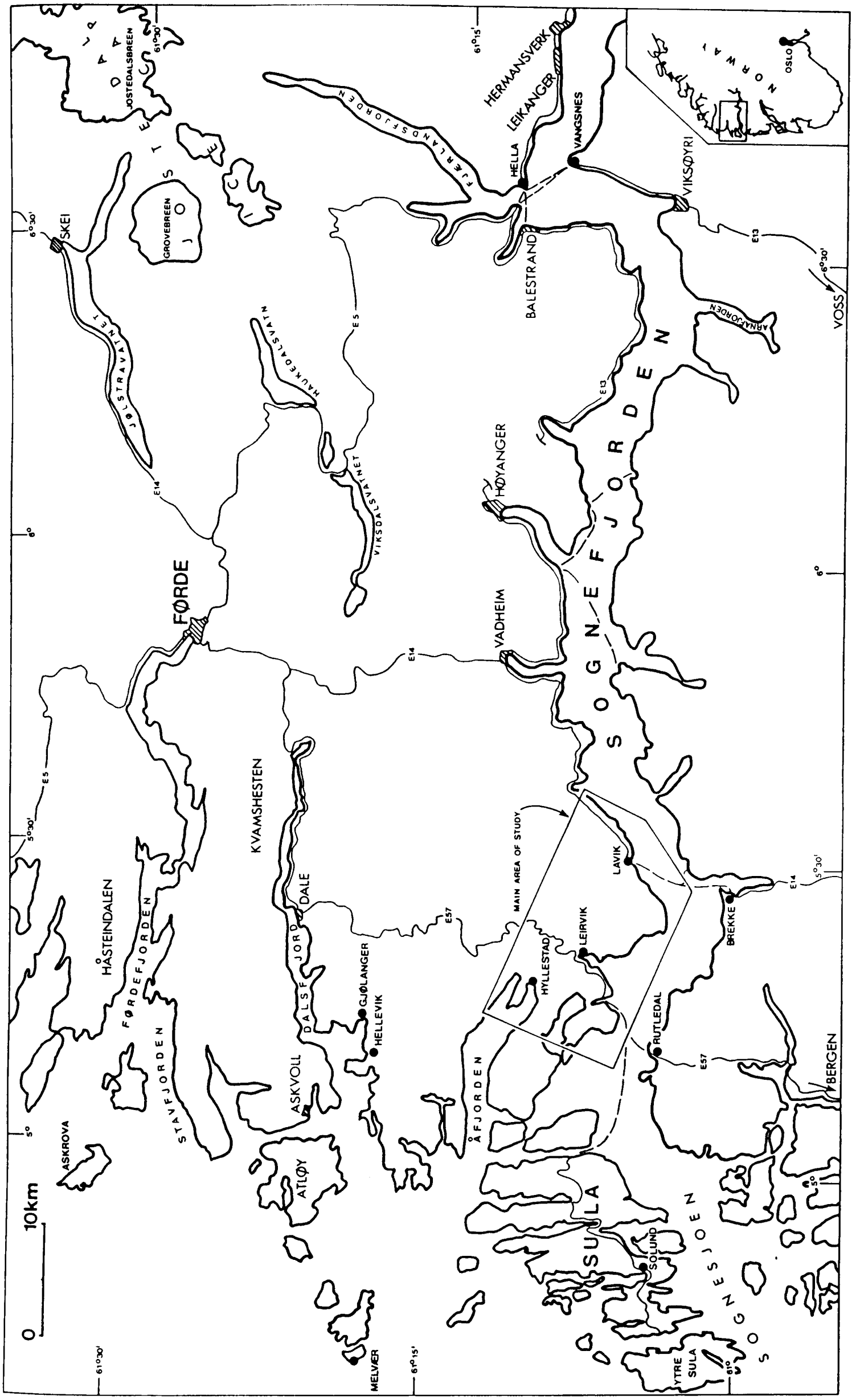

Figure 1.1: Map of part of southwestern Norway showing the field area and localities mentioned in the text.

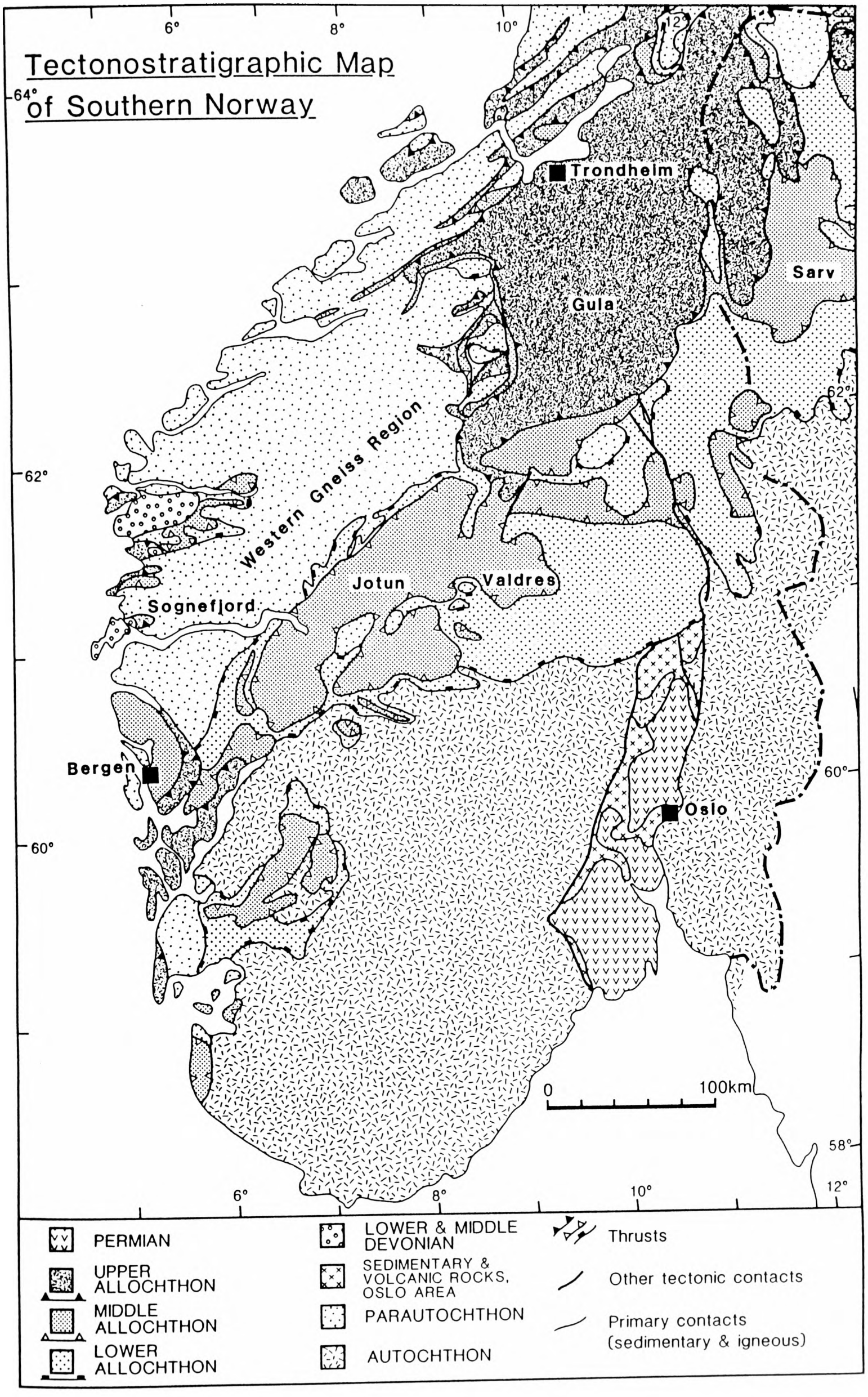

Figure 1.2: Tectonostratigraphic sketch-map of Southern Norway based on Gee et al, 1985.



Figure 1.3: View of Höyanger and Höyangerfjord looking south to peneplain on the far shore of Sognefjord.



Figure 1.4: View of Lifjell looking northwest from Kolgrovheia. Devonian conglomerate forms the cliffs in the middle distance, the moderately-dipping contact can be clearly seen at the break in slope. Highly sheared granitic rocks appear in the foreground.



Figure 1.5: The Sogneskollen granite viewed from Risnes, looking south.

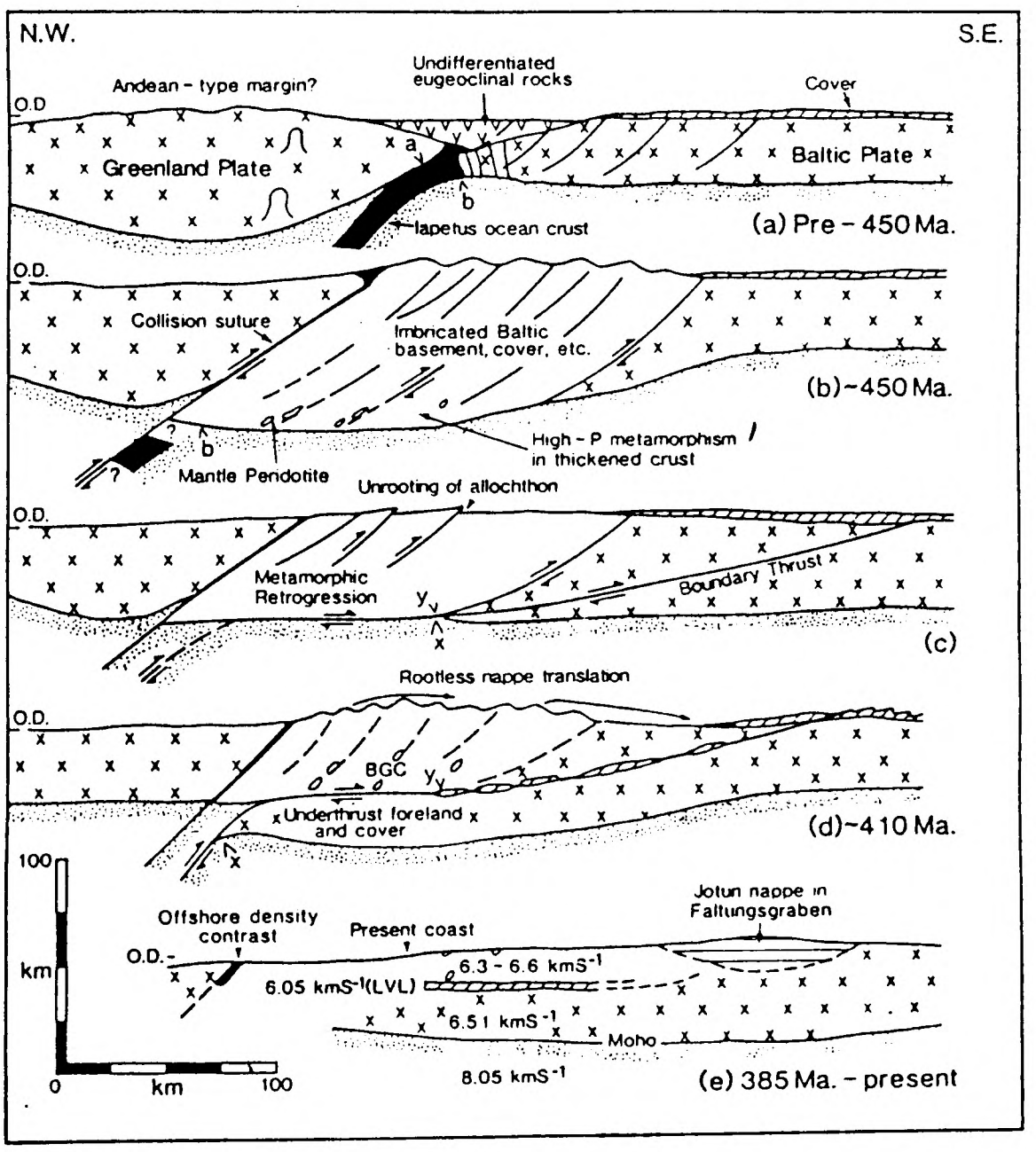

Figure 1.6: Evolutionary tectonic model for the Western Gneiss Region, from Cuthbert et al, 1983.

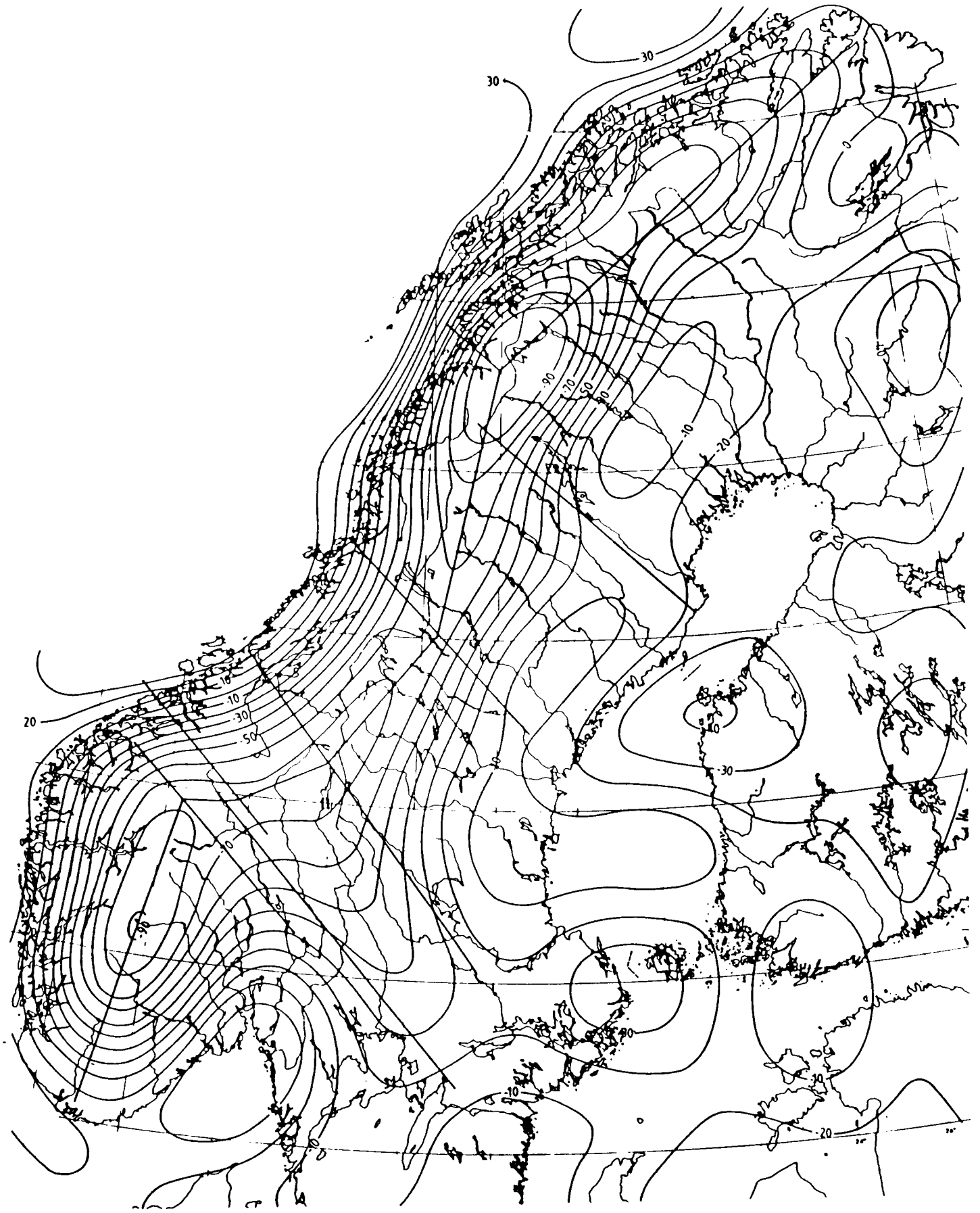

Figure 1.7: Regional low-pass gravity map of Scandinavia, filtered to show only broad-scale gravity features with wavelengths greater than 250 km. From Wolff, 1983.

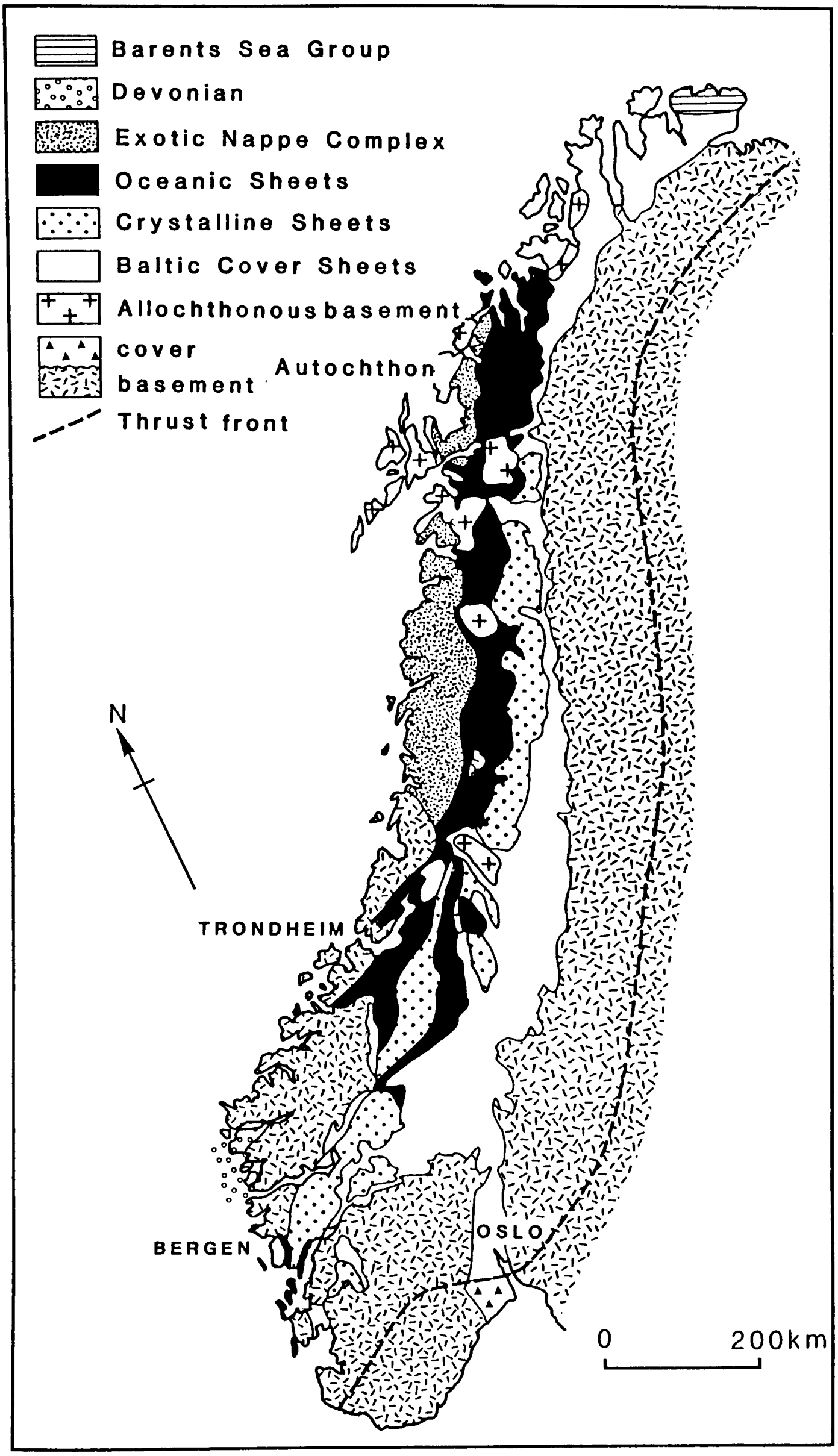

Figure 1.8: Terrane map of the Scandinavian Caledonides, after Hossack and Cooper, 1986.

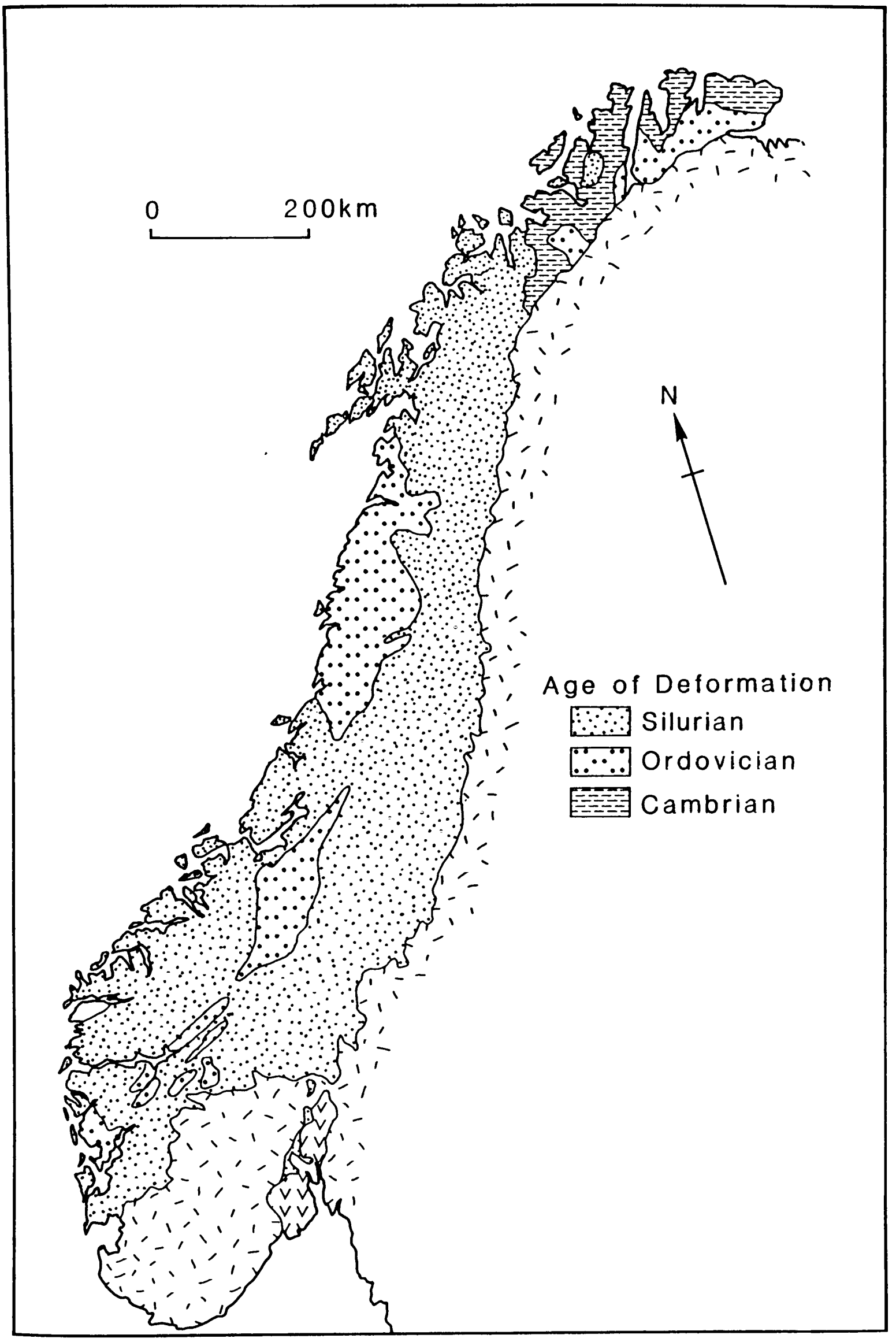

Figure 1.9: Sketch map of Scandinavian Caledonides showing timing of deformation within the allochthon and parautochthon, after Gee and Roberts, 1983.

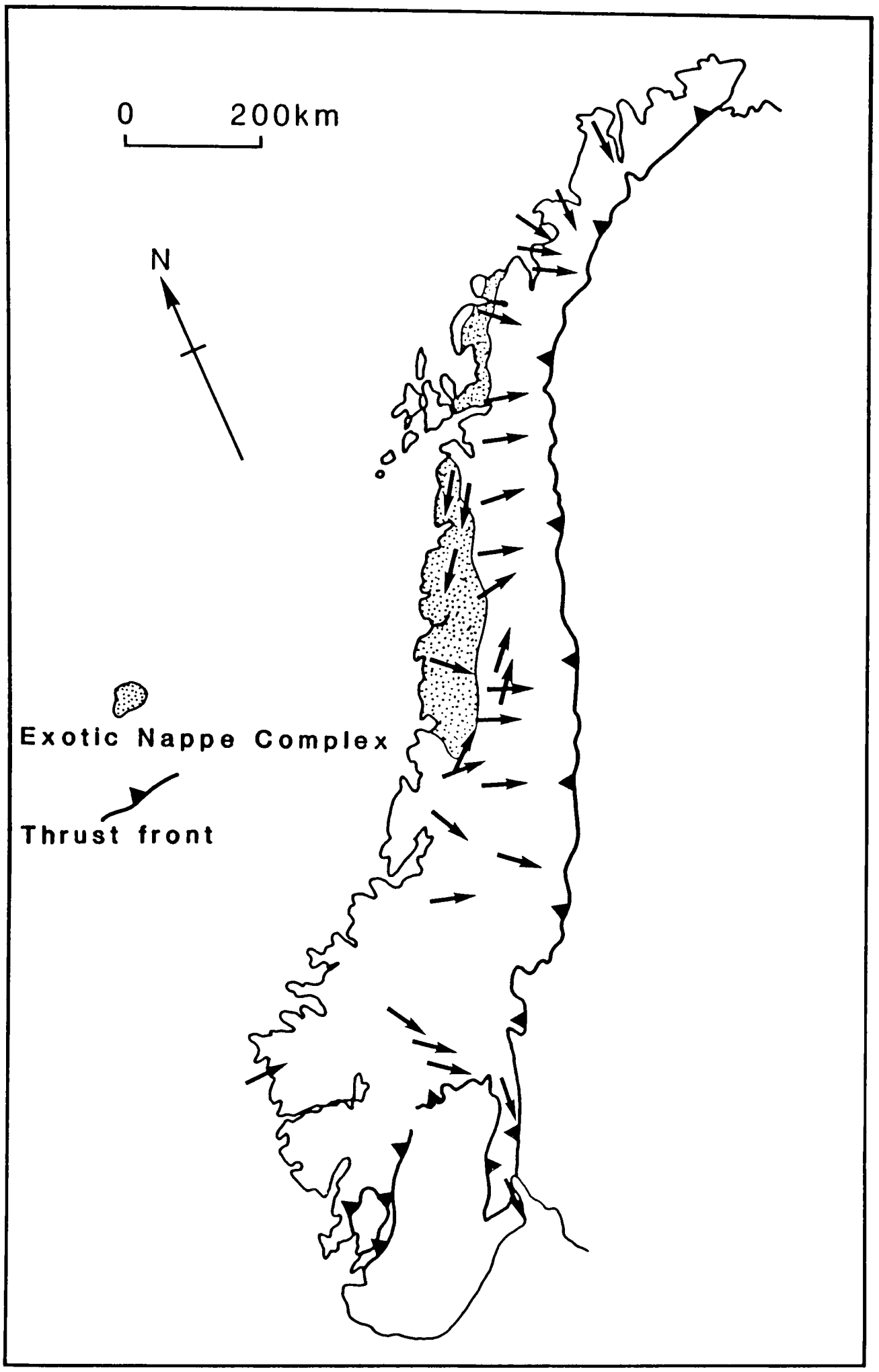

Figure 1.10: Slip vectors for thrusting in the Scandinavian Caledonides, from Hossack and Cooper, 1986.

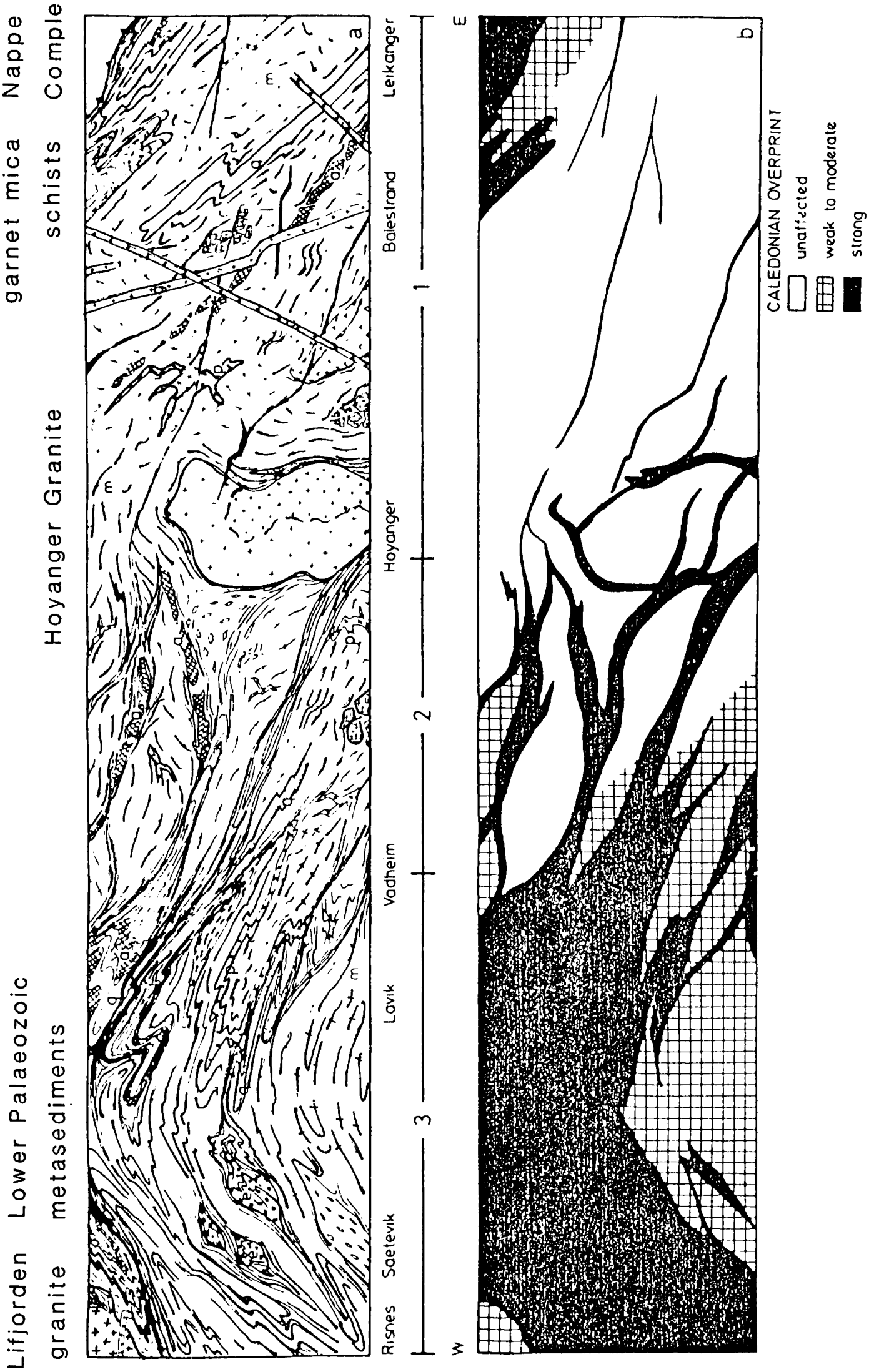

Figure 1.11: Schematic cross-sections along Sognefjord showing (top) lithological and structural relations (a=amphibolite lenses and dykes, c=cataclasite zone, e=eclogite lenses, g=granitic dyke, m=migmatites, q=quartzite, p=pegmatite veins), and (bottom) degree of Caledonian overprinting, from Dietler et al, 1985.

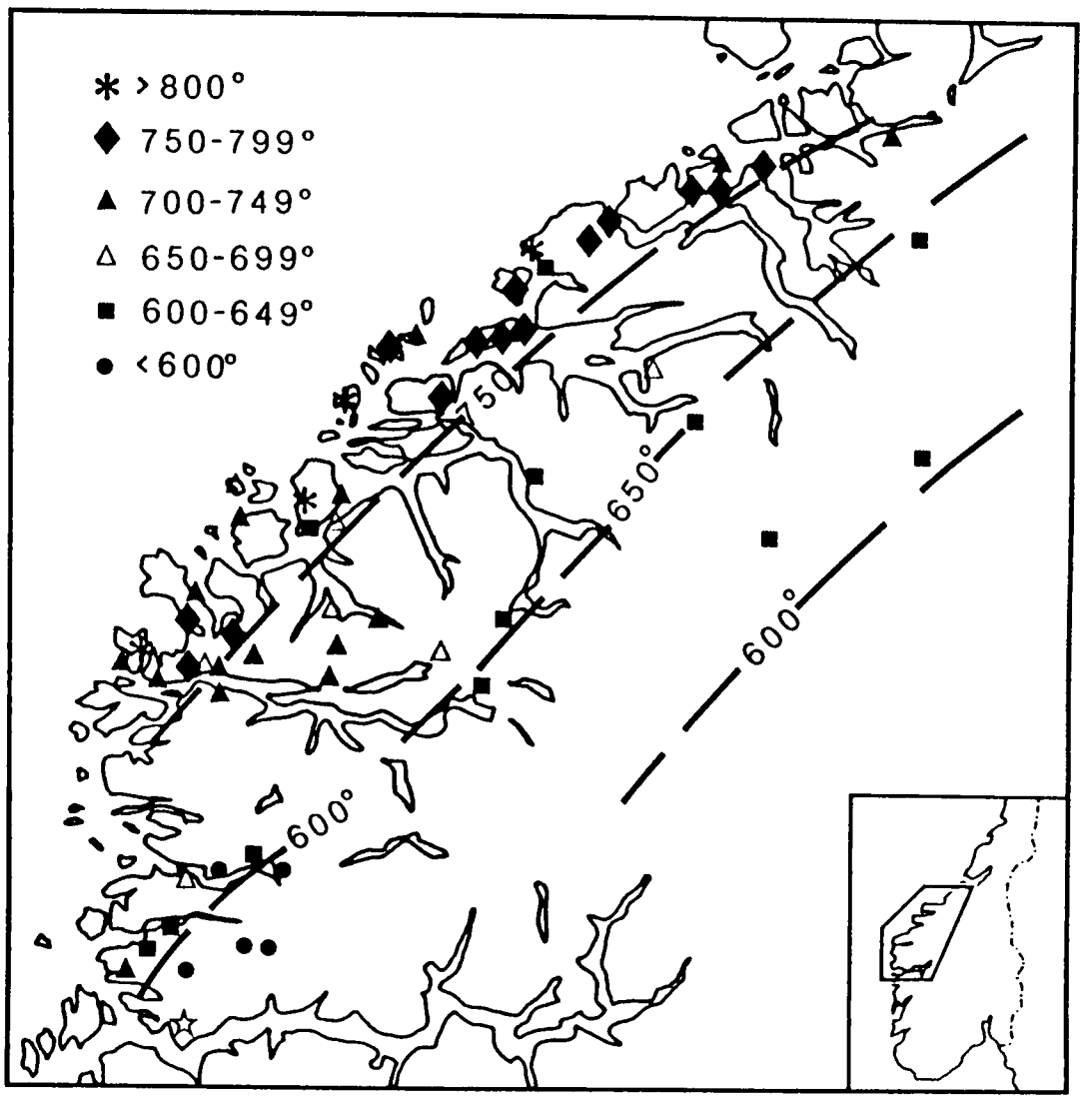

Figure 1.12: Regional distribution of T_{max} in the Western Gneiss Region, based on the geothermometer of Ellis and Green (1979) at an assumed pressure of 15 kbar, after Griffin et al, 1985. Star at bottom left indicates locality of eclogites in this study, for which calculated conditions are 600 °C, 15 kbar.

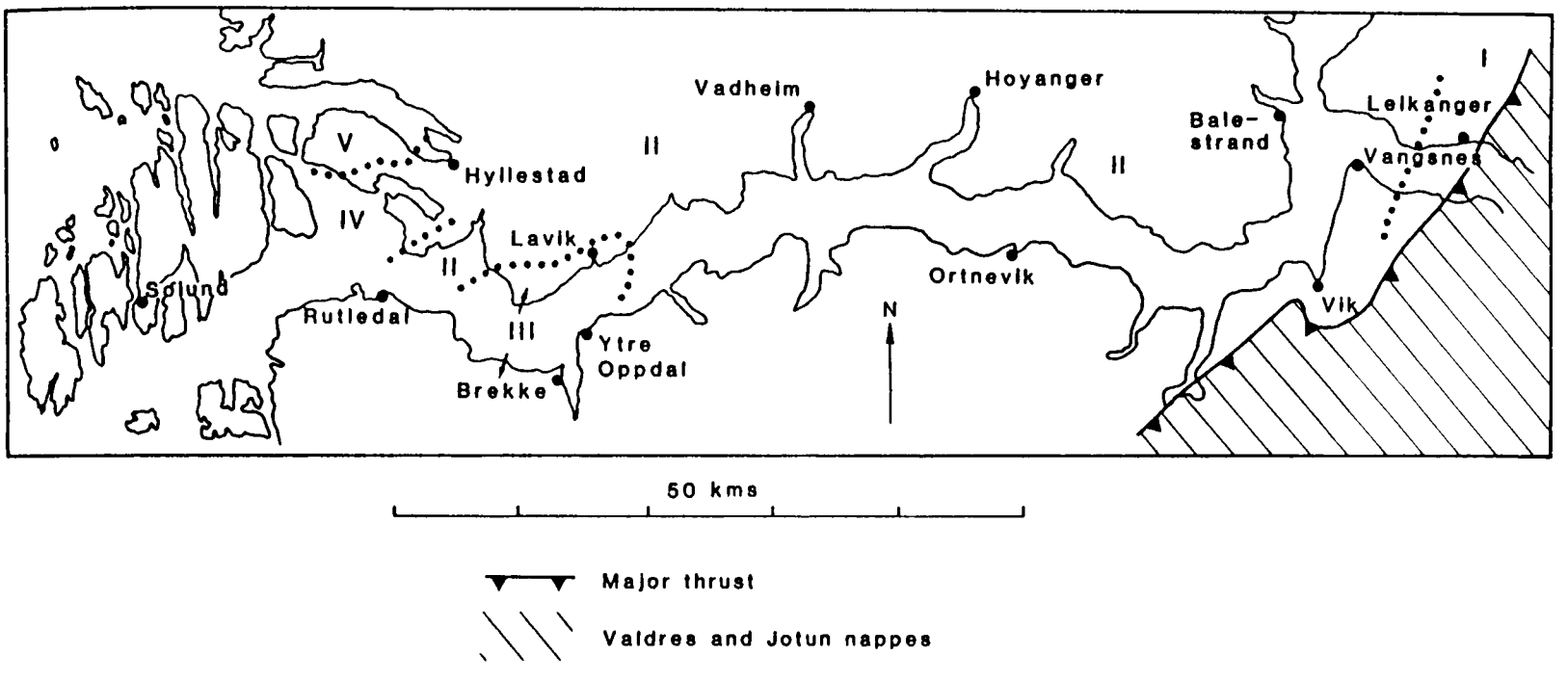

Figure 1.13: Metamorphic zones based mainly on assemblages in basic dykes in Sognefjord. Zone I: upper greenschist overprint on albite-epidote-amphibolite; zone II: albite-epidote-amphibolite overprint on amphibolite facies (possibly to eclogite facies metamorphism near Vadheim); zone III: amphibolite facies overprint on eclogite facies metamorphism; zone IV: units overlying the basement gneisses, comprising rocks of amphibolite, epidote-amphibolite, and greenschist facies metamorphism, zone V: low greenschist metamorphism in Devonian conglomerates. Zones I-III (Leikanger to Lavik) show an E-W increase in early Caledonian metamorphism. The progressively lower grade late Caledonian overprint to the west of Brensdal, seen in zones III-V, has been related to extensional collapse along the Nordfjord-Sogn Detachment (Norton, 1987).

See also figure 2.2 for other localities mentioned in the text

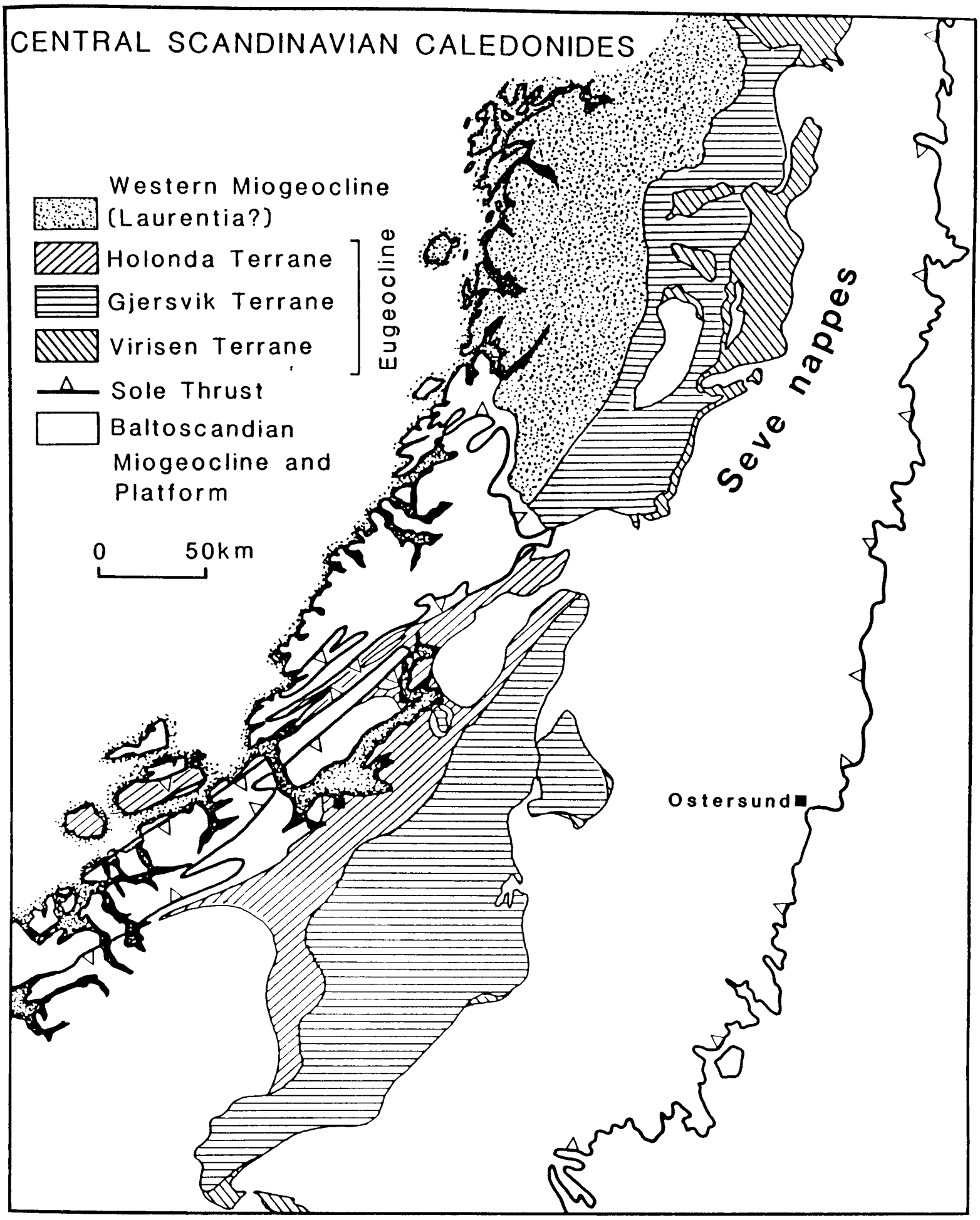

Figure 1.14: Simplified suspect terrane map of central Scandinavian Caledonides, after Stephens and Gee, 1985.

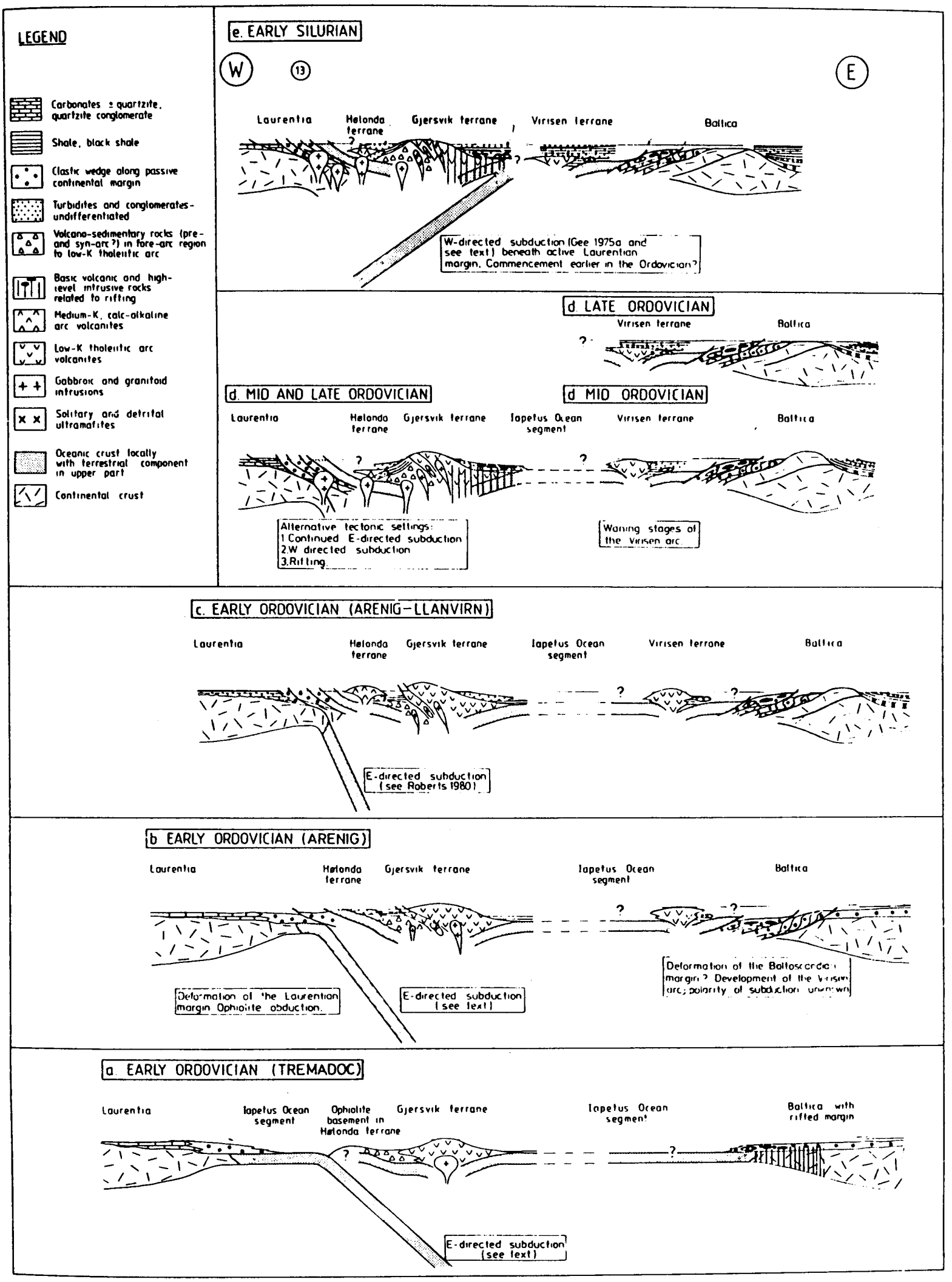

Figure 1.15: Schematic sections showing the tectonic evolution of the central Scandinavian Caledonides, from Stephens and Gee, 1985.

Figure 1.16: Schematic evolution of the southwest Scandinavian Caledonides, from Andresen and Færseth, 1982. (A) shows a possible configuration to explain pre-Ashgill deformation in the Sunnhordland Nappe Complex (SNC). (B) shows continentally derived granodiorites intruding the Karmöy Ophiolite which suggests an Andean-type plate margin. (C) shows deposition of the Dyvikvågen Group in a fault-controlled basin. The dashed line represents a thrust which placed the SNC, with a slice of underlying Precambrian, over the Dyrskard-Kvitenut-Revsegg (DKR) allochthon. A new subhorizontal shear zone developed at the base of the DKR allochthon, and southeasterly displacement of the two nappe complexes along this thrust placed the entire nappe pile on top of the Vidda Group.

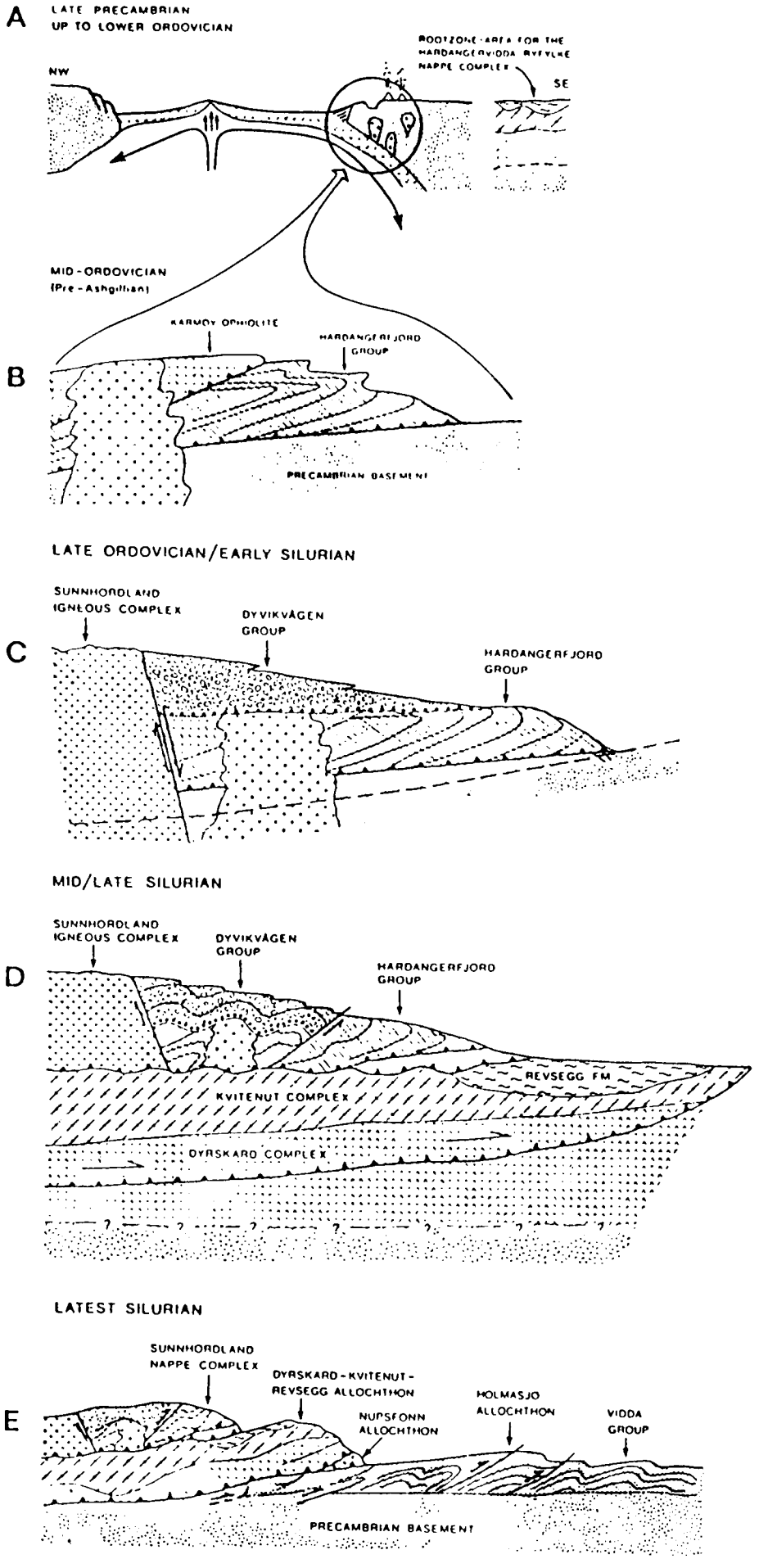
A
LATE PRECAMBRIAN
UP TO LOWER ORDOVICIAN
NW
SE
MID-ORDOVICIAN
(Pre-Ashgillian)
B
KARMØY OPHIOLITE
HARDANGERFJORD GROUP
PRECAMBRIAN BASEMENT
LATE ORDOVICIAN/EARLY SILURIAN
C
SUNNHORDLAND IGNEOUS COMPLEX
DYVIKVÅGEN GROUP
HARDANGERFJORD GROUP
MID/LATE SILURIAN
D
SUNNHORDLAND IGNEOUS COMPLEX
DYVIKVÅGEN GROUP
HARDANGERFJORD GROUP
REVSEGG FM
KVITENUT COMPLEX
DYRSKARD COMPLEX
LATEST SILURIAN
E
SUNNHORDLAND NAPPE COMPLEX
DYRSKARD-KVITENUT-REVSEGG ALLOCHTHON
NUPSFONN ALLOCHTHON
HOLMASJO ALLOCHTHON
VIDDA GROUP
PRECAMBRIAN BASEMENT

Figure 1.16

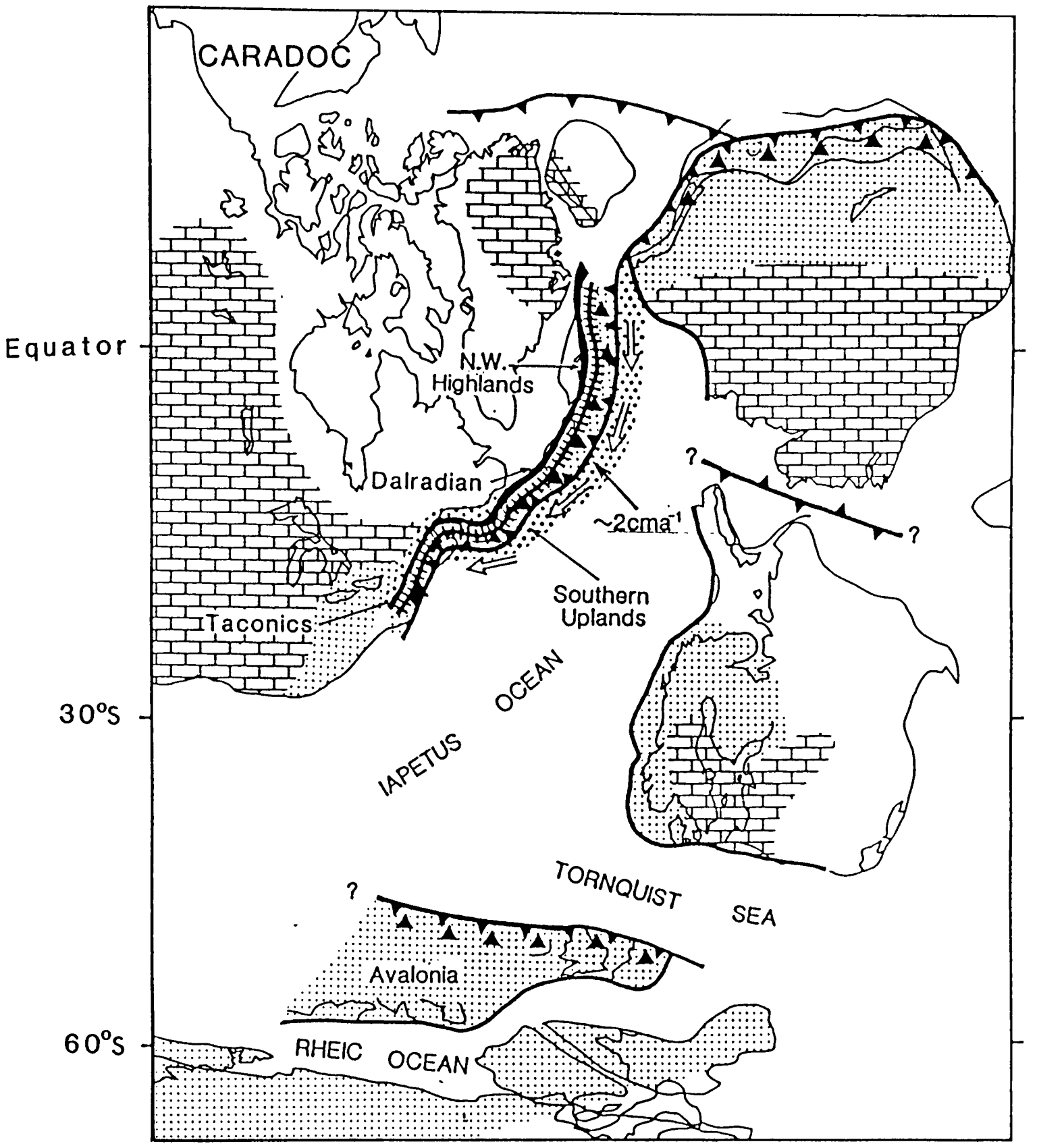

Figure 1.17: Palaeogeographic reconstruction of the Caledonides during the Caradoc from McKerrow et al, 1989. White arrows show direction of sediment transport from the Mongolian arc to the Southern Upland trench, black arrow shows relative motion between Laurentia and Iapetus of 2 cm.a^{-1}. Brick ornament: carbonate platform; coarse dots: thick clastic sediments; fine dots: shelf clastic sediments. Volcanic arcs are shown by black triangles.

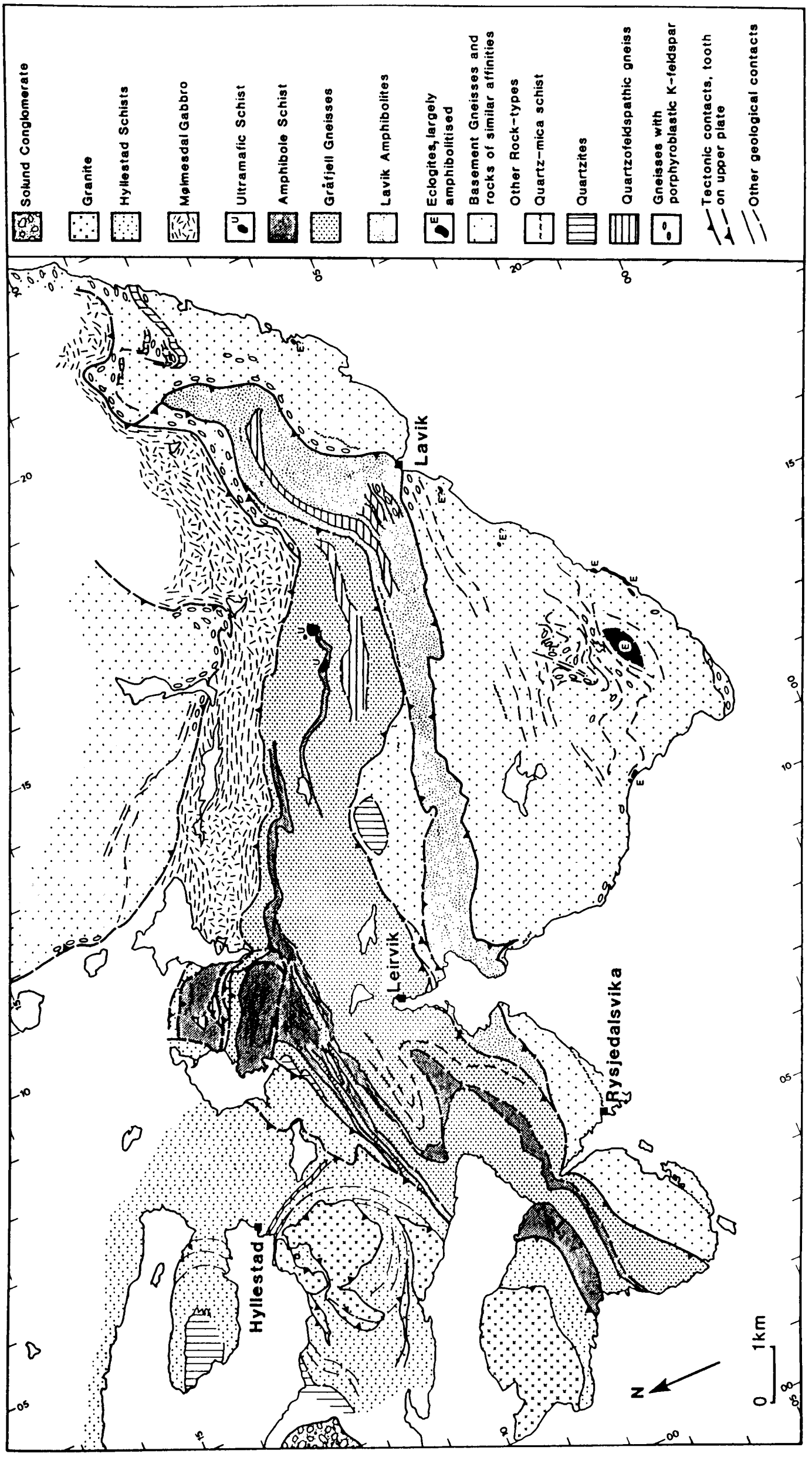

Figure 2.1: Geological sketch map of Hyllestad-Lavik area, Sognefjord.

Figure 2.2: Sketch map of Hyllestad-Lavik area showing place names used in the text.

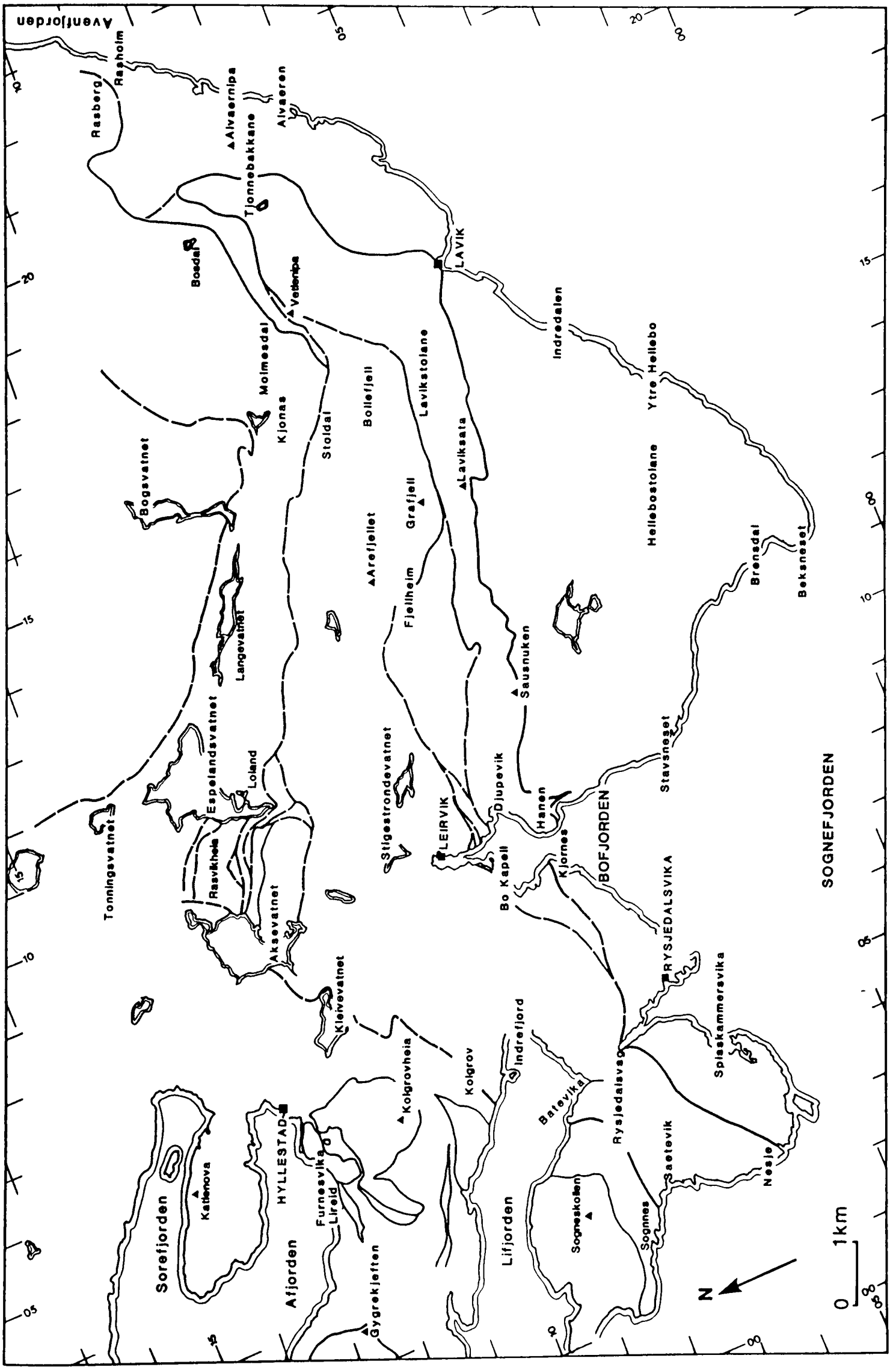



Figure 2.3: Field photograph looking NE showing recrystallized mylonitic foliation developed in Basement Gneisses to the west of Brensdal. Note intrafolial minor folds with truncated lower limbs at upper left; also "nipple" and box folds tipping small fracture at the lower right. Minor structures have top-to-NW asymmetry. The age of the foliation is probably syn-D_3 (see text).



Figure 2.4: Field photograph of un-Caledonized migmatites between Brensdal and Leirvik (cf. figure 2.7)



Figure 2.5: Field photograph of virtually undeformed basic dyke in Basement Gneisses with very little Caledonian overprint.



Figure 2.6: Field photograph of basement migmatites at Austerheim, between Vadheim and Höyanger. Caledonian overprinting is intermediate in intensity between the strong deformation seen further west, at Lavik, and the heterogeneous deformation to the east of Höyanger (cf. figure 2.7).



Figure 2.7: Field photograph of cross-cutting leucosomes in un-Caledonized Precambrian basement, SW of Vangsnes.

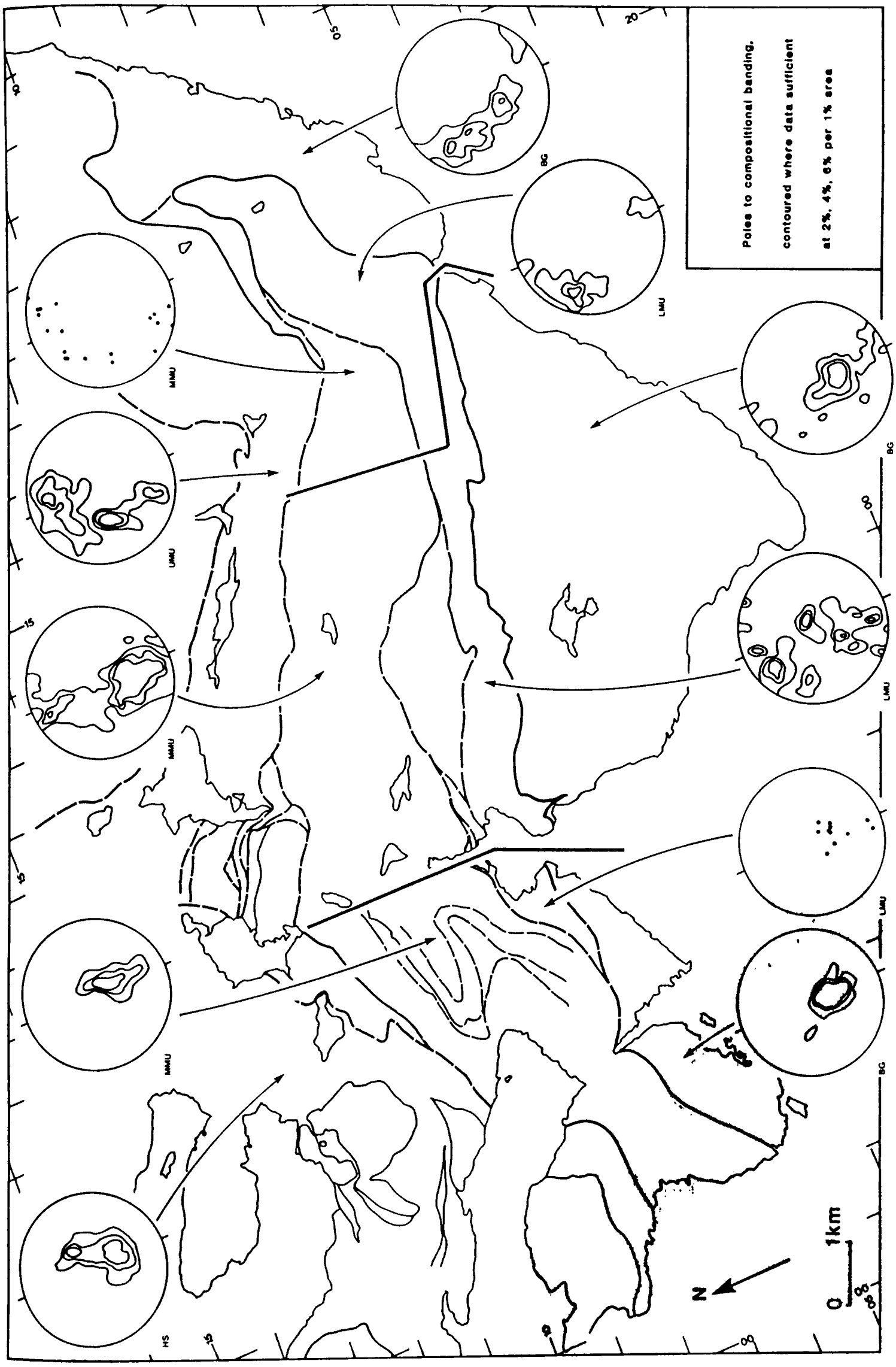

Figure 2.8: Sketch map of Hyllestad-Lavik area showing structural elements.

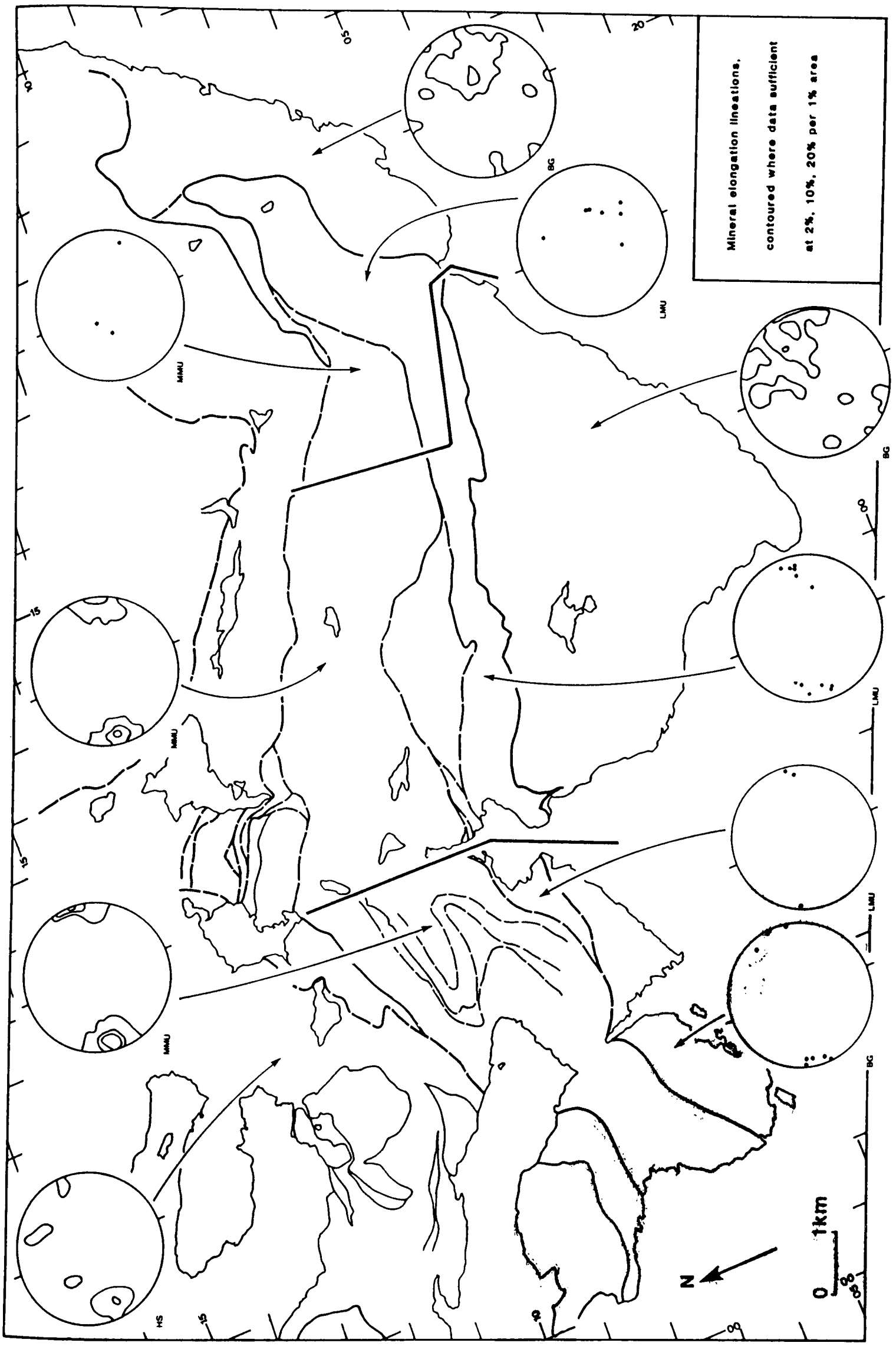

Figure 2.8 (con)

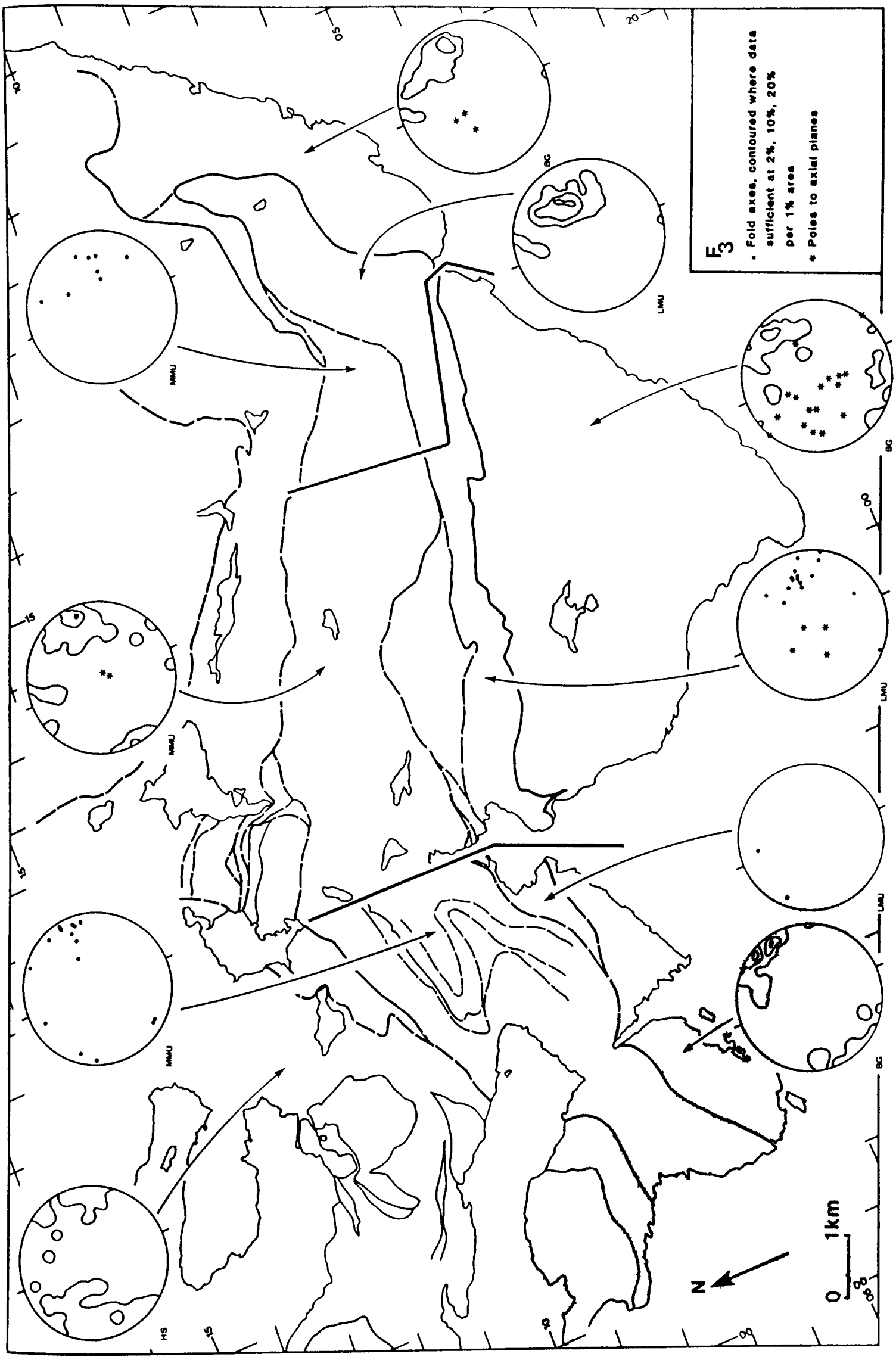

Figure 2.8 (con)



Figure 2.9: Field photograph of tight F_2 fold with axial planar cleavage in strongly Caledonized quartzose migmatites of Basement Gneisses near Lavik.



Figure 2.10: Field photograph of large F_2 isocline in quartzo-feldspathic Caledonized migmatites of Basement Gneisses near Alværen.



Figure 2.11: Field photograph showing F_2 isocline refolded by F_3 in strongly Caledonized quartzofeldspathic migmatites of Basement Gneisses.



Figure 2.12: Field photograph showing refolded F_2 folds in Basement Gneisses near Laviksåta.

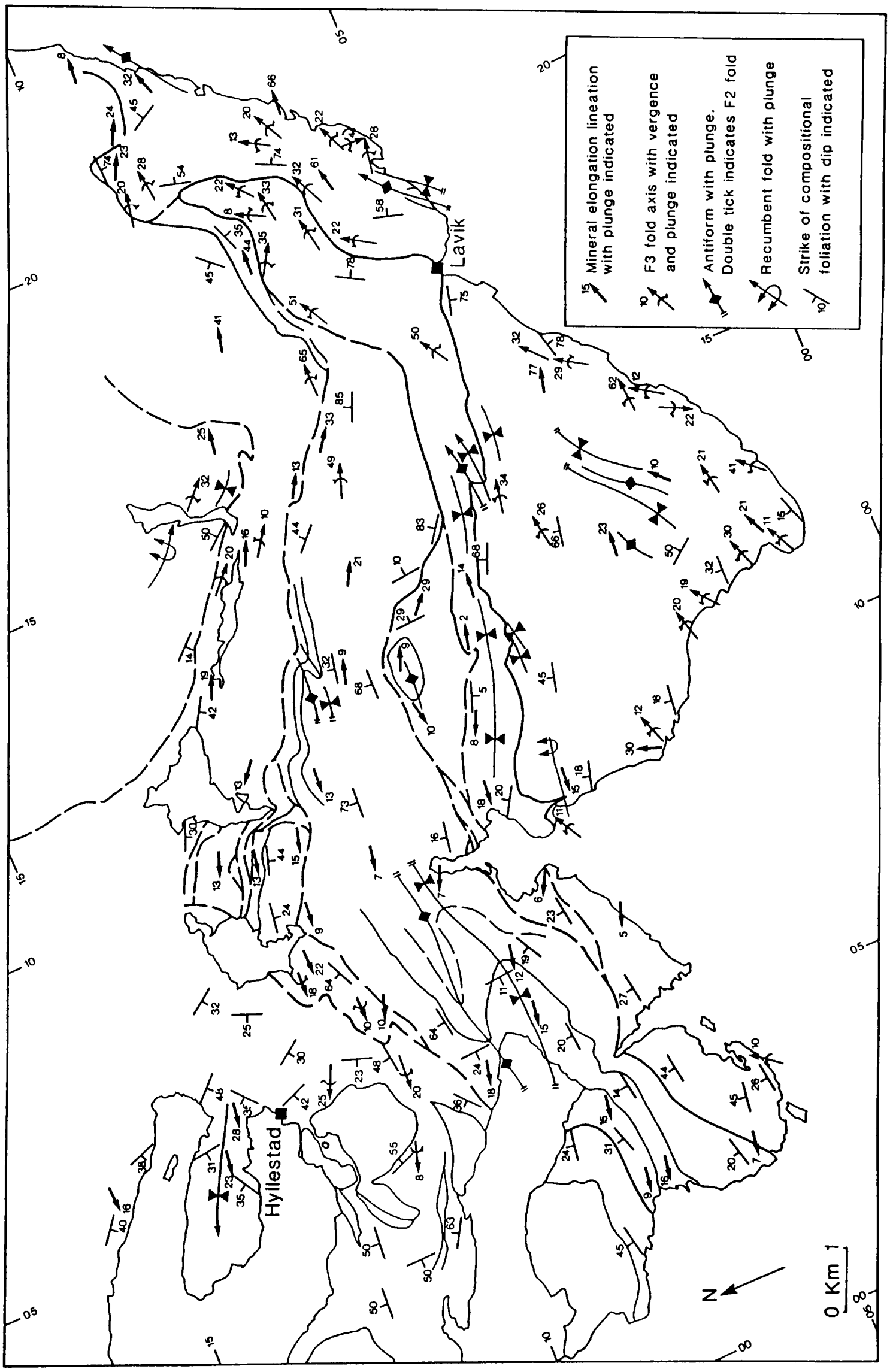

Figure 2.13: Map of the area showing representative structural elements.



Figure 2.14: Field photograph showing large NW-vergent F_3 fold pair in Basement Gneisses at Beksneset. Note discordant accommodation folds to left of Simon Harley.



Figure 2.15: Field photograph showing NW-vergent F_3 folds at Nesje in Basement Gneisses.

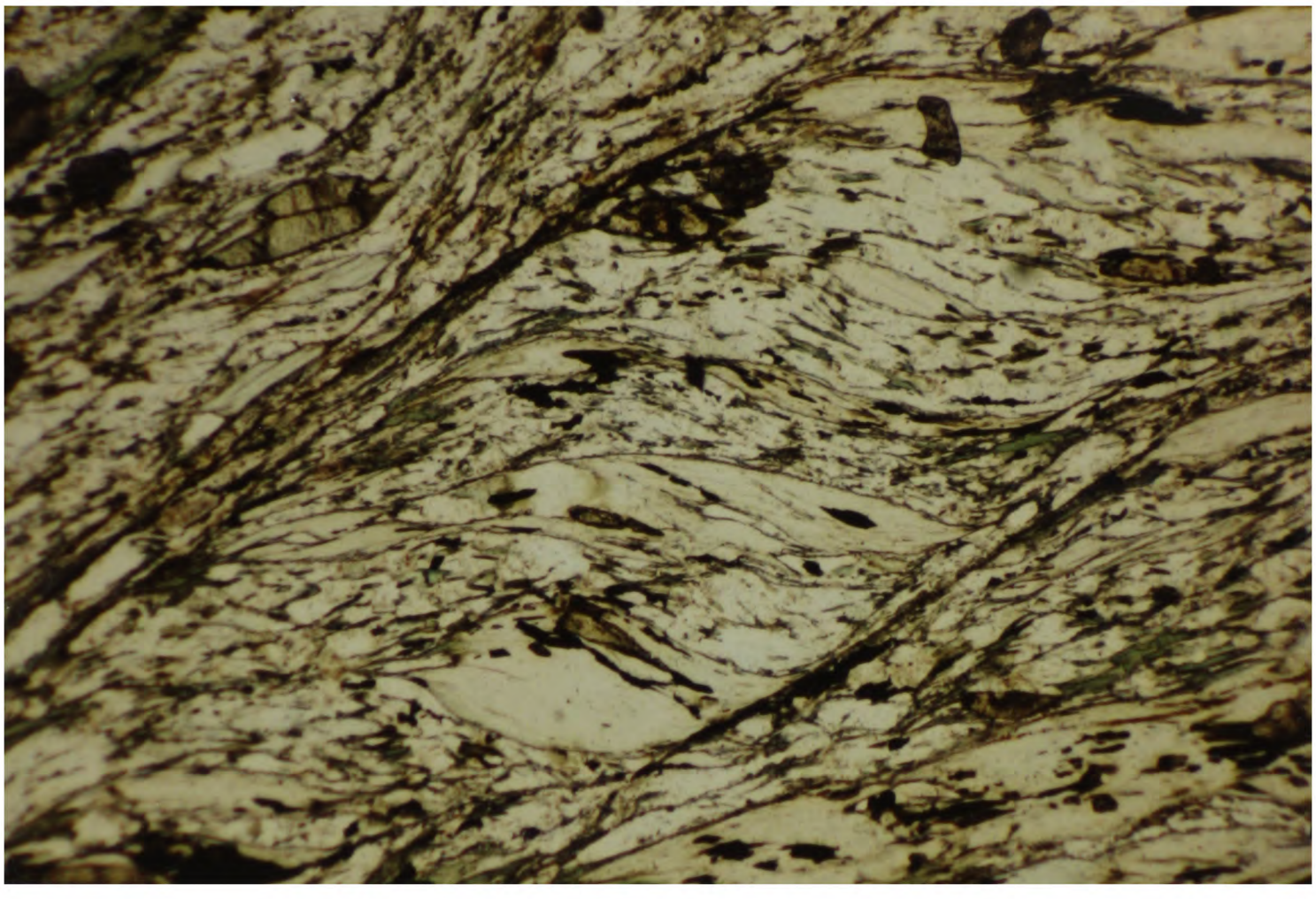

Figure 2.16: Photomicrograph showing extensional crenulation cleavage in Basement Gneisses from Nesje.



Figure 2.17: Field photograph of tension gashes in vertical shear zone in Basement Gneisses near Leirvik.

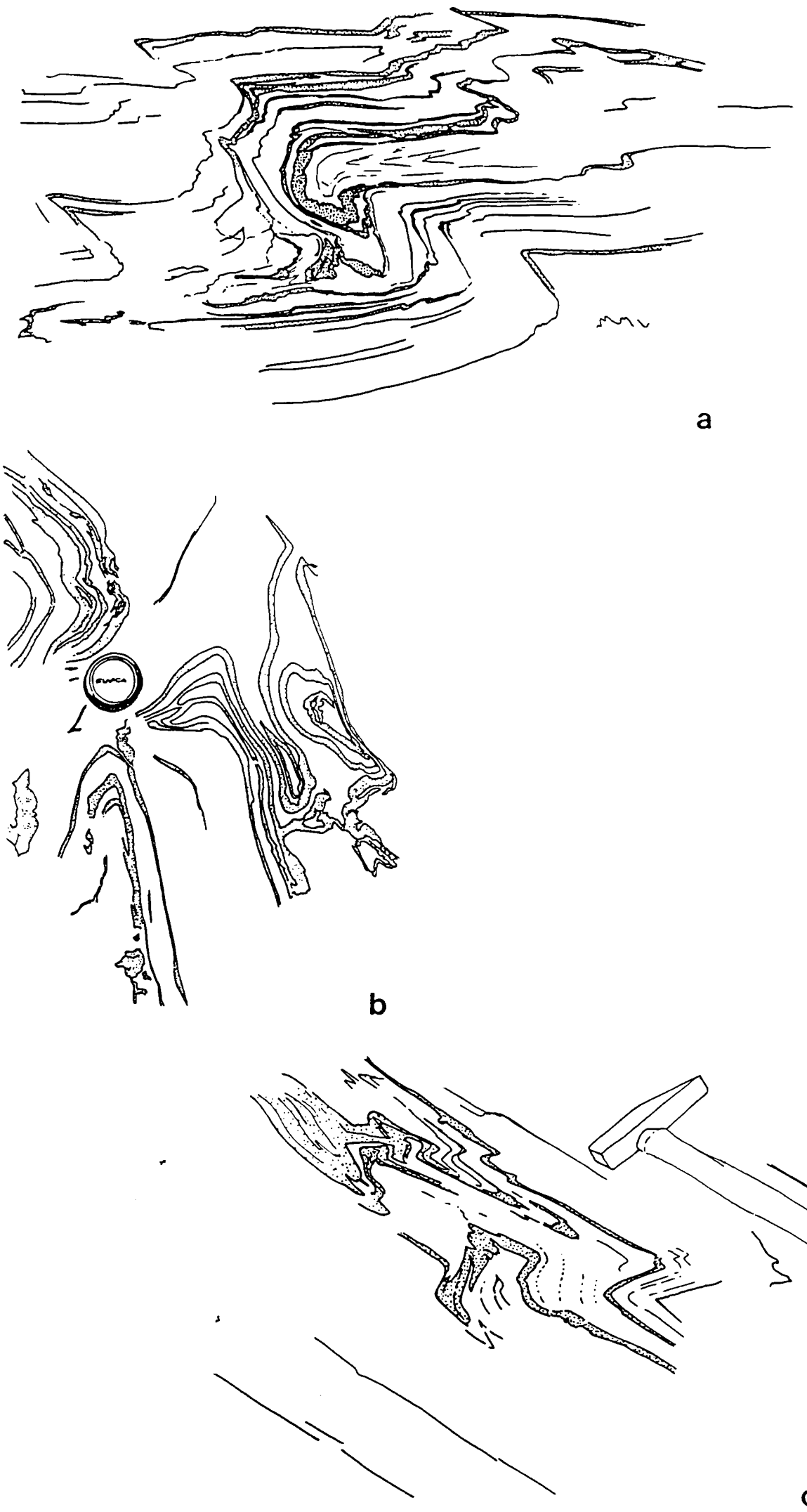

Figure 2.18: F_2 isoclines refolded by F_3 folds (a) Garnet-amphibolites on Lavik-Stöldal road (166057), plagioclase-rich bands stippled (b) Amphibolites on Lavik-Stöldal road (171056), plagioclase-rich bands stippled (c) Quartz-feldspar-biotite gneisses at Bosdal (197085), quartzofeldspathic bands stippled.

Figure 2.19: North-south cross-sections across the area ornament as in figure 2.1.

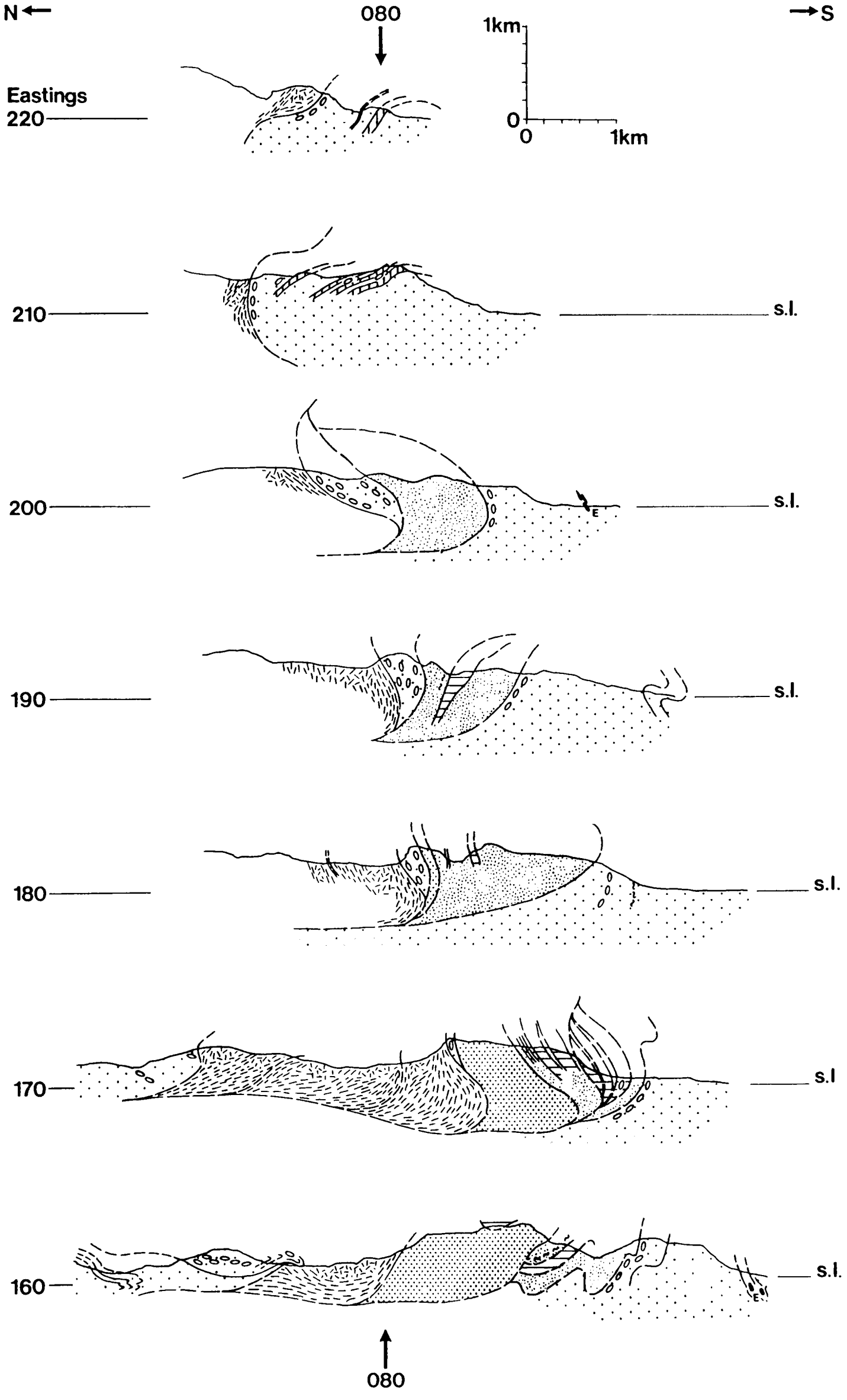

Figure 2.19 (con)

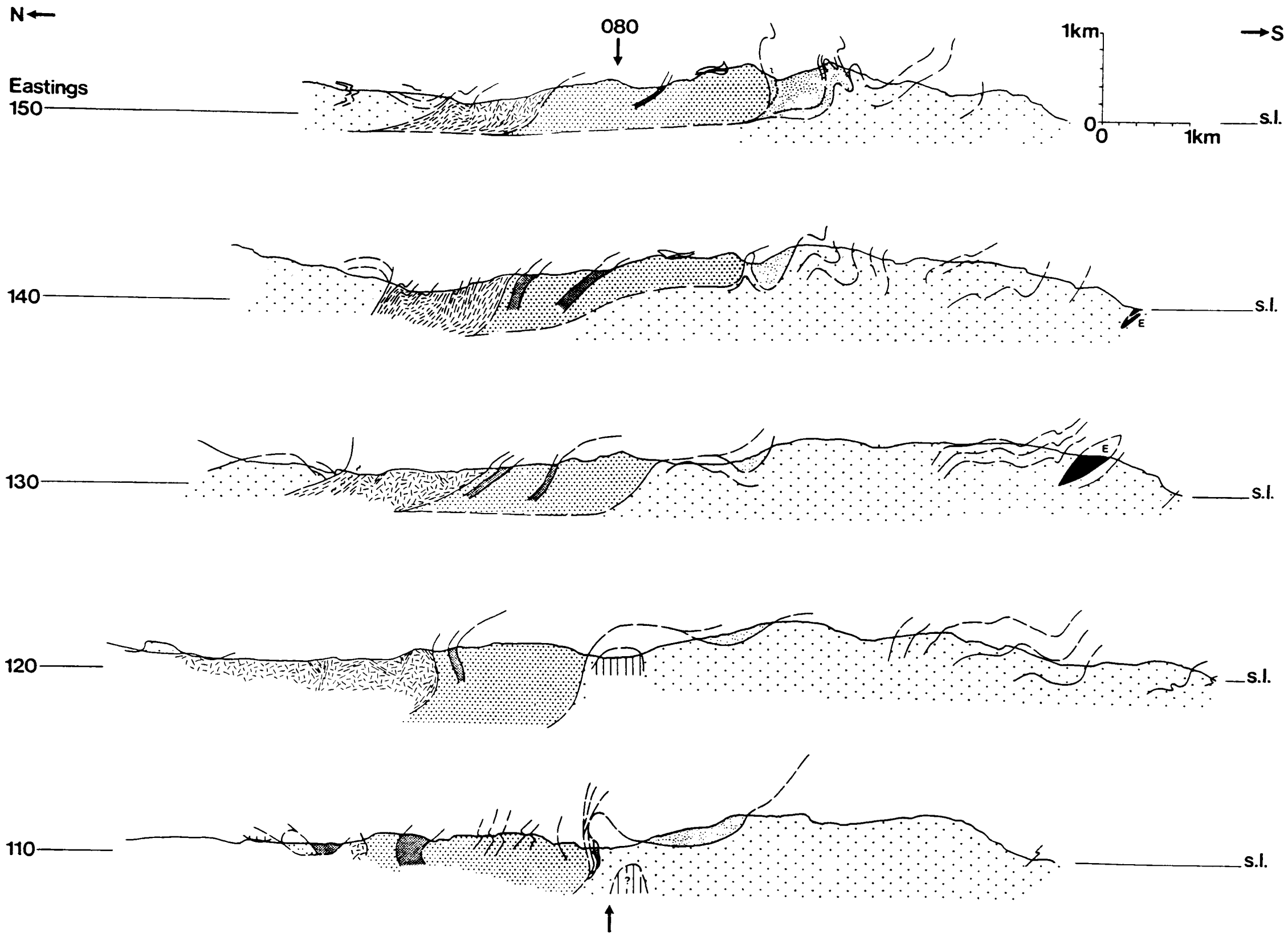

Figure 2.19 (con)

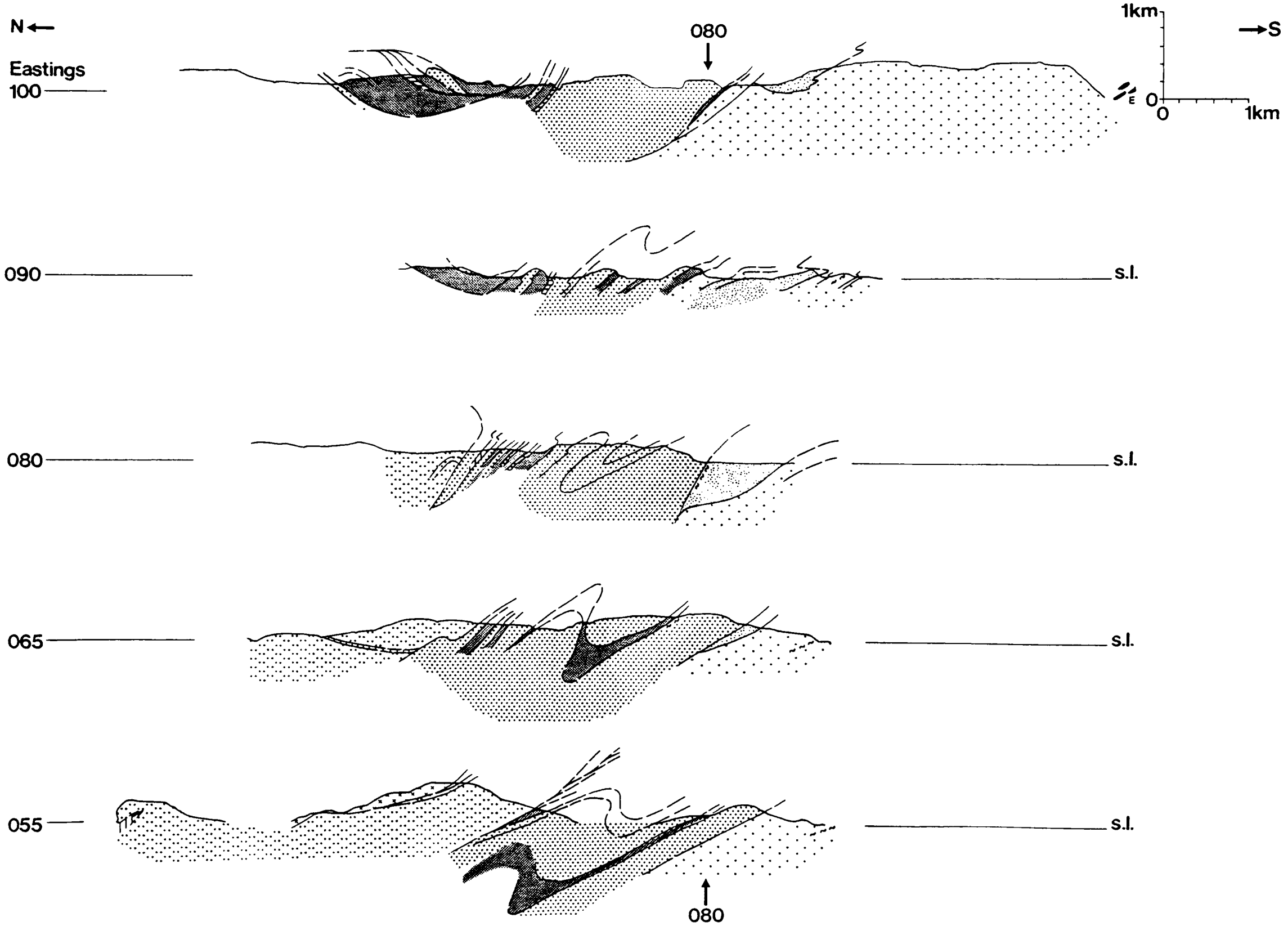



Figure 2.20: Trondhjemite veins in tonalitic gneiss at Leirvik, looking east. The veins have been tightly folded with a top-to-south vergence and the axial planes of the folds are cut by low-angle shear zones with top-to-north shear sense



Figure 2.21: Refolded minor folds (possibly of F_2 type) east of Kleivevatnet.

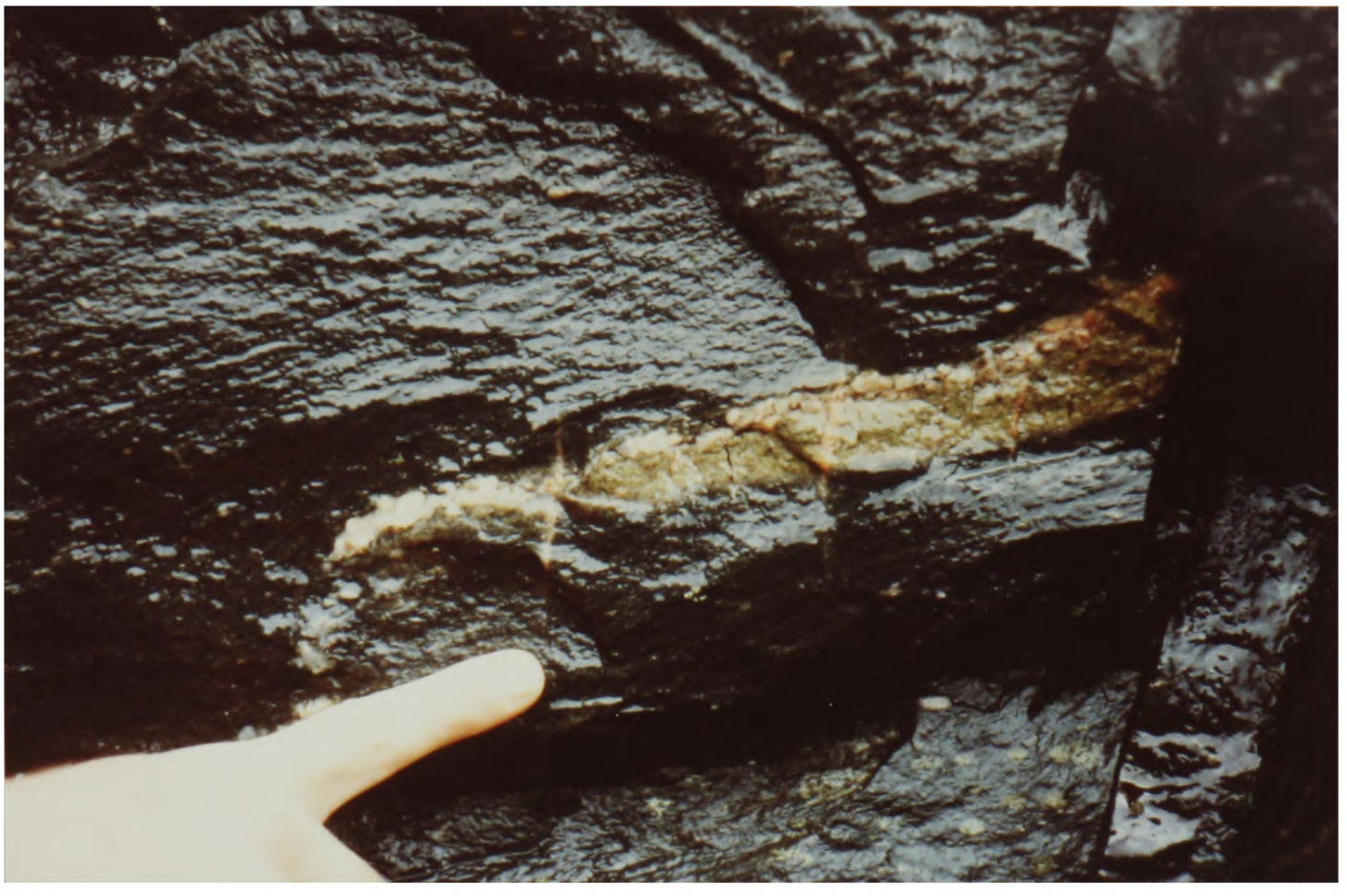

Figure 2.22: Greenish, elongate, saussuritized pod at Rysjedalsvåg, looking east. The longest dimension of the pod is aligned roughly NW-SE and is cross-cut by vertical fractures filled with pink fibrous albite growing perpendicular to the fracture walls.



Figure 2.23: Trondhjemite vein in amphibolitized gabbro at Kjörnas with margins showing top-to west vergence, looking south.



Figure 2.24: Top-to-north shear zone in coarse gabbro at Kjönas with deformation concentrated along the margins of a trondhjemitic vein, looking west. Lens cap is 52mm across.



Figure 2.25: Augen gneiss above Upper Mafic Unit near Lavikdal school with aplitic veins rotated into the mylonitic foliation, looking NW. Compass-clinometer is 10cm long.



Figure 2.26: Boudinaged layer of actinolitic gneiss in meta-volcaniclastic sequence near Sætevik, looking N down-dip, extension of boudinaged layer is E-W. Note quartz-albite knots at boudin necks.



Figure 2.27: Minor faults with offset of few centimetres at Sætevik, looking N.



Figure 2.28: White, massive rocks at top of picture are granite at Soggnes. The contact with the underlying Hyllestad Schists runs from top right to bottom left, dipping NW. Photograph is taken looking roughly NW.



Figure 2.29: Recumbent folds with subhorizontal axes of F_3 type in Hyllestad Schists at Kleivevatnet, looking NE.

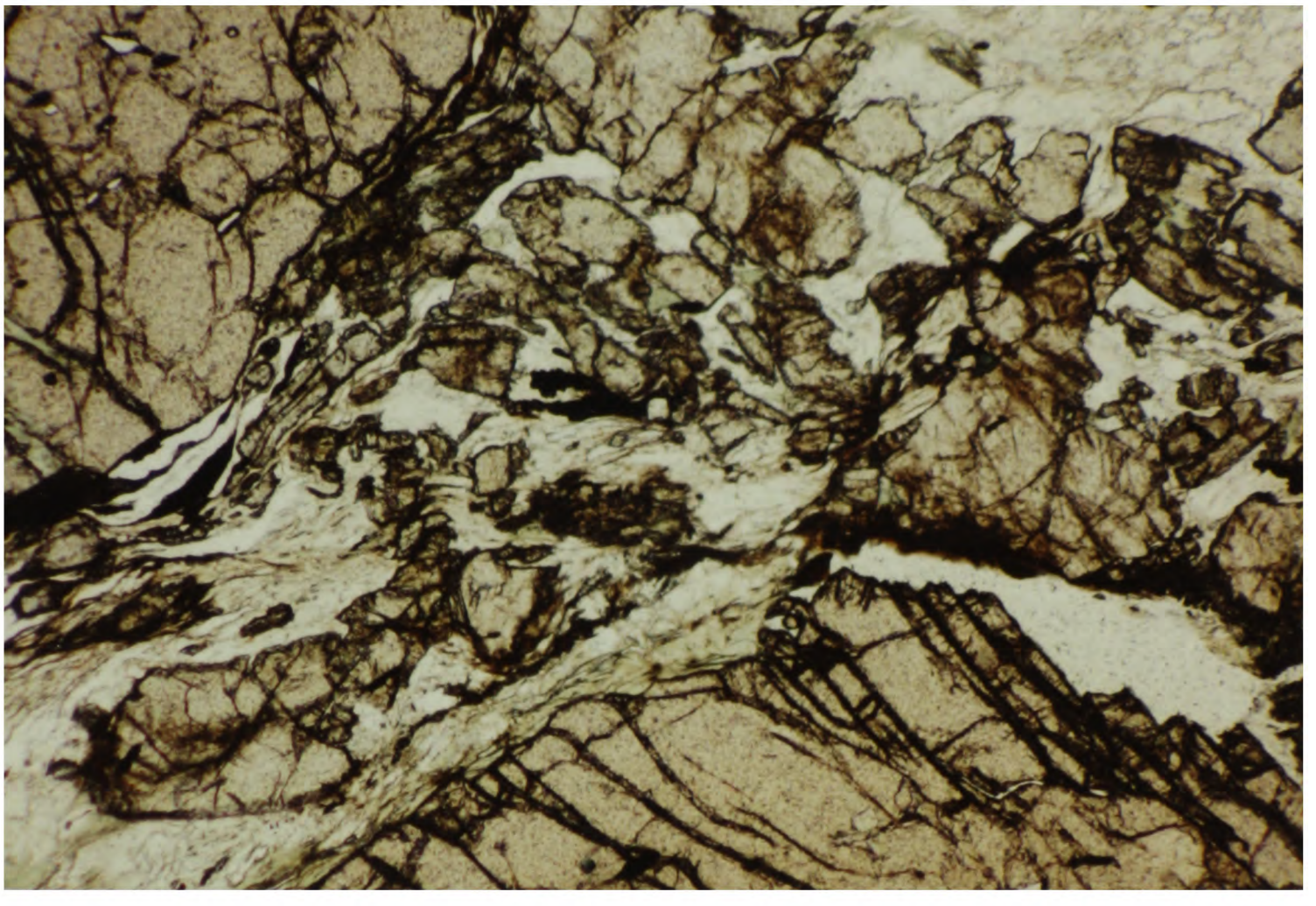

Figure 2.30: Photomicrograph of fractured pre-kinematic kyanite grain, crushed between garnets in kyanite-staurolite-garnet schist from Kleivevatnet. Field of view is 9 mm.

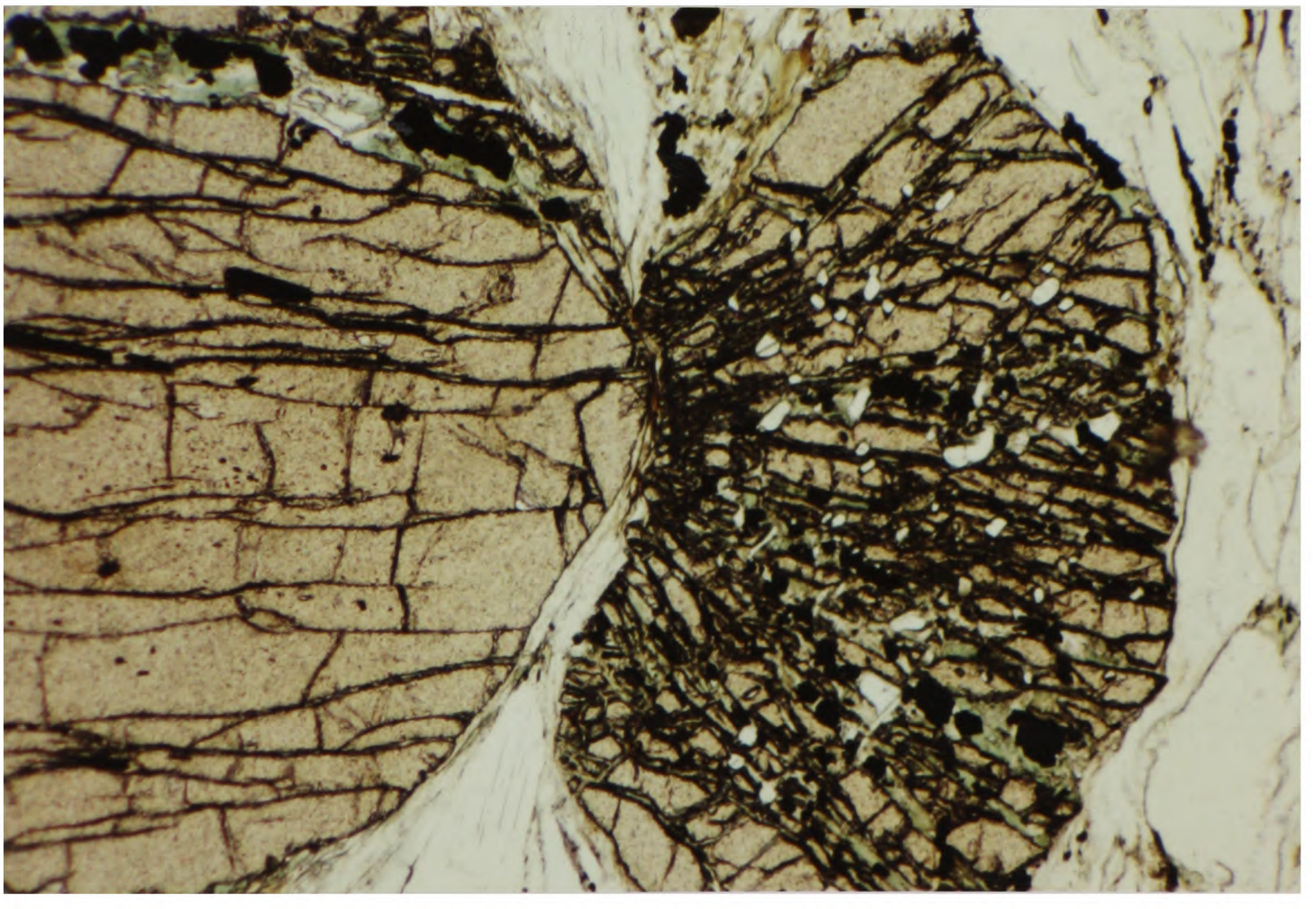

Figure 2.31: Impingement of two garnets in schist from Kleivevatnet. Garnet on right shows radial cracks filled by chlorite and magnetite.

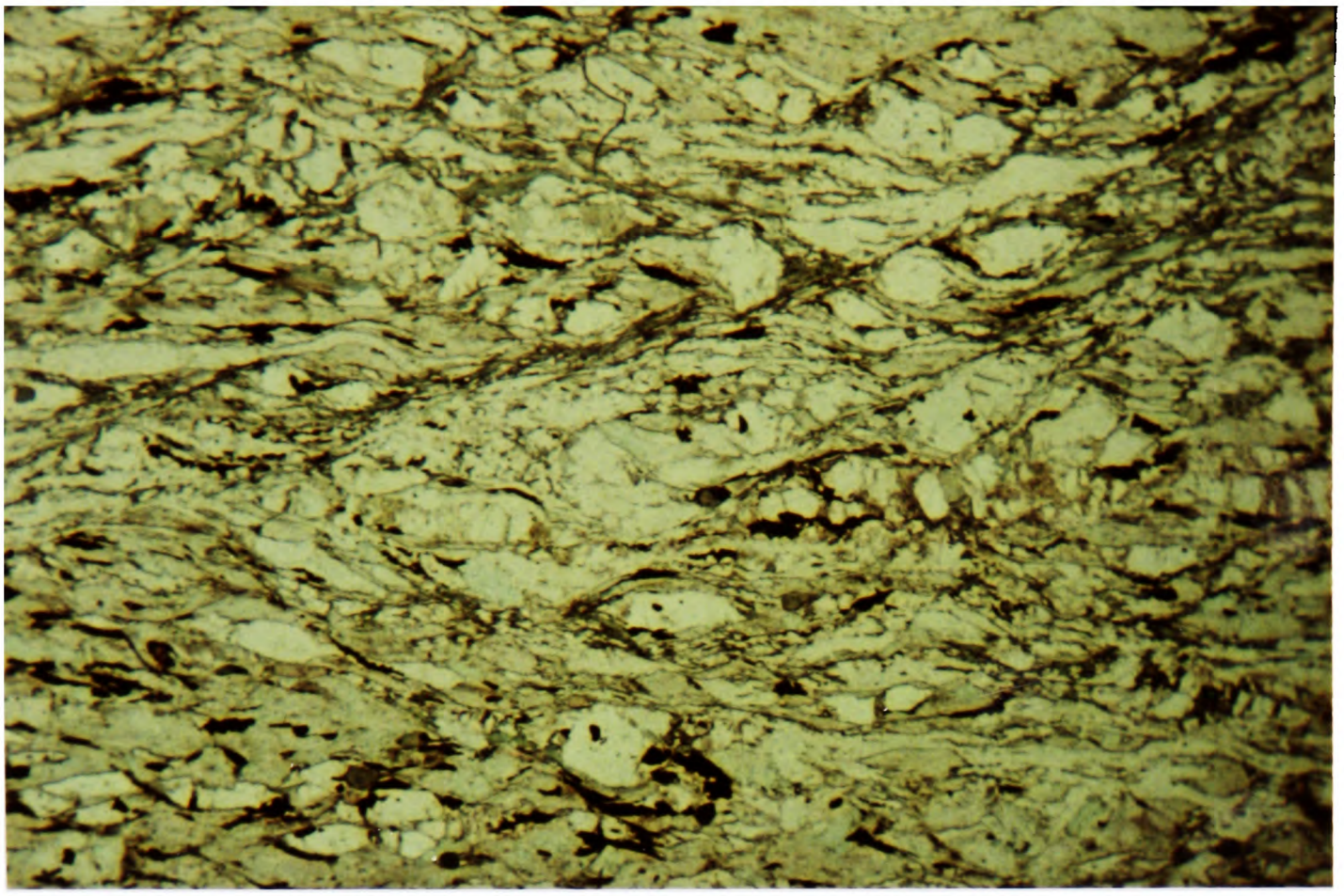

Figure 2.32: Photomicrograph of garnet-chlorite-muscovite schist from near Kleivevatnet. Field of view shows shear bands of extensional crenulation cleavage dipping from right to left (northwestwards) across photo. Deep green grains, centre and bottom left, are tourmaline. Width of field of view is 9 mm.



Figure 2.33: Small "ramp" at Hyllestad, looking S. Garnet chlorite schists, at right, truncate quartzo feldspathic bands. "Ramp" dips towards west. Lineation on underside of schist plunges towards 284°. Structure is probably related to extensional crenulation cleavage in figure 2.32.



Figure 2.34: Folded chloritic schists, to left and just above road, passing into schists interbanded with thin granitic sheets to the right of photo. The fold is truncated by thicker granitic sheets along a shear zone, filled with chloritic gouge, running from the top left of the picture to the bottom right. The shear sense is top-to-west and the structure is related to late extensional crenulation cleavage as seen in fig. 2.32.

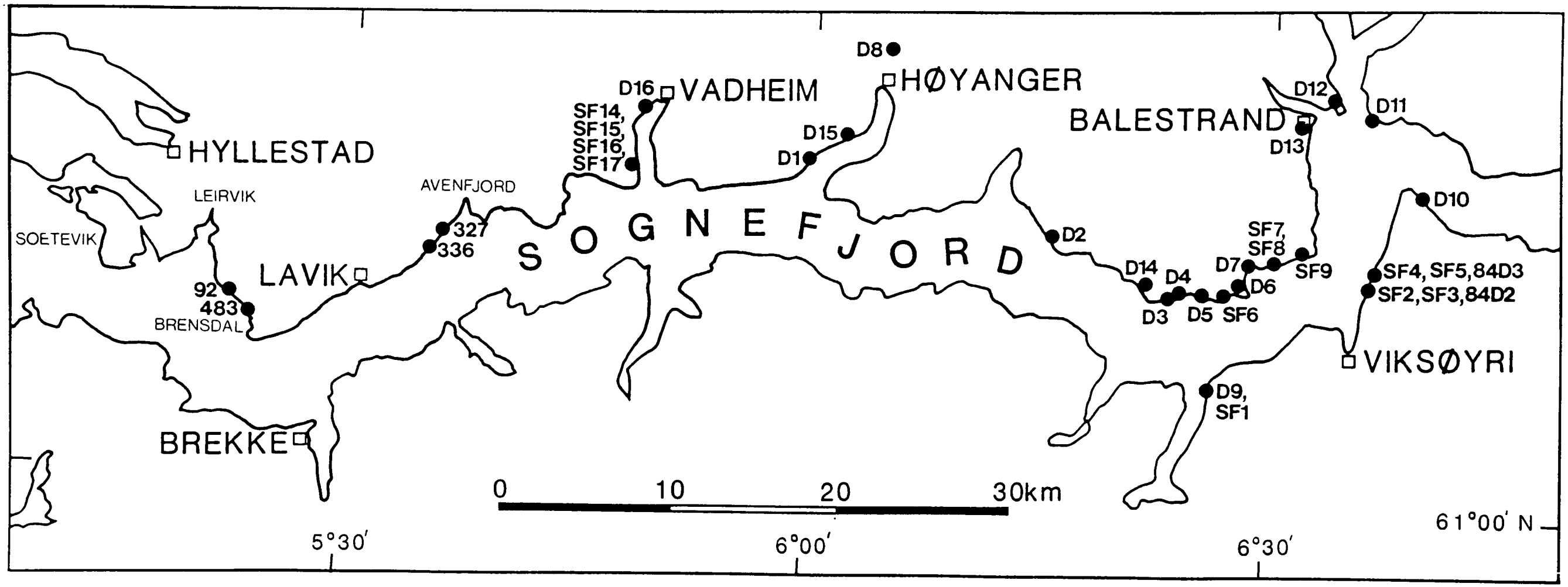

Figure 3.1: Map of Sognefjord, Norway, showing localities of dykes sampled and mentioned in the text.



Figure 3.2: Granitic migmatites in Basement Gneisses at Ytre Hellebö. The orientation of the leucosomes may be tectonically controlled but Caledonian tectonic overprinting is weakly developed.

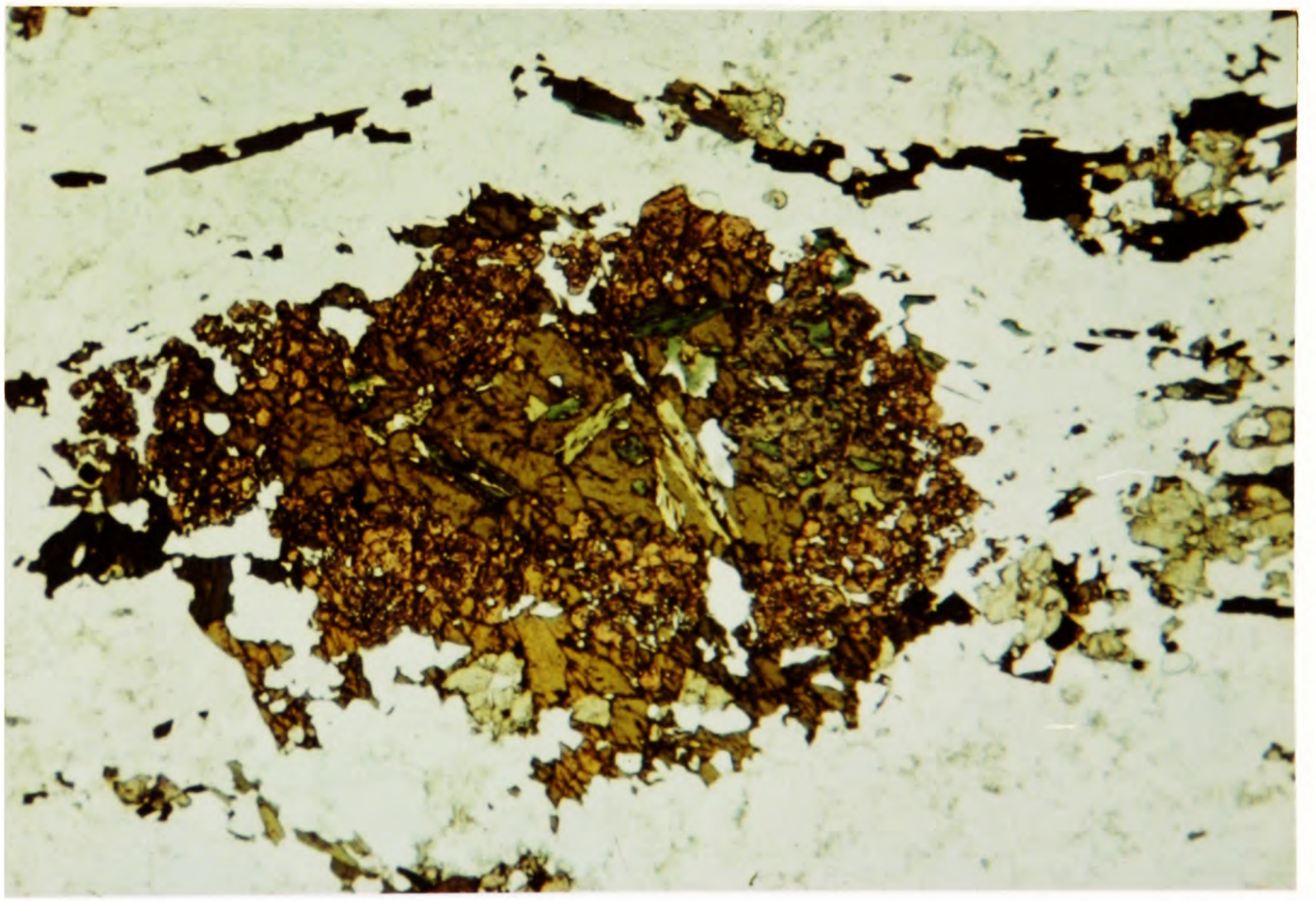

Figure 3.3: Photomicrograph of orthogneiss (SF19) showing olive-green amphibole in quartz-albite matrix. The amphibole is surrounded by a collar of pink garnets. It includes green biotite and deep green chlorite and, on the right, a large grain of sphene. Beneath the amphibole, and in the matrix are several epidote grains. Width of field of view is 9mm.



Figure 3.4: Tight F_2 fold in orthogneiss. Dark green amphiboles are deformed in the hinge region. Pink garnet coronas post-date the deformation of the amphiboles.

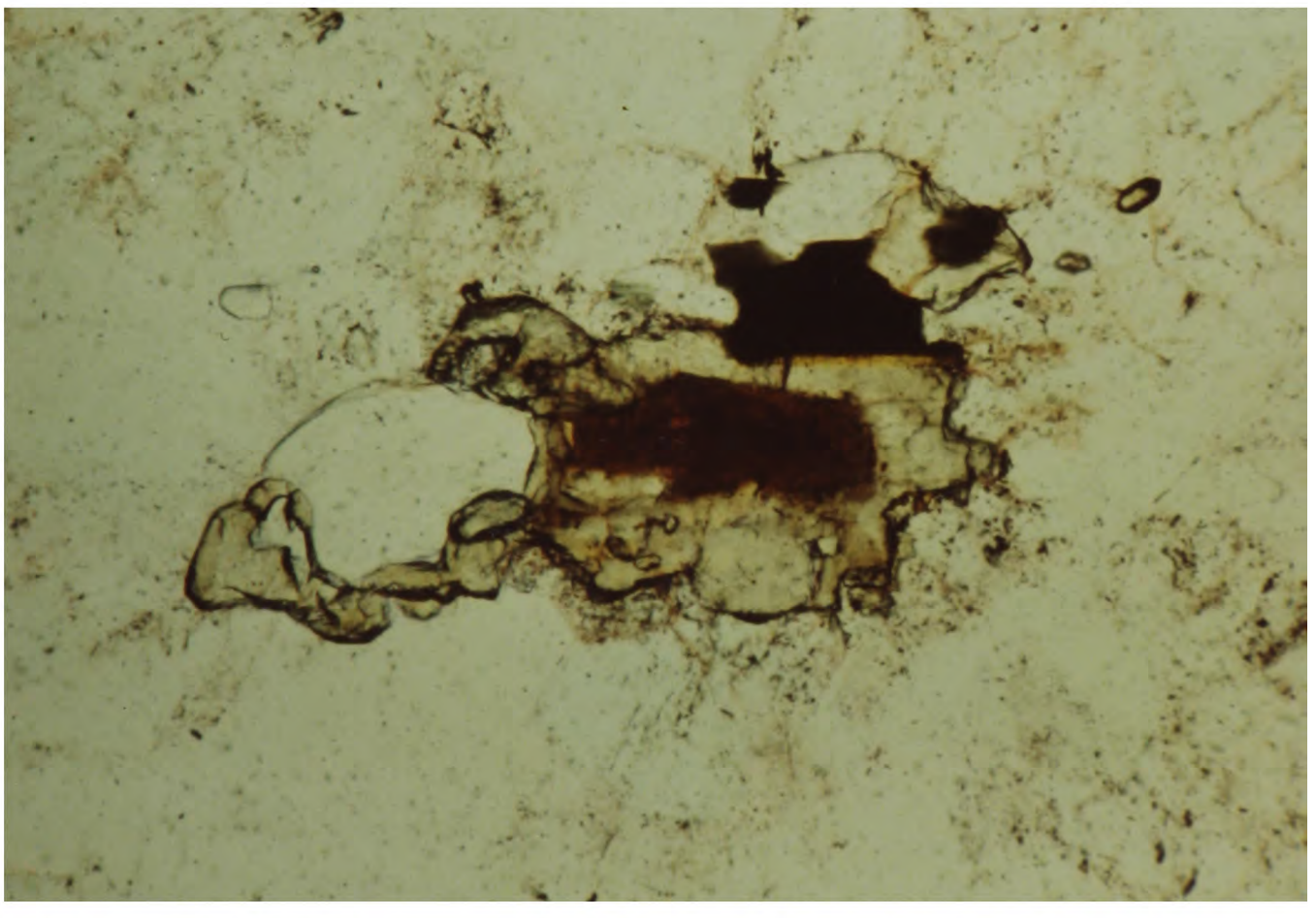

Figure 3.5: Photomicrograph of orthogneiss (SF19) showing epidote grain enclosing metamict allanite grain. Width of field of view is 1.4mm.

Figure 3.6:

a) Chemical zoning profiles across garnets from amphibole-bearing gneisses:

55G - skeletal garnet from metasedimentary gneiss

SF19 - small garnet from corona on amphibole in orthogneiss

Note the high contents of Ca and Mn in 55G and at the rims of SF19.

b) Chemical zoning profiles across garnets from pelitic and semi-pelitic gneisses and migmatites

R1 - skeletal garnet from semi-pelite

446A - traverse along length of garnet elongated in L_2 lineation

FN1 - three profiles from garnets in single sample of semi-pelitic schist. Roman numerals refer to types described in more detail in the text.

(i) "prograde" with increase in Mg at rims and shallow bell-shaped Mn profile

(ii) homogenized profile, chemistry is similar to rim chemistry in (i),

(iii) homogeneous core with a high-Mg, low-Ca plateau and flat, low-Mg, high-Ca rim compositions.

L52 - retrograde profile from garnet in staurolite-bearing schist from near Lavik. In this example the prograde profile has been homogenised (other garnets from the same sample have prograde profiles).

SF165 - slightly "prograde" profile from semi-pelitic schist near contact with Upper Mafic Unit at Råsholm. Below is exaggerated profile for Mn only, illustrating

"twin peaks" produced by rotation of grain during garnet growth (see text).

The high Ca and Mn contents and low Fe of R1 are very similar to those in the amphibole-bearing gneisses in (a). In general, Ca and Mn are lower and Fe is higher in the schists than in the amphibole-bearing gneisses and R1.

c) Chemical zoning profile across small amphibole grain from orthogneiss. Sample SF19.

d) Chemical zoning profile across epidote from semi-pelite showing retrograde zoning in Fe. Sample R1.

GARNETS

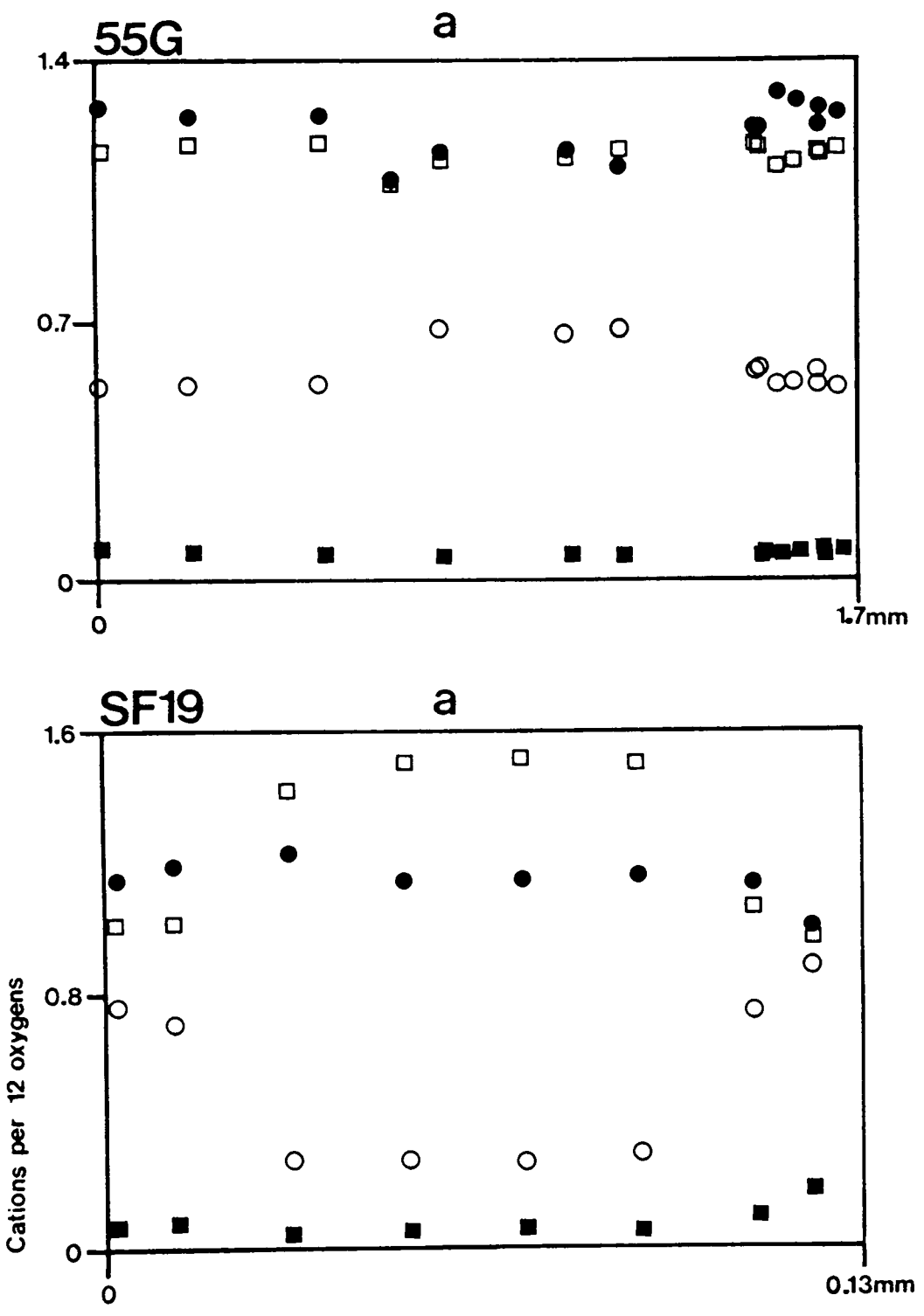

Figure 3.6

GARNETS

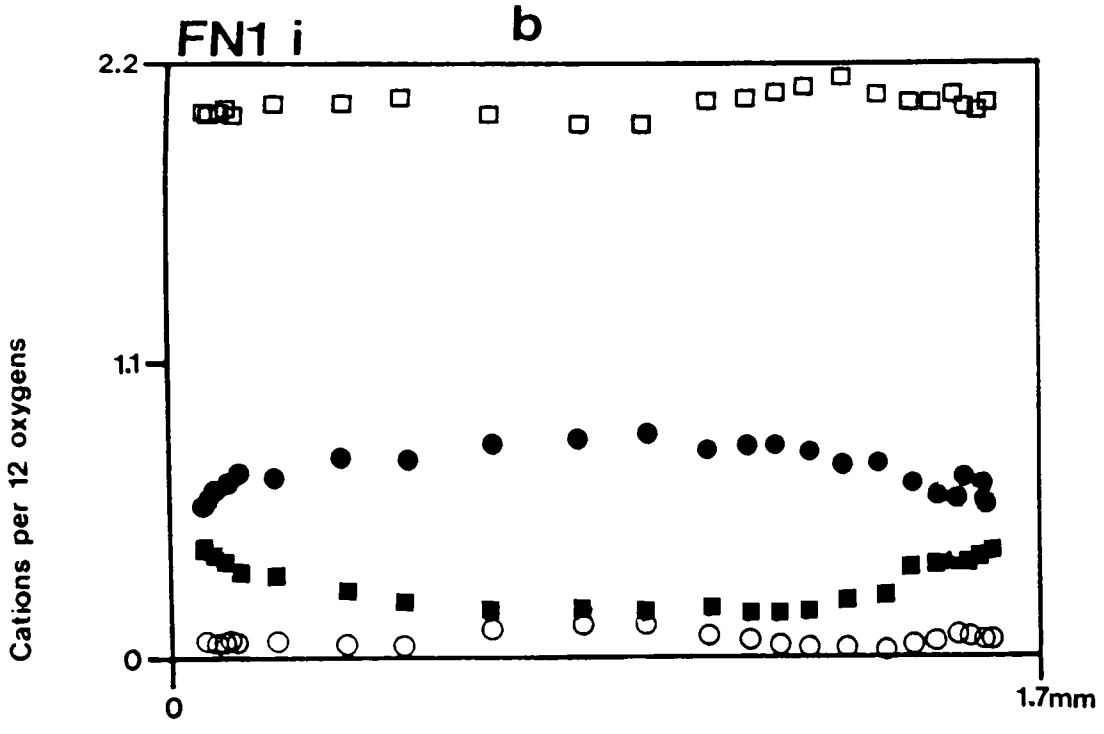

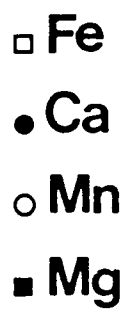

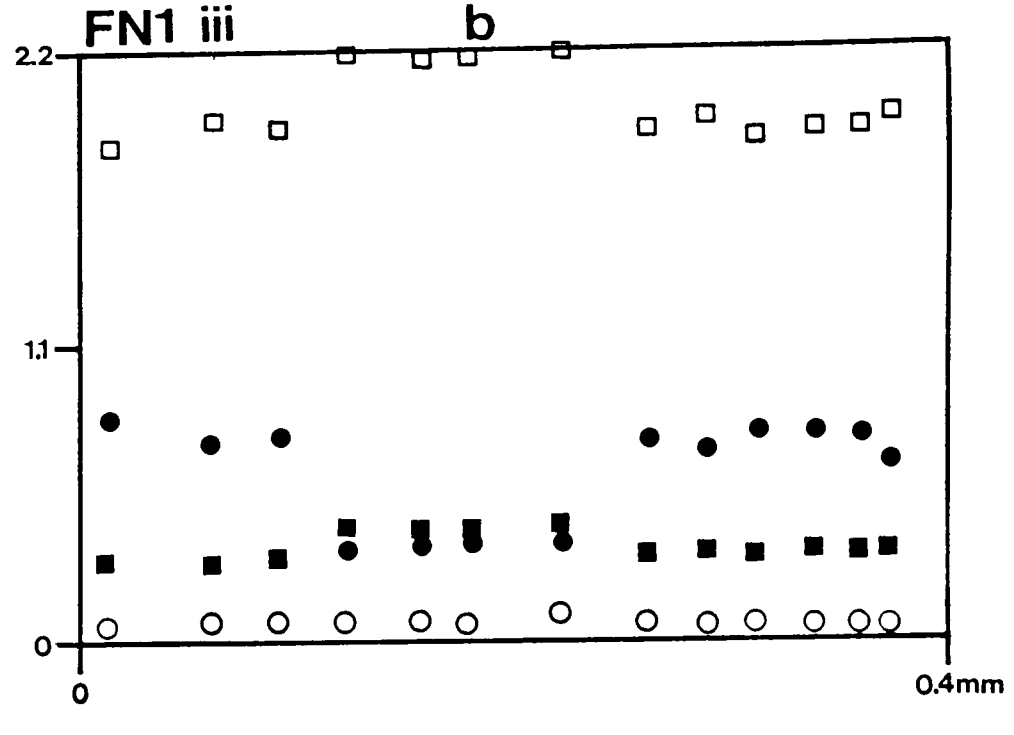

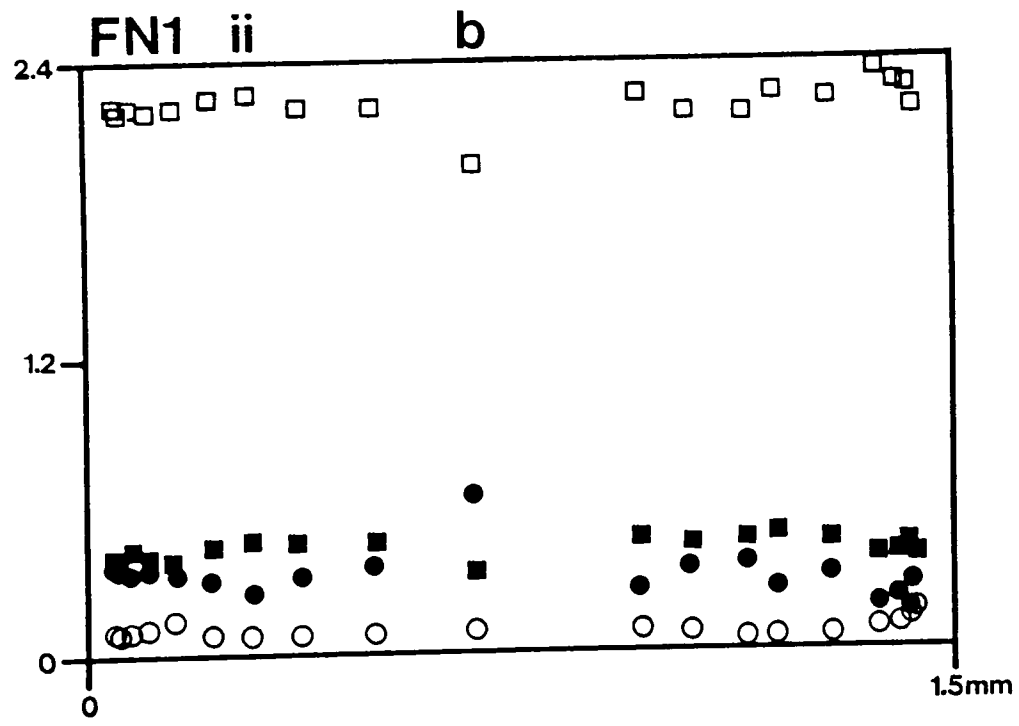

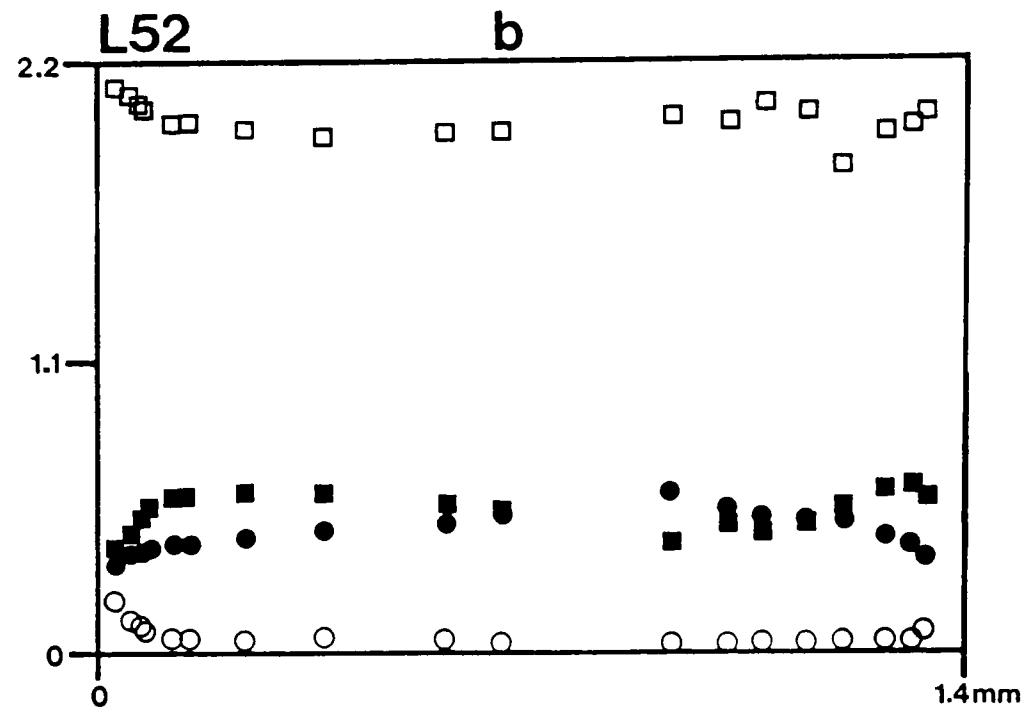

Figure 3.6 (con)

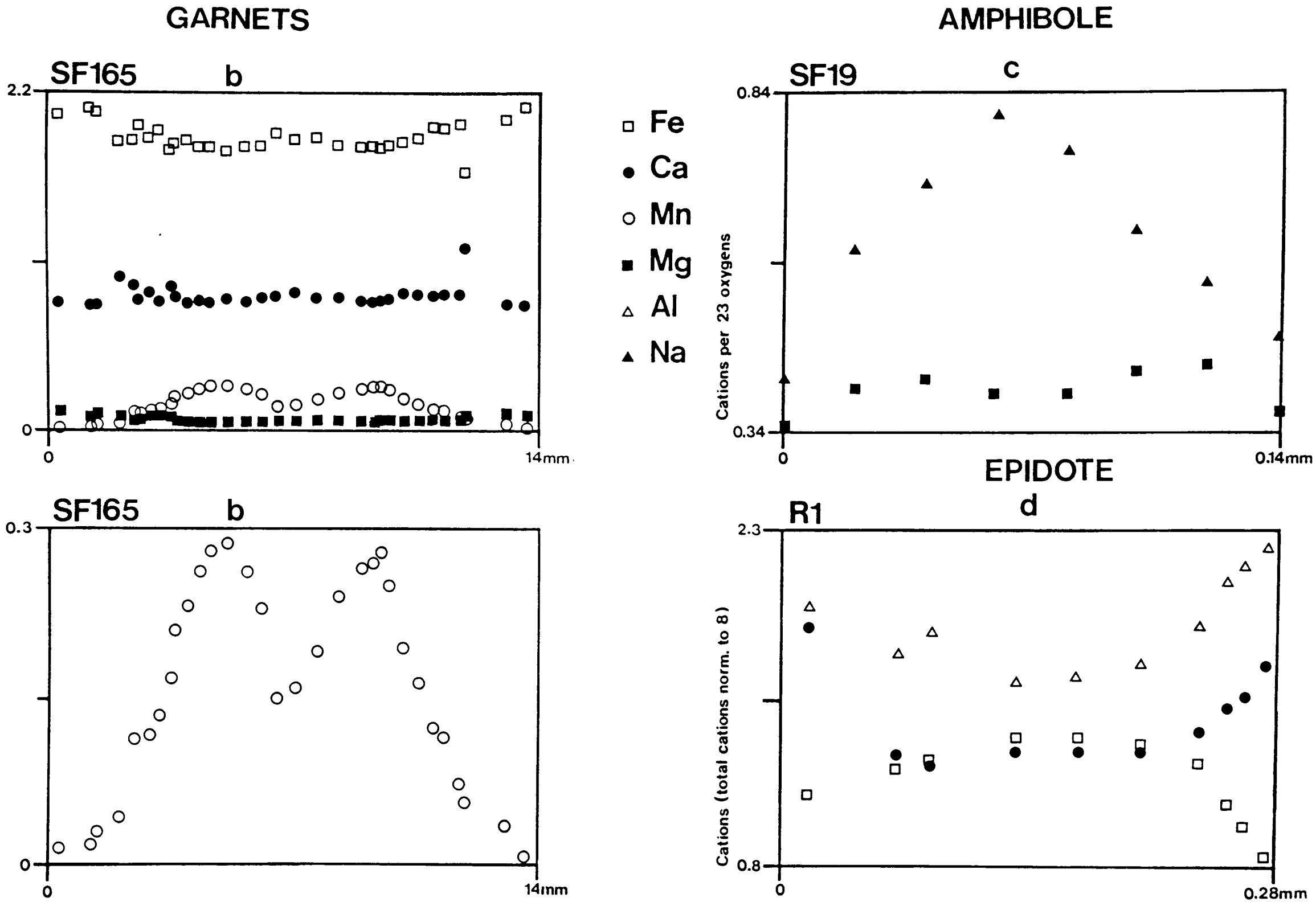

Figure 3.6 (con)

Figure 3.7: Localities for samples analysed on electron microprobe, including those described in chapters 4 to 6.

Basement Gneisses: 55, 149, 446A, FN1, L52A, R1, SF19, SF203, SF165.

Eclogites: 166, SF20, SF21, SF23, SF24, SF68, SF70, SF133, SF138, SF207

Lower Mafic Unit: 176, 449, 446C, L128, L150, SF35, SF110, SF112, SF172, T1

Middle Mafic Unit: 378, 438, 442, 498, R3, S7, SF119

Upper Mafic Unit: B3, K2, K3, KJ6, KJ10, L25, L27, L41, L226, L227, SF156, SF173, SF179, Y22

Hyllestad schists: 427, 472, Å3, Å4, DAN13, H10, H11, H12, H15, H16, H17, H18, R6, R8, SF48, SF51, SF52, SF54, SF55

Other: 368, B12, Y4, Y17

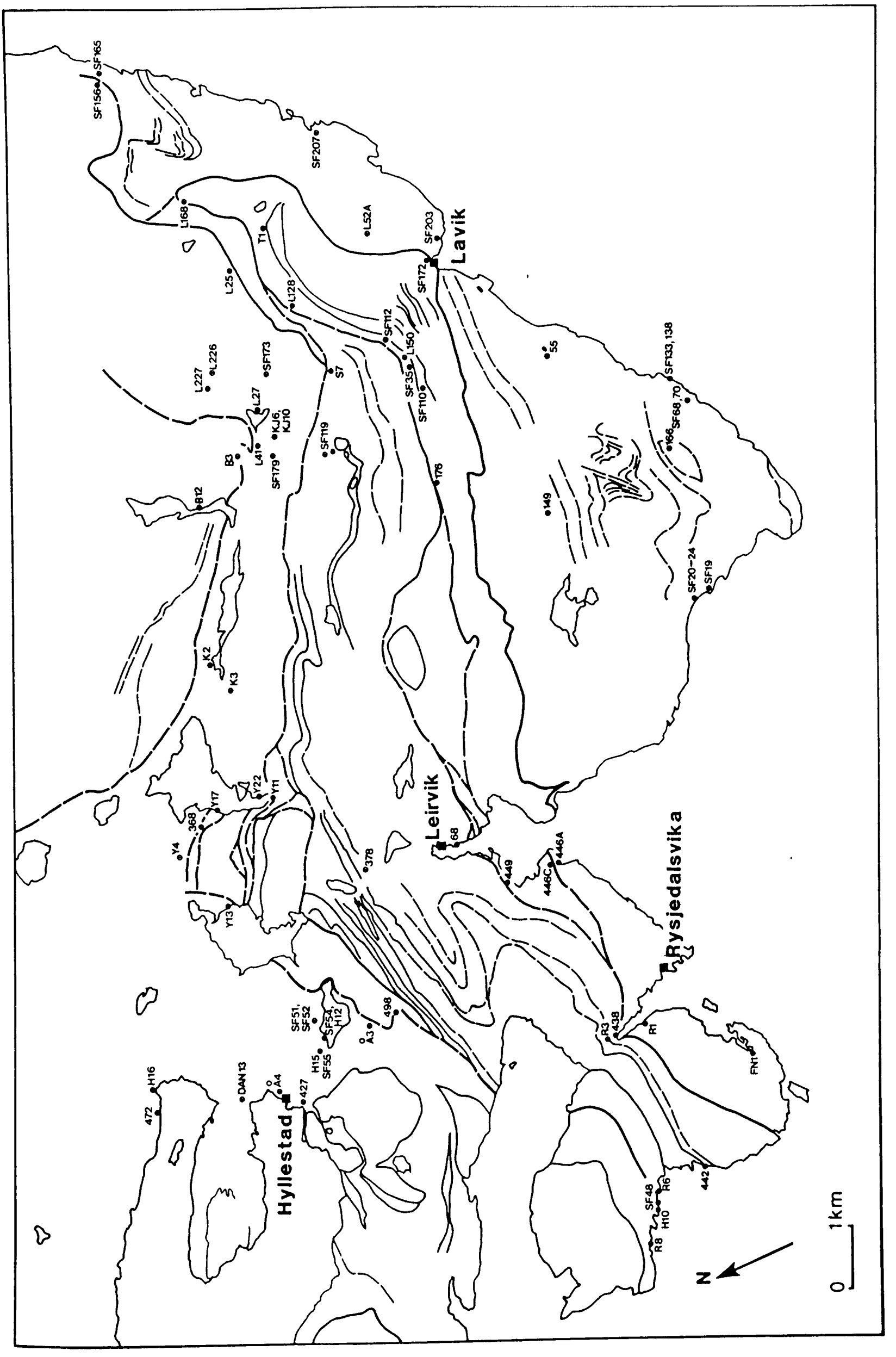
SF165
SF156
SF207
L168
T1
L52A
SF203
Lavik
L25
L128
SF172
SF112
L150
SF35
SF110
L227
L226
SF173
L27
S7
55
SF133, 138
SF68, 70
KJ6, KJ10
L41
SF179
SF119
B3
B12
176
166
149
K2
K3
SF20-24
SF19
Y22
Y11
Y17
368
Y4
Y13
378
68
Leirvik
449
446C
446A
Rysjedalsvika
SF51, SF52
SF54, H12
H15
SF55
498
A3
R3
438
R1
FN1
H16
472
DAN 13
A4
427
Hyllestad
SF48
R6
H10
R8
442
N
0
1km

Figure 3.7

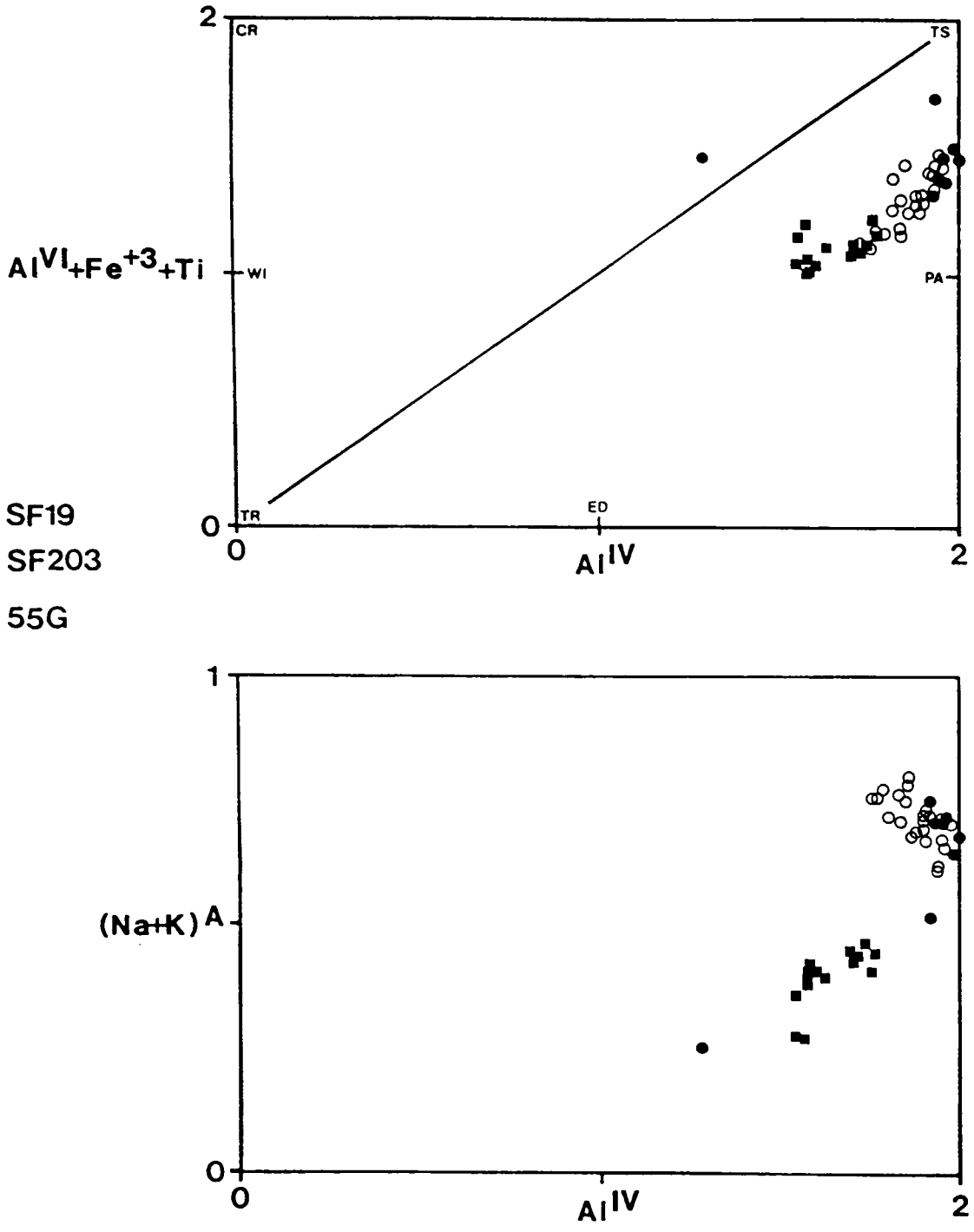

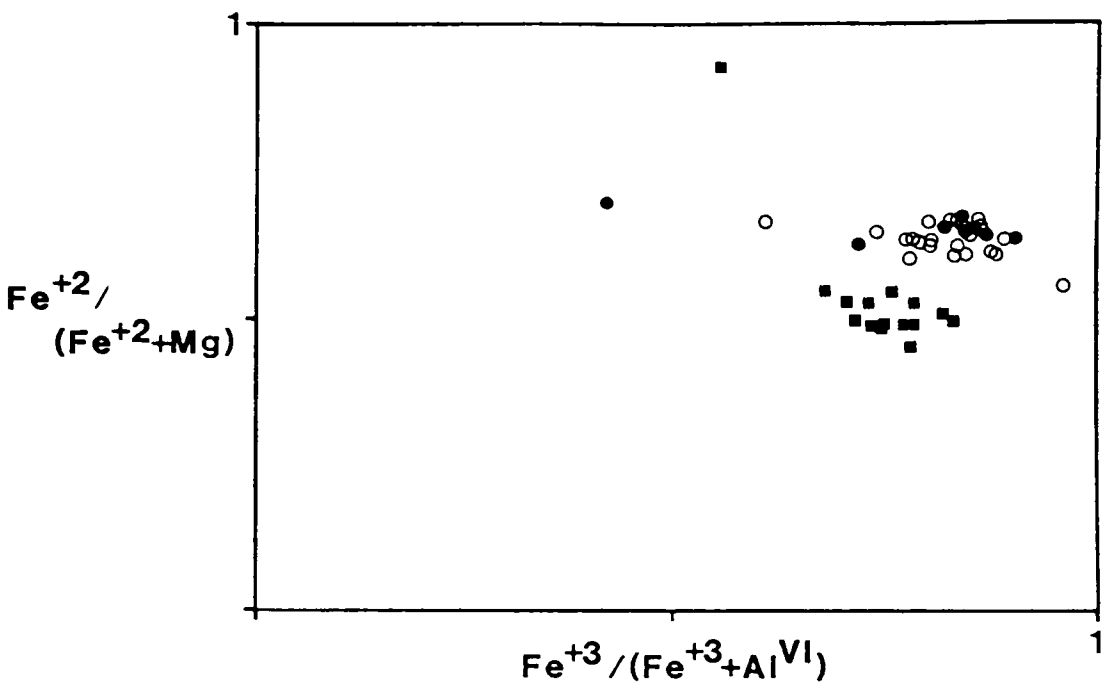

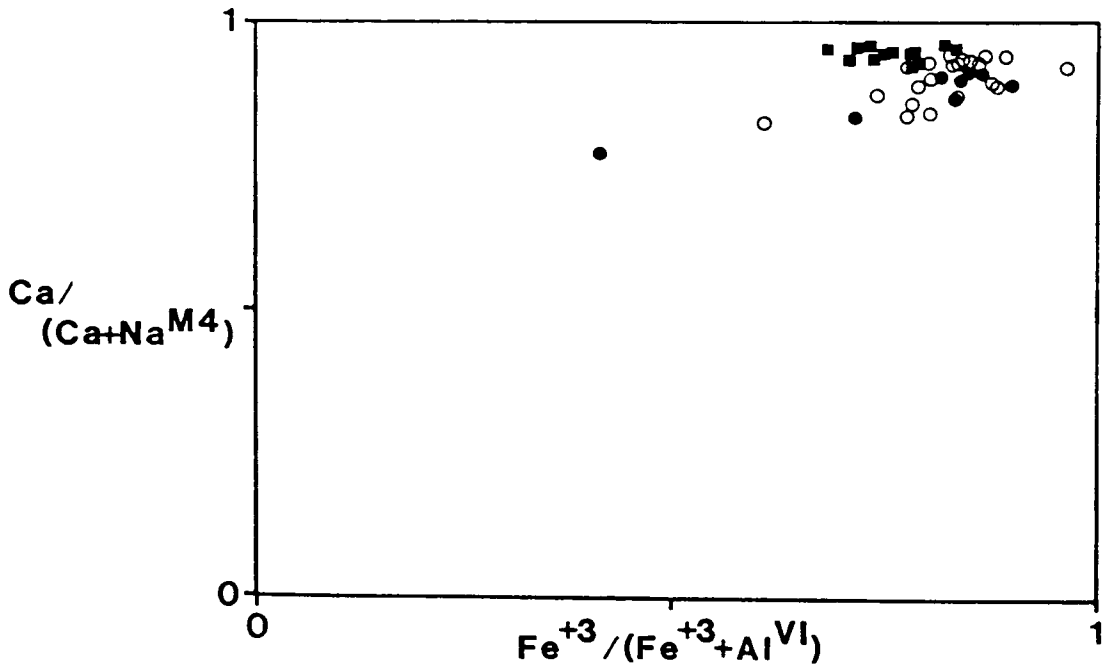

Figure 3.8: Chemical variation in amphiboles from samples in Basement Gneisses. Amphibole analyses are recalculated by the method of Laird and Albee, 1981. See figure 4.16 for abb.

Figure 3.8 (con)

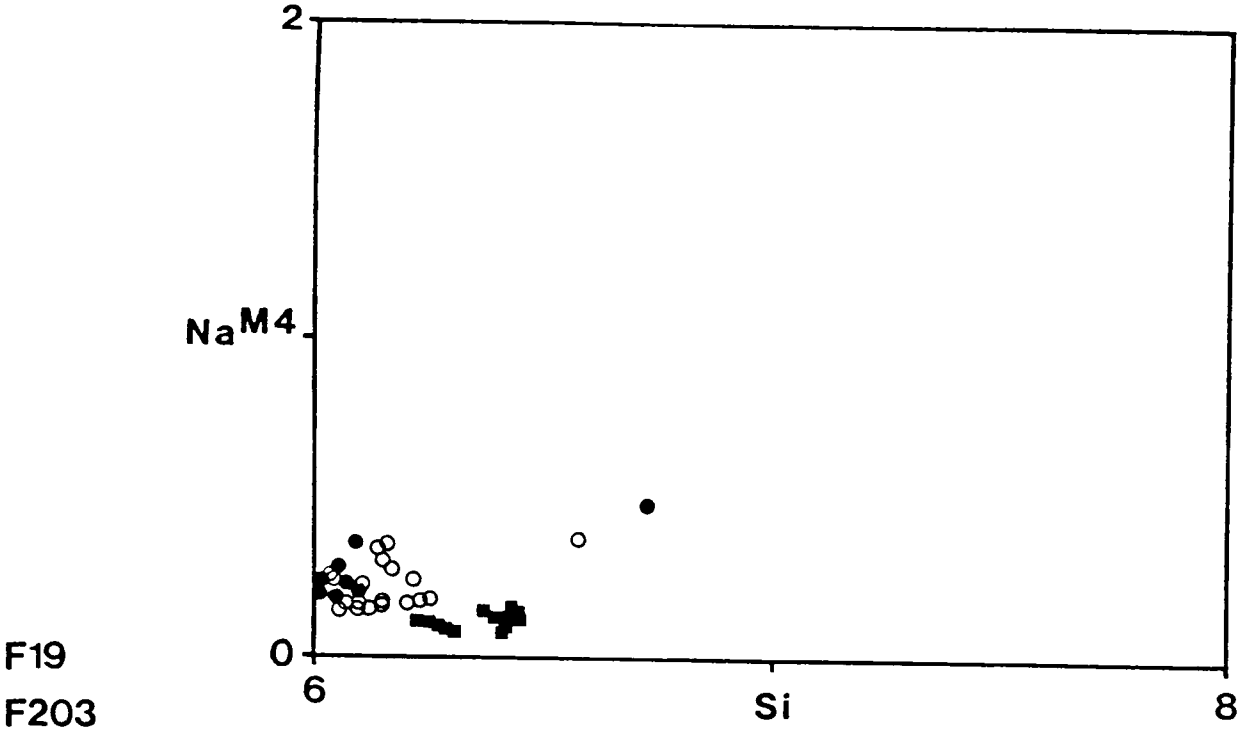

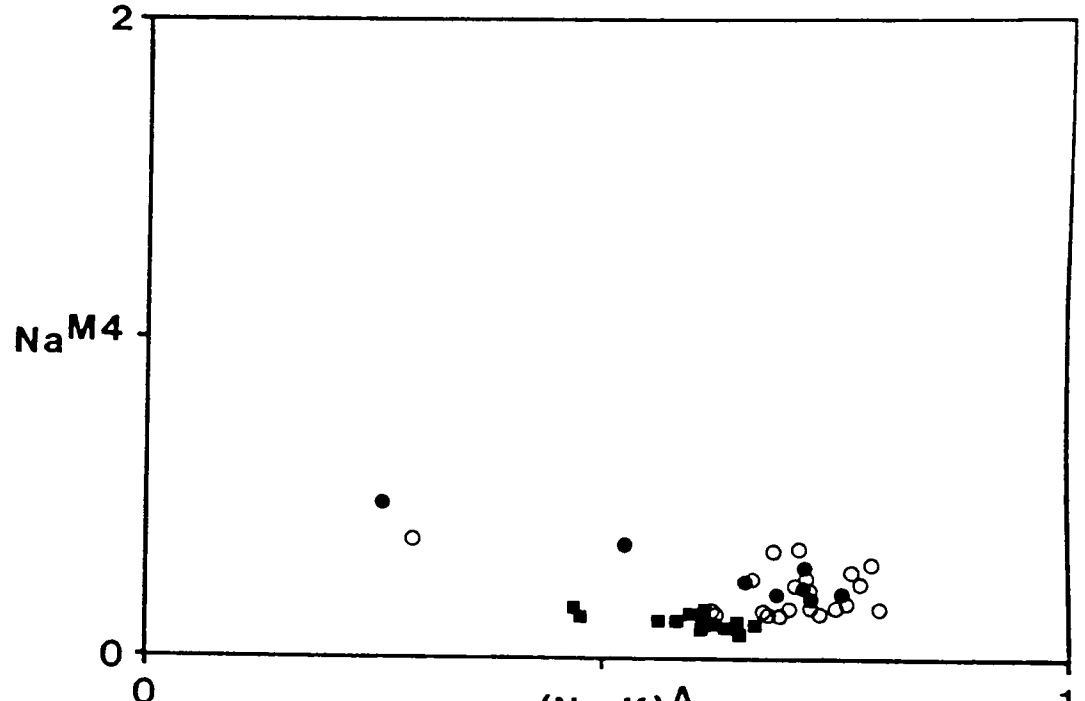

○ SF19
▪ SF203
• 55G

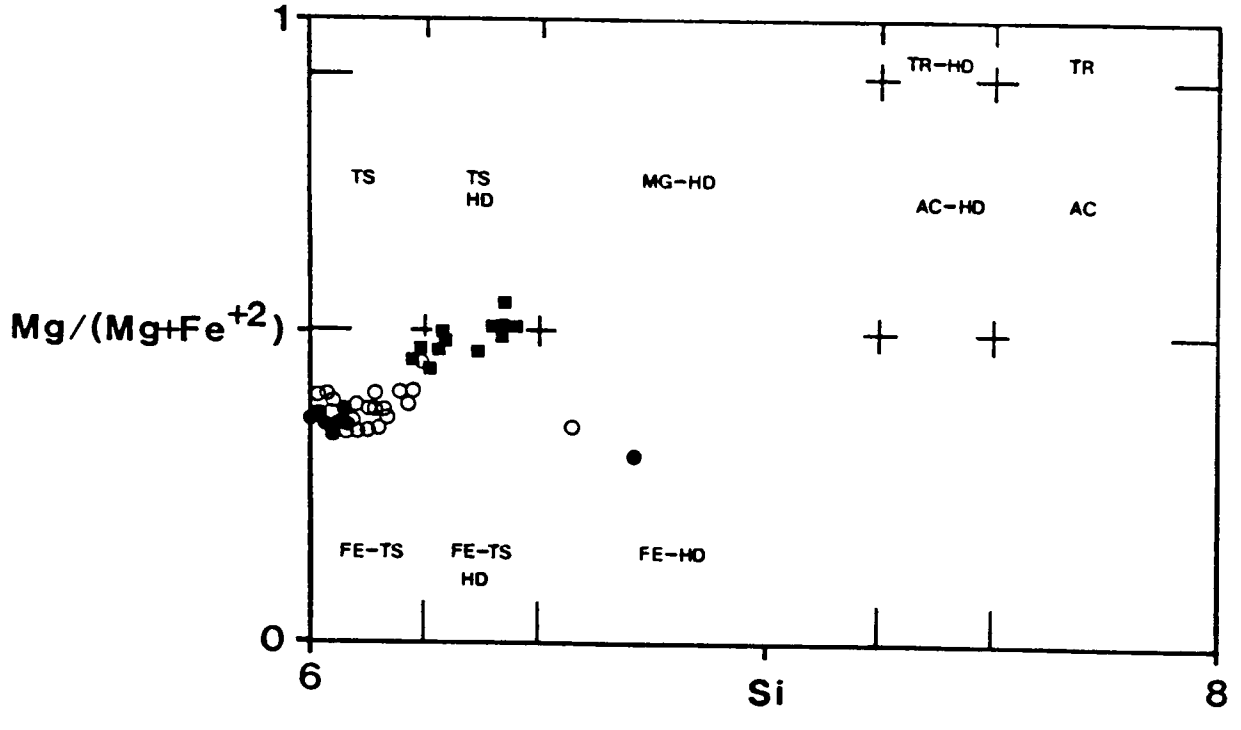

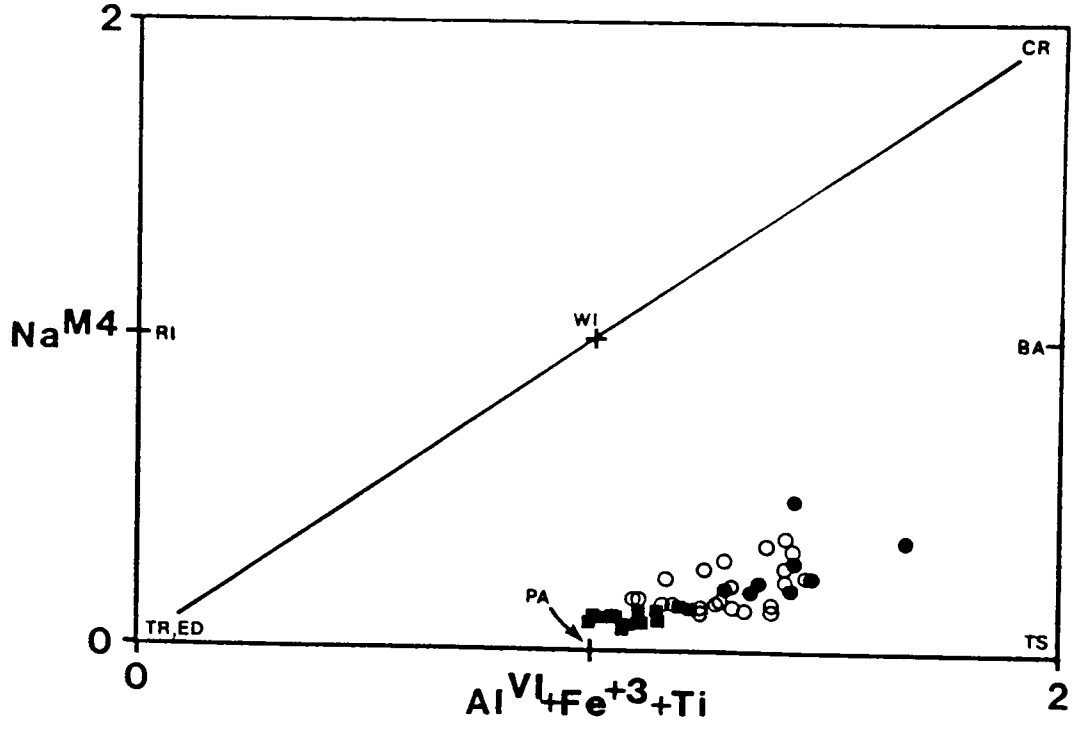

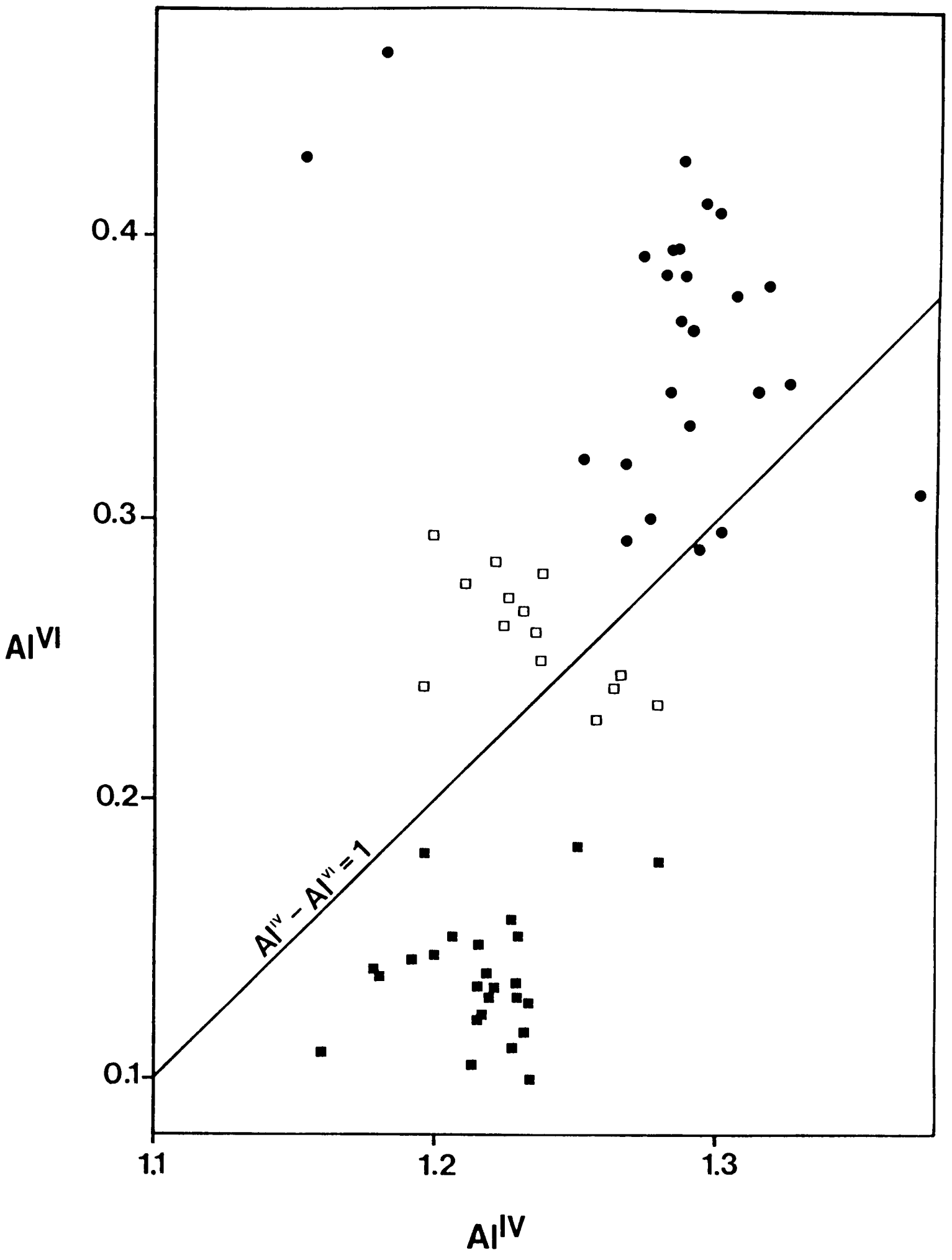

Figure 3.9: Plot of Al distribution between sites in biotites from Basement Gneisses. Annite - phlogopite join is shown for reference. Filled circles: biotite from pelitic schists; open squares: biotite from semi-pelitic gneisses; filled squares: biotites from amphibole-bearing gneisses. Al distribution calculated by the method of Afifi and Essene, 1988.

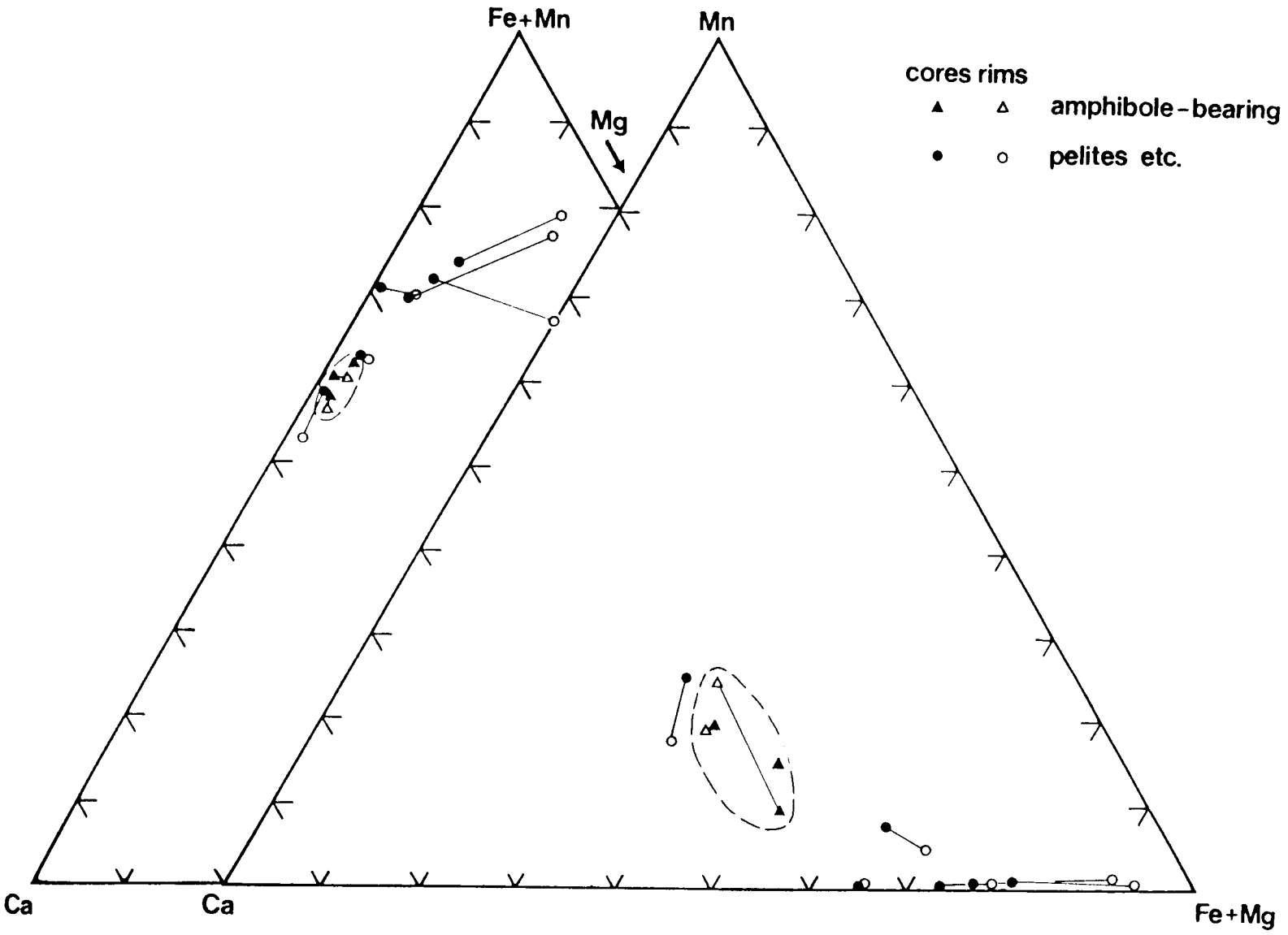

Figure 3.10: Triangular plots comparing garnet compositions in amphibole-bearing and amphibole-absent gneisses from the Basement Gneisses.

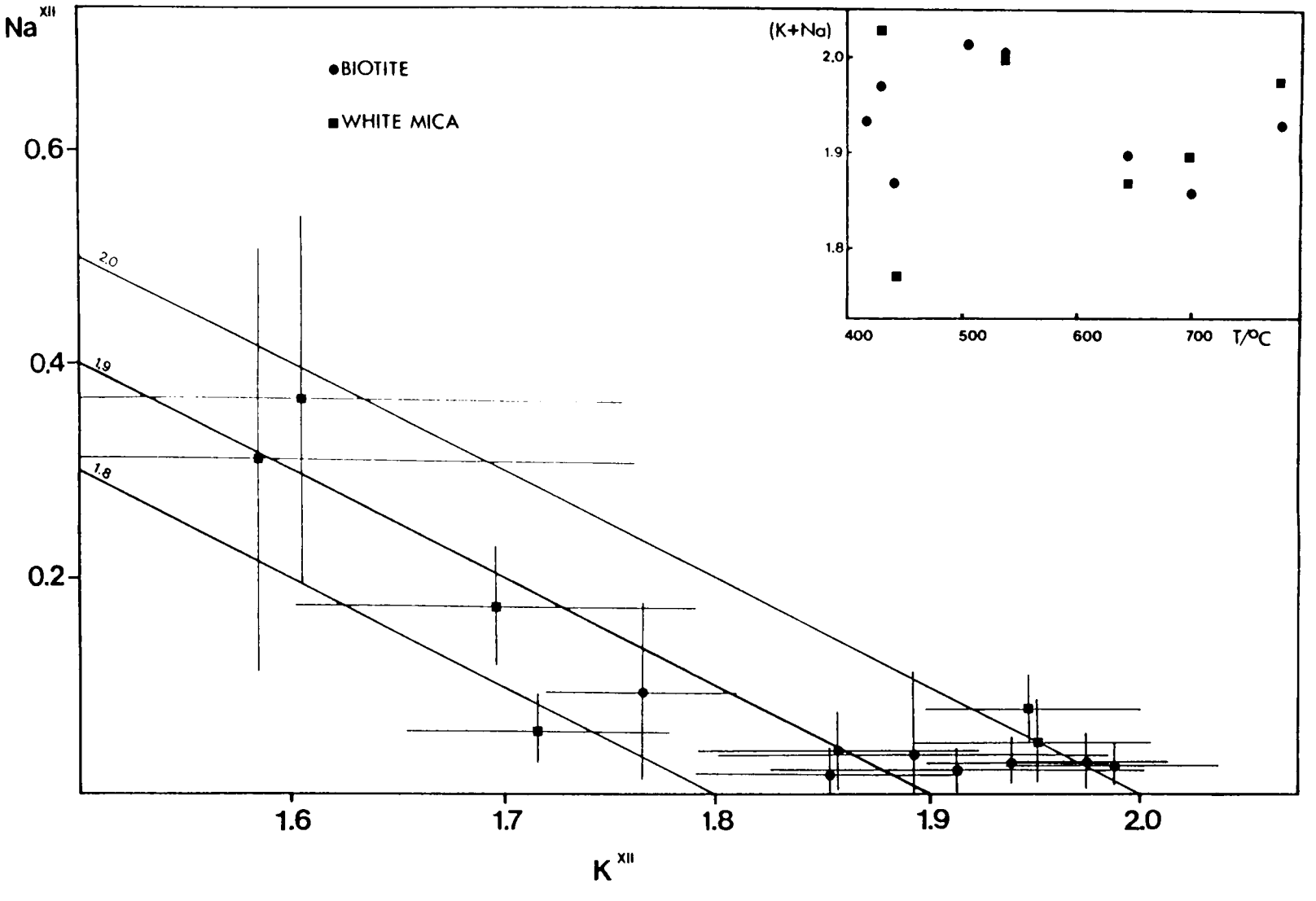

Figure 3.11: Plot of K and Na distribution in XII site of micas from Basement Gneisses with 2σ error bars. Na content is higher in muscovite than in coexisting biotites. Inset: there is no clear relation between XII site vacancies and metamorphic grade, cf. Wang & Banno, 1987. Temperatures have been calculated using the garnet-biotite thermometer as formulated by Ganguly and Saxena, 1984.

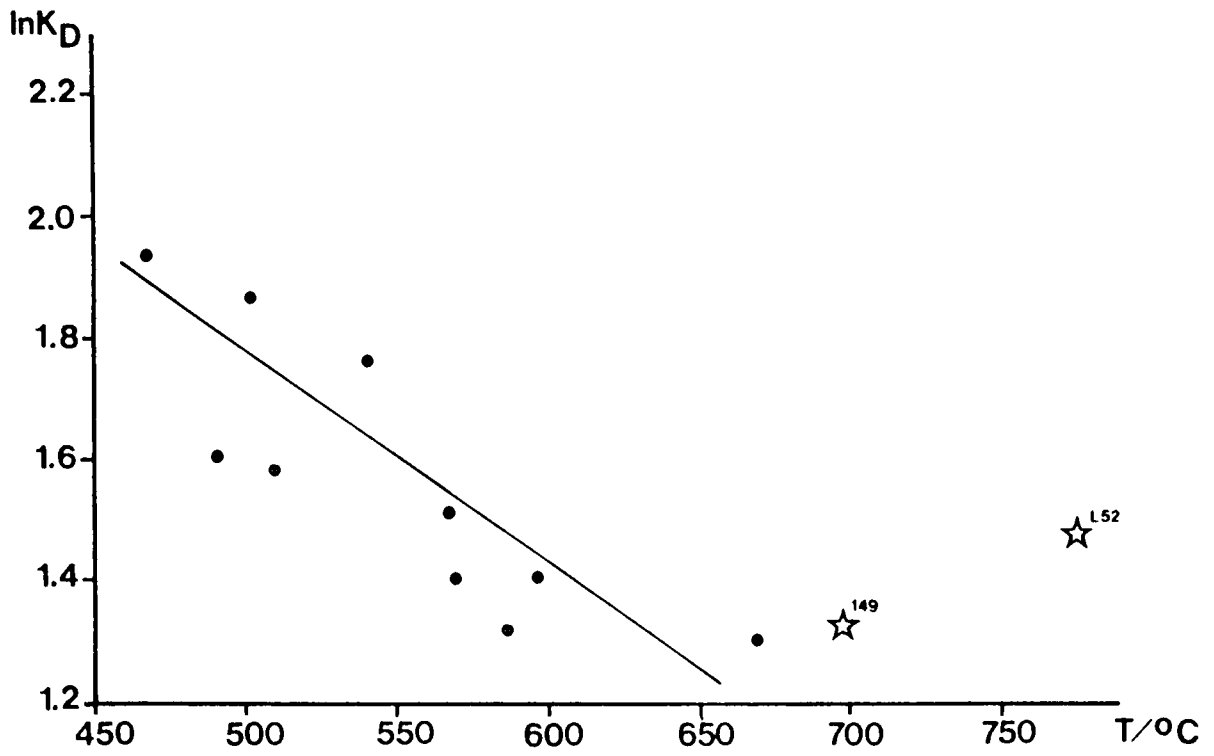

Figure 3.12: Plot to show variation in distribution of Fe and Mg between coexisting staurolite and biotite with temperature. Temperatures have been calculated using the garnet-biotite thermometer as formulated by Ganguly and Saxena, 1984. Filled circles (with "best fit" line): staurolite schists from the Dalradian, taken from Baker, 1985. Stars: data from present work. The poor agreement of data from present work with Baker's results suggests disequilibrium between garnet, staurolite and biotite in samples 149B and L52.

Figure 3.13: Summarized thermobarometric results for samples SF165, 446A, SF203, 55G, R1, SF19, FN1, 149B, and L52 from the Basement Gneisses. These results are listed with others in table 3.4. The range of temperature and pressure for each sample represents peak conditions. The extreme range in estimated conditions for the staurolite schists 149B and L52 is probably a result of disequilibrium between mafic phases. The (partially) diagonally shaded region is the stability range for Fe-staurolite + quartz from Harte, 1975. Pressure estimates should be regarded as maximum limits, as discussed in the text. Arrows indicate a postulated cooling path for post-D_2 uplift.

GS, HS: garnet-biotite thermometers of Ganguly and Saxena, 1984, and Hodges and Spear, 1982, respectively

PER: garnet-amphibole thermometer of Perchuk, 1985 (the calibration of Graham and Powell, 1984, gives rather high temperatures compared with garnet-biotite thermometry, see table 3.4)

P: garnet-staurolite thermometer of Perchuk, 1977

GH: garnet-muscovite thermometer of Green and Hellman, 1982

GS1, GS2, HC, HP: garnet-muscovite-biotite-plagioclase barometer using the formulations of Ghent and Stout, 1981 (equilibria 1 and 2), and Hodges and Crowley, 1985, and the internally consistent data set of Holland and Powell, 1985, respectively.

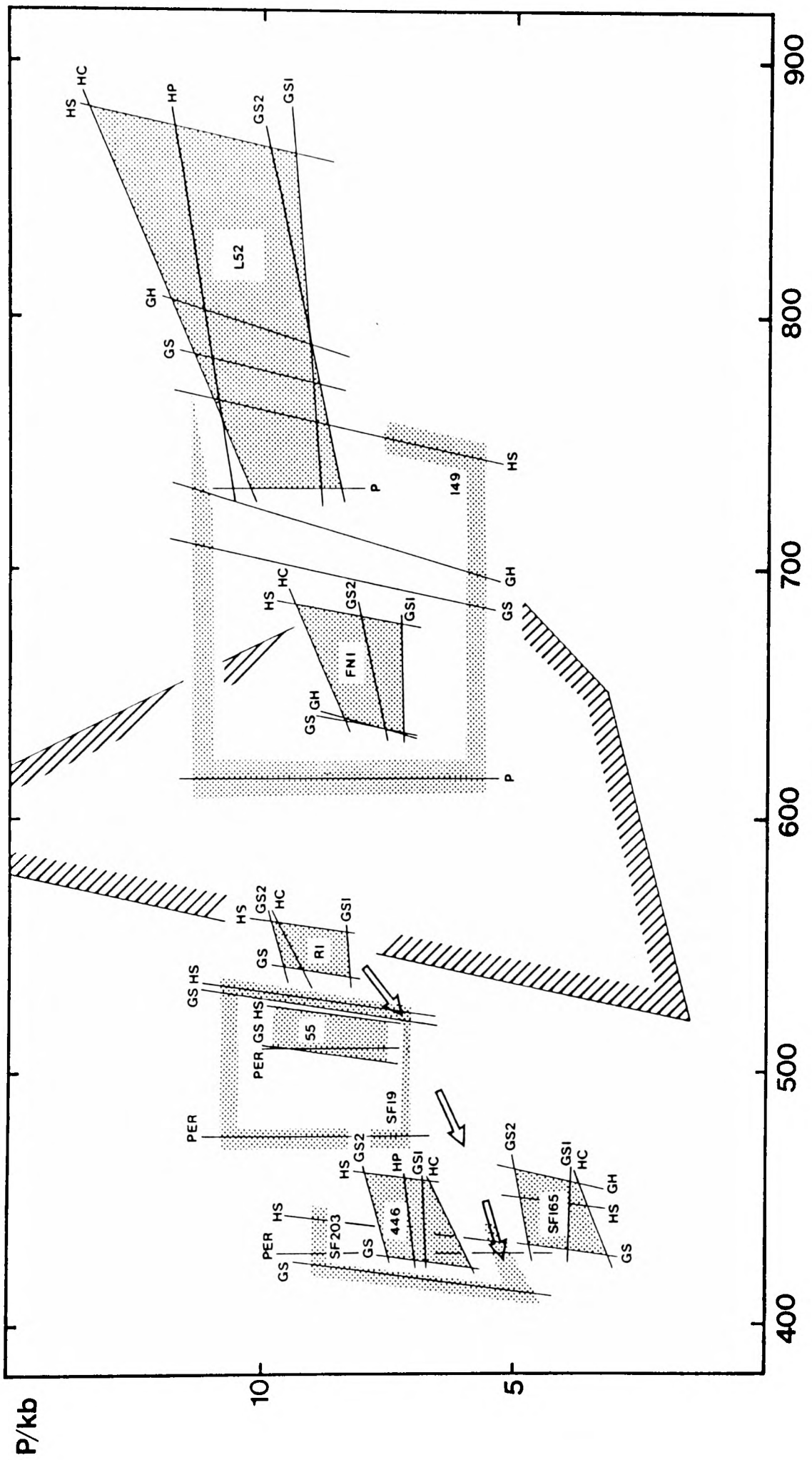
P/kb
T/°C
10
5
600
700
800
900
400
500
HS
HC
HP
GS2
GSI
GH
GS
L52
P
149
FN1
R1
55
SF19
SF203
446
SF165
PER

Figure 3.13



Figure 4.1: Roadside outcrop of eclogite at Brensdal. Eclogite, which has been thoroughly amphibolitized at this locality, occurs as pods and boudins within a white-weathering, well-foliated, quartzose gneiss. An S_2 fold hinge may be discerned in an eclogite pod at the top left of the outcrop. The exposed thickness of the outcrop is about 4m (a geological hammer has been placed at the base of the outcrop).

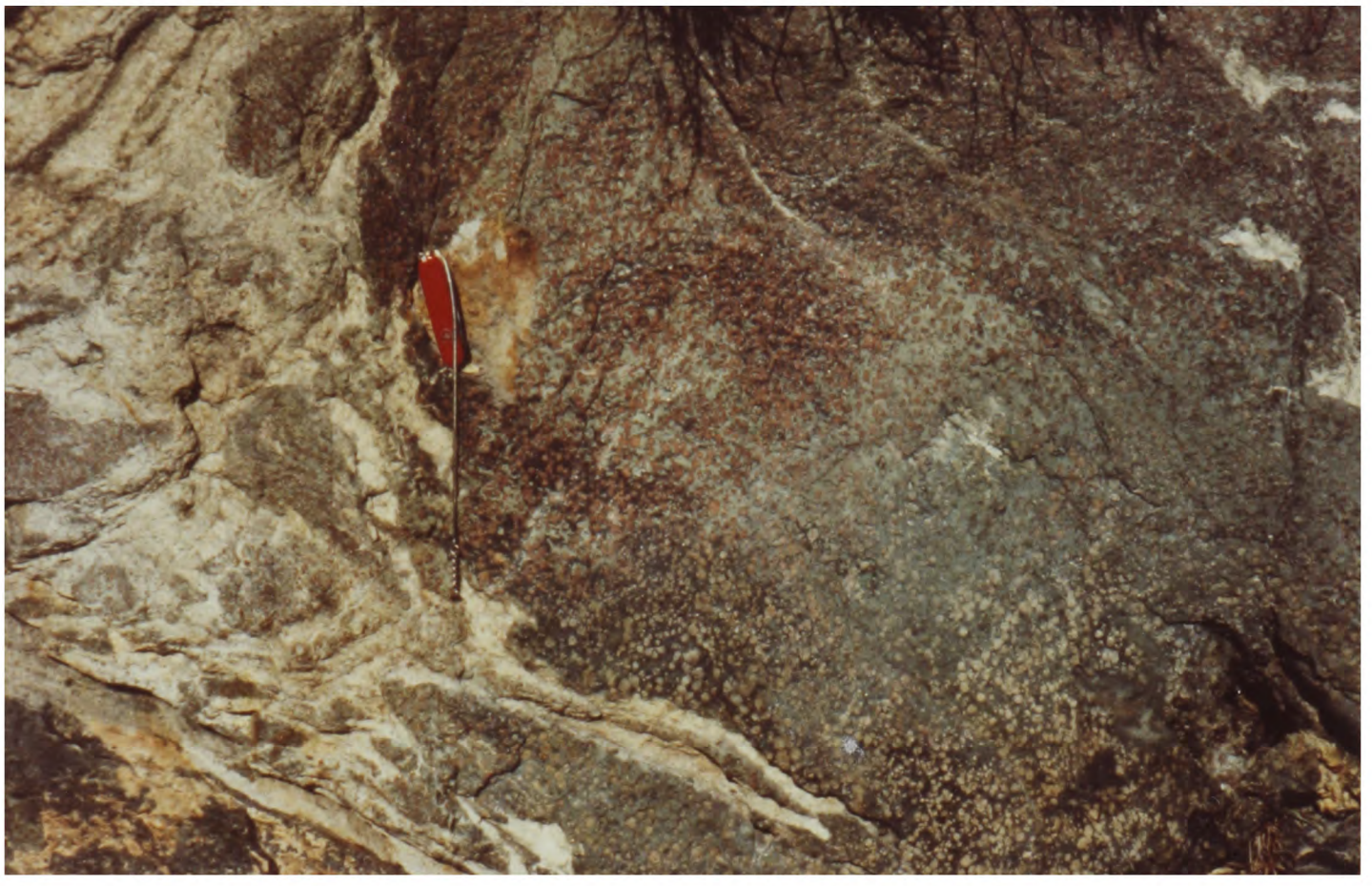

Figure 4.2: Close-up of amphibolitized eclogite pod from Brensdal (see fig. 4.1) showing the irregular margin. The quartz selvage fringing the pod can be clearly seen in the lower part of the picture. Garnets in the bottom right of the photograph have been replaced by epidote, biotite, and chlorite.



Figure 4.3: Large, near-horizontal sheet of eclogitic material at Ytre Hellebö. The margin is irregular (see also fig. 4.2), with invading quartzose veins. Just above the margin, a mylonitic fabric is developed with intrafolial westward-vergent folds. The migmatitic foliation in the Basement Gneisses curves into the contact from above.



Figure 4.4: Vertical sheets of amphibolitized eclogite at Ytre Hellebö, 0.5m thick with quartzose selvages. Interpreted as dolerite dykes intruded into crustal material later and metamorphosed under eclogite facies conditions.

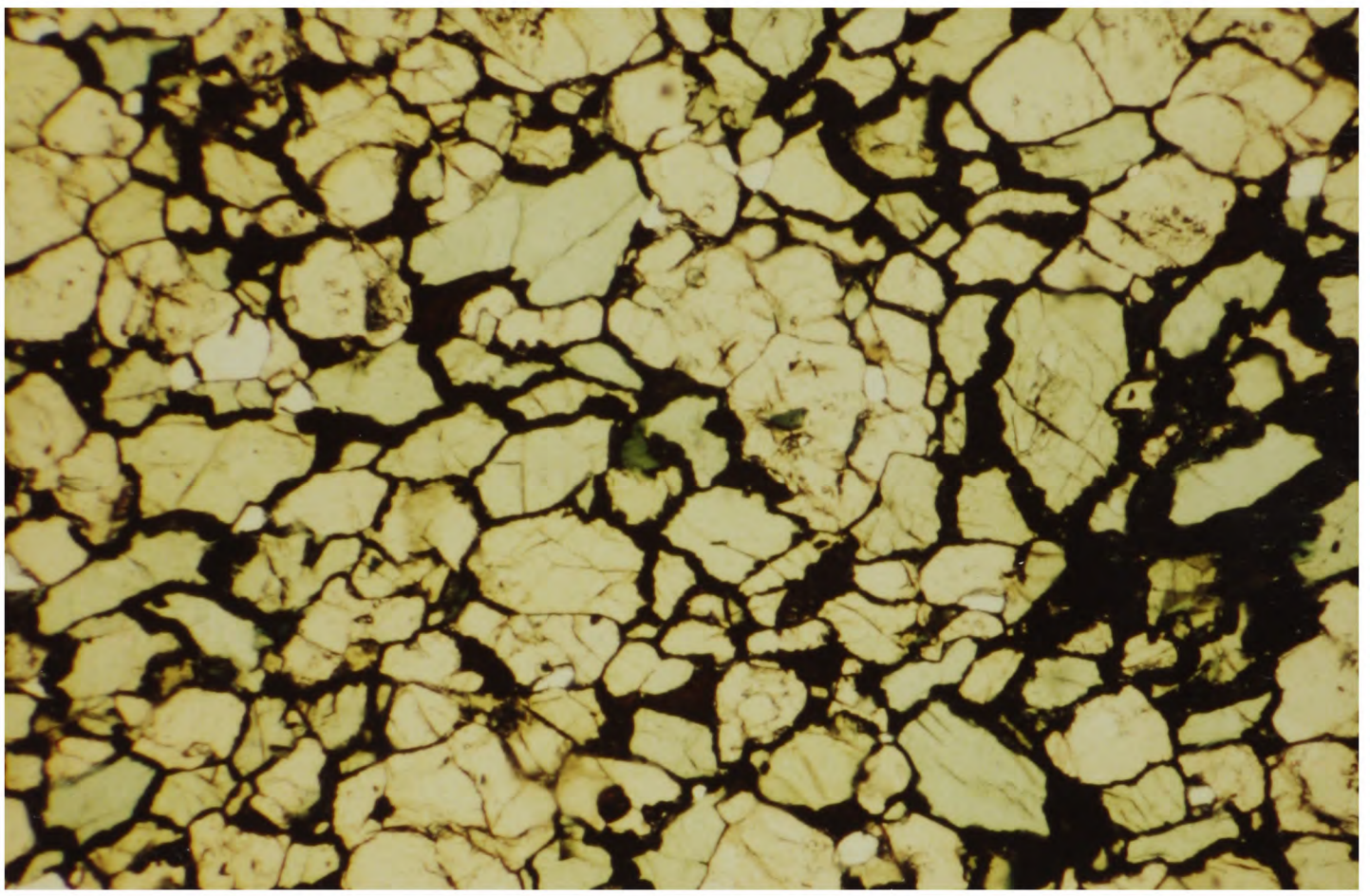

Figure 4.5: Photomicrograph of eclogite from Helleböstölane in PPL, showing initial stages of amphibolitization. Field of view contains mainly omphacite and garnet with a little quartz, and rutile (almost opaque in this picture). Amphibole occurs as dark green inclusions in garnet and in contact with omphacite (e.g. near the centre of the picture). Symplectites of albite and clinopyroxene occur on omphacite rims, particularly on the right of the picture, and appear almost opaque. Field of view is 3.5mm across.

Figure 4.6: Triangular diagram showing relative proportions of almandine (ALM) + spessartine (SP), andradite (AND) + grossular (GR), and pyrope (PYR) for garnets from eclogites and amphibolitized eclogites from Sognefjord, Norway. The compositional ranges for garnets from eclogites of groups A, B, and C are taken from Coleman et al, 1965, who define the groups as follows: Group A: Inclusions in kimberlites, basalts or layers in ultramafic rocks of very deep-seated igneous and metamorphic origin; Group B: Bands or lenses within migmatitic or gneissic terrains, surrounded by amphibolites; Group C: Bands or lenses within alpine-type orogenic zones, associated with glaucophane schists.

Garnets in eclogites from Sognefjord plot in group C, although field relations are those of group B. Zoning from core to rim trends towards group B for most samples. Solid lines join garnet rim and core compositions from each rock. 166A1 and 166A2: eclogites showing little amphibolite overprint from Helleböstölane; SF68 and SF70: amphibolitized eclogites containing relict clinopyroxene from Ytre Hellebö; SF25, SF24, and SF20: amphibolitized eclogites containing no relict clinopyroxene from Brensdal (SF25G and SF25S are from garnets in a gneissose amphibole-rich band and a schistose quartz-rich band, respectively).

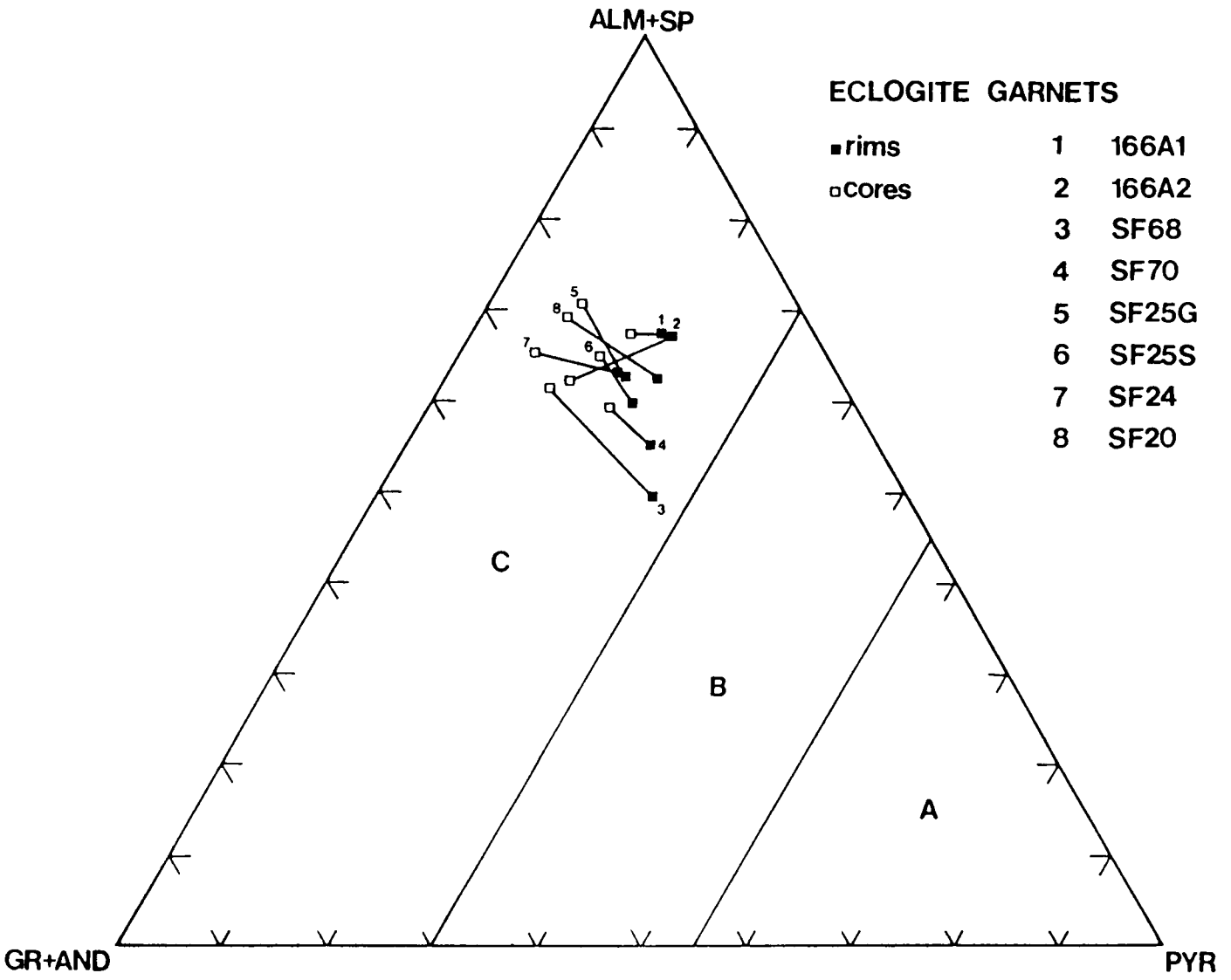
ALM+SP
GR+AND
PYR
C
B
A
1
2
3
4
5
6
7
8
ECLOGITE GARNETS
rims
cores
1 166A1
2 166A2
3 SF68
4 SF70
5 SF25G
6 SF25S
7 SF24
8 SF20

Figure 4.6

Figure 4.7 (a): Chemical zoning profiles for garnets from eclogites and amphibolitized eclogites:

166A: garnet from one of the least altered eclogites. Assemblage includes omphacitic clinopyroxene and minor primary amphibole. Zoning is strongest in Ca, while there is only a slight increase in pyrope content from core to rim. Locality: Helleböstölane.

SF68: garnet from eclogite with amphibole developed at omphacite/garnet contacts. Core compositions are similar to those in 166A but there is more profound zoning in Mg and Mn. Locality: Ytre Hellebö

SF138: zoning in garnet from amphibolitized eclogite. Differs from all other examples in showing a slight increase in Fe/Mg from core to rim. But on the whole there is little zoning by comparison with (for example) SF68. This may be a garnet which has suffered homogenization by intracrystalline diffusion. In such a large grain this process is expected to take tens of millions of years (Spear, 1988). Locality: Ytre Hellebö.

SF25: garnet from gneissic band in eclogitic amphibole from Brensdal. Clinopyroxene has been completely replaced in this rock. Compositions are similar to 166A, but stronger zoning in pyrope and almandine occurs. Locality: Brensdal.

SF24: garnet from amphibolitized eclogite overprinted by greenschist facies metamorphism. It differs from garnets in other eclogitic rocks in having high contents of Mn in the core. The zoning pattern is prograde with increasing Mg towards the grain margins, but there is a slight fall-off at the edge, possibly due to retrogressive re-equilibration with other mafic phases in the matrix. Locality: Brensdal.

(b) Chemical zoning profiles for omphacite from eclogite. The decrease in Mg from core to rim is probably post-retrogressive re-equilibration. Locality: Helleböstölane.

Figure 4.7

CHEMICAL ZONING IN GARNETS

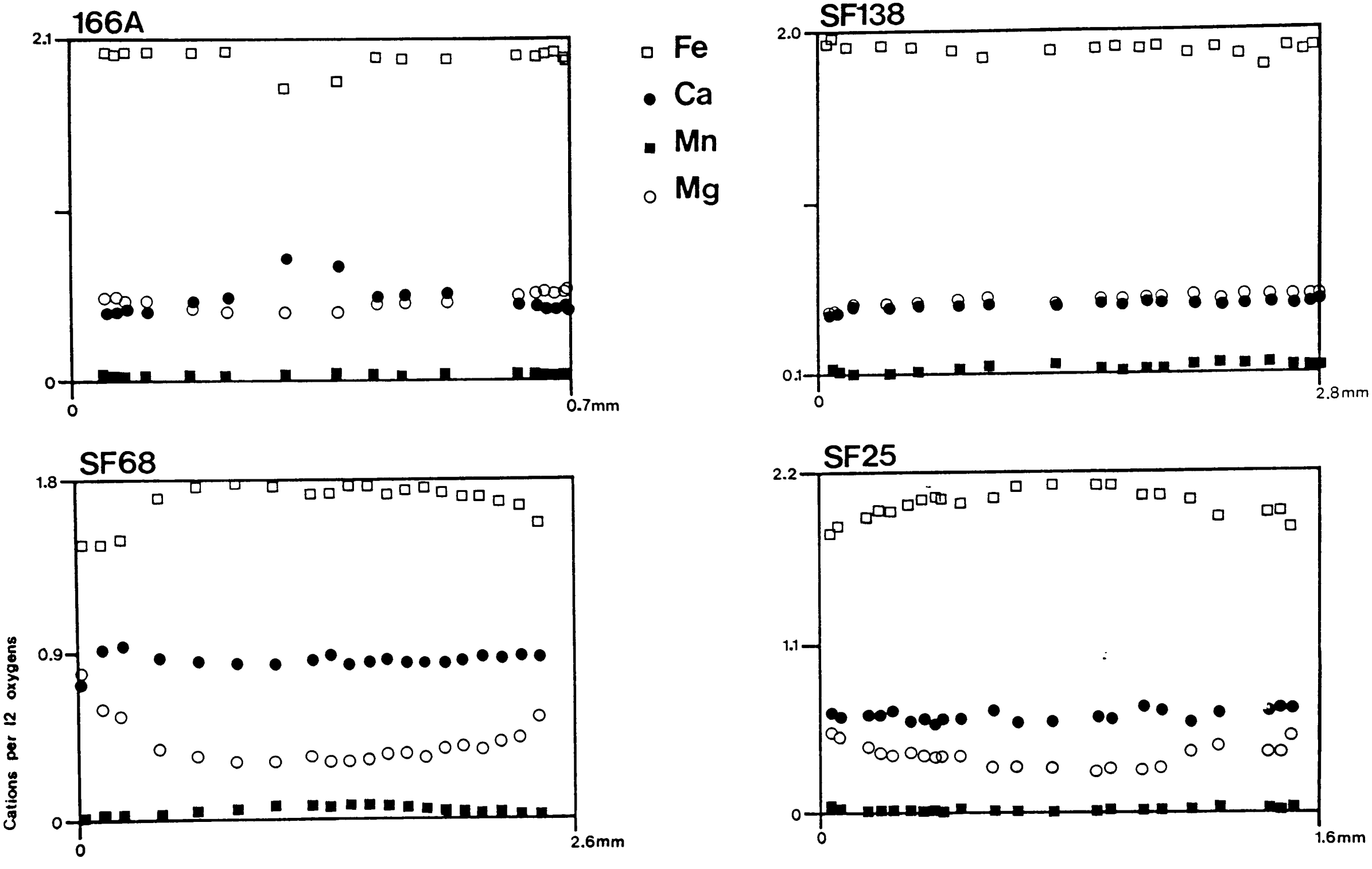

Figure 4.7 (con)

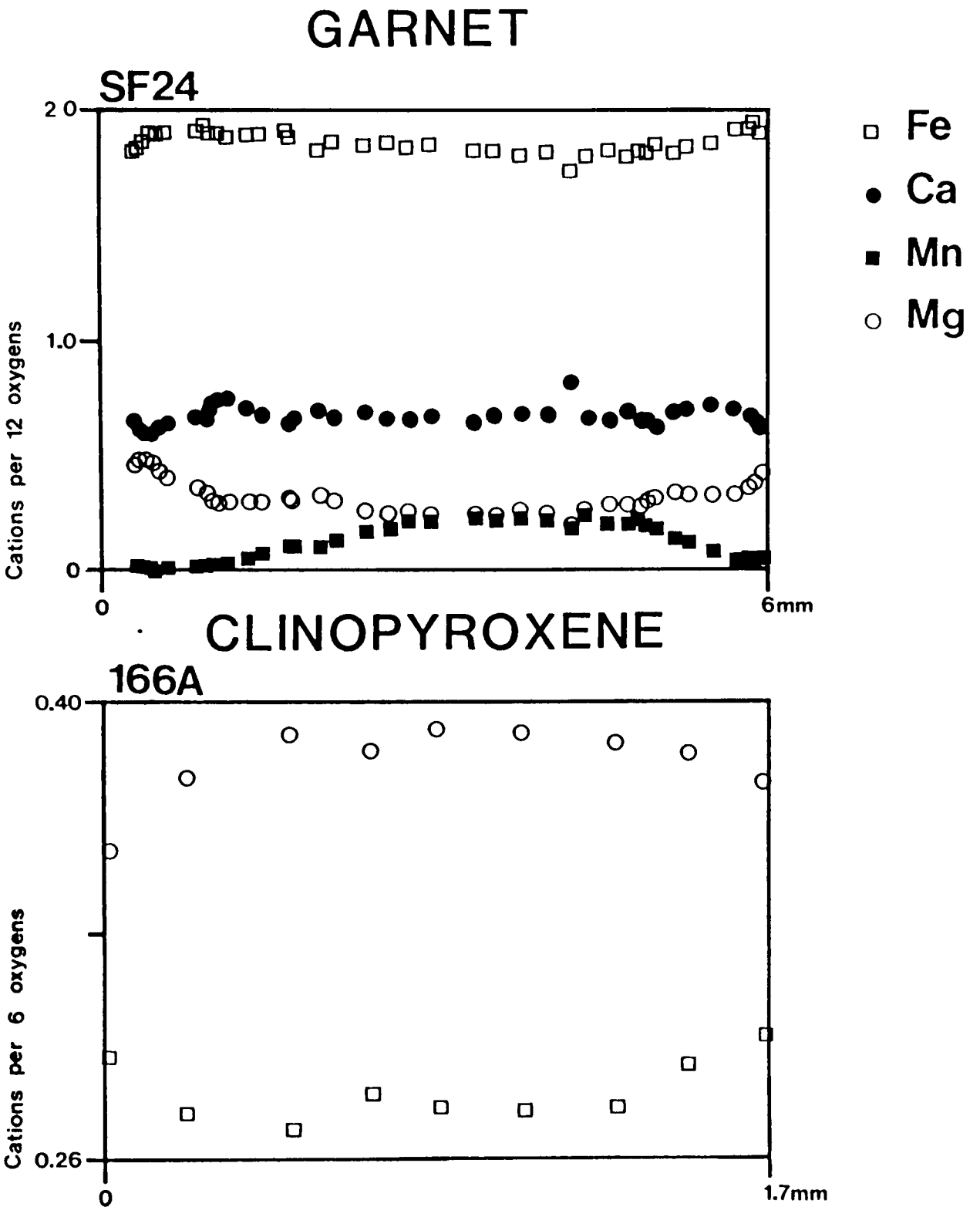

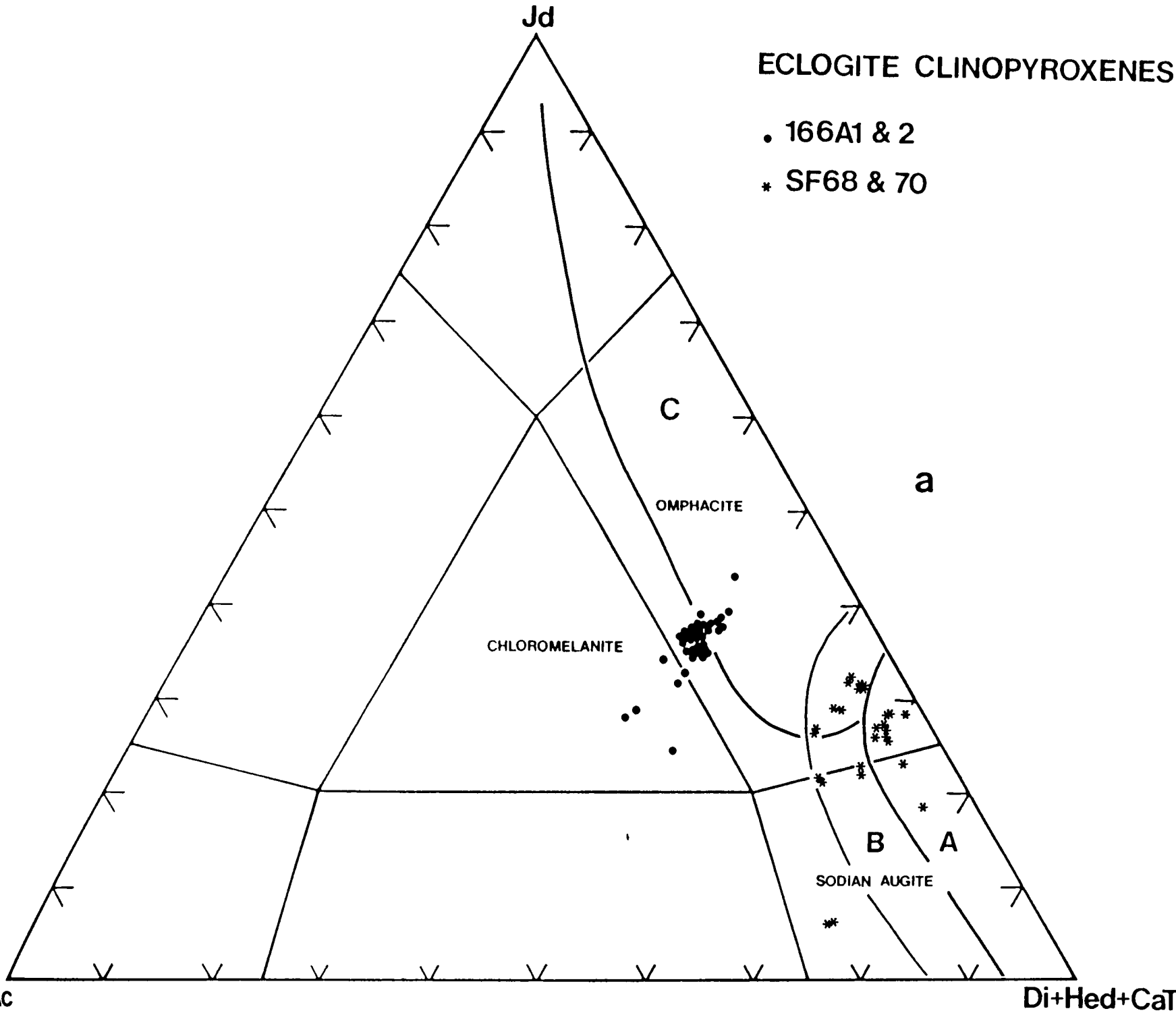

Figure 4.8: Triangular Jd-Ac-(Di+Hed+CaTs) and Na-Al-Ca diagrams showing compositions of clinopyroxenes from eclogites at Helleböstölane and Ytre Hellebö. Fe^{3+} has been calculated by method of Neumann, 1976. Compositional fields shown in a) are from Deer, Howie and Zussman, 1978, (figs. 2, 200, and 211). Fields labelled A, B, and C refer to compositional ranges for clinopyroxenes from types of eclogite as defined by Coleman et al, 1965, see fig. 4.6 for further details.

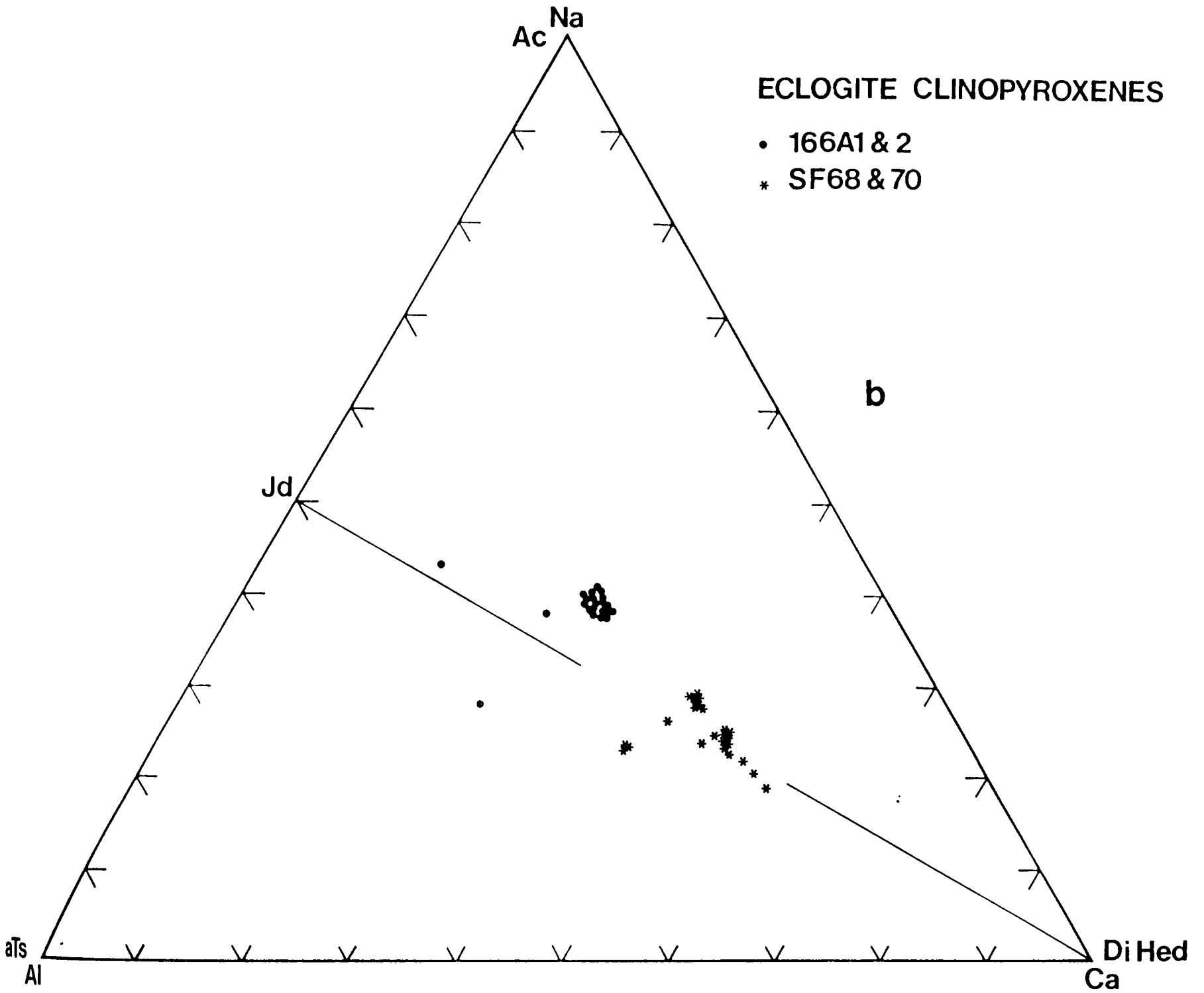

Figure 4.8 (con)

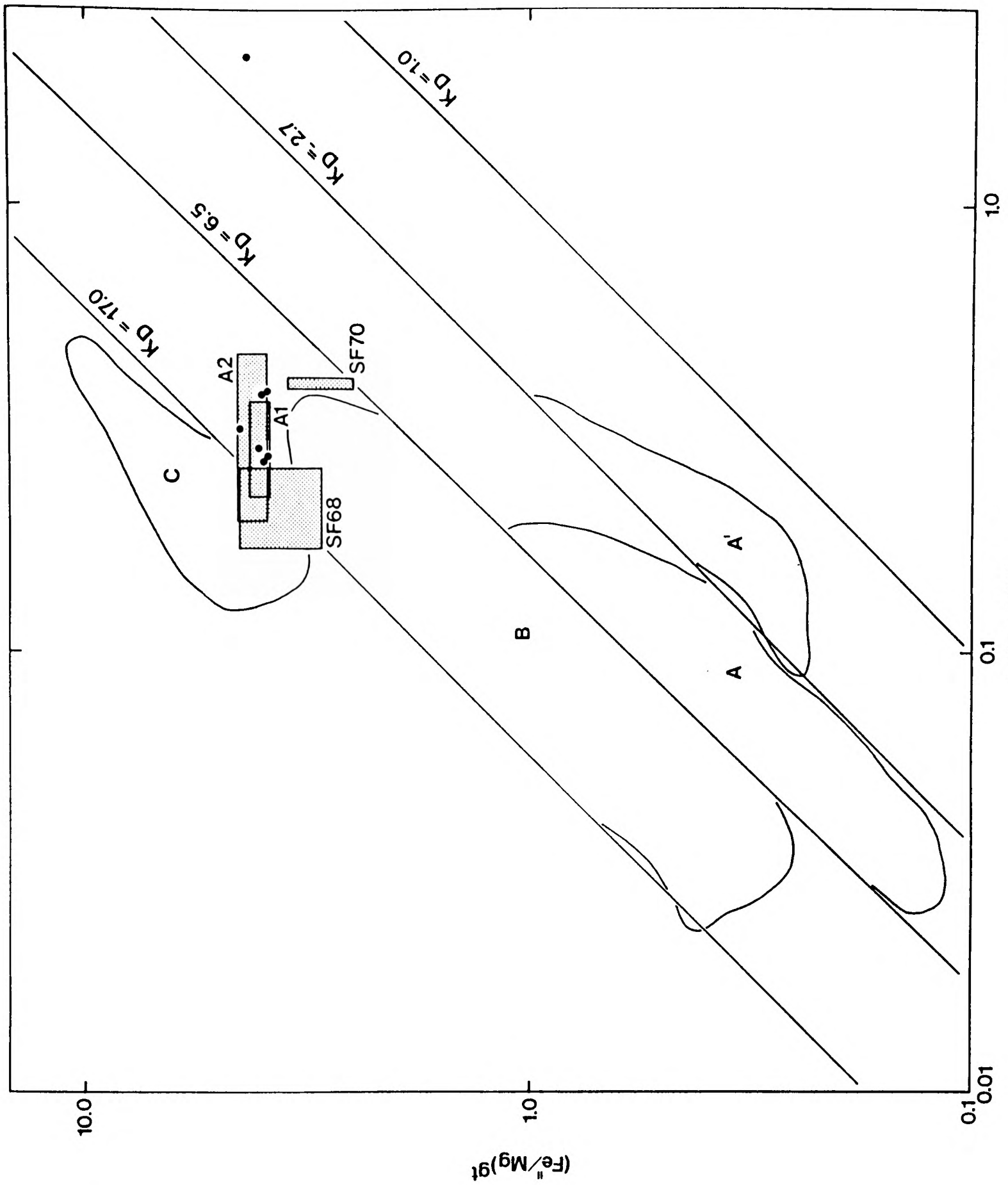

Figure 4.9: Log-scale distribution of Fe^{2+}/Mg between co-existing garnet and clinopyroxene in eclogites from Sognefjord. Where phases are zoned, rim compositions have been used. Fields for A', A, B, and C-type eclogites are based on Miyashiro, 1973 (fig. 12-5). Stippled boxes: average $K_D \pm 2\sigma$ in samples 166A1, 166A2, SF68, and SF70. Dots: Fe^{2+}/Mg distribution between inclusions of clinopyroxene in garnet and adjacent garnet in sample 166A2. Fe^{3+} calculated from electron microprobe analyses by the method of Neumann, 1976.

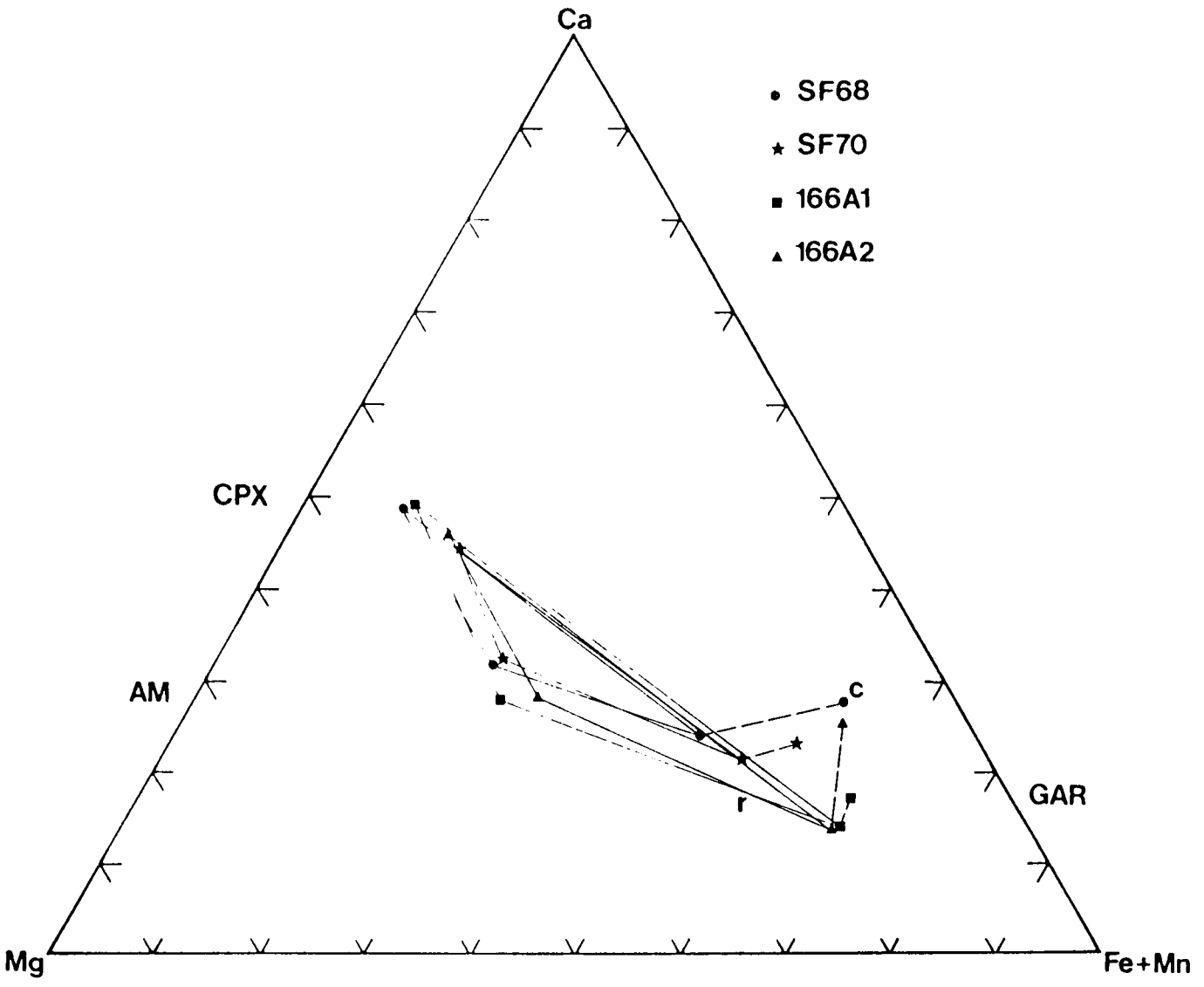

Figure 4.10: Triangular Ca-Mg-(Fe+Mn) diagram for eclogites and amphibolitized eclogites from Sognefjord. For 166A1 and 166A2 clinopyroxene (CPX) + amphibole (AM) + garnet (GAR) compositions are believed to represent a primary assemblage. Amphibole occurs as inclusions in garnet, as well as in the matrix. In SF68 and SF70, amphiboles are secondary, resulting from the breakdown of clinopyroxene and garnet, and form coronas on the rims of omphacite in contact with garnet. This relationship, and the close similarity in garnet core compositions in SF68 and 166A2, suggests that garnet rim compositions have been modified by volume diffusion during corona formation. The difference in clinopyroxene compositions between the two rock groups is mainly in NaAl=Ca(Mg,Fe) exchange, and is not represented on the plot. The dashed lines join rim and core compositions in garnets and do not necessarily represent intermediate compositions; zoning profiles of garnet grains are shown in figures 4.7 and 4.13.

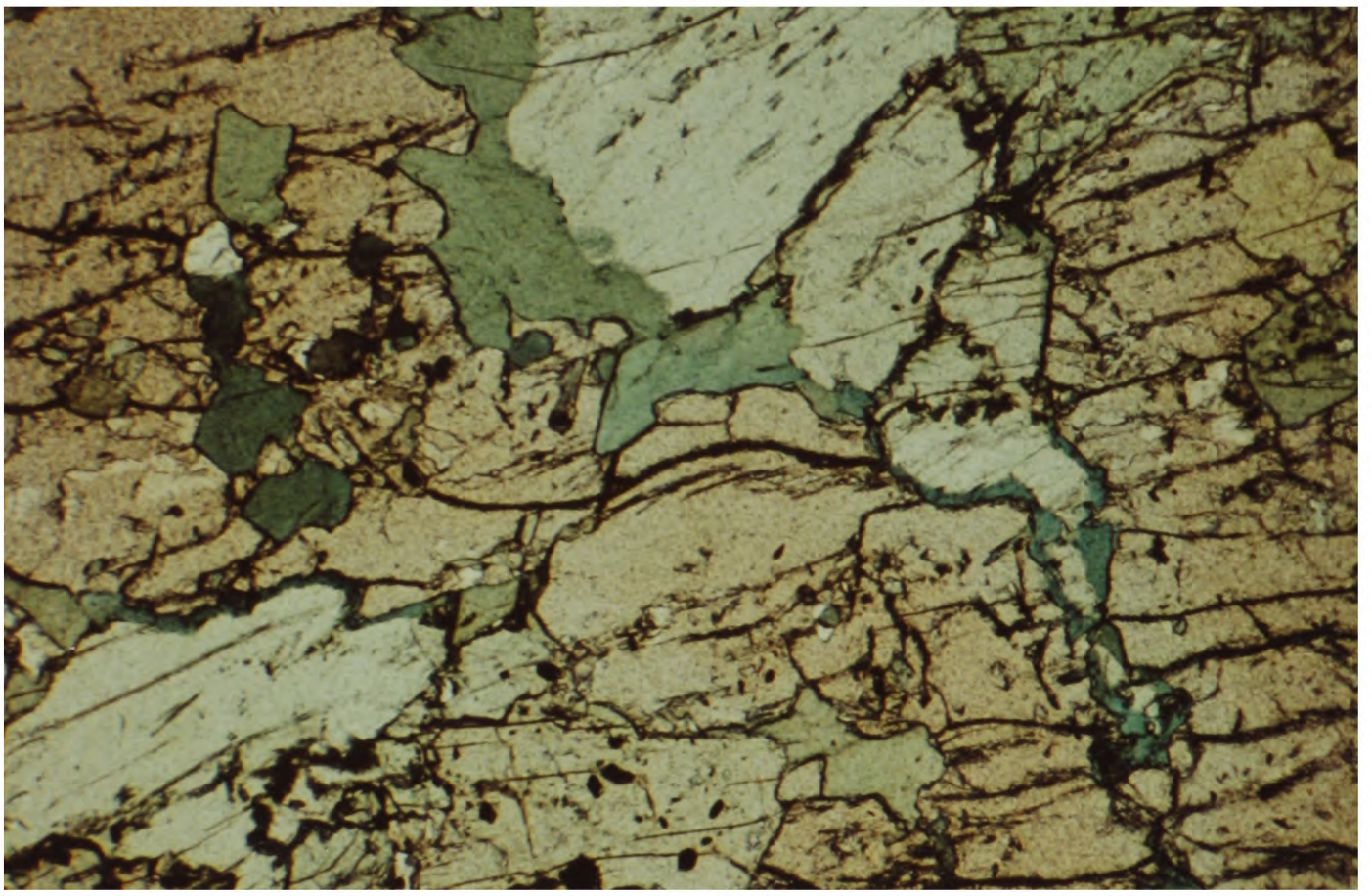

Figure 4.11: Photomicrograph in PPL of partially amphibolitized eclogite from Ytre Hellebö. The field of view shows the development of amphibole at the contact between pale green clinopyroxene and garnet grains, and also along clinopyroxene cleavage planes. Field of view is 3.5mm across. See also fig. 4.13.

Figure 4.12: Compositions of amphiboles from eclogites containing relict clinopyroxene. Fe^{2+} is calculated from electron microprobe analyses by the method of Laird and Albee, 1981. Abbreviations as shown in figure 4.16.
166A: primary amphiboles from eclogites at Helleböstölane, which show little amphibole overprint.
SF68 and SF70: secondary amphiboles from coronas on garnet and clinopyroxene in partially amphibolitized eclogite from Ytre Hellebö. Amphiboles in coronas show lower Na and higher Ca contents than primary eclogite amphiboles (cf figure 4.16).

AMPHIBOLE COMPOSITIONS IN ECLOGITES

● 166A
△ SF68 & 70

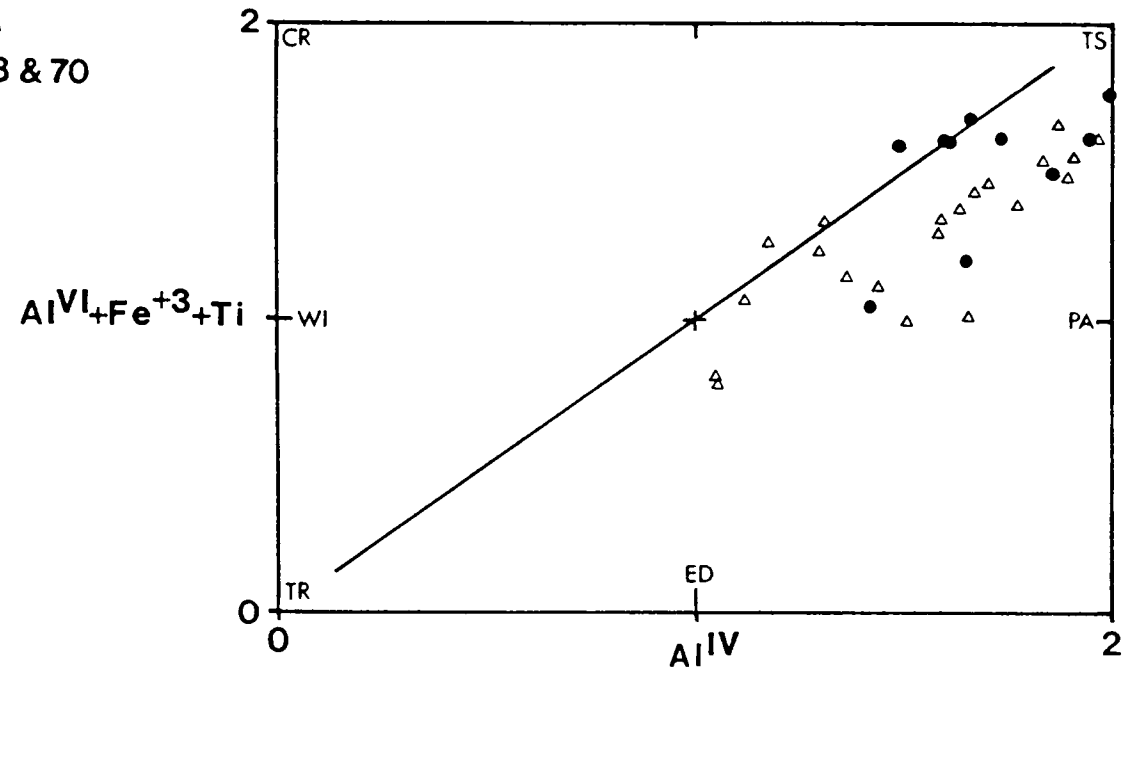

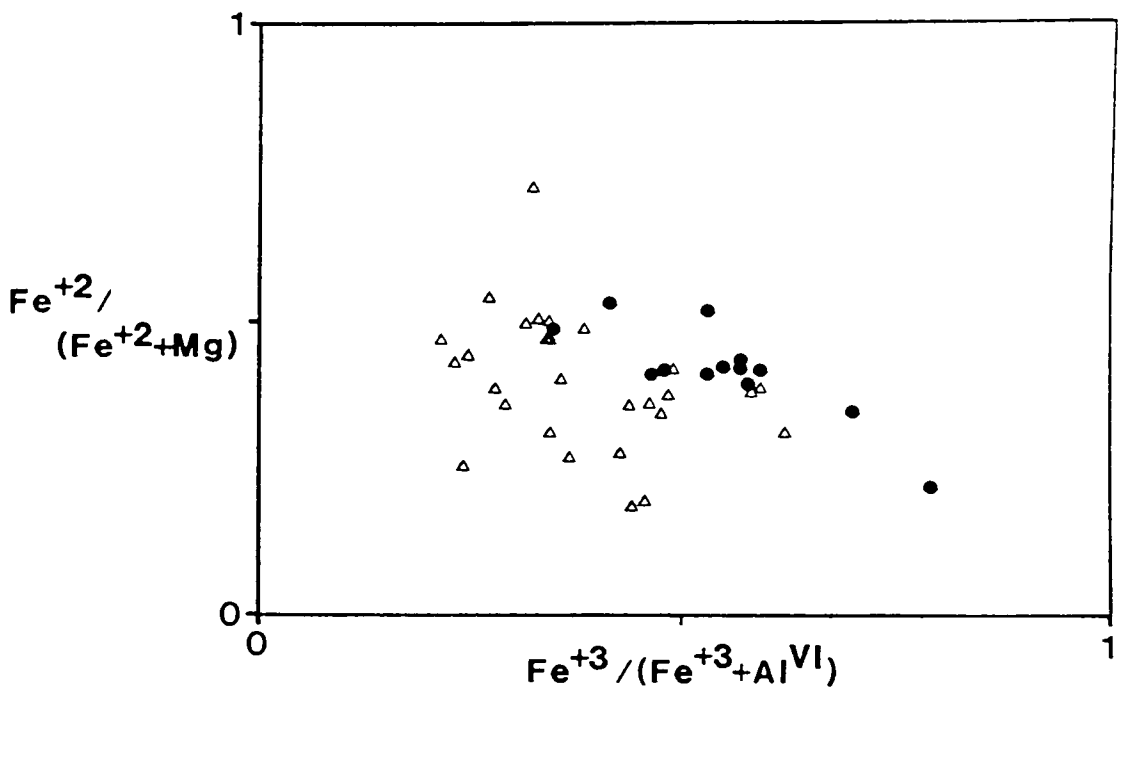

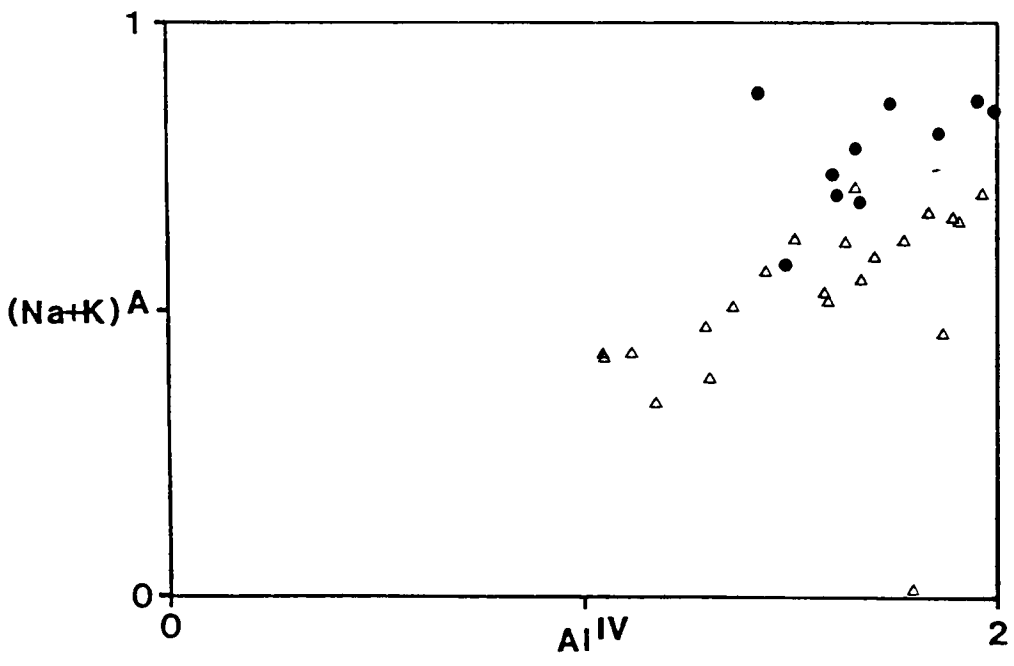

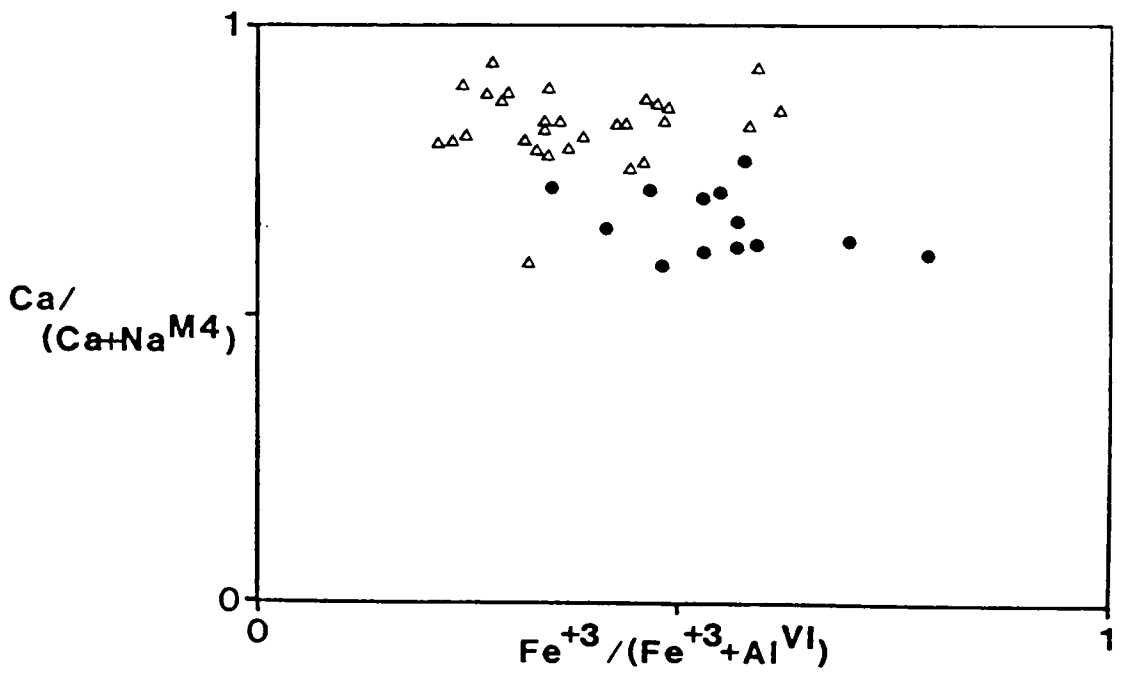

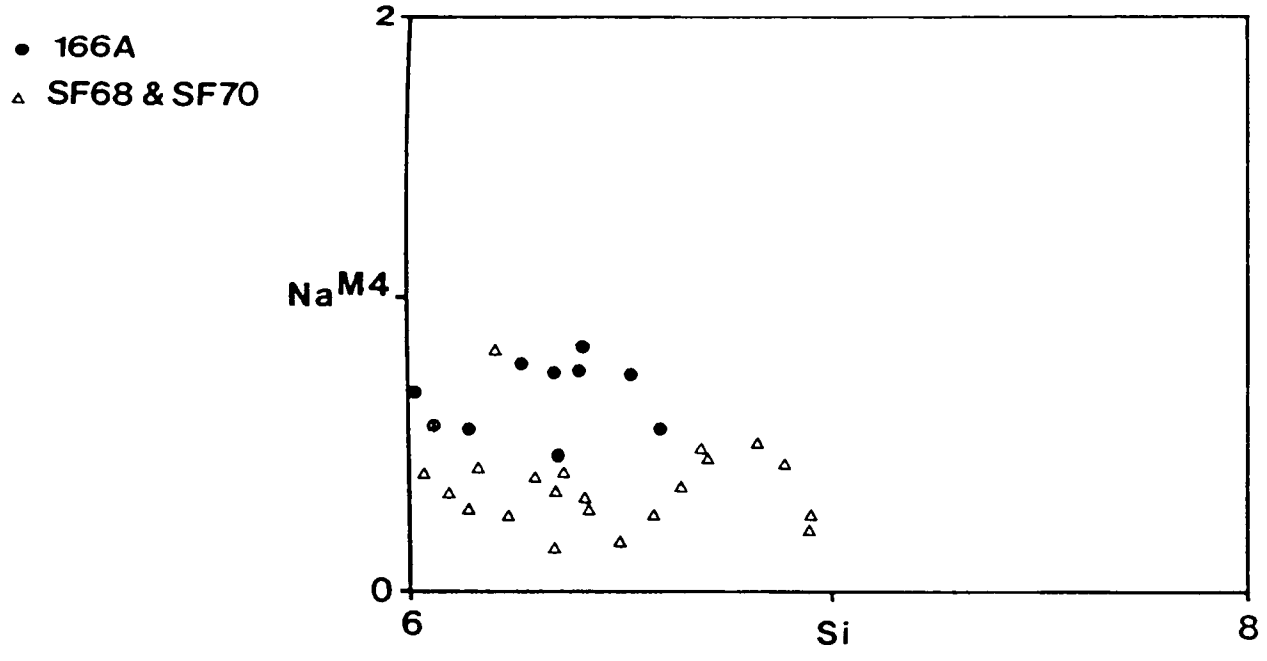
166A
SF68 & SF70
2
0
Na^{M4}
6
Si
8

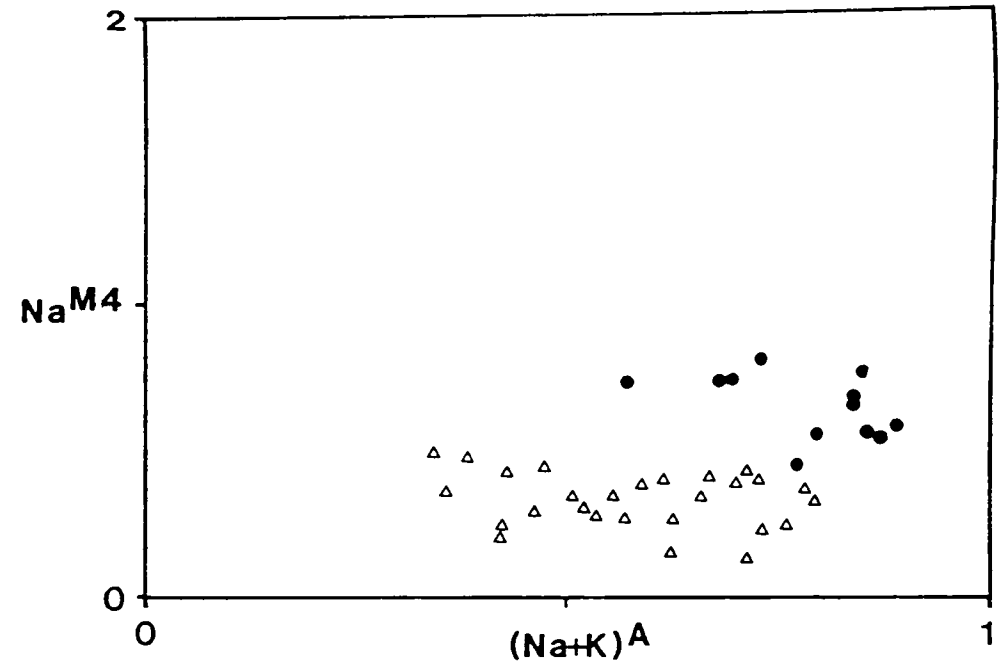
2
0
Na^{M4}
0
$(Na+K)^{A}$
1

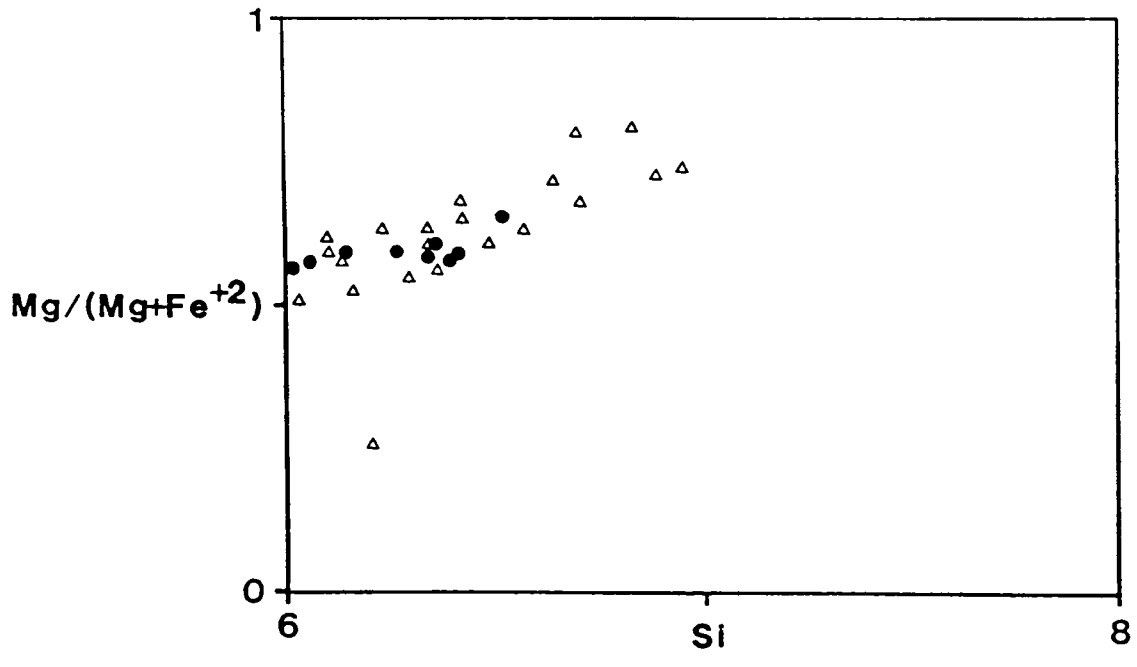
1
0
$Mg/(Mg+Fe^{+2})$
6
Si
8

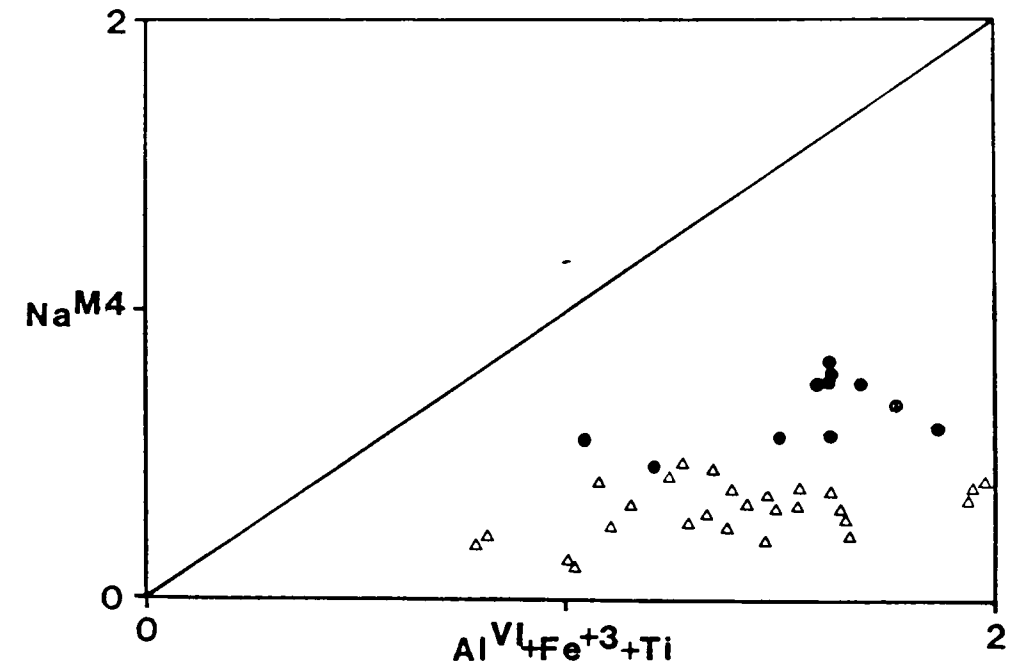
2
0
Na^{M4}
0
$Al^{VI}+Fe^{+3}+Ti$
2

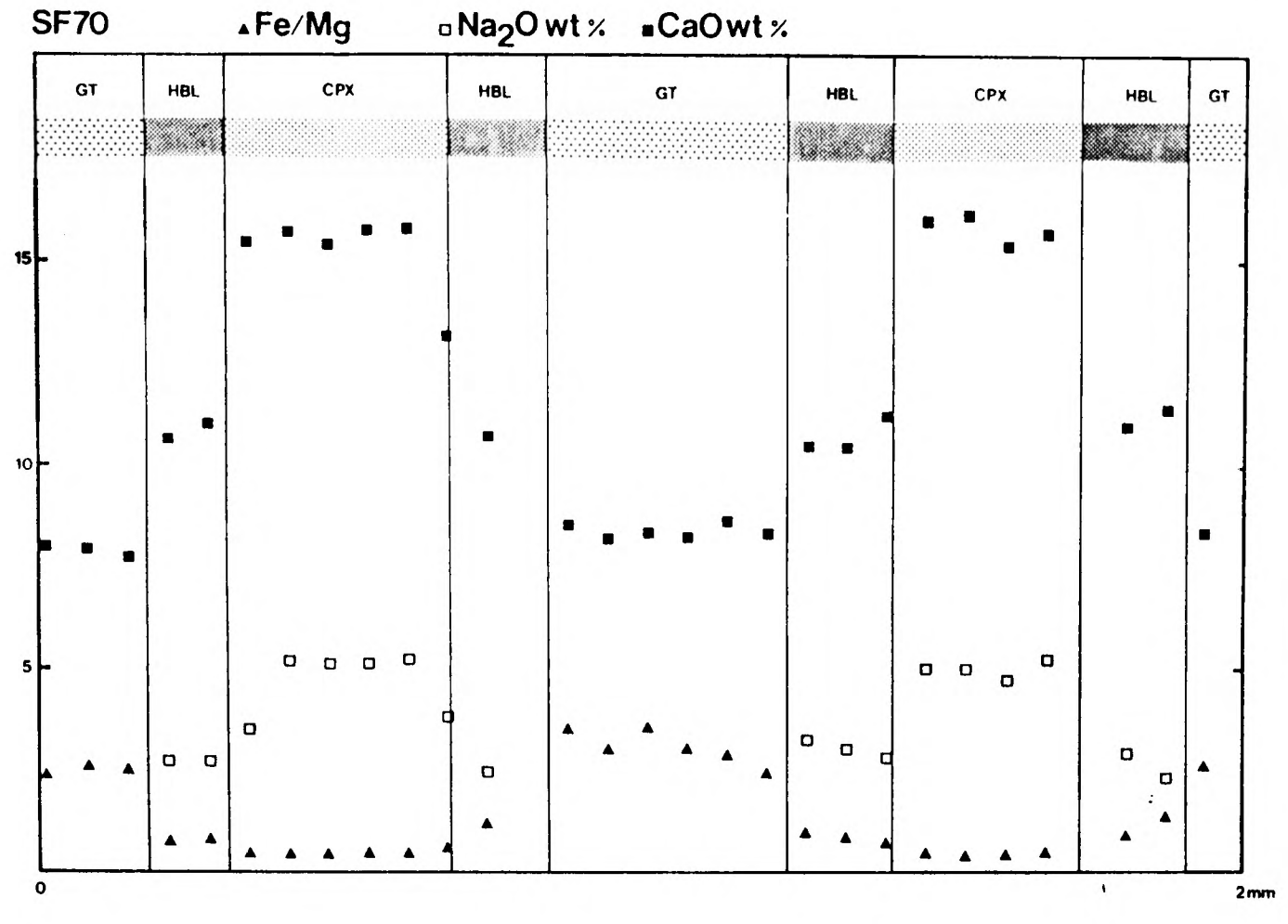

Figure 4.13: Chemical profile across several garnet and clinopyroxene grains with hornblende coronas in amphibolitized eclogite from Ytre Hellebö. The compositions of garnet and clinopyroxene tend towards those of hornblende at grain boundaries suggesting intracrystalline diffusion in primary phases margins during amphibole growth.

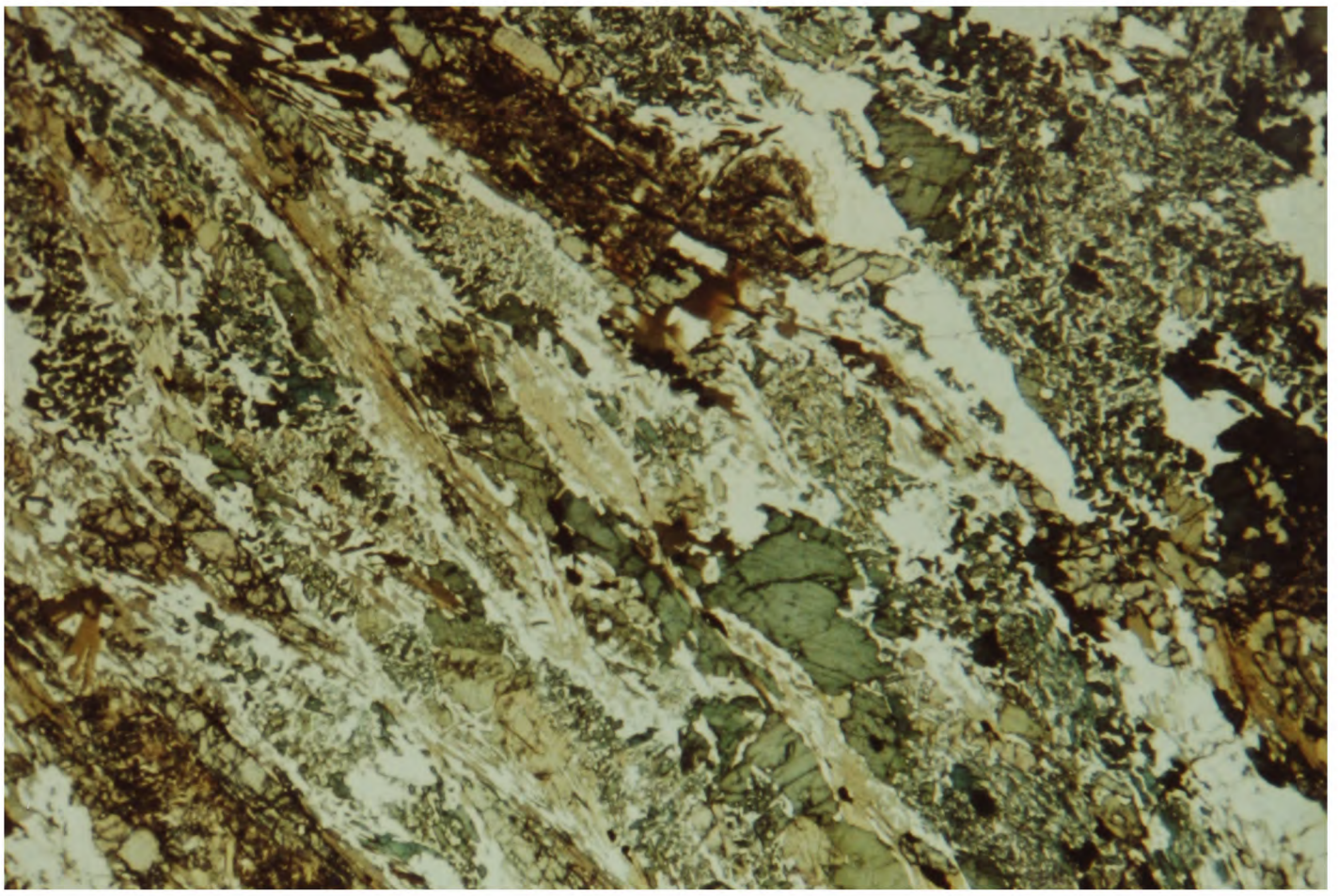

Figure 4.14: Photomicrograph in PPL of amphibolitized eclogite from Brensdal (sample SF21), showing fine-grained intergrowths (symplectites) of albite and hornblende. Field of view is 9mm across.

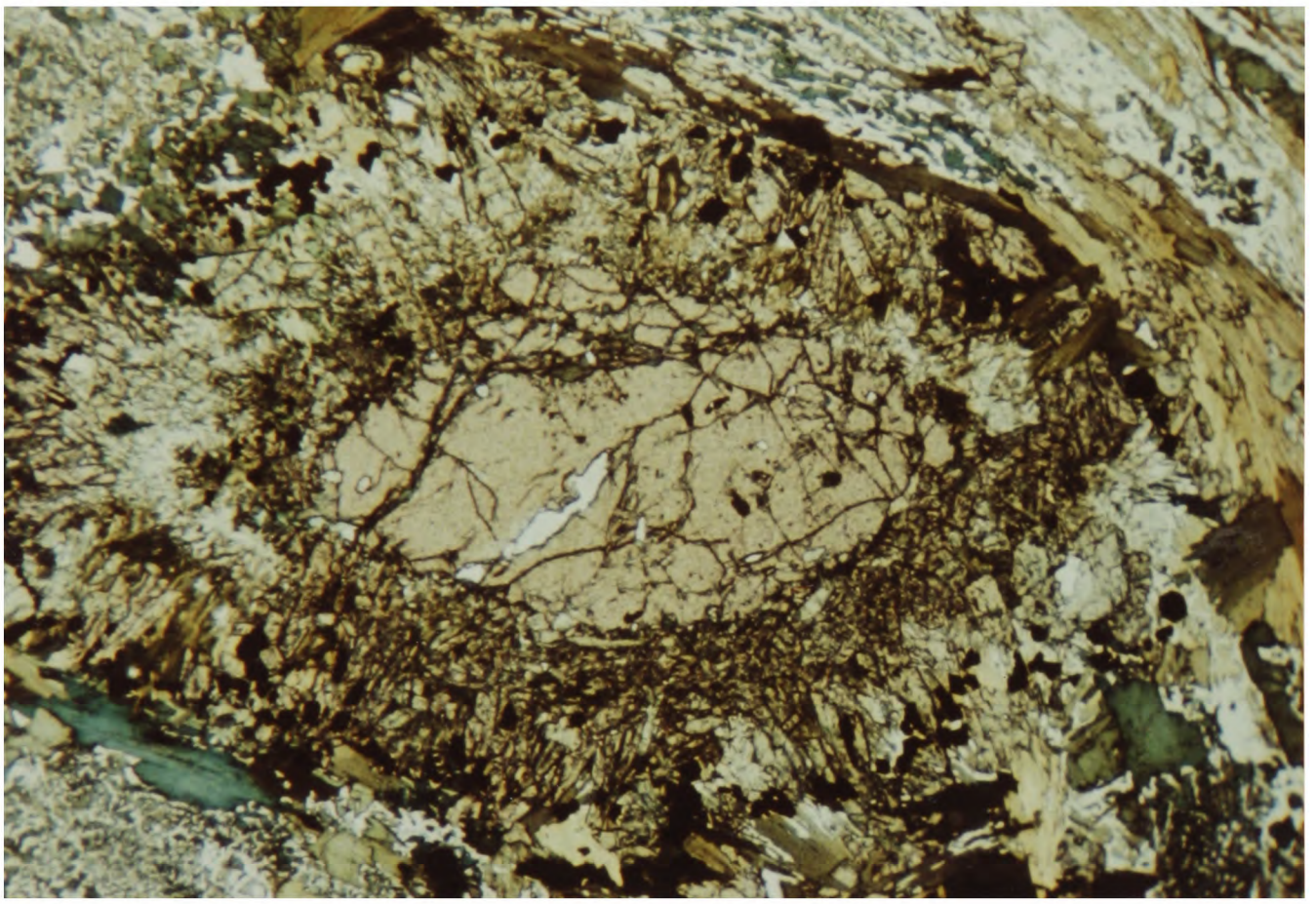

Figure 4.15: Photomicrograph in PPL of amphibolitized eclogite from Brensdal (sample SF21), showing large garnet with corona of radiating epidote and biotite, fringed by a collar of magnetite grains. At its outer limits the corona overgrows an S_2 foliation of biotite, amphibole and amphibole-albite symplectite. The field of view is 9mm.

Figure 4.16: Compositions of amphiboles from eclogites showing thorough amphibolite overprint and containing no relict clinopyroxene. Fe^{3+} calculated by method of Laird and Albee, 1981. Compositional trends are weakly defined. Compare with figure 4.12 where, for example, there is a clear decline in Na^{M4} with amphibolitization. With the increasing amphibolitization represented by this group of rocks, compositional trends are opposed to those seen in figure 4.12 - compare the compositions of amphiboles with respect to examples from SF68 and SF70 in both diagrams. Trends in this plot may reflect the degree of low-temperature alteration of amphiboles (see text).

CR: crossite, ED: edenite, PA: pargasite, RI: richterite, TR: tremolite, TS: tschermakite, WI: winchite.

AMPHIBOLE COMPOSITIONS IN AMPHIBOLITIZED ECLOGITES

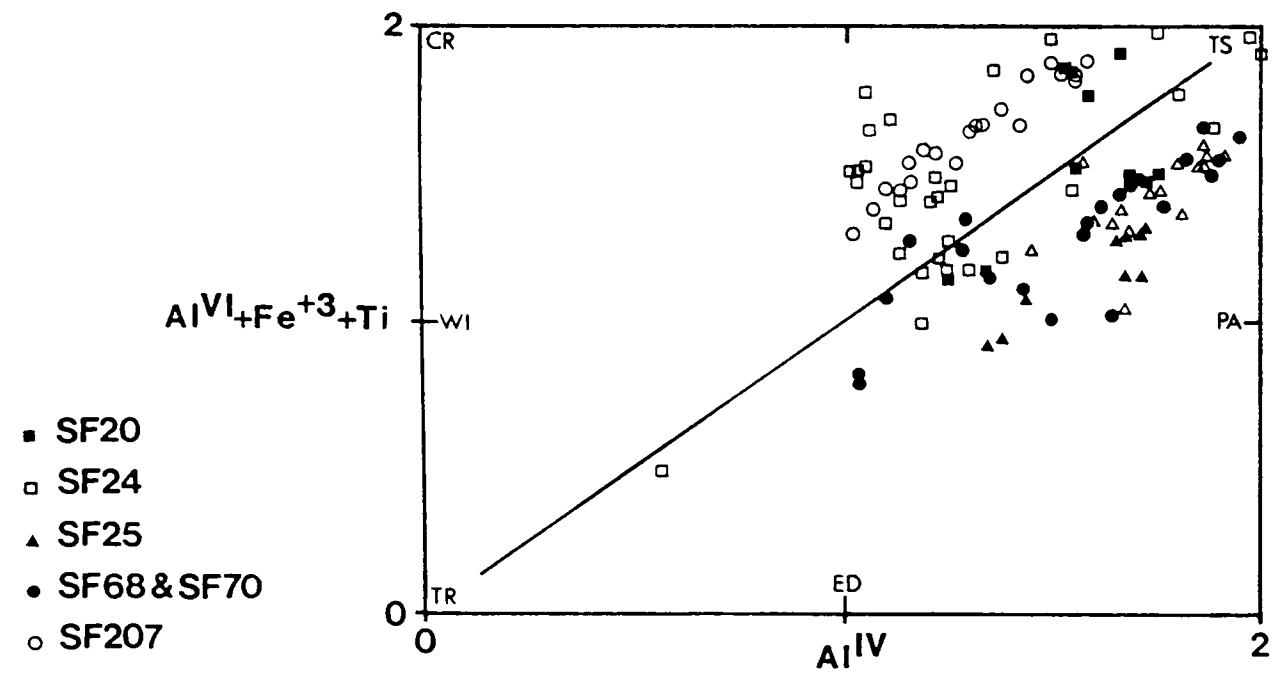

- SF20
- SF24
- SF25
- SF68 & SF70
- SF207
- SF138

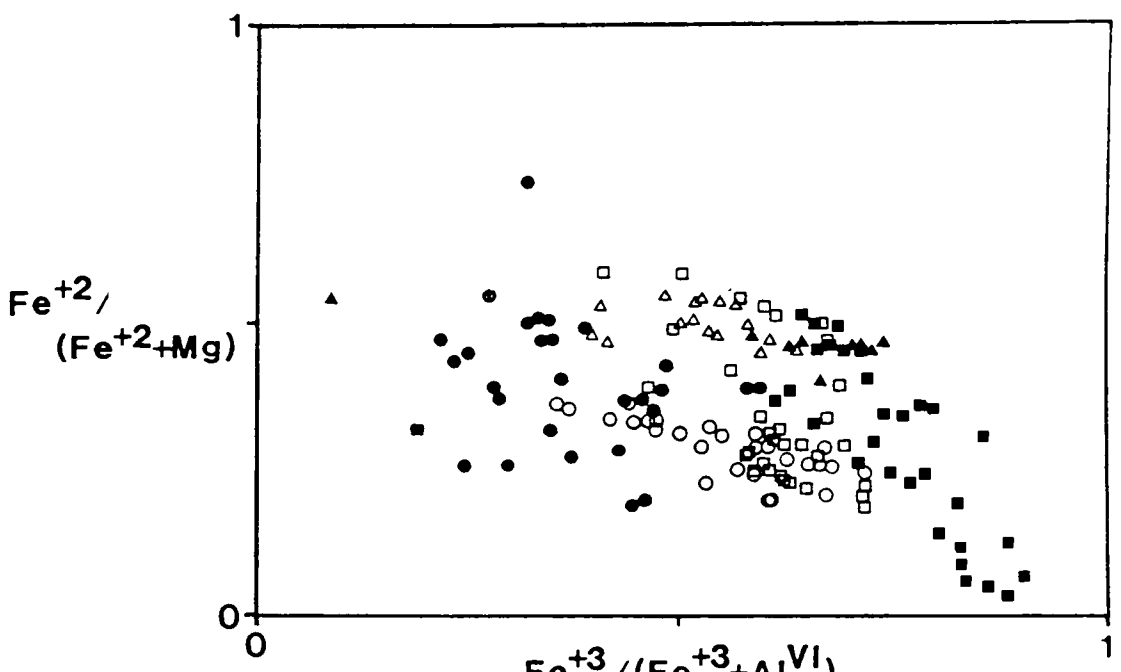

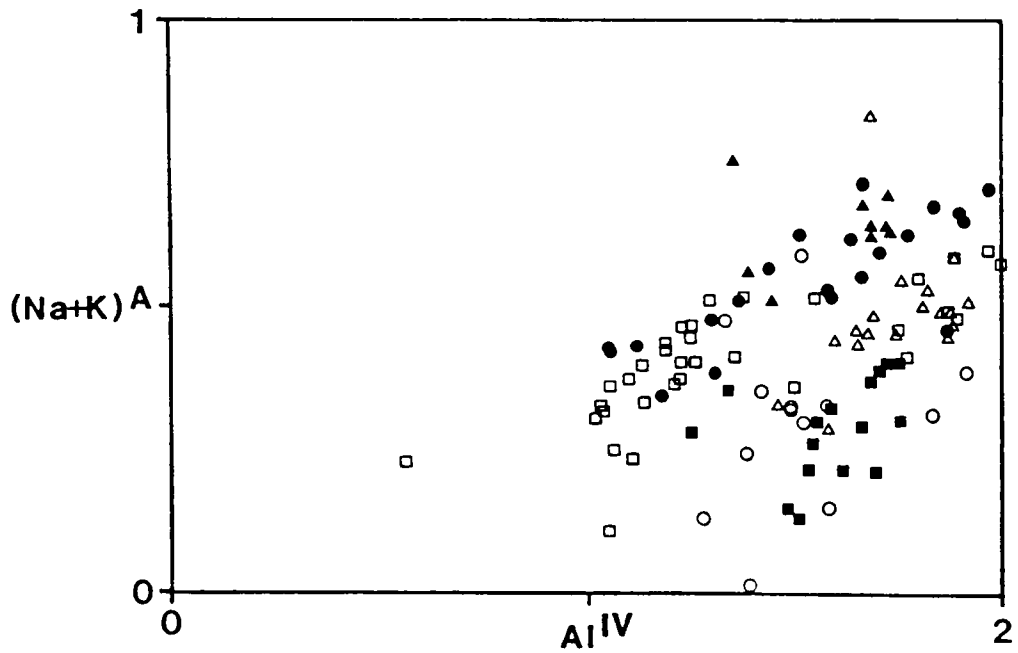

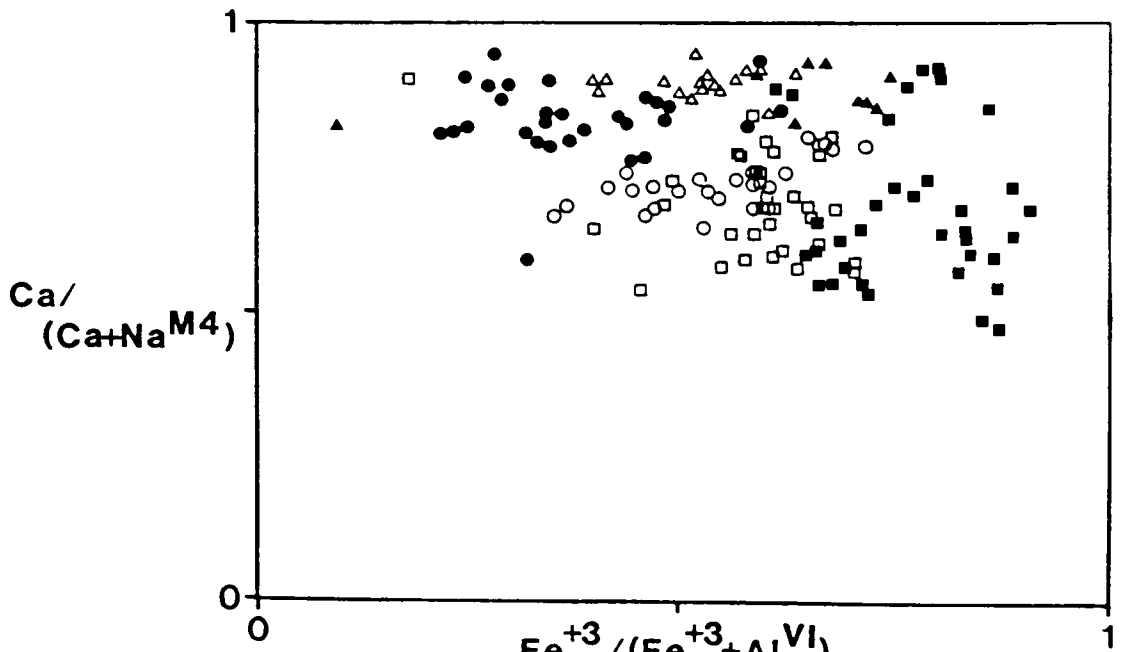

- SF20
- SF24
- SF25
- SF68 & SF70
- SF207
- SF138

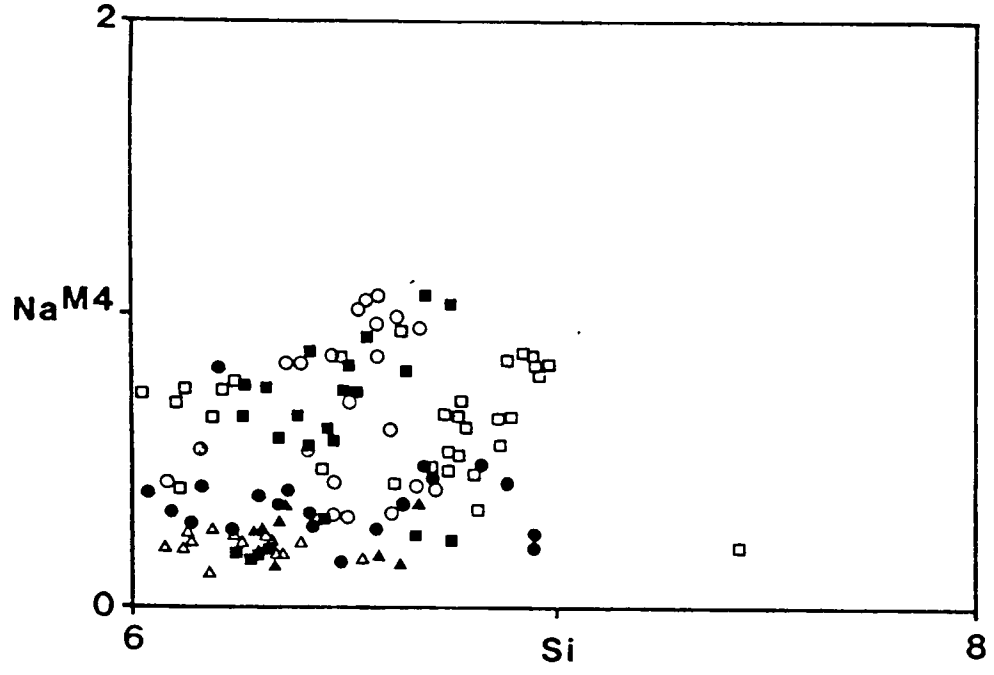

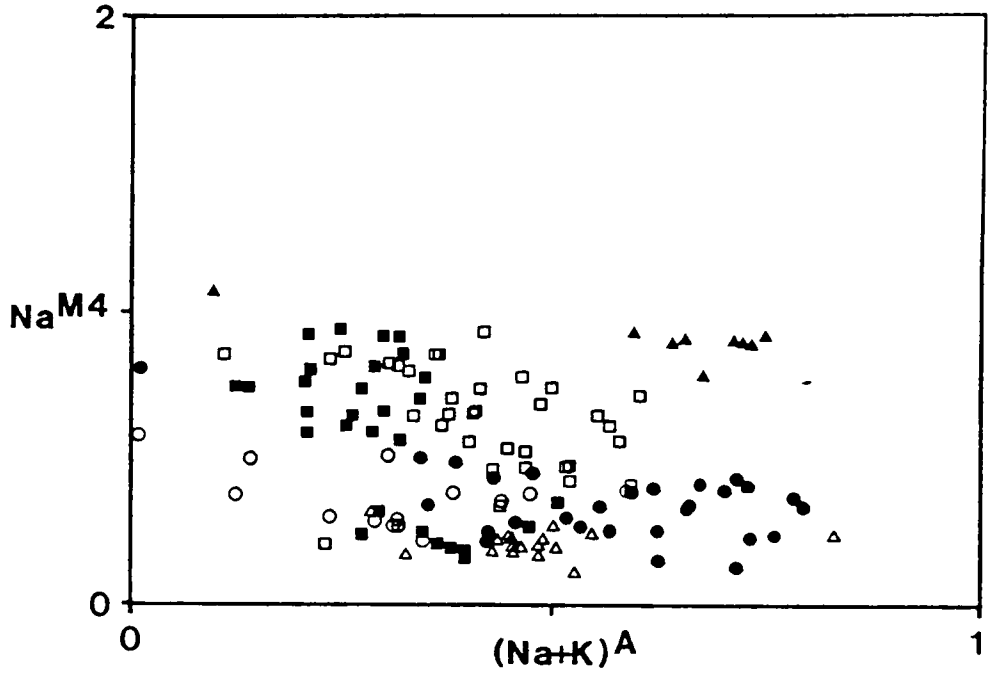

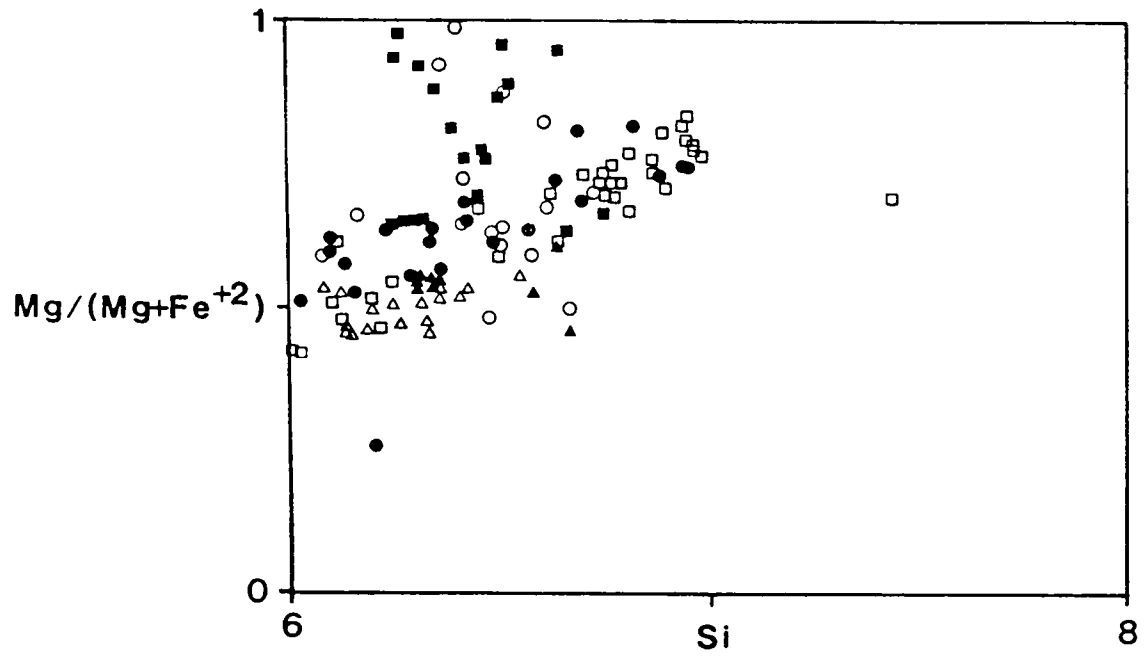

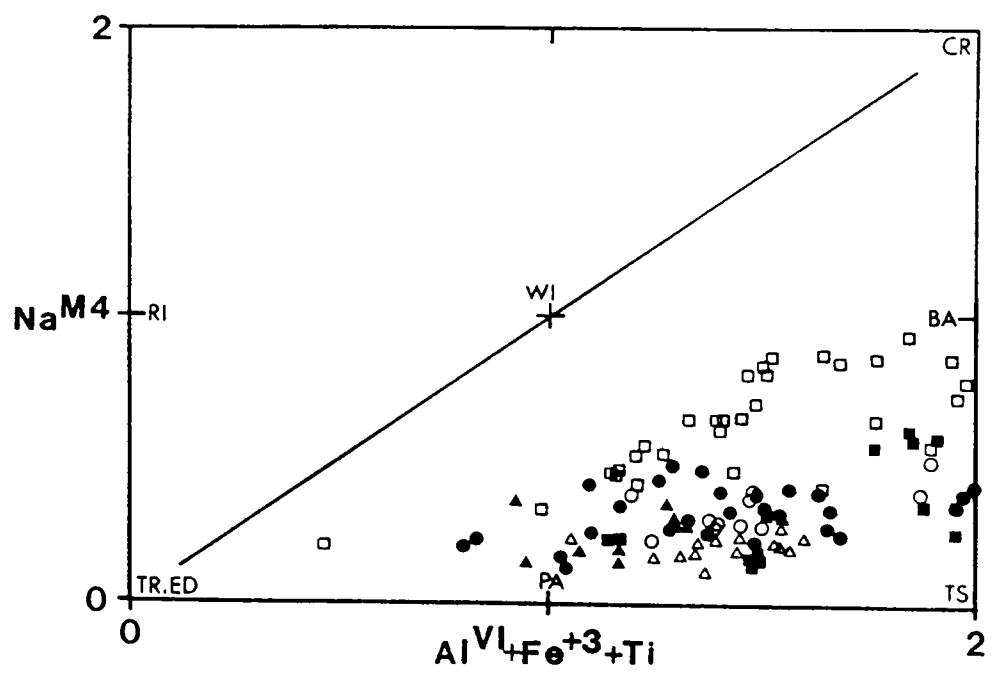

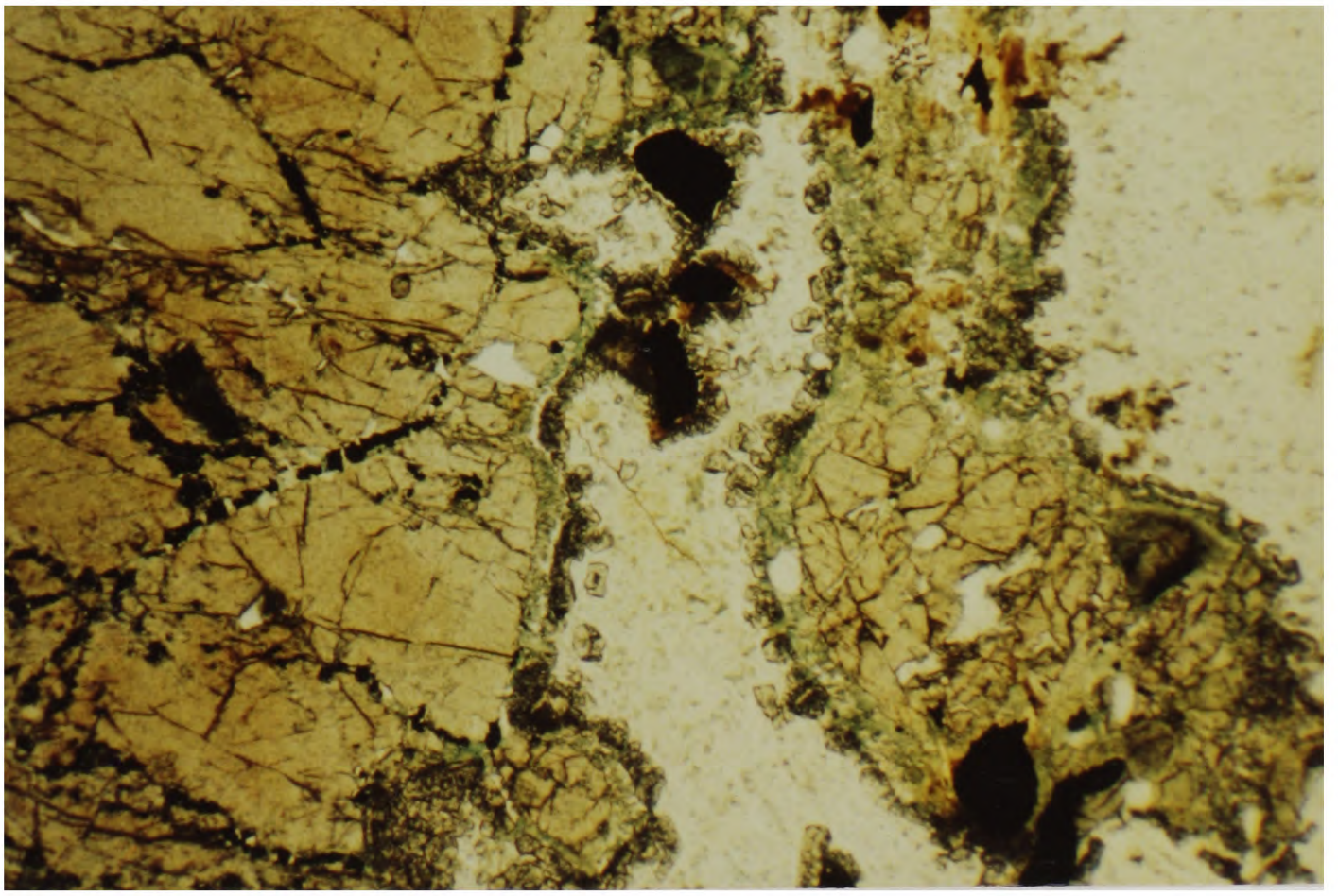

Figure 4.17: Photomicrograph in PPL of orthopyroxene-plagioclase gneiss (sample SF133) from Ytre Hellebö showing collars of garnet grains fringing orthopyroxene and ilmenite. Amphibole is developed between garnet and the pyroxene. Magnetite is developed along cracks in the orthopyroxene. Field of view is 3.5mm across.

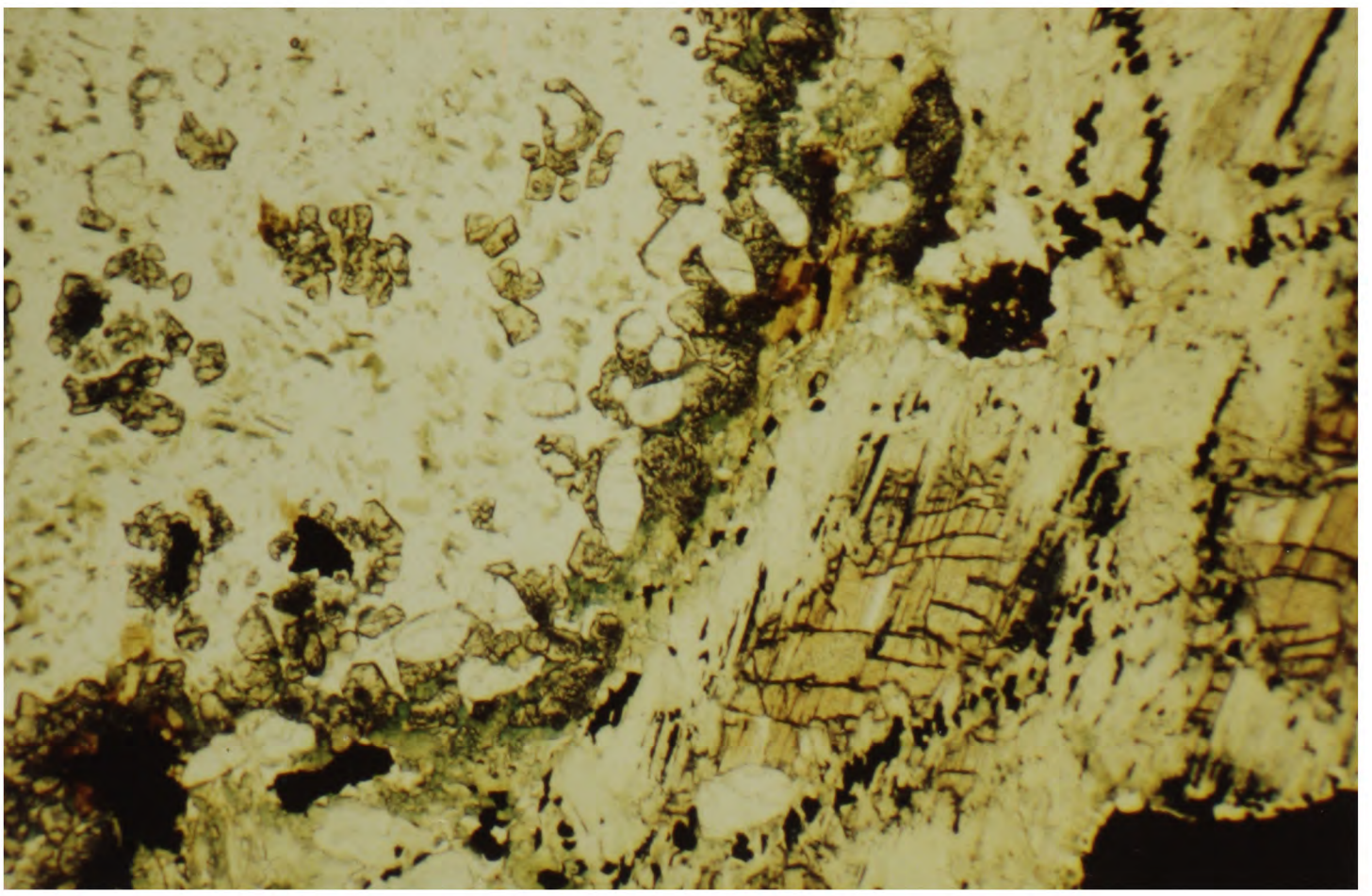

Figure 4.18: Photomicrograph in PPL of orthopyroxene-plagioclase gneiss from Ytre Hellebö (sample HØ1), showing cummingtonite replacing orthopyroxene (left half of picture). At the line of original contact between plagioclase and orthopyroxene, amphibole of deeper green occurs with a collar of garnet grains. Apatite is also particularly abundant at this contact. Field of view is 3.5mm across.

Figure 4.19: Estimated P-T evolution of eclogites from Sognefjord. The star marks the calculated conditions of equilibration of primary eclogite assemblages and the dotted lines show postulated P-T paths leading up to and subsequent to the eclogite metamorphism. Peak eclogite conditions, calculated using the garnet-clinopyroxene thermometer of Ellis and Green (1979) and rim compositions of clinopyroxenes and garnets reached about 600 °C. The P-T trajectory can be only poorly constrained, but inclusions of omphacitic pyroxene in garnets in the least altered eclogites suggest that eclogite mineral assemblages may have existed at temperatures as low as 520 °C. Inclusions are not sufficiently abundant to deduce a detailed P-T evolution by mapping changing garnet-clinopyroxene Fe-Mg K_D during garnet growth (cf Krogh, 1982). The garnet-hornblende thermometer of Graham and Powell (1984) has also been applied to eclogitic rocks in which the primary assemblage has been thoroughly overprinted by garnet amphibolite assemblages (dashed vertical lines). The results appear to suggest that peak temperatures may have been as high as 770°C (samples SF25 and SF138). Lower temperatures (704°C) are obtained from an inclusion of amphibole in garnet in sample SF24. However, as discussed in the text, these temperatures are probably unrealistic since garnet and amphibole compositions have probably not fully equilibrated. Garnets frequently show evidence of resorption, and this is particularly marked in, for example, SF138. In SF20 and SF24, amphiboles also show evidence of disequilibrium and low-grade overprinting and garnet-amphibole temperatures for such rocks are probably unreliable. As discussed in the text, Na^{M4} contents of amphiboles are higher than those recommended for

this calibration. # denotes garnet-amphibole temperatures calculated using inclusions of amphibole in garnet.
A temperature of 650°C (the dash-dot line) is obtained from garnet-amphibole thermometry applied to retrograde corona phases in sample SF133 and may represent a small increase in temperatures during uplift. The P-T trajectory is speculatively indicated as passing through this temperature in the absence of better data.

The light numbered lines refer to mineral equilibria:

1 and 2: lower stabilities of Jd_{100} + quartz and Jd_{20} + quartz respectively (Holland, 1980)

3: Paragonite = $DiJd_{10}$ + Kyanite + H_2O (after Griffin et al, 1985)

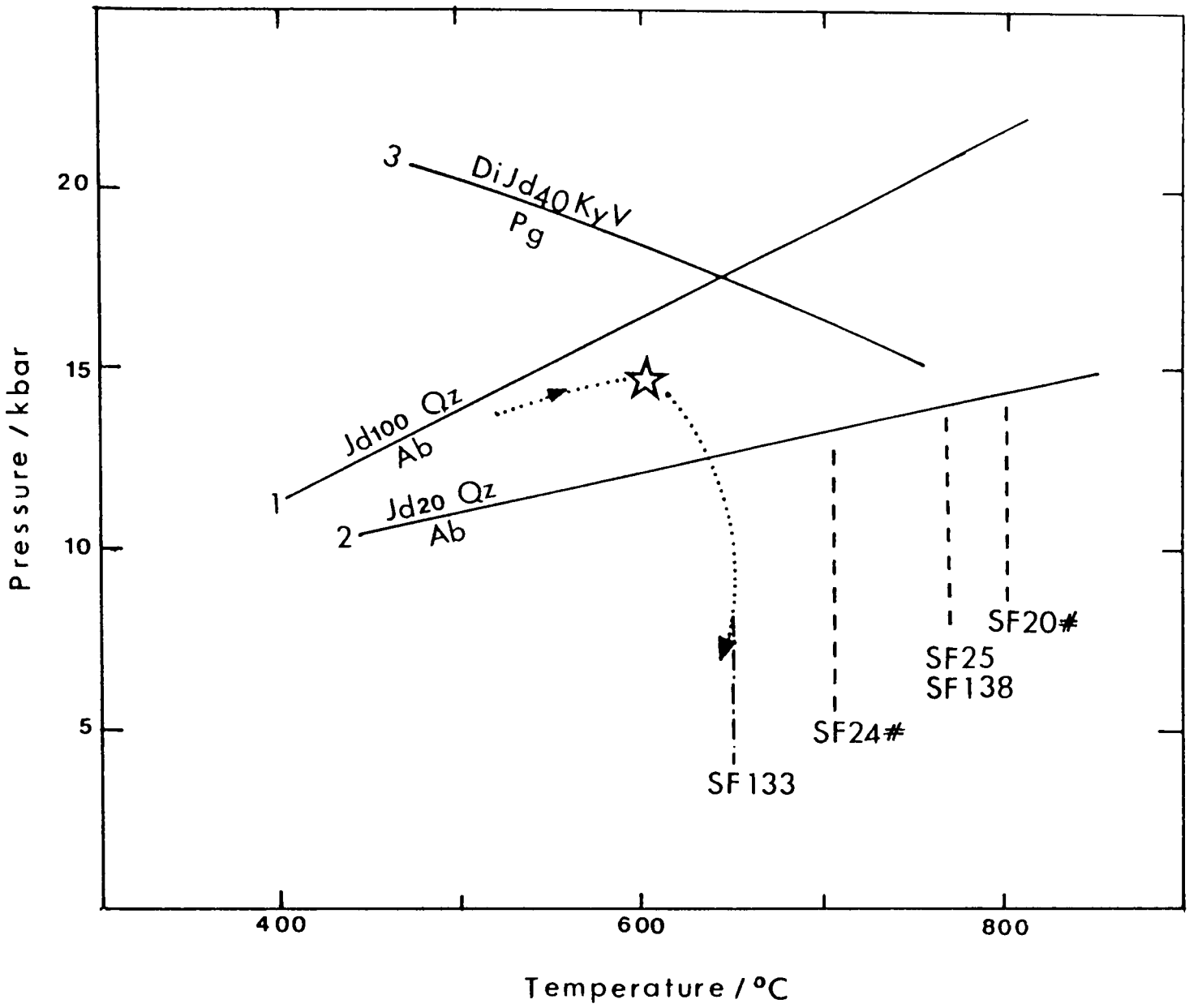
Pressure / kbar
20
15
10
5
3
Di Jd40 Ky V
Pg
Jd100 Qz
Ab
1
Jd20 Qz
Ab
2
SF133
SF24#
SF25
SF138
SF20#
400
600
800
Temperature / °C

Figure 4.19

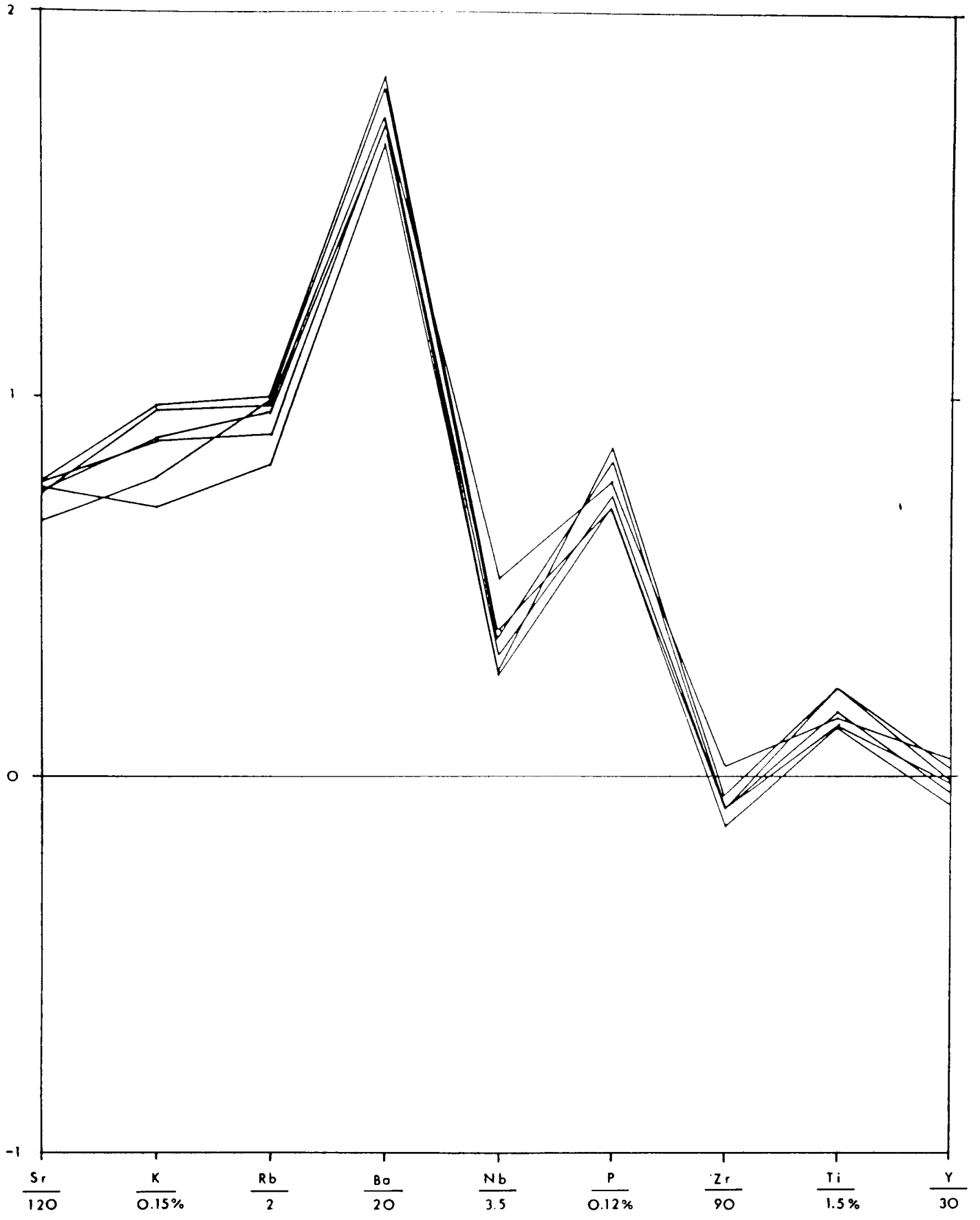

Figure 5.1 (a)

Figure 5.1: "Spider" diagrams comparing trace element chemistry in dykes from a) the Upper Mafic Unit and b) the Basement Gneisses. Values have been normalized to MORB concentrations (Mitchell, pers. com.). The patterns are similar except for lower concentrations of K, Rb, and Zr in the UMU.

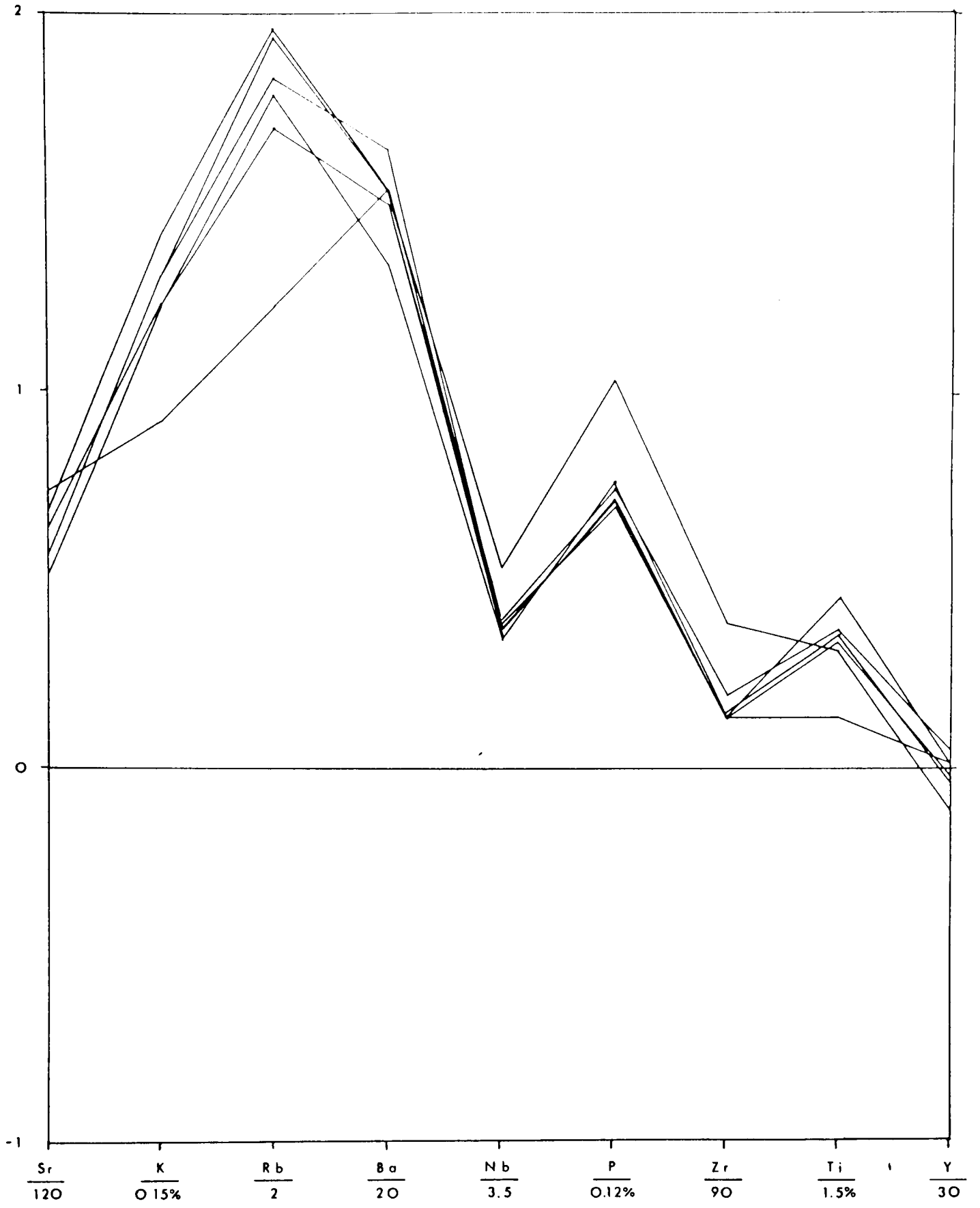

Figure 5.1 (b)

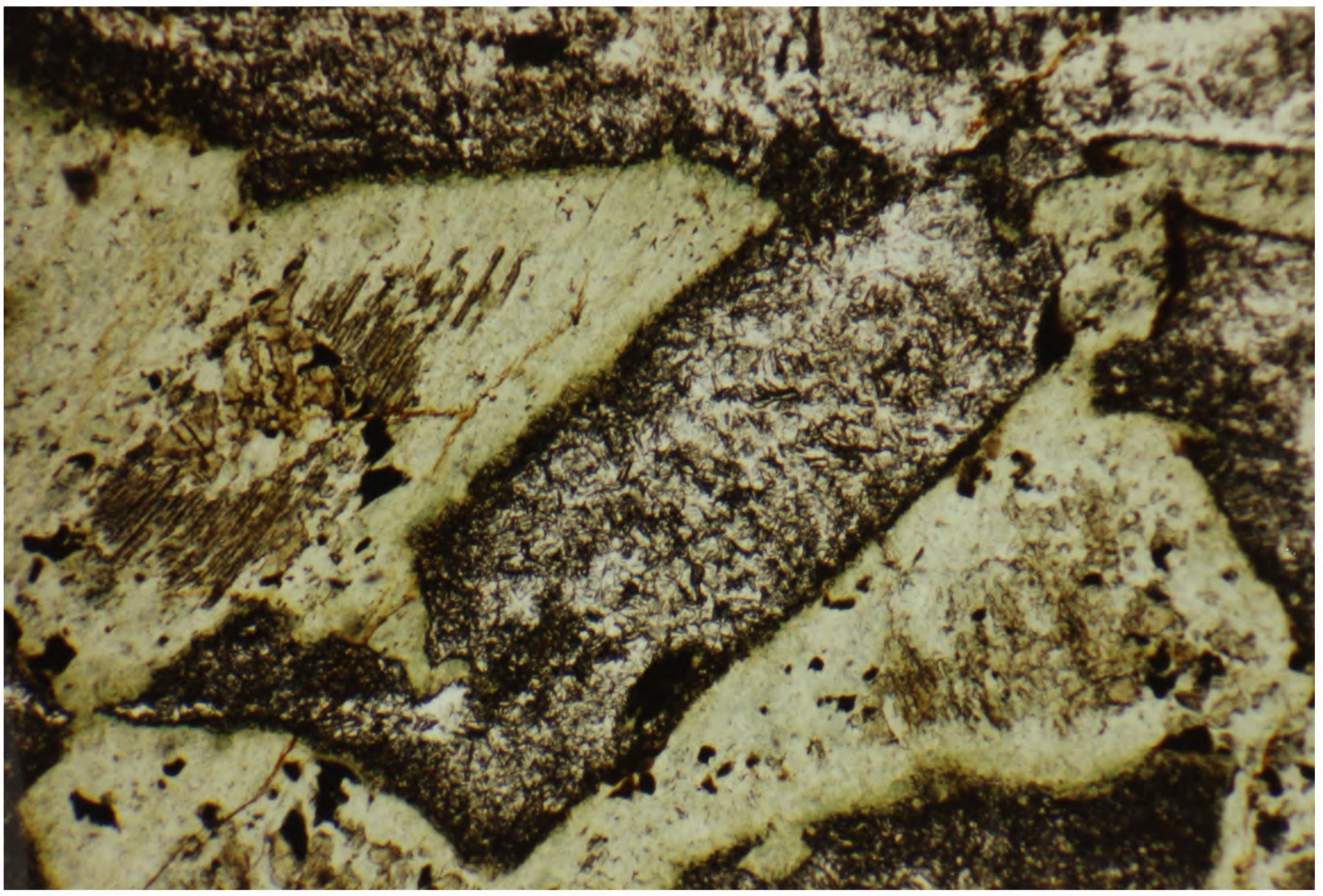

Figure 5.2: Photomicrograph of relict igneous textures and phases in metagabbro from the Lower Mafic Unit at Bosdal. A saussuritized plagioclase lath occupies the central part of the picture. Clinopyroxene shows minor zoning at the rims. Field of view = 9 mm.

Figure 5.3: zoning in garnets and amphiboles from all units: (a)-(c) Lower Mafic Unit, (d)-(f) Middle Mafic Unit, (g)-(j) Upper Mafic Unit. (a)-(f), (h), and (j) are all from mafic garnet amphibolites, (g) is from a sillimanite-schist at Löland, (i) is from a single large garnet in a gabbro from Kjönas, which forms part of the D_2 garnet amphibolite assemblage. Most garnets show some slight (prograde) zoning to higher X_{Mg} at the rims. Amphiboles show the opposite trend, apparently due to a later retrograde overprint.

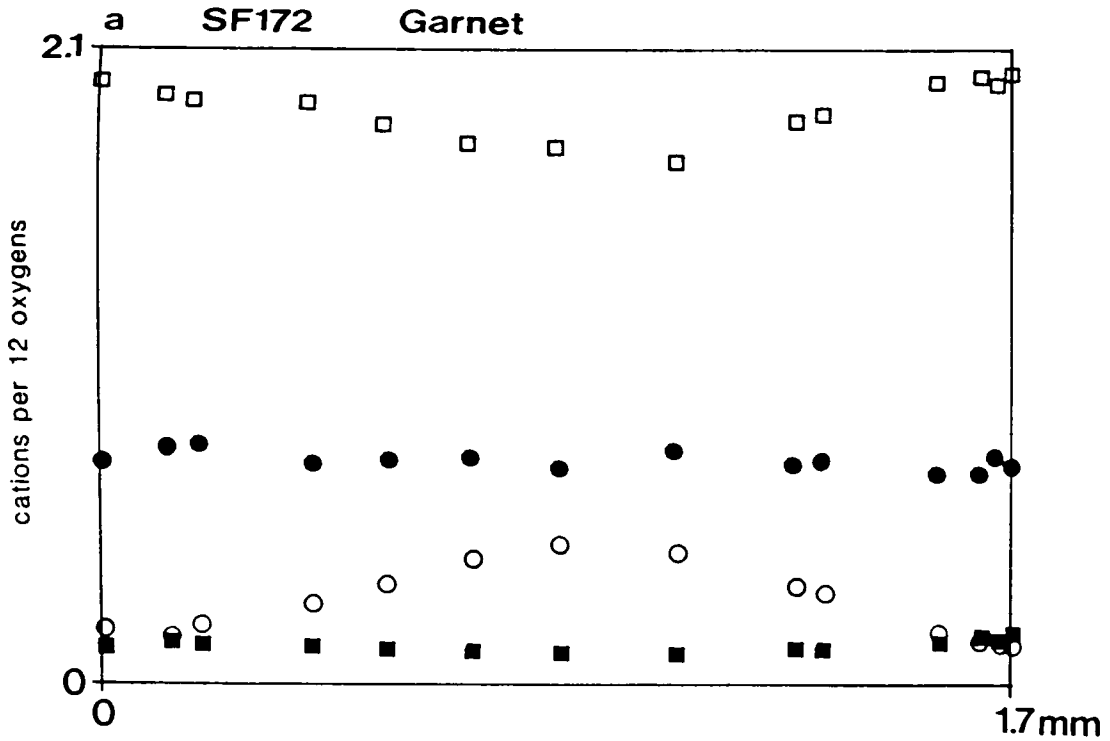

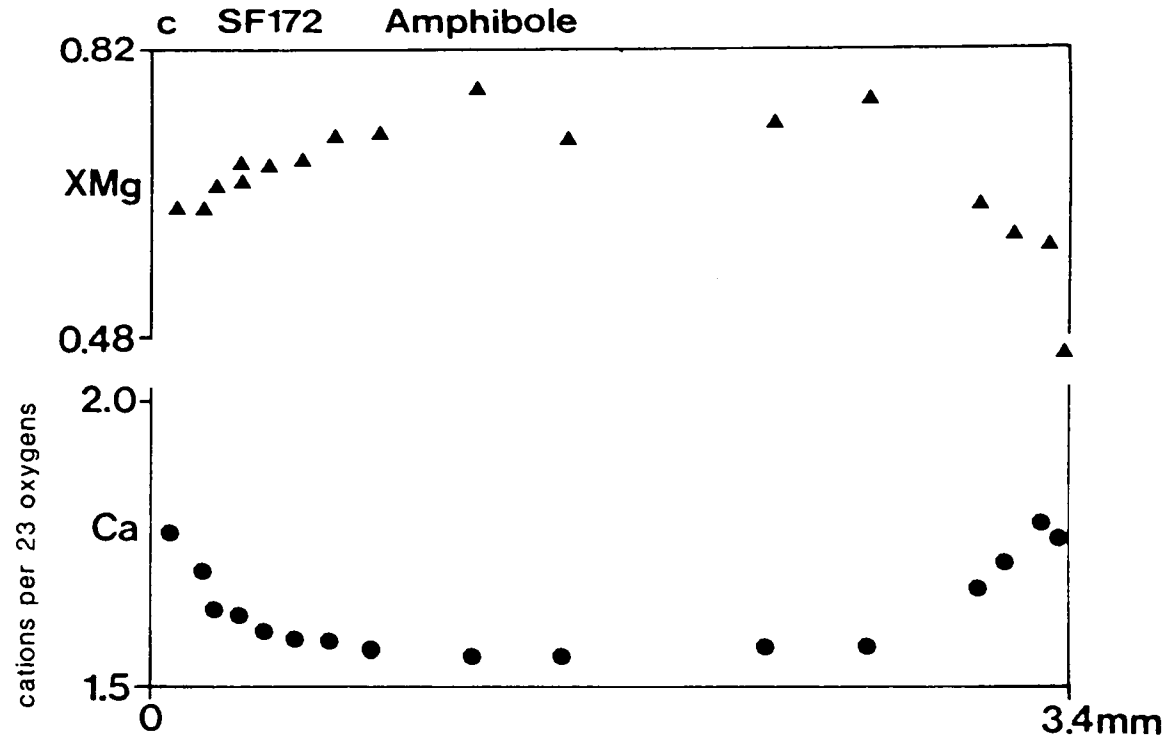

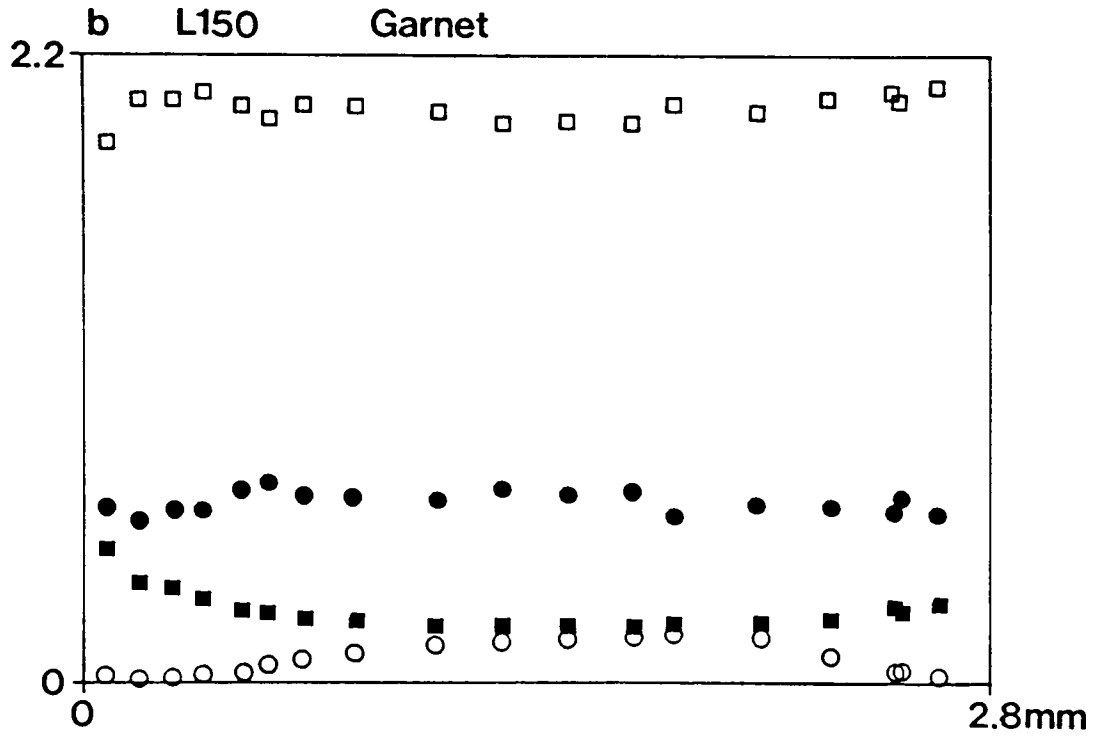

Figure 5.3

- □ Fe^{2+}
- ● Ca
- ○ Mn
- ■ Mg
- ▲ XMg

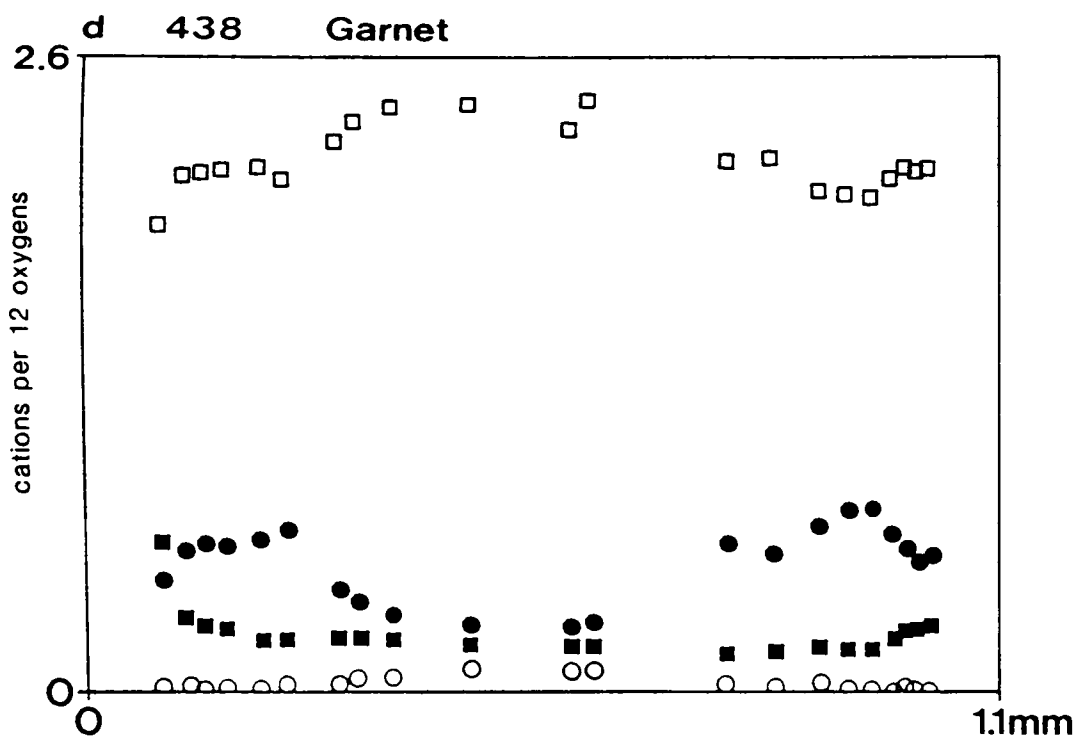

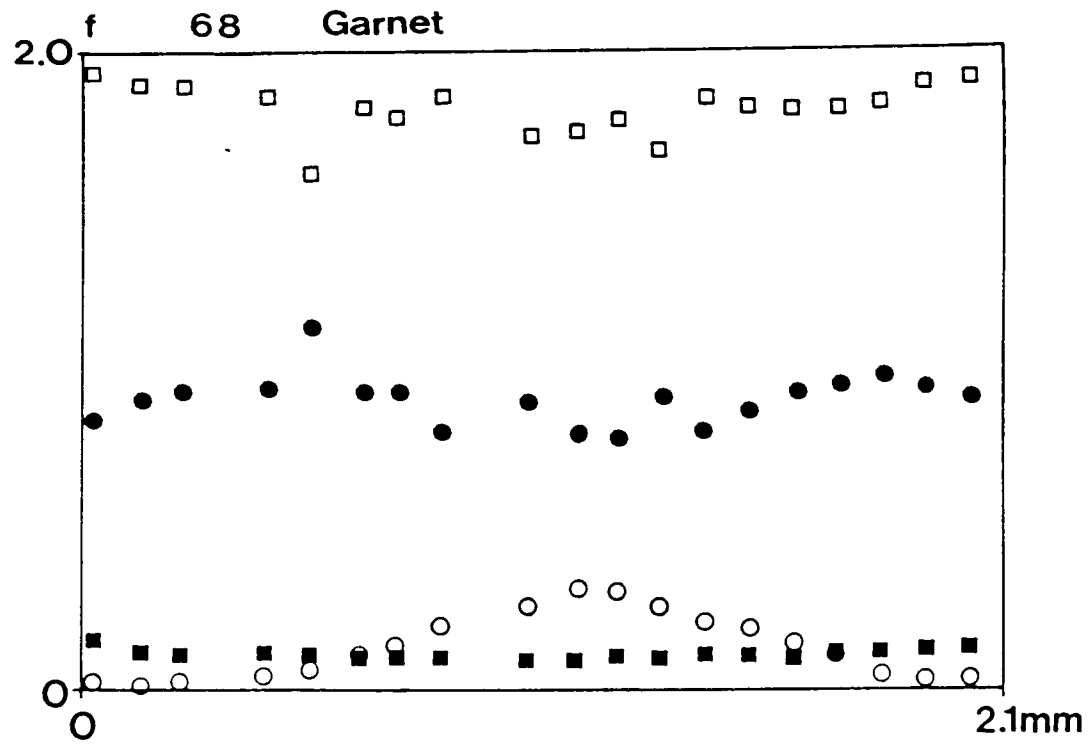

MMU

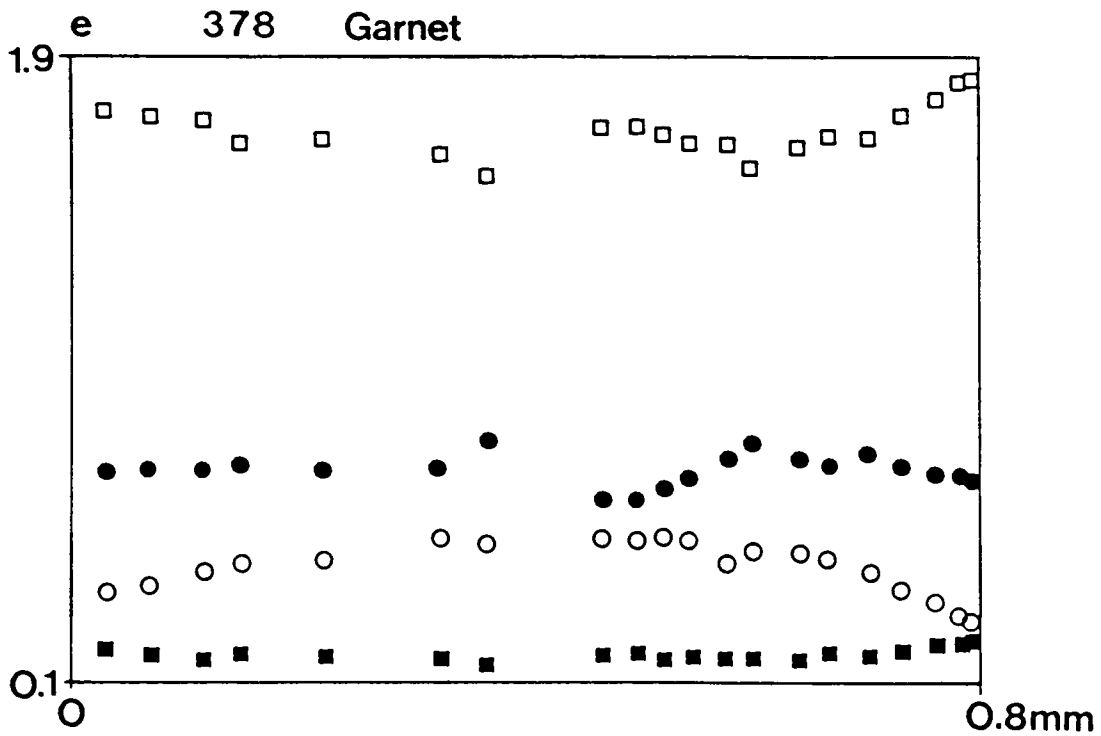

Figure 5.3

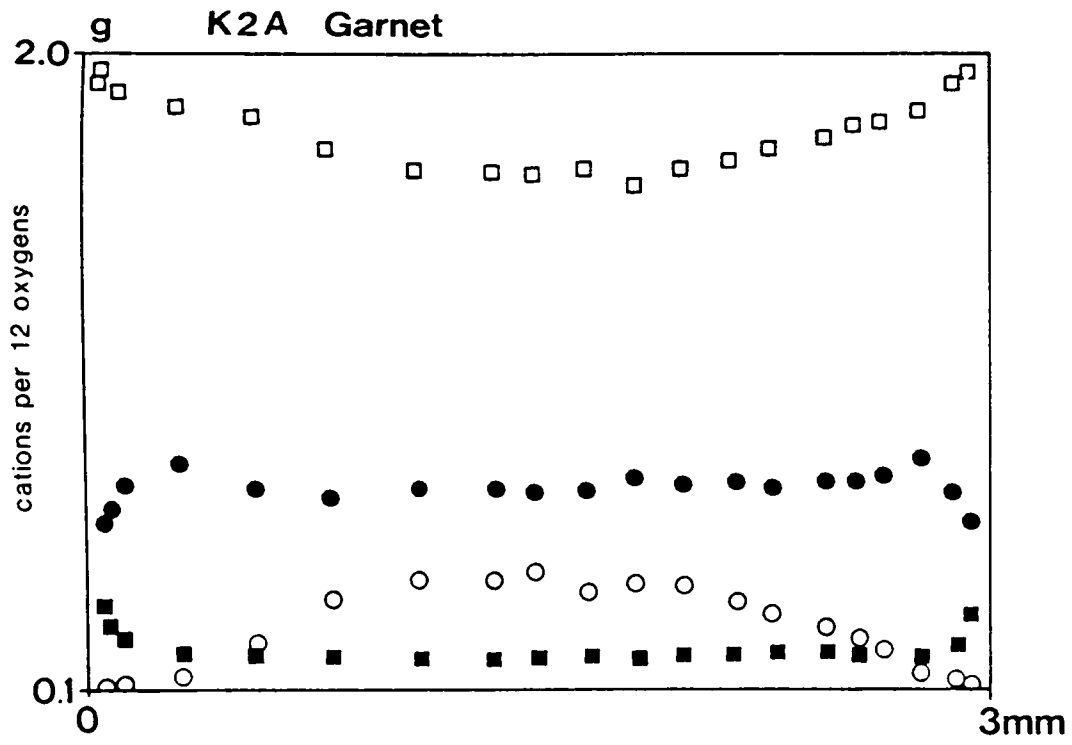

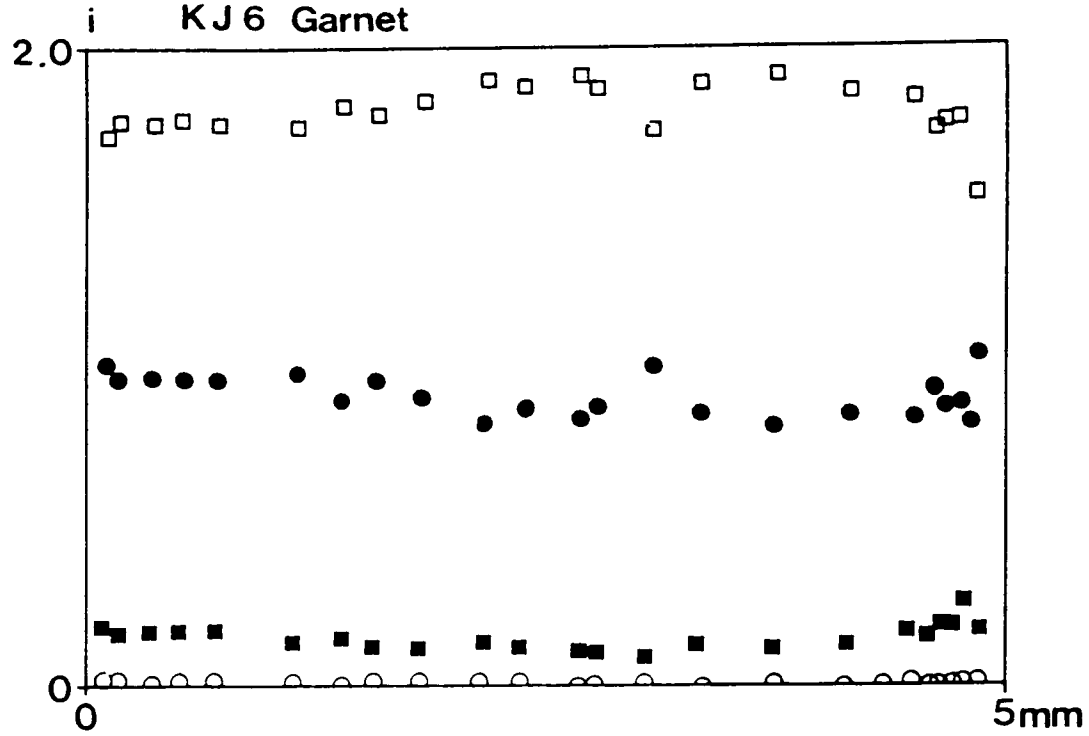

UMU

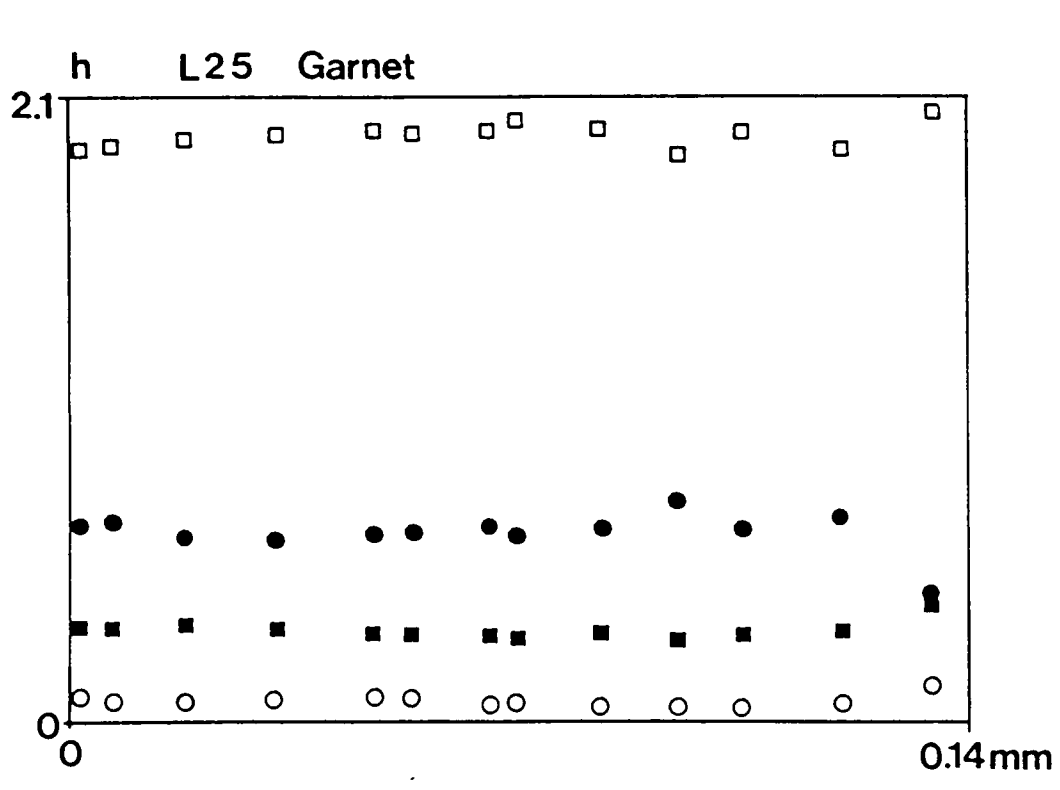

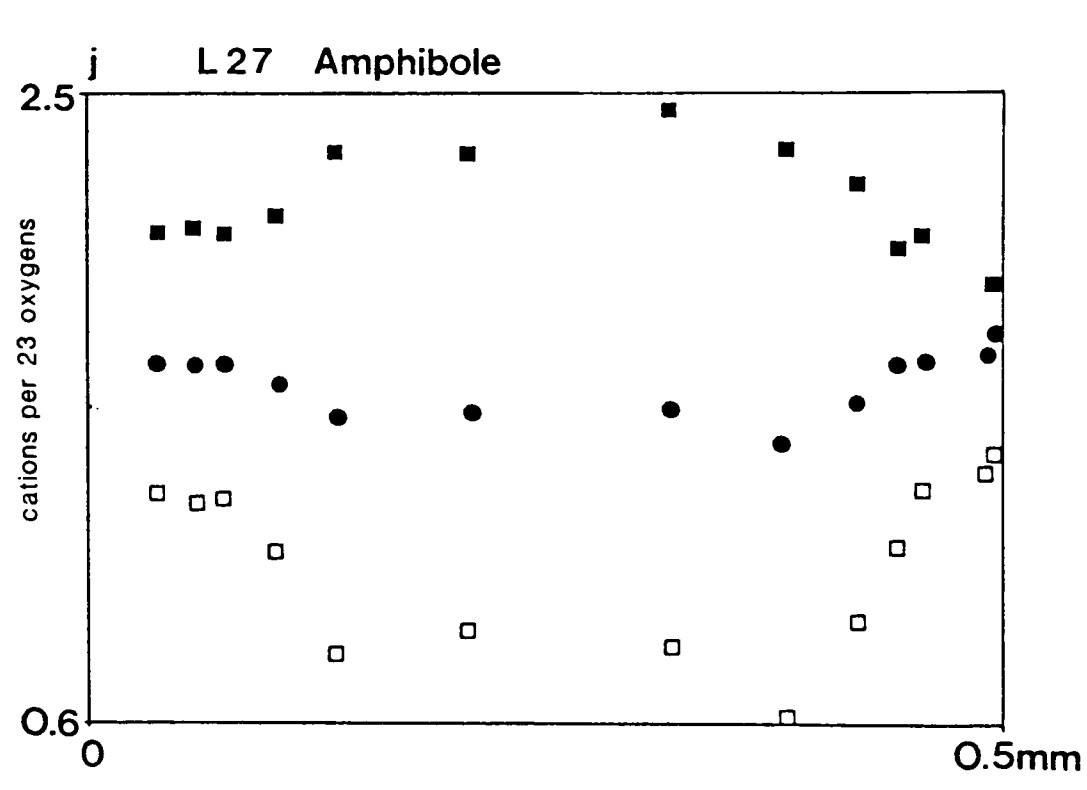

Figure 5.3

Figure 5.4: Amphibole compositions from (a) the Lower and Middle Mafic Units, and (b) the Upper Mafic Unit. Compositional trends from amphibole cores to rims are indicated by arrows. Abbreviations as shown in figure 4.16.

LMU

- ▾ SF112
- ▿ L150
- △ L128
- ● SF172
- ■ 449
- ○ 176
- ◇ SF35
- □ 446C

MMU

- ★ 498

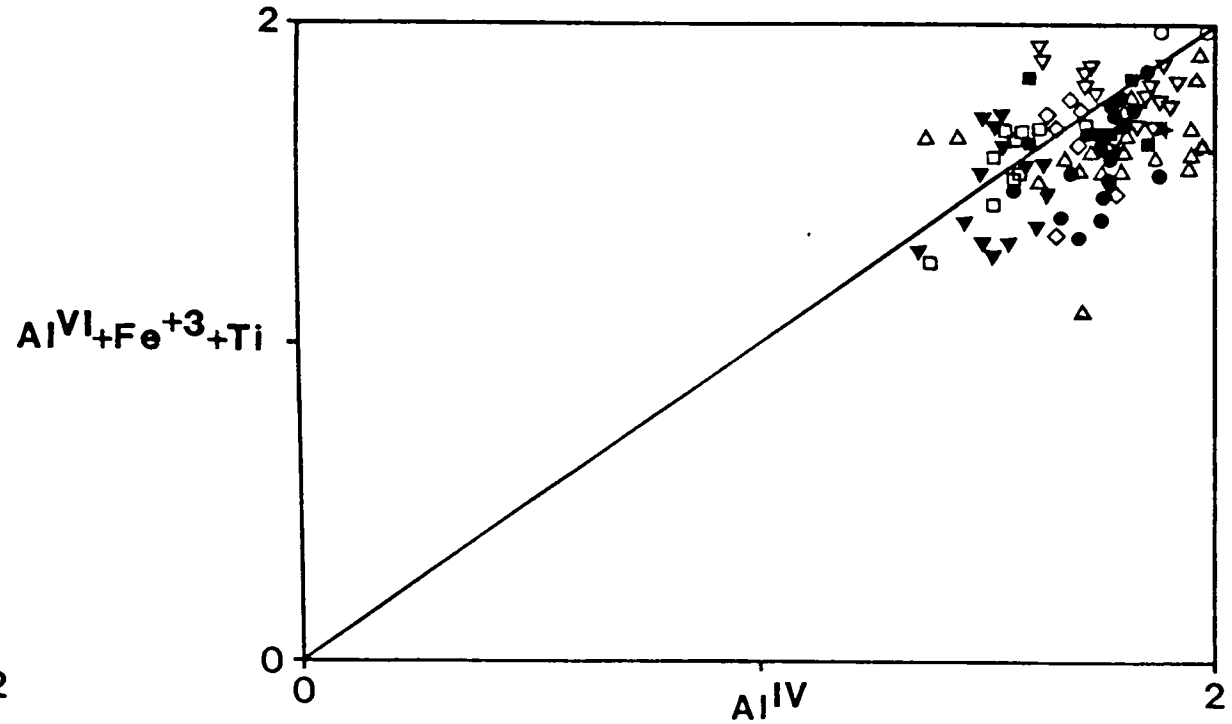

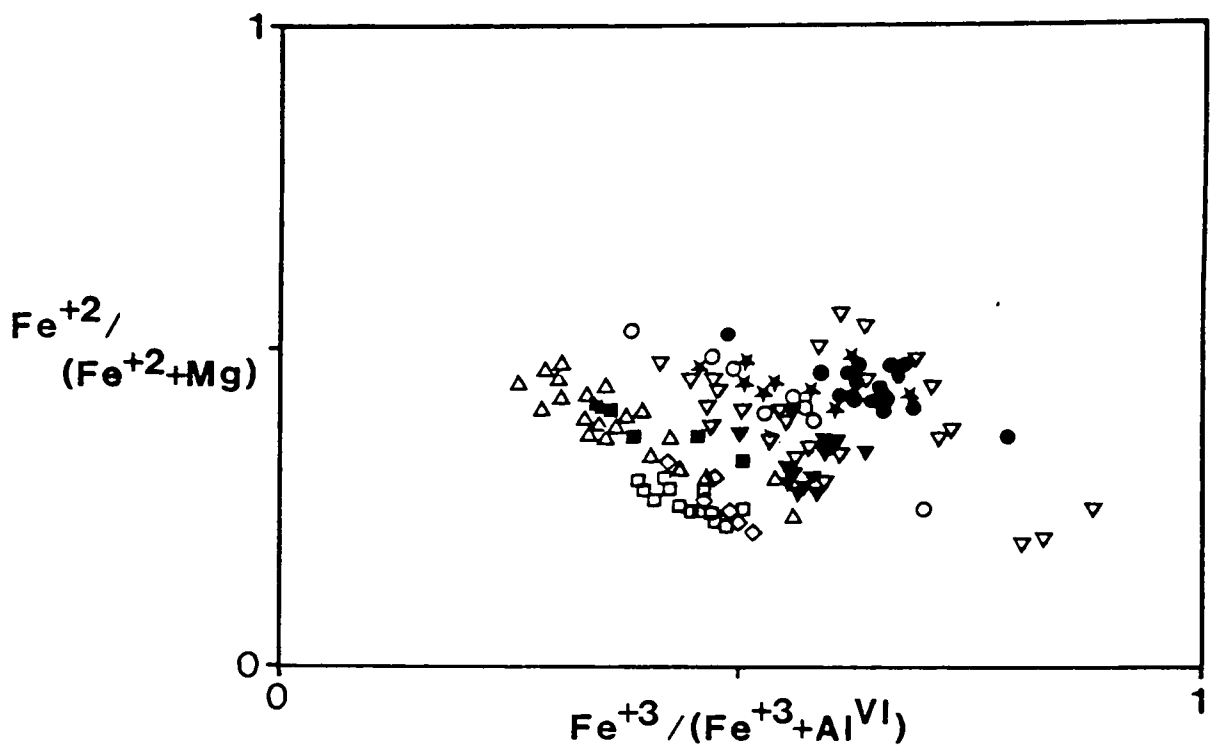

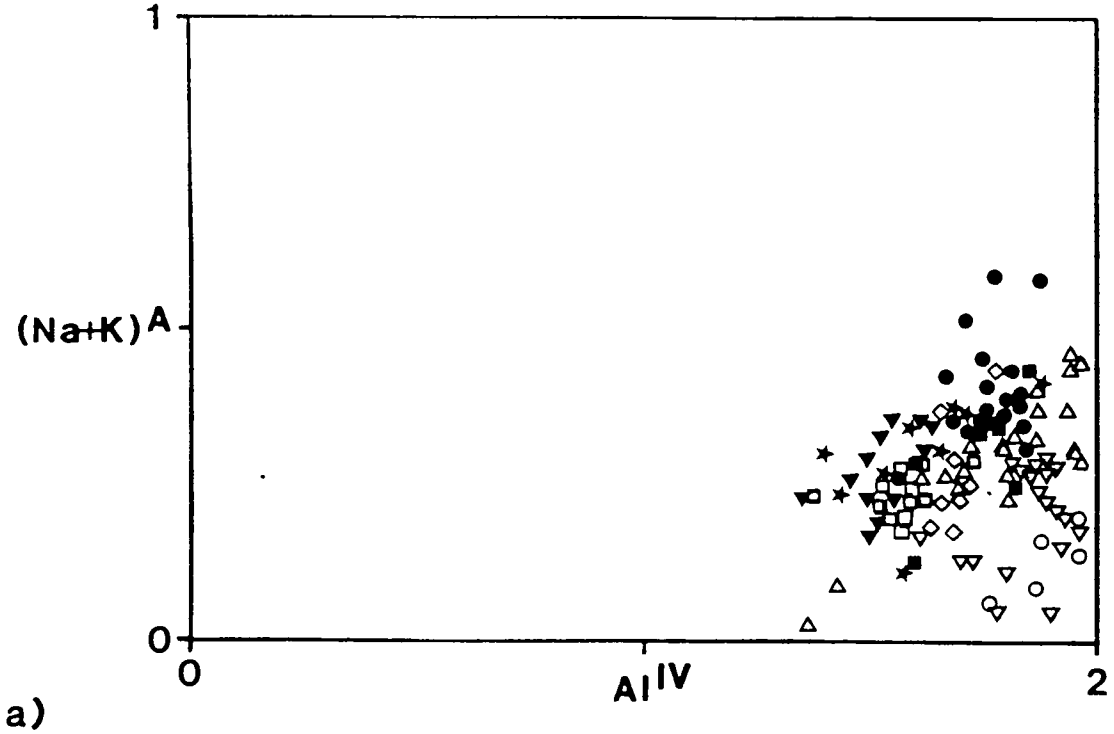

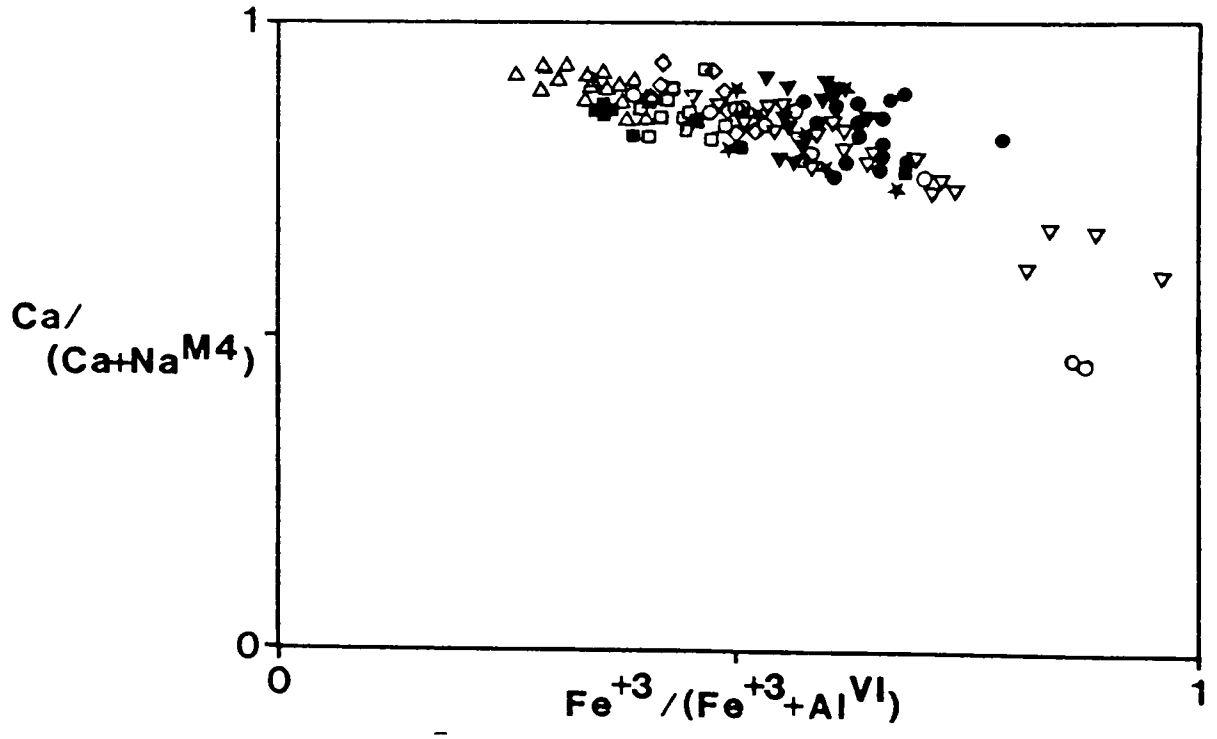

Figure 5.4 (a)

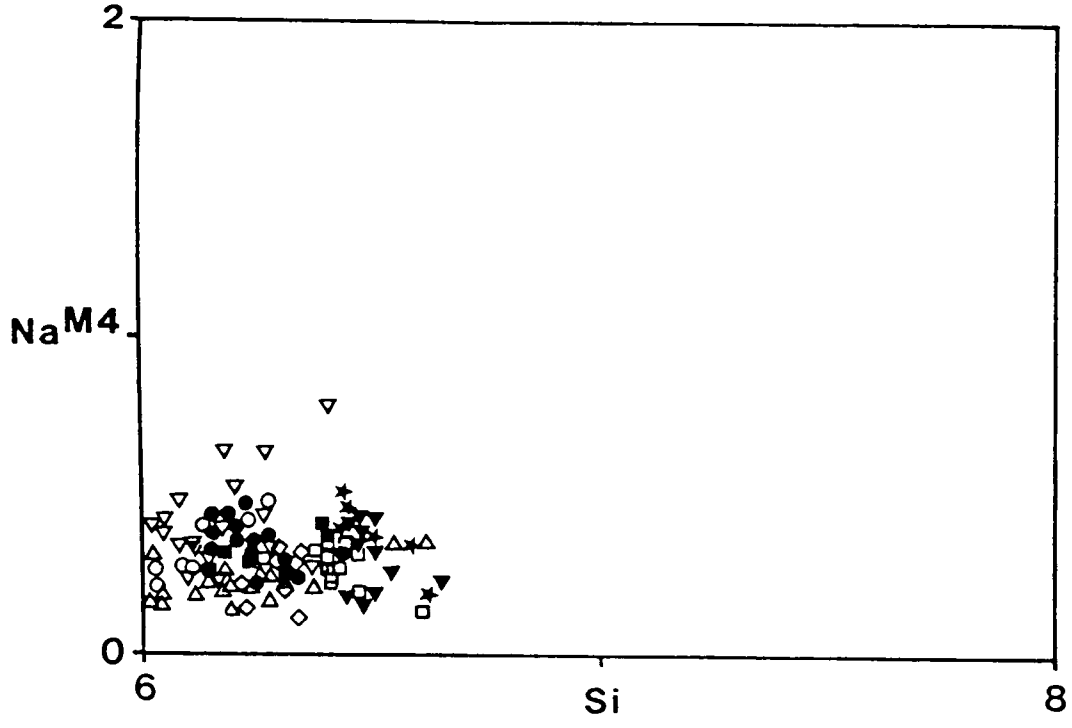

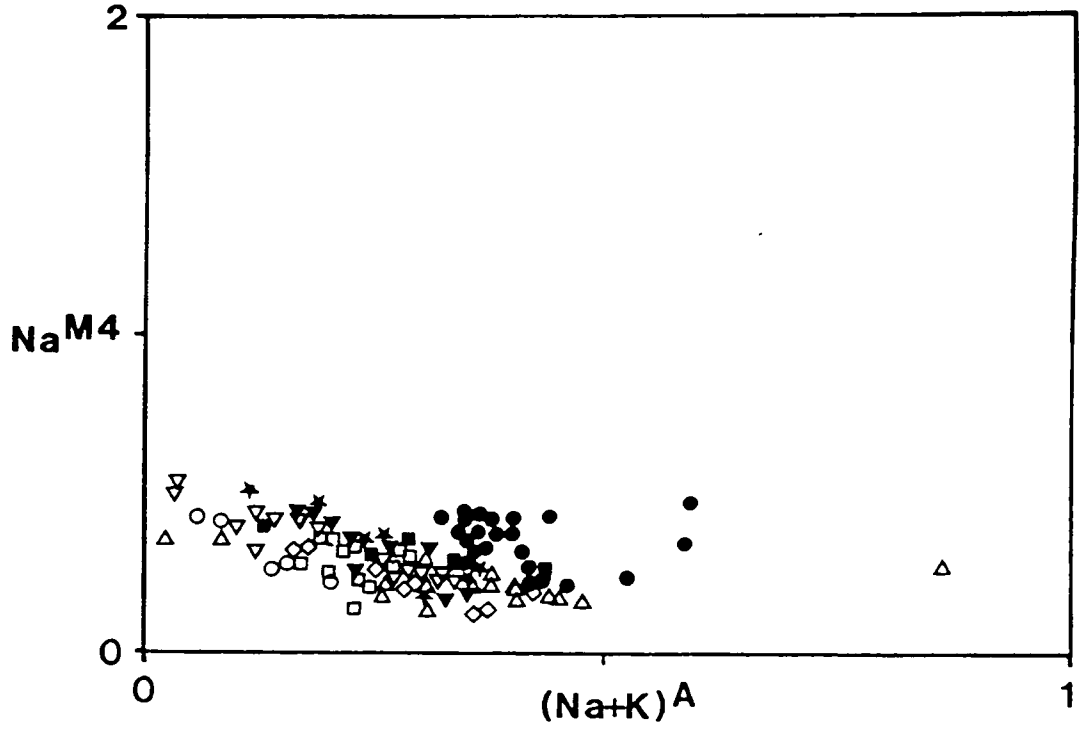

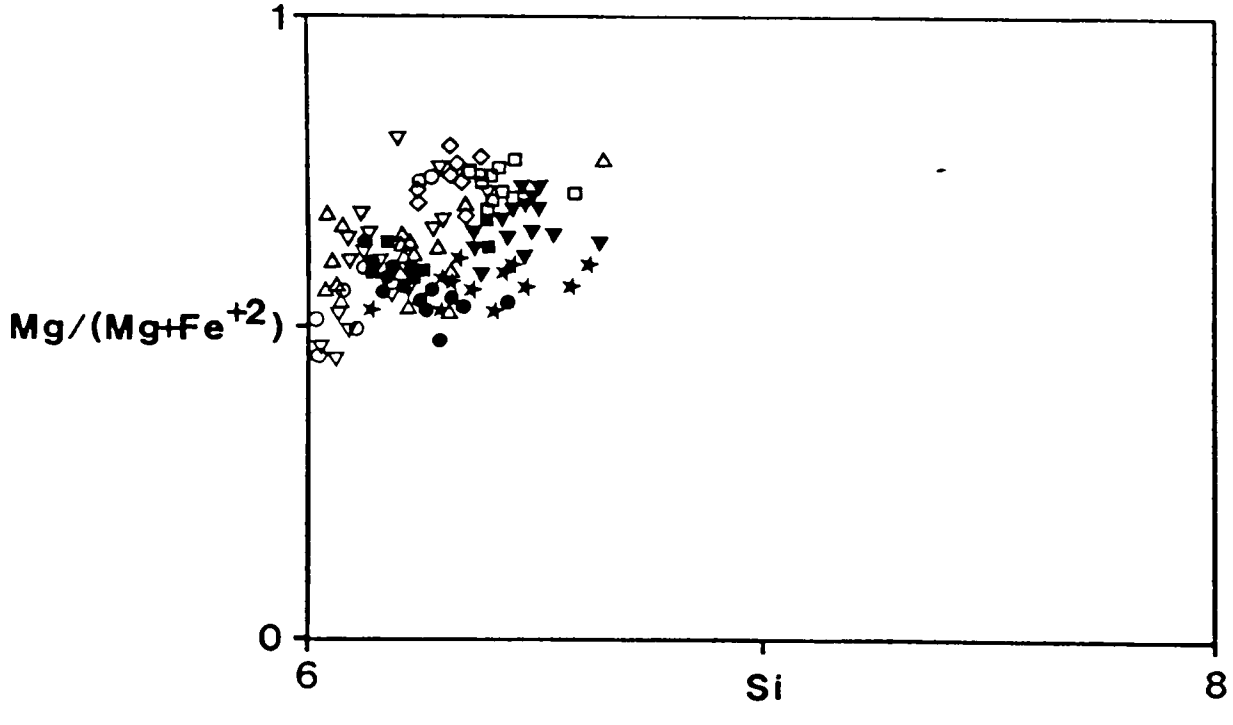

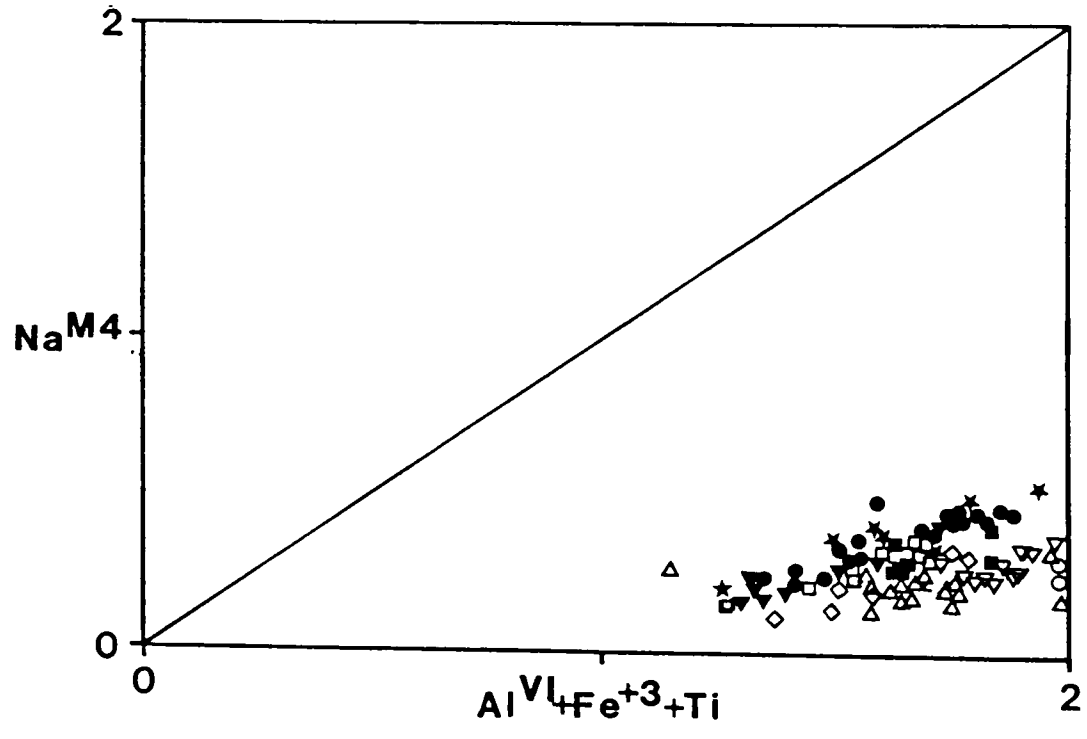

Figure 5.4 (a) (con)

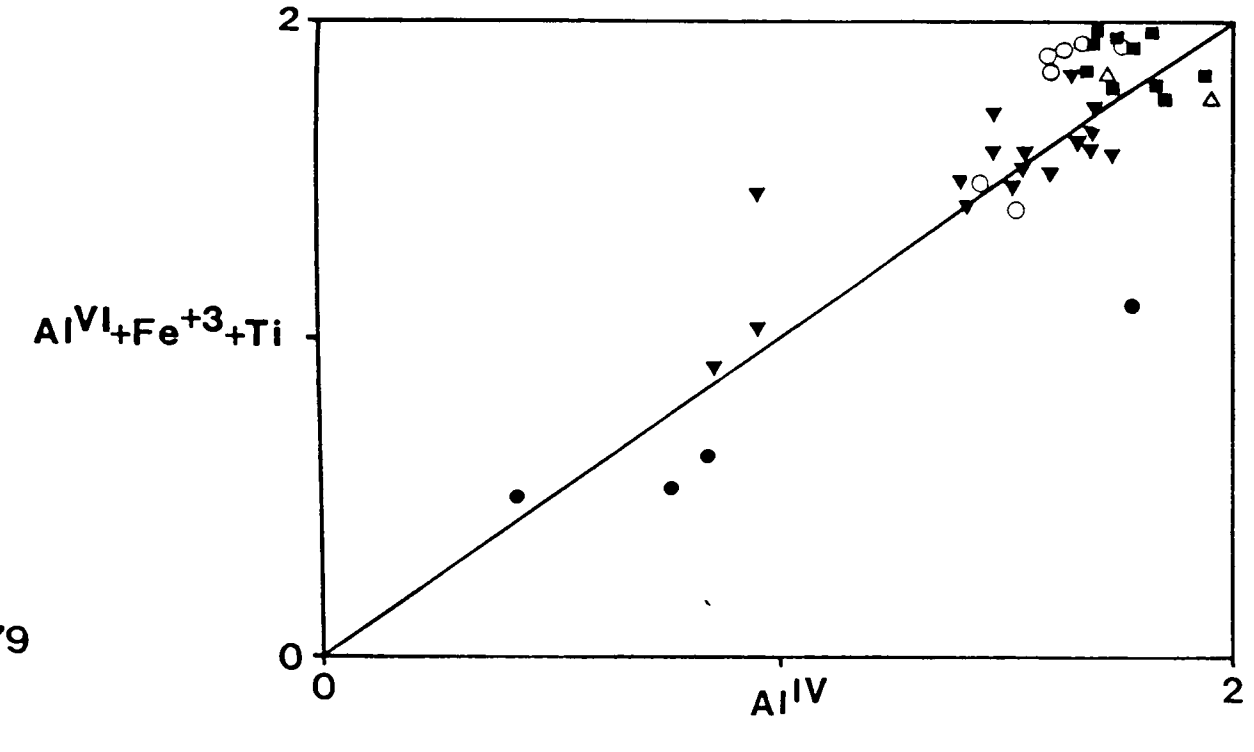

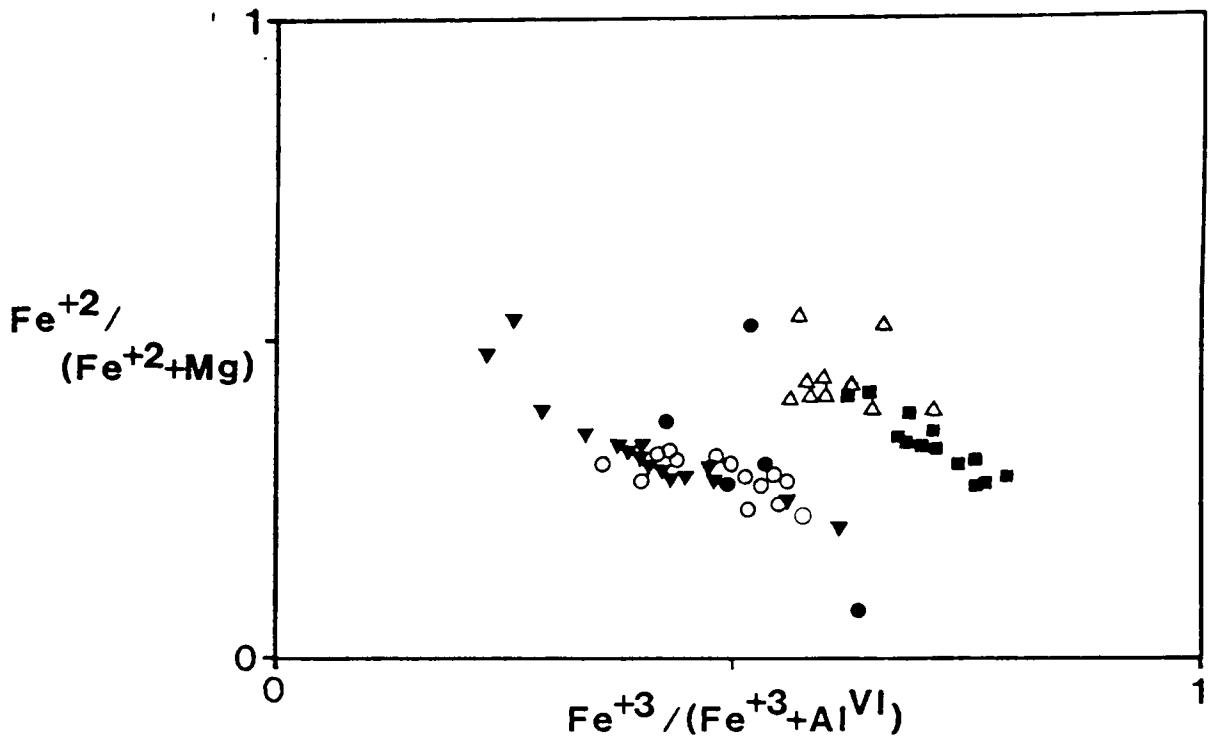

UMU
- ● KJ6
- △ SF179
- ▼ B3
- ■ L25
- ○ K2B

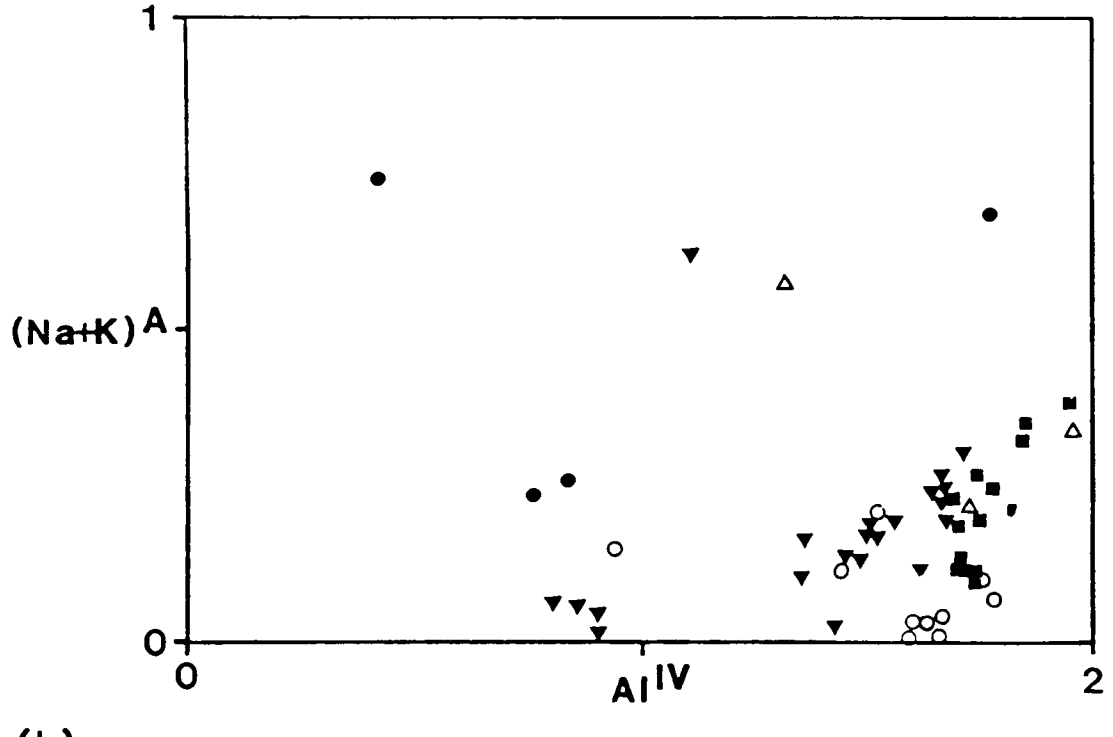

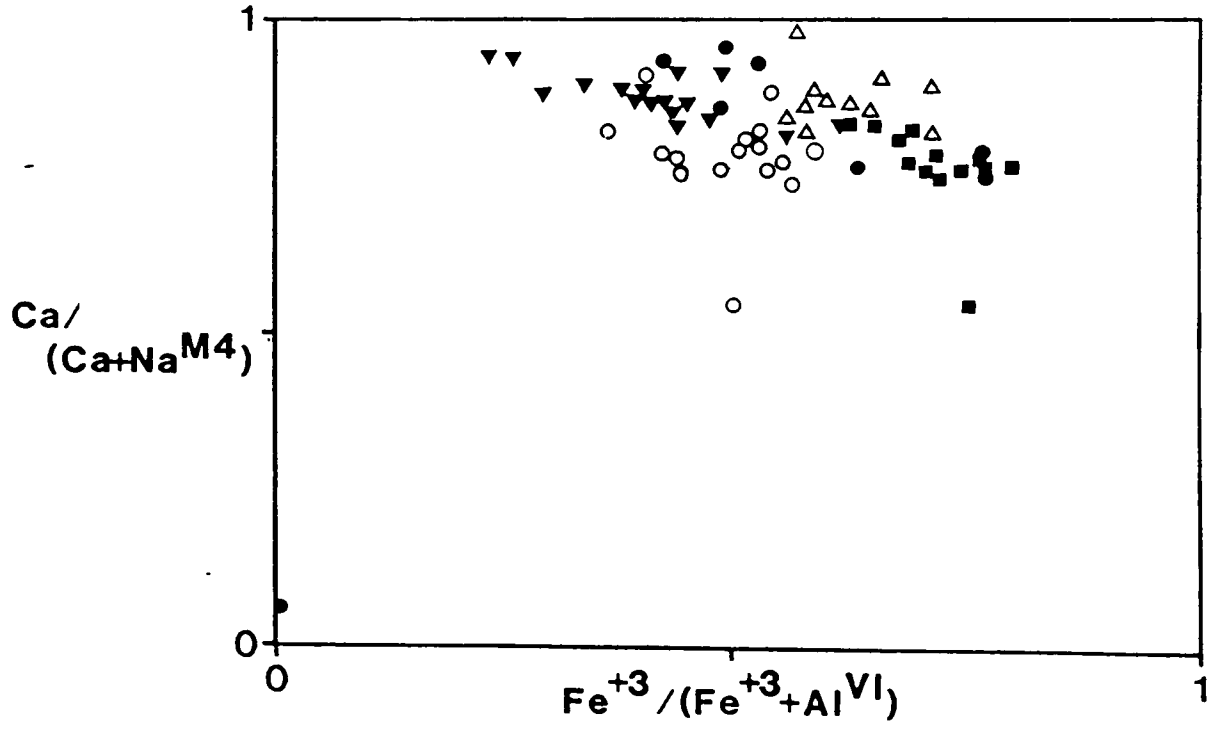

Figure 5.4 (b)

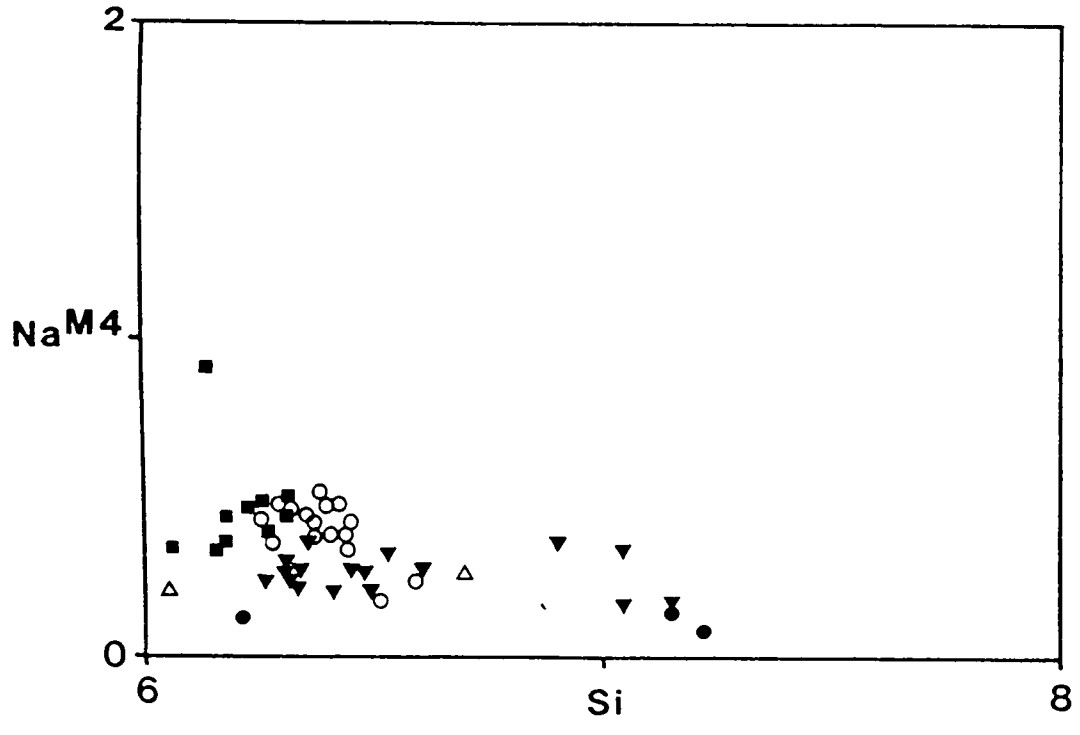

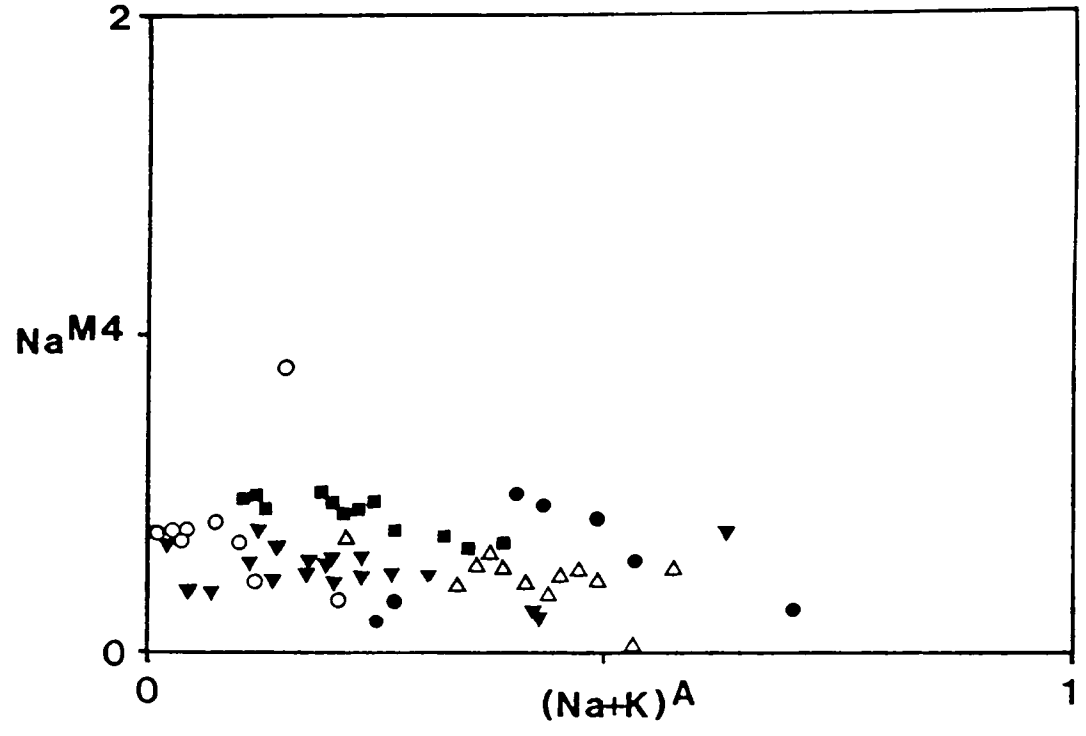

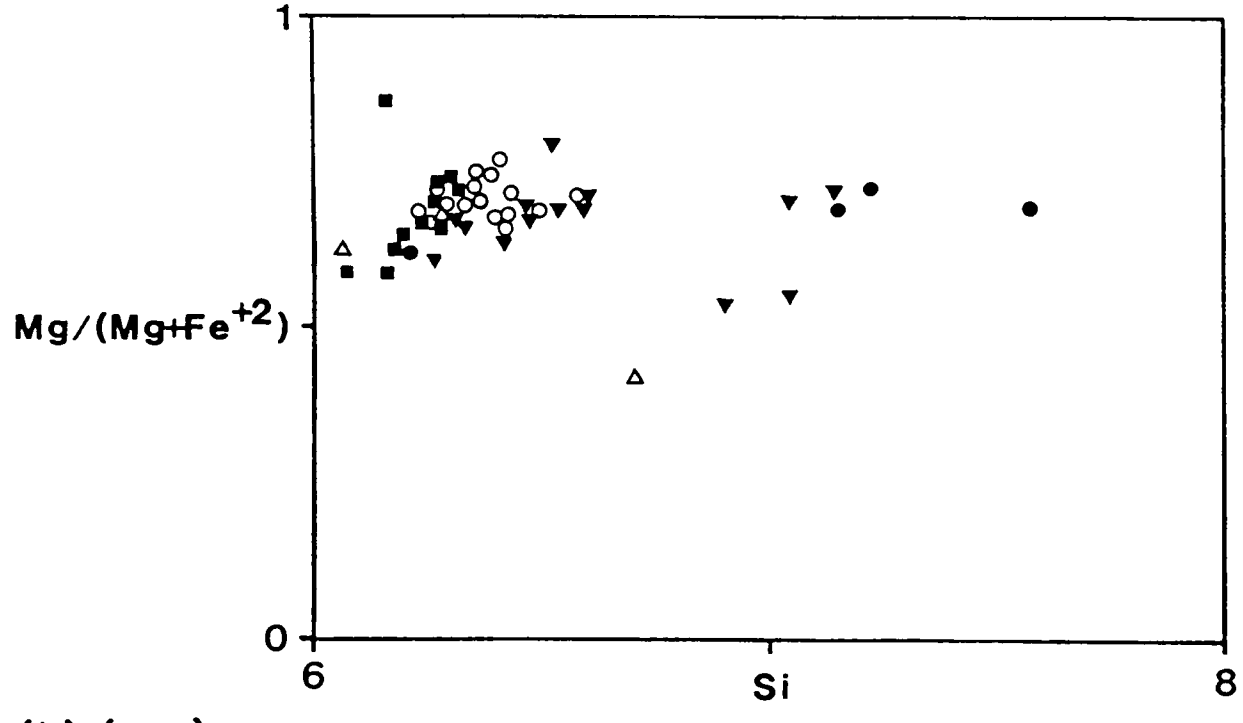

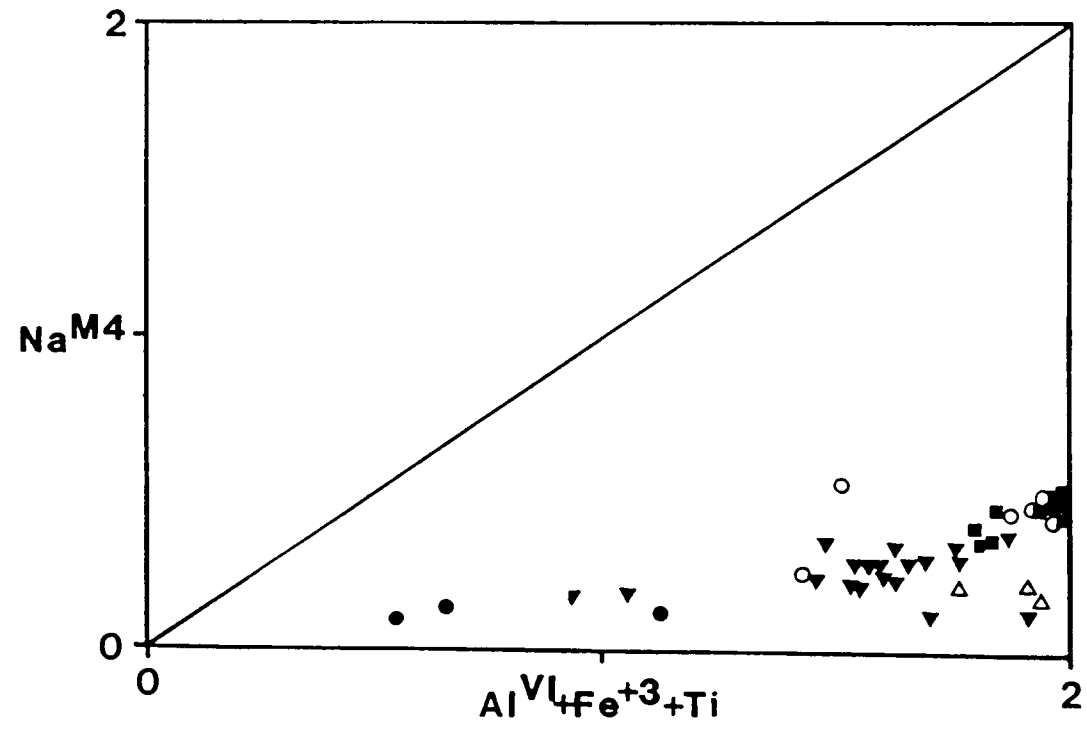

Figure 5.4 (b) (con)



Figure 5.5: Undeformed dolerite dyke in diorite at Mölmesdal

Figure 5.6 (a)

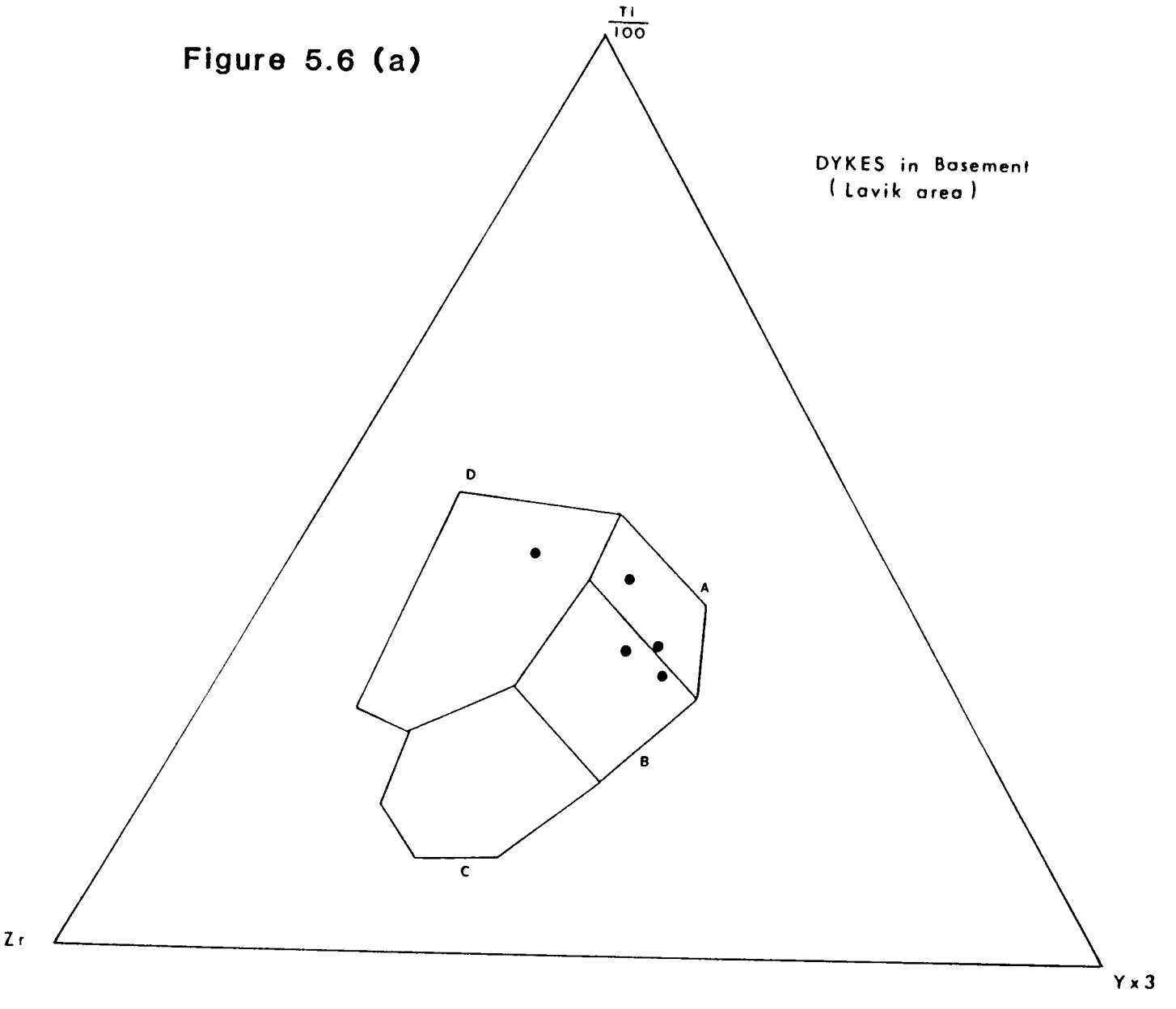

Figure 5.6: Zr-Ti-Y plot of dykes (a) in Upper Mafic Unit and (b) in Basement Gneisses. A=low-K tholeiites; B=Ocean-floor basalts, calc alkali basalts, and low-K basalts; C=calc-alkali basalts; D=within-plate basalts. After Pearce et al (1984).

Figure 5.6 (b)

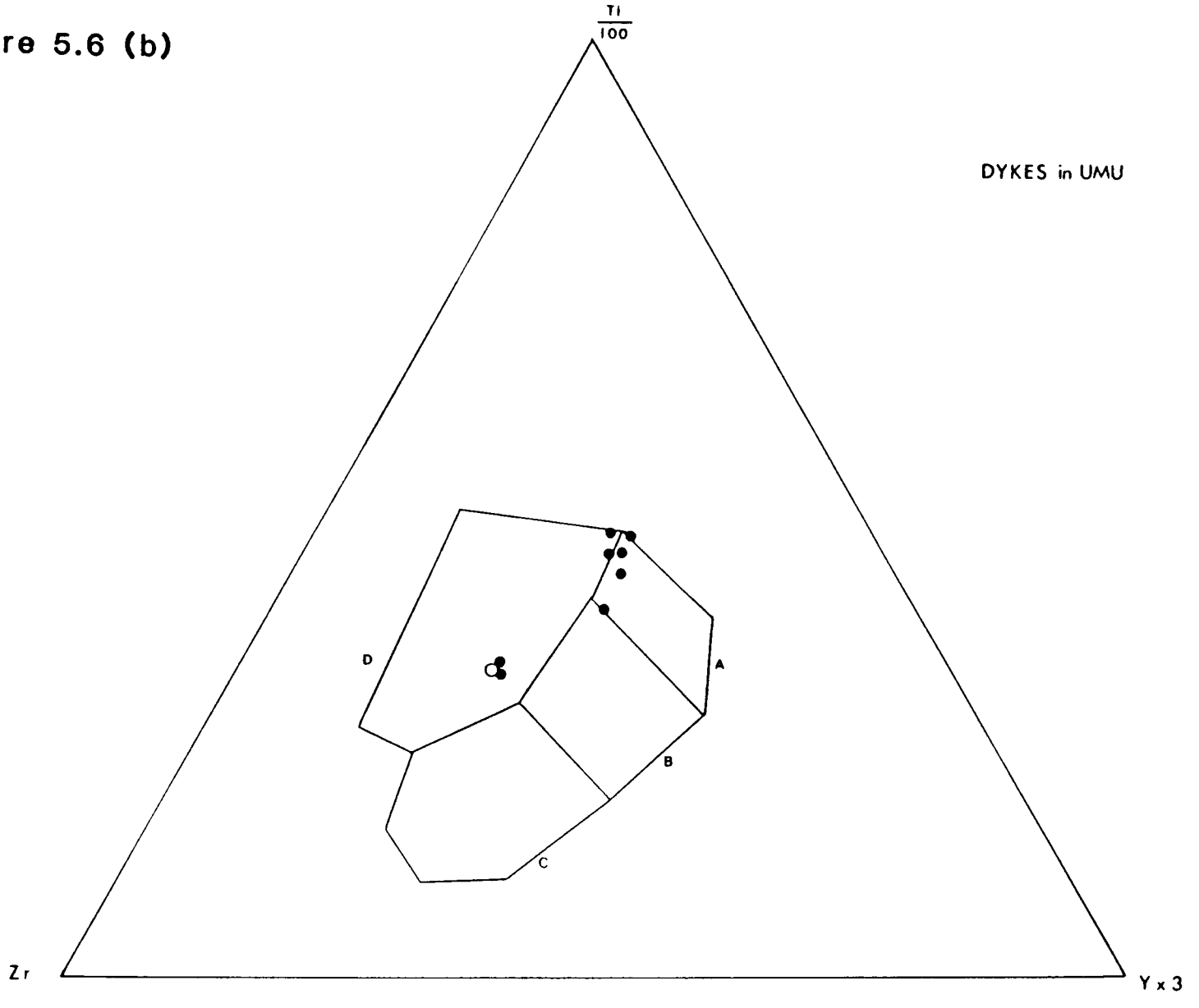

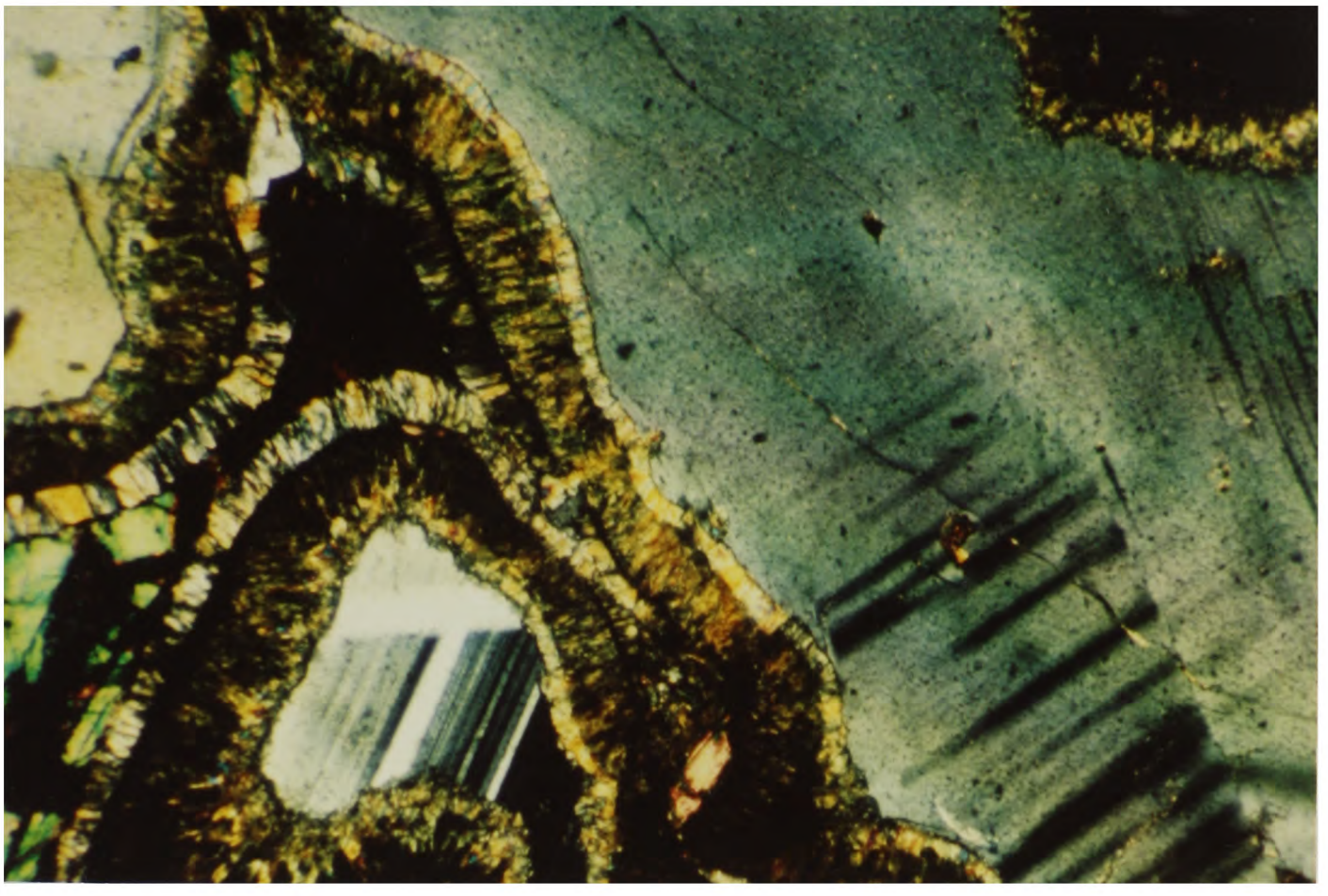

Figure 5.7: Corona gabbros from the Upper Mafic Unit. (a) Photomicrograph (in crossed polarized light) of gabbro with coronas in sample SF173, from Råsholm. On the left, a strongly resorbed olivine cumulus crystal is rimmed by a layer of orthopyroxene with radial habit, an irregular layer of orthopyroxene-spinel symplectite, and pargasitic amphibole. (b) corona gabbro at Kjönas, showing breakdown of orthopyroxene associated with late (low temperature) coronas, and relatively unaffected coarse clinopyroxene intercumulus crystal.



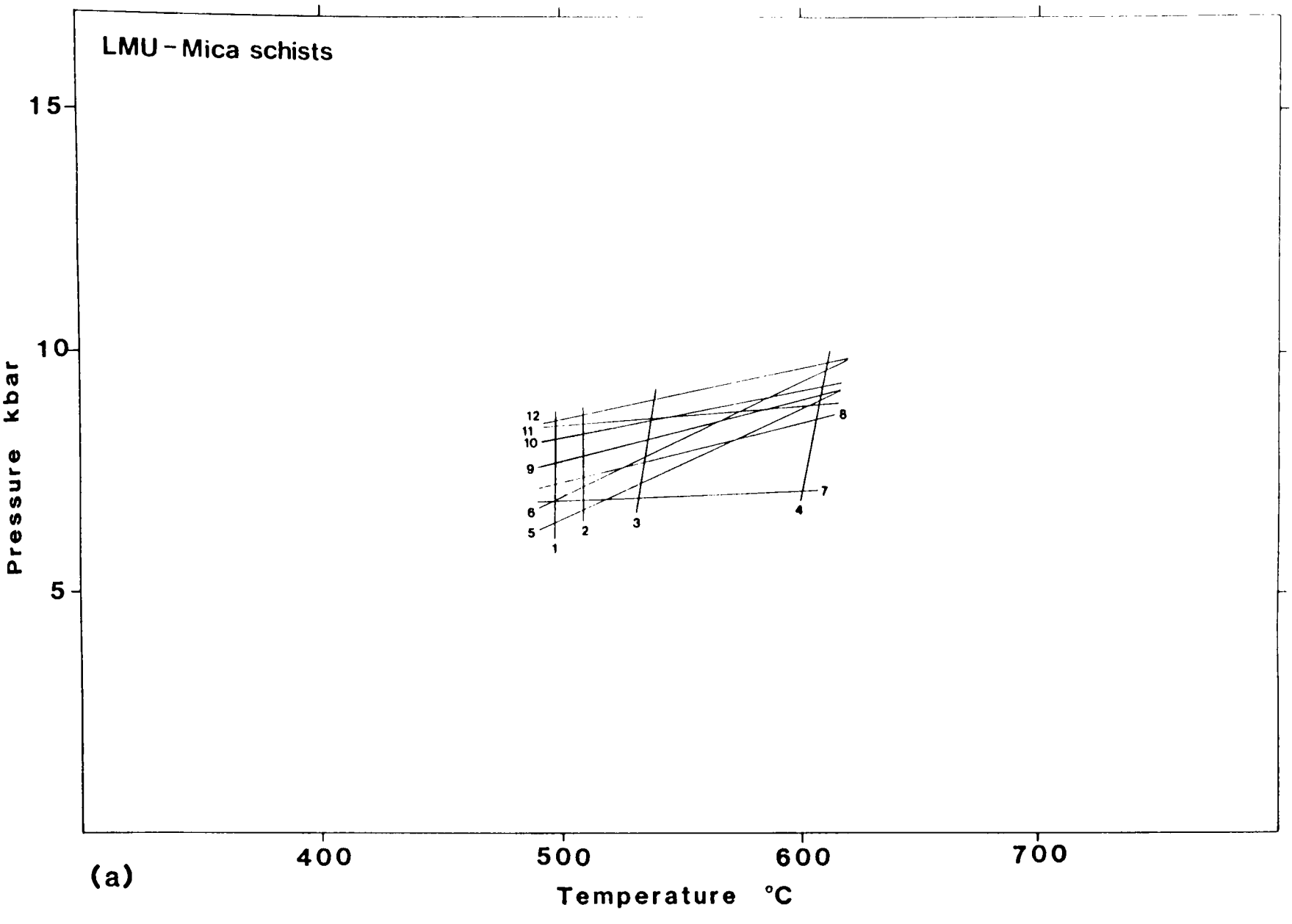

Figure 5.8: Thermobarometric results for LMU

(a) Mica schists; Numbers refer to calculated thermobarometric equilibria for different samples. Garnet-muscovite thermometer of Hynes and Forest (1988); 1=T1, 2=449XZ. Garnet-biotite calibration of Ganguly and Saxena (1984); 3=449XZ, 4=T1 Garnet-mica-plagioclase-quartz barometer of Ghent and Stout (1981); 7,8=449XZ, 9,11=T1. Garnet-mica-plagioclase-quartz barometer of Hodges and Crowley (1985); 5=449Xz, 6=T1; GRIPS barometer of Bohlen and Liotta (1986), 10=T1, 12=449XZ.

(b) Garnet amphibolites. GRIPS: 1=L128; 2=L150, SF110. SF112; 3=449, L168; 4=176; 5=SF172. Garnet-hornblende thermometer of Graham and Powell (1984): 6=SF110, 7=SF172, 8=SF97, 9=SF112, 10=L128, 11=SF112, 12=449, 13=L168, 14=176, 15=L150; dashed lines indicate temperatures calculated by the gt-hbl thermometer using amphibole inclusions and adjacent garnet compositions for L150.

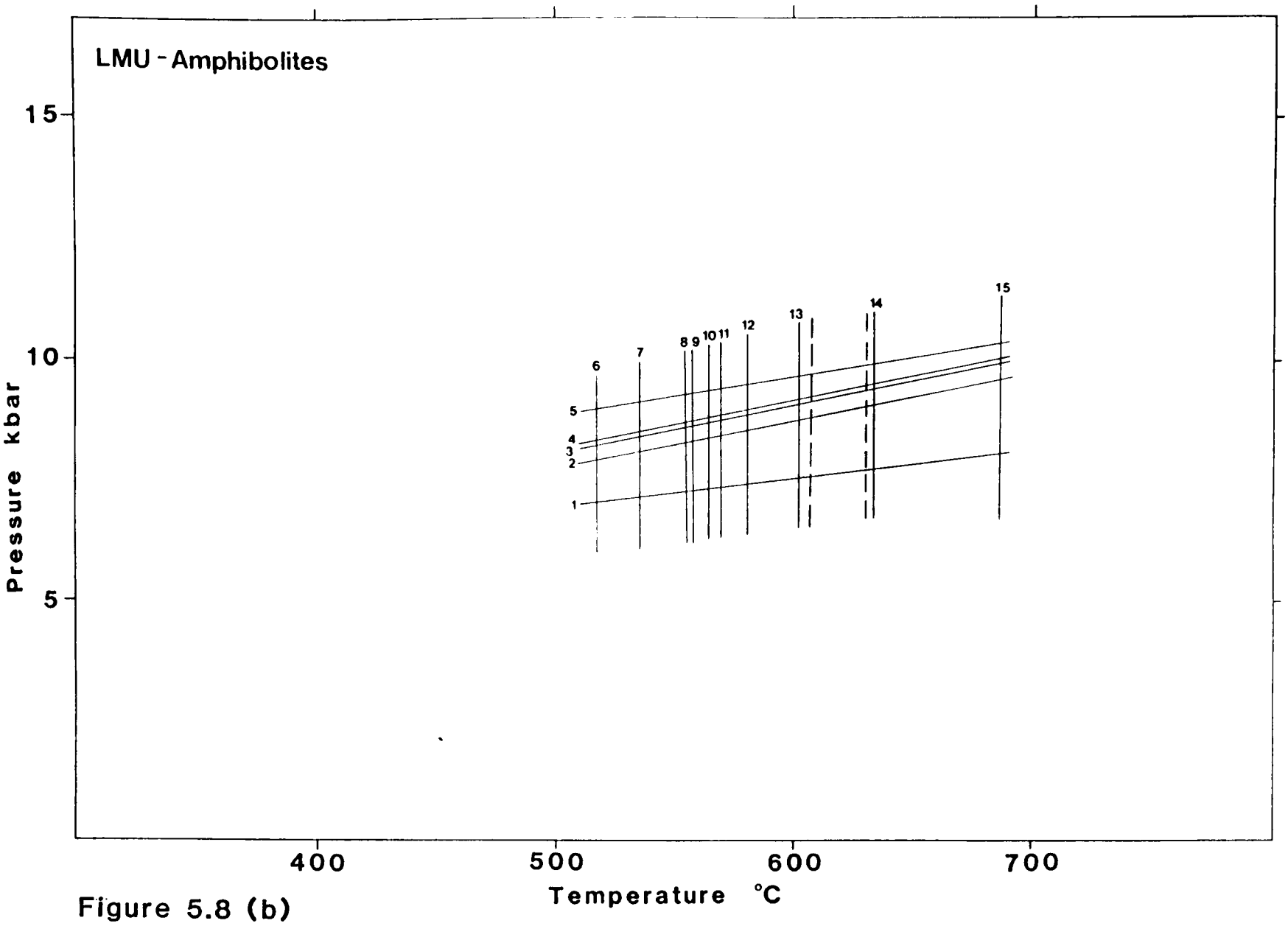
LMU - Amphibolites
15
10
5
Pressure kbar
400
500
600
700
Temperature °C
1
2
3
4
5
6
7
8 9 10 11
12
13
14
15

Figure 5.8 (b)

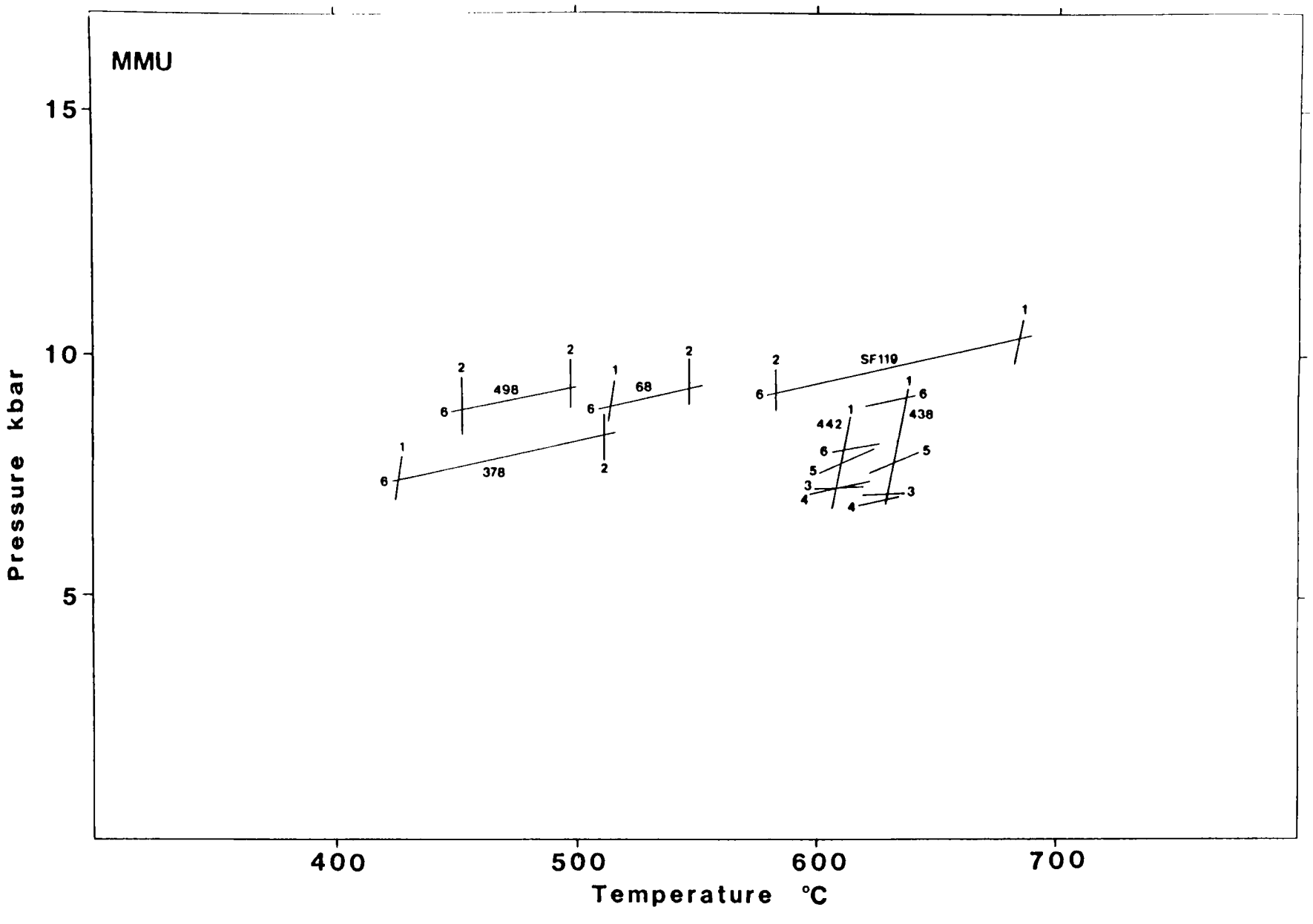

Figure 5.9: Thermobarometric results for Middle Mafic Unit. Sample numbers are indicated on the diagram. Other numbers (1-6) refer to thermobarometric equilibria 1: garnet biotite thermometer of Ganguly and Saxena (1984); 2: garnet-hornblende thermometer of Graham and Powell (1984); 3 and 4: garnet-plagioclase-mica-quartz barometer of Ghent and Stout (1981); 5: garnet-plagioclase mica-quartz barometer of Hodges and Crowley (1985); 6: GRIPS barometer of Bohlen and Liotta (1986)

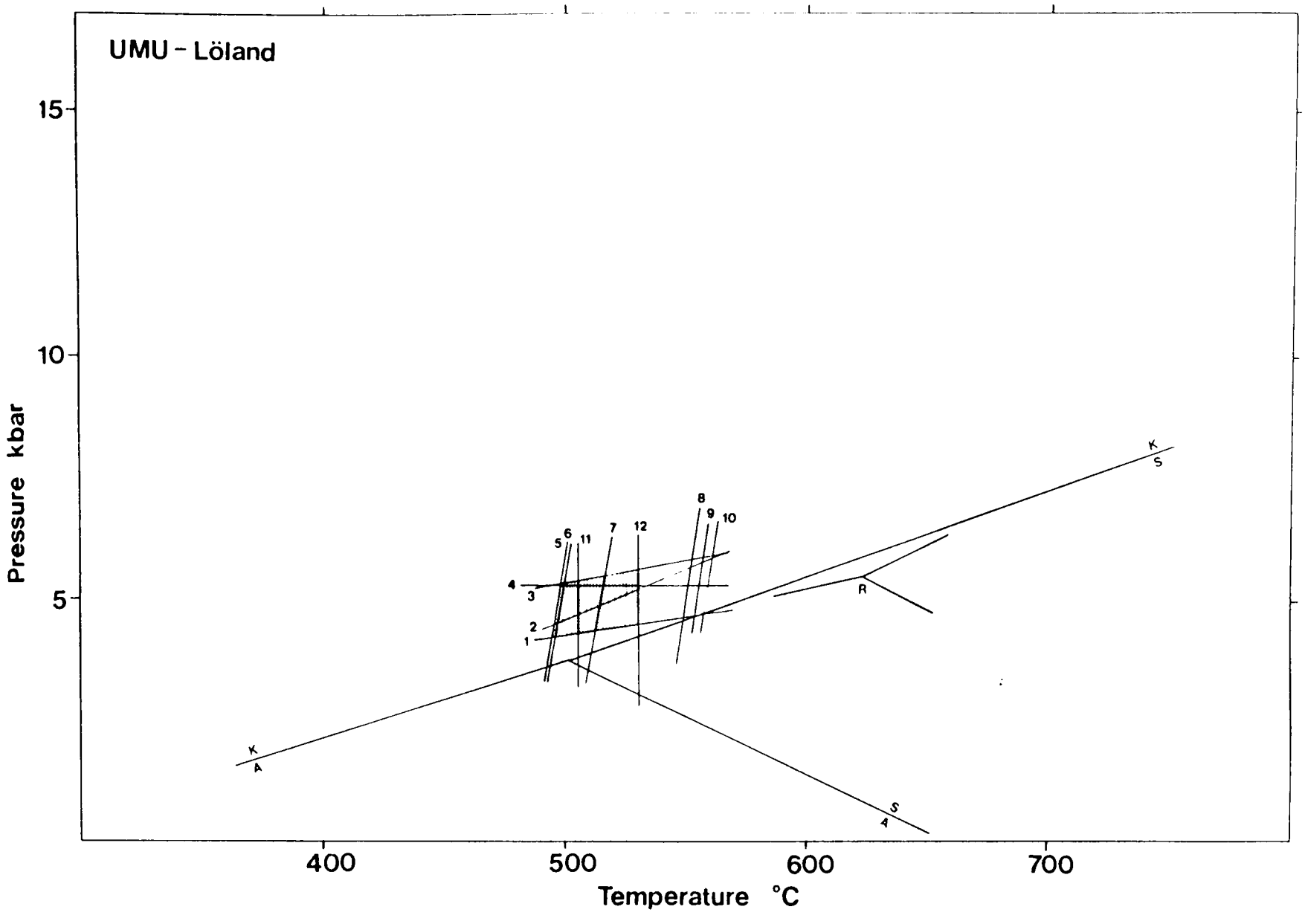

Figure 5.10: (a) Thermobarometric results for rocks at Löland. Numbers 1-4 refer to barometric equilibria applied to sample K2a. 1: GRAIL barometer of Bohlen et al (1983); 2: garnet-plagioclase-mica-quartz barometer of Hodges and Crowley (1985); 3 and 4: garnet-plagioclase-mica-quartz barometer of Ghent and Stout (1981). Numbers 5-7 refer to the garnet-biotite thermometer (Ganguly and Saxena, 1984) for different samples. 5: K2b, 6: K2a, 7: K3. Numbers 8-10 refer to the garnet-biotite thermometer of Hodges and Spear (1982). 8: K3, 9: K2b, 10: K2a. Numbers 11 and 12 refer to the garnet-hornblende thermometer of Graham and Powell (1984). 11: K2b, 12: K3.

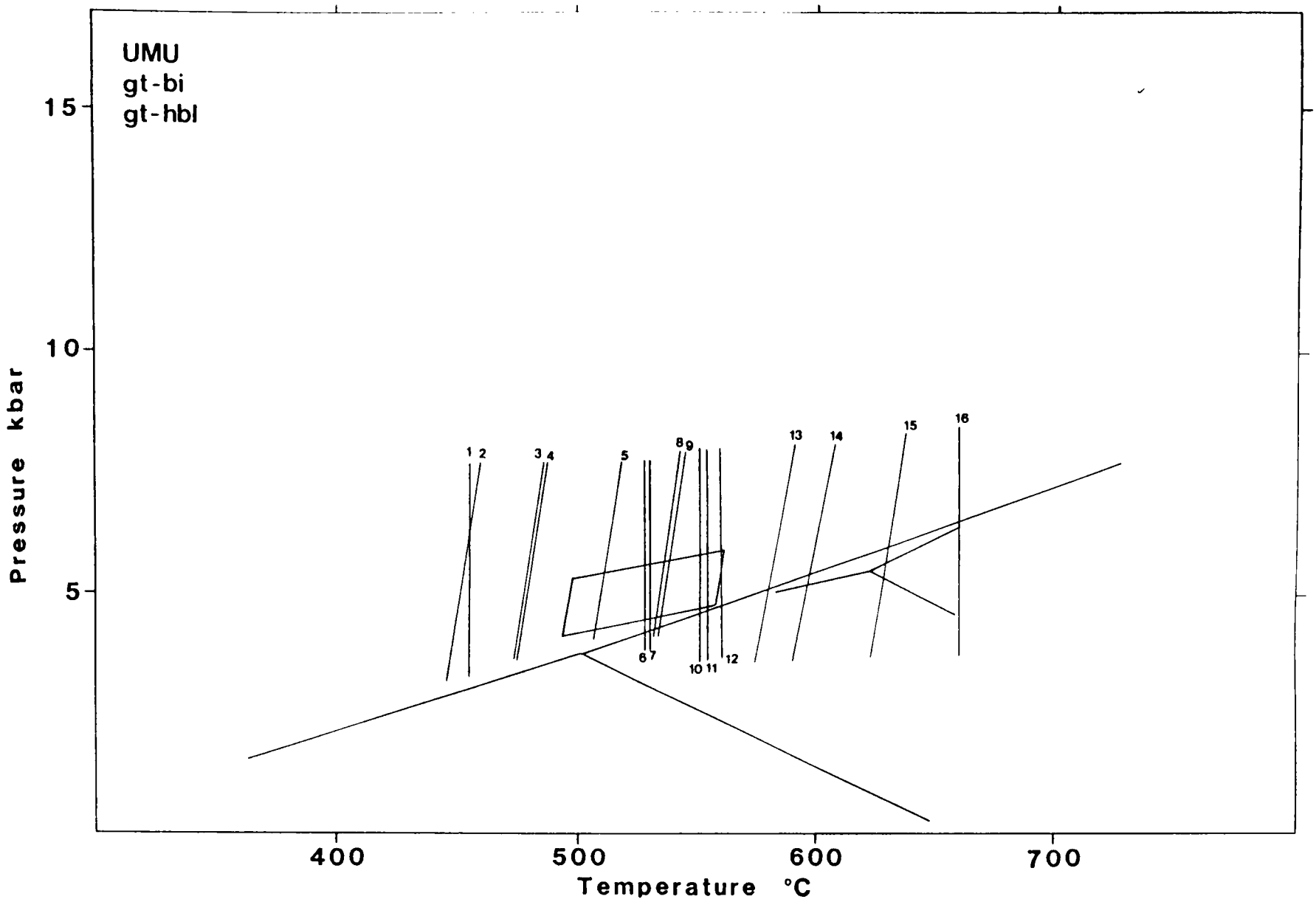

(b) Thermobarometric results for UMU (other than Löland). Garnet-biotite thermometer of Ganguly and Saxena (1984): 2: KJ6, 3: B3, 4: B12, 13: SF156, 14: SF179. Garnet biotite thermometer of Hodges and Spear (1982): 5: KJ6, 8: B3, 9: B12, 15: SF156. Garnet-hornblende thermometer of Graham and Powell (1984): 1: L41b, 6: B3, 7: L27 and SF156, 10: L25, 11: B12, 12: KJ6, 16:SF179

(c) GRIPS barometry for Upper Mafic Unit: numbers refer to samples: 1=K2b, 2=K2a, 3=B3, 4=L27, 5=K3, 6=L25

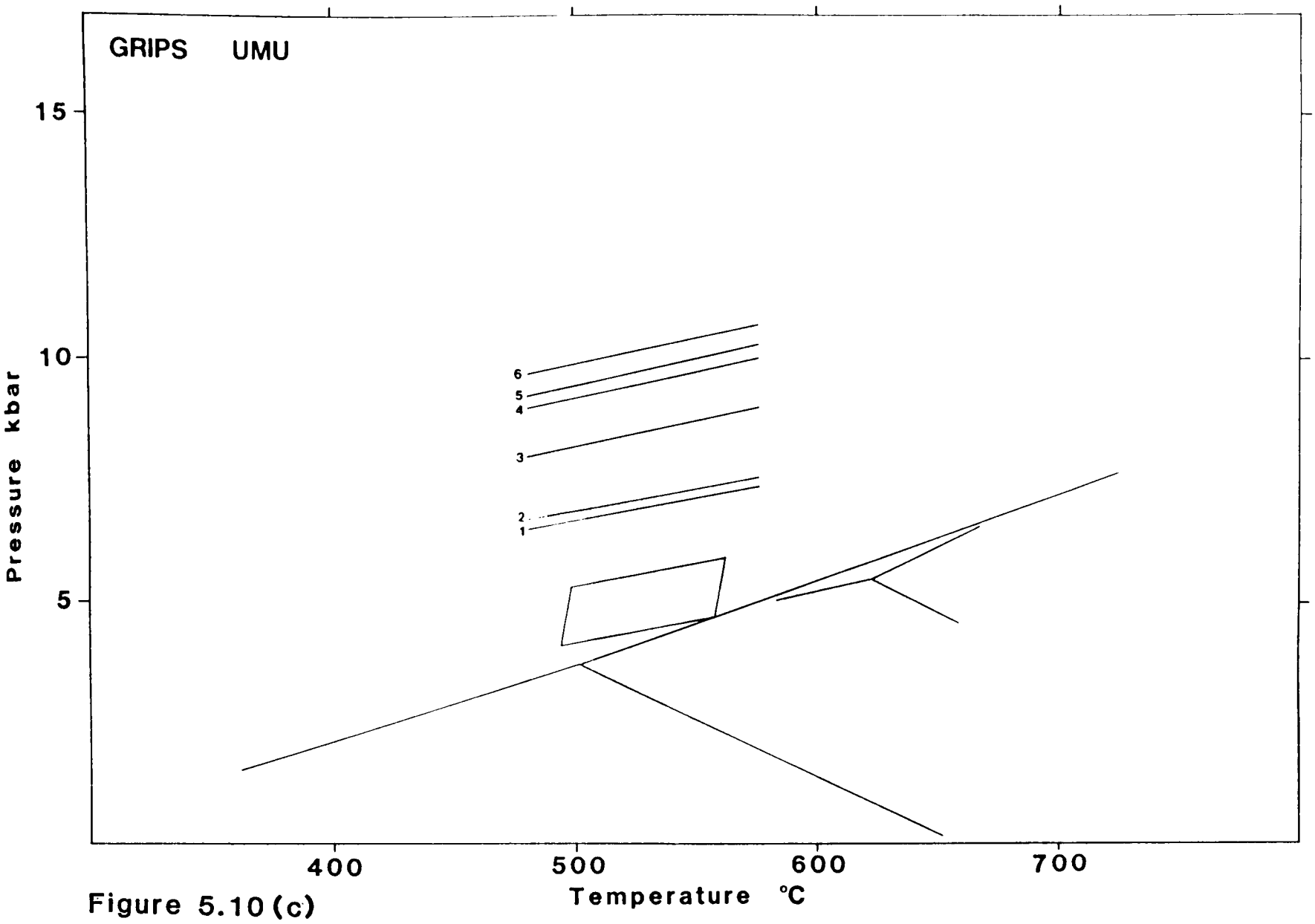
GRIPS UMU
15
10
5
Pressure kbar
6
5
4
3
2
1
400
500
600
700
Temperature °C

Figure 5.10 (c)

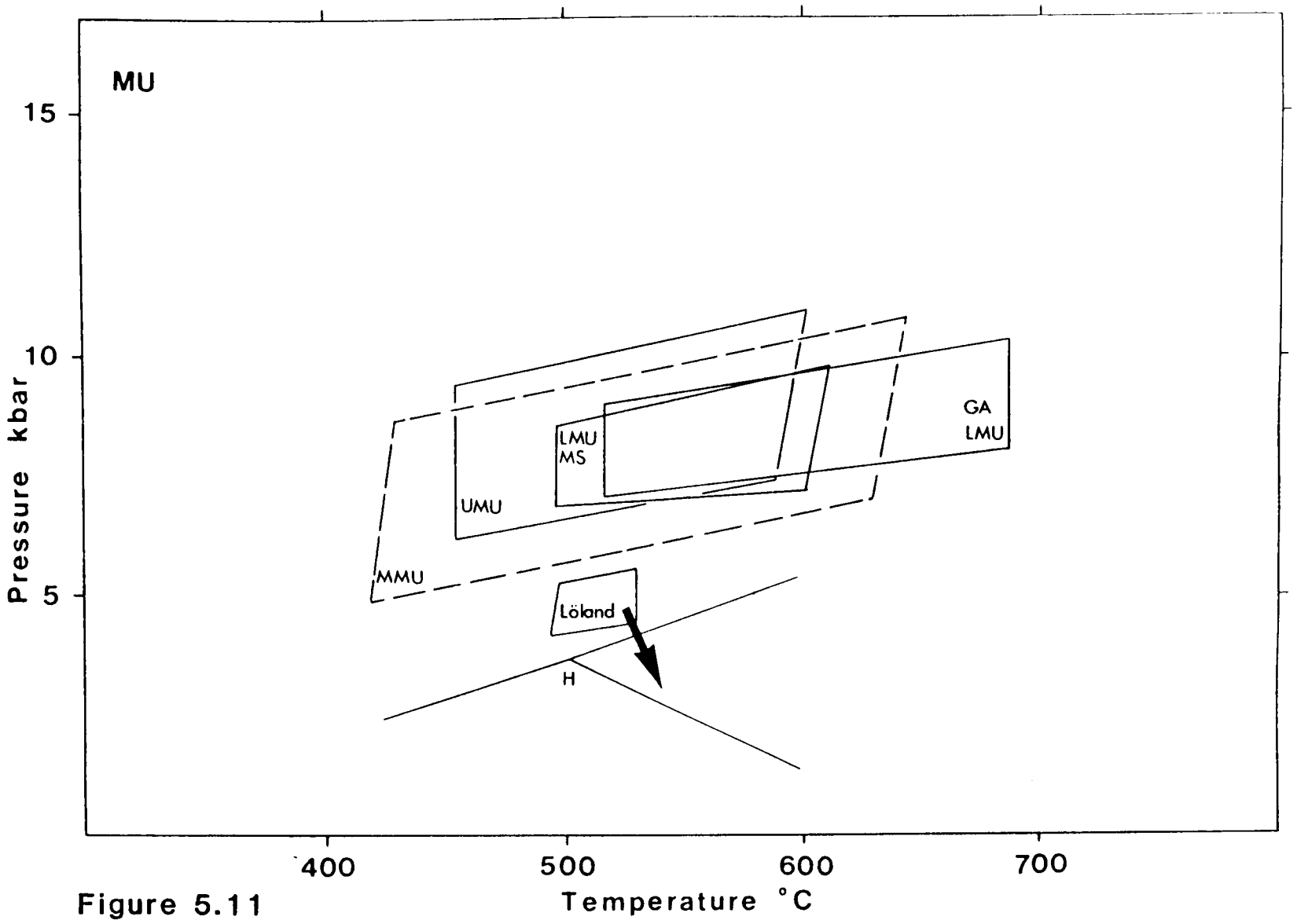

Figure 5.11

Figure 5.11: Summarized P-T plot showing range of estimated temperatures for the different Mafic Units. Boxes show range of P-T conditions calculated from thermobarometers. UMU box is for samples at localities other than Löland (small box at 5 kbar, 500 °C). Most samples give pressure estimates between 5 and 10 kbar, but such estimates are based mainly on the GRIPS barometer, which strictly gives maximum values for most samples (which do not contain rutile. Petrographic studies suggest that the apparently well-constrained P-T conditions recorded at Löland are realistic. The arrow indicates a possible decompression path represented by the breakdown of kyanite to sillimanite in sample K2a. Temperature estimates for all boxes overlap at about 525 °C. Garnet-biotite temperatures calculated by the calibration of Hodges and Spear (1982) are omitted, as are temperatures calculated for some late corona phases in gabbroic rocks which are believed to represent disequilibrium. H=Al_2SiO_5 triple point of Holdaway (1971), MS=mica schists, GA=garnet amphibolites

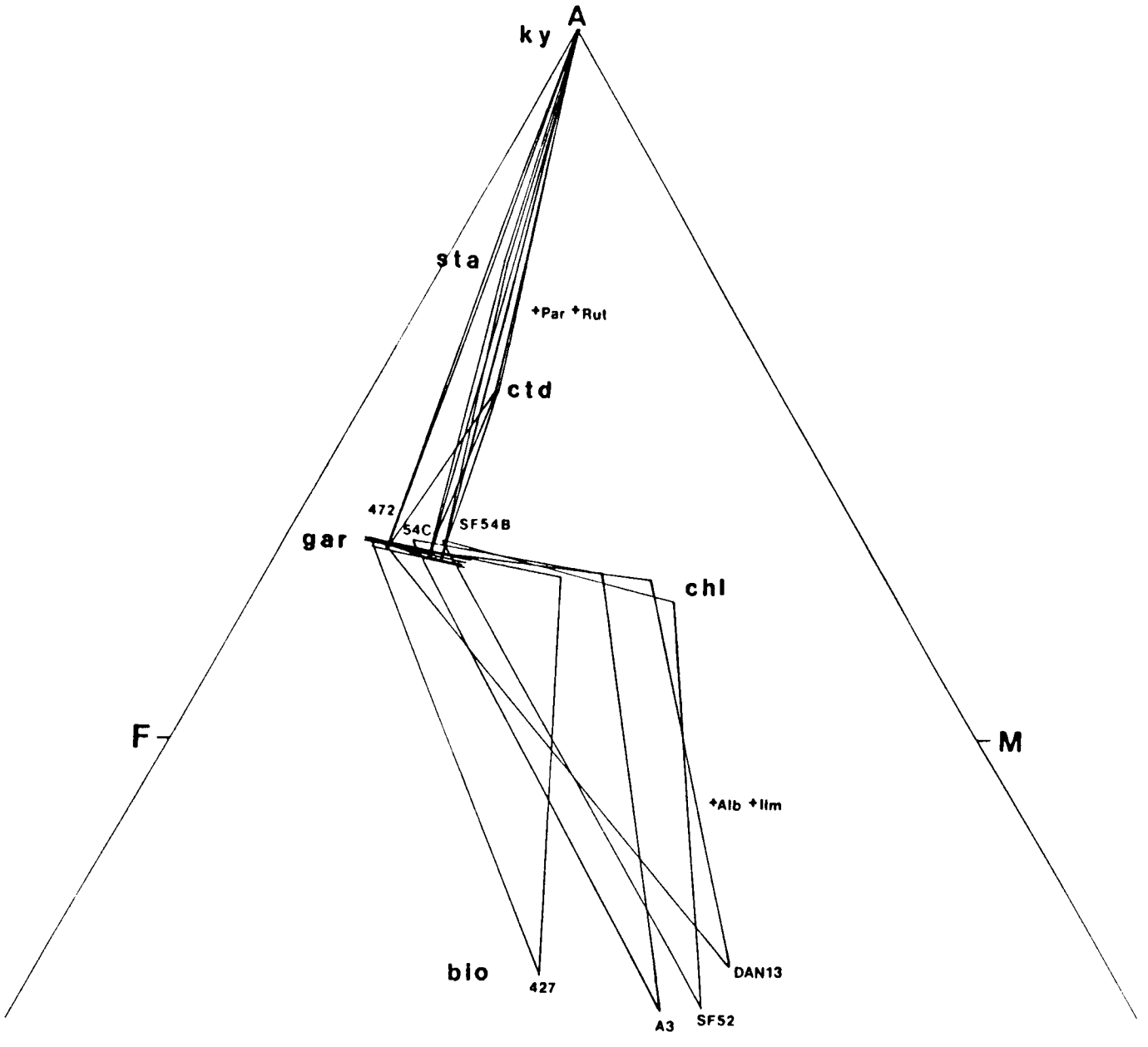

Figure 6.1 (a)

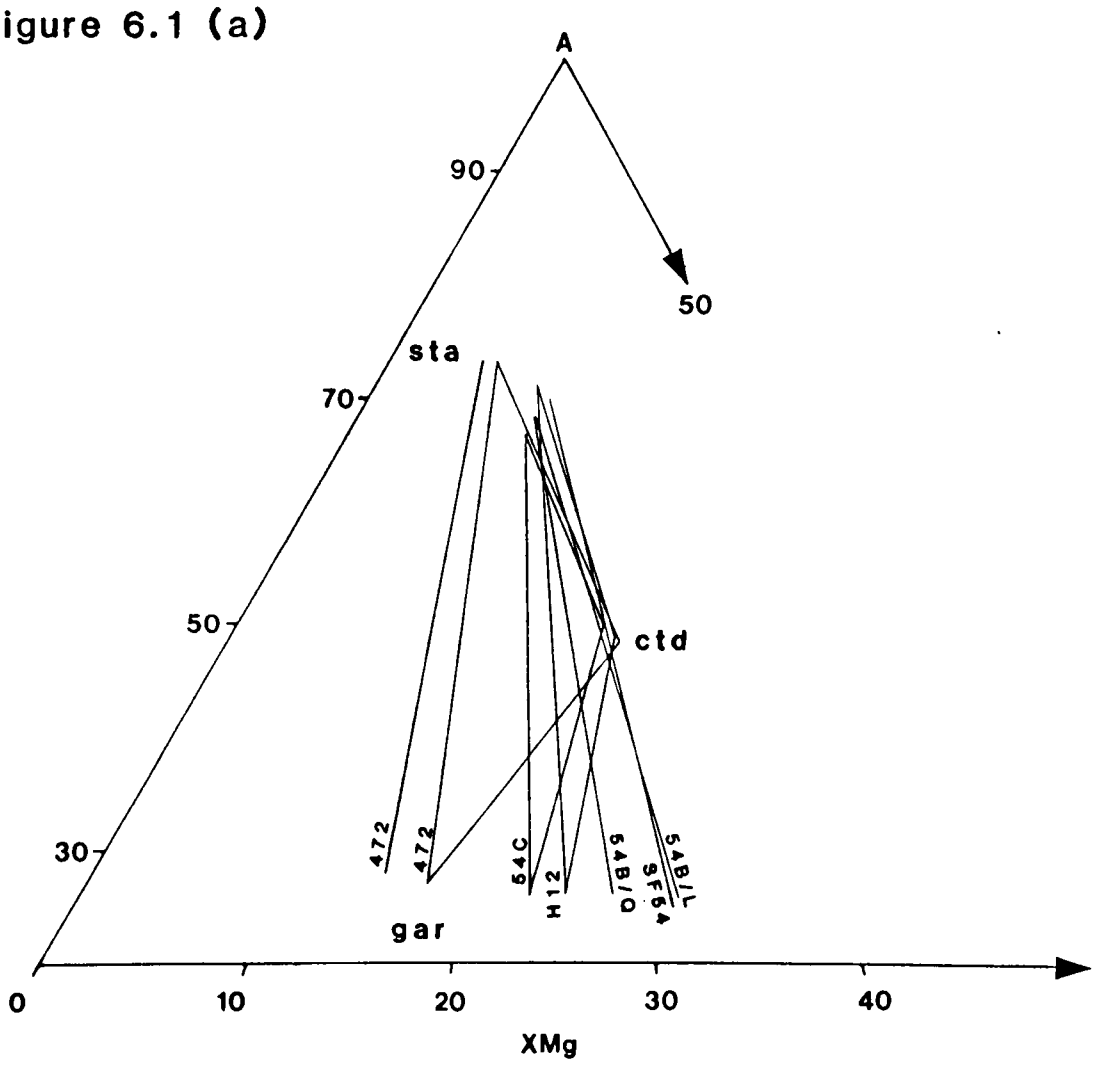

Figure 6.1 (b)

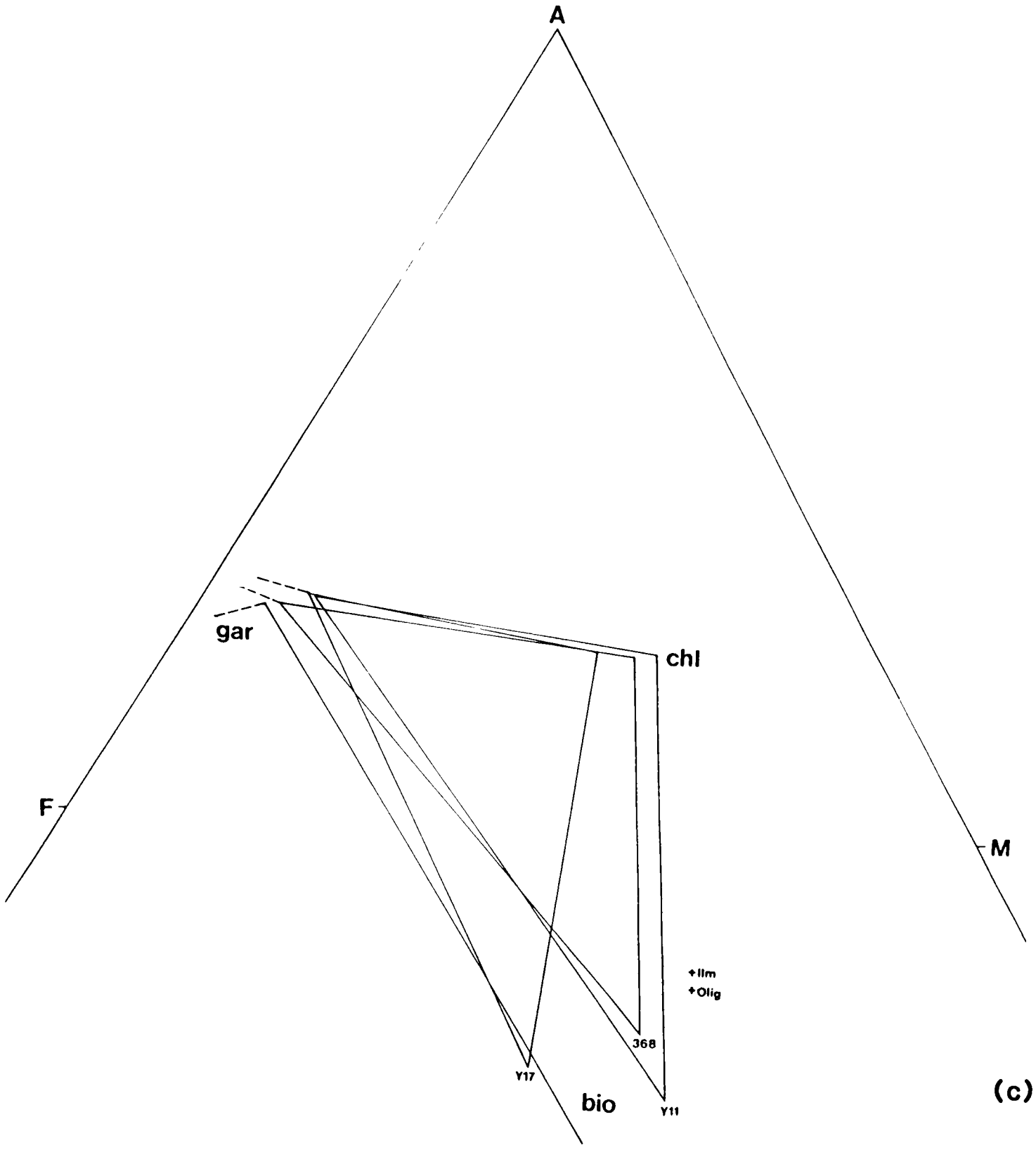

Figure 6.1: Thompson AFM diagram showing assemblages in the Hyllestad schists. All assemblages also include muscovite, quartz, and water. (a) Kyanite-almandine and chlorite-bi-gt schists. A range of garnet compositions is shown representing Fe-rich cores and more magnesian rims. (b) Modified Thompson AFM diagram with expanded FM join, showing compositions of garnet adjacent to staurolite and chloritoid inclusions, as in 6.1a above. Garnet compositions are more magnesian than coexisting staurolites. All rocks also contain kyanite, in some examples it is included in garnet with staurolite, but tie-lines to kyanite are omitted for clarity. (c) Thompson AFM diagram showing compositions of assemblages in schists occurring between Rasvikheia and Espelandsvatnet.

Figure 6.2: Zoning profiles of garnets from various assemblages in the Hyllestad schists. (a) Outline of garnet in sample SF54C, a kyanite-almandine schist from Kleivevatnet, with Mg zoning profiles superimposed. (b) Maps of two garnets in kyanite-almandine schists from Kleivevatnet contoured for XMg. Inclusion relations in one garnet are shown: p=paragonite, k=kyanite, c=chloritoid, s=staurolite. See also figure 6.4. (c) Chemical zoning profiles of Ca, Mg, Mn and Fe^{2+} in garnets from various assemblages from Hyllestad schists.

H16, 472: kyanite-bearing schists; note strong zoning in Mg in 472. For description of inclusion-rich core and "outer zone", see text.

DAN13: garnet-biotite-chlorite schist from Katlenova. Note high core contents of Mn and Ca, and strong zoning in Fe^{2+}.

H18: garnet from amphibole "garbenschiefer", north of Hyllestad. Profile is rather irregular, but core compositions generally lower in Fe and higher in Mn.

R6: garnet-biotite-chlorite schist from Soetevik; compare with DAN13

Y11.2: garnet-biotite schist from Espelandsvatnet, again shows high spessartine component in the core.

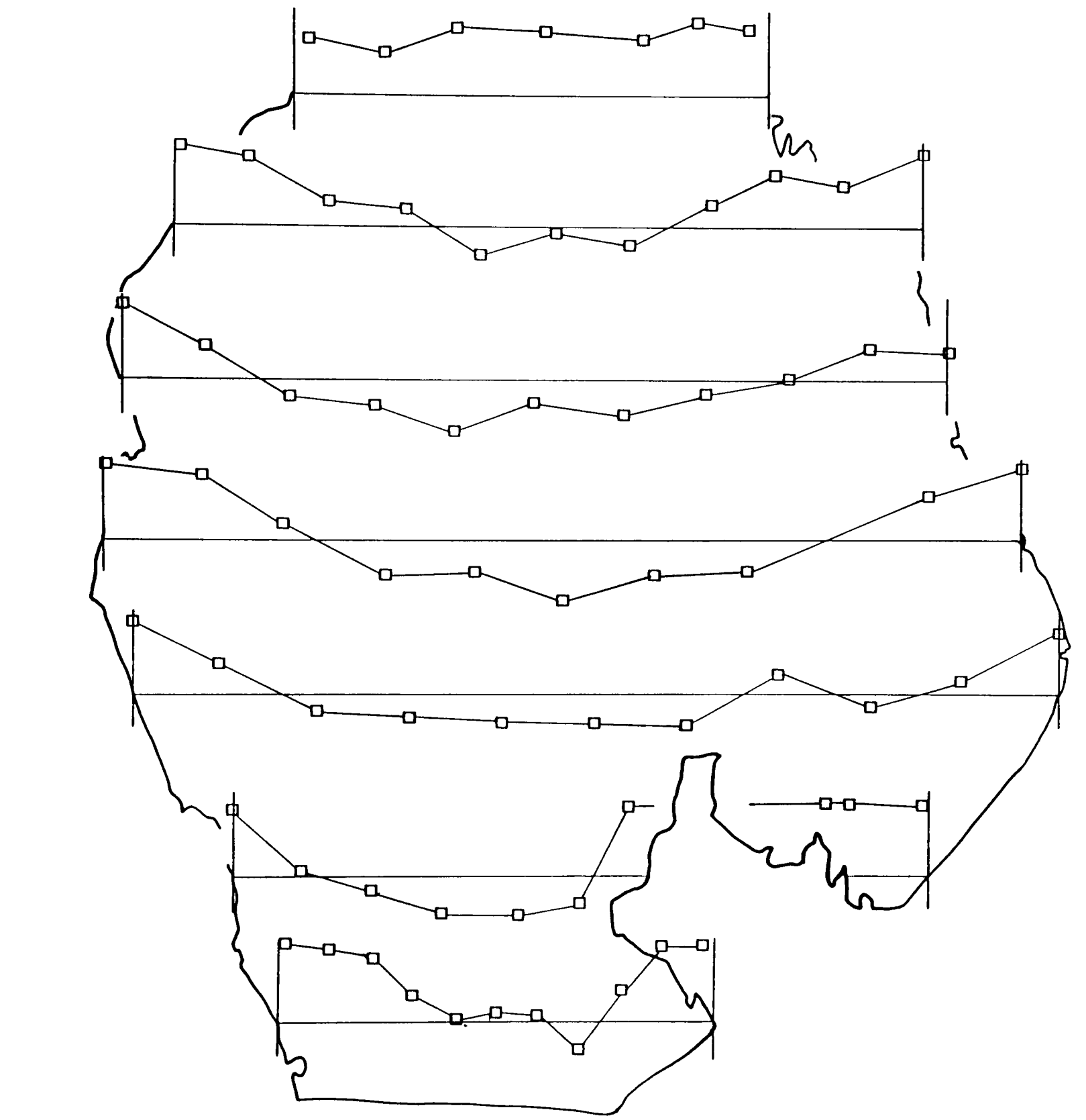

Figure 6.2 (a)

SF54B

$$X_{Mg} = \left[\frac{Mg}{Mg + Fe^{2+}} \right] \times 100$$

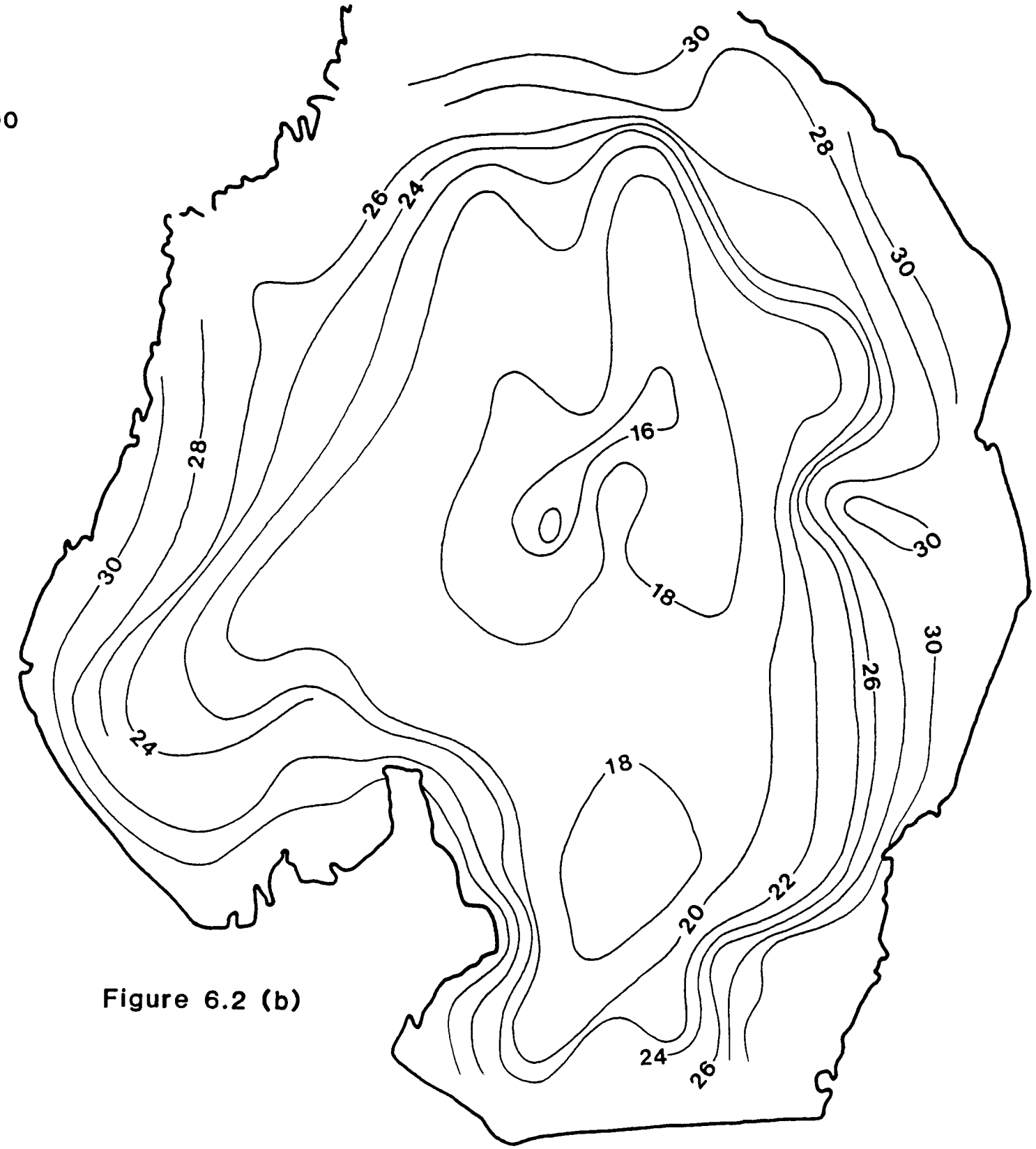

Figure 6.2 (b)

SF54C

$$\left[\frac{Mg}{Mg+Fe^{2+}}\right]\times 100$$

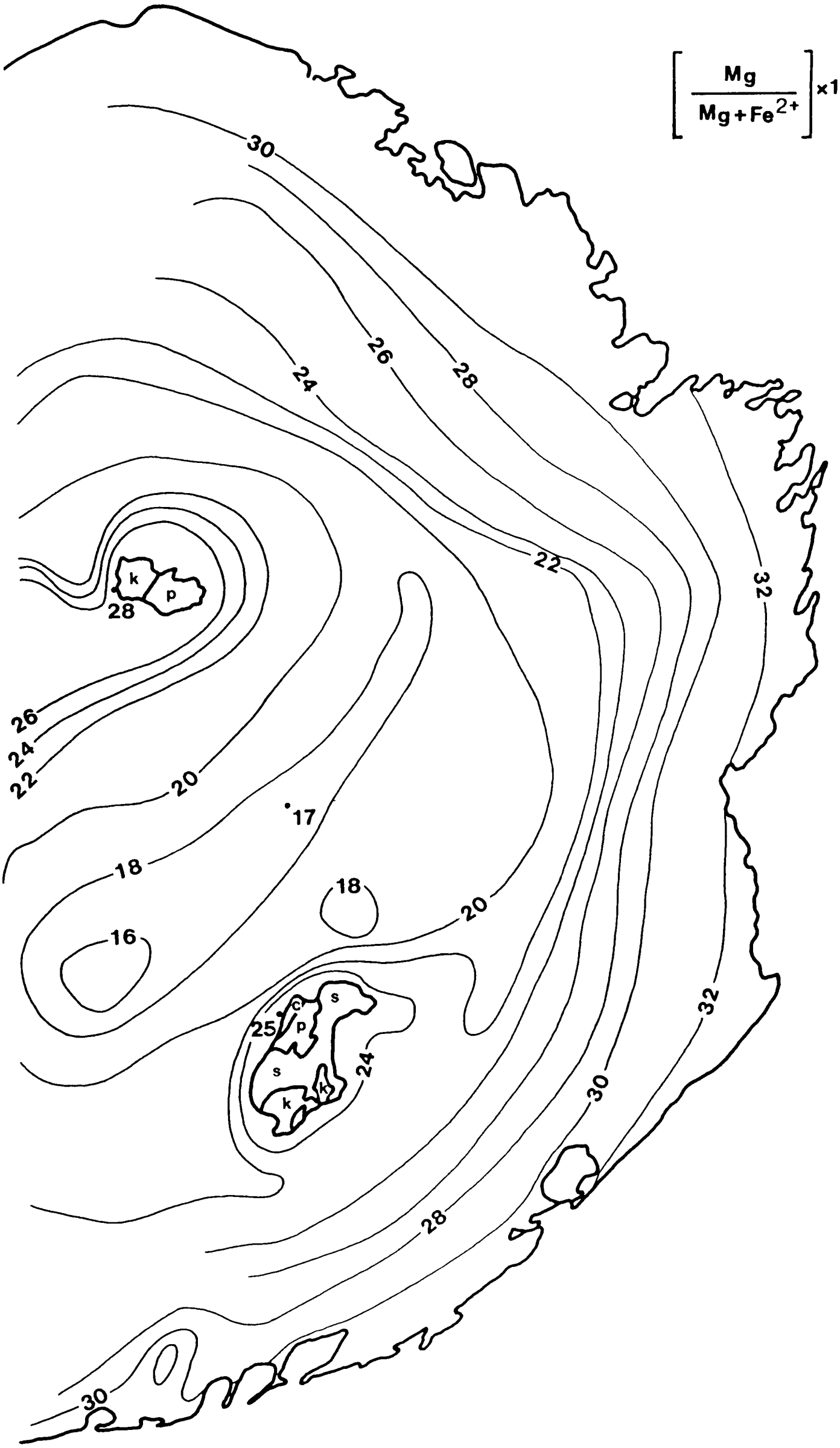

Figure 6.2 (c)

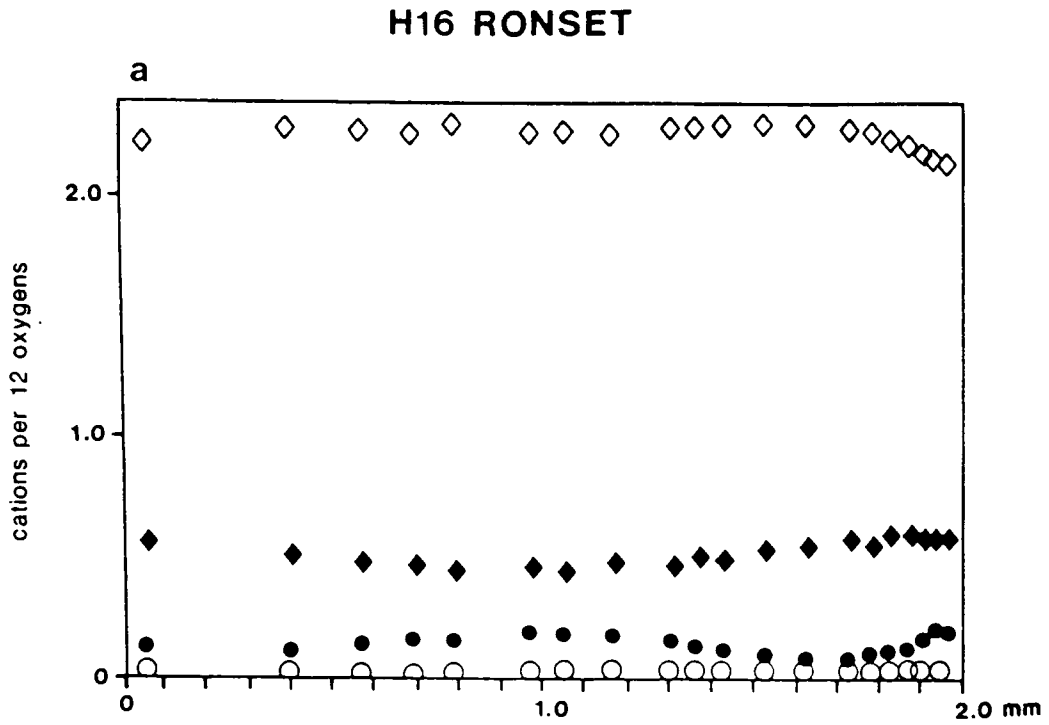

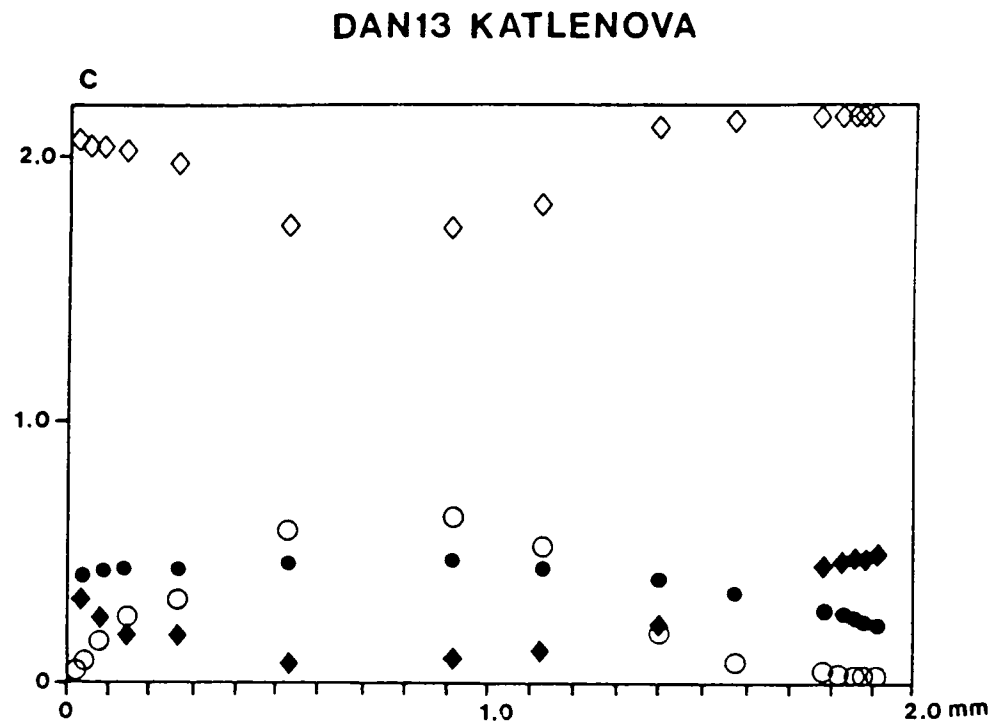

◇ Fe^{2+}

● Ca

◆ Mg

○ Mn

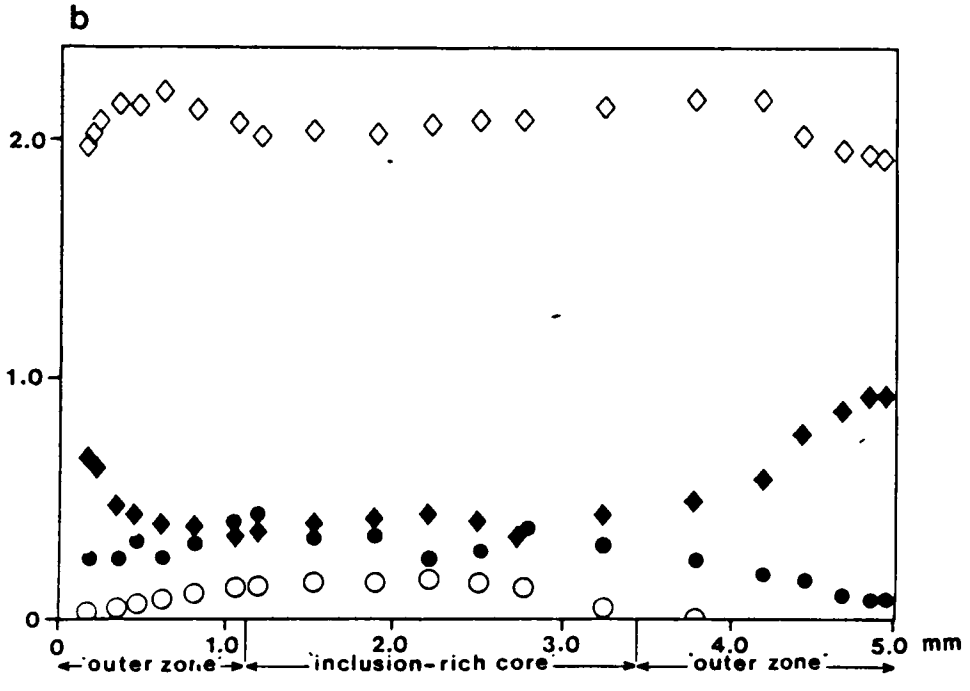

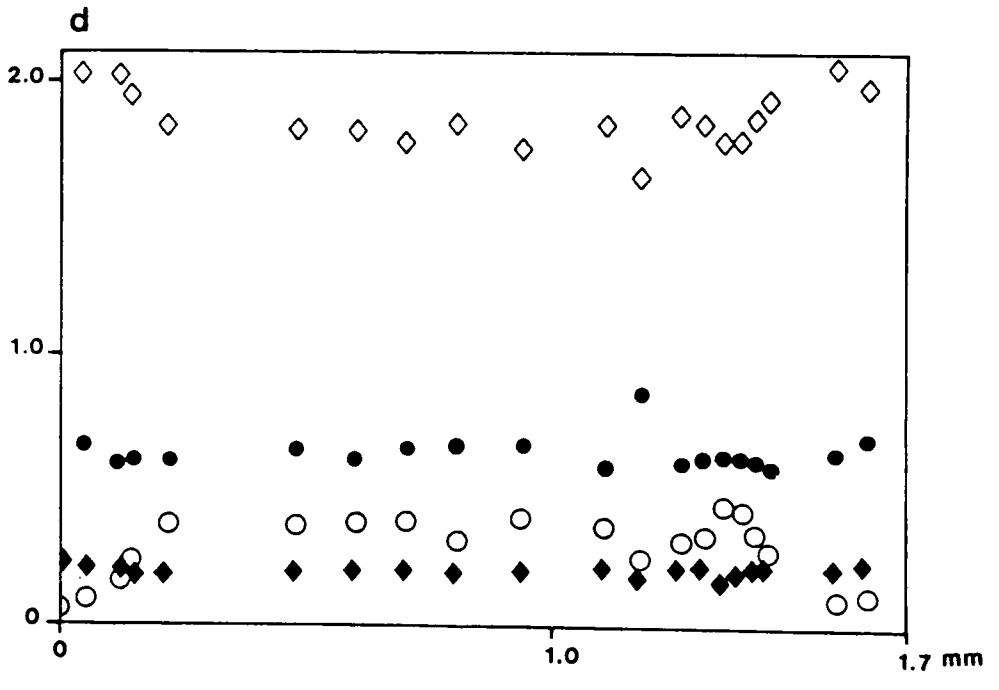

Figure 6.2 (con)

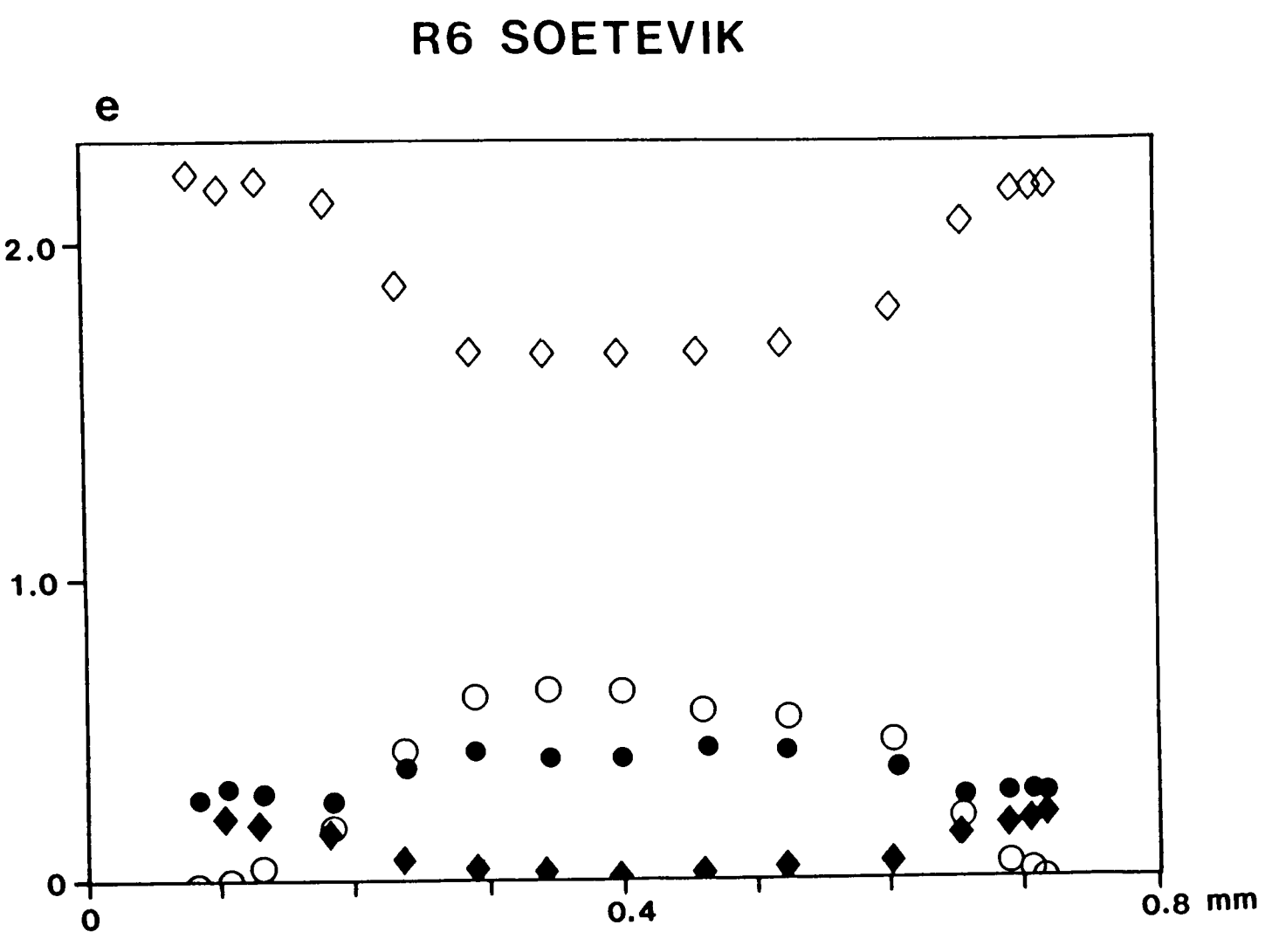

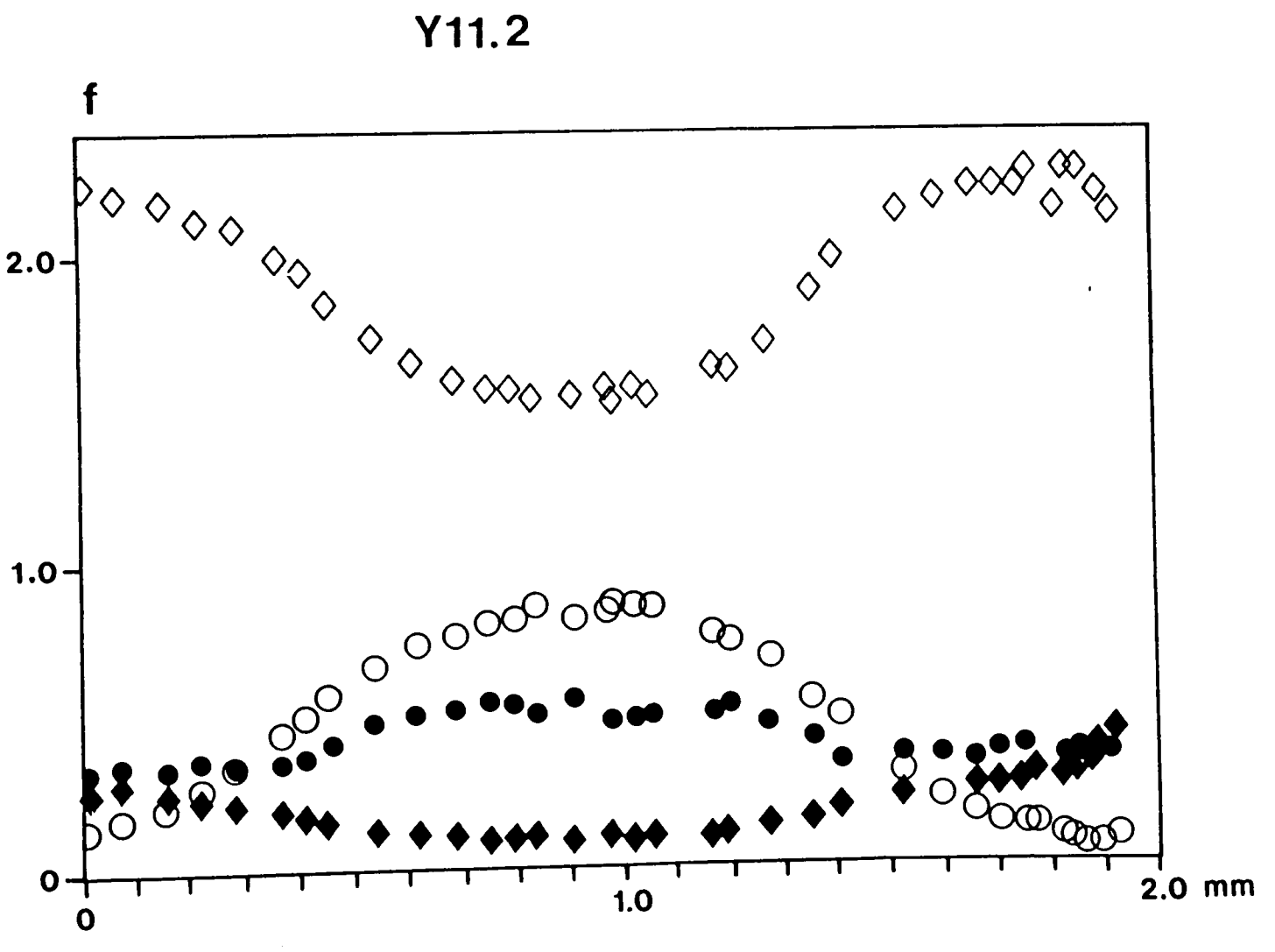

SEQUENTIAL AFM MINERAL FACIES FOR BARROVIAN-TYPE REGIONAL METAMORPHISM.

(N.B. ALL ASSEMBLAGES + MUSC, QZ, H_2O.)

L. GT ZONE

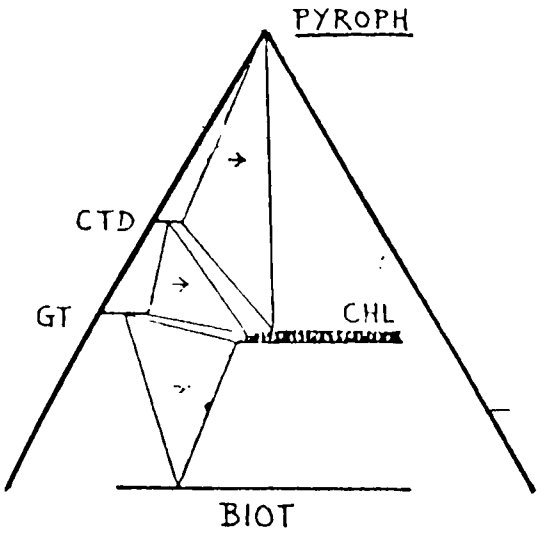

L. GT ZONE

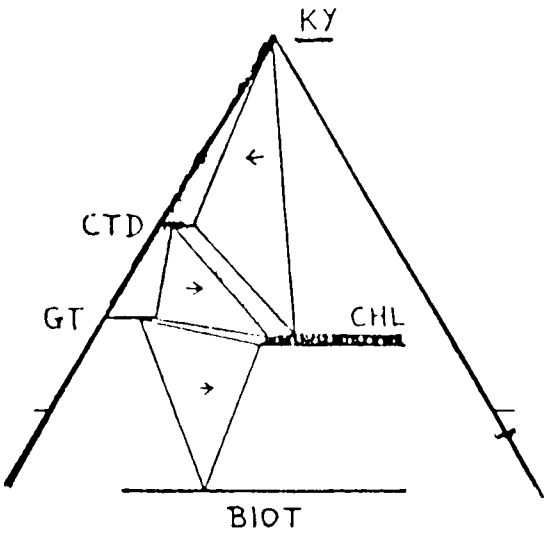

M. GT ZONE

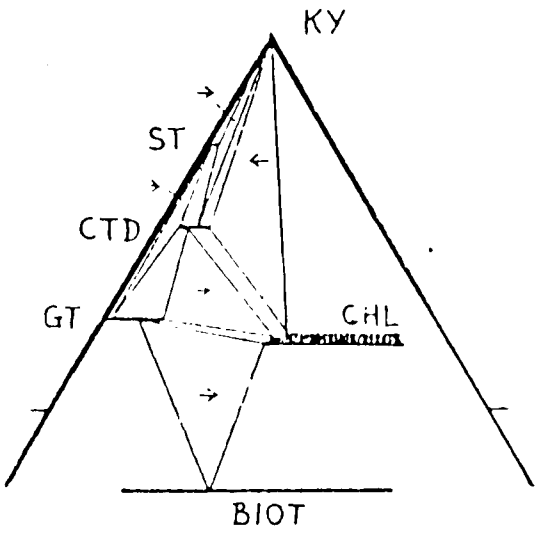

U. GT ZONE

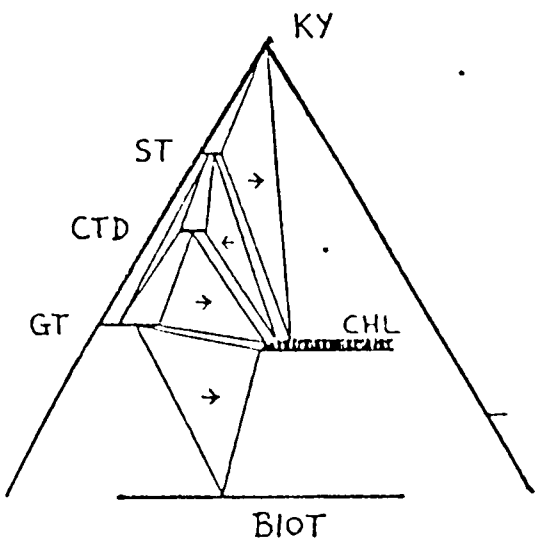

U. GT ZONE

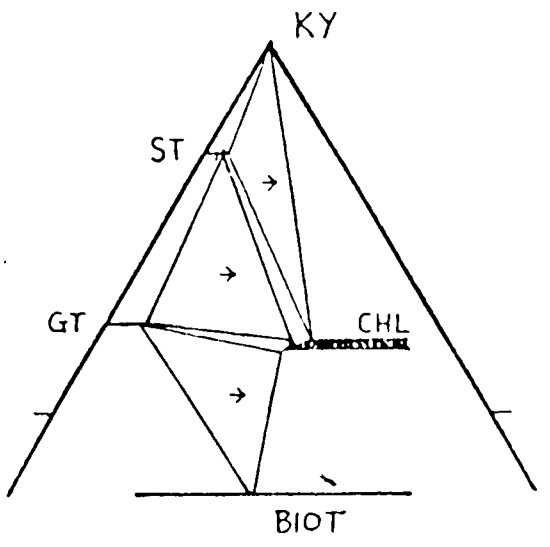

ST ZONE

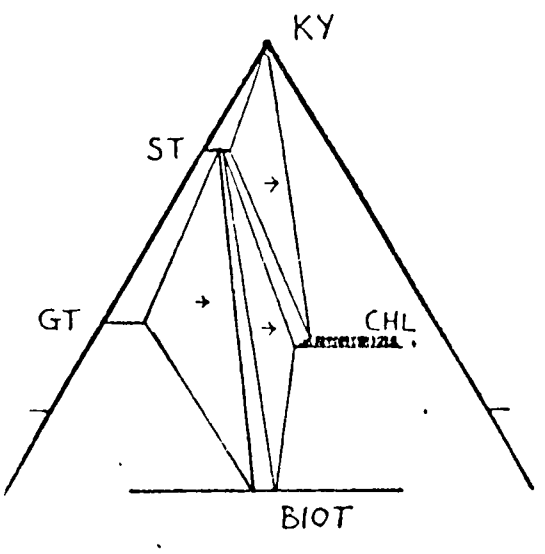

L. KY ZONE

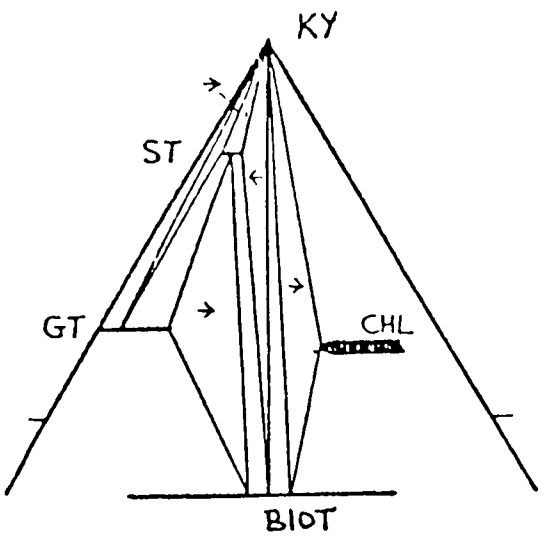

U. KY ZONE

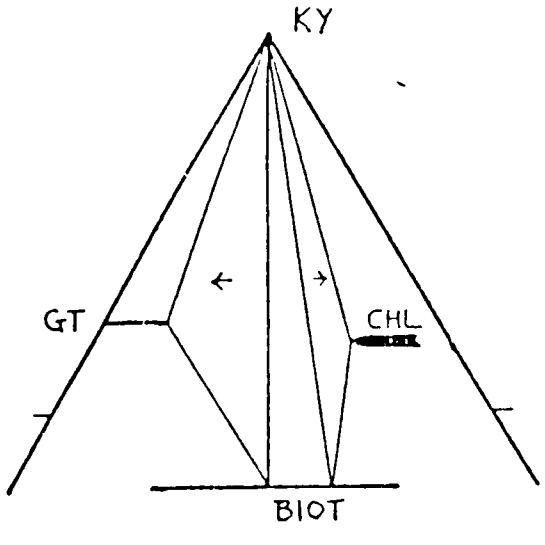

L. SILL ZONE

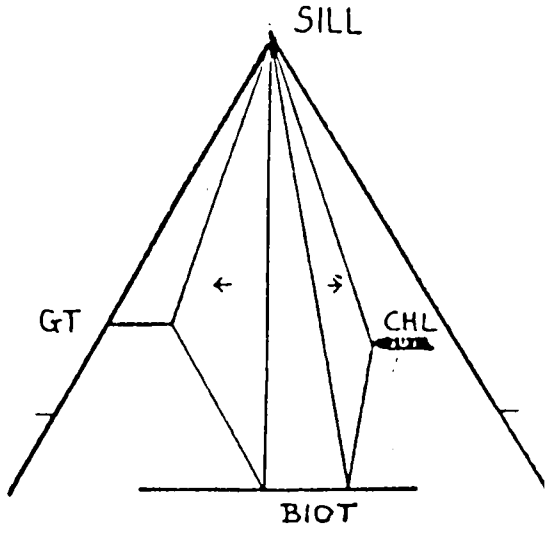

Figure 6.3 Sequential Barrovian assemblages shown on Thompson AFM plots for Dalradian of Scotland (after G.T.R. Droop, pers comm. 1983)

Figure 6.4: Inclusions in garnets from Kleivevatnet (kyanite-garnet schists)

a) DIGIMAP analysis contoured for Al (high values: yellow/red/white, low values: black/blue/green) showing replacement of staurolite inclusion by kyanite. Also visible are paragonite and quartz inclusions. Field of view approximately 2mm. Interpretation of DIGIMAP also shown: Qz=quartz, Gt=garnet, St=staurolite, Ky=kyanite, Chl=chlorite, Pa=paragonite.

b) Photomicrograph of garnet from SF54C showing quartz inclusion-rich core and idioblastic rim. Field of view approximately 9mm.

Figure 6.4 (a)

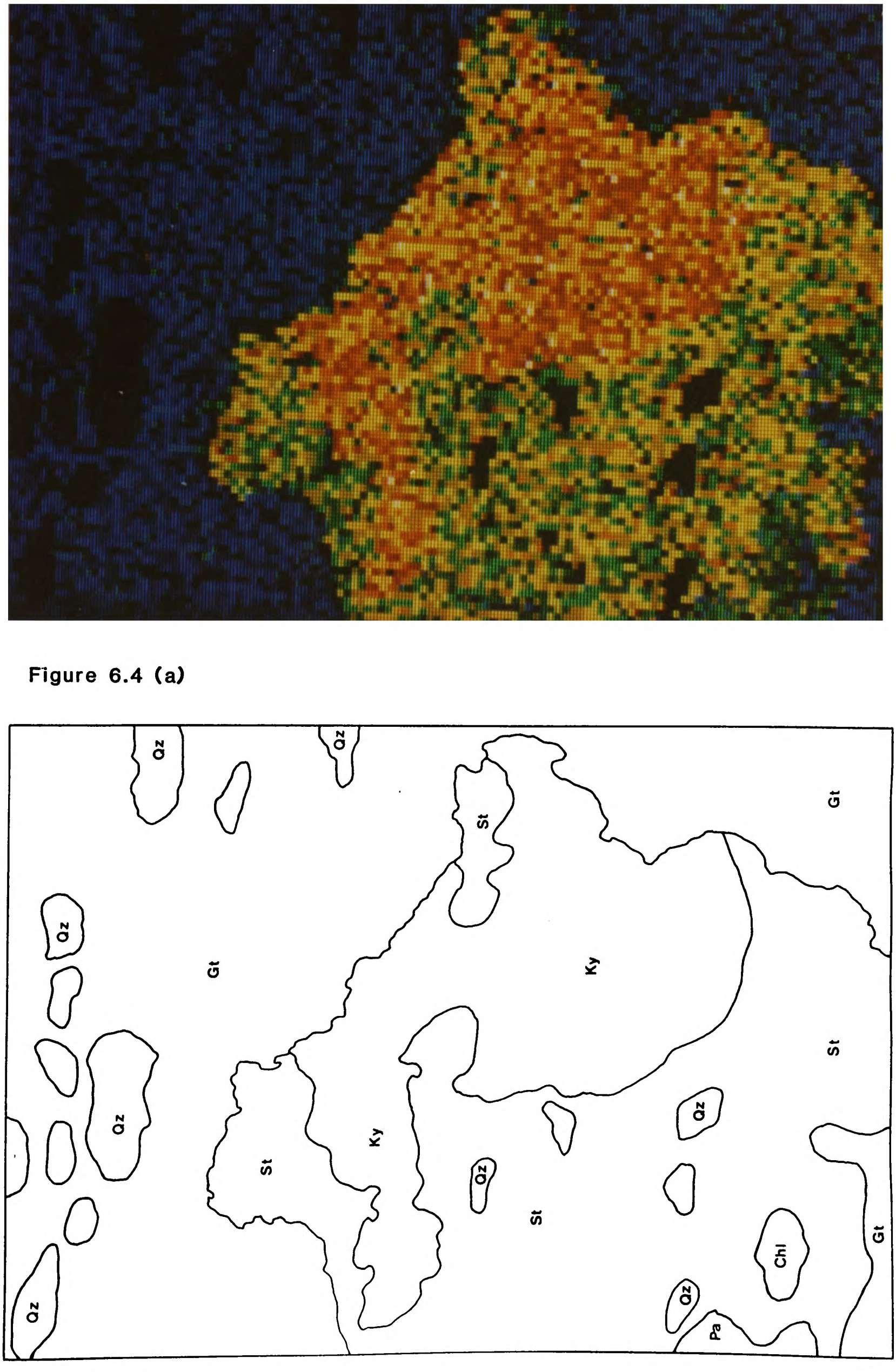

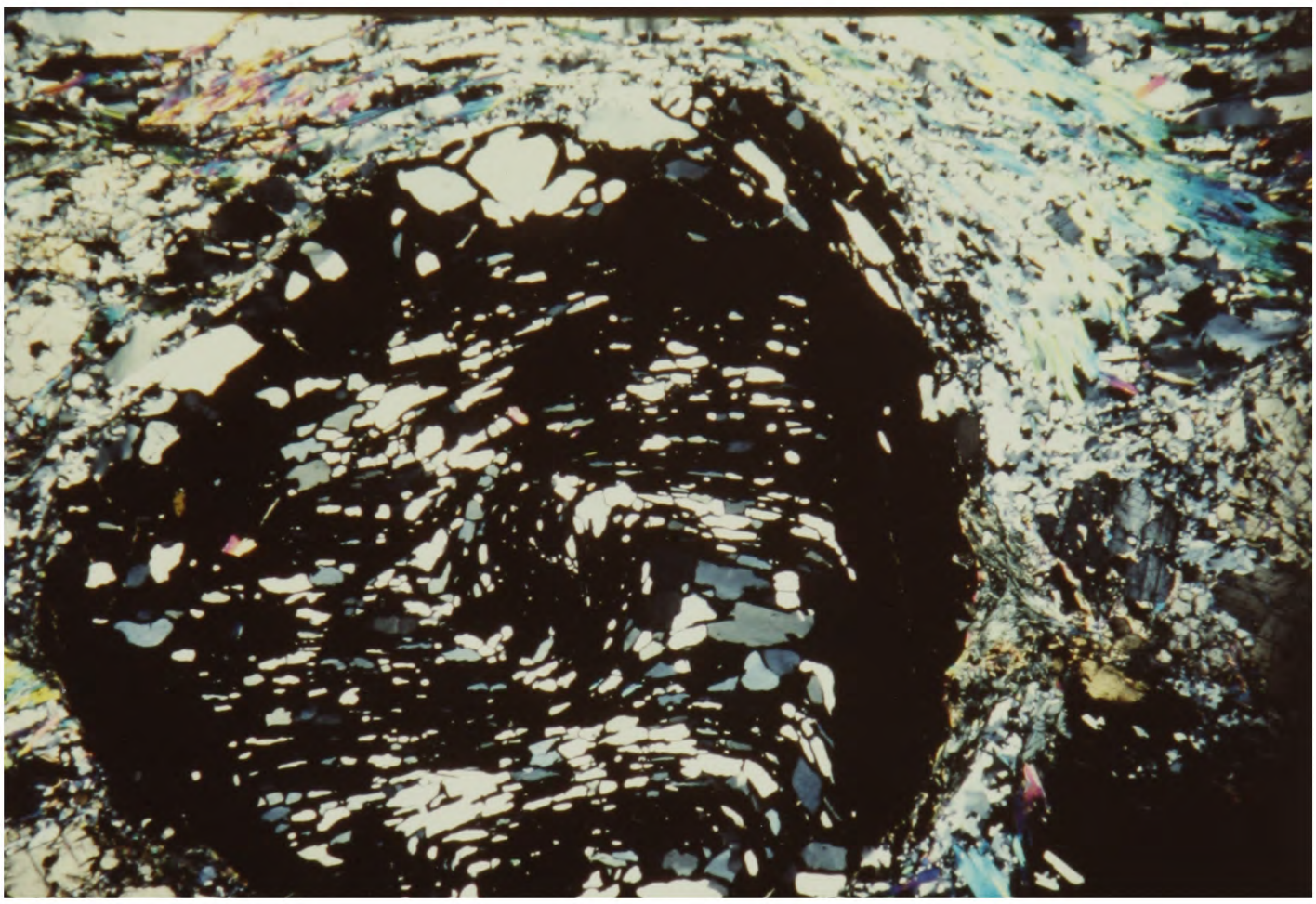

Figure 6.4 (b)

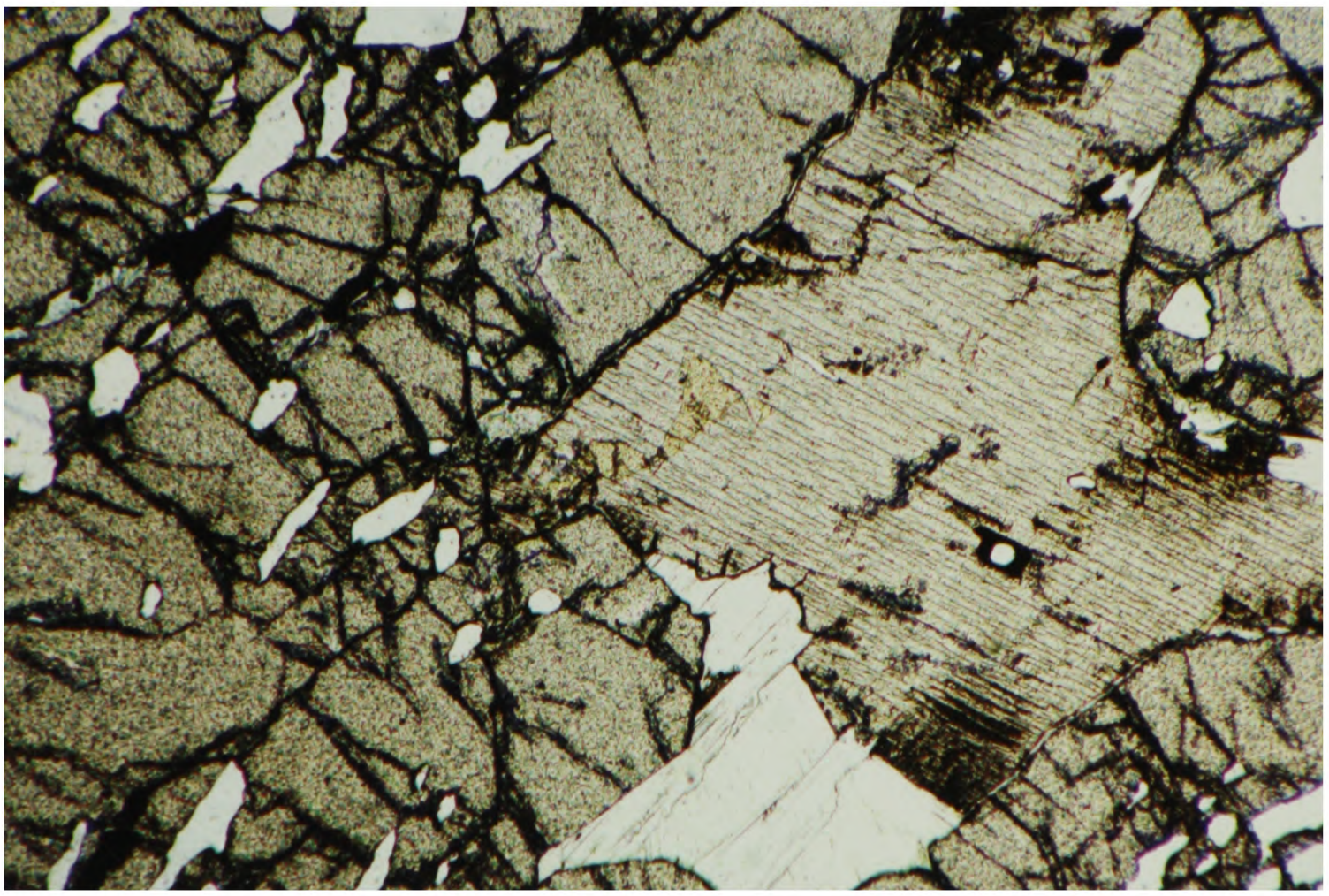

Figure 6.5 Photomicrograph in ppl of sample SF54B showing patchy replacement of staurolite (centre) by kyanite inclusion (large grain to right, with good cleavage) in garnet (most of left of photo). Quartz inclusions occur in garnet to the left. Paragonite occupies an area below the kyanite inclusion. A small amount of late chlorite and magnetite can be seen at upper left. Field of view about 9mm.

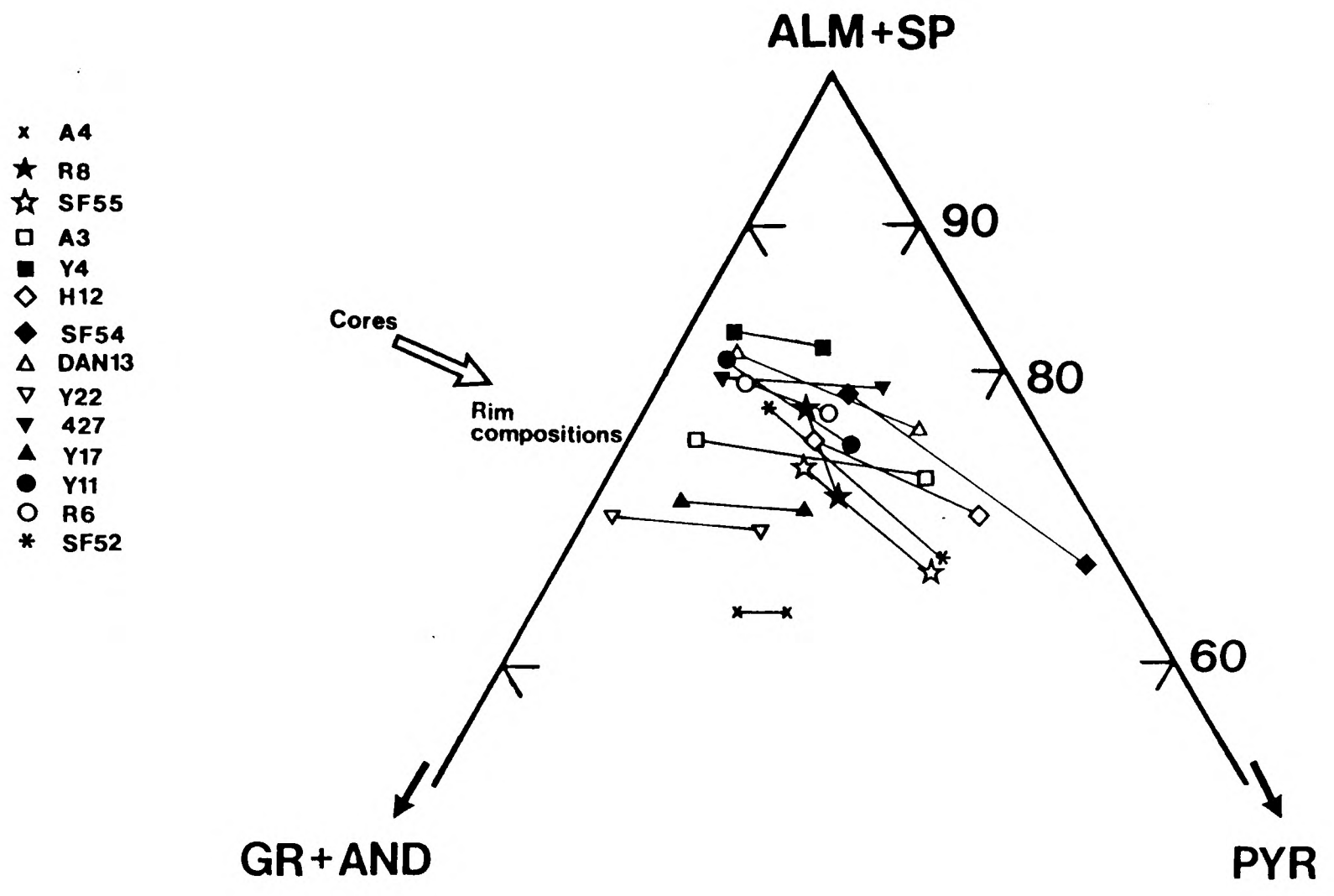

Figure 6.6 Pyrope-almandine-grossular plot of garnets from various assemblages in Hyllestad Schists. Core and rim compositions are given. Mineral assemblages of samples listed are shown in table 6.1

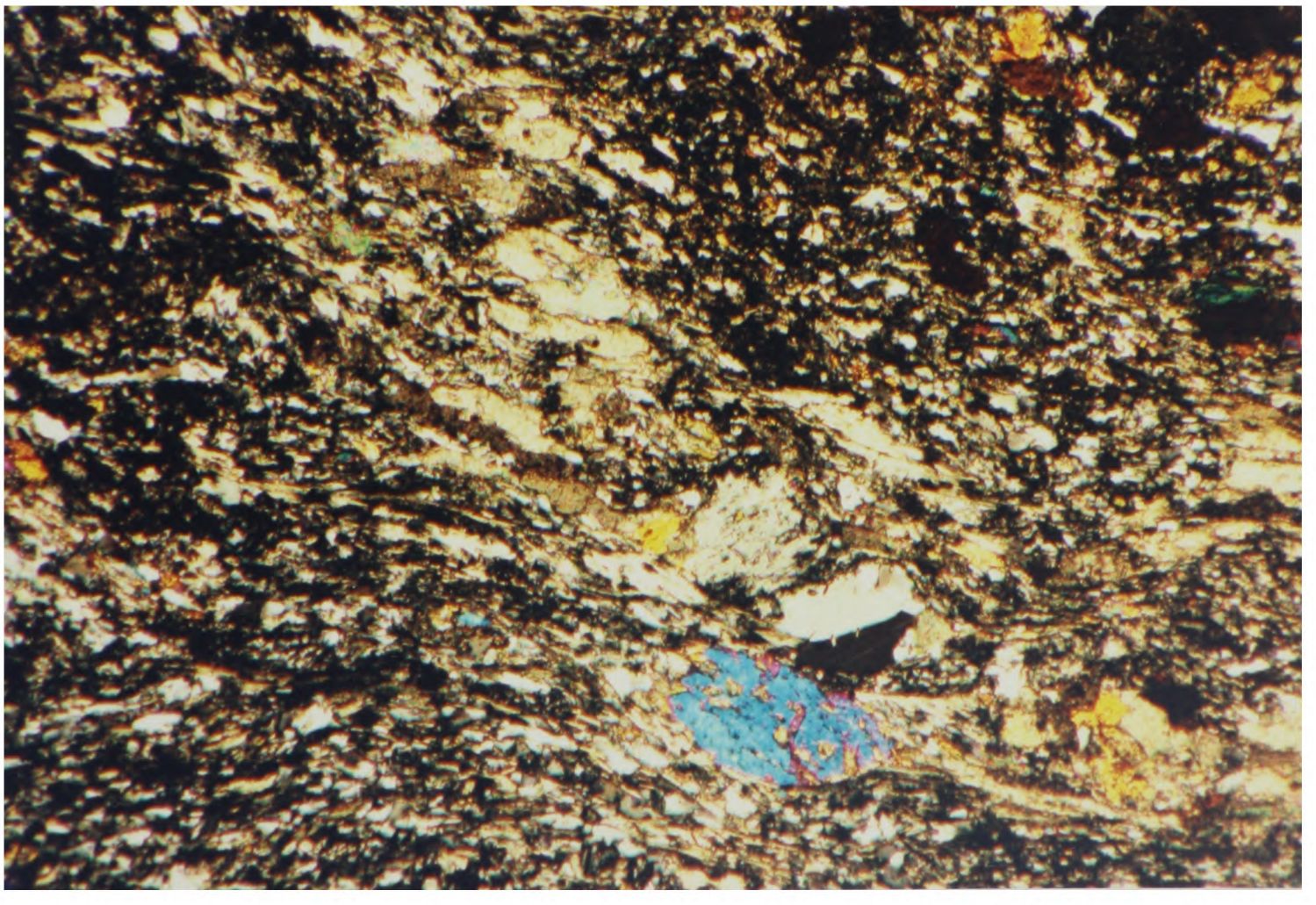

Figure 6.7: Photomicrograph of sheared carbonate rock in boudin necks in sample H10 from Soetevik, showing chlorite replacing tremolite-bearing assemblages. Field of view 9mm.

Figure 6.8: Amphibole compositions from rocks in Hyllestad area. A4: mafic garnet amphibolite from Hyllestad. H17 and H18: garbenschiefer from north of Hyllestad. Y13 and Y22: amphibole-bearing schists from Espelandsvatnet. SF55: garbenschiefer from Kleivevatnet. SF48: chloritoid-garnet-amphibole-bearing schist from Soetevik. See figure 4.16 for abbreviations.

Figure 6.8

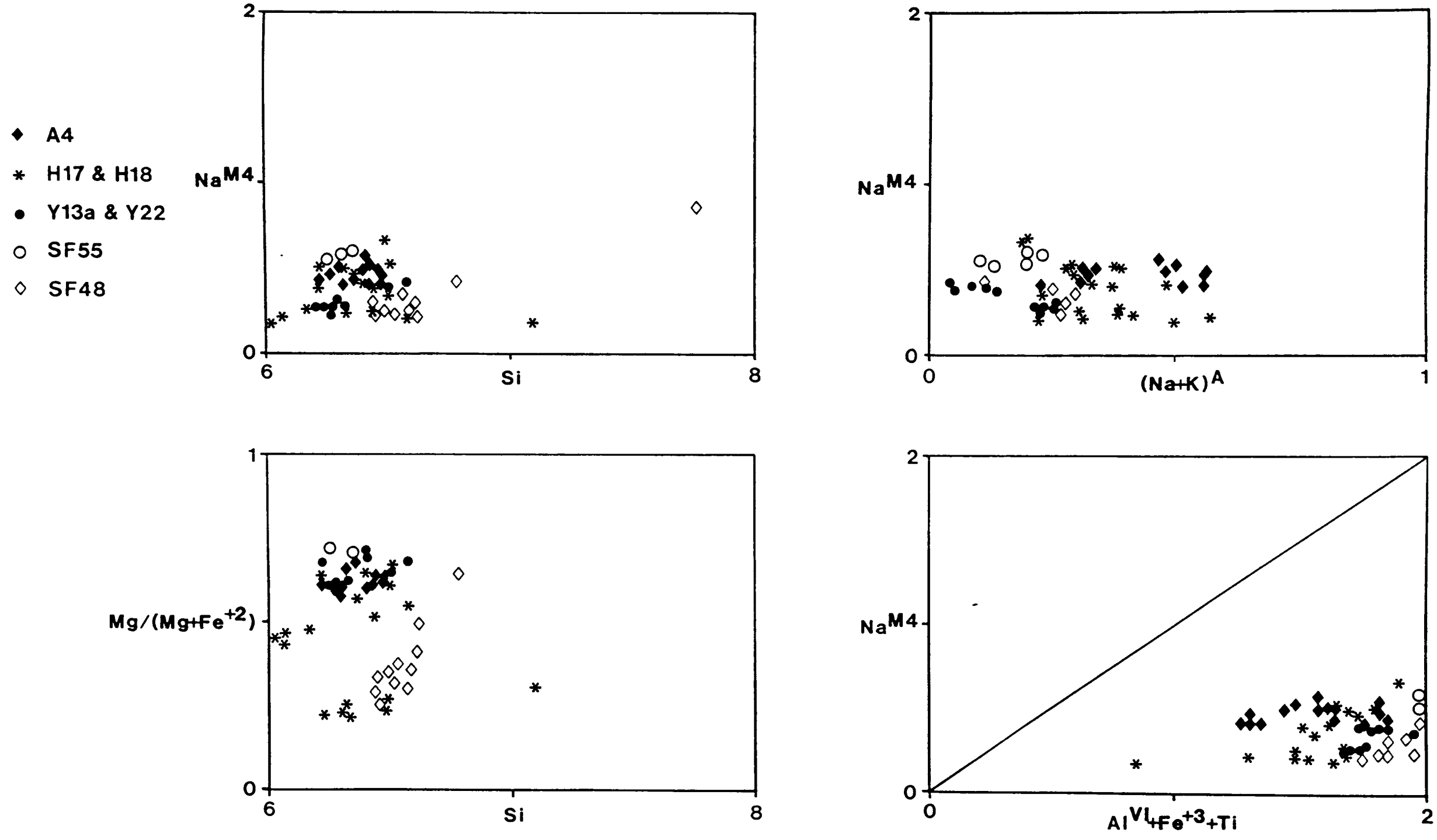
A4
H17 & H18
Y13a & Y22
SF55
SF48
Na^{M4}
2
0
6
Si
8
$(Na+K)^{A}$
1
$Mg/(Mg+Fe^{+2})$
$Al^{VI}+Fe^{+3}+Ti$

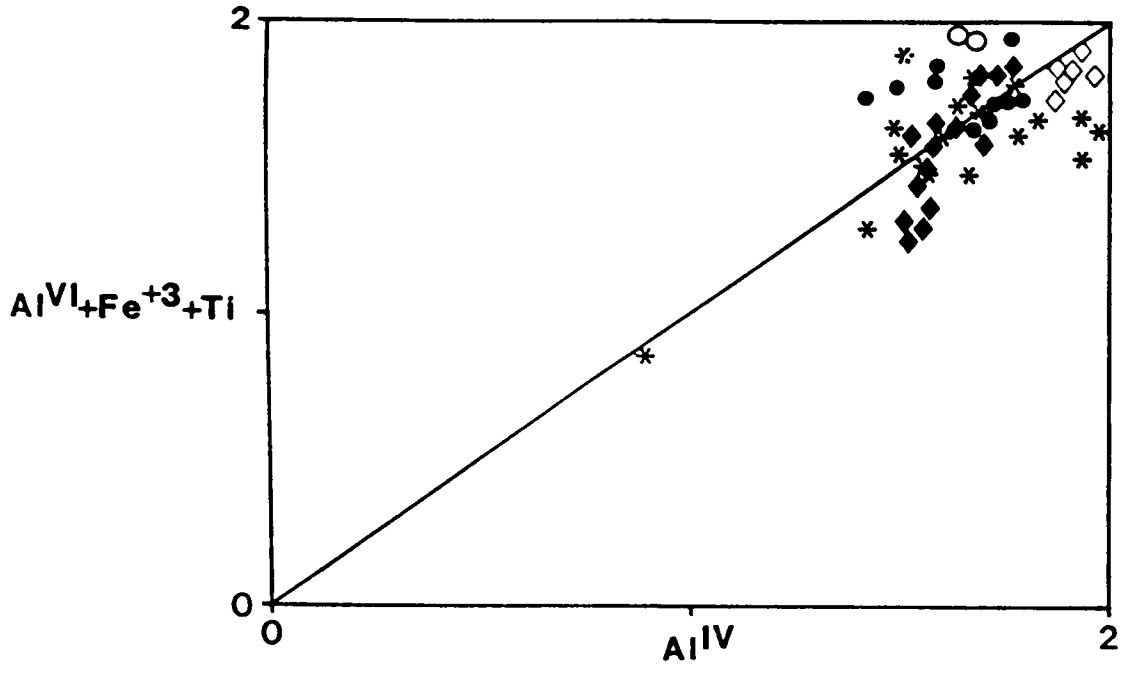
2
0
0
2
$Al^{VI}+Fe^{+3}+Ti$
Al^{IV}

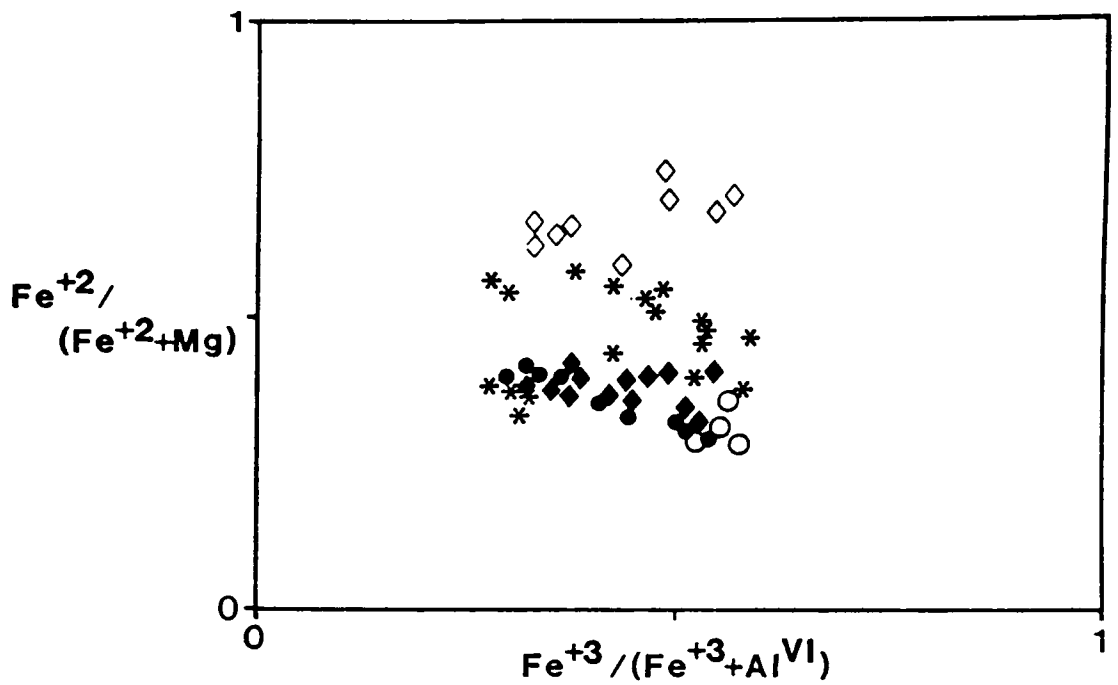
1
0
0
1
$Fe^{+2}/(Fe^{+2}+Mg)$
$Fe^{+3}/(Fe^{+3}+Al^{VI})$

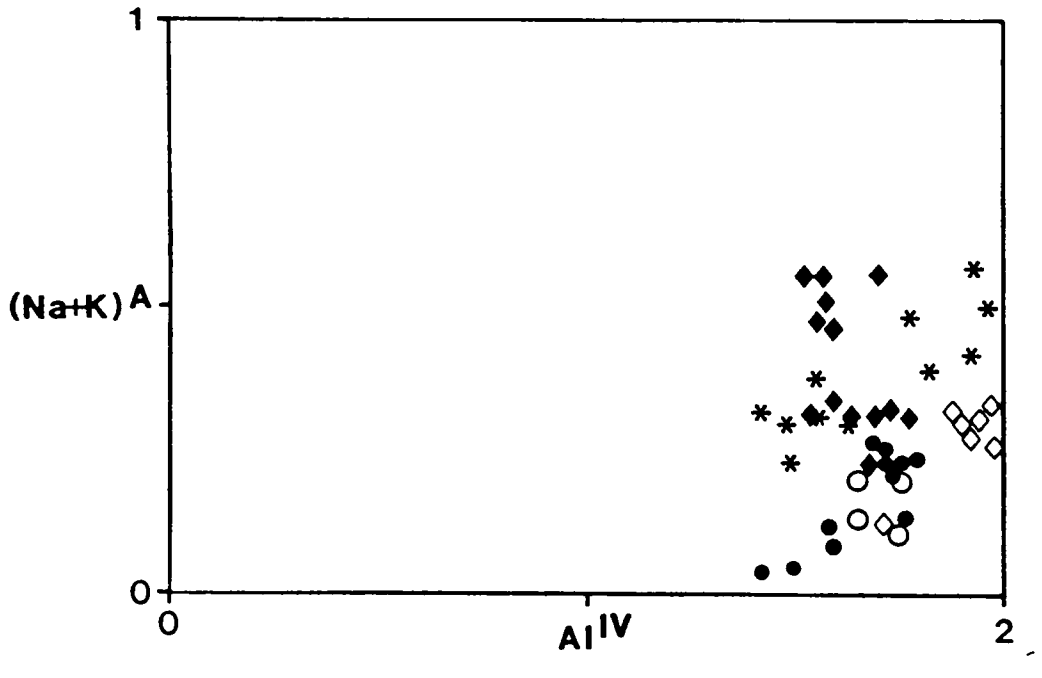
1
0
0
2
$(Na+K)^{A}$
Al^{IV}

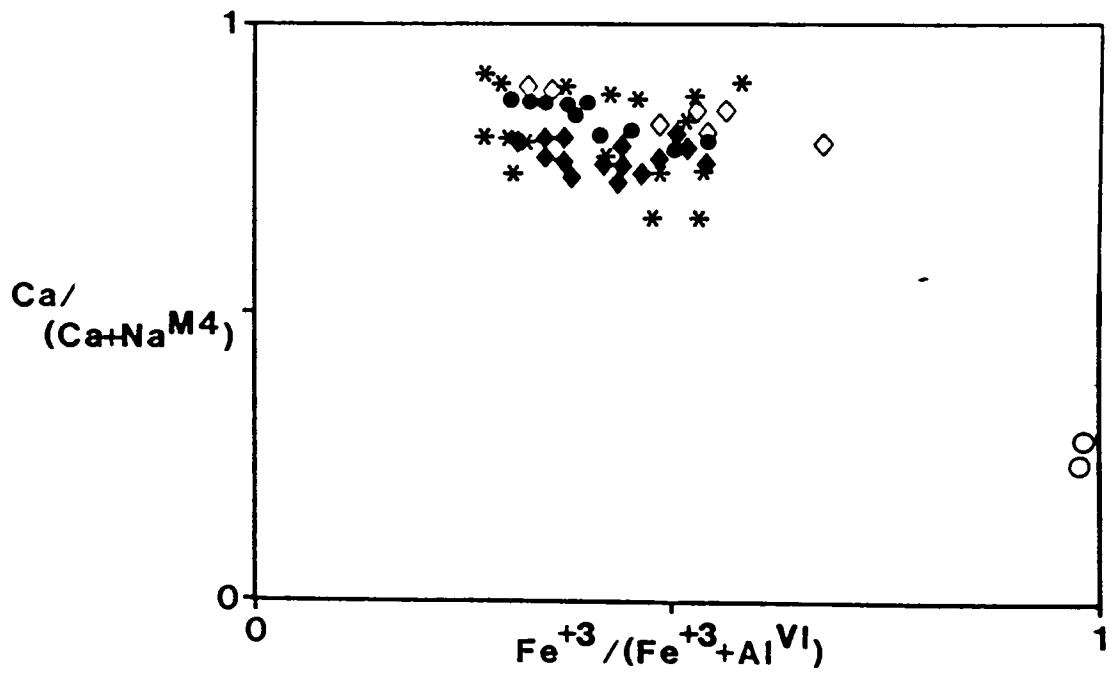
1
0
0
1
$Ca/(Ca+Na^{M4})$
$Fe^{+3}/(Fe^{+3}+Al^{VI})$

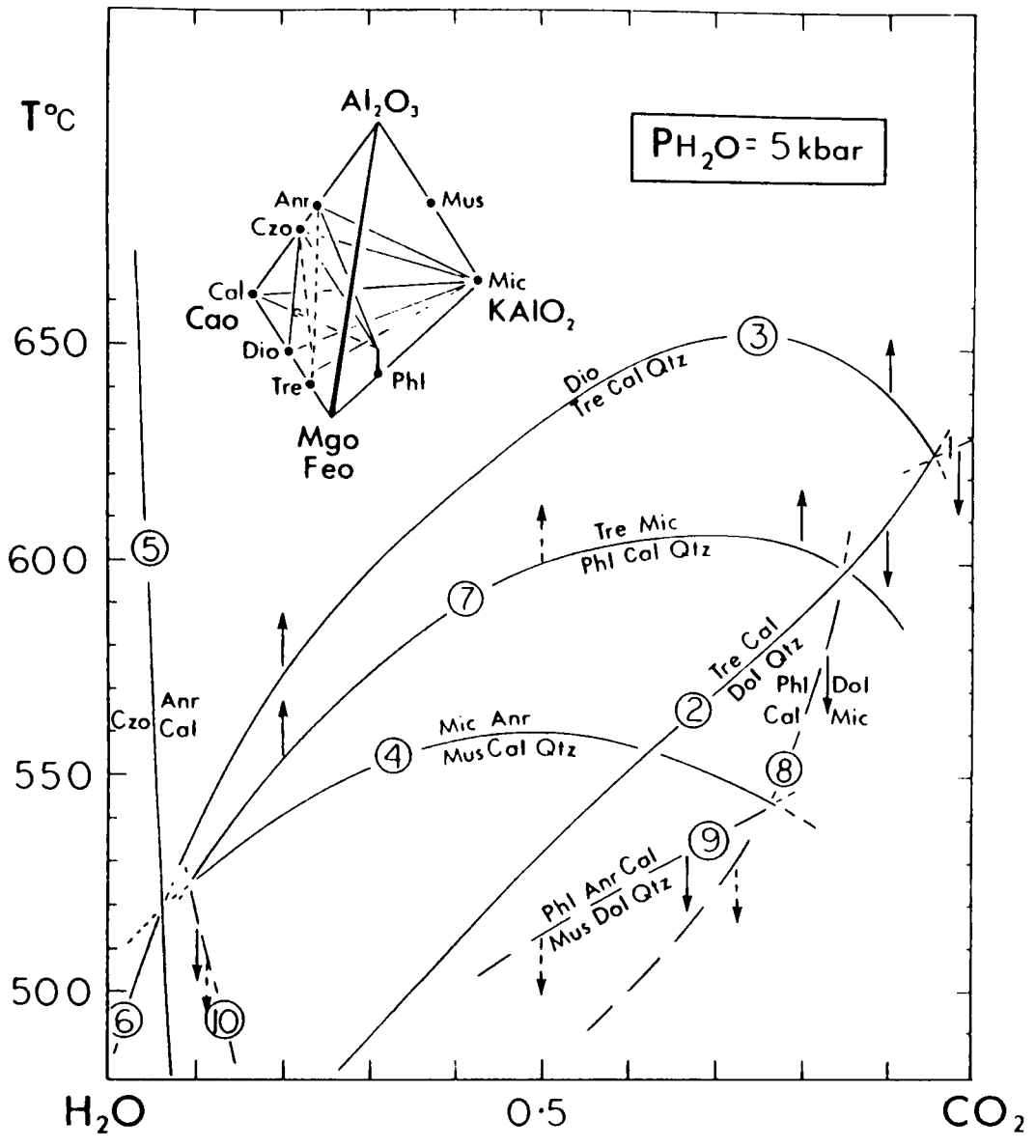

Figure 6.9: T-X(H_2O-CO_2) diagram for some equilibria in the CaO-$KAlO_2$-MgO-Al_2O_3-SiO_2-CO_2-H_2O at 5 kbar, from Thompson (1975) demonstrating temperature limit for carbonates from Kleivevatnet.

Figure 6.10: Selected thermobarometric results for schists from Kleivevatnet, Hyllestad, and Ronset. Also shown are invariant points from grid of Vuichard and Ballèvre (1988) and Al_2SiO_5 triple points of Holdaway (1971) (H) and Richardson et al (1969) (R). The heavy line indicates a P-T-t path calculated for a garnet-chlorite-biotite schist (sample SF52) using the method of Spear and Selverstone (1983). This path is back-calculated from the final P-T conditions which were assumed to be 629 °C at 8 kbar - probably too low a pressure from consideration of other assemblages present.
Geothermometry suggests that most rocks equilibrated at between about 600 and 650 °C, with most results around 630 °C. Rocks from Kleivevatnet give <u>minimum</u> pressures of about 7 kbar (kyanite-bearing rocks), with pressures for chl-bi-gt calculated at about 8-9 kbar. A similar rock from Hyllestad gives much higher pressures, of about 12.5 kbar. These higher pressures are closer to those estimated for observed assemblages in the petrogenetic grids of Vuichard & Ballèvre (1988) and Spear & Cheney (1989).

Numbered equilibria on the figure are:

1-4 Kyanite-almandine schists from Kleivevatnet:

1, 2: minimum and maximum gt-mu temperatures (Hynes & Forest, 1988), 3: minimum pressure from GRAIL (Bohlen et al, 1983), 4: minimum pressure (maximum analysed phengite component) from phengite barometer (Massone & Schreyer, 1987).

5-6 Garnet-kyanite schists from Ronset:

5: gt-mu temperature for sample H16 (sample 472 gives a gt-mu temperature between 1 and 2), 6: minimum phengite pressure.

7-11 Chlorite-biotite-garnet schist from Kleivevatnet

7: gt-mu temperature, 8: gt-bi temperature (Ganguly & Saxena, 1984), 9: pressures calculated from gt-bi-mu-plag-qz equilibrium (Hodges & Crowley, 1985, 10-11: gt-bi-mu-plag-qz equilibria (Ghent & Stout, 1981)

12-16 Chlorite-biotite-garnet schist from Hyllestad

12: gt-bi temperature, 13-15: gt-bi-mu-plag-qz equilibria, 16: gt-mu temperature

17: GRIPS equilibrium (Bohlen & Liotta, 1986) for chlorite-biotite-garnet schist at Kleivevatnet

18: gt-hbl temperature (Graham & Powell, 1984) for garnet-hornblende-mica schist at Kleivevatnet

19: gt-hbl temperature for mafic garnet amphibolite at Hyllestad

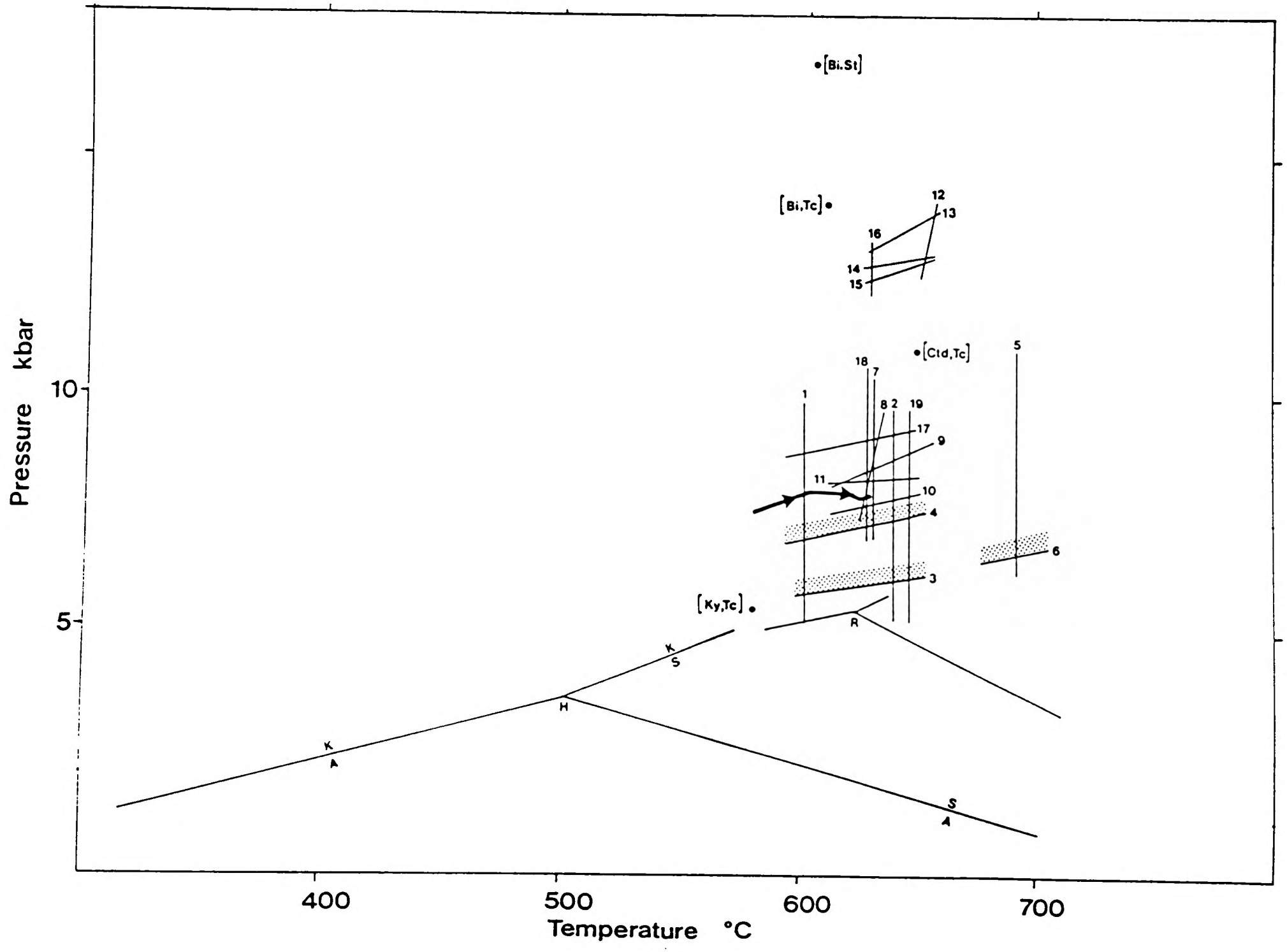
Pressure kbar
10
5
400
500
600
700
Temperature °C
•[Bi.St]
[Bi,Tc]•
12
13
16
14
15
•[Cld,Tc]
5
18
7
1
8 2
19
17
9
11
10
4
6
3
[Ky,Tc]•
R
K
S
H
K
A
S
A

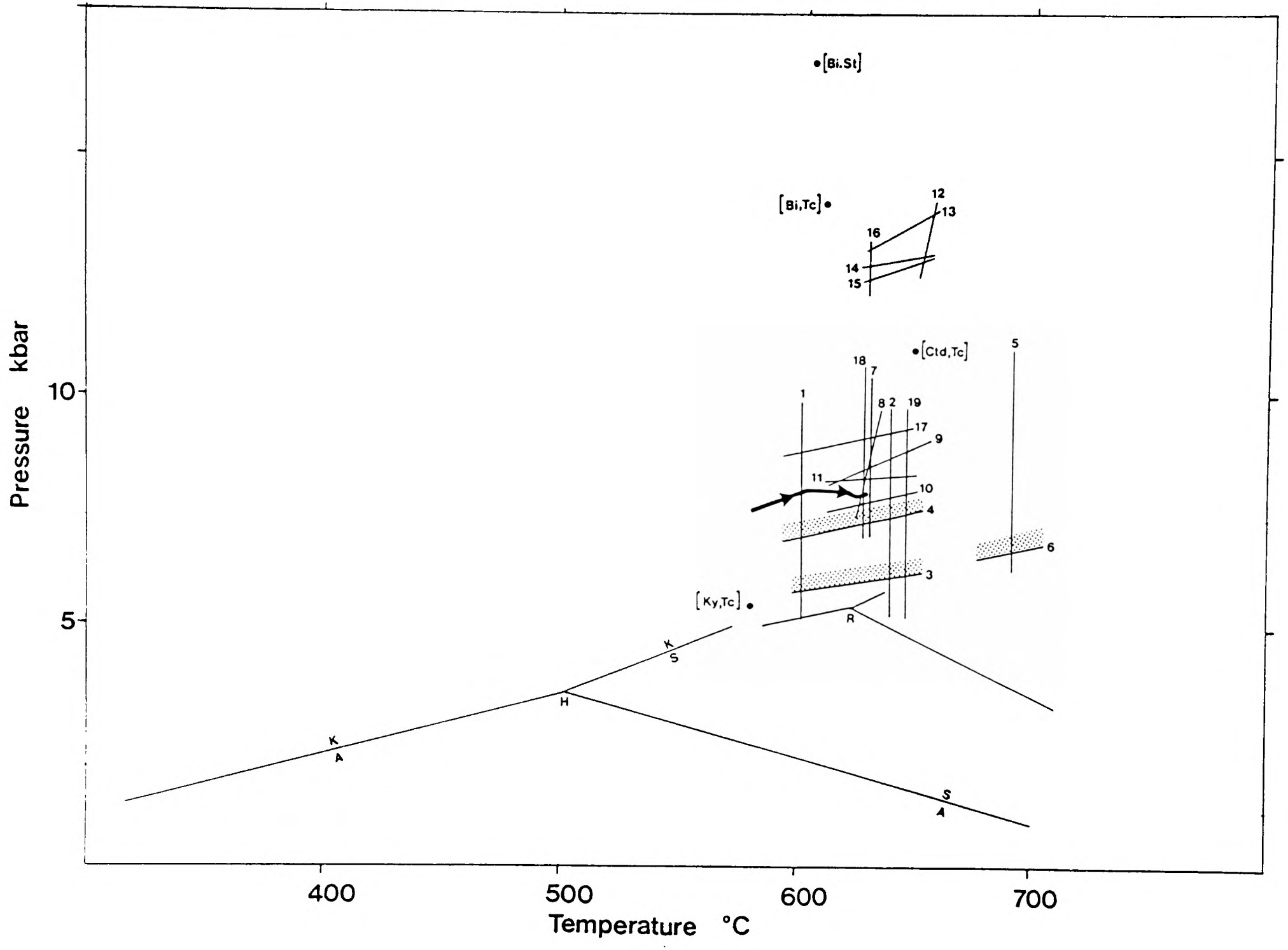
Pressure kbar
10
5
400
500
600
700
Temperature °C
•[Bi.St]
[Bi,Tc]•
12
13
16
14
15
•[Ctd,Tc]
5
18
7
1
8
2
19
17
9
11
10
4
6
3
[Ky,Tc]•
R
K
S
H
K
A
S
A

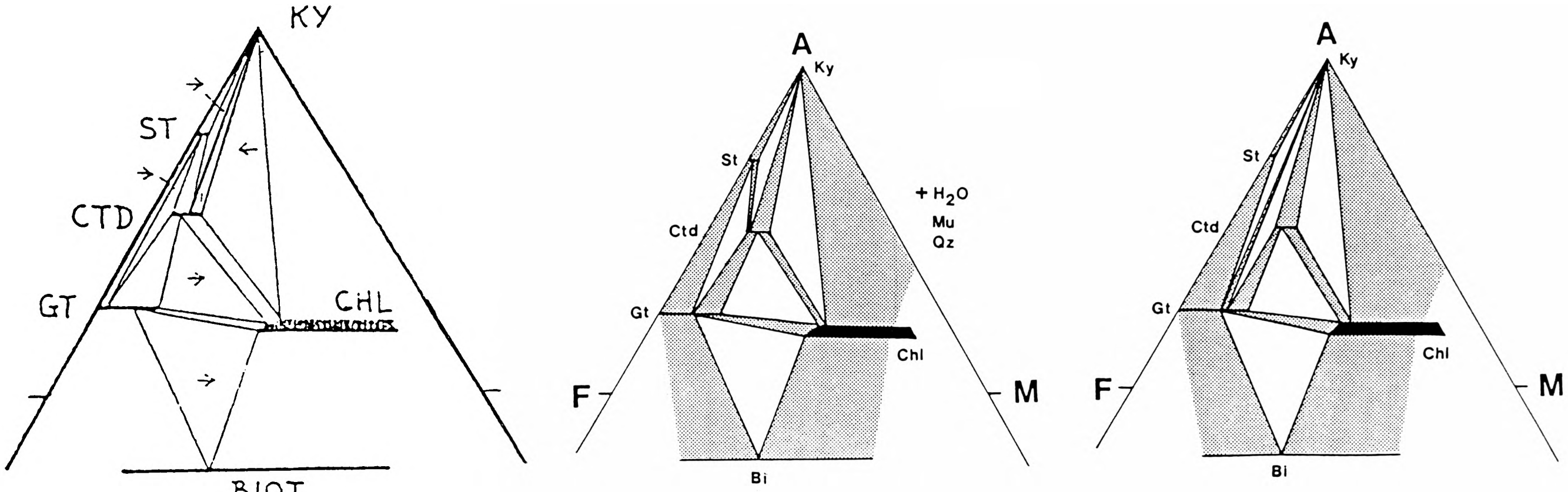

Figure 6.11 Possible sequence of mineral facies for Hyllestad schists, starting in the equivalent of the Barrovian middle garnet zone. A reversal in Fe-Mg partitioning between garnet and staurolite is represented and the reaction st + ctd = gt + ky, inferred from petrographic studies is shown.

Figure 6.12 (a): Petrogenetic grid of Vuichard and Ballèvre (1988) for the system KFMASH. Aluminosilicate phase relations from Holdaway (1971). Ky=kyanite, Tc=talc, St=staurolite, Ctd=chloritoid, Chl=chlorite, Bi=biotite, Gt=garnet, Sill=sillimanite, And=andalusite.

(b) and (c) Schematic modifications to phase relations around [Bi,Tc] invariant point in grid of Vuichard and Ballèvre. Open circles represent singularities, where a reversal in Fe-Mg partitioning between staurolite and garnet occurs, at the intersection of stable and metastable univariant equilibria. However, the reaction grid of Spear and Cheney (1989) has a different topography; the [Bi,Tc] point is metastable (see text). K=kyanite, Tc=talc, S=staurolite, Ct=chloritoid, Ch=chlorite, Bi=biotite, G=garnet.

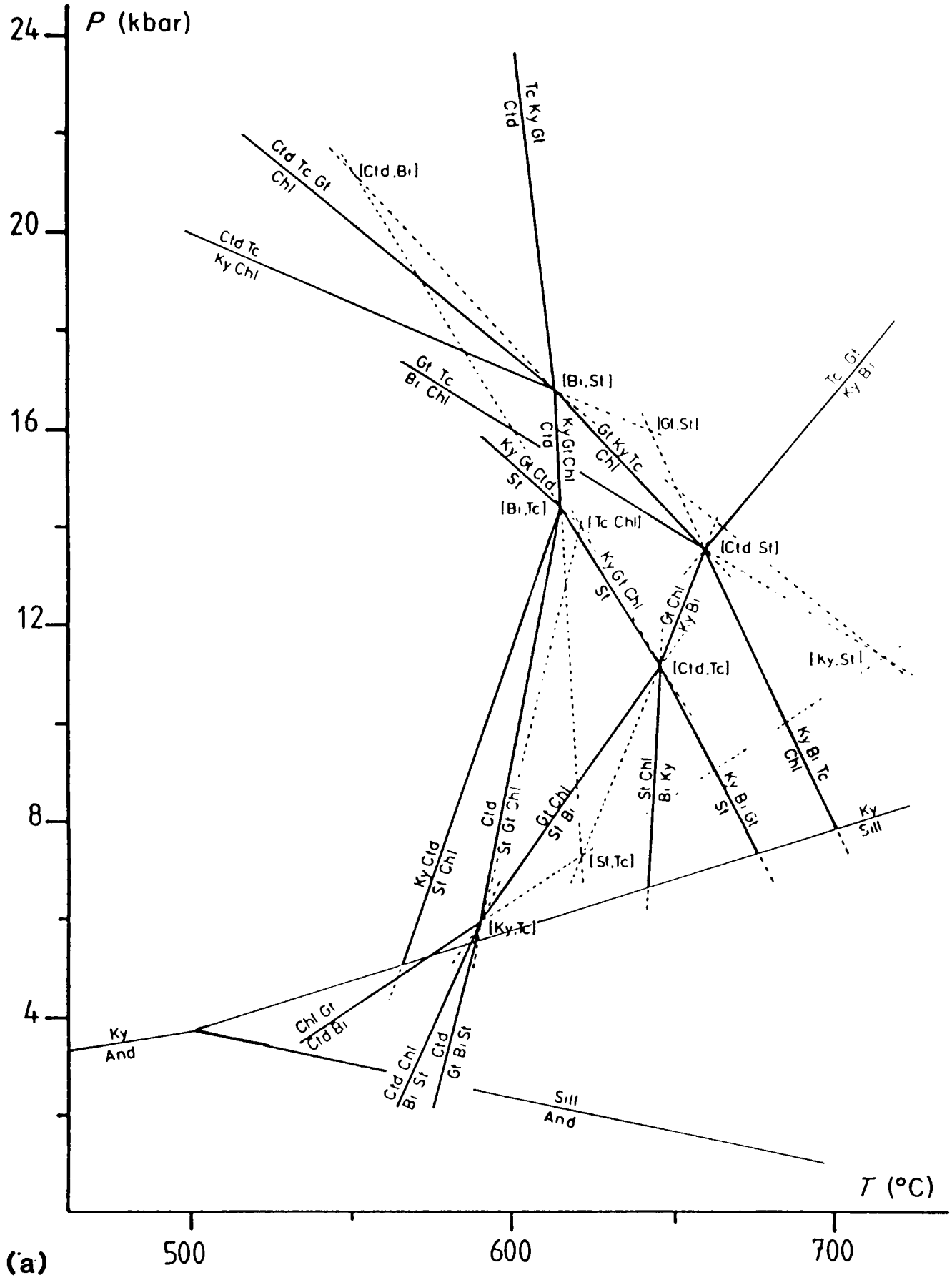
P (kbar)
24
20
16
12
8
4
T (°C)
500
600
700
Tc Ky Gt Ctd
Ctd Tc Gt Chl
[Ctd,Bi]
Ctd Tc Ky Chl
Gt Tc Bi Chl
[Bi,St]
[Gt,St]
Tc Gt Ky Bi
Ctd
Ky Gt Chl
Gt Ky Tc Chl
St
[Bi,Tc]
[Tc Chl]
[Ctd St]
Ky Gt Chl
St
Gt Chl
Ky Bi
[Ctd,Tc]
[Ky,St]
Ky Bi Tc Chl
Ky Ctd St Chl
Ctd
St Gt Chl
Gt Chl
St Bi
St Chl
Bi Ky
Ky Bi Gt
St
Ky Sill
[St,Tc]
[Ky,Tc]
Ky And
Chl Gt Ctd Bi
Ctd Chl Bi St
Ctd Gt Bi St
Sill And

(a)

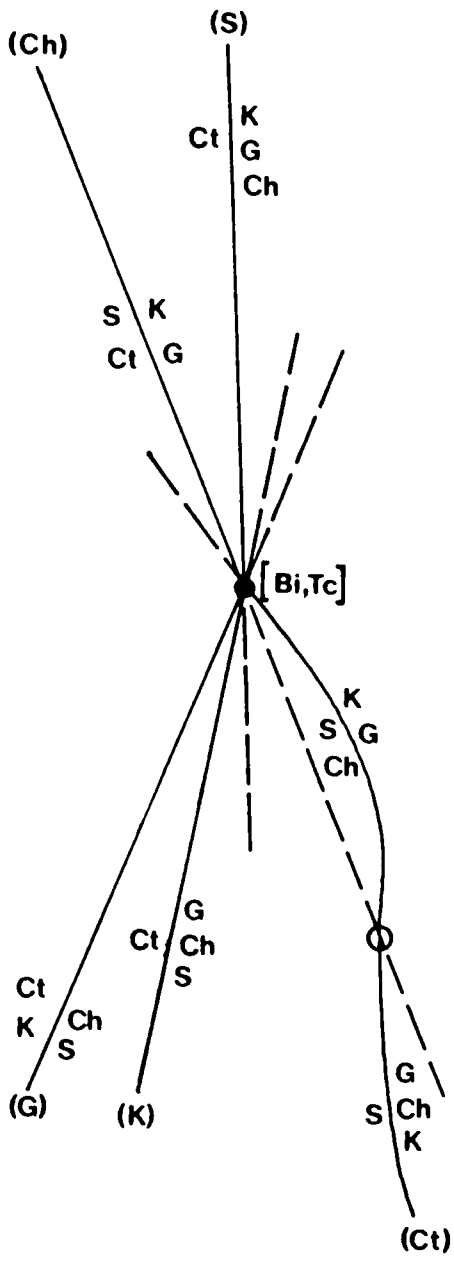
(Ch)
(S)
Ct K G Ch
S K Ct G
[Bi,Tc]
K S G Ch
Ct G Ch S
Ct K Ch S
G S Ch K
(G)
(K)
(Ct)

(b)

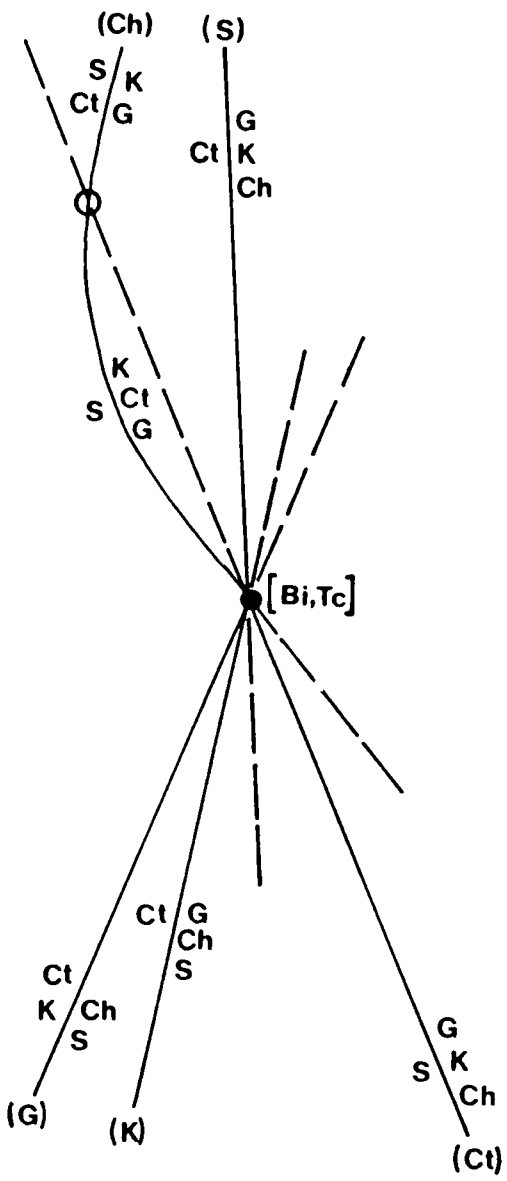
(Ch)
(S)
S K Ct G
Ct G K Ch
K Ct S G
[Bi,Tc]
Ct G Ch S
Ct K Ch S
G K S Ch
(G)
(K)
(Ct)

(c)

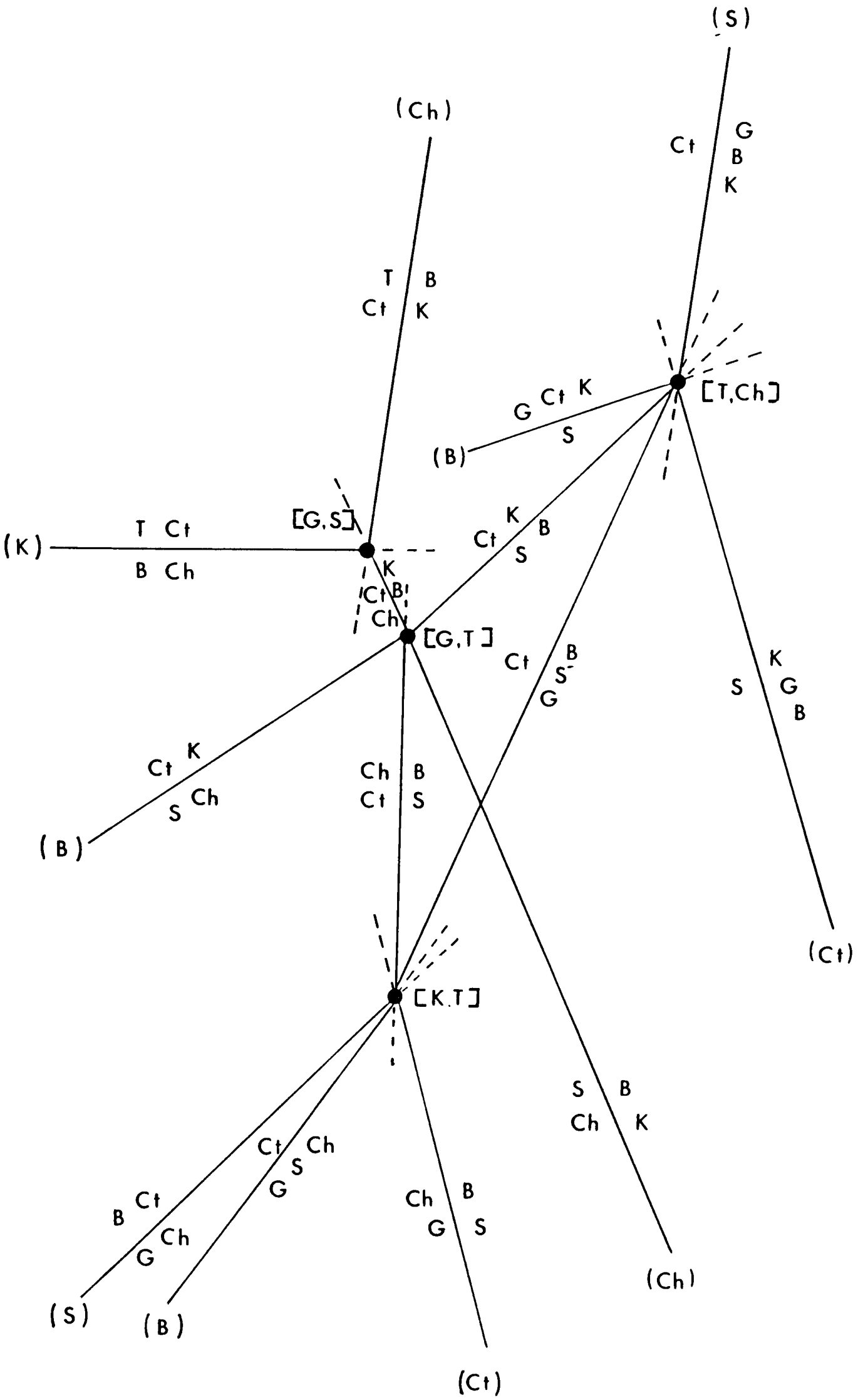

Figure 6.13: Hypothetical variation of petrogenetic grid in KFMASH system. [Bi,Tc] invariant point is assumed to be metastable and stable univariant reaction st = ky + gt + ctd emanates from the [Tc,Chl] invariant point, which is assumed to be stable. Prograde direction of reactions such as chl + gt = ctd + bi are reversed with respect to figure 6.12a.

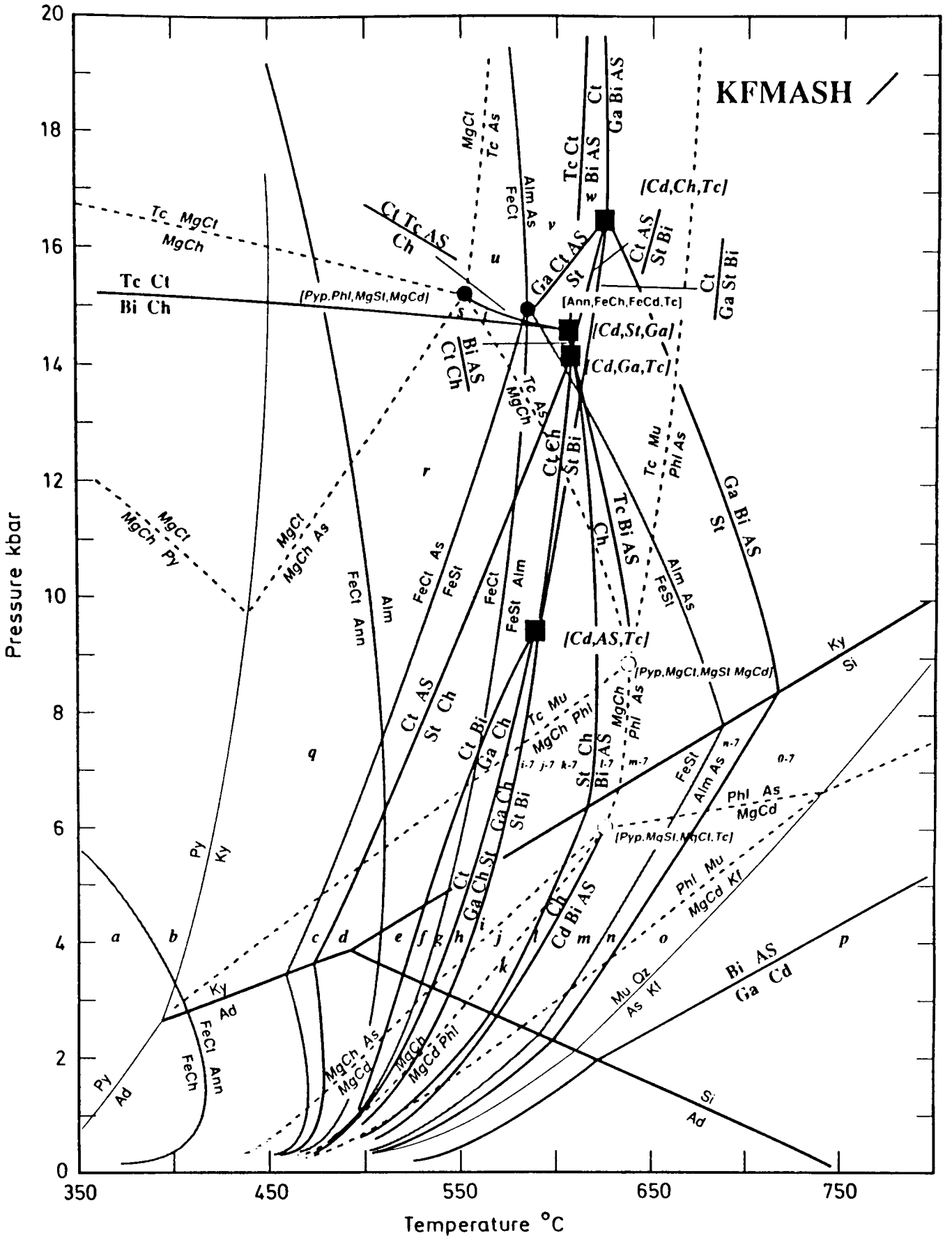

Figure 6.14: Petrogenetic grid for the KFMASH system based on the KFASH and MFASH systems, from Spear and Cheney (1989). Light grey lines=KFASH equilibria, dashed grey lines=KMASH equilibria, heavy black lines=KFMASH equilibria. Solid dots are invariant points in the KFASH or KMASH systems, solid squares are invariant points in the KFMASH system. The equilibrium Ga CT AS St is stable only at high pressures (about 15-16 kbar at 600 °C). Staurolite is the high temperature product of the reaction (cf grid of Vuichard and Ballèvre). The stability of Gt Ch assemblages is limited to a narrow temperature range and pressures less than about 9-10 kbar, but is increased in the system MnKFMASH (see figure 6.15).

Figure 6.15: Contours of XSpess in garnet depicting the effect of MnO (and CaO) on the stability of garnet + chlorite. At XSpess ≥ 0.35, such as those in the cores of garnets in the Hyllestad schists, the stability of garnet + chlorite + biotite overlaps that of Ga + Ct + AS + St.

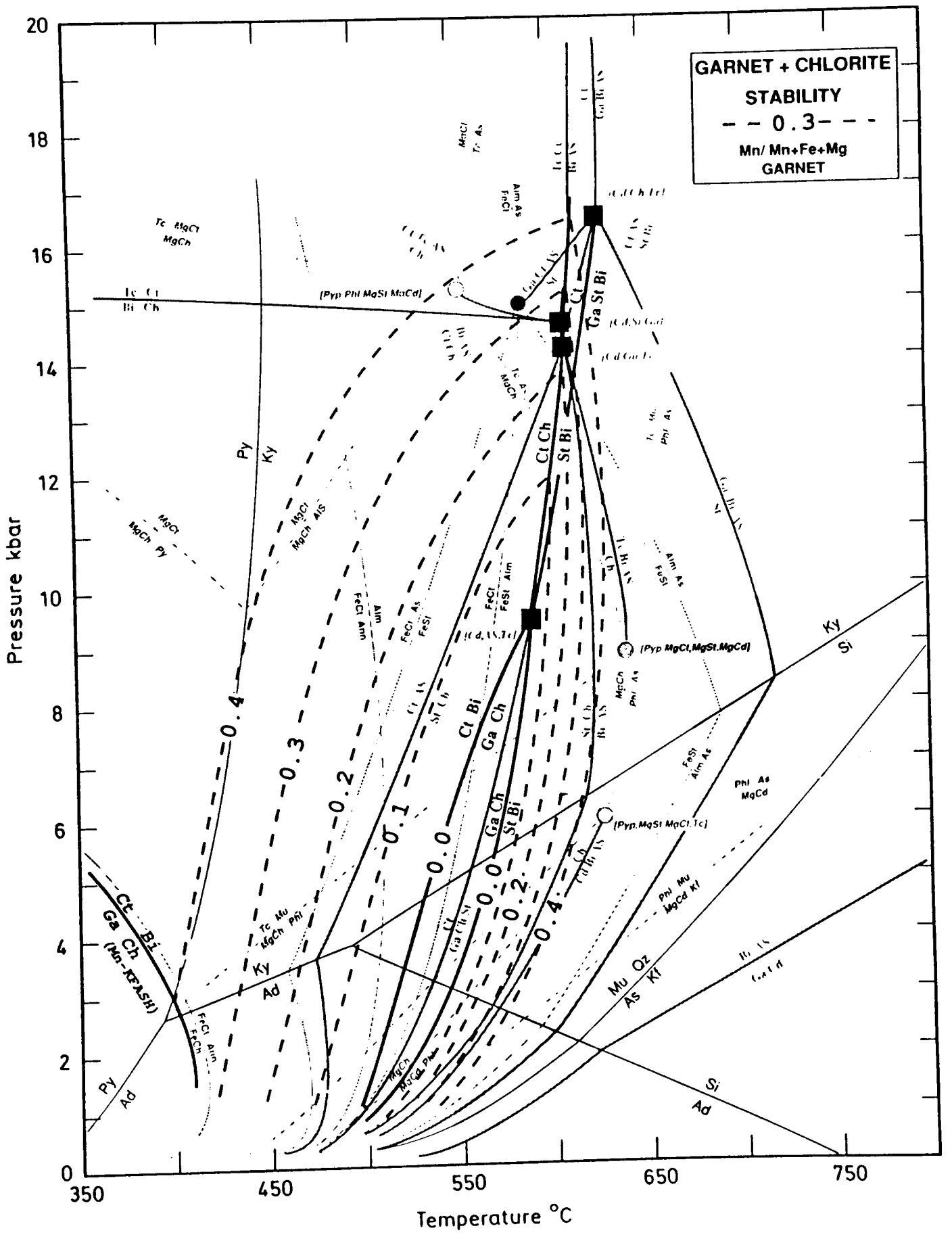

Figure 7.1: Compilation of P-T estimates and inferred P-T-t paths for Basement Gneisses (BG), basement Eclogites (E), Mafic Units (LMU, MMU, UMU, L represents UMU at Löland), and Hyllestad Schists (HK). COR represents estimated conditions of early corona formation in gabbros of the UMU. H=alumino-silicate triple point of Holdaway (1971)
(a) In this model, the various units are assumed to have been juxtaposed during an early compressional event ("D1"?) which was responsible for high-pressure metamorphism in both the basement (E) and in the Hyllestad Schists. Early corona formation in the UMU is assumed to pre-date this (Caledonian) cycle of burial and uplift. The cooling path from COR to deeper burial is highly speculative as no data constraining this part of the P-T evolution has been obtained. It has been included in the diagram to indicate that corona gabbro formation is believed to have been an early feature.

The pre-eclogite facies prograde path is based on temperatures obtained from inclusions of omphacite in garnet at Helleböstölane (pressures on this part of the trajectory are not constrained). The maximum temperature shown for the decompressive path is based on thermometry of rocks associated with eclogites at Ytre Hellebö; analysis of garnet zoning profiles from the Hyllestad Schists suggests that T_{max} may have been lower by about 30 °C, with decompression more nearly adiabatic than shown. In either case HK and E must have evolved along very similar P-T paths in this interpretation. The decompression trajectory between about 600 °C and 500 °C is drawn to pass through the temperature and pressure ranges estimated for the LMU, MMU, UMU, and BG which have been obtained from assemblages interpreted as of D_2 (or at least

pre-D_3) age. This part of the path is very poorly constrained owing to the large scatter of data obtained from these units, but the simplest trajectory which passes through all the calculated P-T ranges is retrograde overall. This is at odds with the apparently prograde nature of D_2 metamorphism in the Mafic Units and BG unless such features as prograde zoning in garnets in these units is a relict of the prograde P-T trajectory. A possible late prograde excursion in the P-T path is recorded by the overprinting of kyanite by sillimanite in a schist at Löland (L). The last stages of the P-T path are essentially unconstrained by geothermobarometry, but the path from D_3 to D_5 seems to involve essentially retrograde metamorphism at low grade.

(b) The second model is tectonically more complex. The same arguments as outlined above apply to the early history of the corona gabbro (COR), but in this interpretation it is assumed not to have been buried at pressures in excess of about 9-10 kbar during the Caledonian deformation cycle. The uplift path of the basement gneisses and eclogites is also very similar to that in (a) above. However, in this case the lack of evidence for high-pressure metamorphism in the Mafic Units is assumed to indicate that they have not suffered deep burial. Thus the high-pressure metamorphism recorded by the Hyllestad Schists must be assumed to have occurred in a different tectonic setting to that of the basement eclogites. The Hyllestad Schists, with pre-existing high-pressure assemblages, and the mafic units were thrust onto the WGR during an early phase of the Caledonian orogeny (during D_1 or early D_2) as part of a thick stack of overthrust rocks. Extensional collapse of the orogen during late D_2 to early D_3 brought the major units into their current relationship.

Extension continued during D_3 and D_5, and may have been responsible for bringing low-grade metasediments and granitic intrusives into contact with high-pressure rocks in the Hyllestad Arc.

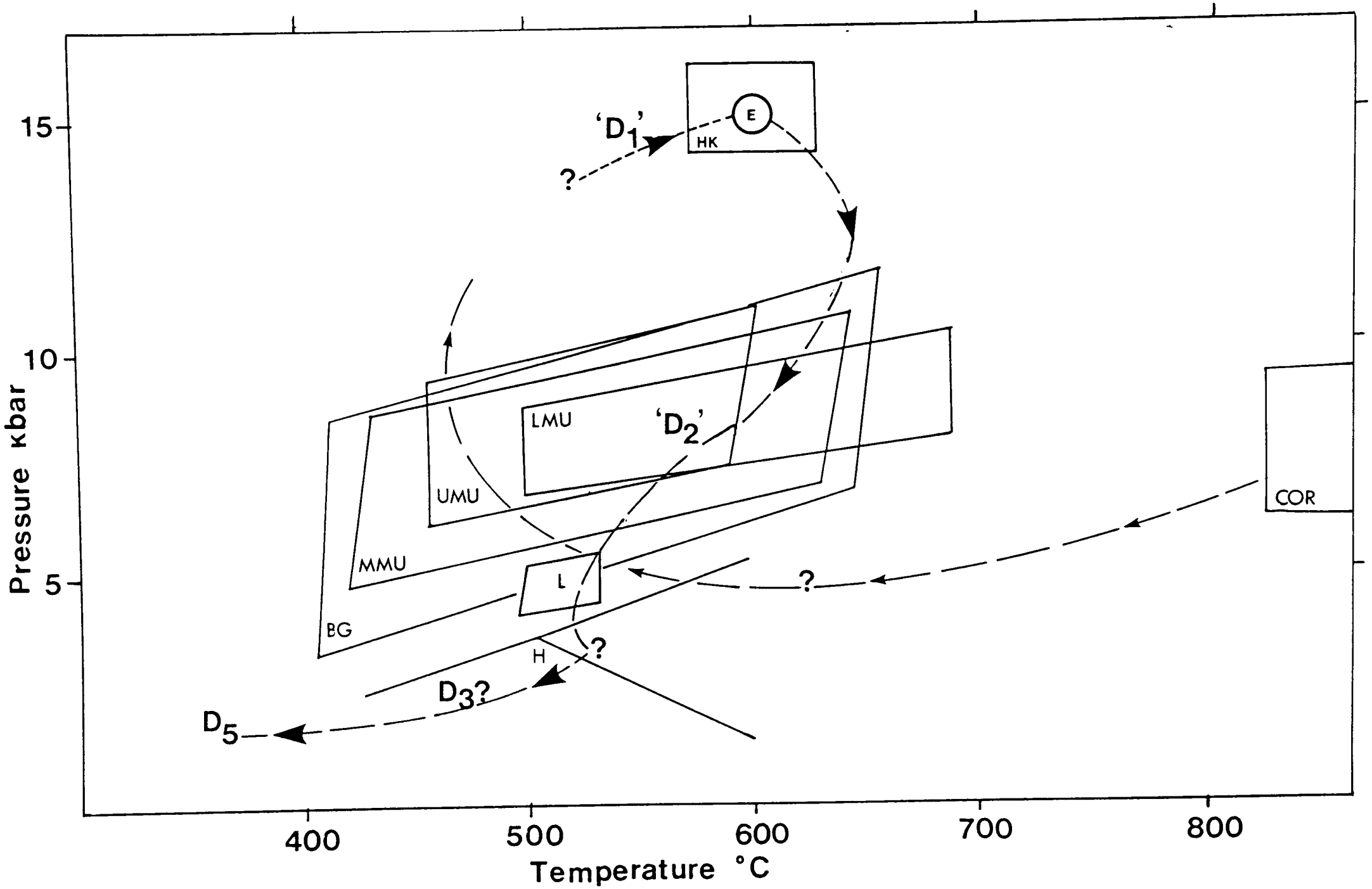
15
10
5
Pressure kbar
'D1'
?
HK
E
LMU
'D2'
UMU
MMU
BG
L
H
?
?
D3?
D5
COR
400
500
600
700
800
Temperature °C

Figure 7.1a

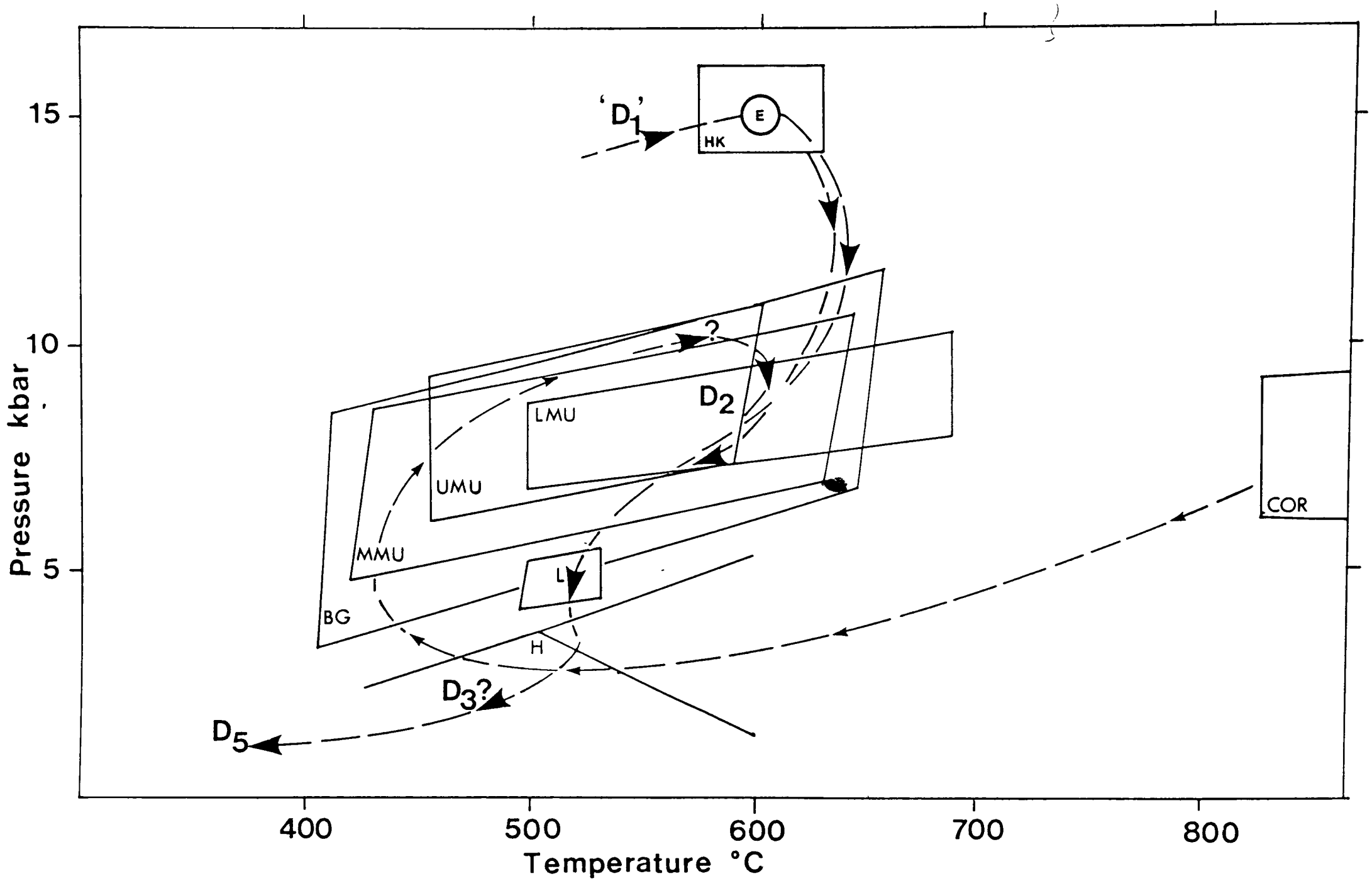
15
10
5
kbar
Pressure
'D1'
E
HK
?
D2
LMU
UMU
MMU
L
BG
H
D3?
D5
COR
400
500
600
700
800
Temperature °C

Figure 7.1b

APPENDIX 1: EQUAL AREA STEREONET PLOTS OF STRUCTURAL DATA

Basement Gneisses

Poles to compositional banding:
i) East of Lavik
ii) Lavik to Leirvik
iii) West of Leirvik

Mineral elongation lineations:
iv) East of Lavik
v) Lavik to Leirvik
vi) West of Leirvik

F_3 folds. Open circles: poles to axial planes; dots: axes
vii) East of Lavik
viii) Lavik to Leirvik
ix) West of Leirvik

F_2 folds. Open circles: poles to axial planes; dots: axes
x) Lavik to Leirvik

Lower Mafic Unit

Poles to compositional banding
xi) East of Lavikstölane
xii) Hanen to Stöldal
xiii) West of Bö Kapell

Mineral elongation lineations
xiv) East of Lavikstölane
xv) Hanen to Stöldal
xvi) West of Bö Kapell

F_3 folds. Open circles: poles to axial planes; dots: axes
xvii) Stöldal to Bosdal
xviii) Hanen to Lavikstölane
xix) West of Bö Kapell

Middle Mafic Unit

Poles to compositional banding
xx) East of Stöldal
xxi) Stöldal to Leirvik
xxii) West of Leirvik

Mineral elongation lineations
xxiii) East of Stöldal
xxiv) Stöldal to Leirvik
xxv) West of Leirvik

F_3 fold axes. Open circles: poles to axial planes; dots: axes
xxvi) East of Stöldal
xxvii) Stöldal to Leirvik
xxviii) West of Leirvik

Upper Mafic Unit etc.

Poles to compositional banding:
xxix) Löland to Råsberg

Poles to joints:

xxx) Open circles: Lower Mafic Unit and Middle Mafic Unit at Djupevik; dots: Upper Mafic Unit between Löland and Langevatnet

Poles to amphibolite grade shear zones:

xxxi) Upper Mafic Unit between Löland and Langevatnet

Poles to low-grade shear zones:

xxxii) Open circles: Lower Mafic Unit and Middle Mafic Unit at Djupevik; dots: Upper Mafic Unit between Löland and Langevatnet

Hyllestad Schists

xxxiii) Poles to compositional banding

xxxiv) Open circles: poles to shear planes. Dots: mineral elongation lineations

xxxv) F_3(?) fold axes

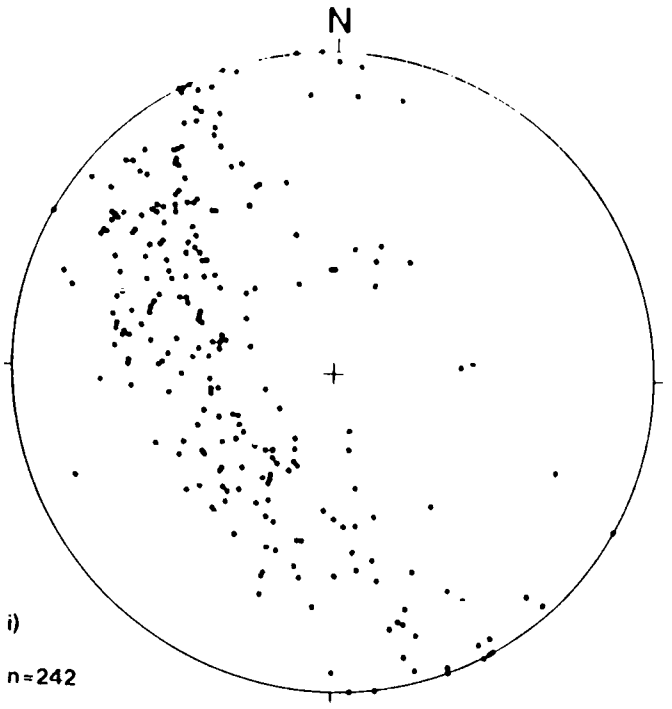

i)

n=242

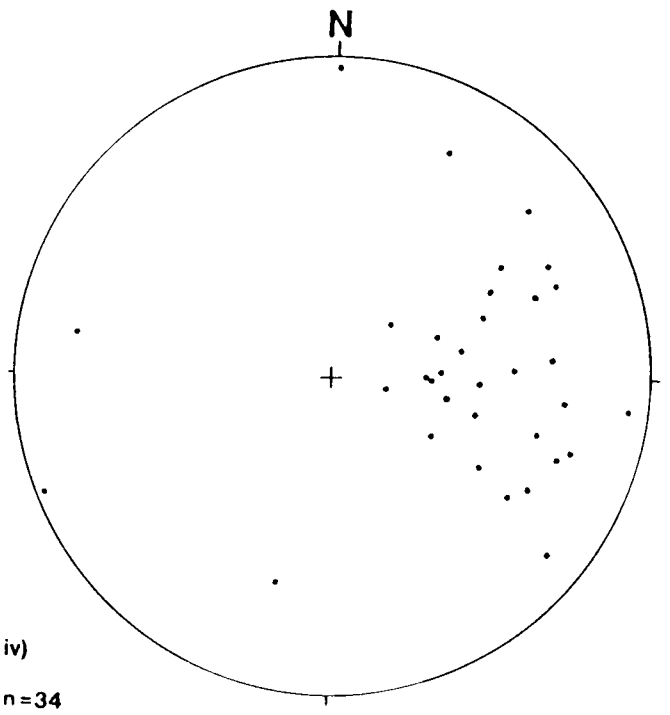

iv)

n=34

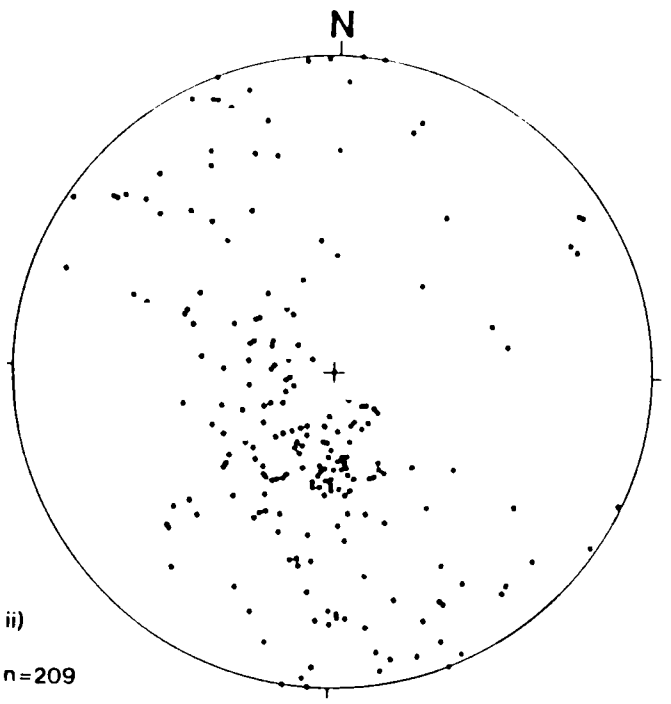

ii)

n=209

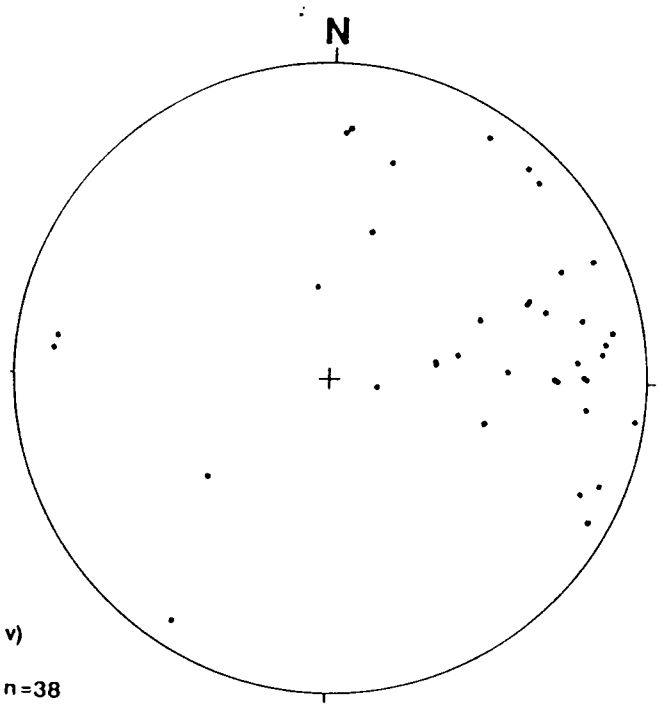

v)

n=38

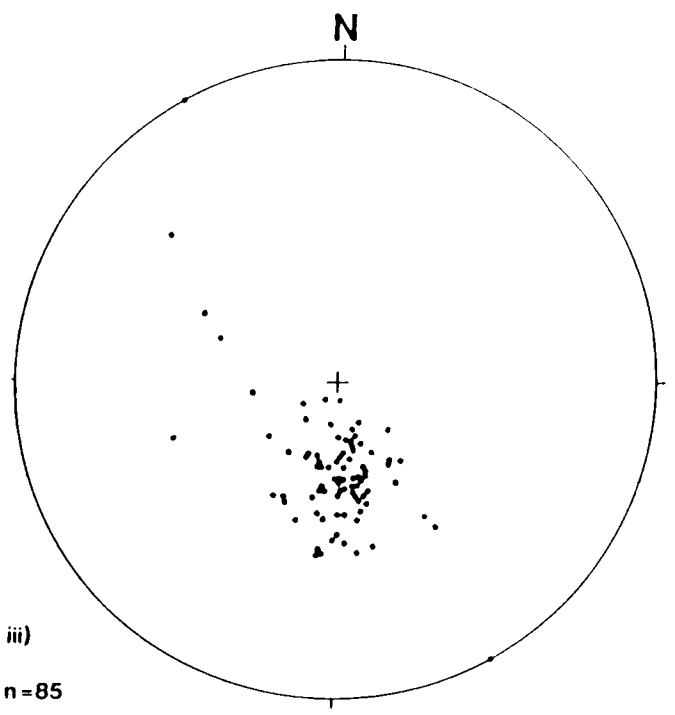

iii)

n=85

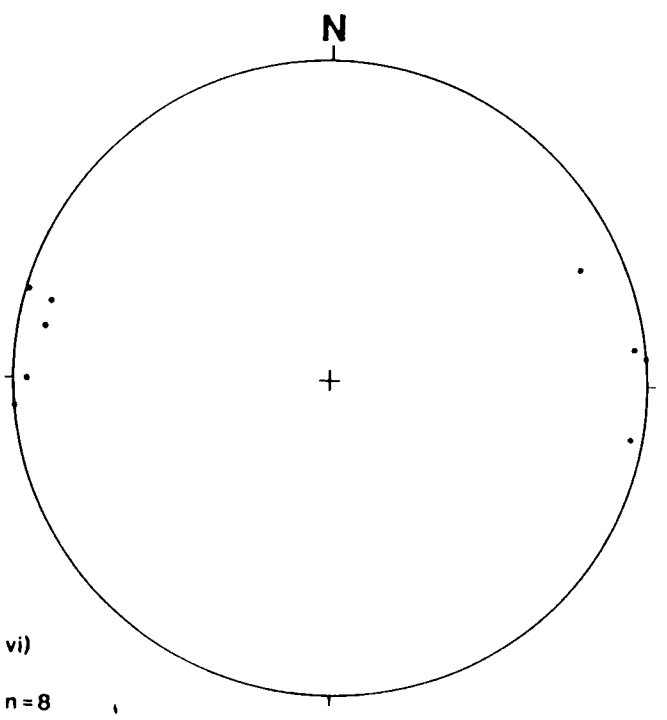

vi)

n=8

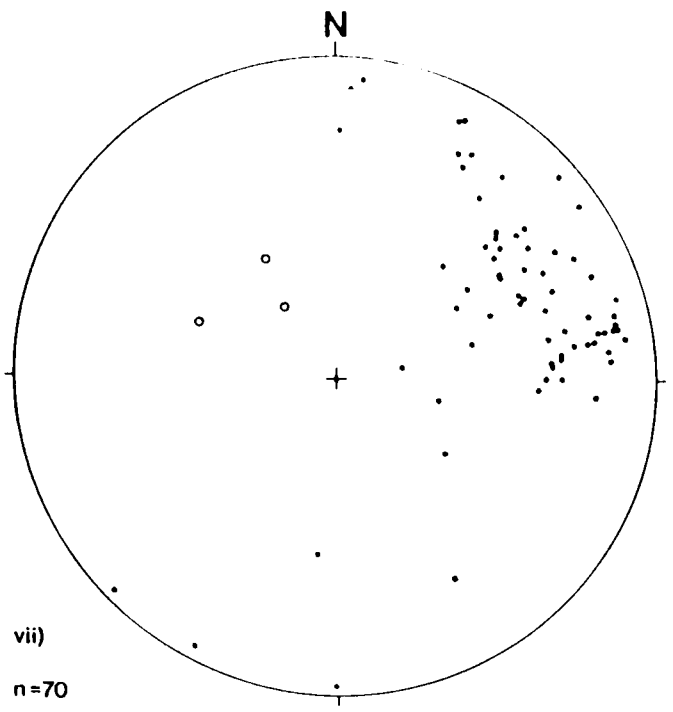

vii)

n=70

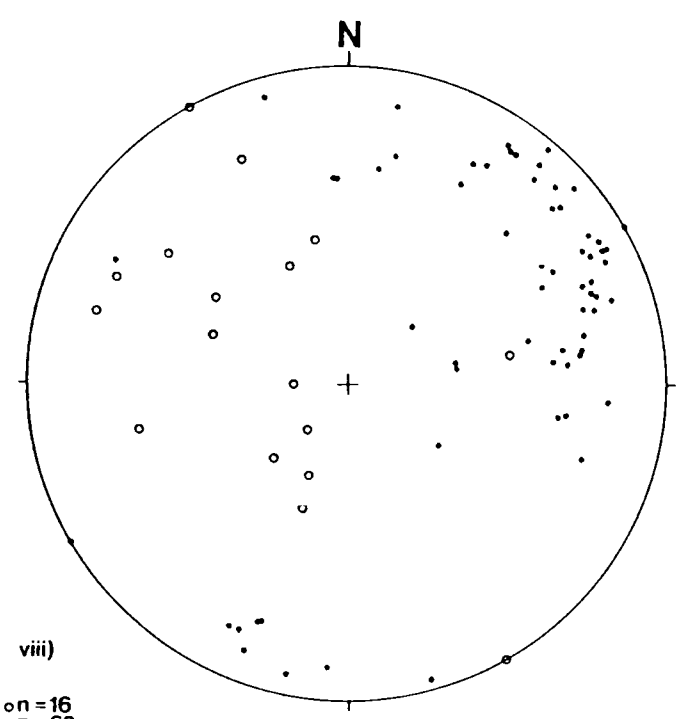

viii)

○ n=16
● n=62

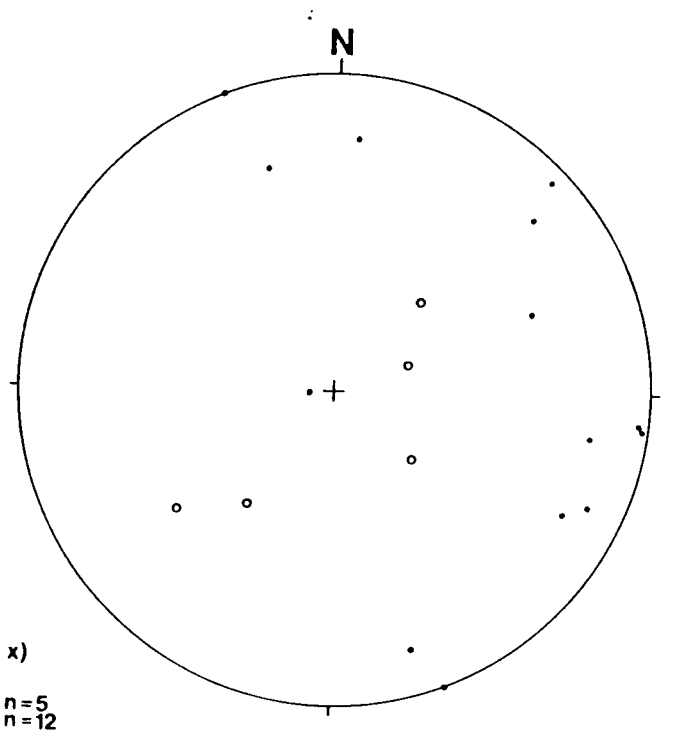

x)

○ n=5
● n=12

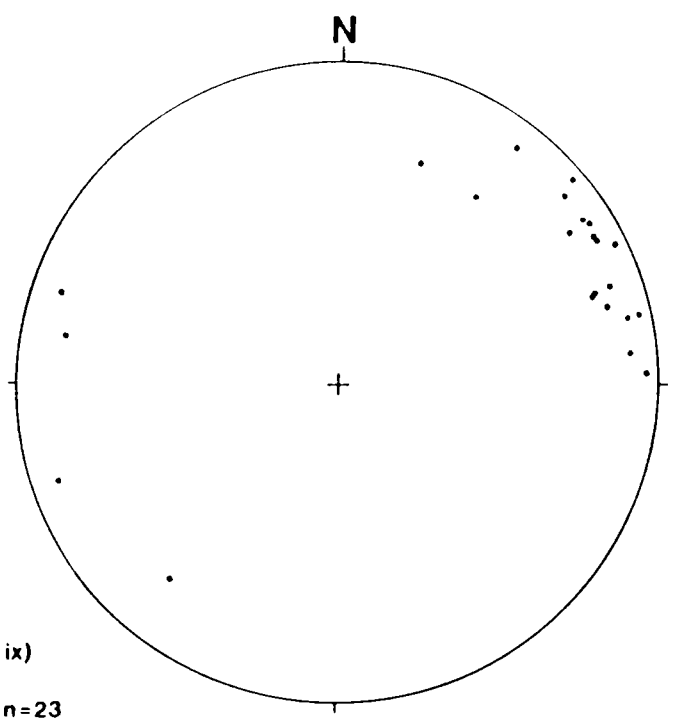

ix)

n=23

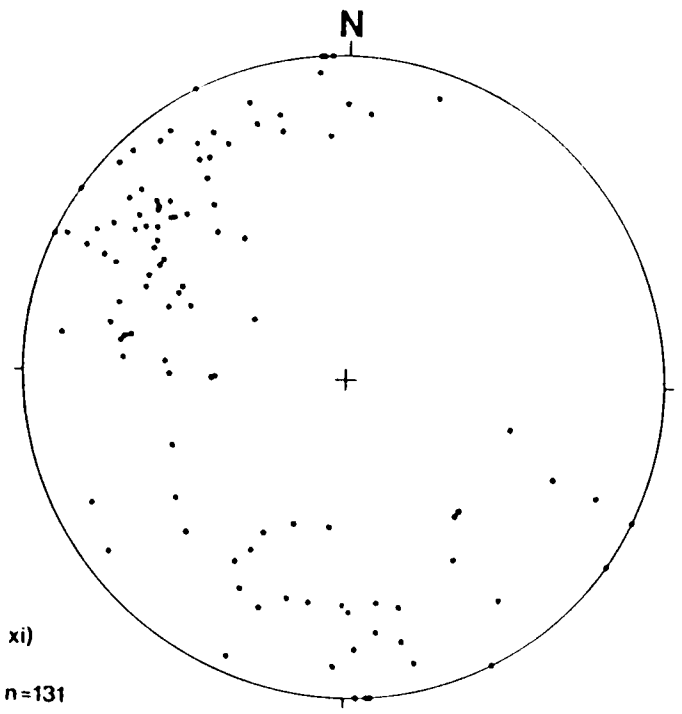

xi)

n=131

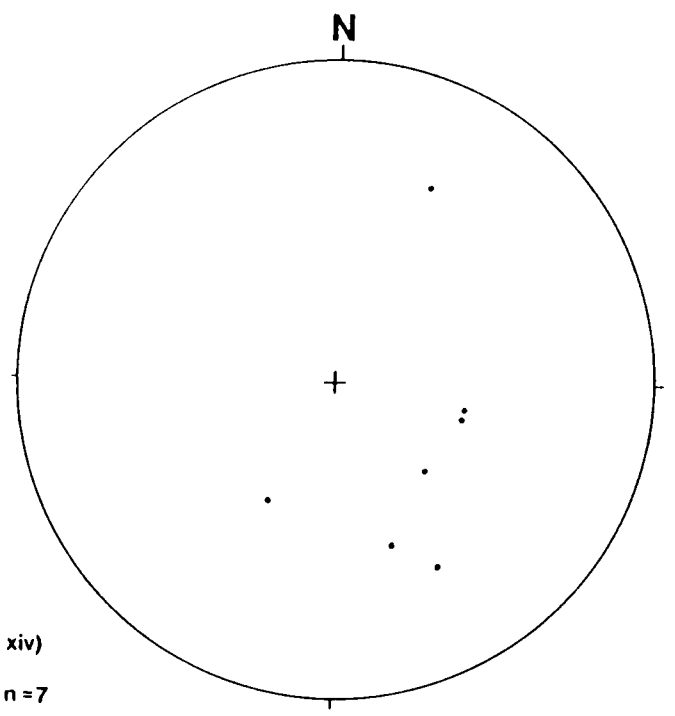

xiv)

n=7

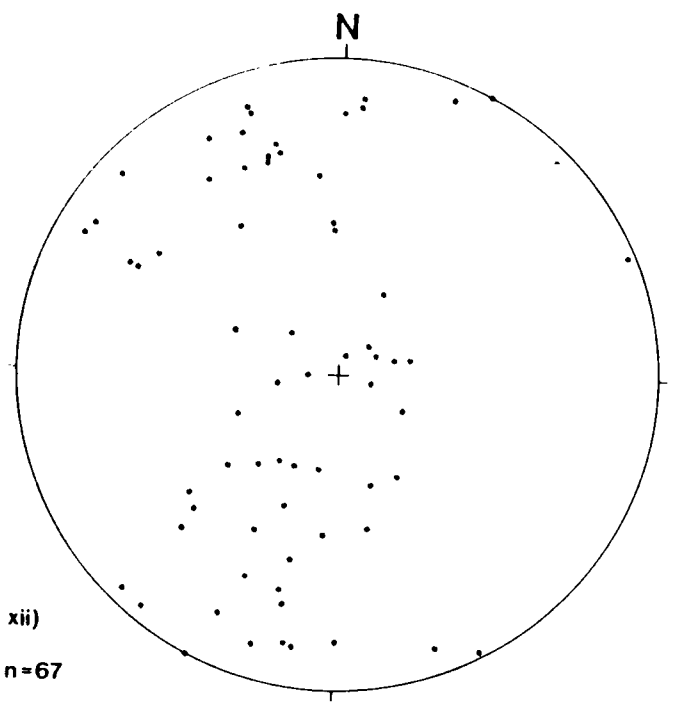

xii)

n=67

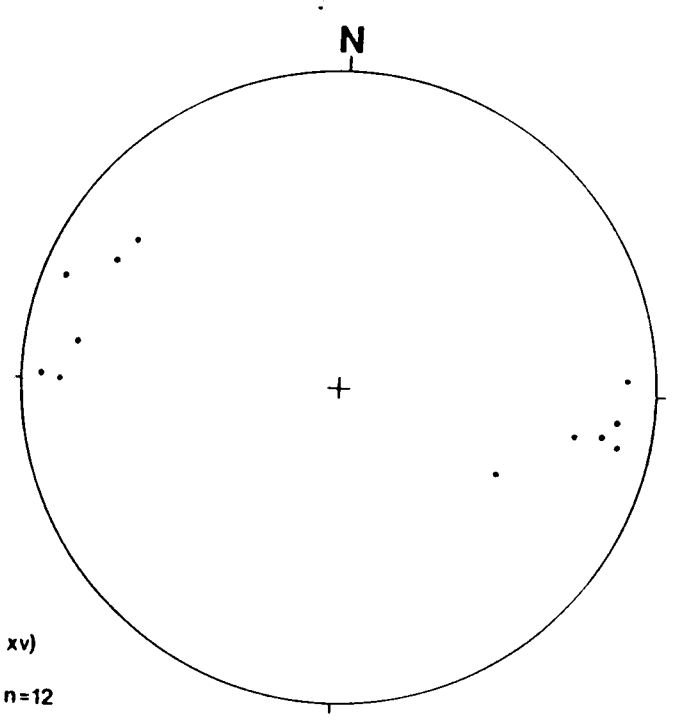

xv)

n=12

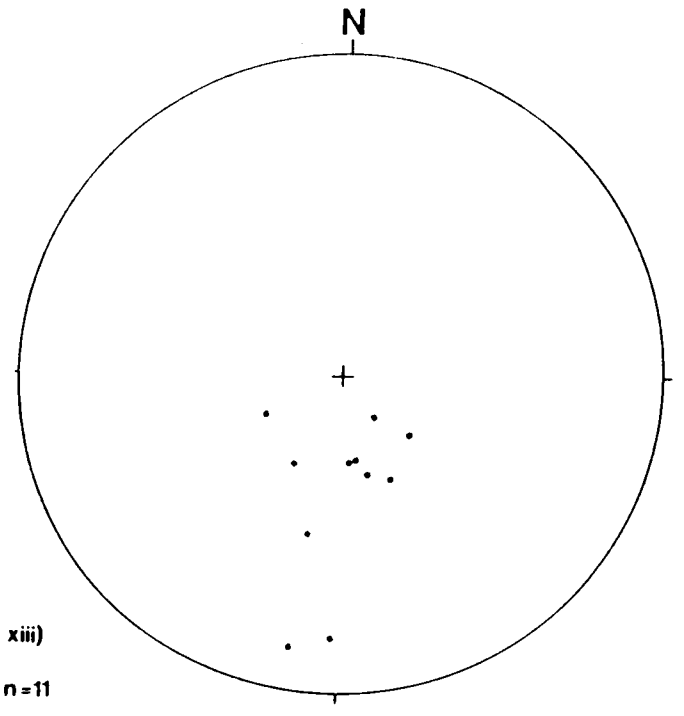

xiii)

n=11

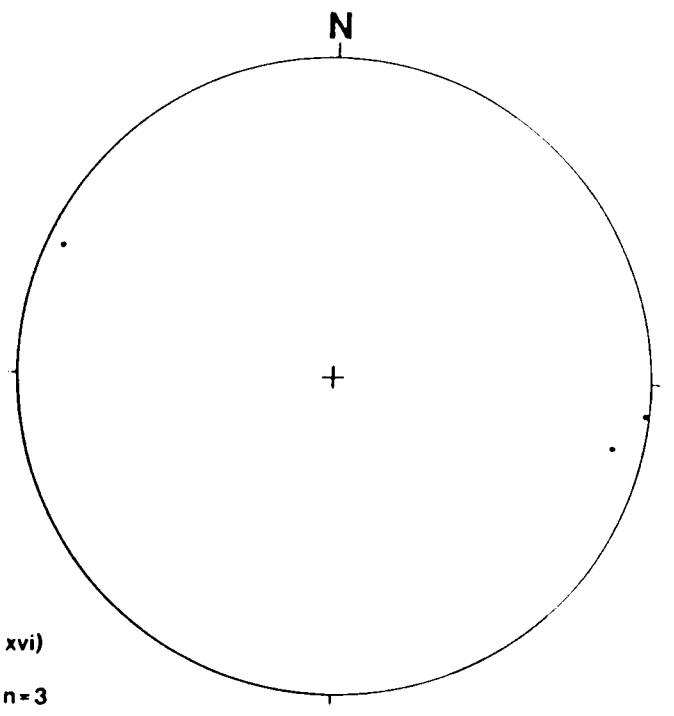

xvi)

n=3

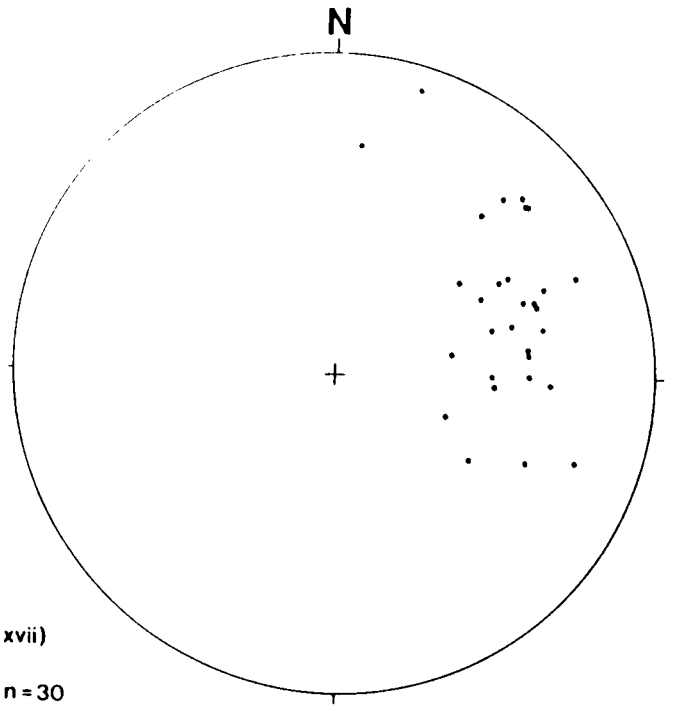

xvii)

n = 30

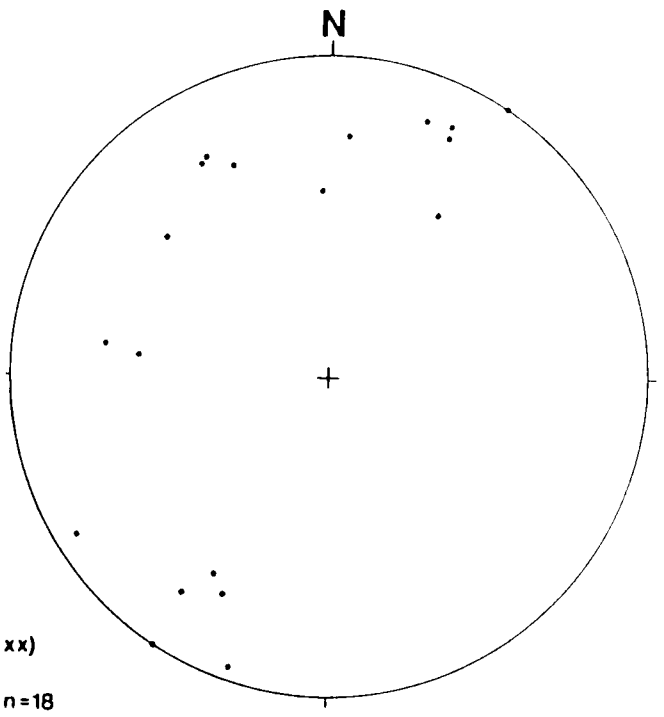

xx)

n = 18

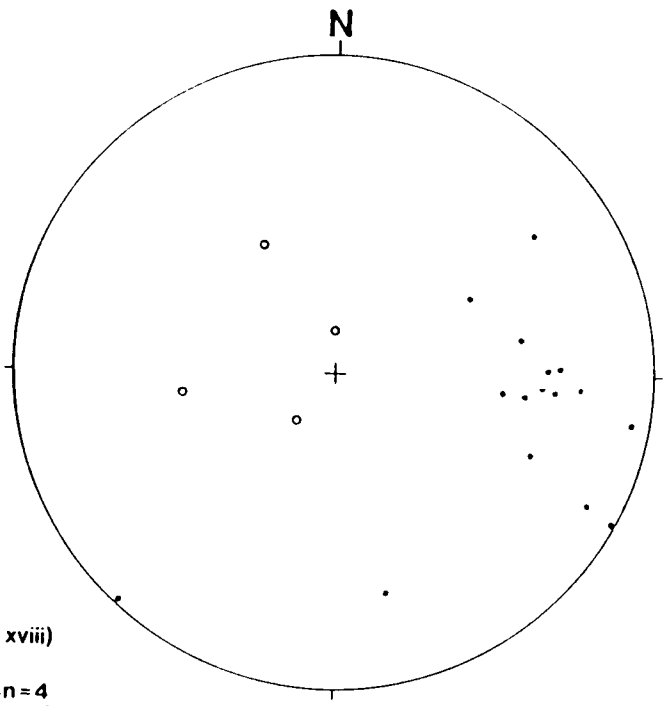

xviii)

o n = 4
• n = 16

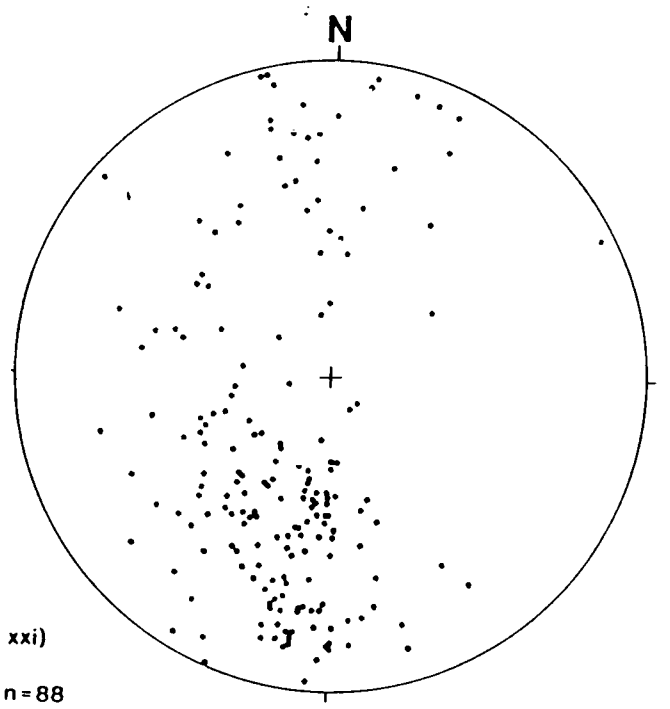

xxi)

n = 88

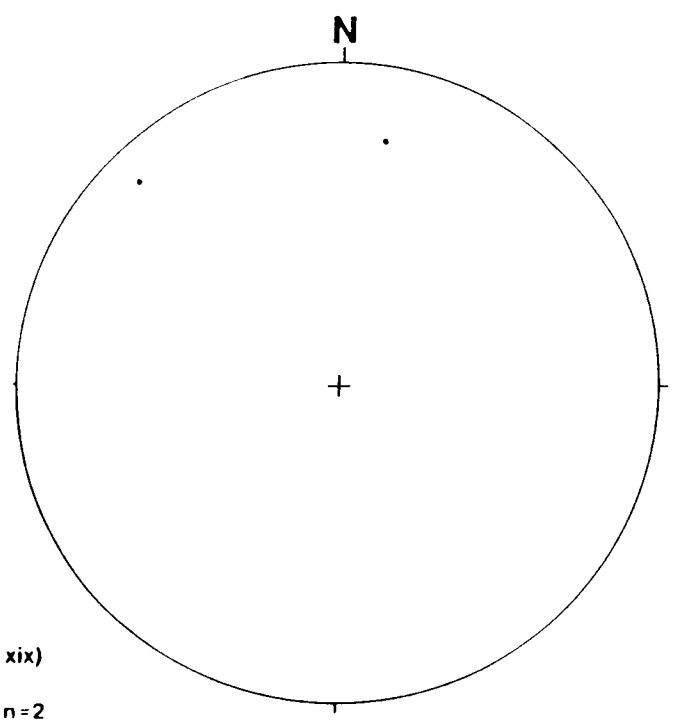

xix)

n = 2

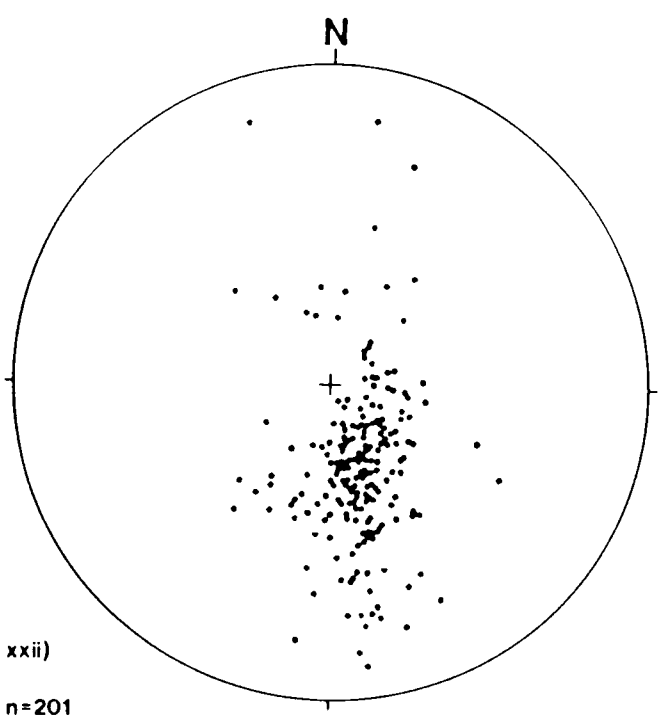

xxii)

n = 201

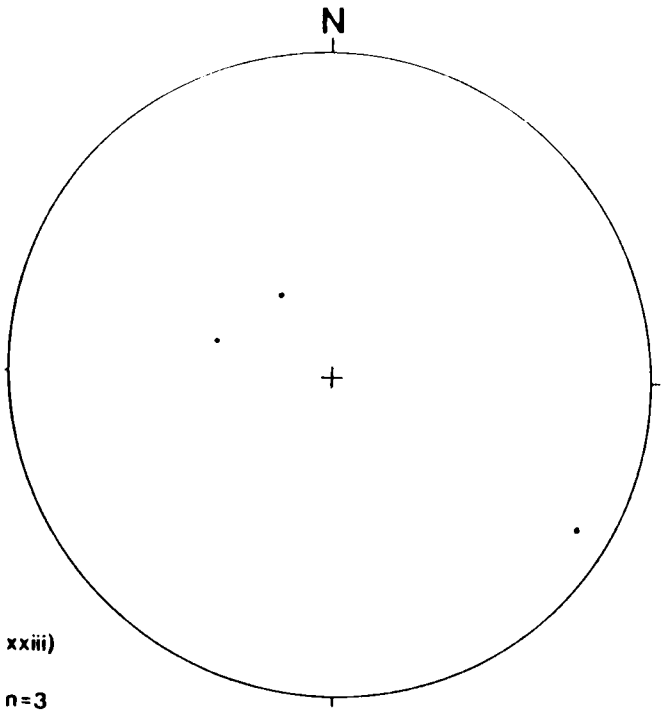

xxiii)

n=3

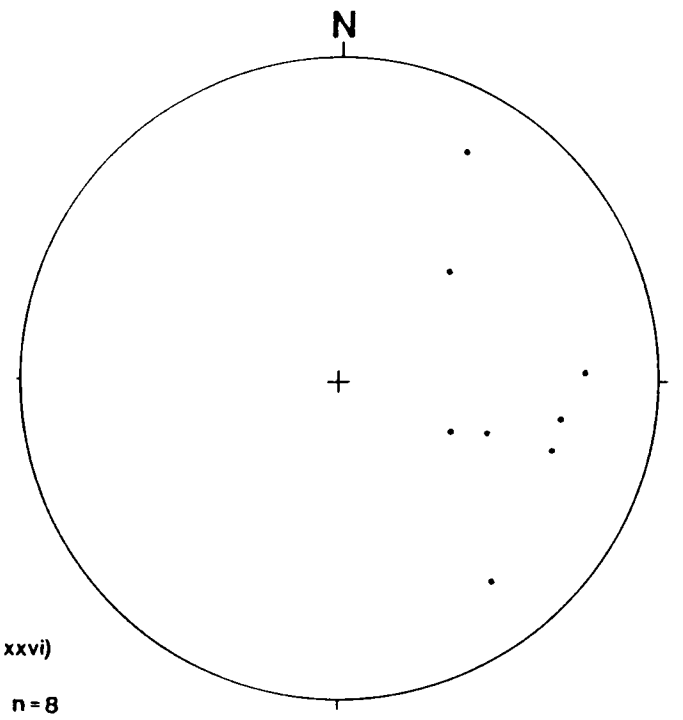

xxvi)

n=8

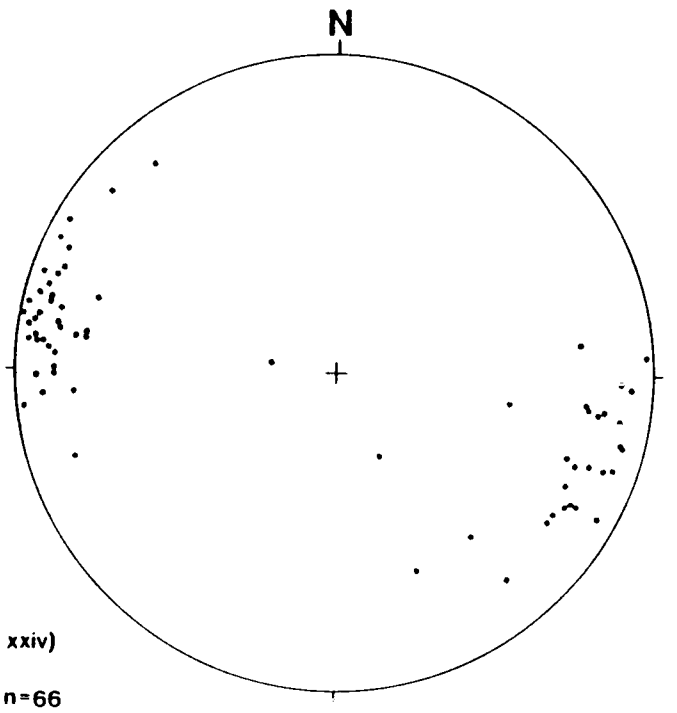

xxiv)

n=66

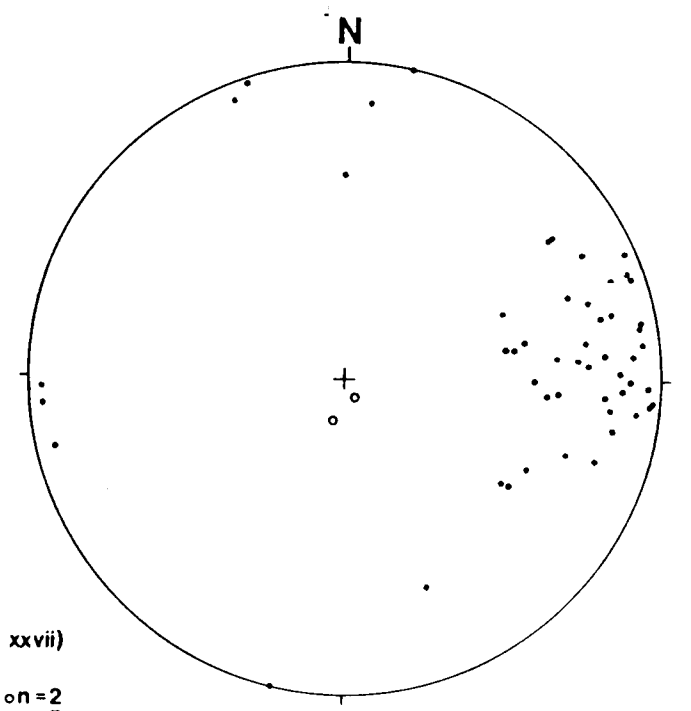

o n=2
• n=5

xxvii)

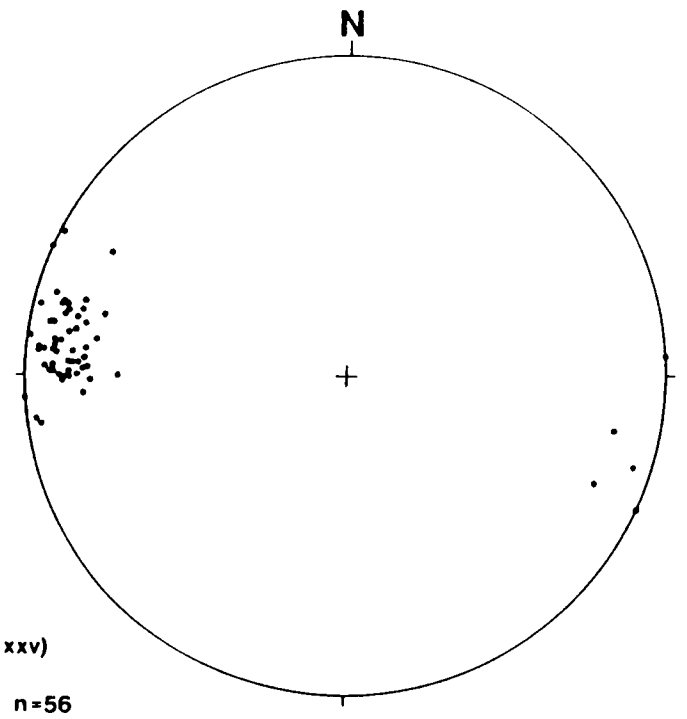

xxv)

n=56

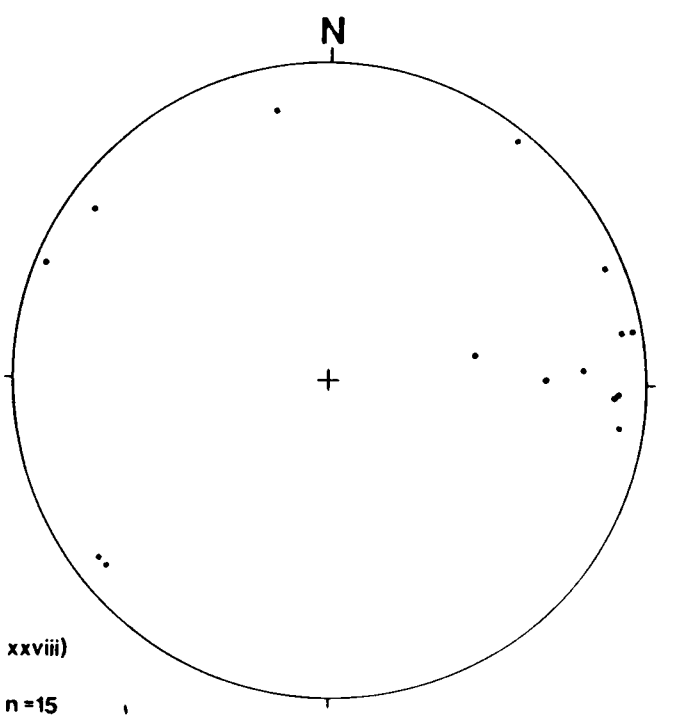

xxviii)

n=15

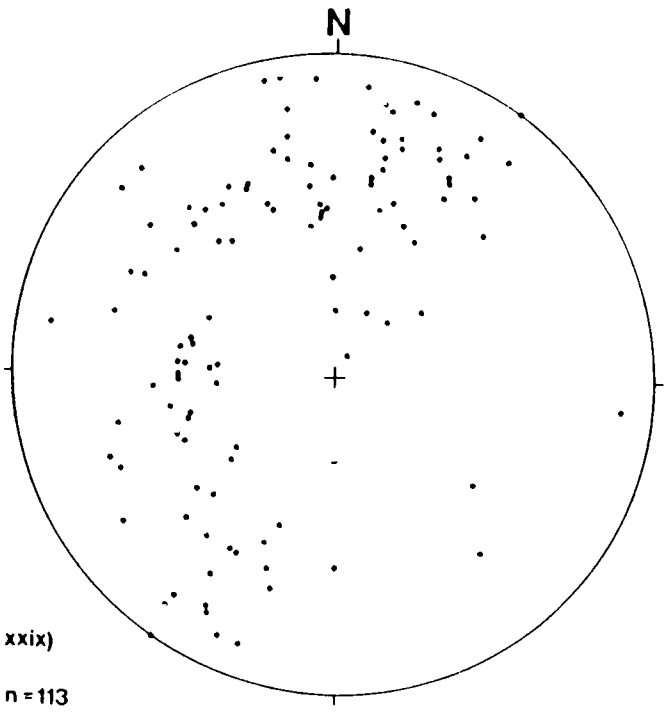

xxix)

n = 113

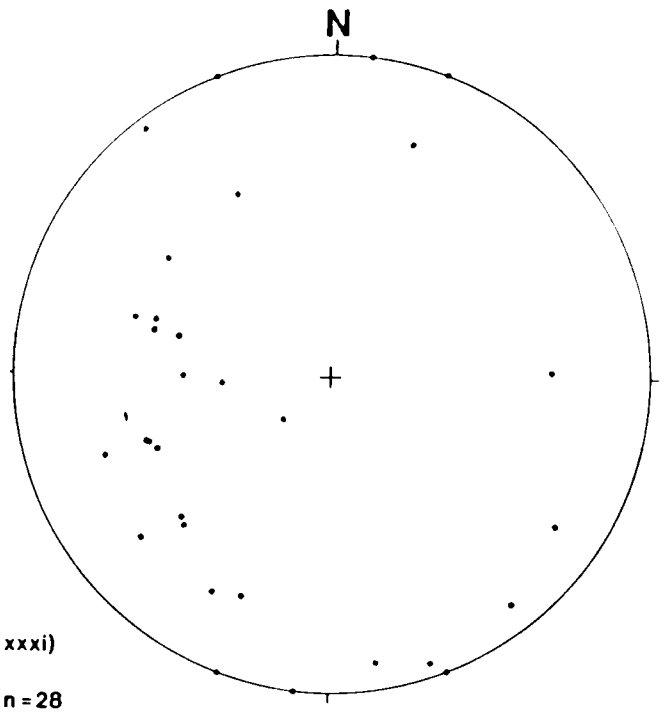

xxxi)

n = 28

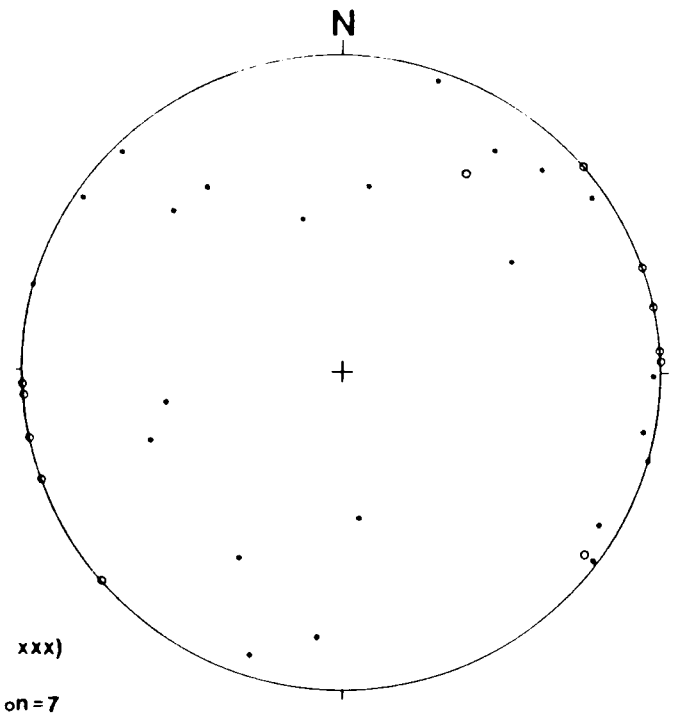

xxx)

o n = 7
• n = 22

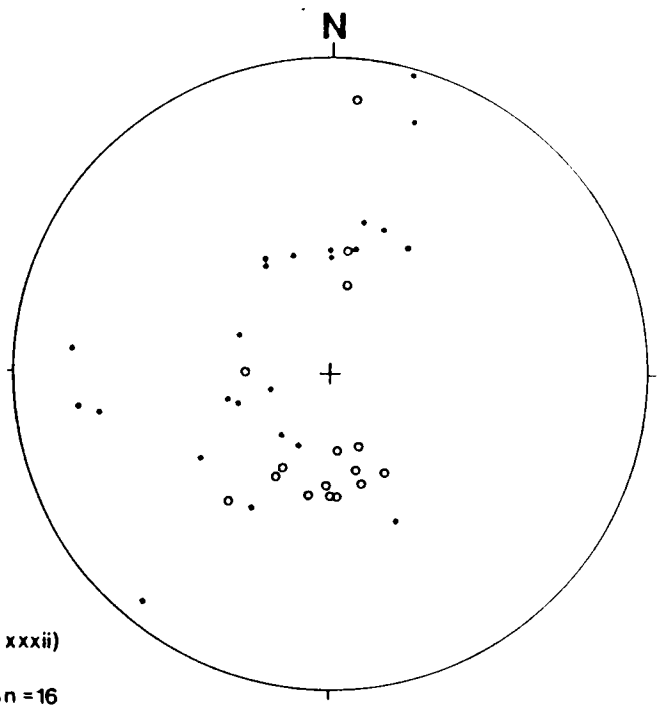

xxxii)

o n = 16
• n = 24

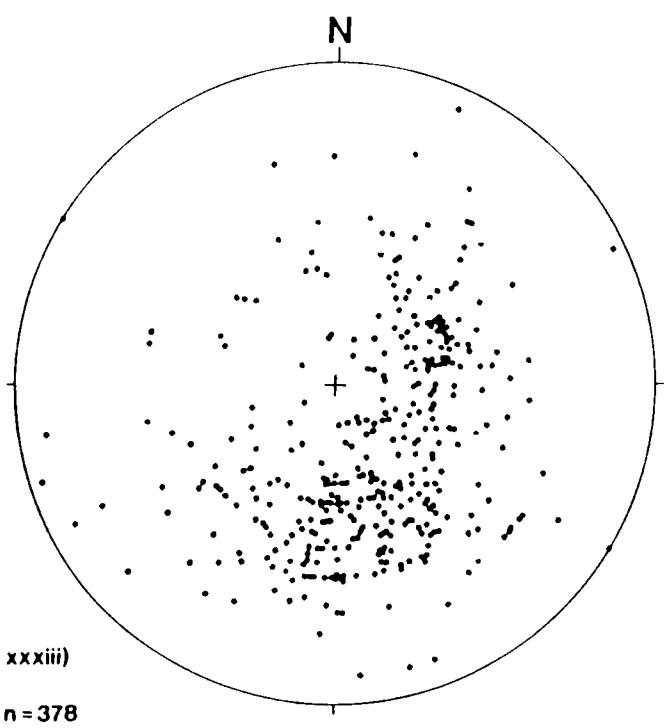

xxxiii)

n = 378

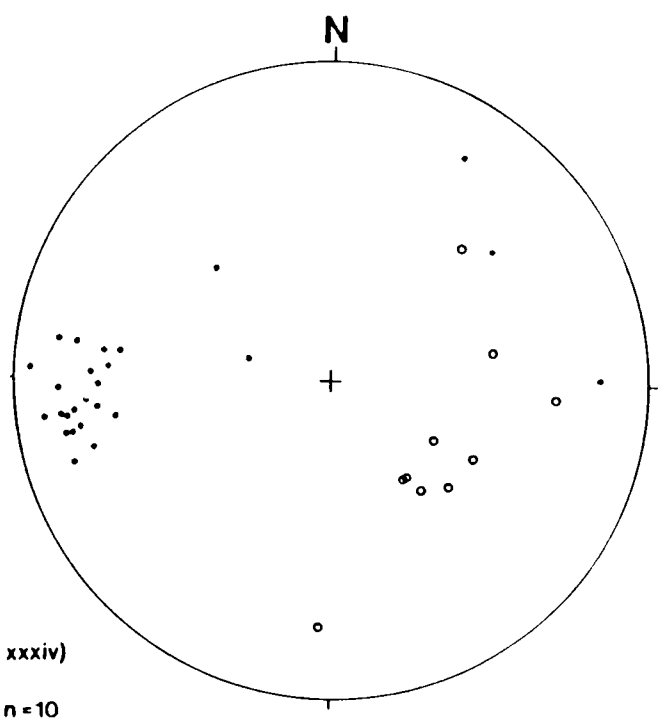

xxxiv)

o n = 10
• n = 26

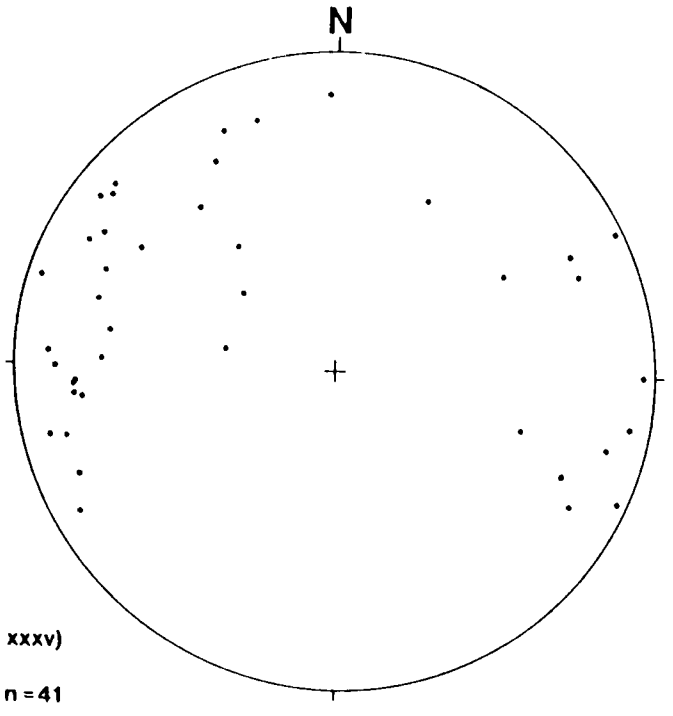

xxxv)

n = 41

Appendix 2: Analytical Techniques

A2.1 Mineral analyses

Mineral analyses were performed on a MICROSCAN 9 electron microprobe at the Department of Earth Sciences, Oxford University. Data was analysed on line by a ZAF correction program following the procedure of Sweatman and Long (1969). Analyses were generally performed at 20 kV with a specimen current of 3.67×10^{-8} A. Spot analyses were carried out on garnets and other silicates where chemical profiles were determined, except for some micas where a raster of between 3 x 3 μm and 10 x 10 μm was used in an attempt to minimise alkali loss.

The following standards and count times were used:

Element	Count time (s)	Standard
Na	30	Jadeite
Mg	15	Periclase
Al	12	Corundum
Si	12	Wollastonite
Ca	10	Wollastonite
K	10	Orthoclase
Ti	10	Rutile
Mn	10	Fowlerite
Fe	10	Haematite
Zn, Ba, & Cr	10	Metals

Analyses presented in tables in the text are not necessarily those used in calculations, which may be averages of several analyses, or analyses of particular grains for which evidence of textural equilibrium with other phases exists.

A2.2 Rock analyses

Major element analyses were carried out on a Philips PW1400 spectrometer with data processing using the X14 package on a PDP11 minicomputer. The analyses were performed on fused glass beads, made of 5.0000 g of spectroflux 100 (lithium tetraborate containing no heavy absorber, dried at 600 °C for six hours) and 1.0000 g of rock powder (pre-ignited at 1000 °C for at least two hours). The flux and rock powder were thoroughly mixed and fused in a zirconia grained 5% Au/Pt crucible at 1225 °C for about 15 minutes. The sample was swirled every three minutes to ensure homogeneity. The melt was then poured into a Pt/Au casting mould, and quenched over a compressed air jet. The crucible was cleaned between samples in boiling 50% HCl for five minutes.

The concentrations of 13 trace elements were determined by the XRF technique. The elements concerned are Rb, Sr, Y, Zr, Nb, Pb, Zn, Cu, Ni, Co, Cr, V, and Ba. Analyses were determined on 10 g pressed powder pellets, using 1.0 ml of "Moviol" as a binding agent, and carried out on a Philips PW1400 spectrometer, with data processing on the PDP11 minicomputer.

Factors affecting the quality of XRF analyses, including the accuracy and precision, and the limits of determination for trace elements, using the above preparation and analytical techniques are discussed by Mitchell (1988). Additional information on silicate analysis is given by Potts (1987).

Appendix 3: Representative mineral analyses
Garnets

Basement gneisses
Orthogneisses

Gt-bi schists

Gt-st schists

Weight % oxides

	55G		446A	R1		SF19		SF203	FN1		SF165		149b	L52A	
	core	rim	rim	core	rim	core	rim	aver	core	rim	core	rim	rim	core	rim
MgO	0.52	0.68	0.97	0.43	0.46	0.44	1.38	0.71	1.18	3.15	0.42	0.96	4.02	2.46	4.89
Al2O3	19.78	19.55	21.05	20.04	20.03	19.32	18.97	19.88	20.99	21.07	20.61	21.11	21.55	21.10	21.47
SiO2	37.71	37.51	37.93	36.98	37.33	38.08	36.42	37.02	37.31	37.89	37.32	37.68	38.34	37.93	38.44
CaO	14.33	14.38	11.63	14.04	15.21	13.57	11.46	12.93	9.63	6.77	10.17	9.45	2.08	6.56	3.29
TiO2	0.19	0.07	0.09	0.21	0.13	nd	nd	0.07	0.12	0.09	0.25	0.11	0.02	0.03	0.09
Cr2O3	nd	nd	nd	nd	nd	nd	nd	0.01	nd	nd	0.00	0.01	nd	0.00	0.00
MnO	8.67	8.36	0.21	11.12	8.34	4.19	12.51	6.89	1.67	0.67	3.95	0.25	0.45	0.12	0.53
FeO	20.63	19.25	28.73	16.53	17.55	25.97	16.97	22.14	29.44	30.78	27.70	31.54	36.08	32.88	32.73
Tot ox	101.84	99.80	100.61	99.35	99.05	101.56	97.71	99.65	100.33	100.42	100.41	101.12	102.52	101.08	101.44

Structural formulae (to 8 cations)

Mg	0.0610	0.0804	0.1146	0.0516	0.0547	0.0513	0.1684	0.0848	0.1399	0.3718	0.0496	0.1132	0.4675	0.2902	0.5696
Al	1.8310	1.8401	1.9674	1.8958	1.8939	1.7982	1.8270	1.8792	1.9744	1.9665	1.9473	1.9752	1.9823	1.9676	1.9762
Si	2.9603	2.9943	3.0064	2.9672	2.9938	3.0069	2.9757	2.9682	2.9772	2.9994	2.9904	2.9904	2.9917	3.0007	3.0018
Ca	1.2053	1.2305	0.9876	1.2072	1.3066	1.1483	1.0036	1.1105	0.8236	0.5739	0.8736	0.8035	0.1739	0.5563	0.2752
Ti	0.0115	0.0043	0.0053	0.0129	0.0076	nd	nd	0.0044	0.0074	0.0052	0.0148	0.0063	0.0010	0.0020	0.0051
Cr	nd	nd	nd	nd	nd	nd	nd	0.0008	nd	nd	0.0000	0.0008	nd	0.0000	0.0000
Mn	0.5763	0.5650	0.0142	0.7556	0.5668	0.2800	0.8659	0.4679	0.1126	0.0452	0.2681	0.0170	0.0295	0.0079	0.0348
Fe	1.3546	1.2855	1.9045	1.1097	1.1768	1.7154	1.1594	1.4842	1.9650	2.0380	1.8563	2.0935	2.3545	2.1754	2.1373
Fe3	0.1972	0.1614	0.0209	0.1241	0.1048	0.1950	0.1973	0.1526	0.0411	0.0289	0.0476	0.0267	0.0250	0.0297	0.0168
Fe2	1.1574	1.1242	1.8836	0.9858	1.0720	1.5204	0.9621	1.3316	1.9239	2.0091	1.8087	2.0663	2.3295	2.1456	2.1204
SUM	8.0000	8.0001	8.0000	8.0000	8.0002	8.0001	8.0000	8.0000	8.0001	8.0000	8.0001	7.9999	8.0004	8.0001	8.0000

Appendix 3 (i) (con)

Eclogites and associated rocks
Amphibolitized eclogites

Eclogites with relict omphacite

Weight % oxides

	SF20		SF24		SF25		SF138	SF68		SF70		166A1		166A2	
	core	rim	core	rim	core	rim		core	rim	core	rim	core	rim	core	rim
MgO	2.08	4.00	2.07	4.18	2.46	4.86	4.93	2.63	6.92	4.55	6.08	3.80	4.60	3.30	4.61
Al2O3	20.37	21.19	21.00	21.05	20.57	21.42	21.02	20.66	21.90	21.40	22.08	21.14	21.22	21.58	20.99
SiO2	36.54	36.79	37.89	37.61	37.90	38.51	39.23	38.53	40.18	39.57	39.85	37.86	38.02	38.46	37.58
CaO	7.69	6.96	8.05	7.20	7.70	7.56	5.74	9.95	9.04	7.47	7.70	6.16	5.16	8.68	5.15
TiO2	0.11	0.05	0.14	0.05	0.07	0.05	0.07	nd	nd	nd	nd	0.14	0.05	0.19	0.10
Cr2O3	0.00	0.01	nd	nd	0.01	0.00	0.00	nd	nd	nd	nd	nd	nd	nd	nd
MnO	5.17	0.21	3.47	0.19	0.16	0.41	2.56	0.74	0.28	1.70	0.39	0.48	0.65	0.69	0.69
FeO	27.14	29.82	28.27	29.00	32.45	27.68	28.17	27.88	23.18	27.44	26.57	30.41	31.31	28.14	30.48
Oxides	99.10	99.04	100.88	99.29	101.32	100.50	101.73	100.40	101.50	102.13	102.67	99.99	100.99	101.06	99.59
Structural formulae (to 8 cations)															
Mg	0.2504	0.4753	0.2444	0.4944	0.2892	0.5646	0.5691	0.3094	0.7813	0.5223	0.6860	0.4489	0.5362	0.3847	0.5445
Al	1.9395	1.9915	1.9599	1.9691	1.9128	1.9682	1.9192	1.9215	1.9555	1.9410	1.9696	1.9742	1.9585	1.9876	1.9626
Si	2.9514	2.9326	2.9998	2.9843	2.9898	3.0009	3.0382	3.0394	3.0432	3.0449	3.0144	2.9993	2.9770	3.0048	2.9812
Ca	0.6655	0.5944	0.6827	0.6122	0.6513	0.6317	0.4766	0.8410	0.7338	0.6156	0.6245	0.5230	0.4326	0.7269	0.4375
Ti	0.0064	0.0031	0.0083	0.0031	0.0041	0.0031	0.0040	nd	nd	nd	nd	0.0084	0.0027	0.0114	0.0062
Cr	0.0000	0.0009	nd	nd	0.0009	0.0000	0.0000	nd	nd	nd	nd	nd	nd	nd	nd
Mn	0.3539	0.0142	0.2330	0.0125	0.0106	0.0272	0.1682	0.0496	0.0179	0.1105	0.0247	0.0319	0.0428	0.0456	0.0462
Fe	1.8330	1.9879	1.8720	1.9245	2.1413	1.8043	1.8247	1.8391	1.4683	1.7657	1.6809	2.0144	2.0502	1.8388	2.0218
Fe3	0.1028	0.0719	0.0320	0.0435	0.0924	0.0278	0.0386	0.0391	0.3475	0.0141	0.0161	0.0181	0.0618	0.0000	0.0499
Fe2	1.7302	1.9161	1.8399	1.8810	2.0489	1.7765	1.7861	1.8000	0.2461	1.7516	1.6648	1.9963	1.9884	1.8388	1.9719
SUM	8.0001	7.9999	8.0001	8.0001	8.0000	8.0000	8.0000	8.0000	8.0000	8.0000	8.0001	8.0001	8.0000	7.9998	8.0000

Appendix 3 (i) (con)

	Opx-gneiss	LMU Garnet amphibolites												
Weight % oxides														
	SF133	176	449	L128		L150		L168	SF97		SF112		SF172	
	corona	rim		core	rim	core	rim	rim	core	rim	core	rim	core	rim
MgO	2.65	3.92	3.22	1.32	4.08	1.66	3.84	1.56	1.22	1.85	1.08	2.32	0.72	1.37
Al2O3	20.96	21.53	20.29	21.48	20.87	20.17	21.39	19.73	21.07	21.52	20.93	21.49	21.02	20.84
SiO2	38.87	38.79	38.53	37.25	37.20	37.40	36.62	38.51	37.45	38.35	36.87	38.34	37.87	38.20
CaO	9.80	5.23	11.36	9.97	7.08	6.76	7.33	8.25	9.69	10.05	9.58	9.83	8.22	8.66
TiO2	0.05	0.00	0.07	0.16	0.04	0.09	0.07	0.14	0.14	0.16	0.19	0.12	0.16	0.14
Cr2O3	nd	0.00	0.00	0.01	0.00	nd	nd	0.00	nd	nd	nd	nd	0.01	0.00
MnO	1.10	0.90	0.41	3.60	0.57	2.42	0.22	1.95	5.19	1.07	7.33	2.58	6.65	1.64
FeO	26.79	30.91	25.57	26.53	29.29	31.34	29.64	31.71	25.99	29.00	24.98	27.28	27.29	31.41
Oxides	100.21	101.28	99.46	100.32	99.12	99.84	99.11	101.85	100.76	102.00	100.97	101.96	101.95	102.26
Structural formulae (to 8 cations)														
Mg	0.3122	0.4575	0.3798	0.1563	0.4847	0.1992	0.4555	0.1841	0.1439	0.2153	0.1283	0.2692	0.0848	0.1605
Al	1.9500	1.9862	1.8910	2.0143	1.9587	1.9154	2.0085	1.8382	1.9730	1.9795	1.9607	1.9724	1.9607	1.9297
Si	3.0668	3.0355	3.0454	2.9626	2.9618	3.0116	2.9171	3.0441	2.9744	2.9922	2.9302	2.9847	2.9962	3.0007
Ca	0.8283	0.4384	0.9618	0.8498	0.6042	0.5829	0.6255	0.6988	0.8244	0.8406	0.8159	0.8201	0.6968	0.7285
Ti	0.0029	0.0000	0.0042	0.0094	0.0021	0.0052	0.0042	0.0083	0.0084	0.0093	0.0114	0.0072	0.0093	0.0083
Cr	nd	0.0000	0.0000	0.0009	0.0000	nd	nd	0.0000	nd	nd	nd	nd	0.0009	0.0000
Mn	0.0733	0.0594	0.0276	0.2422	0.0383	0.1654	0.0151	0.1306	0.3494	0.0709	0.4937	0.1703	0.4456	0.1088
Fe	1.7676	2.0231	1.6903	1.7645	1.9501	2.1109	1.9741	2.0960	1.7265	1.8923	1.6598	1.7761	1.8056	2.0636
Fe3	0.0000	0.0000	0.0595	0.0128	0.0774	0.0678	0.0702	0.1094	0.0526	0.0284	0.0976	0.0358	0.0329	0.0613
Fe2	1.7676	2.0231	1.6308	1.7517	1.8727	2.0431	1.9039	1.9866	1.6739	1.8640	1.5622	1.7404	1.7727	2.0022
SUM	8.0011	8.0000	8.0001	8.0000	7.9999	7.9906	8.0000	8.0001	8.0000	8.0000	8.0000	8.0000	7.9999	8.0001

Appendix 3 (i) (con)

	Mica schist				Orthogneiss		MMU Garnet amphibolites					
Weight % oxides												
	T1		449XZ		SF110		68		378		498	
	core	rim	core	rim	core	rim	core	rim	core	rim	core	rim
MgO	0.79	3.08	2.35	1.58	1.80	2.96	0.81	1.39	1.43	2.00	0.94	1.25
Al2O3	21.14	21.57	20.66	20.99	21.36	21.61	21.24	21.34	20.82	20.60	21.40	21.76
SiO2	38.66	38.33	37.63	37.22	38.65	38.38	37.91	37.99	36.53	37.46	37.93	38.14
CaO	7.95	7.79	5.74	7.74	10.63	7.13	9.40	10.27	7.10	8.45	9.18	9.05
TiO2	0.12	0.07	0.05	0.07	nd	nd	0.19	0.14	0.10	0.10	0.12	0.07
Cr2O3	0.01	0.00	nd	nd	nd	nd	nd	nd	nd	nd	0.00	0.00
MnO	0.72	0.17	0.27	0.28	0.85	1.76	4.13	0.24	7.37	2.89	5.47	2.47
FeO	33.22	31.23	34.42	32.48	28.45	29.87	27.59	29.42	25.51	28.33	26.52	30.01
Oxides	102.63	102.24	101.12	100.36	101.74	101.71	101.27	100.79	98.87	99.84	101.56	102.75
Structural formulae (to 8 cations)												
Mg	0.0930	0.3562	0.2777	0.1885	0.2094	0.3447	0.0952	0.1644	0.1736	0.2386	0.1110	0.1449
Al	1.9591	1.9748	1.9351	1.9783	1.9669	1.9909	1.9843	1.9896	1.9941	1.9423	1.9922	2.0005
Si	3.0383	2.9766	2.9900	2.9754	3.0194	2.9990	3.0044	3.0049	2.9677	2.9970	2.9956	2.9743
Ca	0.6696	0.6484	0.4885	0.6630	0.8896	0.5973	0.7982	0.8708	0.6179	0.7241	0.7765	0.7560
Ti	0.0072	0.0041	0.0031	0.0042	nd	nd	0.0114	0.0084	0.0064	0.0063	0.0073	0.0041
Cr	0.0009	0.0000	nd	nd	nd	nd	nd	nd	nd	nd	0.0000	0.0000
Mn	0.0482	0.0113	0.0185	0.0188	0.0561	0.1162	0.2775	0.0159	0.5069	0.1961	0.3656	0.1630
Fe	2.1836	2.0286	2.2871	2.1718	1.8587	1.9518	1.8290	1.9459	1.7334	1.8955	1.7519	1.9572
Fe3	0.0000	0.0045	0.0718	0.0421	0.0138	0.0101	0.0000	0.0000	0.0318	0.0543	0.0049	0.0211
Fe2	2.1836	1.9842	2.2153	2.1297	1.8449	1.9417	1.8290	1.9459	1.7016	1.8412	1.7470	1.9361
SUM	7.9999	8.0000	8.0000	8.0000	8.0000	7.9999	8.0000	7.9999	8.0000	7.9999	8.0001	8.0000

Appendix 3 (i) (con)

	Mica schists					Orthogneiss			UMU Garnet amphibolites					
Weight % oxides	SF119	438		442	R3		S7		B3		B12		L25	
	rim	core	rim	rim	core	rim	core	rim	core	rim	core	rim	core	rim
MgO	1.99	1.60	3.27	1.94	3.28	1.69	0.23	0.23	1.70	1.97	1.28	2.59	2.47	3.05
Al2O3	21.68	20.70	20.68	21.09	21.70	21.74	20.27	20.41	21.10	21.05	21.74	21.16	20.95	21.34
SiO2	38.10	36.24	37.05	36.95	37.98	38.67	37.75	38.02	37.64	37.88	37.87	37.90	37.39	37.88
CaO	11.26	3.09	3.87	6.47	0.63	9.52	12.21	12.59	11 22	11.44	11.53	9.89	7.39	4.71
TiO2	0.12	0.09	0.14	0.09	0.02	0.18	0.07	0.05	0.16	0.12	0.16	0.11	0.05	0.03
Cr2O3	nd	nd	nd	nd	nd	nd	0.00	0.00	nd	nd	nd	nd	nd	nd
MnO	0.73	1.32	0.46	0.85	2.26	0.33	9.15	7.01	2.19	0.66	1.32	0.62	1.14	1.83
FeO	27.52	35.98	33.57	32.31	36.44	30.10	21.45	23.29	25.99	26.86	25.46	28.12	30.80	32.31
Oxides	101.40	99.02	99.04	99.69	102.31	102.23	101.13	101.60	100.00	99.99	99.36	100.39	100.19	101.15
Structural formulae (to 8 cations)														
Mg	0.2320	0.1950	0.3939	0.2332	0.3848	0.1969	0.0270	0.0268	0.2010	0.2321	0.1525	0.3045	0.2934	0.3590
Al	1.9961	2.0004	1.9697	1.9999	2.0155	1.9978	1.8960	1.8990	1.9743	1.9659	2.0447	1.9679	1.9670	1.9882
Si	2.9762	2.9704	2.9932	2.9723	2.9929	3.0152	2.9958	3.0002	2.9880	2.9998	3.0209	2.9892	2.9777	2.9938
Ca	0.9423	0.2710	0.3351	0.5579	0.0533	0.7951	1.0382	1.0649	0.9542	0.9709	0.9854	0.8359	0.6306	0.3990
Ti	0.0073	0.0053	0.0084	0.0052	0.0010	0.0103	0.0042	0.0031	0.0095	0.0074	0.0095	0.0063	0.0031	0.0020
Cr	nd	nd	nd	nd	nd	nd	0.0000	0.0000	nd	nd	nd	nd	nd	nd
Mn	0.0482	0.0918	0.0315	0.0580	0.1510	0.0218	0.6152	0.4689	0.1472	0.0446	0.0889	0.0416	0.0766	0.1224
Fe	1.7979	2.4662	2.2682	2.1737	2.4015	1 9627	1.4235	1.5371	1.7257	1.7793	1.6981	1.8546	2.0515	2.1356
Fe3	0.0204	0.0240	0.0287	0.0227	0.0000	0.0000	0.1040	0.0977	0.0282	0.0269	0.0000	0.0428	0.0522	0.0160
Fe2	1.7775	2.4422	2.2395	2.1510	2.4015	1.9627	1.3196	1.4394	1.6975	1.7524	1.6981	1.8117	1.9994	2.1196
SUM	8.0000	8.0001	8.0000	8.0000	8.0000	7 9998	7.9999	8.0000	7.9999	8.0000	8.0000	8.0000	7.9999	8.0000

Appendix 3 (i) (con)

	Gabbro	UMU at Löland Mica schists			Gt-amph	Hyllestad schists Garnet-kyanite schists		
Weight % oxides								
	L27		L41b	SF156		KJ6	K2A		K2B	K3	SF54B		SF54C
	core	rim	rim	core	rim	rim	core	rim	rim	rim	core	rim	core
MgO	1.22	2.03	1.99	1.31	2.17	1.61	1.68	2.70	2.16	1.66	2.91	8.12	3.21
Al2O3	21.97	20.99	21.19	21.17	21.49	21.30	21.39	21.05	21.50	21.54	20.91	21.70	20.70
SiO2	38.81	38.04	37.05	38.09	38.16	38.24	38.23	37.85	38.40	38.84	37.31	38.61	37.02
CaO	11.77	7.93	6.68	9.59	10.13	12.34	8.24	7.08	10.41	9.91	3.63	0.92	3.27
TiO2	0.09	0.05	0.05	0.18	0.05	0.14	0.16	0.09	0.07	0.12	0.19	0.02	0.07
Cr2O3	0.00	0.00	0.01	0.01	0.08	0.00	nd	nd	nd	0.00	0.00	0.00	0.00
MnO	2.69	0.91	2.32	2.96	1.45	0.24	6.91	1.58	0.85	0.66	2.80	0.05	2.30
FeO	26.04	31.21	31.98	28.49	26.89	27.52	25.70	30.48	28.60	28.86	32.93	30.97	32.69
Oxides	102.59	101.17	101.26	101.81	100.41	101.38	102.29	100.82	101.99	101.60	100.67	100.39	99.26
Structural formulae (to 8 cations)													
Mg	0.1411	0.2396	0.2346	0.1536	0.2555	0.1873	0.1957	0.3181	0.2508	0.1942	0.3462	0.9374	0.3862
Al	2.0062	1.9559	1.9804	1.9624	1.9991	1.9636	1.9731	1.9625	1.9722	1.9895	1.9673	1.9828	1.9713
Si	3.0069	3.0064	2.9372	2.9947	3.0105	2.9912	2.9914	2.9929	2.9883	3.0425	2.9776	2.9920	2.9897
Ca	0.9769	0.6712	0.5676	0.8076	0.8560	1.0339	0.6908	0.5995	0.8677	0.8319	0.3103	0.0761	0.2833
Ti	0.0051	0.0031	0.0031	0.0104	0.0031	0.0084	0.0092	0.0052	0.0041	0.0072	0.0114	0.0010	0.0042
Cr	0.0000	0.0000	0.0009	0.0009	0.0049	0.0000	nd	nd	nd	0.0000	0.0000	0.0000	0.0000
Mn	0.1767	0.0609	0.1555	0.1971	0.0966	0.0158	0.4581	0.1061	0.0559	0.0440	0.1891	0.0034	0.1573
Fe	1.6872	2.0628	2.1206	1.8733	1.7742	1.7998	1.6817	2.0157	1.8610	1.8907	2.1981	2.0072	2.2080
Fe3	0.0000	0.0346	0.0783	0.0316	0.0000	0.0368	0.0263	0.0394	0.0354	0.0000	0.0437	0.0241	0.0349
Fe2	1.6872	2.0283	2.0423	1.8416	1.7742	1.7630	1.6554	1.9763	1.8257	1.8907	2.1544	1.9831	2.1731
SUM	8.0001	7.9999	7.9999	8.0000	7.9999	8.0000	8.0000	8.0000	8.0000	8.0000	8.0000	7.9999	8.0000

Appendix 3 (i) (con)

Garnet-chlorite schists | Gt-amphibolite

Weight % oxides

	472		H16		SF52		427		DAN13		A3		A4	
	rim	core	rim	core	rim	core	rim	core	rim	core	rim	core	rim	core	rim
MgO	8.09	2.97	8.19	4.00	5.15	2.74	5.92	0.96	3.42	1.03	4.37	0.93	4.84	3.09	3.85
Al2O3	21.38	21.59	22.35	21.05	21.48	21.10	21.69	21.43	21.90	21.74	22.05	21.14	22.30	21.26	21.18
SiO2	38.39	37.86	39.16	37.69	38.48	38.09	38.95	37.88	39.07	37.75	38.73	37.29	38.85	37.93	38.02
CaO	0.75	4.75	1.24	2.24	2.38	5.54	3.66	6.06	2.94	5.60	2.74	7.33	3.09	5.19	7.64
TiO2	0.02	0.07	0.05	0.02	0.03	0.12	0.02	0.10	0.05	0.12	0.05	0.14	0.02	0.10	0.03
Cr2O3	0.00	0.00	0.00	0.00	0.00	0.00	0.00	0.00	0.00	nd	0.00	0.00	0.00	0.09	0.00
MnO	0.03	2.15	0.12	0.51	0.49	8.33	2.93	5.60	0.79	9.58	0.50	5.75	0.41	2.67	0.58
FeO	31.19	31.53	30.41	35.66	33.85	25.17	28.09	29.91	33.73	26.53	33.33	28.04	30.83	31.62	29.27
Oxides	99.84	100.92	101.51	101.18	101.86	101.10	101.26	101.94	101.89	102.34	101.77	100.62	100.34	101.96	100.57

Structural formulae (to 8 cations)

Mg	0.9405	0.3502	0.9331	0.4713	0.5975	0.3228	0.6834	0.1133	0.3994	0.1208	0.5087	0.1109	0.5664	0.3615	0.4504
Al	1.9658	2.0145	2.0150	1.9629	1.9709	1.9669	1.9813	2.0028	2.0241	2.0239	2.0287	1.9958	2.0660	1.9657	1.9602
Si	2.9940	2.9968	2.9951	2.9813	2.9956	3.0114	3.0179	3.0035	3.0627	2.9810	3.0226	2.9870	3.0529	2.9742	2.9844
Ca	0.0626	0.4032	0.1014	0.1901	0.1981	0.4694	0.3036	0.5152	0.2469	0.4740	0.2288	0.6292	0.2602	0.4360	0.6425
Ti	0.0010	0.0041	0.0030	0.0010	0.0020	0.0072	0.0010	0.0061	0.0030	0.0071	0.0030	0.0084	0.0010	0.0061	0.0020
Cr	0.0000	0.0000	0.0000	0.0000	0.0000	0.0000	0.0000	0.0000	0.0000	nd	0.0000	0.0000	0.0000	0.0056	0.0000
Mn	0.0017	0.1439	0.0077	0.0343	0.0321	0.5580	0.1925	0.3759	0.0523	0.6406	0.0330	0.3903	0.0272	0.1774	0.0387
Fe	2.0345	2.0872	1.9448	2.3591	2.2038	1.6643	1.8203	1.9832	2.2115	1.7526	2.1753	1.8784	2.0263	2.0735	1.9219
Fe3	0.0393	0.0000	0.0000	0.0548	0.0315	0.0145	0.0000	0.0000	0.0000	0.0000	0.0000	0.0088	0.0000	0.0484	0.0535
Fe2	1.9953	2.0872	1.9448	2.3043	2.1723	1.6498	1.8203	1.9832	2.2115	1.7526	2.1753	1.8696	2.0263	2.0251	1.8684
SUM	8.0001	7.9999	8.0001	8.0000	8.0000	8.0000	8.0000	8.0000	7.9999	8.0000	8.0001	8.0000	8.0000	8.0000	8.0001

Appendix 3 (i) (con)

	Calc-silicate schists ("garbenschiefer")						Schists at Soetevik						Schists from Espelandsvatnet		
Weight % oxides	SF55		H17		H18		SF51		R6		R8	SF48	Y4		Y11.2
	core	rim	core	rim	core	rim	core	rim	core	rim			core	rim	core
MgO	3.69	5.58	2.74	3.63	1.58	2.31	0.92	1.24	1.19	2.79	3.75	0.99	0.73	2.15	0.77
Al2O3	19.63	19.59	21.31	21.80	20.54	20.99	20.79	20.63	20.96	21.54	21.44	21.28	20.01	21.07	20.26
SiO2	38.14	37.46	38.96	38.76	38.03	38.41	37.74	37.48	37.74	38.53	38.39	37.28	37.07	37.48	37.06
CaO	5.35	4.07	9.10	10.15	7.05	8.96	9.57	10.41	5.67	4.39	5.10	5.13	5.15	3.59	5.46
TiO2	0.10	0.02	0.21	0.05	nd	nd	0.19	0.19	0.07	0.07	0.03	0.09	0.12	0.05	0.08
Cr2O3	0.00	0.00	0.00	0.00	nd	nd	0.01	0.00	0.00	0.00	0.01	0.00	0.00	0.00	0.05
MnO	4.38	0.62	2.86	0.49	6.10	0.54	5.12	1.43	10.10	1.58	1.34	1.35	12.07	0.10	12.28
FeO	27.29	29.92	26.02	25.54	27.35	29.49	27.03	28.99	25.81	34.04	32.45	34.74	25.04	36.37	23.31
Oxides	98.58	97.26	101.21	100.43	100.64	100.69	101.38	100.37	101.54	102.93	102.53	100.86	100.19	100.82	99.27
Structural formulae (to 8 cations)															
Mg	0.4441	0.6739	0.3189	0.4222	0.1875	0.2718	0.1090	0.1474	0.1411	0.3237	0.4343	0.1188	0.0882	0.2569	0.0937
Al	1.8676	1.8701	1.9653	2.0046	1.9336	1.9538	1.9418	1.9375	1.9672	1.9792	1.9622	2.0149	1.9153	1.9891	1.9507
Si	3.0781	3.0334	3.0481	3.0234	3.0368	3.0327	2.9900	2.9868	3.0045	3.0031	2.9808	2.9939	3.0101	3.0010	3.0273
Ca	0.4626	0.3530	0.7628	0.8484	0.6030	0.7581	0.8121	0.8884	0.4836	0.3667	0.4245	0.4418	0.4479	0.3077	0.4777
Ti	0.0063	0.0010	0.0124	0.0031	nd	nd	0.0115	0.0116	0.0041	0.0040	0.0020	0.0052	0.0073	0.0031	0.0052
Cr	0.0000	0.0000	0.0000	0.0000	nd	nd	0.0009	0.0000	0.0000	0.0000	0.0009	0.0000	0.0000	0.0000	0.0030
Mn	0.2993	0.0426	0.1898	0.0325	0.4125	0.0362	0.3436	0.0964	0.6813	0.1041	0.0883	0.0920	0.8305	0.0071	0.8499
Fe	1.8420	2.0260	1.7026	1.6658	1.8266	1.9474	1.7911	1.9319	1.7182	2.2192	2.1069	2.3335	1.7007	2.4352	1.5925
Fe3	0.0480	0.0955	0.0000	0.0000	0.0296	0.0135	0.0558	0.0641	0.0242	0.0137	0.0540	0.0000	0.0673	0.0069	0.0138
Fe2	1.7940	1.9305	1.7026	1.6658	1.7970	1.9338	1.7353	1.8678	1.6940	2.2055	2.0529	2.3335	1.6334	2.4283	1.5787
SUM	8.0000	8.0000	7.9999	8.0000	8.0000	8.0000	8.0000	8.0000	8.0000	8.0000	7.9999	8.0001	8.0000	8.0001	8.0000

Appendix 3 (i) (con)

Weight % oxides

	Y13a	Y17.1		Y22		368	
	rim		core	rim	core	rim	core	rim
MgO	3.57	2.03	1.29	3.26	0.50	1.12	0.94	2.68
Al2O3	21.08	21.12	21.20	21.42	21.02	21.06	20.36	21.25
SiO2	37.51	37.65	38.03	38.30	37.65	37.46	36.97	37.89
CaO	4.15	7.36	8.51	6.02	11.13	11.05	6.20	3.58
TiO2	0.07	0.07	0.23	0.10	0.07	0.07	0.12	0.03
Cr2O3	0.01	0.01	0.00	0.09	0.00	0.00	0.03	0.00
MnO	1.31	1.48	6.01	1.66	11.48	1.40	0.77	1.18
FeO	31.58	30.43	26.68	30.27	18.96	28.00	26.61	34.97
Oxides	99.28	100.16	101.95	101.14	100.81	100.16	100.00	101.60

Structural formulae (to 8 cations)

Mg	0.4264	0.2418	0.1514	0.3825	0.0591	0.1329	0.1129	0.3165
Al	1.9941	1.9874	1.9670	1.9858	1.9678	1.9772	1.9435	1.9834
Si	3.0093	3.0051	2.9935	3.0116	2.9904	2.9830	2.9935	2.9995
Ca	0.3570	0.6297	0.7176	0.5071	0.9469	0.9432	0.5380	0.3039
Ti	0.0042	0.0042	0.0134	0.0062	0.0042	0.0042	0.0073	0.0020
Cr	0.0009	0.0009	0.0000	0.0058	0.0000	0.0000	0.0017	0.0002
Mn	0.0887	0.0999	0.4009	0.1107	0.7720	0.0947	0.6016	0.0792
Fe	2.1194	2.0310	1.7562	1.9903	1.2596	1.8648	1.8015	2.3153
Fe3	0.0000	0.0024	0.0262	0.0000	0.0377	0.0357	0.0539	0.0143
Fe2	2.1194	2.0286	1.7301	1.9903	1.2220	1.8291	1.7475	2.3010
SUM	8.0000	8.0000	8.0000	8.0000	8.0000	8.0000	8.0000	8.0000

Appendix 3 (con)

(ii) Amphiboles

	Basement Gneisses			Eclogites and associated rocks										
	55G	SF19		SF203	SF133	SF20	SF24			SF25	SF68	SF70		SF138
		core	rim	aver		aver	rim	core	incl	aver	aver	nr gt	nr cpx	aver
Na2O	1.57	2.01	1.27	1.36	1.55	2.68	3.21	3.34	3.84	1.94	3.17	2.47	2.71	1.54
MgO	5.24	5.53	5.11	7.45	11.12	9.48	10.98	12.76	6.53	9.04	10.05	8.75	11.15	7.93
Al2O3	11.84	11.58	10.71	10.97	9.35	12.72	11.66	9.40	16.22	10.95	14.70	15.66	13.11	13.55
SiO2	38.31	39.49	42.51	40.59	45.49	41.30	44.09	49.22	39.92	43.67	43.04	41.86	44.16	41.86
K2O	1.87	2.07	1.31	1.16	0.93	0.25	0.33	0.28	0.31	1.37	0.12	0.09	0.09	1.17
CaO	10.49	9.75	9.74	11.23	10.80	8.08	9.82	7.57	8.74	10.49	10.95	10.79	11.00	10.99
TiO2	0.59	0.67	0.60	0.54	0.24	0.43	0.47	0.18	0.35	0.30	0.40	0.18	0.18	0.31
Cr2O3	nd	nd	nd	0.02	0.02	0.01	0.00	0.00	0.02	0.02	nd	nd	nd	0.03
MnO	1.59	1.49	1.42	1.61	0.26	0.11	0.17	0.11	0.36	0.13	0.10	0.20	0.07	0.45
FeO	25.25	24.03	23.43	20.77	18.35	18.37	16.87	14.97	21.41	19.06	14.49	17.98	15.51	19.71
Tot ox	96.75	96.62	96.10	95.71	98.10	93.44	97.62	97.82	97.68	96.97	97.03	97.99	97.99	97.55
	Structural formulae (assuming 23 oxygens)													
Na	0.4899	0.6221	0.3874	0.4177	0.4494	0.8152	0.9123	0.9140	1.1098	0.5739	0.9130	0.7156	0.7757	0.4562
Mg	1.2600	1.3189	1.2017	1.7578	2.4798	2.2147	2.3960	2.6857	1.4509	2.0565	2.2250	1.9483	2.4522	1.8022
Al	2.2497	2.1834	1.9923	2.0467	1.6501	2.3502	2.0123	1.5643	2.8489	1.9695	2.5764	2.7583	2.2799	2.4357
Si	6.1761	6.3173	6.7063	6.4226	6.8076	6.4723	6.4532	6.9502	5.9472	6.6653	6.3972	6.2541	6.5152	6.3797
K	0.3846	0.4221	0.2633	0.2349	0.1775	0.0490	0.0622	0.0501	0.0581	0.2659	0.0223	0.0177	0.0175	0.2272
Ca	1.8112	1.6709	1.6466	1.9046	1.7316	1.3571	1.5409	1.1458	1.3946	1.7163	1.7445	1.7271	1.7390	1.7946
Ti	0.0712	0.0811	0.0717	0.0639	0.0266	0.0508	0.0518	0.0192	0.0390	0.0346	0.0450	0.0203	0.0202	0.0357
Cr	nd	nd	nd	0.0020	0.0019	0.0012	0.0000	0.0000	0.0019	0.0019	nd	nd	nd	0.0036
Mn	0.2177	0.2013	0.1902	0.2161	0.0324	0.0151	0.0216	0.0128	0.0449	0.0169	0.0129	0.0255	0.0084	0.0581
Fe	3.4045	3.2149	3.0914	2.7490	2.2959	2.4072	2.0650	1.7678	2.6672	2.4330	1.8016	2.2464	1.9137	2.5131
SUM	16.0649	16.0320	15.5509	15.8153	15.6528	15.7328	15.5153	15.1099	15.5625	15.7337	15.7377	15.7133	15.7218	15.7060

Appendix 3 (con)

(ii) Amphiboles

					LMU									MMU
	inclusions in gt		SF207 core	rim	166A1 aver	166A2 aver	SF172 aver	core	rim	L128 aver	L150 aver	aver incl	449 aver	68 aver
Na2O	1.59	1.72	1.40	1.65	4.48	4.72	2.17	2.55	1.78	1.65	1.63	1.52	1.70	1.73
MgO	8.20	8.32	12.06	9.85	9.22	8.42	8.41	8.45	8.48	9.13	8.50	7.25	9.44	7.59
Al2O3	16.04	16.06	11.03	12.98	13.33	14.62	13.45	14.08	12.54	16.79	16.07	14.63	16.00	14.88
SiO2	41.42	41.06	45.28	41 75	42.78	41.41	42.36	42.12	41 91	41.72	40.97	41.50	42.59	41.82
K2O	0.99	1.03	0.46	0.44	0.40	0.36	0.67	0.72	0.62	0.43	0.35	0.26	0.51	0.71
CaO	11.26	11.20	6.43	10.33	8.13	8.27	10.14	9.63	10.83	10.93	10.51	8.93	10.47	10.47
TiO2	0.29	0.36	0.20	0.29	0.31	0.48	0.75	0.65	0.83	0.47	0.40	0.37	0.48	0.55
Cr2O3	0.02	0.00	nd	nd	0.00	0.01	0.03	0.03	0.05	0.03	nd	nd	0.02	0.02
MnO	0.24	0.17	0.51	0.27	0.10	0.14	0.35	0.23	0.36	0.11	0.14	0.08	0.11	0.11
FeO	17 80	17.80	15.09	14.81	18.71	18.24	20.04	19.63	20.20	15.08	17.28	22.52	15.75	18.91
Tot ox	97.86	97 72	92.45	92.38	97.47	96.66	98.36	98.09	97.62	96.33	95.86	97.07	97.09	96.78
Na	0.4634	0.5005	0.4165	0.5006	1.3127	1.3946	0.6349	0.7453	0.5275	0.4786	0.4793	0.4515	0.4910	0.5096
Mg	1.8350	1.8652	2.7562	2.2956	2.0755	1.9124	1.8878	1.8985	1.9268	2.0354	1 9268	1.6535	2.0907	1.7222
Al	2.8390	2.8500	1.9952	2.3924	2.3752	2.6258	2.3886	2.5023	2.2543	2.9604	2.8810	2.6389	2.8034	2.6716
Si	6.2174	6.1796	6.9463	6.5252	6.4646	6.3073	6.3822	6.3475	6.3881	6.2414	6.2290	6.3482	6.3296	6.3679
K	0.1899	0.1971	0.0897	0.0882	0.0776	0.0692	0.1284	0.1385	0.1214	0.0816	0.0675	0.0505	0.0972	0.1372
Ca	1.8106	1.8062	1.0563	1.7303	1.3169	1.3497	1.6367	1.5549	1.7692	1 7525	1.7117	1.4639	1.6666	1.7086
Ti	0.0328	0.0411	0.0230	0.0343	0.0357	0.0549	0.0852	0.0737	0.0952	0.0527	0.0462	0.0422	0.0540	0.0635
Cr	0.0019	0.0000	nd	nd	0.0000	0.0008	0.0034	0.0038	0.0058	0.0030	nd	nd	0.0029	0.0024
Mn	0.0307	0.0222	0.0666	0.0357	0.0132	0.0178	0.0451	0.0291	0.0467	0.0136	0.0182	0.0103	0.0140	0.0138
Fe	2.2348	2.2407	1.9358	1.9358	2.3639	2.3236	2.5256	2.4736	2.5756	1.8863	2.1976	2.8816	1.9576	2.4085
SUM	15.6555	15.7026	15.2856	15.5381	16.0353	16.0560	15.7179	15.7672	15.7106	15.5045	15.5573	15.5407	15.5070	15.6053

Appendix 3 (con)

(ii) Amphiboles

	UMU													
	378	B3	B12		K2b	K3		L25		L27		L41b	L227	KJ10b
		core		rim		core	rim	core	rim	core	rim			corona
Na2O	1.62	1.03	1.69	1 47	1.25	1.33	1.83	1.86	2.09	1.32	2.01	1.40	2.09	0.10
MgO	9.67	11.93	10.47	10.28	9.97	9.58	8.69	9.93	8.47	11.48	8.68	8.32	12.51	25.08
Al2O3	12.95	12.37	15.20	15.27	15.43	12.33	13.28	12.64	14.13	9.58	14.91	12.06	12.45	0.20
SiO2	43.31	44.77	43.96	43.71	44.28	46.30	43.80	43.00	41 32	46.59	40.59	43.25	42.22	57.36
K2O	0.43	0.32	0.50	0.57	0.40	0.55	0.57	0.30	0.31	0.50	0.44	0.43	0.97	0.05
CaO	9.97	10.43	10.47	10.91	10.06	7.08	10.51	9.33	10.21	9.73	10.90	9.46	11.33	0.31
TiO2	0.36	0.33	0.50	0.47	0.43	0.47	0.44	0.52	0.58	0.27	0.45	0.49	2.29	0.02
Cr2O3	0.03	0.03	0.04	0.03	nd	nd	nd	0.03	0.02	0.00	0.00	0.00	0.01	nd
MnO	0.35	0.14	0.15	0.21	0.13	0.32	0.35	0.17	0.17	0.17	0.19	0.30	0.22	0.66
FeO	16.53	14.03	14.08	14.57	15.24	19.59	18.22	18.75	19.24	17.76	18.11	21.51	12.08	14.94
Tot ox	95.22	95.38	97.06	97.50	97.20	97.56	97.69	96.54	96.54	97.41	96.29	97.21	96.17	98.71
Na	0.4770	0.2970	0.4821	0.4202	0.3559	0.3808	0.5321	0.5454	0.6180	0.3817	0.5963	0.4129	0.6063	0.0267
Mg	2.1927	2.6570	2.2969	2.2533	2.1838	2.1155	1.9391	2.2422	1.9289	2.5438	1.9789	1.8881	2.7909	5.1784
Al	2.3236	2.1786	2.6372	2.6487	2.6746	2.1535	2.3446	2.2584	2.5452	1.6797	2.6881	2.1659	2.1972	0.0322
Si	6.5895	6.6880	6.4699	6.4308	6.5092	6.8578	6.5568	6.5152	6.3128	6.9276	6.2076	6.5891	6.3208	7.9479
K	0.0836	0.0601	0.0939	0.1074	0.0745	0.1039	0.1087	0.0585	0.0610	0.0955	0.0863	0.0838	0.1851	0.0085
Ca	1.6253	1.6700	1.6507	1.7205	1.5850	1.1243	1.6865	1.5141	1.6708	1.5510	1 7865	1.5442	1.8182	0.0466
Ti	0.0416	0.0370	0.0554	0.0517	0.0479	0.0522	0.0490	0.0598	0.0665	0.0304	0.0521	0.0562	0.2578	0.0018
Cr	0.0039	0.0039	0.0051	0.0039	nd	nd	nd	0.0039	0.0019	0.0000	0.0000	0.0004	0.0017	nd
Mn	0.0451	0.0171	0.0184	0.0258	0.0165	0.0404	0.0443	0.0224	0.0226	0.0220	0.0243	0.0385	0.0275	0.0777
Fe	2.1028	1.7533	1.7326	1.7922	1.8732	2.4268	2.2808	2.3756	2.4588	2.2085	2.3170	2.7405	1.5126	1.7310
SUM	15.4851	15.3620	15.4422	15.4545	15.3206	15.2552	15.5419	15.5955	15.6865	15.4402	15.7371	15.5195	15.7180	15.0508

Appendix 3 (con)

(ii) Amphiboles

Hyllestad schists

		SF179 aver	SF156 rim	A4	H15	H17	H18	SF51	R8	SF48	Y13a	Y22
Na2O	2.42	1.74	0.63	2.59	2.16	2.09	2.26	1.37	2.61	1.45	1.38	1.40
MgO	14.17	7.14	12.55	9.73	9.78	8.55	7.00	9.02	8.73	5.04	8.85	9.73
Al2O3	13.33	16.85	8.15	14.21	15.43	15.08	14.17	14.14	15.04	17.43	16.21	14.95
SiO2	44.76	37.80	49.03	43.59	42.48	42.88	42.51	43.43	43.51	40.48	43.21	43.67
K2O	0.28	0.63	0.23	0.73	0.45	0.45	0.75	0.51	0.47	0.41	0.48	0.47
CaO	11 64	10.37	12.16	9.64	9.02	10.49	9.11	10.95	9.20	10.76	10.55	10.37
TiO2	0.20	0.38	0.37	0.81	0.47	0.34	0.69	0.39	0.43	0.34	0.36	0.37
Cr2O3	nd	0.00	0.03	0.02	nd	nd	nd	0.02	0.02	nd	0.08	0.04
MnO	0.19	0.14	0.22	0.05	0.10	0.12	0.22	0.28	0.09	0.16	0.15	0.16
FeO	11.95	18.68	13.83	15.87	15.31	17 22	19.73	17.31	17.76	21.00	14.90	15.17
Tot ox	98.96	93.75	97.20	97.22	95.19	97.22	96.45	97.43	97.87	97.07	96.16	96.32
Na	0.6766	0.5343	0.1794	0.7455	0.6311	0.6057	0.6689	0.3978	0.7525	0.4287	0.3934	0.4029
Mg	3.0424	1.6815	2.7352	2.1556	2.1993	1.9054	1.5929	2.0074	1 9307	1.1458	1.9391	2.1582
Al	2.2638	3.1390	1.4041	2.4919	2.7443	2.6594	2.5502	2.4895	2.6330	3.1368	2.8091	2.6241
Si	6.4469	5.9725	7.1686	6.4825	6.4086	6.4155	6.4889	6.4846	6.4597	6.1782	6.3523	6.5022
K	0.0516	0.1270	0.0435	0.1376	0.0857	0.0859	0.1469	0.0977	0.0889	0.0791	0.0906	0.0889
Ca	1.7968	1.7549	1.9048	1.5368	1.4579	1.6821	1.4903	1.7514	1.4637	1.7588	1.6613	1.6550
Ti	0.0219	0.0456	0.0404	0.0902	0.0534	0.0381	0.0789	0.0443	0.0478	0.0392	0.0400	0.0419
Cr	nd	0.0005	0.0038	0.0019	nd	nd	nd	0.0028	0.0027	nd	0.0090	0.0048
Mn	0.0231	0.0189	0.0268	0.0061	0.0126	0.0151	0.0288	0.0352	0.0113	0.0207	0.0189	0.0200
Fe	1.4395	2.4682	1.6914	1 9736	1.9319	2.1548	2.5193	2.1615	2.2048	2.6807	1.8316	1.8889
SUM	15.7626	15.7424	15.1980	15.6217	15.5248	15.5620	15.5651	15.4724	15.5950	15.4680	15.1453	15.3869

Appendix 3 (con)

(iii) Biotite

Basement Gneisses

Eclogites and associated rocks LMU

	149b	55G	SF19	SF203	R1	446a	FN1	SF165	L52a	SF133	SF25	SF138	166A1	SF172
Na2O	0.32	0.09	nd	0.07	0.10	0.10	0.13	0.06	0.13	0.17	0.41	0.07	0.29	0.07
MgO	8.80	8.34	9.60	10.61	6.58	9.62	9.39	8.52	9.56	10.95	9.04	9.22	10.24	10.21
Al2O3	19.23	14.41	14.43	14.79	15.88	16.47	18.01	17.58	18.63	14.21	17.87	15.54	18.00	16.12
SiO2	35.81	35.00	35.41	34.96	34.67	35.98	34.94	35.73	35.33	36.14	35.84	35.49	34.58	35.12
K2O	9.06	9.81	9.61	9.44	9.72	9.85	9.37	9.53	9.68	9.45	9.56	9.48	9.33	7.75
CaO	0.01	0.01	0.00	0.10	0.01	0.00	0.05	0.18	nd	0.00	0.56	0.08	0.00	0.55
TiO2	1.40	2.39	2.10	1.92	2.89	2.58	1.72	3.19	1.43	4.04	2.39	2.07	3.37	2.38
Cr2O3	0.08	nd	nd	nd	nd	0.02	nd	0.01	0.02	0.00	0.01	0.01	0.00	0.02
MnO	0.06	1.00	0.00	1.01	0.50	0.34	0.13	0.10	0.07	0.06	0.11	0.28	0.07	0.15
FeO	20.41	23.68	23.22	19.87	23.76	19.81	20.29	21.31	20.55	20.53	19.78	23.43	18.30	22.47
Tot ox	95.17	94.73	94.45	92.76	94.11	94.77	94.02	96.21	95.41	95.55	95.56	95.66	94.17	94.83
Structural formulae (based on 22 oxygens)														
Na	0.0954	0.0280	nd	0.0214	0.0303	0.0308	0.0403	0.0175	0.0372	0.0500	0.1200	0.0218	0.0873	0.0215
Mg	2.0007	1.9738	2.2746	2.5125	1.5620	2.2126	2.1747	1.9369	2.1837	2.4800	2.0568	2.1386	2.3830	2.3572
Al	3.4596	2.6982	2.6837	2.7704	2.9811	2.9958	3.3004	3.1606	3.3653	2.5460	3.2170	2.8516	3.3134	2.9423
Si	5.4652	5.5592	5.5853	5.5561	5.5202	5.5526	5.4311	5.4479	5.4133	5.4940	5.4732	5.5234	5.4003	5.4383
K	1.7643	1.9879	1.9342	1.9135	1.9741	1.9392	1.8573	1.8534	1.8926	1.8320	1.8623	1.8824	1.8591	1.5305
Ca	0.0019	0.0021	0.0000	0.0162	0.0013	0.0008	0.0086	0.0289	nd	0.0000	0.0909	0.0132	0.0000	0.0916
Ti	0.1603	0.2854	0.2497	0.2298	0.3465	0.2990	0.2006	0.3655	0.1647	0.4620	0.2739	0.2418	0.3963	0.2768
Cr	0.0097	nd	nd	nd	nd	0.0026	nd	0.0011	0.0028	nd	0.0015	0.0014	0.0000	0.0029
Mn	0.0081	0.1352	0.0000	0.1359	0.0673	0.0442	0.0166	0.0127	0.0095	0.0080	0.0141	0.0369	0.0089	0.0197
Fe	2.6046	3.1451	3.0632	2.6412	3.1631	2.5574	2.6374	2.7174	2.6340	2.6100	2.5257	3.0496	2.3902	2.9097
SUM	15.5698	15.8149	15.7907	15.7970	15.6459	15.6350	15.6670	15.5419	15.7031	15.4820	15.6354	15.7607	15.8385	15.5894

Appendix 3 (con)

(iii) Biotite

	MMU						UMU							
	L128	T1	449	449XZ	68	378	438	442	B3	B12	SF156	K2a	K2b	K3
Na2O	0.14	0.15	0.03	0.07	0.08	0.10	0.11	0.12	0.28	0.12	0.04	0.30	0.16	0.77
MgO	13.28	6.42	12.55	9.92	9.71	14.56	9.60	10.27	13.50	13.12	11.08	13.13	14.23	10.12
Al2O3	17.29	18.60	16.26	18.29	16.21	16.10	17.58	18.45	16.83	16.57	17.17	19.02	17.92	16.04
SiO2	35.44	35.05	37.08	35.86	35.82	36.29	35.42	35.42	37.27	35.47	35.12	37.17	36.83	35.62
K2O	9.19	9.07	9.43	9.58	9.49	8.21	8.03	9.55	8.80	9.23	8.66	8.88	8.46	8.45
CaO	0.05	0.07	0.05	nd	0.02	0.13	0.03	0.02	0.19	0.06	0.15	0.10	0.03	0.01
TiO2	1.04	2.10	1.85	1.73	2.35	1.92	1.61	1.74	2.30	2.04	1.68	1.41	0.70	2.21
Cr2O3	0.00	0.01	0.03	0.01	0.02	nd	nd	nd	0.03	nd	0.12	nd	nd	nd
MnO	0.03	0.14	0.05	0.04	0.07	0.09	0.03	0.18	0.06	0.02	0.15	0.10	0.11	0.21
FeO	16.89	24.33	17.96	19.73	21.71	16.22	19.99	18.62	15.79	15.46	20.30	15.04	16.05	20.45
Tot ox	93.36	95.94	95.28	95.22	95.48	93.60	92.39	94.36	95.05	92.07	94.47	95.16	94.49	93.89
Struct														
Na	0.0409	0.0455	0.0088	0.0204	0.0247	0.0294	0.0329	0.0343	0.0815	0.0357	0.0108	0.0851	0.0466	0.2323
Mg	3.0448	1.4805	2.8257	2.2568	2.2300	3.2984	2.2370	2.3492	3.0066	3.0325	2.5467	2.9015	3.1798	2.3468
Al	3.1353	3.3925	2.8977	3.2898	2.9470	2.8848	3.2420	3.3384	2.9637	3.0288	3.1229	3.3249	3.1685	2.9417
Si	5.4517	5.4223	5.6027	5.4724	5.5226	5.5159	5.5406	5.4369	5.5680	5.5014	5.4178	5.5099	5.5230	5.5395
K	1.8043	1.7912	1.8172	1.8659	1.8660	1.5913	1.6017	1.8702	1.6766	1 8257	1.7035	1.6789	1.6179	1.6773
Ca	0.0083	0.0112	0.0074	nd	0.0029	0.0216	0.0052	0.0027	0.0297	0.0095	0.0254	0.0166	0.0044	0.0009
Ti	0.1208	0.2447	0.2103	0.1982	0.2721	0.2192	0.1891	0.2006	0.2588	0.2374	0.1951	0.1576	0.0787	0.2590
Cr	nd	0.0010	0.0034	0.0011	0.0029	nd	nd	nd	0.0035	nd	0.0146	nd	nd	nd
Mn	0.0035	0.0179	0.0064	0.0051	0.0093	0.0113	0.0038	0.0230	0.0077	0.0023	0.0199	0.0129	0.0142	0.0282
Fe	2.1728	3.1482	2.2702	2.5176	2.7995	2.0615	2.6144	2.3906	1.9730	2.0047	2.6190	1.8648	2.0131	2.6601
SUM	15.7823	15.5550	15.6498	15.6273	15.6770	15.6334	15.4667	15.6459	15.5691	15.6780	15.6757	15.5522	15.6462	15.6858

Appendix 3 (con)

(iii) Biotite

Hyllestad schists

	KJ6	L226	SF173	SF179	SF52	427	DAN13	A3	H17	H18	SF51	R6	R8	Y4
Na2O	2.02	0.00	0.21	0.42	0.08	0.08	0.17	0.11	0.23	0.14	0.06	0.17	0.16	0.14
MgO	14.57	16.37	14.52	13.57	14.05	9.14	13.62	7.87	16.22	11.46	11.56	12.59	11.76	11.64
Al2O3	19.96	15.00	15.88	16.58	17.90	17.49	18.21	17.76	17.02	15.46	16.68	17.64	16.79	17.64
SiO2	35.43	37.44	35.24	34.81	36.65	38.78	39.41	36.12	36.97	36.46	35.61	37.22	37.51	36.56
K2O	4.72	9.38	9.39	8.00	8.45	9.16	9.34	9.36	8.56	8.64	8.36	9.71	9.54	9.92
CaO	2.50	nd	0.05	0.01	nd	nd	nd	nd	nd	nd	nd	nd	nd	nd
TiO2	0.13	4.06	2.70	2.25	1.28	1.43	1.62	1.78	0.14	0.91	1.70	1.67	1.66	2.19
Cr2O3	0.08	nd	0.03	0.03	nd	nd	0.03	0.04	1.30	1.64	0.02	nd	0.05	0.11
MnO	0.18	0.13	0.08	0.05	0.19	0.15	0.19	0.16	0.01	0.11	0.09	0.19	0.17	0.13
FeO	15.14	13.42	16.02	19.03	15.50	18.37	13.31	19.12	14.08	19.01	20.18	17.11	18.49	16.69
Tot ox	94.74	95.80	94.12	94.74	94.10	94.59	95.89	92.31	94.53	93.84	94.26	96.31	96.13	95.01
Struct														
Na	0.5801	nd	0.0625	0.1232	0.0236	0.0240	0.0490	0.0346	0.0674	0.0429	0.0188	0.0489	0.0459	0.0398
Mg	3.2150	3.5957	3.3049	3.0882	3.1470	2.0560	2.9530	1.8381	3.5974	2.6409	2.6516	2.7948	2.6287	2.6216
Al	3.4826	2.6069	2.8601	2.9855	3.1717	3.1130	3.1240	3.2826	2.9857	2.8181	3.0274	3.0959	2.9703	3.1422
Si	5.2439	5.5198	5.3837	5.3161	5.5067	5.8550	5.7340	5.6628	5.5010	5.6385	5.4814	5.5423	5.6277	5.5238
K	0.8919	1.7640	1.8297	1.5582	1.6205	1.7650	1.7330	1.8716	1.6250	1.7053	1.6412	1.8446	1.8267	1.9120
Ca	0.3959	nd	0.0074	0.0024	nd	nd	nd	nd	nd	nd	nd	nd	nd	nd
Ti	0.0143	0.4505	0.3107	0.2588	0.1449	0.1620	0.1770	0.2104	0.0152	0.1061	0.1972	0.1871	0.1872	0.2490
Cr	0.0099	nd	0.0039	0.0033	nd	nd	0.0030	0.0045	0.1533	0.2010	0.0022	nd	0.0058	0.0129
Mn	0.0227	0.0168	0.0103	0.0059	0.0239	0.0190	0.0230	0.0217	0.0017	0.0146	0.0118	0.0243	0.0221	0.0161
Fe	1.8746	1.6542	2.0470	2.4305	1.9474	2.3200	1.6200	2.5068	1.7526	2.4587	2.5980	2.1312	2.3194	2.1086
SUM	15.7309	15.6079	15.7577	15.6489	15.5857	15.3140	15.4160	15.4331	15.6993	15.6261	15.6296	15.6691	15.6338	15.6260

Appendix 3 (con)

(iii) Biotite

	Y11.2	Y13a	Y17.1	Y22	368
Na2O	0.13	0.11	0.13	0.08	0.23
MgO	13.31	13.02	10.75	13.28	12.90
Al2O3	18.12	17.46	18.58	17.14	19.24
SiO2	36.97	35.90	36.23	36.92	37.62
K2O	9.67	9.50	9.40	9.44	8.94
CaO	nd	nd	nd	nd	nd
TiO2	1.65	1.82	1.85	1.60	1.38
Cr2O3	nd	nd	nd	nd	nd
MnO	0.18	0.09	0.11	0.10	0.17
FeO	14.43	15.69	18.37	16.49	14.83
Tot ox	94.51	93.62	95.51	95.15	95.35
Struct					
Na	0.0384	0.0325	0.0382	0.0230	0.0645
Mg	2.9718	2.9588	2.4160	2.9732	2.8326
Al	3.1994	3.1390	3.3042	3.0350	3.3418
Si	5.5370	5.4759	5.4652	5.5470	5.5434
K	1.8474	1.8484	1.8082	1.8100	1.6801
Ca	nd	nd	nd	nd	nd
Ti	0.1855	0.2090	0.2097	0.1804	0.1532
Cr	0.0066	0.0049	0.0113	0.0108	0.0072
Mn	0.0225	0.0120	0.0145	0.0131	0.0207
Fe	1.8070	2.0009	2.3168	2.0723	1.8275
SUM	15.6156	15.6814	15.5841	15.6648	15.4710

Appendix 3 (con)

(iv) Chlorite

Basement Gneisses					LMU			MMU		UMU				
Weight % oxides	149b	SF203	446a	FN1	L52a	L128	L150	449XZ	438	442	B12	K2a	SF156	KJ6
Na2O	0.11	0.03	0.03	0.00	0.00	0.05	0.02	0.00	0.01	0.09	0.00	0.04	0.00	0.29
MgO	13.97	14.52	2.54	14.64	14.77	19.19	18.56	15.17	13.97	14.88	16.02	18.79	10.60	24.69
Al2O3	22.35	18.33	17.89	22.20	23.08	21.02	22.02	21.96	22.26	21.44	17.47	22.19	20.04	17.81
SiO2	24.13	25.06	23.16	24.01	24.21	26.28	24.86	25.20	23.82	24.21	21.12	26.74	26.62	31.16
K2O	0.72	0.05	0.07	0.04	0.07	0.35	0.04	0.18	0.06	0.08	0.05	1.13	0.86	0.06
CaO	0.02	0.26	0.03	0.03	0.06	0.04	0.02	0.17	0.01	0.05	0.00	0.04	0.04	1.70
TiO2	0.13	0.26	0.02	0.08	0.11	0.14	0.08	0.10	0.08	0.08	0.02	0.33	0.07	0.15
Cr2O3	0.07	nd	0.01	nd	0.02	nd	nd	0.00	nd	nd	nd	nd	0.08	0.01
MnO	0.16	1.63	0.49	0.23	0.12	0.05	0.07	0.13	0.06	0.33	0.12	0.14	0.33	0.07
FeO	25.92	26.27	43.08	24.96	24.97	19.50	20.06	24.62	25.85	24.63	31.06	18.43	30.03	11.68
Tot ox	87.57	86.40	87.32	86.17	87.41	86.61	85.72	87.53	86.12	85.79	85.85	87.81	88.66	87.60
Structural formulae (based on 14 oxygens)														
Na	0.0219	0.0062	0.0077	0.0000	0.0010	0.0107	0.0036	0.0000	0.0026	0.0197	0.0000	0.0080	0.0000	0.0542
Mg	2.2277	2.3874	0.4483	2.3425	2.3256	2.9616	2.9037	2.3807	2.2473	2.3939	2.7137	2.8504	1.6922	3.6077
Al	2.8196	2.3842	2.4946	2.8111	2.8743	2.5657	2.7260	2.7249	2.8331	2.7287	2.3419	2.6626	2.5319	2.0582
Si	2.5814	2.7650	2.7405	2.5785	2.5571	2.7212	2.6102	2.6529	2.5716	2.6129	2.4010	2.7217	2.8522	3.0547
K	0.0976	0.0072	0.0103	0.0048	0.0099	0.0458	0.0055	0.0236	0.0080	0.0112	0.0067	0.1462	0.1169	0.0074
Ca	0.0019	0.0306	0.0034	0.0032	0.0063	0.0039	0.0024	0.0189	0.0011	0.0056	0.0000	0.0040	0.0047	0.1785
Ti	0.0103	0.0213	0.0014	0.0061	0.0087	0.0110	0.0063	0.0083	0.0066	0.0064	0.0015	0.0250	0.0060	0.0107
Cr	0.0061	nd	0.0007	nd	0.0016	nd	nd	0.0000	nd	nd	nd	nd	0.0064	0.0006
Mn	0.0147	0.1525	0.0493	0.0205	0.0107	0.0047	0.0059	0.0113	0.0056	0.0298	0.0114	0.0119	0.0296	0.0056
Fe	2.3188	2.4237	4.2628	2.2417	2.2064	1.6884	1.7613	2.1677	2.3342	2.2234	2.9535	1.5689	2.6907	0.9581
SUM	10.1000	10.1781	10.0190	10.0084	10.0016	10.0130	10.0248	9.9881	10.0101	10.0314	10.4297	9.9987	9.9306	9.9357

Appendix 3 (con)

(iv) Chlorite

Hyllestad schists

	KJ10b	SF52	427	DAN13	A3	H15	H17	SF51	R6	Y11.2	Y13a	Y17.1	368
Na2O	0.00	0.02	0.02	0.02	0.03	0.00	0.00	0.00	0.04	0.05	0.04	0.03	0.00
MgO	26.28	19.59	12.77	17.67	11.61	17.79	16.13	16.13	18.44	20.20	19.14	17.50	19.14
Al2O3	19.92	21.98	22.12	22.68	21.22	21.10	21.97	20.71	22.21	22.50	21.85	22.11	22.17
SiO2	28.68	26.96	24.78	25.78	24.39	25.74	24.60	25.50	26.07	25.36	25.88	25.19	25.71
K2O	0.05	0.70	0.37	0.19	0.15	0.06	0.06	0.06	0.29	0.06	0.24	0.04	0.25
CaO	0.05	0.00	0.00	0.00	0.00	0.00	0.00	0.00	0.00	0.00	0.00	0.00	0.00
TiO2	0.04	0.18	0.16	0.09	0.10	0.07	0.07	0.07	0.13	0.08	0.11	0.07	0.10
Cr2O3	nd	0.00	0.00	0.00	0.00	0.00	0.00	0.00	0.00	0.00	0.00	0.00	0.00
MnO	0.12	0.43	0.31	0.43	0.30	0.29	0.04	0.17	0.37	0.26	0.17	0.23	0.27
FeO	11.48	18.82	24.96	19.26	25.13	19.49	23.63	24.00	20.49	17.43	18.89	21.39	18.80
Tot ox	86.61	88.68	85.48	86.12	82.94	84.54	86.50	86.64	88.04	85.95	86.32	86.56	86.43
Struct													
Na	0.0007	0.0041	0.0040	0.0035	0.0062	0.0000	0.0000	0.0000	0.0036	0.0104	0.0088	0.0069	0.0000
Mg	3.8720	2.9441	2.0580	2.7332	1.9349	2.8128	2.5495	2.5475	1.4062	3.1070	2.9522	2.7207	2.9476
Al	2.3218	2.6129	2.8210	2.7761	2.7972	2.6383	2.7463	2.5870	1.3401	2.7376	2.6653	2.7198	2.7015
Si	2.8354	2.7195	2.6810	2.6762	2.7268	2.7301	2.6083	2.7021	1.3340	2.6170	2.6781	2.6283	2.6572
K	0.0057	0.0907	0.0510	0.0250	0.0219	0.0081	0.0080	0.0083	0.0192	0.0082	0.0319	0.0058	0.0324
Ca	0.0053	0.0000	0.0000	0.0000	0.0000	0.0000	0.0000	0.0000	0.0000	0.0000	0.0000	0.0000	0.0000
Ti	0.0030	0.0136	0.0130	0.0069	0.0080	0.0058	0.0056	0.0059	0.0051	0.0062	0.0089	0.0053	0.0080
Cr	nd	0.0000	0.0000	0.0000	0.0000	0.0000	0.0000	0.0000	0.0000	0.0000	0.0000	0.0000	0.0000
Mn	0.0099	0.0369	0.0280	0.0377	0.0281	0.0258	0.0036	0.0149	0.0161	0.0229	0.0146	0.0206	0.0234
Fe	0.9496	1.5872	2.2580	1.6724	2.3499	1.7293	2.0953	2.1265	0.8769	1.5038	1.6345	1.8662	1.6251
SUM	10.0034	10.0088	9.9140	9.9310	9.8730	9.9501	10.0166	9.9920	9.9920	10.0131	9.9943	9.9736	9.9952

Appendix 3 (con)

(v) Epidote

	Basement Gneisses			Eclogites	MMU	
	SF203	R1 rim	446a	SF25	68	378
Na2O	0.05	0.05	0.00	0.02	0.02	0.02
MgO	0.04	0.08	0.06	0.14	0.06	0.08
Al2O3	23.69	24.53	27.63	24.61	26.18	24.90
SiO2	36.97	37.55	38.11	37.95	38.39	37.75
K2O	0.05	0.05	0.05	0.05	nd	0.05
CaO	22.96	23.06	22.56	22.66	23.07	23.18
TiO2	0.15	0.13	0.24	0.11	0.09	0.15
Cr2O3	0.00	0.03	0.02	0.02	0.02	nd
MnO	0.18	0.16	0.05	0.01	0.03	0.10
FeO	11.40	10.37	6.83	10.85	8.39	9.77
SUM	95.49	96.01	95.55	96.42	96.25	95.98
Structural formulae (based on 25 oxygens)						
Na	0.0156	0.0162	0.000	0.0054	0.0051	0.0054
Mg	0.0098	0.0201	0.014	0.0350	0.0146	0.0200
Al	4.5394	4.7417	5.170	4.7329	4.9740	4.7962
Si	6.0083	6.1589	6.048	6.1919	6.1083	6.1680
K	0.0098	0.0095	0.010	0.0094	nd	0.0094
Ca	3.9984	4.0525	3.836	3.9608	3.9851	4.0581
Ti	0.0186	0.0161	0.028	0.0137	0.0113	0.0184
Cr	0.0000	0.0044	0.002	0.0021	0.0022	nd
Mn	0.0244	0.0226	0.006	0.0018	0.0037	0.0132
Fe	1.3947	1.4227	0.816	1.4809	1.1310	1.3344
SUM	16.0190	16.4647	15.930	16.4339	16.3153	16.4231

Appendix 3 (con)

(vi) Feldspars

	Basement Gneisses					Eclogites and associated rocks					LMU			MMU				UMU
Weight % oxides	SF19	SF203	R1	446a	FN1	SF165	L52a	SF133	SF20	SF25	SF138	L128	L150	449XZ	68	378	438	442	B3 core
Na2O	10.57	0.71	10.09	7.82	7.23	7.41	8.12	7.16	9.57	8.90	9.24	5.95	7.04	8.97	9.76	8.38	7.67	7.23	7.36
MgO	0.06	0.00	0.04	0.02	0.04	1.21	0.06	1.05	0.02	0.93	0.02	0.02	0.03	0.03	0.04	0.02	0.04	0.04	0.02
Al2O3	19.23	18.75	21.59	22.80	26.36	20.30	24.29	22.05	18.32	21.94	22.23	26.59	25.69	23.65	22.05	23.57	24.07	25.04	24.97
SiO2	67.72	64.55	65.78	60.90	60.86	63.91	61.51	54.94	62.95	60.81	64.79	55.48	58.02	62.43	64.16	60.79	61.00	59.24	59.10
K2O	0.26	15.57	0.16	1.10	0.11	0.27	0.11	0.26	0.06	1.20	0.19	0.11	0.07	0.12	0.11	0.08	0.11	0.19	0.08
CaO	1.47	0.00	2.33	4.75	7.19	3.27	5.97	8.90	1.19	3.42	3.53	9.36	7.43	5.23	3.46	5.48	5.61	6.98	7.09
TiO2	0.00	nd	nd	0.02	0.00	0.24	0.02	0.02	0.02	0.17	0.03	nd	0.00	0.01	0.02	nd	nd	nd	nd
MnO	0.08	nd	nd	0.00	0.00	0.27	0.00	0.00	0.01	nd	0.01	nd	0.00	0.00	nd	nd	nd	nd	nd
FeO	0.22	0.07	0.04	0.04	0.07	3.27	0.13	1.77	0.40	2.15	0.31	0.27	0.14	0.08	0.10	0.29	0.16	0.29	0.03
SUM	99.60	99.65	100.03	97.45	101.86	100.13	100.21	96.15	92.54	99.52	100.34	97.78	98.42	100.53	99.70	98.61	98.66	99.01	98.65
Structural formulae (based on 8 oxygens)																			
Na	0.902	0.063	0.859	0.691	0.612	0.639	0.698	0.657	0.876	0.780	0.787	0.530	0.619	0.768	0.838	0.732	0.668	0.631	0.644
Mg	0.004	0.000	0.003	0.001	0.003	0.081	0.004	0.074	0.001	0.063	0.001	0.001	0.002	0.002	0.003	0.001	0.003	0.003	0.001
Al	0.998	1.022	1.117	1.225	1.357	1.066	1.269	1.230	1.020	1.169	1.151	1.439	1.373	1.231	1.151	1.252	1.273	1.329	1.329
Si	2.981	2.986	2.888	2.774	2.657	2.845	2.725	2.599	2.973	2.750	2.846	2.548	2.630	2.756	2.840	2.739	2.737	2.666	2.668
K	0.014	0.919	0.009	0.064	0.006	0.015	0.006	0.016	0.004	0.069	0.011	0.006	0.004	0.007	0.006	0.005	0.006	0.011	0.005
Ca	0.069	0.000	0.110	0.232	0.336	0.156	0.283	0.451	0.060	0.166	0.166	0.461	0.361	0.247	0.164	0.264	0.270	0.337	0.343
Ti	0.000	nd	nd	0.001	0.000	0.008	0.001	0.001	0.001	0.006	0.001	nd	0.000	0.000	0.001	nd	nd	nd	nd
Mn	0.003	nd	nd	0.000	0.000	0.010	0.000	0.000	0.000	nd	0.000	nd	0.000	0.000	nd	nd	nd	nd	nd
Fe	0.008	0.003	0.002	0.002	0.002	0.122	0.004	0.063	0.014	0.081	0.011	0.010	0.005	0.003	0.004	0.011	0.006	0.010	0.001
SUM	4.979	4.994	4.987	4.990	4.973	4.941	4.990	5.091	4.949	5.084	4.975	4.995	4.994	5.015	5.005	5.004	4.963	4.987	4.991

Appendix 3 (con)

(vi) Feldspars

		B12	L25	L27	L41b	SF156		K2a	K2b	K3		KJ6	L226		L227	SF179
	rim					core	rim			core	rim		core	rim		
Na2O	8.17	8.11	9.39	5.39	10.18	7.59	8.53	4.13	6.64	9.29	8.50	3.98	5.56	6.22	3.91	5.53
MgO	0.08	0.00	0.02	0.04	0.04	0.06	0.02	0.02	0.06	0.00	0.00	0.02	0.35	0.02	0.04	0.02
Al2O3	23.56	24.04	21.83	28.17	21.63	25.33	24.61	29.83	26.61	22.60	23.20	30.26	27.83	26.51	30.39	26.59
SiO2	60.41	60.92	64.21	55.95	65.21	60.58	62.05	53.05	57.83	64.68	61.73	52.28	55.58	56.52	51.20	55.61
K2O	0.11	0.10	0.06	0.11	0.06	0.24	0.15	0.07	0.10	0.11	0.16	0.04	0.39	0.12	0.04	0.05
CaO	5.63	5.56	3.18	10.35	2.86	6.55	5.31	12.50	8.72	3.69	4.80	12.83	10.09	8.82	12.98	8.85
TiO2	nd	nd	nd	0.02	0.00	0.02	0.00	nd	nd	0.02	0.00	0.02	0.06	0.04	0.02	0.06
MnO	nd	nd	nd	nd	nd	0.00	0.00	nd	nd	0.14	0.07	0.00	nd	nd	nd	0.01
FeO	0.19	0.06	0.19	0.49	0.16	0.14	0.01	0.10	0.10	0.00	0.10	0.03	0.68	0.25	0.16	0.01
SUM	98.15	98.79	98.88	100.52	100.14	100.51	100.68	99.70	100.06	100.53	98.56	99.46	100.54	98.50	98.74	96.73
Na	0.72	0.706	0.81	0.468	0.87	0.652	0.729	0.363	0.576	0.790	0.740	0.351	0.485	0.549	0.348	0.495
Mg	0.01	0.000	0.00	0.003	0.00	0.004	0.001	0.001	0.004	0.000	0.000	0.001	0.023	0.001	0.003	0.001
Al	1.26	1.272	1.15	1.488	1.12	1.322	1.277	1.595	1.404	1.168	1.228	1.623	1.474	1.423	1.646	1.447
Si	2.73	2.734	2.86	2.506	2.87	2.682	2.732	2.406	2.588	2.835	2.773	2.379	2.498	2.572	2.353	2.568
K	0.01	0.006	0.00	0.006	0.00	0.014	0.008	0.004	0.006	0.006	0.009	0.002	0.023	0.007	0.003	0.003
Ca	0.27	0.268	0.15	0.497	0.13	0.311	0.251	0.607	0.418	0.173	0.231	0.626	0.486	0.430	0.639	0.438
Ti	nd	nd	nd	0.001	0.00	0.001	0.000	nd	nd	0.001	0.000	0.001	0.002	0.001	0.001	0.002
Mn	nd	nd	nd	nd	nd	0.000	0.000	nd	nd	0.005	0.003	0.000	nd	nd	nd	0.001
Fe	0.01	0.002	0.01	0.018	0.01	0.005	0.001	0.004	0.004	0.000	0.004	0.001	0.026	0.009	0.006	0.001
SUM	4.999	4.986	4.976	4.986	5.006	4.989	4.998	4.980	5.000	4.978	4.988	4.984	5.016	4.993	4.998	4.955

Appendix 3 (con)

(vii) Ilmenite

Eclogites and associated rocks	LMU					MMU					UMU						
Weight % oxides	SF133	SF25	SF138	SF172	L150	T1	449	449XZ	68	378	438	K2a	K3	L25	L27	L41b	KJ6	SF179
SiO2	0.00	0.00	nd	0.00	0.00	0.02	0.00	0.00	0.00	0.00	0.00	0.00	0.03	0.00	0.00	0.00	0.25	0.00
TiO2	52.92	52.23	49.09	49.69	49.12	52.26	52.96	52.82	52.11	52.28	52.72	52.11	50.52	50.59	46.70	48.99	49.57	50.48
Al2O3	0.04	0.00	0.08	0.03	0.07	0.08	0.05	0.00	0.05	0.05	0.07	0.03	0.00	0.02	0.00	0.08	0.16	0.03
Cr2O3	0.00	0.02	0.02	0.03	0.00	nd	nd	0.00	nd	nd	0.00	nd	nd	0.00	nd	nd	0.52	0.00
FeO	45.66	47.15	47.44	48.57	48.90	43.13	46.86	46.21	48.01	45.39	45.84	46.84	47.50	48.08	51.00	50.01	46.39	48.70
MnO	0.00	0.36	2.47	1.30	0.43	1.08	nd	1.02	0.36	1.57	0.47	1.41	0.88	0.46	0.51	nd	0.74	0.99
MgO	1.38	0.97	0.07	0.17	0.61	0.00	0.17	0.00	0.08	0.53	0.17	0.06	0.00	0.10	0.56	0.28	0.64	1.23
CaO	0.00	0.00	nd	0.00	0.00	0.00	0.11	0.00	0.06	0.00	0.00	nd	0.00	0.00	0.00	0.00	0.00	0.00
SUM	100.00	100.73	99.20	99.78	99.13	96.57	100.15	100.34	100.67	99.82	99.27	100.45	98.93	99.25	98.77	99.36	98.27	101.43
Structural formulae																		
Si	0.000	0.000	nd	0.000	0.000	0.001	0.000	0.000	0.000	0.000	0.00	0.000	0.001	0.000	0.00	0.000	0.006	0.000
Ti	0.990	0.986	0.930	0.961	0.933	1.021	1.004	1.002	0.982	0.995	1.01	0.991	0.969	0.965	0.89	0.932	0.963	0.956
Al	0.000	0.000	0.000	0.001	0.002	0.002	0.002	0.000	0.002	0.002	0.00	0.001	0.000	0.001	0.00	0.002	0.005	0.001
Cr	0.000	0.000	0.000	0.001	nd	nd	nd	0.000	nd	nd	nd	nd	nd	nd	nd	nd	0.011	0.000
Fe3	0.010	0.000	0.130	0.000	0.065	0.000	0.000	0.000	0.034	0.000	0.00	0.000	0.031	0.069	0.22	0.069	0.000	nd
Fe2	0.940	0.988	0.880	1.045	0.968	0.935	0.985	0.973	0.970	0.959	0.97	0.989	0.981	0.951	0.86	0.987	1.001	1.023
Mn	0.000	0.008	0.050	0.028	0.009	0.024	nd	0.022	0.008	0.034	0.01	0.030	0.019	0.010	0.01	nd	0.016	0.021
Mg	0.050	0.036	0.000	0.006	0.023	0.000	0.006	0.000	0.003	0.020	0.01	0.002	0.000	0.004	0.02	0.010	0.025	0.046
Ca	0.000	0.000	0.000	0.000	0.000	0.000	0.003	0.000	0.002	0.000	0.00	nd	0.000	0.000	0.00	0.000	0.000	0.000
SUM	1.990	2.018	1.990	2.042	2.000	1.982	1.999	1.996	2.000	2.008	1.997	2.012	2.000	2.000	2.000	2.000	2.026	2.047

Appendix 3 (con)

(viii) Muscovite

	Basement Gneisses					Eclogites	LMU	MMU			UMU	Hyllestad schists	
Weight % oxides	149b	R1	446a	FN1	SF165	L52a	SF25	T1	449XZ	438	442	K2a	SF54B inc	SF54B mat
Na2O	1.19	0.19	0.30	0.66	0.22	1.39	0.54	0.41	1.11	0.76	0.46	0.69	6.58	2.04
MgO	1.48	2.30	1.71	1.77	1.87	1.04	2.57	1.34	1.19	0.96	1.49	2.47	0.08	1.29
Al2O3	31.60	26.80	28.95	30.87	30.51	32.80	27.48	32.44	33.26	34.64	33.52	31.54	38.90	33.02
SiO2	46.90	48.40	46.26	46.31	48.62	45.84	48.59	47.15	45.22	47.19	46.70	49.50	46.47	45.52
K2O	9.20	11.11	10.95	9.70	10.02	9.26	10.77	9.98	9.57	9.34	10.23	9.12	1.16	8.22
CaO	0.12	0.02	0.00	0.00	0.08	0.01	0.04	0.00	0.01	0.00	0.00	0.00	0.45	0.00
TiO2	0.49	0.56	0.65	0.64	0.74	0.52	0.47	0.75	0.65	0.50	0.63	0.47	0.17	0.50
Cr2O3	nd	0.01	0.02	0.02	0.00	nd	0.01	0.02	nd	nd	0.01	nd	nd	nd
MnO	0.11	0.05	0.03	0.02	0.01	0.01	0.02	0.03	0.00	nd	0.02	0.01	0.00	0.01
FeO	3.73	4.90	3.64	3.37	2.53	3.15	3.91	2.13	2.52	1.20	2.15	2.10	0.92	2.60
Tot ox	94.83	94.33	92.51	93.36	94.60	94.03	94.40	94.25	93.53	94.59	95.20	95.89	94.72	93.21
Structural formulae (based on 22 oxygens)														
Na	0.3111	0.0498	0.0801	0.1753	0.0577	0.3673	0.1431	0.1067	0.2926	0.1971	0.1185	0.1755	1.6464	0.5385
Mg	0.2977	0.4714	0.3550	0.3621	0.3744	0.2113	0.5235	0.2689	0.2424	0.1902	0.2966	0.4830	0.0146	0.2623
Al	5.0289	4.3473	4.7570	4.9879	4.8276	5.2534	4.4256	5.1500	5.3481	5.4281	5.2801	4.8864	5.9185	5.3028
Si	6.3303	6.6606	6.4465	6.3481	6.5260	6.2281	6.6376	6.3490	6.1669	6.2724	6.2406	6.5057	5.9972	6.1996
K	1.5848	1.9499	1.9478	1.6962	1.7152	1.6055	1.8770	1.7141	1.6649	1.5834	1.7441	1.5295	0.1916	1.4280
Ca	0.0180	0.0035	0.0000	0.0000	0.0109	0.0011	0.0055	0.0000	0.0021	0.0000	0.0005	0.0000	0.0621	0.0000
Ti	0.0496	0.0578	0.0686	0.0660	0.0748	0.0534	0.0485	0.0756	0.0670	0.0496	0.0634	0.0461	0.0162	0.0516
Cr	nd	0.0006	0.0019	0.0023	0.0000	nd	0.0010	0.0024	nd	nd	0.0011	nd	nd	nd
Mn	0.0121	0.0058	0.0039	0.0020	0.0010	0.0008	0.0021	0.0036	0.0000	nd	0.0019	0.0011	0.0000	0.0015
Fe	0.4214	0.5641	0.4239	0.3867	0.2844	0.3583	0.4467	0.2393	0.2872	0.1338	0.2400	0.2303	0.0996	0.2964
SUM	14.0539	14.1108	14.0847	14.0266	13.8720	14.0792	14.1105	13.9096	14.0712	13.8546	13.9868	13.8576	13.9462	14.0807

Appendix 3 (con)

(viii) Muscovite

	SF54C inc	mat	472 mat	H16	SF52	427	DAN13	A3	H17	R6	Y11.2	Y13a	Y17.1	Y22
Na2O	6.38	1.95	1.35	0.94	0.86	0.94	0.51	1.06	6.31	0.74	0.83	0.75	1.94	1.17
MgO	0.11	1.37	1.48	1.25	2.60	1.19	0.75	0.82	0.24	1.90	1.53	1.91	1.33	1.23
Al2O3	38.66	32.80	31.65	31.28	32.33	30.89	33.51	32.17	41.22	31.27	32.14	32.08	30.94	33.83
SiO2	45.74	46.79	46.53	46.33	46.35	47.37	48.23	47.26	47.36	47.68	46.68	47.48	48.96	46.73
K2O	1.37	8.16	8.85	9.96	8.65	9.56	9.27	9.42	1.36	10.15	10.15	10.00	8.33	9.78
CaO	0.26	0.00	0.00	0.00	0.01	0.01	0.01	0.00	0.39	0.00	0.00	0.03	1.05	0.01
TiO2	0.19	0.47	0.43	1.02	0.41	0.82	0.44	0.62	0.19	0.42	0.50	0.47	0.40	0.38
Cr2O3	nd	nd	nd	nd	nd	nd	0.05	0.02	nd	nd	0.03	0.03	0.06	0.02
MnO	0.01	0.00	0.04	0.00	0.02	0.03	0.00	0.01	0.02	0.03	0.02	0.01	0.03	0.01
FeO	1.03	2.66	3.04	3.77	4.60	3.62	2.77	2.16	0.46	3.65	1.91	1.43	1.27	1.25
Tot ox	93.75	94.19	93.37	94.55	95.83	94.43	95.56	93.54	97.53	95.83	93.80	94.19	94.30	94.40
Na	1.6151	0.5077	0.3561	0.2468	0.2217	0.2468	0.1311	0.2772	1.5282	0.1916	0.2189	0.1948	0.5013	0.3039
Mg	0.0223	0.2737	0.3003	0.2538	0.5188	0.2404	0.1485	0.1662	0.0443	0.3784	0.3091	0.3825	0.2645	0.2452
Al	5.9507	5.1992	5.0862	5.0139	5.0945	4.9314	5.2259	5.1359	6.0733	4.9336	5.1405	5.0848	4.8729	5.3450
Si	5.9717	6.2902	6.3417	6.3001	6.1957	6.4142	6.3801	6.4005	5.9189	6.3816	6.3328	6.3842	6.5401	6.2637
K	0.2282	1.3992	1.5394	1.7286	1.4757	1.6523	1.5644	1.6268	0.2168	1.7324	1.7565	1.7145	1.4189	1.6720
Ca	0.0366	0.0000	0.0000	0.0000	0.0018	0.0011	0.0020	0.0000	0.0516	0.0003	0.0000	0.0049	0.1499	0.0012
Ti	0.0182	0.0472	0.0440	0.1048	0.0411	0.0833	0.0440	0.0635	0.0175	0.0420	0.0514	0.0479	0.0405	0.0383
Cr	nd	nd	nd	nd	nd	nd	0.0053	0.0018	nd	nd	0.0032	0.0030	0.0067	0.0016
Mn	0.0015	0.0000	0.0047	0.0000	0.0017	0.0035	0.0000	0.0013	0.0016	0.0029	0.0023	0.0010	0.0030	0.0015
Fe	0.1121	0.2993	0.3468	0.4283	0.5140	0.4104	0.3067	0.2451	0.0476	0.4090	0.2170	0.1610	0.1420	0.1404
SUM	13.9564	14.0165	14.0192	14.0763	14.0650	13.9834	13.8080	13.9183	13.8998	14.0718	14.0317	13.9786	13.9398	14.0128

Appendix 3 (con)

(viii) Muscovite

	368
Na2O	0.68
MgO	2.19
Al2O3	30.93
SiO2	47.38
K2O	9.68
CaO	0.00
TiO2	0.50
Cr2O3	0.03
MnO	0.01
FeO	1.96
Tot ox	93.36
Na	0.1781
Mg	0.4425
Al	4.9516
Si	6.4353
K	1.6779
Ca	0.0000
Ti	0.0514
Cr	0.0037
Mn	0.0010
Fe	0.2223
SUM	13.9638

(ix) Staurolite

Hyllestad schists

Weight % oxides

	SF54B	SF54C	472 inc	472 mat	H12 inc	H12 mat
MgO	2.44	2.07	1.22	1.24	2.15	1.68
Al2O3	53.25	52.93	54.64	53.36	52.57	53.32
SiO2	28.14	28.04	29.50	28.35	28.59	28.51
CaO	nd	nd	0.01	nd	nd	nd
TiO2	0.56	0.58	0.50	0.00	0.63	0.56
MnO	0.01	0.04	0.14	0.45	nd	nd
FeO	12.66	13.54	11.82	12.05	13.69	11.60
ZnO	0.39	0.26	nd	nd	0.69	2.13
tot ox	97.45	97.47	97.83	95.45	98.30	97.80

Structural formulae (based on 24 O)

Mg	0.5041	0.4297	0.2590	0.2592	0.4423	0.3479
Al	8.7081	8.6882	9.1850	8.8333	8.5712	8.7112
Si	3.9031	3.9038	4.2070	3.9814	3.9536	3.9508
Ca	nd	nd	0.0010	nd	nd	nd
Ti	0.0589	0.0611	0.0540	0.0004	0.0651	0.0581
Mn	0.0016	0.0051	0.0170	0.0532	nd	nd
Fe	1.4687	1.5768	1.4100	1.4147	1.5829	1.3440
Zn	0.0399	0.0268	nd	nd	0.0703	0.2184
SUM	14.6844	14.6915	15.1330	14.5422	14.6854	14.6304

(x) Chloritoid

Hyllestad schists

	H12	SF54C	472	SF48
Na2O	0.00	0.02	0.00	0.00
MgO	4.97	4.59	4.89	1.59
Al2O3	40.59	41.02	40.04	40.04
SiO2	24.86	24.40	24.16	24.49
K2O	0.00	0.05	0.03	0.00
CaO	0.00	0.34	0.01	0.00
TiO2	0.01	0.04	0.01	0.02
MnO	0.06	0.07	0.16	0.18
FeO	21.29	20.72	21.18	26.37
tot ox	91.78	91.25	90.47	92.68

Structural formulae (based on 24 O)

Na	nd	0.0069	nd	nd
Mg	1.2110	1.1246	1.2120	0.3935
Al	7.8200	7.9478	7.8510	7.8464
Si	4.0632	4.0096	4.0180	4.0707
K	nd	0.0104	0.0060	nd
Ca	nd	0.0599	0.0010	0.0000
Ti	0.0016	0.0044	0.0010	0.0021
Mn	0.0080	0.0093	0.0230	0.0260
Fe	2.9094	2.8482	2.9460	3.6655
SUM	16.0132	16.0211	16.0580	16.0042

Appendix 3 (con)

(xi) Pyroxene

Eclogites (and associated rocks) UMU

	SF133 aver opx	SF133 aver cpx	SF68 cpx	SF70 cpx core	SF70 cpx rim	166A1 core	166A2	L226	L227	KJ6	SF173 primary cpx	*SF173 primary cpx (rim)	*SF173 corona cpx	SF179 primary cpx
Weight % oxides														
Na2O	0.19	1.74	4.17	5.04	3.85	7.06	7.21	0.67	0.62	0.84	0.62	0.58	0.53	0.48
MgO	15.65	10.48	10.37	9.97	10.62	7.19	6.91	14.56	14.20	13.41	13.58	13.24	13.00	15.89
Al2O3	1.02	1.54	6.49	6.96	8.98	8.53	8.95	2.89	2.86	4.68	4.78	4.16	3.79	4.25
SiO2	51.03	51.40	54.34	56.13	51.84	54.88	54.45	52.03	51.41	50.46	49.91	50.34	49.69	50.27
CaO	1.27	19.80	17.29	16.20	13.28	11.79	11.61	20.56	21.69	18.82	19.49	19.97	20.79	14.80
TiO2	0.13	0.14	0.11	0.06	0.13	0.12	0.13	0.35	0.38	0.90	1.10	1.25	0.90	1.15
Cr2O3	0.01	0.01	nd	0.00	0.00	0.00	0.00	nd	0.02	0.05	0.01	0.00	0.05	0.02
MnO	1.00	0.33	0.00	0.00	0.03	0.00	0.00	0.46	0.29	0.15	0.26	0.25	0.15	0.18
FeO	30.69	14.46	5.75	6.85	11.50	8.97	9.33	7.80	7.20	9.56	9.38	8.80	8.01	9.47
SUM	101.01	99.88	98.50	101.22	100.22	98.53	98.59	99.32	98.67	98.88	99.14	98.65	96.91	96.51
Structural formulae (based on 4 cations)														
Na	0.0144	0.1273	0.2966	0.3486	0.2723	0.4995	0.5101	0.0483	0.0451	0.0614	0.0452	0.0423	0.0392	0.0356
Mg	0.8979	0.5900	0.5673	0.5304	0.5767	0.3910	0.3757	0.8064	0.7913	0.7490	0.7575	0.7436	0.7428	0.9049
Al	0.0465	0.0685	0.2810	0.2927	0.3857	0.3670	0.3849	0.1265	0.1263	0.2069	0.2111	0.1849	0.1710	0.1916
Si	1.9641	1.9416	1.9954	2.0028	1.8894	2.0029	1 9870	1.9334	1 9228	1.8916	1.8686	1.8969	1.9041	1.9203
Ca	0.0524	0.8013	0.6802	0.6195	0.5188	0.4611	0.4541	0.8186	0.8692	0.7561	0.7816	0.8065	0.8536	0.6060
Ti	0.0039	0.0040	0.0030	0.0015	0.0035	0.0032	0.0036	0.0099	0.0107	0.0255	0.0310	0.0355	0.0260	0.0330
Cr	0.0003	0.0002	nd				0.0000	nd	0.0005	0.0016	0.0003	0.0000	0.0016	0.0005
Mn	0.0327	0.0104	0.0000	0.0000	0.0008		0.0000	0.0146	0.0091	0.0047	0.0084	0.0078	0.0049	0.0057
Fe	0.9878	0.4567	0.1765	0.2045	0.3506	0.2738	0.2847	0.2424	0.2251	0.2997	0.2937	0.2821	0.2568	0.3024
Fe3	0.0411	0.1676	0.0190	0.0473	0.1051	0.1220	0.1442	0.0352	0.0515	0.2776	0.0398	0.0000	0.0144	0.0078
Fe2	0.9467	0.2892	0.1575	0.1572	0.2455	0.1519	0.1405	0.2072	0.1737	0.0221	0.2539	0.2821	0.2424	0.2946
SUM	4.0000	4.0000	4.0000	4.0000	3.9978	3.9985	4.0001	4.0001	4.0001	3.9965	3.9974	3.9996	4.0000	4.0000

Fe3 calculated by method of Neumann (1976)

* minor amounts of potassium were also detected in these samples

Appendix 3 (con)

(xi) Pyroxene

	*SF179 primary cpx (rim)	opx
Na2O	0.54	0.10
MgO	12.84	22.00
Al2O3	3.98	1.73
SiO2	49.04	53.20
CaO	21.27	1.32
TiO2	1.01	0.05
Cr2O3	0.02	0.01
MnO	0.26	0.54
FeO	7.50	16.92
SUM	96.51	95.88
Na	0.0405	0.0078
Mg	0.7364	1.2573
Al	0.1806	0.0782
Si	1.8863	2.0403
Ca	0.8768	0.0543
Ti	0.0293	0.0015
Cr	0.0005	0.0002
Mn	0.0084	0.0176
Fe	0.2412	0.5428
Fe3	0.0281	0.0000
Fe2	0.2131	0.5428
SUM	4.0000	4.0000

Fe3 calculated by method of Neumann (1976)

* minor amounts of potassium were also detected in these samples

APPENDIX 4: Abbreviations of mineral names used in the text and figures

A number of different abbreviations have been used in the text, tables, and figures to denote mineral groups, species, and intergrowths. A list of these abbreviations is presented below, many of these are also listed with particular tables or diagrams.

actinolite	act, AC (amphibole composition diagrams only)
Al_2SiO_5	AS
albite	ab, alb
almandine	alm
amphibole	am, amp, amph
andalusite	ad
andradite	and, AND
annite	ann
anorthite	an, anr, anor
apatite	ap, apa, apat
barroisite	bar, BA (amphibole composition diagrams only)
biotite	bi, bio, biot
calcite	cal, calc
chlorite	ch, chl, chlor
chloritoid	cd, ctd
clinopyroxene	cpx
clinozoisite	czo
crossite	CR (amphibole composition diagrams only)
diopsite	di, dio
dolomite	dol
edenite	ED (amphibole composition diagrams only)
epidote	epi, epid
feldspar	fsp
garnet	ga, gt, gar, garn
grossular	grs, gross, GR (garnet composition diagrams only)
haematite	hm
hedenbergite	hed
hornblende	hbl, HD (amphibole composition diagrams only)
ilmenite	il, ilm
jadeite	jd, jad
K-feldspar	Ksp, Kfs, K-fsp
kyanite	ky, kya
labradorite	lab
magnetite	mt, mag
muscovite	mu, mus, musc
myrmekite	myrm
oligoclase	olig
olivine	oli, oliv
opaque ore	opaq
orthopyroxene	opx
paragonite	pa, par
pargasite	PA (amphibole composition diagrams only)
perthite	perth
phengite	phen
phlogopite	phl, phlog
plagioclase	pla, plag
pyrite	pyr
pyrope	PYR (garnet composition diagrams only)
pyrophyllite	pyroph
quartz	q, qz, qtz
richterite	RI (amphibole composition diagrams only)
rutile	rut
sillimanite	si, sil, sill
spessartine	sps, SP (garnet composition diagrams only)
sphene	sph
spinel	spi
staurolite	st, sta, staur
talc	tal, tc
tourmaline	tou, tour
tremolite	tr, tre, TR (amphibole composition diagrams only)
tschermakite	TS (amphibole composition diagrams only)
winchite	WI (amphibole composition diagrams only)
zircon	zir, zirc
zoisite	zo